

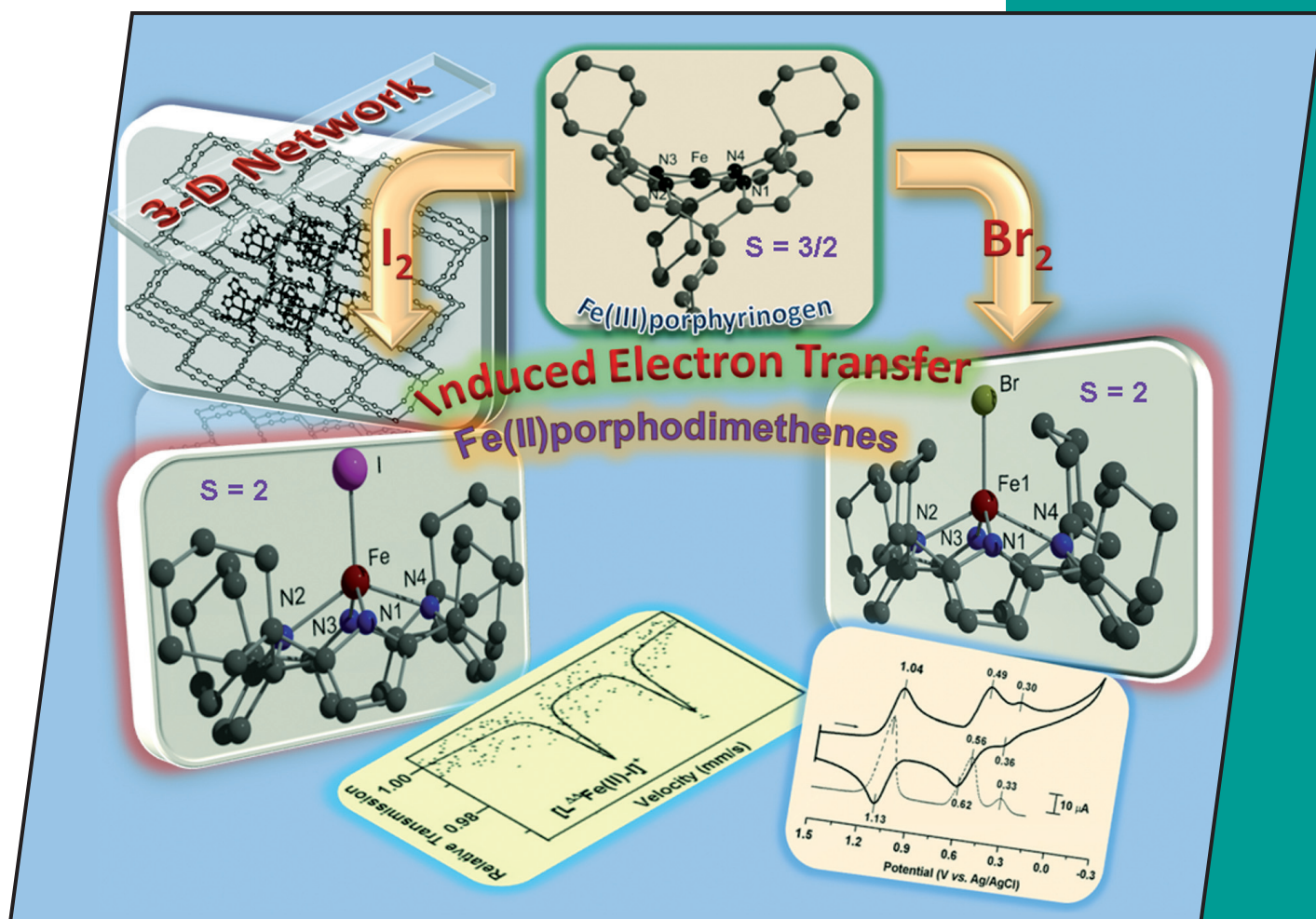
22/2010

1st August Issue

[22]

**EurJIC**  
European Journal of  
Inorganic Chemistry

Eur. J. Inorg. Chem. 2010, 3389–3540

**Cover Picture**

Dibyendu Bhattacharya and Sabyasachi Sarkar

Tetrakis(cyclohexyl)iron(II)porphodimethene with Different Axial Ligands

**Microreview**

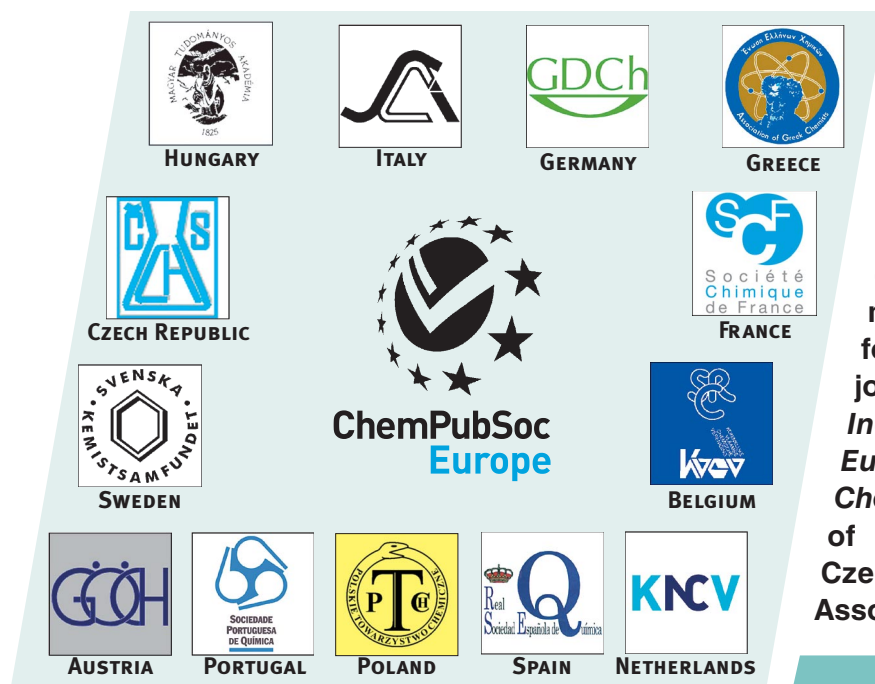
L. Jos de Jongh, Jan Reedijk et al.

Coordination Versatility of Pyrazole-Based Ligands

A Journal of

ChemPubSoc  
Europe

www.eurjic.org

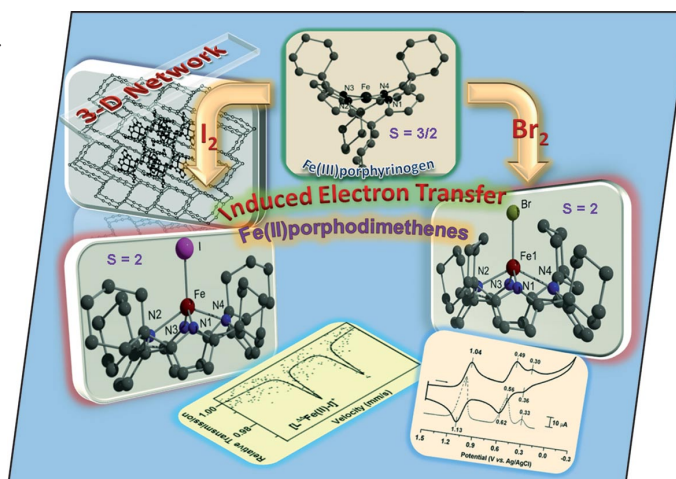


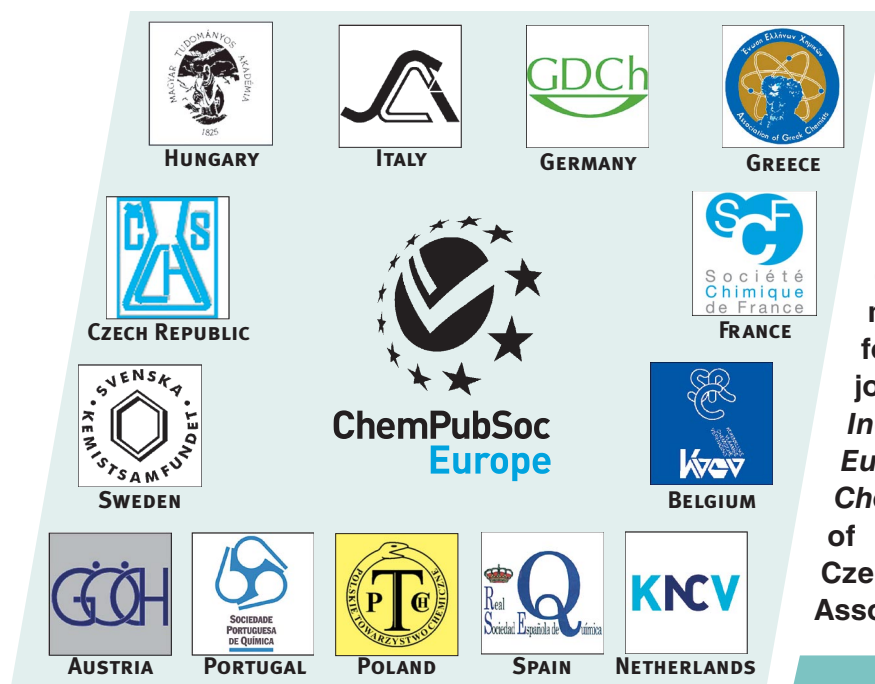
EurJIC is co-owned by 11 societies of ChemPubSoc Europe, a union of European chemical societies for the purpose of publishing high-quality science. All owners merged their national journals to form two leading chemistry journals, the *European Journal of Inorganic Chemistry* and the *European Journal of Organic Chemistry*. Three further members of ChemPubSoc Europe (Austria, Czech Republic and Sweden) are Associates of the two journals.

Other ChemPubSoc Europe journals are *Chemistry – A European Journal*, *ChemBioChem*, *ChemPhysChem*, *ChemMedChem*, *ChemSusChem* and *ChemCatChem*.

## COVER PICTURE

The cover picture shows induced electron-transfer reactions with  $I_2$  or  $Br_2$  as external oxidant,  $Fe^{III}$  as internal oxidant, and coordinated porphyrinogen as internal reductant. As a result of this simultaneous metal- and ligand-based redox reaction, the square-planar iron(III) complex is transformed to a square-pyramidal iron(II) complex, and the tetraanionic porphyrinogen ligand is oxidized to the neutral porphodimethene. The iron(III/II) redox potential of porphodimethene complexes are more positive than that of the heme cofactor. The large quadruple splitting with large isomeric shift indicates a high-spin state ( $S = 2$ ) for the  $[L^{\Delta\Delta}Fe^{II}-I]^+$  cation. Details are discussed in the article by S. Sarkar et al. on p. 3429ff.



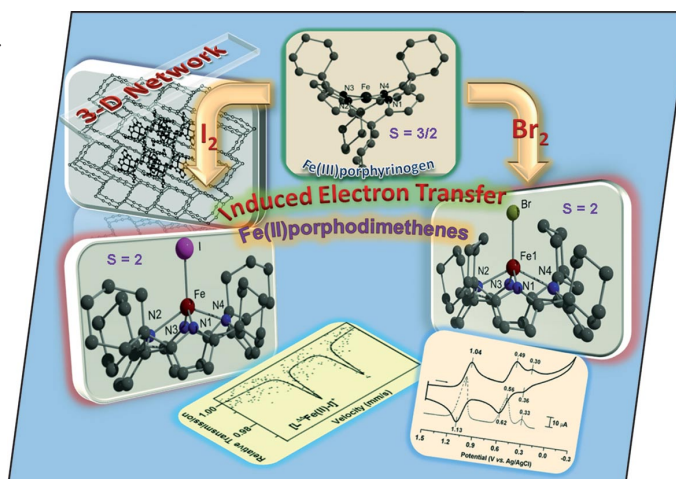


EurJIC is co-owned by 11 societies of ChemPubSoc Europe, a union of European chemical societies for the purpose of publishing high-quality science. All owners merged their national journals to form two leading chemistry journals, the *European Journal of Inorganic Chemistry* and the *European Journal of Organic Chemistry*. Three further members of ChemPubSoc Europe (Austria, Czech Republic and Sweden) are Associates of the two journals.

Other ChemPubSoc Europe journals are *Chemistry – A European Journal*, *ChemBioChem*, *ChemPhysChem*, *ChemMedChem*, *ChemSusChem* and *ChemCatChem*.

## COVER PICTURE

The cover picture shows induced electron-transfer reactions with  $I_2$  or  $Br_2$  as external oxidant,  $Fe^{III}$  as internal oxidant, and coordinated porphyrinogen as internal reductant. As a result of this simultaneous metal- and ligand-based redox reaction, the square-planar iron(III) complex is transformed to a square-pyramidal iron(II) complex, and the tetraanionic porphyrinogen ligand is oxidized to the neutral porphodimethene. The iron(III/II) redox potential of porphodimethene complexes are more positive than that of the heme cofactor. The large quadruple splitting with large isomeric shift indicates a high-spin state ( $S = 2$ ) for the  $[L^{\Delta\Delta}Fe^{II}-I]^+$  cation. Details are discussed in the article by S. Sarkar et al. on p. 3429ff.



# CONTENTS

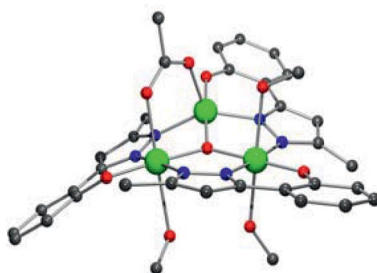
## MICROREVIEW

### Pyrazole Complexes

M. Viciano-Chumillas, S. Tanase,  
L. J. de Jongh,\* J. Reedijk\* ... 3403–3418

Coordination Versatility of Pyrazole-Based Ligands towards High-Nuclearity Transition-Metal and Rare-Earth Clusters

**Keywords:** N ligands / Cluster compounds / Magnetic properties / Transition metals / Rare earths



The coordination chemistry of pyrazole-based ligands is reviewed. The formation of polynuclear clusters and other supramolecular structures such as metallocycles or metallohelicates shows the versatility of the ligand. Magnetic properties of the described compounds are detailed.

## SHORT COMMUNICATIONS

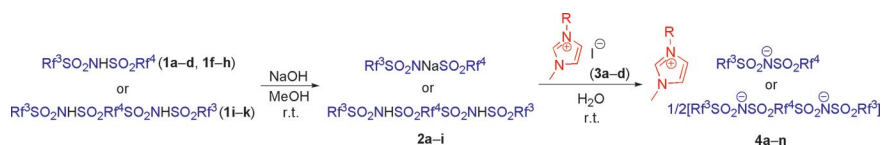
### Fluorinated Ionic Liquids

C.-P. Zhang, Z.-L. Wang,  
Q.-Y. Chen, C.-T. Zhang, Y.-C. Gu,  
J.-C. Xiao\* ..... 3419–3422



Synthesis and Physicochemical Properties of Bis(fluoroalkanesulfon)amide-Based Ionic Liquids

**Keywords:** Ionic liquids / Fluorine / Anions / Bis(fluoroalkanesulfon)amides / Physicochemical properties



A series of bis(fluoroalkanesulfon)amides were synthesized in good yield from the reaction of fluoroalkanesulfonamides and fluoroalkylsulfonyl fluorides. Combination

of these amide anions with imidazolium cations afforded a variety of novel ionic liquids, which demonstrated high densities and wide liquid range.

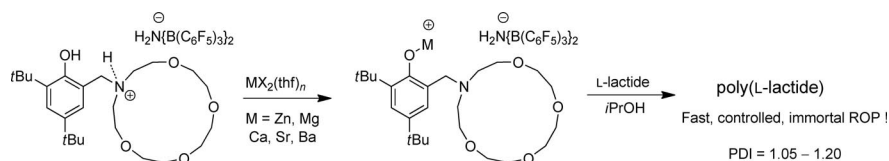
### Alkaline-Earth Metal Cations

Y. Sarazin,\* V. Poirier, T. Roisnel,  
J.-F. Carpentier\* ..... 3423–3428



Discrete, Base-Free, Cationic Alkaline-Earth Complexes – Access and Catalytic Activity in the Polymerization of Lactide

**Keywords:** Alkaline earth metals / Cations / Anions / Ring-opening polymerization / Lactides



A pinch of precious salts: Stable, base-free, discrete cations of alkaline-earth metals (Mg→Ba) and zinc are available in good yields by simple procedures. These highly

Lewis acidic species promote efficiently the controlled, immortal ring-opening polymerization of L-lactide, and the catalytic activity increases with the ionic radius.



## FULL PAPERS

### Iron Porphyrins

D. Bhattacharya, S. Sarkar\* ... 3429–3435

Synthesis, Structural, Redox and Mössbauer Characterization of Four-Electron-Oxidized Tetrakis(cyclohexyl)iron(II)porphodimethene with Different Axial Ligations

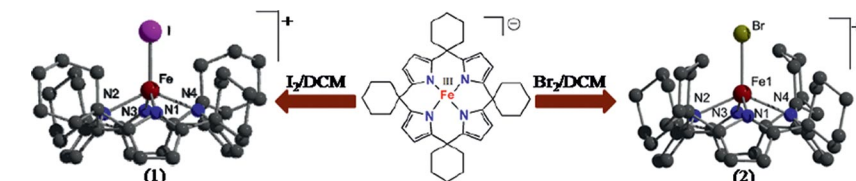
**Keywords:** Crystal engineering / Electron transfer / Iron / Porphyrinoids / Moessbauer spectroscopy

### Perovskite Compounds

R. Cortés-Gil, J. M. Alonso,  
M. L. Ruiz-González,  
J. M. González-Calbet\* ..... 3436–3440

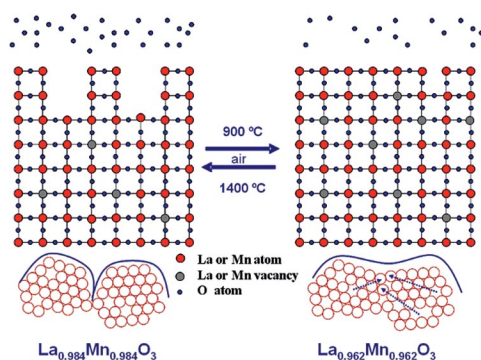
Topotactic Migration of Cationic Vacancies in  $\text{La}_{1-x}\text{Mn}_{1-x}\text{O}_3$

**Keywords:** Lanthanum / Manganese / Perovskite / Microscopy / Surface chemistry



Iron(II)porphodimethene complexes were formed by an electron-transfer reaction between the  $\text{Fe}^{\text{III}}$  and porphyrinogen centers in the  $\text{Fe}^{\text{III}}$  porphyrinogen complex. CV of the oxidized complex shows the reversibly

accessible  $\text{Fe}^{\text{II/III}}$  oxidation states; the redox potential is nearly 1 V more positive than that for a typical heme cofactor, which suggests an oxidizing nature of the tetrapyrrole framework in the  $\text{L}^{\Delta\Delta}$  moiety.



The  $\text{La}_{1-x}\text{Mn}_{1-x}\text{O}_3$  system exhibits reversible topotactic behaviour through an oxidizing–reducing process. On the basis of the surface evolution followed by SEM and

AFM, we present a diffusion mechanism of La and Mn cations through the grain boundaries.

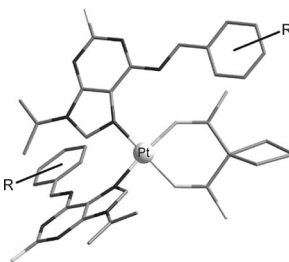
### Cytotoxic Platinum(II) Complexes

L. Dvořák, I. Popa, P. Štarha,  
Z. Trávníček\* ..... 3441–3448

In Vitro Cytotoxic-Active Platinum(II) Complexes Derived from Carboplatin and Involving Purine Derivatives

**Keywords:** Platinum / Nucleobases / Cytotoxicity / Antitumor agents

$[\text{Pt}(\text{cbdc})(\text{HL}_n)_2]$  complexes bearing the cyclobutane-1,1-dicarboxylate (cbdc) dianion and 6-benzylamino-2-chloro-9-isopropylpurine derivatives ( $\text{HL}_n$ ) have been synthesized from  $[\text{Pt}(\text{cbdc})(\text{dmsO})_2]$ , fully characterized and tested for their in vitro cytotoxicity against chronic myelogenous leukaemia and breast adenocarcinoma human cancer cell lines.

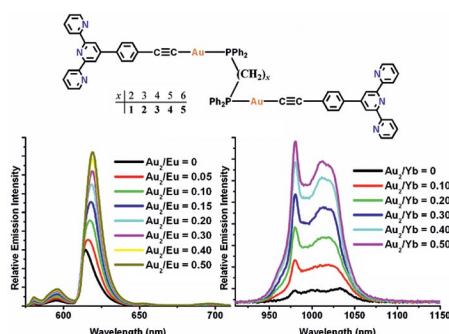


### Gold(I) Acetylides

X.-L. Li,\* K.-J. Zhang, J.-J. Li,  
X.-X. Cheng, Z.-N. Chen ..... 3449–3457

Dual Luminescent Dinuclear Gold(I) Complexes of Terpyridyl-Functionalized Alkyne Ligands and Their Efficient Sensitization of  $\text{Eu}^{\text{III}}$  and  $\text{Yb}^{\text{III}}$  Luminescence

**Keywords:** Gold / Lanthanides / Dinuclear complexes / Sensitized luminescence / Alkynes



The binuclear gold(I) complexes  $[(\text{tpy}-\text{C}_6\text{H}_4\text{C}\equiv\text{CAu})_2\{\mu-\text{Ph}_2\text{P}(\text{CH}_2)_n\text{PPh}_2\}]$  ( $n = 2-6$ ) display dual luminescence at room temperature. Spectrophotometric titration

and quantum yields demonstrate that they can behave as good energy donors for  $\text{Eu}^{\text{III}}$  and  $\text{Yb}^{\text{III}}$  emission.

# CONTENTS

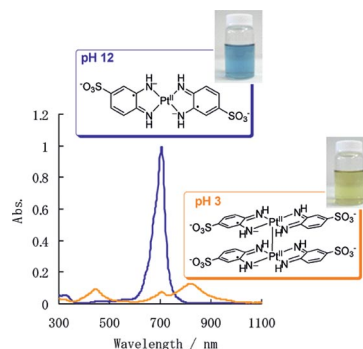
## NIR-Absorbing Complex

A. Masuya, N. Iki,\* C. Kabuto, Y. Ohba,  
S. Yamauchi, H. Hoshino ..... 3458–3465



pH-Responsive Switching of the Near-Infrared Absorption of the Water-Soluble Bis(*o*-diiminobenzosemiquinonato)platinum-(II) Complex

**Keywords:** Absorption / Platinum / Radicals / N ligands / Electronic structure



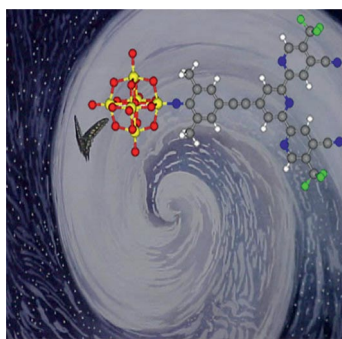
A water-soluble singlet diradical complex of Pt<sup>II</sup> has been prepared that shows intense absorption of near-infrared (NIR) light in basic solutions. The complex shows pH-responsive switching of the NIR absorption upon ligand-centered oxidation followed by dimerization caused by an increase in the red potential of the solution at low pH.

## Enhanced NLO Response in POMs

M. R. S. A. Janjua, W. Guan, L. Yan,  
Z.-M. Su,\* A. Karim,  
J. Akbar ..... 3466–3472

Quantum Chemical Design for Enhanced Second-Order NLO Response of Terpyridine-Substituted Hexamolybdates

**Keywords:** Polyoxometalates / Organic–inorganic hybrid composites / Second-order polarizability / Charge transfer / Density functional calculations



Small variations in the initial configuration of system **1** ( $886.55 \times 10^{-30}$  esu) have produced large variations in the long-term behavior of system **7** ( $4622.92 \times 10^{-30}$  esu). The butterfly effect in quantum mechanics may encapsulate this idea, which leads to a remarkable increase in NLO response.

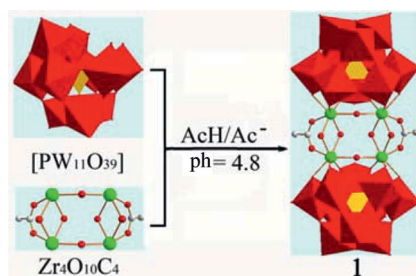
## Zr-Containing POMs

W. Zhang, S.-X. Liu,\* C.-D. Zhang,  
R.-K. Tan, F.-J. Ma, S.-J. Li,  
Y.-Y. Zhang ..... 3473–3477



An Acetate-Functionalized Tetranuclear Zirconium Sandwiching Polyoxometalate Complex

**Keywords:** Polyoxometalates / Sandwich complexes / Zirconium / Clusters / Stabilization



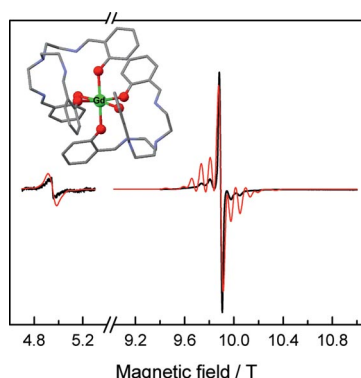
Dimeric zirconium-sandwiching polyoxometalate complex  $K_4H_6[Zr_4(OH)_6(CH_3COO)_2(\alpha-PW_{10}O_{37})_2] \cdot 23H_2O$  (**1**) was prepared from  $ZrCl_4$  and  $K_7[PW_{11}O_{39}]$  and characterized by single-crystal X-ray, thermogravimetric, and elemental analysis, IR, UV, and NMR spectroscopy, and cyclic voltammetry. It is stable in a wide pH range for a long time and has good electrocatalytic activity in the reduction of nitrite.

## Rare-Earth Coordination Chemistry

S. Tanase,\* S. Sottini, V. Marvaud,  
E. J. J. Groenen,  
L.-M. Chamoreau ..... 3478–3483

Anion-Induced Assembly of Hexacoordinate Rare-Earth(III) Complexes

**Keywords:** Rare earths / Schiff bases / Structure elucidation / EPR spectroscopy / Magnetic properties



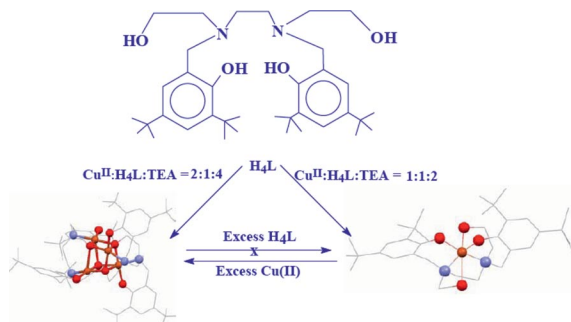
Unusual hexacoordinate complexes with general formula  $[RE\{(Hsal)_3tren\}_2](CF_3SO_3)_3 \cdot nCH_3CN$  [ $RE = Eu$  (**1**),  $Gd$  (**2**), and  $Tb$  (**3**);  $n = 0.5$  or  $1.5$ ] were obtained from the reaction of tris[2-(salicylidene-imino)ethyl]amine,  $(Hsal)_3tren$ , with  $RE-(CF_3SO_3)_3 \cdot nH_2O$  both in the presence and absence of tetrabutylammonium hydroxide. The synthesis, crystal structure, and properties of complexes **1–3** are described in detail.

## Cubane-Type Cu Complex

D. Maity, A. D. Jana, M. Debnath,  
N. G. R. Hearn, M.-H. Sie, H. M. Lee,  
R. Clérac,\* M. Ali\* ..... 3484–3490

A  $\mu_3$ -Alkoxo-Bridged Tetranuclear  $[\text{Cu}_4\text{L}_2]$  Copper(II) Complex of a Hexadentate  $\text{N}_2\text{O}_4$  Donor Ligand with a  $[6 + 0]$   $\text{Cu}_4\text{O}_4$  Cubane Core: Synthesis, Crystal Structure, and Magnetic Properties

**Keywords:** Copper /  $\text{N}_2\text{O}_4$  donor ligands / Magnetic properties



A novel hexacoordinating non-Schiff base ligand ( $\text{H}_4\text{L}$ ) with  $\text{N}_2\text{O}_4$  donor atoms and its mono- and tetranuclear  $\text{Cu}^{\text{II}}$  complexes

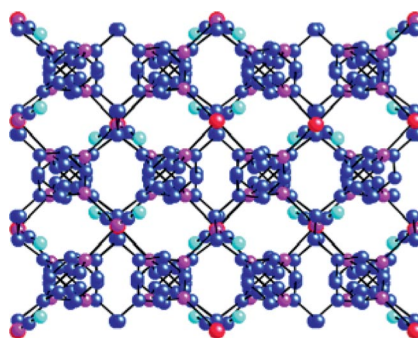
have been synthesized and characterized by single-crystal X-ray diffraction and magnetic measurements.

## Weak Ferromagnetism

N. de la Pinta, G. Madariaga, L. Lezama,  
M. L. Fidalgo, R. Cortés\* ..... 3491–3497

Weak Ferromagnetism Caused by a 2D Effect in Two New Cobalt(II)– and Nickel(II)–1,2-Bis(4-pyridyl)ethane (bpa) Polynuclear Compounds

**Keywords:** Polynuclear structures / Magnetic properties / Structure-magnetism relationship / N ligands / Cyanato ligands / Cobalt / Nickel



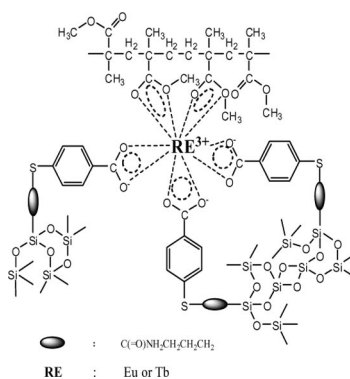
Two new polynuclear compounds have been synthesized by using the cyanato ligand and bpa linker with cobalt and nickel as the transition metals. This combination leads to the formation of  $\text{M}-(\text{gauche-bpa})_2-\text{M}$  ( $\text{M} = \text{Co}$  and  $\text{Ni}$ ) bridges and a global 2D network through interchain hydrogen bonds. Although the bpa intermetallic bridges exhibit slight antiferromagnetic interactions, packing of the chains causes a 2D canting effect.

## Rare Earth Polymeric Hybrids

K. Sheng, B. Yan,\* H.-F. Lu,  
L. Guo ..... 3498–3505

Ternary Rare Earth Inorganic–Organic Hybrids with a Mercapto-Functionalized Si–O Linkage and a Polymer Chain: Coordination Bonding Assembly and Luminescence

**Keywords:** Organic-inorganic hybrid composites / Rare earths / Polymers / Bridging ligands / Sulfur / Luminescence



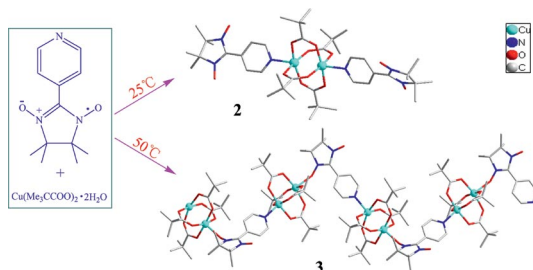
Ternary rare earth/organic/inorganic/polymeric hybrid materials containing both inorganic networks ( $\text{Si}-\text{O}-\text{Si}$ ) and organic polymeric  $\text{C}-\text{C}$  chains have been assembled. The small bridge molecule ligand precursor (mercaptobenzoic acid)-Si is constructed through mercapto functionalization with different coupling reagents and the polymer ligand is synthesized by a polymerization reaction.

## Copper–Radical Complexes

X.-d. Chen, R. Rong, Y. Wang, L.-l. Zhu,  
Q.-h. Zhao, S. G. Ang,  
B.-w. Sun\* ..... 3506–3512

Three Novel Copper–Radical Complexes: Syntheses, Crystal Structures, and Magnetic Properties

**Keywords:** Copper / Magnetic properties / Radicals / Structure elucidation



Paddle-wheel dicopper complex **2** and chain complex **3** were synthesized from the same reactants but at different temperatures: 25 and 50 °C, respectively. Unlike the antiferromagnetic interactions that take

place between radicals and copper(II) ions through the pyridine nitrogen atom, significant ferromagnetic interactions occur when nitroxide coordinates copper ions directly.

# CONTENTS

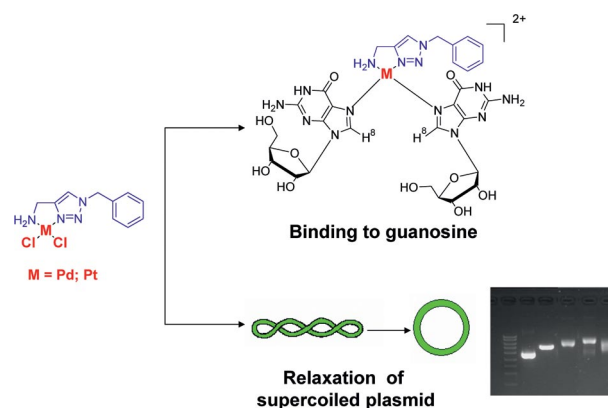
## Click Chelators

A. Chevy, M.-L. Teyssot, A. Maisoniai,  
P. Lemoine,\* B. Viossat, M. Traïkia,  
D. J. Aitken, G. Alves, L. Morel,  
L. Nauton, A. Gautier\* ..... 3513–3519



Click Chelators – The Behavior of Platinum and Palladium Complexes in the Presence of Guanosine and DNA

**Keywords:** Platinum / Palladium / Click chemistry / Conformation analysis / DNA / Antitumor agents



Click chelators comprising platinum and palladium are able to bind guanosine, induce conformational change of the nu-

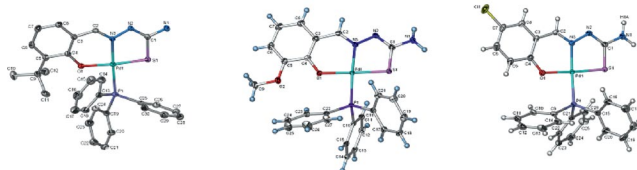
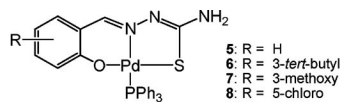
cleotide and relax supercoiled DNA. The similarity between these Pt<sup>II</sup> and Pd<sup>II</sup> complexes with cisplatin is discussed.

## Thiosemicarbazone Pd Complexes

P. Chellan, N. Shunmoogam-Gounden,  
D. T. Hendricks, J. Gut, P. J. Rosenthal,  
C. Lategan, P. J. Smith, K. Chibale,  
G. S. Smith\* ..... 3520–3528

Synthesis, Structure and in Vitro Biological Screening of Palladium(II) Complexes of Functionalised Salicylaldimine Thiosemicarbazones as Antimalarial and Anticancer Agents

**Keywords:** Palladium / Salicylaldimine / Anticancer activity / Antimalarial activity / Thiosemicarbazone



Mononuclear salicylaldiminato(thiosemicarbazone)palladium(II) complexes have been synthesized. The free ligands and their palladium complexes were evaluated for their antimalarial and anticancer activi-

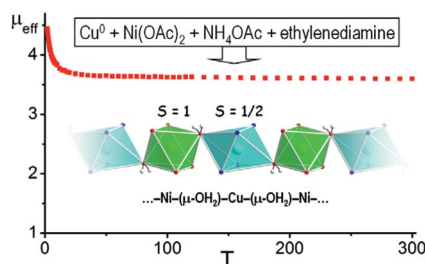
ties. The palladium complexes show enhanced antiplasmodial activity over their free thiosemicarbazone ligands, whilst the opposite effect is observed for in vitro anticancer studies.

## Ferromagnetic Coordination Polymers

O. V. Nesterova, S. R. Petrusenko,  
D. S. Nesterov,\* V. N. Kokozyay,  
B. W. Skelton, J. Jezierska, W. Linert,  
A. Ozarowski ..... 3529–3535

A Cu<sup>II</sup>Ni<sup>II</sup> Complex with Ethylenediamine: Crystal Structure and Ferromagnetic Behaviour of an Aqua-Bridged Heterometallic Chain Containing Ambidentate Ni(OAc)<sub>4</sub><sup>2-</sup> Blocks

**Keywords:** Copper / Nickel / Chain structures / Direct synthesis / Ferromagnetic behaviour / High-field EPR spectroscopy



The first aqua-bridged heterometallic 1D polymer [Cu(en)<sub>2</sub>(μ<sub>2</sub>-H<sub>2</sub>O)<sub>2</sub>Ni(OAc)<sub>4</sub>]<sub>n</sub>·4nH<sub>2</sub>O has been prepared by direct synthesis and was magnetostructurally characterized.

\* Author to whom correspondence should be addressed.

Supporting information on the WWW (see article for access details).

If not otherwise indicated in the article, papers in issue 21 were published online on July 9, 2010





On these pages, we feature a selection of the excellent work that has recently been published in our sister journals. If you are reading these pages on a

computer, click on any of the items to read the full article. Otherwise please see the DOIs for easy online access through Wiley InterScience.



### Drug delivery

B. W. Harper, A. M. Krause-Heuer, M. P. Grant, M. Manohar, K. B. Garbutcheon-Singh, J. R. Aldrich-Wright\*

#### Advances in Platinum Chemotherapeutics

**Evolution of platinum anticancer agents:** Research into platinum-based anticancer compounds has led to the development of a myriad of drugs, with only a small handful gaining approval. This review highlights the current techniques for improving these approved drugs to retain or improve efficacy whilst reducing toxic side-effects. We focus on cancer-specific targeting, drug delivery and the prodrug approach.



*Chem. Eur. J.*  
DOI: 10.1002/chem.201000148

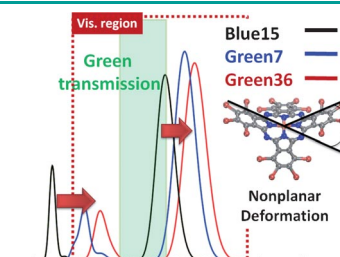


### Phthalocyanines

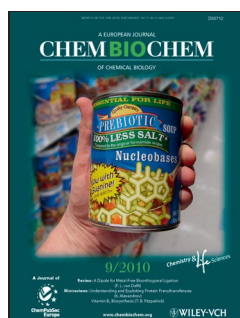
S. U. Lee,\* J. C. Kim, H. Mizuseki, Y. Kawazoe

#### The Origin of the Halogen Effect on the Phthalocyanine Green Pigments

**Going green!** Nonplanar deformation of the tetraazatetrabenzoporphyrin chromophore of the halogenated copper-phthalocyanine (*na,m*β(Hal)-CuPc) molecule is the main role of halogenation in the manufacture of phthalocyanine green pigments. The present study may serve as an important reference point for designing novel halogen-free green pigments.



*Chem. Asian J.*  
DOI: 10.1002/asia.200900601

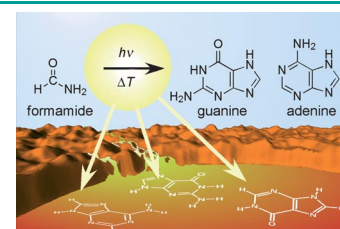


### Prebiotic Syntheses

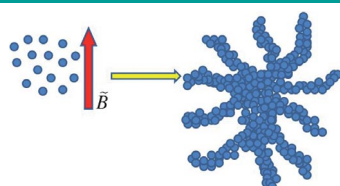
H. L. Barks, R. Buckley, G. A. Grievies, E. Di Mauro, N. V. Hud,\* T. M. Orlando\*

#### Guanine, Adenine, and Hypoxanthine Production in UV-Irradiated Formamide Solutions: Relaxation of the Requirements for Prebiotic Purine Nucleobase Formation

**Relaxed requirements:** We demonstrate the formation of adenine, hypoxanthine, and guanine from heated (130 °C), UV-irradiated formamide solutions in the absence of an inorganic catalyst. Evidence is also provided that “classical” HCN pathways for purine nucleobase production are also active in heated and UV-irradiated formamide reactions.



*ChemBioChem*  
DOI: 10.1002/cbic.201000074



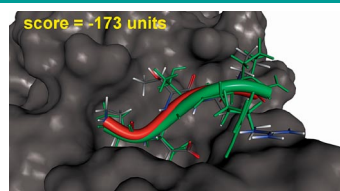
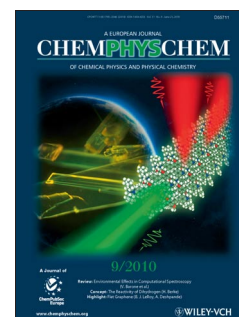
*ChemPhysChem*  
DOI: 10.1002/cphc.201000056

### Magnetic Nanoparticles

W. Zhang, J. Sun, T. Bai, C. Wang, K. Zhuang, Y. Zhang, N. Gu\*

#### Quasi-One-Dimensional Assembly of Magnetic Nanoparticles Induced by a 50 Hz Alternating Magnetic Field

**We've got the power:** Spoke-like assemblies of magnetic nanoparticles are fabricated by the exposure of a colloidal suspension to an alternating magnetic field of power frequency 50 Hz (see picture). In such a low-frequency alternating magnetic field, the assemblies retain super-paramagnetism.



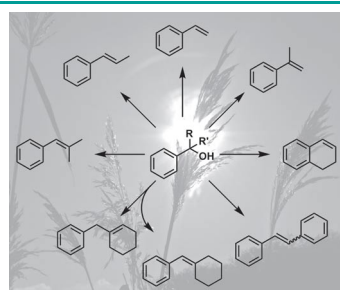
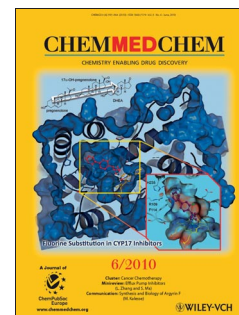
*ChemMedChem*  
DOI: 10.1002/cmdc.201000090

### Drug Design

O. Korb, H. M. Möller, T. E. Exner\*

#### NMR-Guided Molecular Docking of a Protein–Peptide Complex Based on Ant Colony Optimization

**The combination** of NMR experimental data and docking tools can greatly increase the reliability of predicted docking poses. For the complex of the antibody SM3 with its epitope, the PLANTS docking program and the ChemPLP scoring function complemented with intra-ligand trNOE and STD distance constraints are able to correctly predict the complex structure as the best-ranked docking pose.



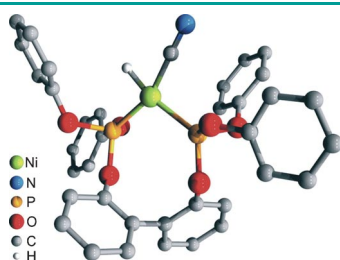
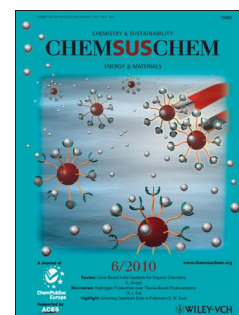
*ChemSusChem*  
DOI: 10.1002/cssc.201000055

### Biorenewables

T. J. Korstanje, J. T. B. H. Jastrzebski, R. J. M. Klein Gebbink\*

#### Catalytic Dehydration of Benzylic Alcohols to Styrenes by Rhenium Complexes

**The oxygen content of biomass-based materials** can be reduced by selective dehydration of hydroxyl groups. As a first step towards biomass-based chemicals, rhenium-based catalysts are shown to be active in the dehydration of various benzylic alcohols to styrene moieties. The turnover frequencies are superior to the benchmark catalyst sulfuric acid, without sacrificing any selectivity.



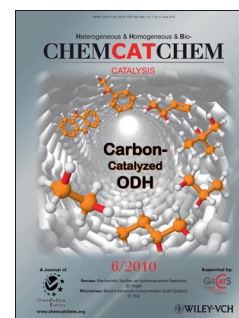
*ChemCatChem*  
DOI: 10.1002/cctc.201000034

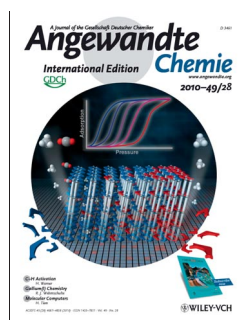
### Homogeneous Catalysis

L. Bini, C. Müller, D. Vogt\*

#### Mechanistic Studies on Hydrocyanation Reactions

**Cyano' the times:** This Review summarizes the state of the art in transition metal-catalyzed alkene hydrocyanation to form nitriles, with special emphasis on mechanistic studies. Ligand electronic and steric effects play a dominant role in determining the catalyst performance. Although the majority of the existing techniques concern nickel-catalyzed hydrocyanation, catalysis with complexes of other metals, such as cobalt and copper, is also discussed.



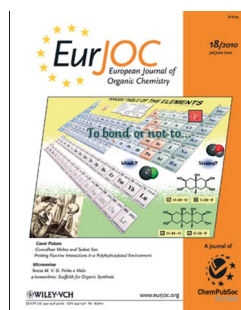
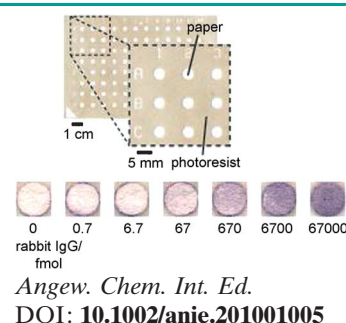


### Clinical Analytics

C.-M. Cheng, A. W. Martinez, J. Gong, C. R. Mace, S. T. Phillips, E. Carrilho, K. A. Mirica, G. M. Whitesides\*

#### Paper-Based ELISA

**Paper works:** Paper-based indirect ELISA (see picture) has been demonstrated through the detection of rabbit IgG and the HIV-1 envelope antigen gp41. This technique combines the sensitivity and specificity of ELISA with the low cost and ease-of-use of paper-based platforms.

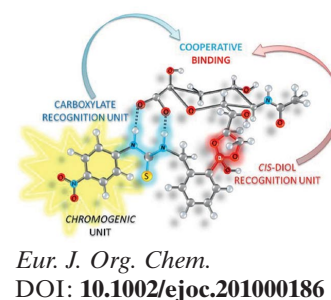


### Sialic Acid Recognition

M. Regueiro-Figueroa, K. Djanashvili, D. Esteban-Gómez, A. de Blas, C. Platas-Iglesias,\* T. Rodríguez-Blas\*

#### Towards Selective Recognition of Sialic Acid Through Simultaneous Binding to Its *cis*-Diol and Carboxylate Functions

Receptors containing phenylboronic acid and urea or thiourea units recognize sialic acids through a cooperative two-site binding mode based on 1) ester formation through interaction at the phenylboronic acid function of the receptor and 2) hydrogen-bond interaction between the thiourea moiety and the carboxylate group of the saccharide.



**New Journal**

Heterogeneous, Homogeneous and BioCatalysis

[www.chemcatchem.org](http://www.chemcatchem.org)

**FREE ONLINE ACCESS**

In 2010 for all users from institutions that have registered

Ask your librarian to register for complimentary online access TODAY

[www.interscience.wiley.com/newjournals](http://www.interscience.wiley.com/newjournals)

Founding Societies:

A journal of



# Coordination Versatility of Pyrazole-Based Ligands towards High-Nuclearity Transition-Metal and Rare-Earth Clusters

Marta Viciano-Chumillas,<sup>[a,b]</sup> Stefania Tanase,<sup>[a]†</sup> L. Jos de Jongh,<sup>\*[b]</sup> and Jan Reedijk<sup>\*[a]</sup>

**Keywords:** N ligands / Cluster compounds / Magnetic properties / Transition metals / Rare earths

The synthesis of transition-metal and rare-earth clusters has become a very active research field, mainly because these compounds can behave as molecule-based magnets. The formation of such compounds strongly depends on the choice of the bridging ligand. This review covers the progress made by pyrazole-based ligands in the formation of new transition-

metal and rare-earth clusters. Synthetic approaches, structural diversity and magnetic properties are described. The formation of other interesting supramolecular structures, such as metallocycles or metallohelicates is also described to emphasize the richness of this type of ligands.

## Introduction

Polynuclear clusters have become an appealing research field because of their relevance in bioinorganic chemistry as functional models for the active site of metalloenzymes,<sup>[1,2]</sup> and also because of their interesting magnetic properties.<sup>[3,4]</sup> These paramagnetic clusters can behave as molecule-based magnets, exhibiting a remnant moment below a critical temperature.<sup>[3–5]</sup> The choice of the bridging ligand is crucial for the formation of these cluster compounds. Carboxylates, Schiff base derivatives and more recently oximes have been widely studied as bridging ligands.<sup>[6–9]</sup> The use of pyrazole-based ligands is still limited.<sup>[10–12]</sup> Therefore, in this review, the coordination versatility of pyrazole-based ligands for the formation of polymetallic compounds, especially dealing with high-nuclearity clusters, is presented. Synthetic approaches, structural diversity and magnetic properties are described.

Pyrazoles are five-membered heterocyclic aromatic rings consisting of three carbon atoms and two nitrogen atoms at the positions 1 and 2 (Figure 1). The N(1)–H has an acid character due to the proton, whereas the N(2) has a basic character due to the lone pair in the  $sp^2$  orbital. Tautomerism exists in the case of symmetrical substitution or non-substitution on the ring, unless the substituent is in position

1. This is because breaking the N–C bond is more difficult than breaking the N–H bond. Five-membered heterocycles, such as pyrazoles, are  $\pi$ -excessive. Consequently, they are poorer  $\pi$ -acceptors and better  $\pi$ -donors than six-membered heterocycles. Hence, they can act as a hard donor site.<sup>[13,14]</sup> Numerous synthetic routes have been used to obtain pyrazole-based ligands. Two routes are the most common: the condensation of a 1,3-diketone (1,3-dicarbonyl) with hydrazine derivatives and the 1,3-dipolar cycloaddition of diazoalkane with alkynes.<sup>[15]</sup>

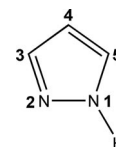


Figure 1. Pyrazole (Hpz).

Pyrazoles can behave either as monodentate or as bidentate ligands, after deprotonation of the N(1)–H group. The pyrazolato anion can act as an *endo* ( $\eta^2$ ) or an *exo*-bidentate ( $\eta^1$ – $\eta^1$ ) bridging ligand (Figure 2). This coordination ability or nucleophilicity is controlled by the nature of the metal ion and the substituents on the pyrazole ring. Substituents at the 3- and 5-positions modify the steric properties,

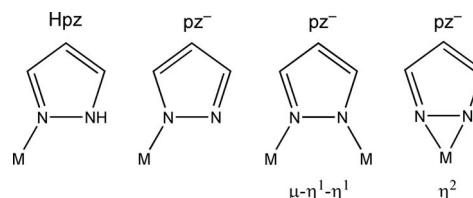


Figure 2. Common coordination modes of the pyrazole ligand and the corresponding anionic ligand.

[a] Leiden Institute of Chemistry, Gorlaeus Laboratories, Leiden University, P. O. Box 9502, 2300 RA Leiden, The Netherlands  
Fax: +31-71-527-4671  
E-mail: reedijk@chem.leidenuniv.nl

[b] Leiden Institute of Physics, Kamerlingh Onnes Laboratory, Leiden University, P. O. Box 9504, 2300 RA Leiden, The Netherlands  
Fax: +31-71-527-5404  
E-mail: jongh@physics.leidenuniv.nl

[†] Current address: Van 't Hoff Institute for Molecular Sciences, University of Amsterdam, Science Park 904, 1098 XH Amsterdam, The Netherlands



whereas substituents at the 4-position can mainly influence the electronic properties.

The study of the coordination chemistry of pyrazole ligands began in 1889 with the report of a silver(I) complex,  $[\text{Ag}(\text{pz})_n]$ .<sup>[16]</sup> Much later, Trofimenko and co-workers stimulated the research with the introduction of poly(pyrazolyl)-borate chelating ligands in coordination chemistry.<sup>[17–20]</sup> After this discovery, numerous papers and reviews have been written illustrating the rich coordination chemistry of pyrazole-based ligands.<sup>[13,14,21–24]</sup> In the literature, three major reviews devoted to polynuclear compounds have been reported.<sup>[10–12]</sup> The first review was published in 1997 highlighting the catalytic activity of polynuclear heteroatom-bridged pyrazole complexes.<sup>[12]</sup> Two other reviews have appeared more recently.<sup>[10,11]</sup> One deals with di-, oligo- and polynuclear transition-metal complexes with substituted pyrazole ligands having chelating side arms.<sup>[11]</sup> The other review describes the structural diversity of pyrazole ligands for the formation of all types of metal compounds in all ranges of nuclearities.<sup>[10]</sup> In this review, the aim is to provide an overview of the pyrazole-based ligands used to form

transition-metal and rare-earth clusters, with a more detailed description of their magnetic properties and with a focus on the ability of the pyrazole ligand to provide a pathway for magnetic exchange interactions. Deprotonated pyrazoles can link two metal ions, which results in a metal–metal distance of 3.5–4.5 Å. Substituents on the pyrazole ring can induce changes in the intermetallic distances, hence controlling the magnetic exchange interactions. Therefore, the compounds discussed in this manuscript are grouped depending on the type of substituents on the pyrazole ligand. In this work, pyrazoles substituted at the *N*1 position, polymers and dinuclear compounds are not discussed.

## Polynuclear Compounds

### Pyrazole Ligands with Non-Coordinating Substituents

Most cluster compounds incorporate the pyrazole ligand or its derivatives with non-coordinating substituents, such as Br, NO<sub>2</sub>, Me, Mes (2,4,6-trimethylphenyl), and so on, at



*Jan Reedijk (1943) is Professor of Chemistry (since 1979) at Leiden University, NL. After his Ph.D. (1968) he lectured at Delft University of Technology until 1979. His research interests include coordination and bioinorganic chemistry of transition-metal ions applied to catalysis, materials, medicine, ion-exchange and surface chemistry. He has (co)-authored over 1100 refereed research publications and patents (1965–2009) and has supervised (1973–2009) about 80 postdocs, 90 graduate students and over 250 MSc students. He was a founding editor of the European Journal of Inorganic Chemistry (EurJIC) and was on its board from 1998 to 2008.*



*L. Jos de Jongh graduated in experimental physics at the University of Amsterdam (1968), where he also received a Ph.D. in 1973 with a thesis entitled “Experiments on simple magnetic model systems” (edited as a Monograph in Physics by Taylor & Francis, London, 1974; also published in Adv. Phys. 2001, 50, 947). He then joined the Leiden University, becoming Professor of Experimental Physics in 1986. His research interests span low-dimensional magnetism, magnetic nanoparticles and molecular clusters, nanowires, phase transitions, superconductivity, experimental techniques at low temperatures and high magnetic fields.*

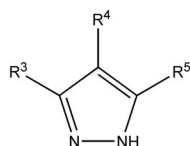


*Stefania Tanase (1972) received her Ph.D. from the University of Bucharest (Romania) in 2002. She has worked in the group of Prof. Jan Reedijk at Leiden University (2001–2009) on oxidation catalysis, bioinorganic chemistry and materials. In 2004, she was awarded a VENI research grant by the Netherlands Organization for Scientific Research. Currently, she is working at University of Amsterdam in the group of Prof. Gadi Rothenberg. Her research interests include sustainable conversion of lignin into bulk chemicals and bio-inspired oxidation catalysis using heterogeneous catalysts.*



*Marta Viciano-Chumillas (1980) obtained her MSc degree from Universitat de València (Spain) in 2003. In September 2005 she joined the group of Prof. Dr. Jan Reedijk at Leiden University as a PhD student, who together with Prof. L. Jos de Jongh and Dr. Stefania Tanase supervised her PhD work. She successfully defended her thesis entitled “Phenol-pyrazole ligands in the design of manganese(III) compounds: Synthesis, characterization and study of the magnetic properties” at Leiden University, October 2009.*

the 3-, 4-, or 5-position of the pyrazole ring (HR-pz). Figure 3 shows some of the pyrazole ligands discussed in this section.



HL1a: R <sup>3</sup> = R <sup>4</sup> = R <sup>5</sup> = H	HL1h: R <sup>3</sup> = H; R <sup>4</sup> = H; R <sup>5</sup> = Mes
HL1b: R <sup>3</sup> = H; R <sup>4</sup> = Me; R <sup>5</sup> = H	HL1i: R <sup>3</sup> = H; R <sup>4</sup> = H; R <sup>5</sup> = <i>t</i> Bu
HL1c: R <sup>3</sup> = H; R <sup>4</sup> = Cl; R <sup>5</sup> = H	HL1j: R <sup>3</sup> = H; R <sup>4</sup> = H; R <sup>5</sup> = 4-F-Ph
HL1d: R <sup>3</sup> = H; R <sup>4</sup> = Br; R <sup>5</sup> = H	HL1k: R <sup>3</sup> = Me; R <sup>4</sup> = H; R <sup>5</sup> = Me
HL1e: R <sup>3</sup> = H; R <sup>4</sup> = I; R <sup>5</sup> = H	HL1l: R <sup>3</sup> = CF <sub>3</sub> ; R <sup>4</sup> = H; R <sup>5</sup> = CF <sub>3</sub>
HL1f: R <sup>3</sup> = H; R <sup>4</sup> = NO <sub>2</sub> ; R <sup>5</sup> = H	HL1m: R <sup>3</sup> = <i>t</i> Bu; R <sup>4</sup> = H; R <sup>5</sup> = <i>t</i> Bu
HL1g: R <sup>3</sup> = H; R <sup>4</sup> = CHO; R <sup>5</sup> = H	

Figure 3. Some of the pyrazole ligands with non-coordinating substituents discussed in this review.

Trinuclear complexes are the most common clusters with pyrazole ligands or pyrazole derivatives containing non-coordinating substituents. These compounds can adopt two different types of structure. The first type is a linear structure, formed when the pyrazole is deprotonated, and it bridges the metal ions (Figure 4a); other ligands are found at the terminal positions (i.e. halogens, acetylacetonate, non-deprotonated pyrazoles or cyclopentadienyl ligands). Some examples reported contain nickel(II),<sup>[25,26]</sup> cobalt(II),<sup>[27,28]</sup> palladium(II) ions,<sup>[28]</sup> and palladium(II)/cobalt(II) mixtures.<sup>[28]</sup> Weak antiferromagnetic interactions were observed between the paramagnetic metal ions in all cases.

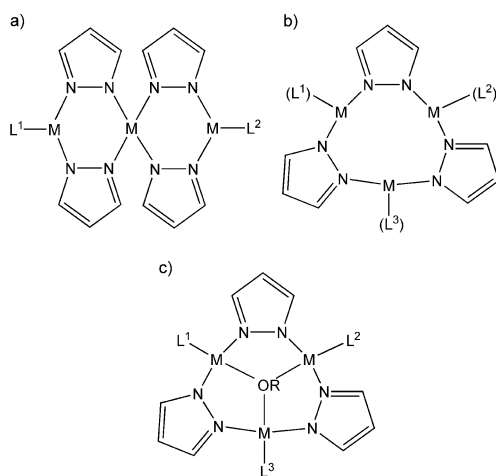


Figure 4. Structural types of trinuclear pyrazole-bridged compounds.

The second possible type of structure for trinuclear compounds is the triangle (Figure 4b, c). Monovalent group 11 ions [copper(I) (Figure 5), silver(I) and gold(I)] and mercury(II) ions form compounds with a general formula [M(R-pz)<sub>3</sub>]<sub>3</sub>.<sup>[29–42]</sup> In the case of gold(I/III), compounds of type [M<sub>3</sub>(R-pz)<sub>3</sub>(L)<sub>2</sub>] are formed.<sup>[43–45]</sup> Nevertheless, compounds with other nuclearities can also be formed, such as tetranuclear or hexanuclear compounds.<sup>[30,39]</sup> In some cases, the distance between the trinuclear units is small, which

leads to the formation of dimers of trinuclear units.<sup>[46–49]</sup> Trinuclear heterobimetallic gold(I)–silver(I) compounds have been synthesized with 3,5-diphenylpyrazole and other type of bridging ligands.<sup>[50,51]</sup> Compounds with the general formula [M<sub>3</sub>(R-pz)<sub>6</sub>] are formed with divalent metal ions, such as palladium(II),<sup>[52]</sup> platinum(II)<sup>[53]</sup> or platinum(II/III) ions.<sup>[53]</sup>

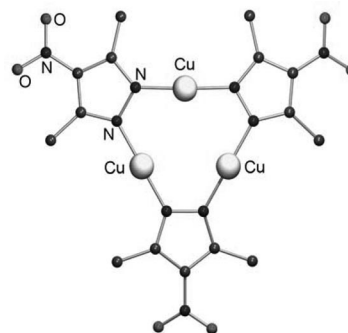


Figure 5. Molecular structure of [Cu<sub>3</sub>(L1f)<sub>3</sub>].<sup>[30]</sup>

[M<sub>3</sub>-μ<sub>3</sub>-O(R')]<sup>m+</sup> (R' = H, Me; m = 4, 5, 7) centred triangles are reported with several transition-metal ions, such as iron(III), cobalt(II/III) and copper(II) ions (Figure 4c). Compounds X<sub>4</sub>[Fe<sub>3</sub>(μ<sub>3</sub>-O)(L1f)<sub>6</sub>Cl<sub>3</sub>]Cl<sub>2</sub> (X<sup>+</sup> = HNet<sub>3</sub><sup>+</sup>, Bu<sub>4</sub>N<sup>+</sup>, PPh<sub>4</sub><sup>+</sup>) have a structure which resembles the basic carboxylates because of the presence of six pyrazole ligands.<sup>[54]</sup> Mössbauer spectroscopy, magnetic susceptibility and EPR studies revealed the presence of antiferromagnetic interactions between the iron(III) ions and the achievement of a ground state of S<sub>T</sub> = 1/2.<sup>[54]</sup> In this case, the pyrazole ligands mediate stronger antiferromagnetic interactions than the analogous carboxylates.<sup>[54]</sup> Another example is a mixed-valence cobalt(II/III) compound, [Co<sub>3</sub>(μ<sub>3</sub>-OH)(L1a)<sub>4</sub>-(dbm)<sub>3</sub>]·2THF (Hdbm = dibenzoylmethane), with a μ<sub>3</sub>-hydroxide bridge.<sup>[55]</sup> Numerous compounds were synthesized with the copper(II) ion. Many of them were reported by Raptis and co-workers,<sup>[56–62]</sup> who studied the influence of non-coordinating substituents on the pyrazole ring and of the terminal ligands, L. The general formula of these complexes is [Cu<sub>3</sub>(μ<sub>3</sub>-OR')(R-pz)<sub>3</sub>L<sub>3</sub>]<sup>m+</sup> (R' = H, Me; L = Cl<sup>−</sup>, Br<sup>−</sup>, HL1a, RCO<sub>2</sub><sup>−</sup>, HL1g, H<sub>2</sub>O, EtOH; R-pz<sup>−</sup> = L1a<sup>−</sup>, L1f<sup>−</sup>, L1h<sup>−</sup> and m = 0, 1, 2) (Figure 6).<sup>[56–72]</sup> Most of the trinuclear centred copper(II) triangles are synthesized from a copper(II) salt and the pyrazole ligand in a molar ratio 1:1 or 1:2, in the presence of base and with use of different counterions.<sup>[56]</sup> Other possible synthetic routes are: (i) the substitution of the terminal ligand or the centred anion in a preformed trinuclear compound; (ii) the addition of a bridging ligand such as carboxylate, an acid, a base or NaBr to a trinuclear copper(II) compound.<sup>[56,59,60,63,65]</sup> The control of the pH is crucial in the formation of the triangular structure, since numerous species often exist in solution. In some cases, compounds of higher nuclearity, or polymers that retain the trinuclear structure are obtained.<sup>[61,63–67,72]</sup> Another synthetic route to obtain trinuclear-centred copper(II) compounds is by oxidation of mononuclear copper(I) complexes.<sup>[68]</sup> Apparently, the introduction of substit-

uents at the 4-position of the aromatic ring does not affect the formation of trinuclear copper(II) complexes. The use of 3,5-substituted pyrazoles precludes the formation of the triangle, because of the steric effects of such side groups in the ligand. In these cases, mononuclear or dinuclear copper(II) complexes were obtained.<sup>[59,64]</sup> So far, in only one case with substituents at the 3,5-positions, the trinuclear structure is retained.<sup>[69]</sup> By following similar procedures as those described for the synthesis of O(R')-centred copper(II) triangles (R' = H, Me), but with different amounts of the counterion, compounds with the formula  $[\text{Cu}_3(\mu_3\text{-X})_2(\text{R-pz})_3\text{X}_3]^{2-}$  ( $\text{X}^- = \text{Cl}^-$ ,  $\text{Br}^-$  and  $\text{R-pz}^- = \text{L1a}^-$ – $\text{L1f}^-$ ) are formed (Figure 6).<sup>[56–59,61]</sup> Trinuclear copper(II) compounds with two types of bridging ligands, such as hydroxide and chloride ligands for  $[\text{Cu}_3(\mu_3\text{-OH})(\mu\text{-Cl})\text{Cl}(\text{L1a})_3(\text{HL1a})_2]^{[73]}$  and oxide and perchlorate ligands for  $[\text{Cu}_3(\mu_3\text{-O})(\text{ClO}_4)(\text{L1a})_3(\text{HL1a})_3]\cdot\text{CH}_3\text{OH}$ ,<sup>[74]</sup> were also reported. In

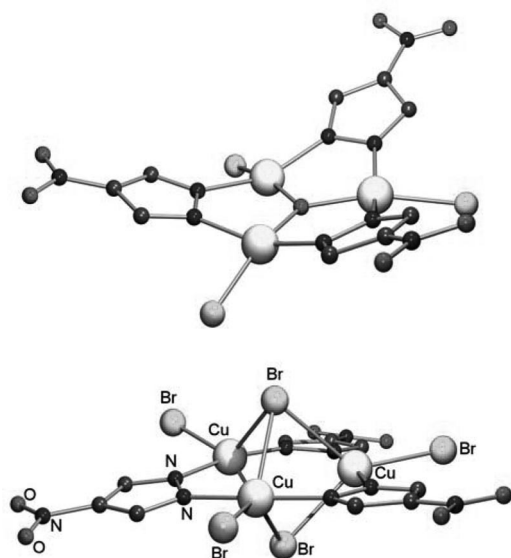


Figure 6. Molecular structure of anion  $[\text{Cu}_3(\mu_3\text{-O})(\text{L1f})_3\text{Cl}_3]^{2-}$ <sup>[70]</sup> (top) and anion  $[\text{Cu}_3(\mu_3\text{-Br})_2(\text{L1f})_3\text{Br}_3]^{2-}$ <sup>[57]</sup> (bottom).

these trinuclear copper(II) compounds, the introduction of substituents on the pyrazole ring does not induce any significant structural differences, such as  $\text{Cu}\cdots\text{Cu}$  distances or  $\text{Cu}-\mu_3\text{-Y}$  [ $\text{Y} = \mu\text{-O}^{2-}$ ,  $\text{OH}^-$ ,  $\text{OMe}^-$ ,  $\mu\text{-X}$  ( $\text{X}^- = \text{Cl}^-$ ,  $\text{Br}^-$ )] distances. The main structural difference between all the trinuclear copper(II) triangles is the central bridging atom that induces the distortion of the  $\text{Cu}-\mu\text{-Y}-\text{Cu}$  angle when going from  $\mu\text{-O}^{2-}$  through  $\text{OH}^-$  to  $\mu\text{-X}$  ( $\text{X}^- = \text{Cl}^-$ ,  $\text{Br}^-$ ).

Magnetic susceptibility and EPR studies were performed for some of the trinuclear copper(II) compounds (Table 1).<sup>[56,57,65,68,69,71,73]</sup> Strong antiferromagnetic interactions between the copper(II) ions are operative in the case of the compounds with a  $\text{Cu}-\mu_3\text{-Y}-\text{Cu}$  angle of approximately  $120^\circ$  ( $\text{Y}^{2-} = \text{O}^{2-}$ ). Generally, a decrease in the magnitude of the antiferromagnetic exchange interaction is observed when the  $\text{Cu}-\mu_3\text{-Y}-\text{Cu}$  angle decreases ( $\text{Y}^- = \text{OH}^-$ ), and ferromagnetic interactions become operative when the  $\text{Cu}-\mu_3\text{-Y}-\text{Cu}$  angle is approximately  $80^\circ$  ( $\text{Y}^- = \text{Cl}^-$ ,  $\text{Br}^-$ ). This change in the magnetic behaviour is explained by the principles of the orbital complementarity and overlapping.<sup>[57]</sup> In some of the O(R)-centred copper(II) triangles, small values of magnetic susceptibility (values lower than those expected for a  $S_T = 1/2$ ) at low temperature are found.<sup>[69,73]</sup> This common phenomenon can be described by the presence of antisymmetric exchange between the copper(II) ions in view of the magnetic susceptibility and EPR studies.<sup>[69]</sup>

Mononuclear and trinuclear copper(I/II) complexes with pyrazole ligands were used as starting materials to synthesize compounds of higher nuclearity by addition of other bridging ligands (i.e. carboxylate, pyridazine or nitrate ligands).<sup>[29,61,75,76]</sup> Pyrazole-based ligands have also been used as additional bridging ligands with mononuclear compounds to form tetranuclear copper(II) compounds<sup>[77]</sup> or to bridge two trinuclear units, thus forming hexanuclear copper(II) compounds with the formula  $[\text{PPN}][\text{Cu}_6(\mu_3\text{-O})_2(\text{R-pz})_6(4\text{-R}'\text{-3,5-Ph}_2\text{-pz})_3]$  ( $\text{R-pz}^- = \text{L1a}^-$ ,  $\text{L1c}^-$ ,  $\text{L1d}^-$ ;  $\text{R}' = \text{H}$ ,  $\text{Cl}$ ).<sup>[62]</sup> In these hexanuclear copper(II) compounds, DFT calculations and magnetic studies indicated that the low-

Table 1. Magnetic and structural data for trinuclear copper(II) compounds.<sup>[a]</sup>

Compound	$\text{Cu}-\text{Y}-\text{Cu}^{[b]}$	$\text{Cu}_3-\mu_3-\text{Y}^{[c]}$	$J/\text{cm}^{-1}[d]$	$g^{[e]}$	$g^{[f]}$	Ref.
$(\text{PPN})_2[\text{Cu}_3(\mu_3\text{-O})(\text{L1a})_3\text{Cl}_3]$	119.59, 119.59, 120.82	n.r.	–250	2.1	n.r.	[56]
$(\text{PPN})_2[\text{Cu}_3(\mu_3\text{-OH})(\text{L1a})_3\text{Cl}_3]$	118.54, 117.26, 104.38	0.524	n.r.	n.r.	n.r.	[56]
$[\text{Cu}_3(\mu_3\text{-OH})(\text{L1a})_3(\text{MeCO}_2)_2(\text{HL1a})]$	118.0, 115.5, 102.6	0.563	< 0	n.r.	$g_{xx} = 2.015$ , $g_{yy} = 2.050$ , $g_{zz} = 2.200$	[65]
$[\text{Cu}_3(\text{OH})\text{Cl}_2(\text{L1a})_3(\text{py})_2]\cdot\text{py}$	102.2, 113.3, 70.93	n.r.	–74, –11.5	2.17	n.r.	[73]
$[\text{Cu}_3(\text{OH})(\text{L1a})_3(\text{HL1a})_2(\text{NO}_3)_2]\cdot\text{H}_2\text{O}$	112.0, 115.0, 116.4	0.478	< 0	n.r.	2.1	[68]
$[\text{Cu}_3(\mu_3\text{-OH})(\text{L1a})_3(\text{HL1a})_2(\text{Me}_3\text{CCO}_2)_2](\text{Me}_3\text{CCOOH})_2$	116.32, 111.98, 108.40	0.567	–117.7, –90.3, –90.3	2.047	n.r.	[71]
$(\text{Bu}_4\text{N})_2[\text{Cu}_3(\mu_3\text{-Cl})_2(\text{L1a})_3\text{Cl}_3]$	86.05	n.r.	+14.3	2.07	$g_\perp = 2.05$ , $g_\parallel = 2.11$	[56,57]
$(\text{Bu}_4\text{N})_2[\text{Cu}_3(\mu_3\text{-Br})_2(\text{L1f})_3\text{Br}_3]$	77.41–81.07	n.r.	+1.55	$g_\perp = 2.46$ , $g_\parallel = 2.42$	$g_\perp = 2.01$ , $g_\parallel = 2.08$	[57]
$[\text{Cu}_3(\mu_3\text{-OMe})\text{Cl}(\text{L1h})_3(\text{HL1h})_2]\text{Cl}$	105.77, 105.09, 101.87	n.r.	–100	2.19	$g_\perp = 2.21$ , $g_\parallel = 1.47$	[69]
$[\text{Cu}_3(\mu_3\text{-OMe})\text{Br}(\text{L1h})_3(\text{HL1h})_2]\text{Br}$	107.43, 104.61, 104.40	n.r.	–103	2.20	$g_\perp = 2.19$ , $g_\parallel = 1.59$	[69]

[a]  $\text{PPN}^+$  = bis(triphenylphosphoranylidene)ammonium cation; ligand abbreviations HL1a–HL1f are given in Figure 3; n.r. = not reported. [b]  $\text{Cu}-\text{Y}-\text{Cu}$  angle ( $\text{Y} = \text{O}^{2-}$ ,  $\text{HO}^-$ ,  $\text{Cl}^-$ ,  $\text{Br}^-$ ). [c] Distance of  $\mu_3\text{-Y}$  from the  $\text{Cu}_3$  plane. [d] The  $J$  values describe the magnetic exchange interactions depending on the geometrical parameters of each compound; the reported  $J$  values have been converted according to the Hamiltonian  $\hat{H} = -\sum J_{ij}S_iS_j$  for comparison. [e]  $g$  values obtained from the fitting of the magnetic susceptibility data. [f]  $g$  values obtained from EPR measurements.

symmetry distortion within each trinuclear unit and the antisymmetric exchange at low temperatures are important to determine the magnetic behaviour.<sup>[78]</sup>

Another class of trinuclear compounds that is not very common is formed by the linear heterobimetallic compounds with the formula (cyclam)M[( $\mu$ -Cl)U(L1k)<sub>4</sub>]<sub>2</sub> (M = Ni, Cu, Zn, Co; cyclam = 1,4,8,11-tetraazacyclotetradecane). They are synthesized from the homoleptic dimer [U(L1k)<sub>4</sub>]<sub>2</sub> and the compound [M(cyclam)Cl<sub>2</sub>]. In the case of nickel(II) and cobalt(II) compounds, weak ferromagnetic interactions between the metal ions are present with *J* values between 2.8–19 cm<sup>-1</sup> (Ni<sup>II</sup>–U<sup>IV</sup>) and 15–48 cm<sup>-1</sup> (Co<sup>II</sup>–U<sup>IV</sup>).<sup>[79,80]</sup>

The use of lanthanide ions with pyrazole ligands is still very limited, especially in the synthesis of high-nuclearity compounds rather than the common polymeric structures. It has been observed that the size of the lanthanide ions can sometimes determine the type of structure and nuclearity of the resulting compounds under similar reaction conditions.<sup>[81,82]</sup> [Nd<sub>3</sub>(L1a)(HL1a)<sub>2</sub>](HL1a)(tech)<sub>2</sub> (tech = 1,2,3,4-tetrahydroquinoline) is a triangular compound in which the pyrazole ligand displays several coordination modes, including *endo* ( $\eta^2$ ) and *exo* ( $\eta^1$ - $\eta^1$ ) modes.<sup>[82]</sup> Another example is a tetranuclear europium(II) compound, [Eu<sub>4</sub>(L1m)<sub>8</sub>], which has a linear structure formed by a dimer of dinuclear units. In this compound, the pyrazole ligand binds the metal ions in the *endo* ( $\eta^2$ ) and *exo* ( $\eta^2$ - $\eta^2$ ) coordination modes (Figure 7).<sup>[81]</sup>

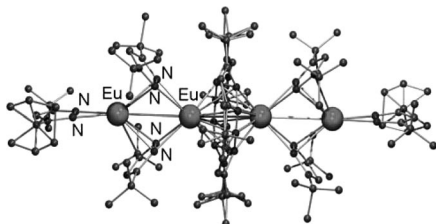


Figure 7. Molecular structure of [Eu<sub>4</sub>(L1m)<sub>8</sub>].<sup>[81]</sup>

Tetranuclear copper(II) compounds are generally synthesized from a copper(II) salt, the pyrazole ligand, another type of ligand and a base. In these compounds, the pyrazolate anion bridges two dinuclear units.<sup>[83,84]</sup> For example, the compound with the formula [Cu<sub>4</sub>(L1a)<sub>4</sub>L<sub>2</sub>](ClO<sub>4</sub>) (HL = 1,3-diamino-2-propanol), has a dinuclear unit formed by two copper(II) ions bridged by a pyrazolate ligand and by 1,3-diamino-2-propanolato.<sup>[83]</sup> Another example is the compound [Cu<sub>4</sub>L<sub>2</sub>(L1a)<sub>4</sub>(CH<sub>3</sub>OH)<sub>2</sub>](ClO<sub>4</sub>)<sub>2</sub> {L = 1,1-bis(2-pyridyl)-1-methoxymethanol}.<sup>[84]</sup> Magnetic susceptibility studies define both compounds as dinuclear complexes with weak antiferromagnetic interactions between the dinuclear copper(II) units, ascribed to the countercomplementary behaviour of the bridging pyrazole that decreases the value of the magnetic exchange imposed by the other bridging ligand.<sup>[83,84]</sup> Another example is the compound [Cu<sub>4</sub>F<sub>2</sub>( $\mu_4$ -F)(L1j)<sub>5</sub>(HL1j)<sub>4</sub>], which contains a  $\mu_4$ -F bridge between the four copper(II) ions that interact antiferromagnetically.<sup>[85]</sup> A tetranuclear zirconium(IV) compound is obtained by conversion of a dinuclear compound in wet toluene.<sup>[86]</sup> Tet-

ranuclear heterobimetallic compounds with palladium(II) ions and silver(I) or gold(I) ions have also been reported,<sup>[52,87]</sup> as well as those with zinc(II) and sodium(I) ions.<sup>[88]</sup> Some of the tetranuclear compounds that are reported in the literature were minor side products that were only characterized by X-ray crystallography.<sup>[89,90]</sup>

The reaction of CuX<sub>2</sub> (X<sup>-</sup> = Cl<sup>-</sup>, Br<sup>-</sup>, NO<sub>3</sub><sup>-</sup>) with 3(5)-*tert*-butylpyrazole (HL1i) and sodium methoxide in methanol affords the heptanuclear compounds [{Cu<sub>3</sub>(HL1i)<sub>6</sub>( $\mu_3$ -X)( $\mu_3$ -OH)<sub>3</sub>]<sub>2</sub>Cu]X<sub>6</sub> (X<sup>-</sup> = Cl<sup>-</sup>, Br<sup>-</sup>, NO<sub>3</sub><sup>-</sup>).<sup>[91,92]</sup> With CuF<sub>2</sub> under the same reaction conditions, a hexanuclear cyclic copper(II) compound is formed (see metallocycles).<sup>[93]</sup> Using a ligand with large steric hindrance at the 3,5-positions of the pyrazole ring precludes the formation of these heptanuclear species and affords a trinuclear compound (as described above).<sup>[69]</sup> The heptanuclear copper(II) compounds are double-cubanes in which a vertex of a copper(II) ion coordinated by six hydroxide ligands is shared. Antiferromagnetic interactions between the copper(II) ions were found in all compounds, and the variation of the magnetic exchange interaction is in agreement with magnetostructural correlations on the basis of the Cu–O–Cu angles (the so-called Haase correlation)<sup>[94]</sup> for the [Cu<sub>4</sub>( $\mu_3$ -OR)<sub>4</sub>]<sup>4+</sup> and [Cu<sub>2</sub>( $\mu$ -OH)]<sup>3+</sup> species, leading to a ground state of *S*<sub>T</sub> = 1/2.<sup>[91,92]</sup>

[Fe<sub>8</sub>( $\mu_4$ -O)<sub>4</sub>(L1a)<sub>12</sub>Cl<sub>4</sub>] is an octanuclear iron(III) compound with a Fe<sub>4</sub>O<sub>4</sub> cubane structure, where the inner iron(III) ions are connected with the outer iron(III) ions through pyrazole bridges and with the chloride ligands at terminal positions.<sup>[95]</sup> This compound is the first example of an all-iron(III) cubane.<sup>[95]</sup> The compound has an unusual stability due to the [Fe<sub>4</sub>O<sub>4</sub>]<sup>4+</sup> core. Replacement of the terminal chloride ligands with other ligands and the introduction of the fourth substituent on the pyrazole ring (HL1b and HL1c) were reported.<sup>[96]</sup> These compounds exhibit similar redox properties, demonstrating that the [Fe<sub>4</sub>O<sub>4</sub>]<sup>4+</sup> core is redox-active.<sup>[96]</sup> Strong antiferromagnetic interactions between the iron(III) ions are present in the compound [Fe<sub>8</sub>( $\mu_4$ -O)<sub>4</sub>(L1a)<sub>12</sub>Cl<sub>4</sub>]. The fit of the experimental magnetic data indicates strong antiferromagnetic coupling between the inner and the outer iron(III) ions (*J* = –50.55 cm<sup>-1</sup>), whereas much weaker coupling is observed between the iron(III) ions within the core (*J* = –2.1 cm<sup>-1</sup>).<sup>[96]</sup> The stronger antiferromagnetic interactions between the inner and the outer iron(III) ions are in agreement with the larger Fe–O–Fe angles, approximately 119°, as compared with the Fe–O–Fe angles within the inner core, approximately 98°. DFT studies were performed to confirm the parameters obtained from a fit of the experimental magnetic susceptibility data.<sup>[96]</sup> A gallium(III) analogue was synthesized.<sup>[97]</sup> Other examples of octanuclear clusters involve molybdenum(V/VI)<sup>[98]</sup> or zinc(II) ions.<sup>[99]</sup> The compound [Ni(bma)(H<sub>2</sub>O)<sub>3</sub>][Ni<sub>8</sub>(OH)<sub>6</sub>(L1a)<sub>12</sub>·6DMSO] {bma = bis(2-benzimidazolylmethyl)amine} consists of an anionic structure composed from an octanuclear nickel(II) unit, [Ni<sub>8</sub>(OH)<sub>6</sub>(L1a)<sub>12</sub>]<sup>-</sup>, and a cation formed by a mononuclear nickel(II) entity, [Ni(bma)(H<sub>2</sub>O)<sub>3</sub>]<sup>+</sup>. In the former case, the eight nickel(II) ions form a cube and the Ni···Ni···Ni angles



are around 90°. Antiferromagnetic interactions are present between the nickel(II) ions in the octanuclear anion, leading to  $S = 0$ , but the ground state of the molecule is  $S_T = 1$ , resulting from the mononuclear counterion.<sup>[100]</sup> DFT calculations were performed to estimate the magnetic exchange interactions.<sup>[100]</sup>

Chandrasekhar and co-workers have employed the combination of phosphonates and pyrazoles (HL1a, HL1k, HL1l and HL1m) as ligands to form a tetranuclear cadmium(II) compound<sup>[101]</sup> and copper(II) complexes of different nuclearities,<sup>[102–105]</sup> ranging from tetranuclear to hexadecanuclear (Figure 8). All compounds display antiferromagnetic interactions of different strengths.<sup>[102–105]</sup>

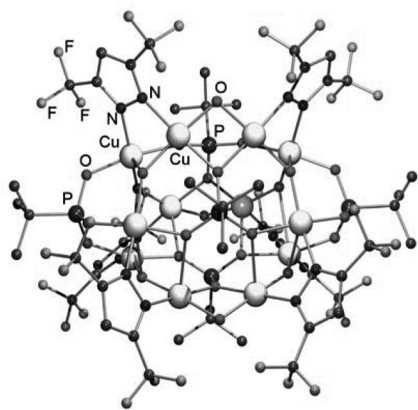


Figure 8. Molecular structure of the neutral compound  $[(\text{Cu}_{12}\text{L}11)_6(\mu_3\text{-OH})_6(\mu\text{-OH})_3(\mu_3\text{-}t\text{BuPO}_3)_2(\mu_6\text{-}t\text{BuPO}_3)_3]$ .<sup>[104]</sup>

The combination of two pyrazole moieties, i.e. bis-(pyrazole) ligands, was successfully used to form tetranuclear copper(II) compounds<sup>[106]</sup> and also porous coordination polymers with palladium(II), platinum(II), silver(I) or copper(I) ions.<sup>[107–110]</sup>

### Pyrazole Ligands with Substituents Containing Donor Atoms

Substituents with donor atoms on the pyrazole ring can increase the number of possible metal-binding sites that may lead to polynuclear type of compounds. Commonly, the substituents are placed at the 3- and 5-positions of the aromatic ring. Variation of the side arm chain lengths gives some control over metal–metal separation, while the number and type of side arm donor sites allow the determination of electronic and coordinative properties.<sup>[12,22]</sup> Recently, a review has been published by Meyer and co-workers, dealing with polynuclear transition-metal complexes with compartmental pyrazolate ligands.<sup>[11]</sup> The main part of the review was dedicated to dinuclear compounds.

### Pyrazole Ligands with N-Donor Substituents, Amines

Figure 9 shows the ligands used for the compounds described in this section. An important part of this research has been developed by Meyer and co-workers,<sup>[111–126]</sup> who

have studied the coordination ability of the 3,5-disubstituted pyrazole ligands with chelating side arms, mainly with N-donor atoms. These ligands differ in the chain lengths of the chelating side arms and the number of donor sites.

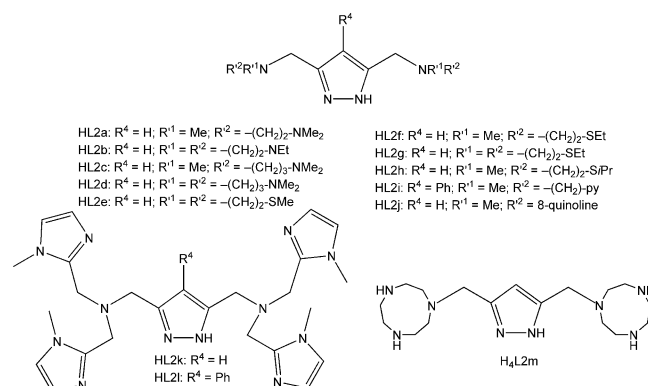


Figure 9. Pyrazole-based ligands with N-donor substituents, amines.

Tetranuclear nickel(II) compounds with the general formula  $[\text{Ni}_4\text{L}_2]^{6+}$  were synthesized with stoichiometric amounts of the metal salt, the pyrazole-based ligand ( $\text{HL} = \text{HL2c}\text{--}\text{HL2h}$ , see Figure 9), the base and an appropriate amount of the bridging ligand, such as azide and/or carboxylate.<sup>[115–120]</sup> Another synthetic approach employed the reaction of dinuclear complexes with labile co-ligands and with azides.<sup>[116,118,120]</sup> In some cases, the assembly of these dinuclear nickel(II) units can lead to other topologies such as 1D chains.<sup>[115,123]</sup> The similar central core of the tetranuclear nickel(II) structures is formed by dinuclear nickel(II) units,  $[\text{Ni}_2\text{L}]^{3+}$ , which are connected by azide and carboxylate bridges (Figure 10).<sup>[115–120]</sup> Table 2 shows the values of the magnetic exchange interactions for the tetranuclear nickel(II) compounds discussed above. In most of the tetranuclear compounds, overall antiferromagnetic interactions are present between the nickel(II) ions (high-spin), leading to a ground state of  $S_T = 0$ , except for the first four compounds in Table 2, in which ferromagnetic interactions between the nickel(II) ions are dominant.<sup>[116]</sup> Ferromagnetic exchange interactions between nickel(II) ions are found in the presence of end-on azido bridges. In the case of end-to-end azido bridges, weak antiferromag-

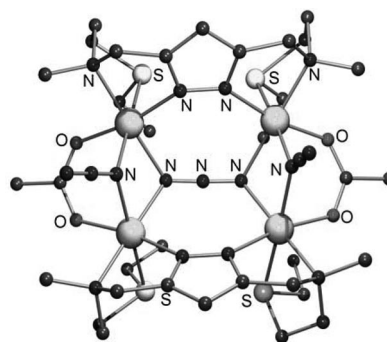


Figure 10. Molecular structure of the cation  $[\text{Ni}_4(\text{L}2\text{f})_2(\mu\text{-}1,1\text{-N}_3)_2(\mu_4\text{-}1,1,3,3\text{-N}_3)(\text{O}_2\text{CMe})_2]^+$ .<sup>[117]</sup>

Table 2. Magnetic data for a selection of tetranuclear nickel(II) compounds.

Compound <sup>[a]</sup>	$J/\text{cm}^{-1[\text{b}]}$	$g$	Ref.
$[\text{Ni}_4(\text{L2c})_2(\mu-1,1-\text{N}_3)_2(\mu-1,3-\text{N}_3)_2](\text{ClO}_4)_2 \cdot 2\text{CH}_3\text{O} \cdot 0.5\text{H}_2\text{O}$	+1.8; +4.2	2.21	[116]
$[\text{Ni}_4(\text{L2c})_2(\mu-1,1-\text{N}_3)_2(\mu-1,3-\text{N}_3)_2](\text{ClO}_4)_2 \cdot 2\text{C}_3\text{H}_6\text{O} \cdot \text{C}_5\text{H}_{12}$	+2.5; +2.5	2.16	[116]
$[\text{Ni}_4(\text{L2c})_2(\mu-1,1-\text{N}_3)_2(\mu-1,3-\text{N}_3)_2](\text{BPh}_4)_2 \cdot 2\text{C}_3\text{H}_6\text{O}$	+3.4; -1.0	2.22	[116]
$[\text{Ni}_4(\text{L2d})_2(\mu-1,1-\text{N}_3)_2(\mu-1,3-\text{N}_3)_2](\text{BPh}_4)_2 \cdot 2\text{C}_3\text{H}_6\text{O}$	+0.9; -5.8	2.27	[116]
$[\text{Ni}_4(\text{L2d})_2(\mu-1,1-\text{N}_3)_2(\mu-1,3-\text{N}_3)_2](\text{BPh}_4)_2$	+2.0; +4.7	2.19	[116]
$[\text{Ni}_4(\text{L2g})_2(\mu_3-1,1,3-\text{N}_3)_2(\text{MeOH})_2](\text{ClO}_4)_4$	-42.6; -24.0; +32.1	2.19	[115]
$[\text{Ni}_4(\text{L2f})_2(\mu-1,1-\text{N}_3)_2(\mu_4-1,1,3,3-\text{N}_3)(\text{O}_2\text{CMe})_2] \cdot \text{ClO}_4 \cdot \text{C}_3\text{H}_6\text{O}$	-110; +106; +2	2.15	[117]
$[\text{Ni}_4(\text{L2f})_2(\mu-1,1-\text{N}_3)_2(\mu_4-1,1,3,3-\text{N}_3)(\text{O}_2\text{CPh})_2] \cdot \text{ClO}_4 \cdot \text{NaClO}_4 \cdot 2\text{C}_3\text{H}_6\text{O} \cdot \text{H}_2\text{O}$	-111; +51; +9	2.15	[117]
$[\text{Ni}_4(\text{L2h})_2(\mu-1,1-\text{N}_3)_2(\mu_4-1,1,3,3-\text{N}_3)(\text{O}_2\text{CMe})_2] \cdot \text{ClO}_4$	-133; +129; +26	2.15	[117]
$[\text{Ni}_4(\text{L2h})_2(\mu-1,1-\text{N}_3)_2(\mu_4-1,1,3,3-\text{N}_3)(\text{O}_2\text{CAda})_2] \cdot \text{ClO}_4 \cdot \text{C}_3\text{H}_6\text{O}$	-111; +86; +5	2.15	[117]
$[\text{Ni}_4(\text{L2e})_2(\mu_4-1,1,3,3-\text{N}_3)(\text{O}_2\text{CAda})_4] \cdot \text{ClO}_4$	-39; +98; -12	2.15	[117]
$[\text{Ni}_4(\text{L2g})_2(\mu_4-1,1,3,3-\text{N}_3)(\text{O}_2\text{CAda})_4] \cdot \text{ClO}_4$	-50; +66; +7	2.15	[117]
$[\text{Ni}_4(\text{L2d})_2(\mu-1,1-\text{N}_3)_2(\mu-1,3-\text{N}_3)_2](\text{BPh}_4)_2 \cdot 2\text{C}_3\text{H}_6\text{O}$	-16.2; +2	2.01	[118]
$[\text{Ni}_2(\text{L2c})_2(\mu-1,1-\text{N}_3)_2(\mu_3-1,1,3-\text{N}_3)(\text{N}_3)_2] \cdot 2\text{CH}_2\text{Cl}_2$	-19.7; +6	2.29	[118]
$[\text{Ni}_4(\text{L2g})_2(\mu-1,3-\text{N}_3)(\mu_3-1,1,3-\text{N}_3)_2(\text{O}_2\text{CMe})](\text{ClO}_4)_2$	+57; -51; -18; +6	2.29	[119]
$[\text{Ni}_4(\text{L2g})_2(\mu-1,3-\text{N}_3)(\mu_3-1,1,3-\text{N}_3)_2(\text{O}_2\text{CPh})](\text{ClO}_4)_2$	+25; -61; -12; +5	2.38	[119]
$[\text{Ni}_4(\text{L2h})_2(\mu-1,3-\text{N}_3)(\mu_3-1,1,3-\text{N}_3)_2(\text{O}_2\text{CPh})](\text{ClO}_4)_2$	+27; -53; -3; +6	2.30	[119]
$[\text{Ni}_4(\text{L2g})_2(\text{OCN}_2\text{H}_4)_2(\text{OCN}_2\text{H}_3)_2](\text{ClO}_4)_2$	+3.4	2.25	[121]

[a] The azide nomenclature does not follow the rules of IUPAC. Here  $\mu-1,1-\text{N}_3$  and  $\mu-1,3-\text{N}_3$  is used for the end-on and end-to-end bridge, respectively. [b] The  $J$  values describe the magnetic exchange interactions depending on the geometrical parameters of each compound; the  $J$  values reported have been converted according to the Hamiltonian  $\hat{H} = -\sum J_{ij} S_i S_j$  for comparison. Ligand abbreviations are given in Figure 9.

netic or ferromagnetic exchange interactions can occur.<sup>[116–120]</sup> The sign of the magnetic exchange constant between the nickel(II) ions depends mainly on the Ni–N<sub>3</sub>–Ni torsion angle and the Ni–N–N angle values. This has been previously established by common magnetostructural correlations based on the azide bridge.<sup>[116–120]</sup> So, if the Ni–N<sub>3</sub>–Ni torsion angle is around 90°, ferromagnetic interactions should be operative. Besides exploring azide as bridging ligand, other ligands, such as urea<sup>[121]</sup> and cyanide,<sup>[124]</sup> have been used in combination with HL2a and HL2b ligands, respectively. With urea as a ligand, a tetranuclear nickel(II) compound is formed, in which the presence of two low-spin nickel(II) ions and two high-spin nickel(II) ions that interact ferromagnetically is confirmed by magnetic susceptibility studies.<sup>[121]</sup>

The coordination ability of the HL2a ligand towards other metal ions, such as copper(II) or zinc(II) ions, was also explored. The pyrazolato ligand bridges the two metal ions, and in some cases, the dinuclear structures,  $[\text{M}_2\text{L2a}]^+$  ( $\text{M} = \text{Cu}^{\text{II}}$  and  $\text{Zn}^{\text{II}}$ ), are linked by carbonates incorporated from air,<sup>[111,114]</sup>  $\mu_4$ -peroxido,<sup>[122]</sup> phosphato<sup>[113]</sup> or oxazetidinylacetato ligands.<sup>[112]</sup> An octanuclear copper(I) compound, which can be described as a  $[(\text{MesCu})_4(\mu_4-\text{O})]^{2-}$  ( $\text{Mes} = 2,4,6\text{-trimethylphenyl}$ ) anion with two dinuclear copper(I)–pyrazole clamps containing the HL2i ligand, has also been reported.<sup>[126]</sup> The use of more bulky pyrazole ligands (i.e. HL2j) affords tetranuclear copper(I) compounds, which were studied by NMR spectroscopy.<sup>[127]</sup>

The incorporation of other functional groups in the amino substituents of the pyrazole ring, such as imidazole (HL2j<sup>[125]</sup> and HL2l<sup>[128]</sup> ligands) or 1,4,7-triazacyclononane (HL2m ligand),<sup>[129]</sup> has also been studied. In most of the cases, pH potentiometric studies in aqueous solution were performed in combination with the crystallographic characterization of the different polynuclear species formed in the presence of the copper(II) ion.<sup>[125,129]</sup>

## Pyrazole Ligands with N-Donor Substituents, Pyridines

2-Pyridylpyrazole derivatives (Figure 11) have been proven to be good ligands for obtaining different assemblies, such as metallohelicates<sup>[130,131]</sup> or clusters.<sup>[132–140]</sup> Together with another bridging ligand, for example, phosphonate, they provide a good approach to isolate a decanuclear copper(II) cage with the formula  $[\text{Cu}_5(\mu_3\text{-OH})_2(\text{rBuPO}_3)_3(\text{L3a})_2(\text{MeOH})_2] \cdot 10\text{MeOH} \cdot 2\text{H}_2\text{O}$ .<sup>[141]</sup> The reaction of an iron(II) salt with the 3-(2-pyridyl)pyrazole ligand formed by the decomposition of the ligand tris[3-(2-

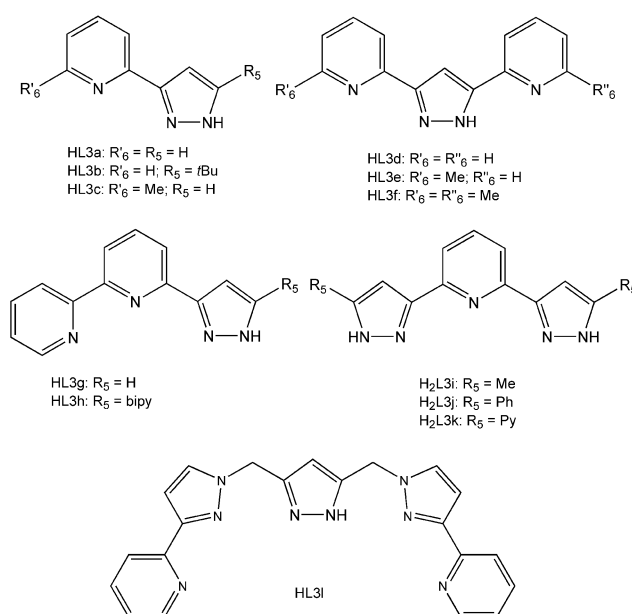


Figure 11. Pyrazole-based ligands with N-donor substituents, pyridines.

pyridyl)pyrazol-1-yl}hydroborate] (Tp<sup>Py</sup>), leads to a tetranuclear compound,  $[\text{Fe}_4(\text{HL3a})_2(\text{L3a})_6(\mu\text{-O})_2](\text{PF}_6)_2 \cdot 4\text{CH}_3\text{CN}$ .<sup>[135]</sup>

The coordination ability of the 3-(2-pyridyl)pyrazole ligand (HL3a) and its derivatives (HL3f, HL3g and HL3h) is also confirmed by the formation of copper(II) tetranuclear grids with the core  $[\text{Cu}_4\text{L}_6]^{2+}$  or  $[\text{Cu}_4\text{L}_4]^{4+}$  (Figure 12) in an isolated fashion or in 1D chains.<sup>[133,134,136,138,140]</sup> In such types grids, strong antiferromagnetic interactions are present between the copper(II) ions. The antiferromagnetic magnetic behaviour and its strength were explained on the basis of the number of pyrazole bridges, the distorted geometry of the pyrazole ligands and the orientation of the magnetic orbitals of the copper(II) ion.<sup>[133,134,136,138,140]</sup> Other grid-type structures are formed with cobalt(II) and manganese(II) ions.<sup>[140]</sup> Different typologies and nuclearities can also be found with the cobalt(II) ion and the HL3f ligand,<sup>[137]</sup> the copper(II) ion and the HL3l ligand,<sup>[142]</sup> and the copper(I) and copper(II) ions with the HL3c ligand.<sup>[139]</sup>

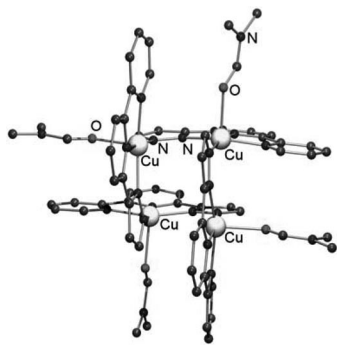


Figure 12. Molecular structure of the cation,  $[\text{Cu}_4(\text{L3g})_4(\text{dmf})_4]^{2+}$ .<sup>[136]</sup>

Coordination of 5-*tert*-butyl-3-(pyrid-2-yl)-1*H*-pyrazole (HL3b) to copper(II) and cobalt(II/III) leads to metallocycles (see below). In the case of copper(II) salts with non-coordinated anions, a cubane-based structure is formed,  $[\text{Cu}_4(\mu_3\text{-OH})_4(\text{L3b})_4](\text{ClO}_4)_4 \cdot x\text{CH}_2\text{Cl}_2$  ( $x = 1-2$ ).<sup>[143]</sup> Small antiferromagnetic interactions between the copper(II) ions are present, as expected on the basis of Hatfield and Hodgson's studies of the correlation with the bridging angle.<sup>[144]</sup> The Cu–O–Cu angles found in this compound are within the range in which both antiferromagnetic and ferromagnetic interactions can be present. Using bis(pyrazole)pyridine ligands ( $\text{H}_2\text{L3i}$  and  $\text{H}_2\text{L3j}$ ) affords octanuclear copper(I) compounds<sup>[145]</sup> and hexanuclear silver(I) compounds.<sup>[146]</sup> The binding of ligand  $\text{H}_2\text{L3k}$  to cobalt(II) affords an octanuclear cobalt(II) compound ring and a nonanuclear cobalt(II/III) compound grid.<sup>[147]</sup> Both compounds display antiferromagnetic interactions resulting in a total ground-state spin of  $S_T = 0$  [for the octanuclear cobalt(II) compound] and 4 [for the nonanuclear cobalt(II/III) compound], in which the latter displays SMM behaviour.<sup>[147]</sup>

## Pyrazole Ligands with O-Donor Substituents, Alcohols

The ligands described in this section,  $\text{H}_2\text{L4a-H}_2\text{L4d}$  (Figure 14), have been used by Winpenny and co-workers to explore the coordination chemistry of nickel(II) and manganese(II/III) ions.<sup>[148–153]</sup>  $[\text{Mn}_{14}\text{O}_2(\text{OH})_4(\text{L4c})_{18}(\text{HL4c})_4(\text{NO}_3)_4(\text{H}_2\text{O})_4]$  is a mixed-valent compound containing two manganese(III) and twelve manganese(II) ions.<sup>[148]</sup> Strong antiferromagnetic interactions between the metal centres lead to a ground state of  $S_T = 0$ .<sup>[148]</sup> After the synthesis of this cluster and the wheel  $[\text{Ni}_{24}(\text{OH})_8(\text{L4a})_{16}(\text{O}_2\text{CMe})_{24}(\text{HL4a})_{16}]$  that is described below as a metallocycle,<sup>[149]</sup> derivatives of pyrazolinol-type ligands (HL4b, HL4c, HL4d) were synthesized to study their binding to nickel(II) ions in the presence of pivalate (*piv*<sup>−</sup>) bridging ligands. As a result, different topologies were obtained with nuclearities ranging from  $[\text{Ni}_4\text{Na}_4]$ ,  $[\text{Ni}_5\text{Na}_4]$ ,  $[\text{Ni}_5\text{Li}_6]$  and  $[\text{Ni}_8\text{M}_2]$  ( $\text{M} = \text{K}^{\text{I}}, \text{Rb}^{\text{I}}, \text{Cs}^{\text{I}}$ ) to  $[\text{Ni}_8]$ .<sup>[150]</sup> In these compounds, the presence of antiferromagnetic interactions between the nickel(II) ions gives the zero-spin or low-spin ground states in most of the cases. For  $[\text{Ni}_5\text{Li}_6]$ , weak ferromagnetic interactions are operative within the cluster, which yields a ground state of  $S_T \geq 1$ .<sup>[150]</sup>  $[\text{Ni}_8\text{M}_2]$  and  $[\text{Ni}_8]$  clusters are formed by two pseudo-cubanes linked by  $\mu\text{-O}$  bridges.<sup>[150]</sup> The magnetic behaviour of both types of clusters are explained in terms of the magnetostructural correlations within the  $[\text{Ni}_4(\mu_3\text{-O})_4]$  core, in which Ni–O–Ni angles smaller than  $99^\circ$  favour ferromagnetic interactions, whereas larger angles promote antiferromagnetic interactions.<sup>[150]</sup> The incorporation of alkali metals in the final structure of some of the compounds allowed the extension of this study.<sup>[151]</sup> Thus, reactions were performed with the dinuclear complex  $[\text{Ni}_2(\text{H}_2\text{O})(\text{piv})_4(\text{Hpiv})_4]$  (*Hpiv* = trimethylacetic acid) as a starting material and with HL4c, to form  $[\text{Ni}_6\text{Mg}_2(\text{OH})_2(\text{L4c})_4(\text{piv})_{10}(\text{HL4c})_4(\text{MeOH})_2]$  and  $[\text{Ni}_8\text{M}]$  ( $\text{M} = \text{Sr}^{\text{II}}, \text{Ba}^{\text{II}}$ ) clusters.<sup>[151]</sup> The first compound is formed by two nickel(II) triangles bridged by magnesium(II) ions. Ferromagnetic exchange interactions are present between the nickel(II) ions forming the triangle. The nonanuclear compounds,  $[\text{Ni}_8\text{Sr}(\text{OH})_2(\text{L4c})_6(\text{piv})_{10}(\text{HL4c})_5(\text{Hpiv})_2(\text{CH}_3\text{CN})]$  and  $[\text{Ni}_8\text{Ba}(\text{OH})_2(\text{L4c})_6(\text{piv})_{10}(\text{HL4c})_{5.3}(\text{Hpiv})_{0.7}(\text{CH}_3\text{CN})_2]$ , are formed by two tetranuclear nickel(II) units bridged by strontium(II) and barium(II) ions, respectively.<sup>[151]</sup> Dominant antiferromagnetic interactions are present between the nickel(II) ions leading to two independent ground states both with  $S_T = 2$ , corresponding to the two tetranuclear units.<sup>[151]</sup> The use of silver(I) as a second metal ion resulted in the serendipitous formation of the large antiferromagnetic cluster  $[\text{Ni}_{21}\text{Ag}(\mu_4\text{-OH})_4(\mu_3\text{-OH})_6(\text{L4d})_{13}(\text{piv})_{20}(\text{Hpiv})_4(\text{CH}_3\text{CN})_{3.5}(\text{H}_2\text{O})_{0.5}]$ .<sup>[152]</sup> The exploration of new carboxylic acids, i.e. *tert*-butylbenzoic acid and benzoic acid as well as azido ligands, has demonstrated the unpredictability of the pyrazolinone ligands with three new compounds,  $\text{Na}[\text{Ni}_8\text{Na}(\text{OH})_2\text{F}_8(\text{tBuPhCO}_2)_8(\text{HL4a})_8]$ ,  $[\text{Ni}_8\text{Na}_2(\text{N}_3)_{12}(\text{tBuPhCO}_2)_2(\text{L4a})_4(\text{HL4a})_6(\text{EtOAc})_6]$  and  $[\text{Ni}_8\text{Na}_2(\text{N}_3)_{12}(\text{PhCO}_2)_2(\text{L4a})_4(\text{HL4a})_6(\text{EtOAc})_6]$ .<sup>[153]</sup> Figure 13 shows the molecular structure of  $[\text{Ni}_8\text{Na}_2(\text{N}_3)_{12}(\text{PhCO}_2)_2(\text{L4a})_4(\text{HL4a})_6(\text{EtOAc})_6]$ , in which

ferromagnetic interactions between the nickel(II) ions are propagated through the azide ligands; micro-SQUID measurements indicate a single-molecule magnet behaviour.<sup>[153]</sup>

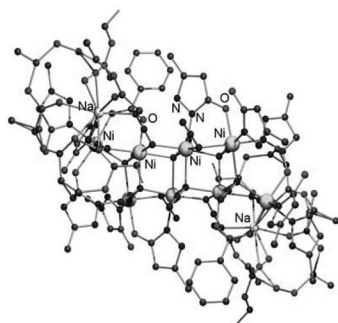


Figure 13. Molecular structure of the compound  $[\text{Ni}_8\text{Na}_2(\text{N}_3)_{12}(\text{PhCO}_2)_2(\text{L4a})_4(\text{HL4a})_6(\text{EtOAc})_6]$ .<sup>[153]</sup>

### Pyrazole Ligands with O-Donor Substituents, Phenols

The phenol-pyrazole-based ligands used for the compounds described in this section are shown in Figure 14. An octanuclear manganese(III) compound with the formula  $[\text{Mn}_8(\mu_4\text{-O})_4(\text{L5d})_8(\text{thf})_4]$  was reported by some of us, in which strong antiferromagnetic interactions are operative between all the manganese(III) ions (Figure 15).<sup>[154]</sup> This compound resembles other octanuclear iron(III) compounds with a cubane core, described above.<sup>[95,96]</sup> The stability of the cluster core with different phenol-pyrazole ligands ( $\text{H}_2\text{L5a}$ ,  $\text{H}_2\text{L5d}$ ,  $\text{H}_2\text{L5e}$ ) has been studied in various solvents.<sup>[154,155]</sup> When ligands with small substituents on the pyrazole ring ( $\text{H}_2\text{L5a}$ ,  $\text{H}_2\text{L5d}$ ) are used, the core  $[\text{Mn}_8(\mu_4\text{-O})_4(\text{L})_8]$  ( $\text{L} = 5\text{a}^{2-}$ ,  $5\text{d}^{2-}$ ) is retained.<sup>[155]</sup> However, the use of bulkier groups (ethyl) drives the formation of a hexanuclear compound with the formula  $[\text{Mn}_6(\mu_3\text{-O})_4(\mu_3\text{-Br})_2(\text{HL5e})_6(\text{L5e})]$ .<sup>[155]</sup> Strong antiferromagnetic interactions are operative in all octanuclear compounds, because the core motif does not change considerably and the magnetic behaviour is ruled mainly by the Mn–O–Mn angles. By contrast, in the hexanuclear compound  $[\text{Mn}_6(\mu_3\text{-O})_4(\mu_3\text{-Br})_2(\text{HL5e})_6(\text{L5e})]$ , weak ferromagnetic interactions are found. This behaviour was explained in terms of a canted structure in which all the Jahn–Teller magnetic axes have different orientations.<sup>[155]</sup>

Trinuclear oxide-centred compounds have also been obtained with phenol-pyrazole ligands.<sup>[156–162]</sup> They have the general formula  $[\text{Mn}_3(\mu_3\text{-O})(\text{R-pz})_3(\text{L})_x(\text{S})_y]^{0/-}$  ( $\text{H}_2\text{R-pz} = \text{H}_2\text{L5a}–\text{H}_2\text{L5d}$ ,  $\text{H}_2\text{L5f}$ ,  $\text{H}_2\text{L5g}$ ;  $\text{L} = \text{azide}$ , carboxylate ligand;  $\text{S} = \text{methanol}$ , ethanol;  $x = 1, 2$ ;  $y = 0–4$ ).<sup>[156–162]</sup> The doubly deprotonated phenol-pyrazole ligands are in the same plane as the  $[\text{Mn}_3(\mu_3\text{-O})]^{7+}$  core, whereas bridging ligands, such as azide or carboxylates and alcoholic solvents, are present at the axial positions of the manganese(III) ions. The introduction of a substituent on the fifth position of the pyrazole ring such as methyl or phenyl ( $\text{H}_2\text{L5d}$ ,  $\text{H}_2\text{L5f}$ ) drives the carboxylate to bind to two manganese(III) ions from the same trinuclear unit, instead of bridging the trinuclear

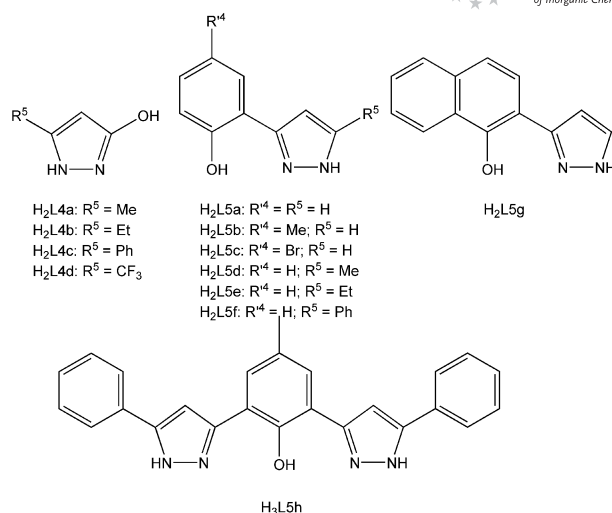


Figure 14. Pyrazole-based ligands with O-donor substituents, alcohols and phenols.

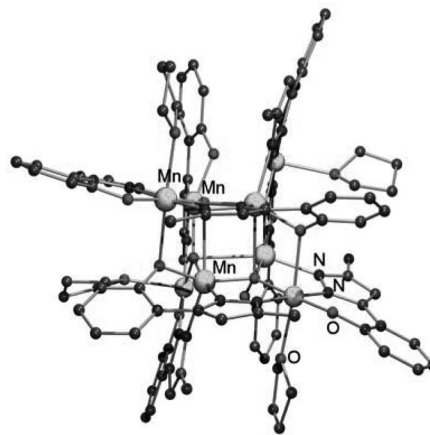


Figure 15. Molecular structure of  $[\text{Mn}_8(\mu_4\text{-O})_4(\text{L5d})_8(\text{thf})_8]$ .<sup>[154]</sup>

clear manganese(III) units.<sup>[160,161]</sup> If the carboxylate ligand is small, i.e. acetate, these trinuclear manganese(III) units can form chains, because of the hydrogen bonds established between the carboxylate and the solvent molecules.<sup>[160,161]</sup> When the carboxylate ligand is bulkier, such as benzoate, the trinuclear units become isolated, and no intermolecular hydrogen bonding interactions are observed.<sup>[161]</sup> In the absence of a substituent on the fifth position of the pyrazole ( $\text{H}_2\text{L5a}$ ,  $\text{H}_2\text{L5b}$ ,  $\text{H}_2\text{L5c}$ ,  $\text{H}_2\text{L5g}$ ), the trinuclear units are linked by a bridging ligand,<sup>[156–160,162]</sup> acetate or azide, forming 1D chains. In all these trinuclear manganese(III) compounds, overall antiferromagnetic interactions are present in the trinuclear unit. Ferromagnetic interactions between the trinuclear units are operative in most of the 1D chains,<sup>[156–160]</sup> showing long-range magnetic ordering or single-chain-magnet behaviour. It was found that ferromagnetic interactions between the manganese(III) ions of the trinuclear unit are favourable when the Mn–O–Mn angle values are smaller than  $120^\circ$  (value for an equilateral triangle) (Table 3, Figure 16).<sup>[160,161]</sup>



Table 3. Selected magnetic and structural data for trinuclear oxide-bridged manganese(III) compounds containing phenol-pyrazole ligands.

Compound	$J_1$ /cm <sup>-1</sup> [a]	$J_2$ /cm <sup>-1</sup> [a]	$zJ'$ /cm <sup>-1</sup>	$g$	Mn–O–Mn <sup>[b]</sup>	Ref.
[Mn <sub>3</sub> (μ <sub>3</sub> -O)(L5a) <sub>3</sub> (MeOH) <sub>3</sub> (O <sub>2</sub> CMe)] <sub>n</sub>	-3.01	-3.01	+0.32	1.88	119.88; 119.15; 119.98	[159,160]
[Mn <sub>3</sub> (μ <sub>3</sub> -O)(L5b) <sub>3</sub> (MeOH) <sub>4</sub> (O <sub>2</sub> CMe)] <sub>n</sub>	-3.21	-3.21	+0.68	1.93	120.42; 119.41; 120.14	[159]
[Mn <sub>3</sub> (μ <sub>3</sub> -O)(L5b) <sub>3</sub> (EtOH) <sub>4</sub> (O <sub>2</sub> CMe)] <sub>n</sub>	-1.87	-5.61	-0.014	1.99	120.43; 118.44; 121.13	[156]
[Mn <sub>3</sub> (μ <sub>3</sub> -O)(L5c) <sub>3</sub> (MeOH) <sub>3</sub> (N <sub>3</sub> )] <sub>n</sub> ·2 <i>n</i> MeOH	-3.87	-8.20	-0.07	2.12	119.91; 119.17; 119.35	[157]
[Mn <sub>3</sub> (μ <sub>3</sub> -O)(L5c) <sub>3</sub> (MeOH) <sub>3</sub> (N <sub>3</sub> )] <sub>n</sub>	-4.66	-7.35	-0.30	2.12	120.33; 118.75; 120.61	[157]
[Mn <sub>3</sub> (μ <sub>3</sub> -O)(L5c) <sub>3</sub> (MeOH) <sub>3</sub> (O <sub>2</sub> CMe)] <sub>n</sub>	-1.58	-5.50	-0.27	2.04	120.56; 119.18; 120.20	[158]
[Mn <sub>3</sub> (μ <sub>3</sub> -O)(L5c) <sub>3</sub> (EtOH) <sub>3</sub> (O <sub>2</sub> CMe)] <sub>n</sub>	-1.02	-4.39	-0.31	2.02	120.3; 119.3; 120.4	[158]
[Mn <sub>3</sub> (μ <sub>3</sub> -O)(L5c) <sub>3</sub> (EtOH) <sub>3</sub> (O <sub>2</sub> CMe)] <sub>n</sub>	-0.72	-3.13	-0.18	2.02	119.54; 120.15; 120.22	[158]
[Mn <sub>3</sub> (μ <sub>3</sub> -O)(L5d) <sub>3</sub> (O <sub>2</sub> CMe)(MeOH) <sub>3</sub> ]·1.5MeOH	-7.1	+4.4	–	1.98	120.61; 116.10; 120.85	[160]
[Mn <sub>3</sub> (μ <sub>3</sub> -O)(L5a) <sub>3</sub> (MeOH) <sub>4</sub> (N <sub>3</sub> )] <sub>n</sub> · <i>n</i> MeOH	-6.2	-3.7	–	2.01	120.79; 118.96; 120.11	[160]
[Mn <sub>3</sub> (μ <sub>3</sub> -O)(L5d) <sub>3</sub> (O <sub>2</sub> CMe)(EtOH)]·EtOH	-10.3	+10.9	–	1.87	112.65; 122.73; 124.28	[161]
<i>n</i> Bu <sub>4</sub> N[Mn <sub>3</sub> (μ <sub>3</sub> -O)(L5d) <sub>3</sub> (O <sub>2</sub> CPh) <sub>2</sub> ]	-4.2	-10.3	–	1.88	124.67; 117.91; 117.35	[161]
<i>n</i> Bu <sub>4</sub> N[Mn <sub>3</sub> (μ <sub>3</sub> -O)(L5f) <sub>3</sub> (O <sub>2</sub> CPh) <sub>2</sub> ]	-4.8	-10.2	–	1.93	117.75; 125.58; 116.66	[161]
[Mn <sub>3</sub> (μ <sub>3</sub> -O)(L5g) <sub>3</sub> (MeOH) <sub>2</sub> (O <sub>2</sub> CMe)] <sub>n</sub>	-2.2	-6.4	–	1.99	121.50; 119.43; 119.03	[162]

[a] The  $J$  values describe the magnetic exchange interactions depending on the geometrical parameters of each compound according to the Hamiltonian  $\hat{H} = -\sum J_{ij}S_iS_j$ . [b] Mn–μ<sub>3</sub>-O–Mn angle. Ligand abbreviations are given in Figure 14.

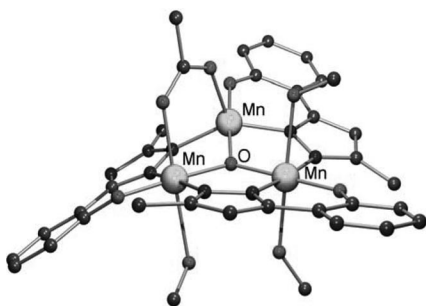


Figure 16. Molecular structure of [Mn<sub>3</sub>(μ<sub>3</sub>-O)(L5d)<sub>3</sub>(O<sub>2</sub>CMe)(MeOH)<sub>3</sub>]·1.5MeOH.<sup>[160]</sup>

Another example of a trinuclear compound is Na{Mn(HL5f)(L5f)(MeOH)<sub>2</sub>}<sub>2</sub>HCO<sub>2</sub>.<sup>[163]</sup> The two manganese units are bridged by a sodium(I) ion, which derives from the use of sodium methoxide as a base. Remarkably, a formate ion, which is coordinated to the sodium(I) ion is spontaneously formed by the decomposition of methanol and/or sodium methoxide.<sup>[163]</sup>

A tetranuclear nickel(II) compound with the formula [Ni<sub>4</sub>(OH)(OMe)<sub>3</sub>(HL5d)<sub>4</sub>(MeOH)<sub>3</sub>]·MeOH has been reported with the ligand H<sub>2</sub>L5d.<sup>[164]</sup> Ferromagnetic interactions between the nickel(II) ions are present, leading to a ground state of  $S_T = 4$ .

Tao and co-workers extended the chemistry of these types of ligands to other transition-metal ions, such as the copper(II) ion.<sup>[165]</sup> The result is the formation of large cages with the formula (HNEt<sub>3</sub>)<sub>2</sub>[Cu<sub>21</sub>(CH<sub>3</sub>CN)<sub>2</sub>(H<sub>2</sub>O)(μ-N<sub>3</sub>)<sub>6</sub>(μ<sub>3</sub>-N<sub>3</sub>)<sub>2</sub>(L5a)<sub>18</sub>]·3H<sub>2</sub>O·2EtOH and [Cu<sub>16</sub>(EtOH)<sub>2</sub>(H<sub>2</sub>O)<sub>2</sub>(L5b)<sub>16</sub>]·9.5H<sub>2</sub>O.<sup>[165]</sup> Predominant antiferromagnetic interactions were found between the copper(II) ions in both compounds, although some ferromagnetic interactions are present between some of the copper(II) ions in (HNEt<sub>3</sub>)<sub>2</sub>[Cu<sub>21</sub>(CH<sub>3</sub>CN)<sub>2</sub>(H<sub>2</sub>O)(μ-N<sub>3</sub>)<sub>6</sub>(μ<sub>3</sub>-N<sub>3</sub>)<sub>2</sub>(L5a)<sub>18</sub>]·3H<sub>2</sub>O·2EtOH.<sup>[165]</sup> Monte Carlo simulations were performed to evaluate the magnitude of the magnetic exchange interactions:  $J_1 > 340$  cm<sup>-1</sup>,  $J_2 = -290(20)$  cm<sup>-1</sup>,  $J_3 = -3(1)$  cm<sup>-1</sup>

and  $J_1 = -368(2)$  cm<sup>-1</sup>,  $J_2 = -53(2)$  cm<sup>-1</sup> for (HNEt<sub>3</sub>)<sub>2</sub>[Cu<sub>21</sub>(CH<sub>3</sub>CN)<sub>2</sub>(H<sub>2</sub>O)(μ-N<sub>3</sub>)<sub>6</sub>(μ<sub>3</sub>-N<sub>3</sub>)<sub>2</sub>(L5a)<sub>18</sub>]·3H<sub>2</sub>O·2EtOH and [Cu<sub>16</sub>(EtOH)<sub>2</sub>(H<sub>2</sub>O)<sub>2</sub>(L5b)<sub>16</sub>]·9.5H<sub>2</sub>O, respectively.<sup>[165]</sup> A phenol-bis(pyrazole) ligand (H<sub>3</sub>L5h) was used to synthesize a mixed-valence manganese(II/III) linear trinuclear compound, [Mn<sub>3</sub>(HL5h)<sub>2</sub>(O<sub>2</sub>CMe)<sub>3</sub>(MeOH)<sub>3</sub>].<sup>[166]</sup> Antiferromagnetic interactions between the manganese(II/III) ions are present in the molecule, leading to a ground state of  $S_T = 3$ .<sup>[166]</sup>

### Pyrazole Ligands with Other Functional Groups with N- and/or O-Donor Substituents

In this section, compounds with ligands that cannot be described by the previous classifications will be presented (Figure 17).

The functionalization of the pyrazole ligand with acid groups as substituents on the pyrazole ring, like 3,5-pyrazoledicarboxylic acid (H<sub>3</sub>L6a), introduces numerous coordination sites. Coordination polymers have been obtained by hydrothermal synthesis with a variety of transition-metal ions,<sup>[167–169]</sup> lanthanides<sup>[170]</sup> or a combination of 3d- and 4f-metal ions, such as Cu<sup>II</sup>Ln<sup>III</sup><sub>2</sub>.<sup>[171,172]</sup> An example with the 3,5-pyrazoledicarboxylic acid as a ligand is a trinuclear copper(II) compound with formula [Cu<sub>3</sub>(L6a)<sub>2</sub>(H<sub>2</sub>O)<sub>4</sub>]<sub>n</sub>.<sup>[167]</sup> Strong antiferromagnetic interactions between the copper(II) ions are mediated by the pyrazole ligand, whereas weaker ferromagnetic and antiferromagnetic interactions between the copper(II) ions are mediated by the carboxylate ligands in a *syn-anti*-equatorial-equatorial and a *syn-anti*-axial-equatorial type of bridge, respectively.<sup>[167]</sup> The use of an additional ligand, like imidazole (HIm), allows the formation of a tetranuclear copper(II) compound with a U-shaped core, [Cu<sub>4</sub>(L6a)<sub>4</sub>(Im)<sub>4</sub>]·4Dma·9H<sub>2</sub>O, in which weak antiferromagnetic interactions are present.<sup>[173]</sup> Decomposition of an amide-pyrazole derivative ligand to an L6a<sup>3-</sup> ligand during the synthesis resulted in the formation of trinuclear linear copper(II) compounds.<sup>[174]</sup> Magnetic susceptibility studies revealed weak antiferromagnetic

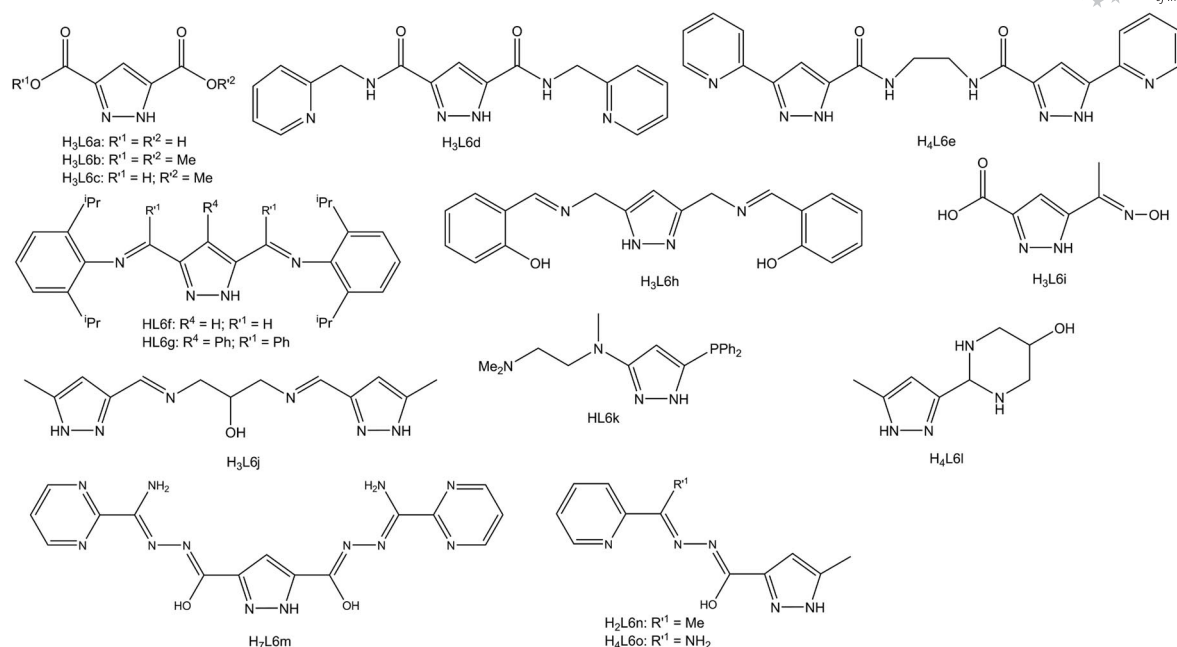


Figure 17. Pyrazole-based ligands containing other functional groups with N- and/or O-donor substituents.

interactions ascribed to the large separation between the copper(II) ions.<sup>[174]</sup> The HL6b ligand has been used in the synthesis of a linear trinuclear copper(II) compound.<sup>[175]</sup> Hydrolysis of the HL6b ligand during the synthesis resulted also in the formation of a tetranuclear copper(II) compound with the HL6c ligand. Weak antiferromagnetic interactions between the copper(II) ions were observed in this case.<sup>[176]</sup>

Pyrazole-3,5-dicarboxamides are often used as intermediates in the synthesis of pyrazoles with chelating amine side arms. Therefore, the coordination ability of this type of ligands has also been studied, because when the amide is deprotonated, the metal ion can coordinate through the nitrogen atoms, whereas if it remains protonated, the coordination would be through the oxygen atom. The ligand *N,N'*-bis(2-pyridylmethyl)pyrazole-3,5-dicarboxamide (H<sub>3</sub>L6d) forms tetranuclear [2 × 2] grids with the general formula [M<sub>4</sub>(HL6d)<sub>4</sub>]·8H<sub>2</sub>O (M = Cu<sup>II</sup>, Ni<sup>II</sup>).<sup>[177]</sup> Magnetic susceptibility and EPR studies were performed only for the copper(II) compound.<sup>[177]</sup> The nickel(II) compound is diamagnetic, whilst antiferromagnetic interactions between the copper(II) ions are mediated by the pyrazole bridges. Other examples of tetranuclear nickel(II) and copper(II) compounds have been reported with the ligand H<sub>4</sub>L6e.<sup>[178,179]</sup> These compounds have different topology depending on the metal ion used: linear for nickel(II) ions and helical for copper(II) ions.<sup>[179]</sup> Weak and strong antiferromagnetic interactions have been found between the nickel(II) and copper(II) ions, respectively.<sup>[179]</sup> Heterobimetallic compounds with the same ligand are also reported.<sup>[178]</sup>

Diimine-pyrazole ligands are known to stabilize large clusters.<sup>[180–183]</sup> Two hexanuclear nickel(II) compounds have been reported, which are composed of three bimetallic

units, [Ni<sub>2</sub>(L6f)X<sub>3</sub>] (X<sup>−</sup> = Cl<sup>−</sup>, Br<sup>−</sup>), bridged by a halogen (Figure 18).<sup>[180,181]</sup> Also, hexanuclear copper(II) compounds are obtained with the same type of ligands.<sup>[182]</sup> EPR and magnetic susceptibility studies revealed strong antiferromagnetic interactions between the copper(II) ions. The coordination of this type of ligands (HL6g) with cobalt(II) ions affords tetranuclear complexes, in which antiferromagnetic interactions are operative.<sup>[183]</sup> A linear tetranuclear manganese(III) compound has been reported with H<sub>3</sub>L6h, in which the salicylideneamine moiety acts as a chelating ligand and the pyrazole ligand bridges the manganese(III) ions.<sup>[184]</sup> Weak antiferromagnetic interactions between the manganese(III) ions are observed.<sup>[184]</sup> N-heterocyclic carbene groups have been found at the 3,5-position of pyrazole rings. The same ligands used in combination with silver(I) yielded tetranuclear and octanuclear compounds depending on the substituents of the carbene ligand.<sup>[185]</sup>

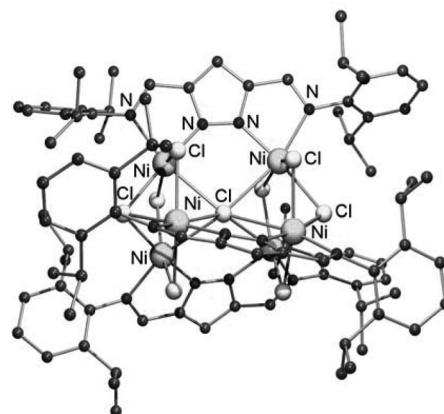


Figure 18. Molecular structure of [Ni<sub>2</sub>(L6f)Cl<sub>3</sub>].<sup>[180,181]</sup>

The coordination ability of ligands containing two different substituent groups on the pyrazole ring has also been explored.<sup>[186,187]</sup> As a result, a linear trinuclear copper(II) compound has been synthesized with the H<sub>3</sub>L6i ligand that contains both an oxime and an acid substituent groups. Strong antiferromagnetic interactions between the copper(II) ions are operative in this compound.<sup>[187]</sup> Another example is a tetranuclear nickel(II) compound with the HL6k ligand, in which the nickel(II) ions are in low-spin electronic configuration.<sup>[186]</sup> Polytopic hydrazone-based ligands (H<sub>2</sub>L6n and H<sub>4</sub>L6o) containing the pyrazole group have been used for the synthesis of three different tetranuclear copper(II) grids.<sup>[188,189]</sup> In the case of nickel(II) ion and H<sub>7</sub>L6m, a trinuclear compound is formed, in which the magnetic interactions between the nickel(II) centres are negligible.<sup>[190]</sup> A linear tetranuclear copper(II) compound was synthesized containing two different types of pyrazolate ligands, H<sub>3</sub>L6j and H<sub>3</sub>L6l.<sup>[191]</sup> Strong antiferromagnetic interaction between the copper(II) ions is present, as confirmed by magnetic susceptibility and EPR studies.<sup>[191]</sup>

## Other Architectures

### Metallocycles

Metal-directed self-assembly processes often form well-defined architectures.<sup>[192–195]</sup> Cyclic metal–organic compounds with a central cavity, or metallocycles, are one of these structural examples found in supramolecular chemistry.<sup>[192–195]</sup> Some examples with pyrazole-based ligands have been reported in the literature.<sup>[29,85,93,196–199]</sup> An octanuclear copper(II) wheel, [Cu<sub>8</sub>(L1k)<sub>8</sub>(OH)<sub>8</sub>] (HL1k = 3,5-dimethylpyrazole), was formed by oxidation of [Cu(L1k)]<sub>n</sub>, which is catalytically active in some oxidation reactions.<sup>[29]</sup> The reaction of the wheel with primary alcohols affords octaalkoxido derivatives.<sup>[29]</sup> Removing the chloride anion from [Cu<sub>3</sub>(μ<sub>3</sub>-O)(L1a)<sub>3</sub>Cl<sub>3</sub>]<sup>2-</sup> and [Cu<sub>3</sub>(μ<sub>3</sub>-Cl)<sub>2</sub>(L1a)<sub>3</sub>Cl<sub>3</sub>]<sup>2-</sup> affords the rings [*cis*-Cu(μ-OH)(L1a)]<sub>n</sub> (*n* = 6, 8, 9, 12 and 14), where the distorted square-planar copper(II) ions are connected by μ-pz ligands outside the ring and μ-OH ligands inside the ring.<sup>[197]</sup> Two of these units encapsulate different ions (chloride, carbonate and sulfate) that are stabilized by numerous weak hydrogen bonds. The ring size does not depend on the encapsulated anion.<sup>[197]</sup> Copper(II) cages of smaller nuclearity have also been reported.<sup>[85,196]</sup> An example is the compound [{Cu<sub>3</sub>(HL1i)<sub>4</sub>(L1i)<sub>2</sub>(μ-F)<sub>2</sub>(μ<sub>3</sub>-F)}<sub>2</sub>]F<sub>2</sub> (HL1i = 5-*tert*-butylpyrazole), in which antiferromagnetic interactions are present between the copper(II) ions, the stronger path being the one mediated by the [Cu(μ-F)<sub>2</sub>]<sup>2+</sup> bridges.<sup>[93]</sup> Another example is the hexanuclear copper(II) cage [Au(PPh<sub>3</sub>)<sub>2</sub>][Cu<sub>6</sub>(μ-OH)<sub>6</sub>(L1l)<sub>6</sub>Cl] {HL1l = 3,5-bis(trifluoromethyl)pyrazole}, in which strong antiferromagnetic interactions are present between the copper(II) ions.<sup>[198]</sup> The zinc(II) ion has also been found to be suitable for the synthesis of a neutral macrocycle,<sup>[199]</sup> in which the mercaptoethanolato ligands are inside the ring and the pyrazole ligands are outside; a channel with a diameter of 4.7 Å is generated from this structure.

Pyrazole ligands bearing substituents with donor atoms are also capable of forming metallocycles.<sup>[85,149,200–202]</sup> The 3(5)-pyrid-2-yl-5-(3)-(*tert*-butyl)pyrazole ligand (HL3b) affords a metallocrown with the formula [Cu(μ-F){μ-(L3b)}<sub>6</sub>(H<sub>2</sub>O)<sub>2</sub>·8CH<sub>2</sub>Cl<sub>2</sub>] (Figure 19).<sup>[201]</sup> This metallocycle contains a water molecule in the cavity stabilized by hydrogen bonding. Therefore, the binding of guest molecules, such as Na<sup>+</sup>, K<sup>+</sup>, NH<sub>4</sub><sup>+</sup>, MeNH<sub>3</sub><sup>+</sup> and four amino acids, in the cavity was studied.<sup>[200]</sup> Larger guests cannot bind inside the cavity; therefore, they bind exogenously to the two bowl-shaped cavities.<sup>[200]</sup> Strong hydrogen bonds stabilize all these structures.<sup>[200,201]</sup> Magnetic susceptibility studies reveal antiferromagnetic interactions that are barely affected by the guest binding.<sup>[200]</sup> The use of weakly coordinating anions of the copper(II) salt affords tetranuclear compounds.<sup>[85]</sup> Other metal ions such as cobalt(II) afford the mixed-valence Co(II/III) metallocrown, [Co<sub>6</sub>(μ-OH)<sub>6</sub>{μ-(L3b)}<sub>6</sub>]<sup>m+</sup> (*m* = 2 or 3).<sup>[202]</sup> A large cage is formed by 24 high-spin nickel(II) ions in [Ni<sub>24</sub>(OH)<sub>8</sub>(L4a)<sub>16</sub>(O<sub>2</sub>CMe)<sub>24</sub>·(HL4a)<sub>16</sub>] (HL4a = 3-methyl-3-pyrazolin-5-one).<sup>[149]</sup> It is described as an octamer of chemically trinuclear-based building blocks. Antiferromagnetic interactions between the nickel(II) ions are present, and even at low temperature many excited states are populated.<sup>[149]</sup>

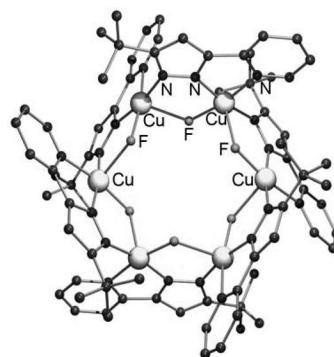


Figure 19. Molecular structure of the metallocycle [Cu(μ-F){μ-(L3b)}<sub>6</sub>].<sup>[200]</sup>

### Metallohelicates

Another group of supramolecular architectures is formed by metallohelicates, based not only on coordinative bonds, but also on intermolecular non-covalent interactions, such as electrostatic interactions, hydrogen bonding and π–π stacking.<sup>[203,204]</sup> Only a few examples have been reported thus far involving pyrazole ligands.<sup>[130,131,205]</sup> The first reported compound is [{Ru(L3a)<sub>3</sub>}<sub>2</sub>Cu<sub>3</sub>]ClO<sub>4</sub>.<sup>[205]</sup> It was synthesized by adding a copper salt to the [Ru(HL3a)<sub>3</sub>](ClO<sub>4</sub>)<sub>2</sub> in the presence of triethylamine. Other metallohelicates contain the ligand 3,5-bis(2-pyridyl)pyrazole (HL3d). The compounds [{M(μ-L3d)}<sub>2</sub>{M(μ-OH)}](SCN)<sub>3</sub>·6H<sub>2</sub>O (M = Ni<sup>II</sup>, Zn<sup>II</sup>) were synthesized under solvothermal conditions.<sup>[130]</sup> In such compounds, the [Ni<sub>3</sub>(μ-OH)]<sup>5+</sup> cluster core is wrapped by two terminal [Ni(μ-L3d)<sub>3</sub>]<sup>-</sup> units with SCN<sup>-</sup> as a counteranion.<sup>[130]</sup> These compounds were used



in combination with CuSCN to obtain other compounds,  $[\text{Cu}_{12}(\text{CN})_{11}(\text{SCN})_4][\{\text{M}(\mu\text{-L3d})_3\}_2\{\text{M}(\mu\text{-OH})\}]$  ( $\text{M} = \text{Ni}^{\text{II}}, \text{Zn}^{\text{II}}$ ),<sup>[130]</sup> in which the double-helical strands are stabilized by hydrogen bonding. Antiferromagnetic interactions between the nickel(II) ions were found in  $[\{\text{Ni}(\mu\text{-L3d})_3\}_2\{\text{Ni}(\mu\text{-OH})\}](\text{SCN})_3 \cdot 6\text{H}_2\text{O}$  and  $[\text{Cu}_{12}(\text{CN})_{11}(\text{SCN})_4][\{\text{Ni}(\mu\text{-L3d})_3\}_2\{\text{Ni}(\mu\text{-OH})\}]$ .<sup>[130]</sup> Another example is the compound  $[\{\text{Fe}(\mu\text{-L3d})_3\}_2\text{Fe}_3(\mu\text{-O})](\text{NCS})_2 \cdot 10\text{H}_2\text{O}$  (Figure 20), where the  $[\text{Fe}_3\text{O}]^{4+}$  core with high-spin iron(II) ions is wrapped by two  $[\text{Fe}(\text{L3d})_3]^-$  units with low-spin iron(II) ions.<sup>[131]</sup> Mössbauer spectroscopy confirmed the oxidation states of the iron(II) ions, and antiferromagnetic interactions between high-spin iron(II) ions were found to be present in the core.<sup>[131]</sup>

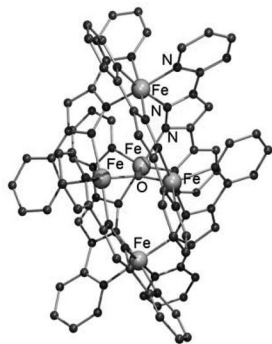


Figure 20. Molecular structure of  $[\{\text{Fe}(\mu\text{-L3d})_3\}_2\text{Fe}_3(\mu\text{-O})](\text{NCS})_2 \cdot 10\text{H}_2\text{O}$ .<sup>[131]</sup>

## Conclusions

To conclude, pyrazole-based ligands are very versatile ligands, as they are able to form different architectures, ranging from polynuclear clusters to metallocycles or metallo-helicates. The incorporation of other coordinating groups to the pyrazole ring increases the number of coordination sites and therefore the variety of polymetallic compounds that can be formed. In addition to the ability to bridge two or more metal ions, pyrazole ligands also provide an effective magnetic exchange pathway between them. The magnetic properties of the obtained compounds show large diversity, varying from (strongly) antiferromagnetic to ferromagnetic.

## Acknowledgments

This work was financially supported by the EC-Research Training Network “QuEMolNa” (No. MRTN-CT-2003-504880) and the EC Network of Excellence “MAGMANet” (No. 515767-2). S. T. acknowledges the Netherlands Organization for Scientific Research (NWO) for a Veni grant.

- [1] C. S. Mullins, V. L. Pecoraro, *Coord. Chem. Rev.* **2008**, 252, 416–443.
- [2] S. Mukhopadhyay, S. K. Mandal, S. Bhaduri, W. H. Armstrong, *Chem. Rev.* **2004**, 104, 3981–4026.

- [3] G. Aromí, E. K. Brechin, *Struct. Bonding (Berlin)* **2006**, 122, 1–67.
- [4] D. Gatteschi, R. Sessoli, J. Villain, *Molecular Nanomagnets*, Oxford University Press, Oxford, **2006**.
- [5] O. Kahn, *Molecular Magnetism*, Wiley-VCH, New York, **1993**.
- [6] G. Aromí, S. M. J. Aubin, M. A. Bolcar, G. Christou, H. J. Epley, K. Folting, D. N. Hendrickson, J. C. Huffman, R. C. Squire, H. L. Tsai, S. Wang, M. W. Wemple, *Polyhedron* **1998**, 17, 3005–3020.
- [7] G. Christou, *Polyhedron* **2005**, 24, 2065–2075.
- [8] C. J. Milios, T. C. Stamatatos, S. P. Perlepes, *Polyhedron* **2006**, 25, 134–194.
- [9] C. J. Milios, A. Vinslava, W. Wernsdorfer, A. Prescimone, P. A. Wood, S. Parsons, S. P. Perlepes, G. Christou, E. K. Brechin, *J. Am. Chem. Soc.* **2007**, 129, 6547–6561; and ref. therein.
- [10] M. A. Halcrow, *Dalton Trans.* **2009**, 2059–2073.
- [11] J. Klingele, S. Dechert, F. Meyer, *Coord. Chem. Rev.* **2009**, 253, 2698–2741.
- [12] G. La Monica, G. A. Ardizzoia, *Prog. Inorg. Chem.* **1997**, 46, 151–238.
- [13] E. C. Constable, P. J. Steel, *Coord. Chem. Rev.* **1989**, 93, 205–223.
- [14] J. Reedijk in *Heterocyclic Nitrogen-Donor Ligands, Vol. II* (Eds.: G. Wilkinson, R. D. Gillard, J. A. McCleverty), Pergamon, Oxford, **1987**, pp. 73–98.
- [15] R. Fusco in *Chemistry of Heterocyclic Compounds: Pyrazoles, Pyrazolines, Indazoles and Condensed Rings, Vol. 22* (Eds.: R. H. B. Wiley, L. C., R. Fusco, C. H. Jarboe), John Wiley & Sons, Ltd., New York, **1967**, pp. 1–174.
- [16] E. Büchner, *Ber. Dtsch. Chem. Ges.* **1889**, 22, 842–847.
- [17] S. Trofimenko, *Chem. Rev.* **1972**, 72, 497–509.
- [18] S. Trofimenko, *Adv. Chem.* **1976**, 289–301.
- [19] S. Trofimenko, *Prog. Inorg. Chem.* **1986**, 34, 115–210.
- [20] S. Trofimenko, *Chem. Rev.* **1993**, 93, 943–980.
- [21] M. A. Halcrow, *Coord. Chem. Rev.* **2005**, 249, 2880–2908.
- [22] R. Mukherjee, *Coord. Chem. Rev.* **2000**, 203, 151–218.
- [23] J. Reedijk, *Recl. Trav. Chim. Pays-Bas* **1970**, 89, 605–619.
- [24] A. P. Sadimenko, S. S. Basson, *Coord. Chem. Rev.* **1996**, 147, 247–297.
- [25] M. Maekawa, M. Munakata, T. Kuroda, Y. Nozaka, *Inorg. Chim. Acta* **1993**, 208, 243–244.
- [26] S. J. Rettig, A. Storr, D. A. Summers, R. C. Thompson, J. Trotter, *Can. J. Chem.* **1997**, 75, 949–958.
- [27] M. K. Ehlert, S. J. Rettig, A. Storr, R. C. Thompson, J. Trotter, *Can. J. Chem.* **1993**, 71, 1425–1436.
- [28] H. N. Miras, H. Zhao, R. Herchel, C. Rinaldi, S. Perez, R. G. Raptis, *Eur. J. Inorg. Chem.* **2008**, 4745–4755.
- [29] G. A. Ardizzoia, M. A. Angaroni, G. La Monica, F. Cariati, S. Cenini, M. Moret, N. Masciocchi, *Inorg. Chem.* **1991**, 30, 4347–4353.
- [30] G. A. Ardizzoia, S. Cenini, G. La Monica, N. Masciocchi, A. Maspero, M. Moret, *Inorg. Chem.* **1998**, 37, 4284–4292.
- [31] H. V. R. Dias, H. V. K. Diyabalanage, M. G. Eldabaja, O. Elbjerrami, M. A. Rawashdeh-Omary, M. A. Omary, *J. Am. Chem. Soc.* **2005**, 127, 7489–7501.
- [32] H. V. R. Dias, C. S. P. Gamage, J. Keltner, H. V. K. Diyabalanage, I. Omari, Y. Eyobo, N. R. Dias, N. Roehr, L. McKinney, T. Poth, *Inorg. Chem.* **2007**, 46, 2979–2987.
- [33] H. V. R. Dias, S. A. Polach, Z. Y. Wang, *J. Fluorine Chem.* **2000**, 103, 163–169.
- [34] M. W. Dodge, W. F. Wacholtz, J. T. Mague, *J. Chem. Crystallogr.* **2005**, 35, 5–12.
- [35] M. K. Ehlert, S. J. Rettig, A. Storr, R. C. Thompson, J. Trotter, *Can. J. Chem.* **1992**, 70, 2161–2173.
- [36] M. K. Ehlert, A. Storr, R. C. Thompson, *Can. J. Chem.* **1992**, 70, 1121–1128.
- [37] N. Masciocchi, S. Galli, E. Alberti, A. Sironi, C. Di Nicola, C. Pettinari, L. Pandolfo, *Inorg. Chem.* **2006**, 45, 9064–9074.
- [38] T. Morawitz, H. W. Lerner, M. Bolte, *Acta Crystallogr., Sect. E* **2006**, 62, M1474–M1476.



- [39] H. H. Murray, R. G. Raptis, J. P. Fackler, *Inorg. Chem.* **1988**, 27, 26–33.
- [40] M. A. Omary, M. A. Rawashdeh-Omary, M. W. A. Gonser, O. Elbjeirami, T. Grimes, T. R. Cundari, *Inorg. Chem.* **2005**, 44, 8200–8210.
- [41] R. G. Raptis, J. P. Fackler, *Inorg. Chem.* **1988**, 27, 4179–4182.
- [42] M. C. Torralba, P. Ovejero, M. J. Mayoral, M. Cano, J. A. Campo, J. V. Heras, E. Pinilla, M. R. Torres, *Helv. Chim. Acta* **2004**, 87, 250–263.
- [43] R. G. Raptis, J. P. Fackler, *Inorg. Chem.* **1990**, 29, 5003–5006.
- [44] G. Yang, J. R. Martinez, R. G. Raptis, *Inorg. Chim. Acta* **2009**, 362, 1546–1552.
- [45] G. Yang, R. G. Raptis, *J. Chem. Soc., Dalton Trans.* **2002**, 3936–3938.
- [46] H. V. R. Dias, H. V. K. Diyabalanage, *Polyhedron* **2006**, 25, 1655–1661.
- [47] M. K. Ehlert, S. J. Rettig, A. Storr, R. C. Thompson, J. Trotter, *Can. J. Chem.* **1990**, 68, 1444–1449.
- [48] N. Masciocchi, M. Moret, P. Cairati, A. Sironi, G. A. Ardizzoia, G. La Monica, *J. Am. Chem. Soc.* **1994**, 116, 7668–7676.
- [49] A. A. Mohamed, L. M. Pérez, J. P. Fackler, *Inorg. Chim. Acta* **2005**, 358, 1657–1662.
- [50] A. A. Mohamed, A. Burini, J. P. Fackler, *J. Am. Chem. Soc.* **2005**, 127, 5012–5013.
- [51] A. A. Mohamed, R. Galassi, F. Papa, A. Burini, J. P. Fackler, *Inorg. Chem.* **2006**, 45, 7770–7776.
- [52] K. Umakoshi, Y. Yamauchi, K. Nakamiya, T. Kojima, M. Yamasaki, H. Kawano, M. Onishi, *Inorg. Chem.* **2003**, 42, 3907–3916.
- [53] K. Umakoshi, T. Kojima, Y. H. Kim, M. Onishi, Y. Nakao, S. Sakaki, *Chem. Eur. J.* **2006**, 12, 6521–6527.
- [54] D. Piñero, P. Baran, R. Boča, R. Herchel, M. Klein, R. G. Raptis, F. Renz, Y. Sanakis, *Inorg. Chem.* **2007**, 46, 10981–10989.
- [55] M. Łukasiewicz, Z. Ciunik, J. Mazurek, J. Sobczak, A. Staron, S. Wołowicz, J. J. Ziołkowski, *Eur. J. Inorg. Chem.* **2001**, 1575–1579.
- [56] P. A. Angaridis, P. Baran, R. Boča, F. Cervantes-Lee, W. Haase, G. Mezei, R. G. Raptis, R. Werner, *Inorg. Chem.* **2002**, 41, 2219–2228.
- [57] R. Boča, L. Dlhán, G. Mezei, T. Ortiz-Perez, R. G. Raptis, J. Telser, *Inorg. Chem.* **2003**, 42, 5801–5803.
- [58] G. Mezei, J. E. McGrady, R. G. Raptis, *Inorg. Chem.* **2005**, 44, 7271–7273.
- [59] G. Mezei, R. G. Raptis, *Inorg. Chim. Acta* **2004**, 357, 3279–3288.
- [60] G. Mezei, R. G. Raptis, J. Telser, *Inorg. Chem.* **2006**, 45, 8841–8843.
- [61] G. Mezei, M. Rivera-Carrillo, R. G. Raptis, *Inorg. Chim. Acta* **2004**, 357, 3721–3732.
- [62] G. Mezei, M. Rivera-Carrillo, R. G. Raptis, *Dalton Trans.* **2007**, 37–40.
- [63] M. Casarin, A. Cingolani, C. Di Nicola, D. Falcomer, M. Monari, L. Pandolfo, C. Pettinari, *Cryst. Growth Des.* **2007**, 7, 676–685.
- [64] M. Casarin, C. Corvaja, C. Di Nicola, D. Falcomer, L. Franco, M. Monari, L. Pandolfo, C. Pettinari, F. Piccinelli, *Inorg. Chem.* **2005**, 44, 6265–6276.
- [65] M. Casarin, C. Corvaja, C. di Nicola, D. Falcomer, L. Franco, M. Monari, L. Pandolfo, C. Pettinari, F. Piccinelli, P. Tagliatesta, *Inorg. Chem.* **2004**, 43, 5865–5876.
- [66] C. Di Nicola, F. Garau, Y. Y. Karabach, L. Martins, M. Monari, L. Pandolfo, C. Pettinari, A. J. L. Pombeiro, *Eur. J. Inorg. Chem.* **2009**, 666–676.
- [67] C. Di Nicola, Y. Y. Karabach, A. M. Kirillov, M. Monari, L. Pandolfo, C. Pettinari, A. J. L. Pombeiro, *Inorg. Chem.* **2007**, 46, 221–230.
- [68] F. B. Hulsbergen, R. W. M. Tenhoedt, G. C. Verschoor, J. Reedijk, A. L. Spek, *J. Chem. Soc., Dalton Trans.* **1983**, 539–545.
- [69] X. M. Liu, M. P. de Miranda, E. J. L. McInnes, C. A. Kilner, M. A. Halcrow, *Dalton Trans.* **2004**, 59–64.
- [70] M. Rivera-Carrillo, I. Chakraborty, G. Mezei, R. D. Webster, R. G. Raptis, *Inorg. Chem.* **2008**, 47, 7644–7650.
- [71] J. H. Zhou, Z. Liu, Y. Z. Li, Y. Song, X. T. Chen, X. Z. You, *J. Coord. Chem.* **2006**, 59, 147–156.
- [72] S. Contaldi, C. Di Nicola, F. Garau, Y. Y. Karabach, L. Martins, M. Monari, L. Pandolfo, C. Pettinari, A. J. L. Pombeiro, *Dalton Trans.* **2009**, 4928–4941.
- [73] M. Angaroni, G. A. Ardizzoia, T. Beringhelli, G. La Monica, D. Gatteschi, N. Masciocchi, M. Moret, *J. Chem. Soc., Dalton Trans.* **1990**, 3305–3309.
- [74] W. Z. Shen, L. Yi, P. Cheng, S. P. Yan, D. Z. Liao, Z. H. Jiang, *Inorg. Chem. Commun.* **2004**, 7, 819–822.
- [75] H. V. R. Dias, H. V. K. Diyabalanage, C. S. P. Gamage, *Chem. Commun.* **2005**, 1619–1621.
- [76] K. Sakai, Y. Yamada, T. Tsubomura, M. Yabuki, M. Yamaguchi, *Inorg. Chem.* **1996**, 35, 542–544.
- [77] T. Kogane, T. Yamamoto, M. Hayashi, R. Hirota, C. A. Horiuchi, *Polyhedron* **1995**, 14, 2475–2482.
- [78] E. M. Zueva, M. M. Petrova, R. Herchel, Z. Travnicek, R. G. Raptis, L. Mathivathanan, J. E. McGrady, *Dalton Trans.* **2009**, 5924–5932.
- [79] S. A. Kozimor, B. M. Bartlett, J. D. Rinehart, J. R. Long, *J. Am. Chem. Soc.* **2007**, 129, 10672–10674.
- [80] J. D. Rinehart, B. M. Bartlett, S. A. Kozimor, J. R. Long, *Inorg. Chim. Acta* **2008**, 361, 3534–3538.
- [81] G. B. Deacon, A. Gitlits, P. W. Roesky, M. R. Burgstein, K. C. Lim, B. W. Skelton, A. H. White, *Chem. Eur. J.* **2001**, 7, 127–138.
- [82] C. C. Quitmann, V. Bezugly, F. R. Wagner, K. Muller-Buschbaum, *Z. Anorg. Allg. Chem.* **2006**, 632, 1173–1186.
- [83] E. Kavlakoglu, A. Elmali, Y. Elerman, I. Svoboda, *Polyhedron* **2002**, 21, 1539–1545.
- [84] J. Manzur, A. M. Garcia, M. T. Garland, V. Acuna, O. González, O. Peña, A. M. Atria, E. Spodine, *Polyhedron* **1996**, 15, 821–827.
- [85] Q. F. Mokuolu, D. Foguet-Albiol, L. F. Jones, J. Wolowska, R. M. Kowalczyk, C. A. Kilner, G. Christou, P. C. McGowan, M. A. Halcrow, *Dalton Trans.* **2007**, 1392–1399.
- [86] M. Sanz, M. E. G. Mosquera, T. Cuenca, *Dalton Trans.* **2009**, 2616–2622.
- [87] K. Umakoshi, T. Kojima, Y. Arikawa, M. Onishi, *Chem. Eur. J.* **2006**, 12, 5094–5104.
- [88] A. Karmakar, J. B. Baruah, R. B. Shankar, *CrystEngComm* **2009**, 11, 832–840.
- [89] M. K. Ehlert, S. J. Rettig, A. Storr, R. C. Thompson, J. Trotter, *Acta Crystallogr., Sect. C-Cryst. Struct. Commun.* **1994**, 50, 1023–1026.
- [90] P. E. Kruger, F. Launay, V. McKee, *Chem. Commun.* **1999**, 639–640.
- [91] X. M. Liu, J. A. McAllister, M. P. de Miranda, B. J. Whitaker, C. A. Kilner, M. Thornton-Pett, M. A. Halcrow, *Angew. Chem. Int. Ed.* **2002**, 41, 756–758.
- [92] X. M. Liu, J. A. McAllister, M. P. de Miranda, E. J. L. McInnes, C. A. Kilner, M. A. Halcrow, *Chem. Eur. J.* **2004**, 10, 1827–1837.
- [93] X. M. Liu, A. C. McLaughlin, M. P. de Miranda, E. J. L. McInnes, C. A. Kilner, M. A. Halcrow, *Chem. Commun.* **2002**, 2978–2979.
- [94] L. Merz, W. Haase, *J. Chem. Soc., Dalton Trans.* **1980**, 875–879.
- [95] R. G. Raptis, I. P. Georgakaki, D. C. R. Hockless, *Angew. Chem. Int. Ed.* **1999**, 38, 1632–1634.
- [96] P. Baran, R. Boča, I. Chakraborty, J. Giapintzakis, R. Herchel, Q. Huang, J. E. McGrady, R. G. Raptis, Y. Sanakis, A. Simopoulos, *Inorg. Chem.* **2008**, 47, 645–655.
- [97] M. V. Capparelli, P. Hodge, B. Piggott, *Chem. Commun.* **1997**, 937–938.

- [98] M. K. Ehlert, S. J. Rettig, A. Storr, R. C. Thompson, J. Trotter, *Inorg. Chem.* **1993**, 32, 5176–5182.
- [99] H. Z. Wu, H. X. Li, M. L. Cheng, W. H. Zhang, Y. Zhang, H. P. Lang, *Inorg. Chem. Commun.* **2008**, 11, 8–10.
- [100] J. Y. Xu, X. Qiao, H. B. Song, S. P. Yan, D. Z. Liao, S. Gao, Y. Journaux, J. Cano, *Chem. Commun.* **2008**, 6414–6416.
- [101] V. Chandrasekhar, P. Sasikumar, R. Boomishankar, *Dalton Trans.* **2008**, 5189–5196.
- [102] V. Chandrasekhar, S. Kingsley, *Angew. Chem. Int. Ed.* **2000**, 39, 2320–2322.
- [103] V. Chandrasekhar, L. Nagarajan, *Dalton Trans.* **2009**, 6712–6714.
- [104] V. Chandrasekhar, L. Nagarajan, R. Clerac, S. Ghosh, T. Senapati, S. Verma, *Inorg. Chem.* **2008**, 47, 5347–5354.
- [105] V. Chandrasekhar, L. Nagarajan, R. Clerac, S. Ghosh, S. Verma, *Inorg. Chem.* **2008**, 47, 1067–1073.
- [106] P. E. Kruger, B. Moubaraki, G. D. Fallon, K. S. Murray, *J. Chem. Soc., Dalton Trans.* **2000**, 713–718.
- [107] J. He, Y. G. Yin, T. Wu, D. Li, X. C. Huang, *Chem. Commun.* **2006**, 2845–2847.
- [108] S. Y. Yu, H. P. Huang, S. H. Li, Q. Jiao, Y. Z. Li, B. Wu, Y. Sei, K. Yamaguchi, Y. J. Pan, H. W. Ma, *Inorg. Chem.* **2005**, 44, 9471–9488.
- [109] J. P. Zhang, S. Horike, S. Kitagawa, *Angew. Chem. Int. Ed.* **2007**, 46, 889–892.
- [110] J. P. Zhang, S. Kitagawa, *J. Am. Chem. Soc.* **2008**, 130, 907–917.
- [111] J. Ackermann, F. Meyer, H. Pritzkow, *Z. Anorg. Allg. Chem.* **2004**, 630, 2627–2631.
- [112] B. Bauer-Siebenlist, S. Dechert, F. Meyer, *Chem. Eur. J.* **2005**, 11, 5343–5352.
- [113] B. Bauer-Siebenlist, F. Meyer, E. Farkas, D. Vidovic, J. A. Cuesta-Seijo, R. Herbst-Irmer, H. Pritzkow, *Inorg. Chem.* **2004**, 43, 4189–4202.
- [114] B. Bauer-Siebenlist, F. Meyer, D. Vidovic, H. Pritzkow, *Z. Anorg. Allg. Chem.* **2003**, 629, 2152–2156.
- [115] S. Demeshko, G. Leibel, S. Dechert, S. Fuchs, T. Pruschke, F. Meyer, *ChemPhysChem* **2007**, 8, 405–417.
- [116] S. Demeshko, G. Leibel, S. Dechert, F. Meyer, *Dalton Trans.* **2006**, 3458–3465.
- [117] S. Demeshko, G. Leibel, W. Maringgele, F. Meyer, C. Mennrich, H. H. Klauss, H. Pritzkow, *Inorg. Chem.* **2005**, 44, 519–528.
- [118] G. Leibel, S. Demeshko, B. Bauer-Siebenlist, F. Meyer, H. Pritzkow, *Eur. J. Inorg. Chem.* **2004**, 2413–2420.
- [119] F. Meyer, S. Demeshko, G. Leibel, B. Kersting, E. Kaifer, H. Pritzkow, *Chem. Eur. J.* **2005**, 11, 1518–1526.
- [120] F. Meyer, P. Kircher, H. Pritzkow, *Chem. Commun.* **2003**, 774–775.
- [121] F. Meyer, M. Konrad, E. Kaifer, *Eur. J. Inorg. Chem.* **1999**, 1851–1854.
- [122] F. Meyer, H. Pritzkow, *Angew. Chem. Int. Ed.* **2000**, 39, 2112–2115.
- [123] F. Meyer, U. Ruschewitz, P. Schober, B. Antelmann, L. Zsolnai, *J. Chem. Soc., Dalton Trans.* **1998**, 1181–1186.
- [124] F. Meyer, R. F. Winter, E. Kaifer, *Inorg. Chem.* **2001**, 40, 4597–4603.
- [125] A. Prokofieva, A. I. Prikhod'ko, E. A. Enyedy, E. Farkas, W. Maringgele, S. Demeshko, S. Dechert, F. Meyer, *Inorg. Chem.* **2007**, 46, 4298–4307.
- [126] M. Stollenz, C. Gross, F. Meyer, *Chem. Commun.* **2008**, 1744–1746.
- [127] M. Stollenz, M. John, H. Gehring, S. Dechert, C. Grosse, F. Meyer, *Inorg. Chem.* **2009**, 48, 10049–10059.
- [128] A. Prokofieva, S. Dechert, C. Grosse, G. M. Sheldrick, F. Meyer, *Chem. Eur. J.* **2009**, 15, 4994–4997.
- [129] M. Raidt, M. Neuburger, T. A. Kaden, *Dalton Trans.* **2003**, 1292–1298.
- [130] J. Z. Hou, M. Li, Z. Li, S. Z. Zhan, X. C. Huang, D. Li, *Angew. Chem. Int. Ed.* **2008**, 47, 1711–1714.
- [131] K. Yoneda, K. Adachi, K. Nishio, M. Yamasaki, A. Fuyuhiko, M. Katada, S. Kaizaki, S. Kawata, *Angew. Chem. Int. Ed.* **2006**, 45, 5459–5461.
- [132] V. Chandrasekhar, S. Kingsley, A. Vij, K. C. Lam, A. L. Rheingold, *Inorg. Chem.* **2000**, 39, 3238–3242.
- [133] T. L. Hu, J. R. Li, C. S. Liu, X. S. Shi, J. N. Zhou, X. H. Bu, J. Ribas, *Inorg. Chem.* **2006**, 45, 162–173.
- [134] J. C. Jeffery, P. L. Jones, K. L. V. Mann, E. Psillakis, J. A. McCleverty, M. D. Ward, C. M. White, *Chem. Commun.* **1997**, 175–176.
- [135] P. L. Jones, J. C. Jeffery, J. A. McCleverty, M. D. Ward, *Polyhedron* **1997**, 16, 1567–1571.
- [136] K. L. V. Mann, E. Psillakis, J. C. Jeffery, L. H. Rees, N. M. Harden, J. A. McCleverty, M. D. Ward, D. Gatteschi, F. Totti, F. E. Mabbs, E. J. L. McInnes, P. C. Riedi, G. M. Smith, *J. Chem. Soc., Dalton Trans.* **1999**, 339–348.
- [137] J. P. Picart, F. J. Sánchez, J. Casabó, J. Rius, A. Alvarez-Larena, J. Ros, *Inorg. Chem. Commun.* **2002**, 5, 130–133.
- [138] J. Pons, F. J. Sanchez, J. Casabó, A. Alvarez-Larena, J. F. Piniella, J. Ros, *Inorg. Chem. Commun.* **2003**, 6, 833–836.
- [139] K. J. Singh, J. R. Long, P. Stavropoulos, *Inorg. Chem.* **1998**, 37, 1073–1079.
- [140] J. I. van der Vlugt, S. Demeshko, S. Dechert, F. Meyer, *Inorg. Chem.* **2008**, 47, 1576–1585.
- [141] V. Chandrasekhar, L. Nagarajan, K. Gopal, V. Baskar, P. Kogerler, *Dalton Trans.* **2005**, 3143–3145.
- [142] A. K. Singh, J. I. van der Vlugt, S. Demeshko, S. Dechert, F. Meyer, *Eur. J. Inorg. Chem.* **2009**, 3431–3439.
- [143] L. F. Jones, C. A. Kilner, M. A. Halcrow, *Polyhedron* **2007**, 26, 1977–1983.
- [144] V. H. Crawford, H. W. Richardson, J. R. Wasson, D. J. Hodgson, W. E. Hatfield, *Inorg. Chem.* **1976**, 15, 2107–2110.
- [145] Y. Zhou, W. Chen, *Dalton Trans.* **2007**, 5123–5125.
- [146] Y. B. Zhou, W. Z. Chen, D. Q. Wang, *Dalton Trans.* **2008**, 1444–1453.
- [147] T. Shiga, T. Matsumoto, M. Noguchi, T. Onuki, N. Hoshino, G. N. Newton, M. Nakano, H. Oshio, *Chem. Asian J.* **2009**, 4, 1660–1663.
- [148] G. Aromí, A. Bell, S. J. Teat, A. G. Whittaker, R. E. P. Winpenny, *Chem. Commun.* **2002**, 1896–1897.
- [149] A. L. Dearden, S. Parsons, R. E. P. Winpenny, *Angew. Chem. Int. Ed.* **2001**, 40, 151–154.
- [150] G. Aromí, A. R. Bell, M. Helliwell, J. Raftery, S. J. Teat, G. A. Timco, O. Roubeau, R. E. P. Winpenny, *Chem. Eur. J.* **2003**, 9, 3024–3032.
- [151] G. Aromí, O. Roubeau, M. Helliwell, S. J. Teat, R. E. P. Winpenny, *Dalton Trans.* **2003**, 3436–3442.
- [152] G. Aromí, A. Bell, S. J. Teat, R. E. P. Winpenny, *Chem. Commun.* **2005**, 2927–2929.
- [153] A. Bell, G. Aromí, S. J. Teat, W. Wernsdorfer, R. E. P. Winpenny, *Chem. Commun.* **2005**, 2808–2810.
- [154] S. Tanase, G. Aromí, E. Bouwman, H. Kooijman, A. L. Spek, J. Reedijk, *Chem. Commun.* **2005**, 3147–3149.
- [155] M. Viciano-Chumillas, G. de Ruiter, S. Tanase, J. M. M. Smits, R. de Gelder, I. Mutikainen, U. Turpeinen, L. J. de Jongh, J. Reedijk, *Dalton Trans.* **2010**, 39, 4991–4998.
- [156] Y. L. Bai, J. Tao, W. Wernsdorfer, O. Sato, R. B. Huang, L. S. Zheng, *J. Am. Chem. Soc.* **2006**, 128, 16428–16429.
- [157] C. M. Liu, D. Q. Zhang, D. B. Zhu, *Chem. Commun.* **2008**, 368–370.
- [158] C. M. Liu, D. Q. Zhang, D. B. Zhu, *Inorg. Chem.* **2009**, 48, 4980–4987.
- [159] J. Tao, Y. Z. Zhang, Y. L. Bai, O. Sato, *Inorg. Chem.* **2006**, 45, 4877–4879.
- [160] M. Viciano-Chumillas, S. Tanase, I. Mutikainen, M. Turpeinen, L. J. de Jongh, J. Reedijk, *Inorg. Chem.* **2008**, 47, 5919–5929.
- [161] M. Viciano-Chumillas, S. Tanase, I. Mutikainen, U. Turpeinen, L. J. de Jongh, J. Reedijk, *Dalton Trans.* **2009**, 7445–7453.

- [162] M. Viciano-Chumillas, S. Tanase, O. Roubeau, S. J. Teat, L. J. de Jongh, J. Reedijk, *Eur. J. Inorg. Chem.* **2010**, 947–951.
- [163] M. Viciano-Chumillas, M. Marqués-Giménez, S. Tanase, I. Mutikainen, M. Turpeinen, J. M. M. Smits, R. de Gelder, L. J. de Jongh, J. Reedijk, unpublished results.
- [164] G. Aromí, E. Bouwman, E. Burzuri, C. Carbonera, J. Krzyszek, F. Luis, C. Schlegel, J. van Slageren, S. Tanase, S. J. Teat, *Chem. Eur. J.* **2008**, *14*, 11158–11166.
- [165] Y.-L. Bai, V. Tangoulis, R. B. Huang, L.-S. Zheng, J. Tao, *Chem. Eur. J.* **2009**, *15*, 2377–2383.
- [166] L. A. Barrios, G. Aromí, J. Ribas, J. S. Uber, O. Roubeau, K. Sakai, S. Masaoka, P. Gamez, J. Reedijk, *Eur. J. Inorg. Chem.* **2008**, 3871–3876.
- [167] P. King, R. Clerac, C. E. Anson, C. Coulon, A. K. Powell, *Inorg. Chem.* **2003**, *42*, 3492–3500.
- [168] P. King, R. Clerac, C. E. Anson, A. K. Powell, *Dalton Trans.* **2004**, 852–861.
- [169] Y. H. Xing, G. H. Zhou, Y. An, X. Q. Zeng, M. F. Ge, *Synth. React. Inorg. Met.-Org. Nano-Metal Chem.* **2008**, *38*, 514–517.
- [170] J. Zhao, L. S. Long, R. B. Huang, L. S. Zheng, *Dalton Trans.* **2008**, 4714–4716.
- [171] Y. Wang, Y. Song, Z. R. Pan, Y. Z. Shen, Z. Hu, Z. J. Guo, H. G. Zheng, *Dalton Trans.* **2008**, 5588–5592.
- [172] X. H. Zhou, Y. H. Peng, X. D. Du, C. F. Wang, J. L. Zuo, X. Z. You, *Cryst. Growth Des.* **2009**, *9*, 1028–1035.
- [173] X. Feng, L.-Y. Wang, J.-S. Zhao, B. Liu, J.-G. Wang, X.-G. Shi, *Inorg. Chim. Acta* **2009**, *362*, 5127–5132.
- [174] W. L. Driessen, L. Chang, C. Finazzo, S. Gorter, D. Rehorst, J. Reedijk, M. Lutz, A. L. Spek, *Inorg. Chim. Acta* **2003**, *350*, 25–31.
- [175] M. Angaroni, G. A. Ardizzoia, G. La Monica, E. M. Beccalli, N. Masciocchi, M. Moret, *J. Chem. Soc., Dalton Trans.* **1992**, 2715–2721.
- [176] H. Zhang, D. G. Fu, F. Ji, G. X. Wang, K. B. Yu, T. Y. Yao, *J. Chem. Soc., Dalton Trans.* **1996**, 3799–3803.
- [177] J. Klingele, A. I. Prikhod'ko, G. Leibel, S. Demeshko, S. Dechert, F. Meyer, *Dalton Trans.* **2007**, 2003–2013.
- [178] L. Kovbasyuk, H. Pritzkow, R. Kramer, I. O. Fritsky, *Chem. Commun.* **2004**, 880–881.
- [179] R. Kramer, I. O. Fritsky, H. Pritzkow, L. A. Kovbasyuk, *J. Chem. Soc., Dalton Trans.* **2002**, 1307–1314.
- [180] G. Noël, J. C. Röder, S. Dechert, H. Pritzkow, L. Bolk, S. Mecking, F. Meyer, *Adv. Synth. Catal.* **2006**, *348*, 887–897.
- [181] J. C. Röder, F. Meyer, H. Pritzkow, *Chem. Commun.* **2001**, 2176–2177.
- [182] A. Sachse, G. Noël, S. Dechert, S. Demeshko, A. Honecker, A. Alfonsov, V. Kataev, F. Meyer, *Eur. J. Inorg. Chem.* **2008**, 5390–5396.
- [183] A. Sachse, S. Demeshko, F. Meyer, *Dalton Trans.* **2009**, 7756–7764.
- [184] K. Shindo, Y. Mori, K. Motoda, H. Sakiyama, N. Matsumoto, H. Okawa, *Inorg. Chem.* **1992**, *31*, 4987–4990.
- [185] U. J. Scheele, M. Georgiou, M. John, S. Dechert, F. Meyer, *Organometallics* **2008**, *27*, 5146–5151.
- [186] M. Konrad, S. Wuthe, F. Meyer, E. Kaifer, *Eur. J. Inorg. Chem.* **2001**, 2233–2240.
- [187] L. Penkova, S. Demeshko, M. Haukka, V. A. Pavlenko, F. Meyer, I. O. Fritsky, *Z. Anorg. Allg. Chem.* **2008**, *634*, 2428–2436.
- [188] S. Roy, T. N. Mandal, A. K. Barik, S. Pal, R. J. Butcher, M. S. El Fallah, J. Tercero, S. K. Kar, *Dalton Trans.* **2007**, 1229–1234.
- [189] S. Roy, T. N. Mandal, A. K. Barik, S. Gupta, M. S. El Fallah, J. Tercero, R. J. Butcher, S. K. Kar, *Dalton Trans.* **2009**, 8215–8226.
- [190] K. V. Shuvaev, T. S. M. Abedin, C. A. McClary, L. N. Dawe, J. L. Collins, L. K. Thompson, *Dalton Trans.* **2009**, 2926–2939.
- [191] S. Pal, A. K. Barik, S. Gupta, A. Hazra, S. K. Kar, S. M. Peng, G. H. Lee, R. J. Butcher, M. S. El Fallah, J. Ribas, *Inorg. Chem.* **2005**, *44*, 3880–3889.
- [192] P. A. Gale, *Coord. Chem. Rev.* **2000**, *199*, 181–233.
- [193] F. P. Schmidtchen, M. Berger, *Chem. Rev.* **1997**, *97*, 1609–1646.
- [194] V. L. Pecoraro, A. J. Stemmler, B. R. Gibney, J. J. Bodwin, H. Wang, J. W. Kampf, A. Barwinski, *Prog. Inorg. Chem.* **1997**, *45*, 83–177.
- [195] J. M. Lehn, *Angew. Chem. Int. Ed. Engl.* **1988**, *27*, 89–112.
- [196] F. Escartí, C. Miranda, L. Lamarque, J. Latorre, E. García-España, M. Kumar, V. J. Arán, P. Navarro, *Chem. Commun.* **2002**, 936–937.
- [197] G. Mezei, P. Baran, R. G. Raptis, *Angew. Chem. Int. Ed.* **2004**, *43*, 574–577.
- [198] A. A. Mohamed, A. Burini, R. Galassi, D. Paglialunga, J. R. Galán-Mascarós, K. R. Dunbar, J. P. Fackler, *Inorg. Chem.* **2007**, *46*, 2348–2349.
- [199] D. T. Puerta, S. M. Cohen, *Chem. Commun.* **2003**, 1278–1279.
- [200] L. F. Jones, S. A. Barrett, C. A. Kilner, M. A. Halcrow, *Chem. Eur. J.* **2008**, *14*, 223–233.
- [201] L. F. Jones, C. A. Kilner, M. P. De Miranda, J. Wolowska, M. A. Halcrow, *Angew. Chem. Int. Ed.* **2007**, *46*, 4073–4076.
- [202] L. F. Jones, C. A. Kilner, M. A. Halcrow, *Chem. Eur. J.* **2009**, *15*, 4667–4675.
- [203] M. Albrecht, *Chem. Rev.* **2001**, *101*, 3457–3497.
- [204] C. Piguet, G. Bernardinelli, G. Hopfgartner, *Chem. Rev.* **1997**, *97*, 2005–2062.
- [205] M. H. W. Lam, S. T. C. Cheung, K. M. Fung, W. T. Wong, *Inorg. Chem.* **1997**, *36*, 4618–4619.

Received: April 14, 2010

Published Online: July 5, 2010

After publication in Early View, the address of one of the affiliations has been changed.



# Synthesis and Physicochemical Properties of Bis(fluoroalkanesulfon)amide-Based Ionic Liquids

Cheng-Pan Zhang,<sup>[a]</sup> Zong-Ling Wang,<sup>[a,b]</sup> Qing-Yun Chen,<sup>[a]</sup> Chun-Tao Zhang,<sup>[b]</sup> Yu-Cheng Gu,<sup>[c]</sup> and Ji-Chang Xiao<sup>\*[a]</sup>

**Keywords:** Ionic liquids / Fluorine / Anions / Bis(fluoroalkanesulfon)amides / Physicochemical properties

A series of bis(fluoroalkanesulfon)amides were synthesized in good yield from the reaction of fluoroalkanesulfonamides and fluoroalkylsulfonyl fluorides. Ionic liquids based

on these amide anions and an imidazolium cation demonstrated high densities and a wide temperature range for the liquid state.

## Introduction

Ionic liquids have attracted significant attention in recent years.<sup>[1]</sup> Due to their favorable properties such as high ionic mobility, negligible vapor pressure, wide electrochemical window, good thermal stability, and high conductivity, numerous ionic liquids have been synthesized and used as solvents for electrochemistry, biochemistry, polymer chemistry, organic synthesis, and catalytic process as well as separation science.<sup>[1,2]</sup> Reactions conducted in ionic liquids often show improved reactivity and selectivity.<sup>[2]</sup> In addition, ionic liquids could be used as high-performance lubricants.<sup>[3]</sup> Thus, much attention has been paid to the application of ionic liquids in tribology. Ionic liquid crystals are new liquid-crystalline compounds,<sup>[4]</sup> which are considered to be novel materials not only displaying lamellar mesophases but also exhibiting nematic columnar phases. Studies on liquid-crystalline ionic liquids have shown that the choice of the anion has a strong influence on the mesophase behavior.<sup>[4]</sup> Piperidinium, piperazinium, and morpholinium cations combined with different types of anions exhibit rich mesomorphic behavior.<sup>[5]</sup> Indeed, besides liquid-crystalline behavior, the physicochemical properties of ionic liquids are much influenced by the type of anion. For example, ionic liquids containing the bis(trifluoromethanesulfon)amide anion are very hydrophobic. A high charge/discharge capacity and a wide operating temperature range could be obtained for lithium batteries by employing bis(fluoroalkanesulfon)amide-based ionic liquids as electrolytes.<sup>[6]</sup>

Thus, it is inferred that bis(fluoroalkanesulfon)amides might be the suitable anion to endow ionic liquids with useful properties. However, only a few bis(fluoroalkanesulfon)amides have been reported so far.<sup>[7]</sup> To expand the research on amide-type ionic liquids, we explored the preparation of bis(fluoroalkanesulfon)amides and investigated the synthesis and physicochemical properties of these amide-based ionic liquids.

## Results and Discussion

As shown in Table 1, treatment of fluoroalkanesulfonamide with the corresponding fluoroalkylsulfonyl fluoride gave the symmetrically substituted amide (entries 1–5). Triethylamine was used as the solvent as well as the catalyst and reagent for the reaction. Hydrodeiodination inevitably happened under these basic conditions,<sup>[8]</sup> affording the corresponding hydrogenolysis amide (entries 2–4). A longer reaction time was needed with elongation of the fluoroalkyl chain. The reaction of fluoroalkanesulfonamides with different chain length and fluoroalkylsulfonyl fluoride resulted in the formation of asymmetrically substituted amides (entries 6–8). Diamides **1i–1k** were readily obtained from the reaction of the disulfonyl fluorides with trifluoromethanesulfonamide (entries 9–11). Bis(fluoroalkanesulfon)amide salts **5** with short alkyl chain are slightly soluble in water, which leads to the loss of the salts while being washed with water during workup (entries 7–9). However, washing with water is necessary for complete removal of water-soluble fluorides and iodides. Otherwise, large amounts of HF and I<sub>2</sub> would be generated during the acidification stage, making further purification difficult. For those amides with high boiling point and high fluorine content, extraction with F113 (CF<sub>2</sub>ClCFCl<sub>2</sub>) became a relatively efficient procedure for the isolation of the final product (entries 4–5, 11).

[a] Key Laboratory of Organofluorine Chemistry, Shanghai Institute of Organic Chemistry, Chinese Academy of Sciences, 345 Lingling Road, Shanghai 200032, China  
Fax: +86-21-64166128  
E-mail: jchxiao@mail.sioc.ac.cn

[b] Hunan University of Chinese Medicine, Changsha, Hunan Province 410208, China

[c] Syngenta, Jealott's Hill International Research Centre, Bracknell, Berkshire, RG42 6EY, UK

Supporting information for this article is available on the WWW under <http://dx.doi.org/10.1002/ejic.201000171>.



Table 1. Preparation of symmetric and asymmetric amides.

$$\text{Rf}^1\text{SO}_2\text{NH}_2 + \text{Rf}^2\text{SO}_2\text{F} \xrightarrow[\text{reflux}]{\text{NEt}_3} \left[ \begin{array}{c} \text{Rf}^3\text{SO}_2\text{N}(\text{HNEt}_3)\text{SO}_2\text{Rf}^4 \\ \text{or} \\ \text{Rf}^3\text{SO}_2\text{NH}(\text{HNEt}_3)\text{SO}_2\text{Rf}^4\text{SO}_2\text{NH}(\text{HNEt}_3)\text{SO}_2\text{Rf}^3 \end{array} \right] \xrightarrow{\text{H}_2\text{SO}_4} \begin{array}{c} \text{Rf}^3\text{SO}_2\text{NHSO}_2\text{Rf}^4 \text{ (1a-h)} \\ \text{or} \\ \text{Rf}^3\text{SO}_2\text{NHSO}_2\text{Rf}^4\text{SO}_2\text{NHSO}_2\text{Rf}^3 \text{ (1i-k)} \end{array}$$

5

Entry	Rf <sup>1</sup> [a]	Rf <sup>2</sup> SO <sub>2</sub> F	Time (h)	Rf <sup>3</sup> SO <sub>2</sub> NHSO <sub>2</sub> Rf <sup>4</sup> or Rf <sup>3</sup> SO <sub>2</sub> NHSO <sub>2</sub> Rf <sup>4</sup> SO <sub>2</sub> NHSO <sub>2</sub> Rf <sup>3</sup>	Yield (%) <sup>[b]</sup>
1	Cl(CF <sub>2</sub> ) <sub>2</sub>	Cl(CF <sub>2</sub> ) <sub>2</sub> SO <sub>2</sub> F	12	[Cl(CF <sub>2</sub> ) <sub>2</sub> SO <sub>2</sub> ] <sub>2</sub> NH (1a)	81
2	I(CF <sub>2</sub> ) <sub>2</sub> O(CF <sub>2</sub> ) <sub>2</sub>	I(CF <sub>2</sub> ) <sub>2</sub> O(CF <sub>2</sub> ) <sub>2</sub> SO <sub>2</sub> F	29	[H(CF <sub>2</sub> ) <sub>2</sub> O(CF <sub>2</sub> ) <sub>2</sub> SO <sub>2</sub> ] <sub>2</sub> NH (1b)	86
3	I(CF <sub>2</sub> ) <sub>4</sub> O(CF <sub>2</sub> ) <sub>2</sub>	I(CF <sub>2</sub> ) <sub>4</sub> O(CF <sub>2</sub> ) <sub>2</sub> SO <sub>2</sub> F	36	[H(CF <sub>2</sub> ) <sub>4</sub> O(CF <sub>2</sub> ) <sub>2</sub> SO <sub>2</sub> ] <sub>2</sub> NH (1c)	82
4 <sup>[c]</sup>	I(CF <sub>2</sub> ) <sub>6</sub> O(CF <sub>2</sub> ) <sub>2</sub>	I(CF <sub>2</sub> ) <sub>6</sub> O(CF <sub>2</sub> ) <sub>2</sub> SO <sub>2</sub> F	60	[H(CF <sub>2</sub> ) <sub>6</sub> O(CF <sub>2</sub> ) <sub>2</sub> SO <sub>2</sub> ] <sub>2</sub> NH (1d)	41
5 <sup>[c]</sup>	Cl(CF <sub>2</sub> ) <sub>6</sub> O(CF <sub>2</sub> ) <sub>2</sub>	Cl(CF <sub>2</sub> ) <sub>6</sub> O(CF <sub>2</sub> ) <sub>2</sub> SO <sub>2</sub> F	50	[Cl(CF <sub>2</sub> ) <sub>6</sub> O(CF <sub>2</sub> ) <sub>2</sub> SO <sub>2</sub> ] <sub>2</sub> NH (1e)	46
6	CF <sub>3</sub> (CF <sub>2</sub> ) <sub>3</sub>	I(CF <sub>2</sub> ) <sub>2</sub> O(CF <sub>2</sub> ) <sub>2</sub> SO <sub>2</sub> F	42	CF <sub>3</sub> (CF <sub>2</sub> ) <sub>3</sub> SO <sub>2</sub> NHSO <sub>2</sub> (CF <sub>2</sub> ) <sub>2</sub> O(CF <sub>2</sub> ) <sub>2</sub> H (1f)	88
7	Cl(CF <sub>2</sub> ) <sub>2</sub>	I(CF <sub>2</sub> ) <sub>2</sub> O(CF <sub>2</sub> ) <sub>2</sub> SO <sub>2</sub> F	29	Cl(CF <sub>2</sub> ) <sub>2</sub> SO <sub>2</sub> NHSO <sub>2</sub> (CF <sub>2</sub> ) <sub>2</sub> O(CF <sub>2</sub> ) <sub>2</sub> H (1g)	70
8	CF <sub>3</sub>	I(CF <sub>2</sub> ) <sub>2</sub> O(CF <sub>2</sub> ) <sub>2</sub> SO <sub>2</sub> F	37	CF <sub>3</sub> SO <sub>2</sub> NHSO <sub>2</sub> (CF <sub>2</sub> ) <sub>2</sub> O(CF <sub>2</sub> ) <sub>2</sub> H (1h)	69
9	CF <sub>3</sub>	FSO <sub>2</sub> (CF <sub>2</sub> ) <sub>2</sub> O(CF <sub>2</sub> ) <sub>2</sub> SO <sub>2</sub> F	27	CF <sub>3</sub> SO <sub>2</sub> NHSO <sub>2</sub> (CF <sub>2</sub> ) <sub>2</sub> O(CF <sub>2</sub> ) <sub>2</sub> SO <sub>2</sub> NHSO <sub>2</sub> CF <sub>3</sub> (1i)	64
10	CF <sub>3</sub>	FSO <sub>2</sub> (CF <sub>2</sub> ) <sub>2</sub> O(CF <sub>2</sub> ) <sub>4</sub> O(CF <sub>2</sub> ) <sub>2</sub> SO <sub>2</sub> F	43	CF <sub>3</sub> SO <sub>2</sub> NHSO <sub>2</sub> (CF <sub>2</sub> ) <sub>2</sub> O(CF <sub>2</sub> ) <sub>4</sub> O(CF <sub>2</sub> ) <sub>2</sub> SO <sub>2</sub> NHSO <sub>2</sub> CF <sub>3</sub> (1j)	94
11 <sup>[c]</sup>	CF <sub>3</sub>	FSO <sub>2</sub> (CF <sub>2</sub> ) <sub>2</sub> O(CF <sub>2</sub> ) <sub>8</sub> O(CF <sub>2</sub> ) <sub>2</sub> SO <sub>2</sub> F	48	CF <sub>3</sub> SO <sub>2</sub> NHSO <sub>2</sub> (CF <sub>2</sub> ) <sub>2</sub> O(CF <sub>2</sub> ) <sub>8</sub> O(CF <sub>2</sub> ) <sub>2</sub> SO <sub>2</sub> NHSO <sub>2</sub> CF <sub>3</sub> (1k)	66

[a] Rf<sup>1</sup>SO<sub>2</sub>NH<sub>2</sub> were synthesized according to our previous work.<sup>[9]</sup> [b] Isolated yield. [c] Purified by column chromatography.

Reaction of these bis(fluoroalkanesulfon)amides with NaOH in methanol could convert them into the corresponding sodium salts (Table 2). Subsequent anion exchange reaction with imidazolium iodides afforded the room-temperature ionic liquids **4a–n** in good yields. It was found that the ionic liquids, even sodium salts **2a–i**, were soluble in a variety of organic solvents, thus making the purification simple and efficient. The good solubility might result from the coexistence of the long lipophilic fluoroalkyl chain and the hydrophilic amide group. However, the ionic liquids with short fluoroalkyl chain became slightly soluble in water, leading to their inevitable loss during workup. Therefore, the yield of **4a** and **4k** was relatively lower as compared with other ionic liquids (entries 1, 11).

Densities and thermal properties are given in Table 3. All of these ionic liquids exhibited higher density than the commonly used ones, which might be the result of the increase

in fluorine content. For instance, with *N,N*-dimethylimidazolium as the cation, elongation of the fluoroalkyl chain would increase the density (entries 2, 6, and 7, entries 8 and 10, entries 11 and 13), which is much higher than that observed with bis(trifluoromethanesulfon)amide as the anion.<sup>[10]</sup> On the other hand, the variation of the density showed a trend similar to that in common ionic liquids (entries 2–5, entries 11 and 12, entries 13 and 14). For example, with [H(CF<sub>2</sub>)<sub>2</sub>O(CF<sub>2</sub>)<sub>2</sub>SO<sub>2</sub>]<sub>2</sub>N<sup>−</sup> as the anion, changing the alkyl group from methyl (in **4b**) to butyl (in **4e**) caused the density to decrease from 1.82 to 1.68 g/cm<sup>3</sup> (entries 2–5). Another important feature of these ionic liquids is their low glass transition temperature and good thermal stability. *N,N*-dimethylimidazolium-based ionic liquids are usually solid at ambient temperature even when bis(trifluoromethanesulfon)amide is used as the anion. However, all of ionic liquids **4a–n** are liquid at room temperature, showing

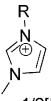
Table 2. Synthesis of ionic liquids.

$$\begin{array}{c} \text{Rf}^3\text{SO}_2\text{NHSO}_2\text{Rf}^4 \text{ (1a-d, 1f-h)} \\ \text{or} \\ \text{Rf}^3\text{SO}_2\text{NHSO}_2\text{Rf}^4\text{SO}_2\text{NHSO}_2\text{Rf}^3 \text{ (1i-k)} \end{array} \xrightarrow[\text{MeOH, r.t.}]{\text{NaOH}} \begin{array}{c} \text{Rf}^3\text{SO}_2\text{NNaSO}_2\text{Rf}^4 \\ \text{or} \\ \text{Rf}^3\text{SO}_2\text{NHSO}_2\text{Rf}^4\text{SO}_2\text{NHSO}_2\text{Rf}^3 \end{array} \xrightarrow[\text{H}_2\text{O, r.t.}]{\text{Imidazolium salt (3a-d)}} \begin{array}{c} \text{Rf}^3\text{SO}_2\text{NHSO}_2\text{Rf}^4 \\ \text{or} \\ 1/2[\text{Rf}^3\text{SO}_2\text{NHSO}_2\text{Rf}^4\text{SO}_2\text{NHSO}_2\text{Rf}^3] \end{array}$$

Entry	Rf <sup>3</sup> SO <sub>2</sub> NNaSO <sub>2</sub> Rf <sup>4</sup> or Rf <sup>3</sup> SO <sub>2</sub> NHSO <sub>2</sub> Rf <sup>4</sup> SO <sub>2</sub> NNaSO <sub>2</sub> Rf <sup>3</sup>	Yield (%) <sup>[a]</sup>	Imidazolium salt (3a-d)	Rf <sup>3</sup> SO <sub>2</sub> NHSO <sub>2</sub> Rf <sup>4</sup> or 1/2[Rf <sup>3</sup> SO <sub>2</sub> NHSO <sub>2</sub> Rf <sup>4</sup> SO <sub>2</sub> NHSO <sub>2</sub> Rf <sup>3</sup> ]	Yield (%) <sup>[a]</sup>
1	[Cl(CF <sub>2</sub> ) <sub>2</sub> SO <sub>2</sub> ] <sub>2</sub> NNa ( <b>2a</b> )	72	R = CH <sub>3</sub> ( <b>3a</b> )	[mmim][Cl(CF <sub>2</sub> ) <sub>2</sub> SO <sub>2</sub> ] <sub>2</sub> N <sup>+</sup> ( <b>4a</b> )	58
2	[H(CF <sub>2</sub> ) <sub>2</sub> O(CF <sub>2</sub> ) <sub>2</sub> SO <sub>2</sub> ] <sub>2</sub> NNa ( <b>2b</b> )		R = CH <sub>3</sub> ( <b>3a</b> )	[mmim][H(CF <sub>2</sub> ) <sub>2</sub> O(CF <sub>2</sub> ) <sub>2</sub> SO <sub>2</sub> ] <sub>2</sub> N <sup>+</sup> ( <b>4b</b> )	87
3	[H(CF <sub>2</sub> ) <sub>4</sub> O(CF <sub>2</sub> ) <sub>2</sub> SO <sub>2</sub> ] <sub>2</sub> NNa ( <b>2b</b> )	93	R = C <sub>2</sub> H <sub>5</sub> ( <b>3b</b> )	[emim][H(CF <sub>2</sub> ) <sub>4</sub> O(CF <sub>2</sub> ) <sub>2</sub> SO <sub>2</sub> ] <sub>2</sub> N <sup>+</sup> ( <b>4c</b> )	91
4	[H(CF <sub>2</sub> ) <sub>2</sub> O(CF <sub>2</sub> ) <sub>2</sub> SO <sub>2</sub> ] <sub>2</sub> NNa ( <b>2b</b> )		R = <i>n</i> -C <sub>3</sub> H <sub>7</sub> ( <b>3c</b> )	[pmim][H(CF <sub>2</sub> ) <sub>2</sub> O(CF <sub>2</sub> ) <sub>2</sub> SO <sub>2</sub> ] <sub>2</sub> N <sup>+</sup> ( <b>4d</b> )	87
5	[H(CF <sub>2</sub> ) <sub>2</sub> O(CF <sub>2</sub> ) <sub>2</sub> SO <sub>2</sub> ] <sub>2</sub> NNa ( <b>2b</b> )		R = <i>n</i> -C <sub>4</sub> H <sub>9</sub> ( <b>3d</b> )	[bmim][H(CF <sub>2</sub> ) <sub>2</sub> O(CF <sub>2</sub> ) <sub>2</sub> SO <sub>2</sub> ] <sub>2</sub> N <sup>+</sup> ( <b>4e</b> )	91
6	[H(CF <sub>2</sub> ) <sub>4</sub> O(CF <sub>2</sub> ) <sub>2</sub> SO <sub>2</sub> ] <sub>2</sub> NNa ( <b>2c</b> )	73	R = CH <sub>3</sub> ( <b>3a</b> )	[mmim][H(CF <sub>2</sub> ) <sub>4</sub> O(CF <sub>2</sub> ) <sub>2</sub> SO <sub>2</sub> ] <sub>2</sub> N <sup>+</sup> ( <b>4f</b> )	95
7	[H(CF <sub>2</sub> ) <sub>6</sub> O(CF <sub>2</sub> ) <sub>2</sub> SO <sub>2</sub> ] <sub>2</sub> NNa ( <b>2d</b> )	77	R = CH <sub>3</sub> ( <b>3a</b> )	[mmim][H(CF <sub>2</sub> ) <sub>6</sub> O(CF <sub>2</sub> ) <sub>2</sub> SO <sub>2</sub> ] <sub>2</sub> N <sup>+</sup> ( <b>4g</b> )	89
8	CF <sub>3</sub> (CF <sub>2</sub> ) <sub>3</sub> SO <sub>2</sub> NNaSO <sub>2</sub> (CF <sub>2</sub> ) <sub>2</sub> O(CF <sub>2</sub> ) <sub>2</sub> H ( <b>2e</b> )	75	R = CH <sub>3</sub> ( <b>3a</b> )	[mmim][CF <sub>3</sub> (CF <sub>2</sub> ) <sub>3</sub> SO <sub>2</sub> NNaSO <sub>2</sub> (CF <sub>2</sub> ) <sub>2</sub> O(CF <sub>2</sub> ) <sub>2</sub> H] ( <b>4h</b> )	95
9	Cl(CF <sub>2</sub> ) <sub>2</sub> SO <sub>2</sub> NNaSO <sub>2</sub> (CF <sub>2</sub> ) <sub>2</sub> O(CF <sub>2</sub> ) <sub>2</sub> H ( <b>2f</b> )	87	R = CH <sub>3</sub> ( <b>3a</b> )	[mmim][Cl(CF <sub>2</sub> ) <sub>2</sub> SO <sub>2</sub> NNaSO <sub>2</sub> (CF <sub>2</sub> ) <sub>2</sub> O(CF <sub>2</sub> ) <sub>2</sub> H] ( <b>4i</b> )	71
10	CF <sub>3</sub> SO <sub>2</sub> NNaSO <sub>2</sub> (CF <sub>2</sub> ) <sub>2</sub> O(CF <sub>2</sub> ) <sub>2</sub> H ( <b>2g</b> )	75	R = CH <sub>3</sub> ( <b>3a</b> )	[mmim][CF <sub>3</sub> SO <sub>2</sub> NNaSO <sub>2</sub> (CF <sub>2</sub> ) <sub>2</sub> O(CF <sub>2</sub> ) <sub>2</sub> H] ( <b>4j</b> )	76
11	CF <sub>3</sub> SO <sub>2</sub> NNaSO <sub>2</sub> (CF <sub>2</sub> ) <sub>2</sub> O(CF <sub>2</sub> ) <sub>2</sub> SO <sub>2</sub> NNaSO <sub>2</sub> CF <sub>3</sub> ( <b>2h</b> )		R = CH <sub>3</sub> ( <b>3a</b> )	[mmim] <sub>2</sub> [CF <sub>3</sub> SO <sub>2</sub> NNaSO <sub>2</sub> (CF <sub>2</sub> ) <sub>2</sub> O(CF <sub>2</sub> ) <sub>2</sub> SO <sub>2</sub> NNaSO <sub>2</sub> CF <sub>3</sub> ] ( <b>4k</b> )	51
12	CF <sub>3</sub> SO <sub>2</sub> NNaSO <sub>2</sub> (CF <sub>2</sub> ) <sub>2</sub> O(CF <sub>2</sub> ) <sub>4</sub> O(CF <sub>2</sub> ) <sub>2</sub> SO <sub>2</sub> NNaSO <sub>2</sub> CF <sub>3</sub> ( <b>2i</b> )	85	R = <i>n</i> -C <sub>4</sub> H <sub>9</sub> ( <b>3d</b> )	[bmim] <sub>2</sub> [CF <sub>3</sub> SO <sub>2</sub> NNaSO <sub>2</sub> (CF <sub>2</sub> ) <sub>2</sub> O(CF <sub>2</sub> ) <sub>4</sub> O(CF <sub>2</sub> ) <sub>2</sub> SO <sub>2</sub> NNaSO <sub>2</sub> CF <sub>3</sub> ] ( <b>4l</b> )	72
13	CF <sub>3</sub> SO <sub>2</sub> NNaSO <sub>2</sub> (CF <sub>2</sub> ) <sub>2</sub> O(CF <sub>2</sub> ) <sub>4</sub> O(CF <sub>2</sub> ) <sub>2</sub> SO <sub>2</sub> NNaSO <sub>2</sub> CF <sub>3</sub> ( <b>2i</b> )		R = CH <sub>3</sub> ( <b>3a</b> )	[mmim] <sub>2</sub> [CF <sub>3</sub> SO <sub>2</sub> NNaSO <sub>2</sub> (CF <sub>2</sub> ) <sub>2</sub> O(CF <sub>2</sub> ) <sub>4</sub> O(CF <sub>2</sub> ) <sub>2</sub> SO <sub>2</sub> NNaSO <sub>2</sub> CF <sub>3</sub> ] ( <b>4m</b> )	76
14	CF <sub>3</sub> SO <sub>2</sub> NNaSO <sub>2</sub> (CF <sub>2</sub> ) <sub>2</sub> O(CF <sub>2</sub> ) <sub>8</sub> O(CF <sub>2</sub> ) <sub>2</sub> SO <sub>2</sub> NNaSO <sub>2</sub> CF <sub>3</sub> ( <b>2i</b> )	94	R = <i>n</i> -C <sub>4</sub> H <sub>9</sub> ( <b>3d</b> )	[bmim] <sub>2</sub> [CF <sub>3</sub> SO <sub>2</sub> NNaSO <sub>2</sub> (CF <sub>2</sub> ) <sub>2</sub> O(CF <sub>2</sub> ) <sub>8</sub> O(CF <sub>2</sub> ) <sub>2</sub> SO <sub>2</sub> NNaSO <sub>2</sub> CF <sub>3</sub> ] ( <b>4n</b> )	85

[a] Isolated yield.

Table 3. The properties of bis(fluoroalkanesulfon)amide-based ionic liquids.

Entry	 $\text{R}^3\text{SO}_2\text{NSO}_2\text{R}^4$ or $1/2[\text{R}^3\text{SO}_2\text{NSO}_2\text{R}^4\text{SO}_2\text{NSO}_2\text{R}^3]$	$\rho$ (g cm <sup>-3</sup> ) <sup>[a]</sup>	$T_g$ (°C) <sup>[b]</sup>	$T_d$ (°C) <sup>[c]</sup>	$\mu$ (mm <sup>2</sup> s <sup>-1</sup> ) <sup>[d]</sup>
1	<b>4a</b>	1.89	-103.4	398.9	160.3
2	<b>4b</b>	1.82	-97.6	414.0	164.1
3	<b>4c</b>	1.75	-99.4	393.0	127.1
4	<b>4d</b>	1.73	-97.3	398.0	133.2
5	<b>4e</b>	1.68	-97.6	393.0	158.4
6	<b>4f</b>	1.92	-86.4	393.1	236.2
7	<b>4g</b>	1.95	-83.2	407.9	465.1
8	<b>4h</b>	1.75	-94.1	402.0	217.9
9	<b>4i</b>	1.85	-101.0	406.1	175.0
10	<b>4j</b>	1.71	-81.9	422.7	70.0
11	<b>4k</b>	1.81	-80.6	444.9	712.5
12	<b>4l</b>	1.66	-86.5	447.5	667.0
13	<b>4m</b>	1.89	-113.8	446.0	1359.7
14	<b>4n</b>	1.71	-71.1	443.3	968.8

[a] Pycnometer, 25 °C. [b] Determined by DSC. DSC data were recorded in the range -150 to 200 °C with a heating rate of 10 °C/min. [c] Determined by TGA.  $T_d$  was  $T_{\text{onset}}$ . [d] Ubbelohde viscosity meter, 25 °C.

a rather low glass transition temperature below -80 °C. Moreover, they are all thermally stable to >390 °C, as determined by thermogravimetric analysis (TGA), demonstrating a wide temperature range for the liquid state. It can be inferred that the bis(fluoroalkanesulfon)amide anions contribute to this peculiar thermal behavior. Moreover, the viscosity of these ionic liquids was influenced by the anions and cations. Elongation of the fluoroalkyl chain in amides increased their viscosity (Table 3, entries 1, 2, 6, and 7, entries 8–10, entries 11 and 13, entries 12 and 14). Changing the alkyl group on the cation from methyl to ethyl, propyl, or butyl resulted in a decrease of the viscosity (entries 2–5, entries 11–12, and entries 13–14).

## Conclusion

A series of bis(fluoroalkanesulfon)amides were synthesized in good yield from the reaction of fluoroalkanesulfonamides and fluoroalkylsulfonyl fluorides. The combination of bis(fluoroalkanesulfon)amide anions with imidazolium cations afforded a variety of novel ionic liquids, which demonstrated high densities from 1.66 to 1.95 g/cm<sup>3</sup> and a wide liquid range. Further investigations on the applications of these ionic liquids in lithium batteries are going on.

## Experimental Section

**General:** Unless otherwise stated, NMR spectra were recorded in deuterated acetone at 300 MHz (<sup>1</sup>H NMR) and 282 MHz (<sup>19</sup>F NMR). All chemical shifts were reported in ppm relative to TMS and CFCl<sub>3</sub> (positive for downfield shifts) as external standards. Analytical pure Et<sub>3</sub>N and MeOH were used without any purification. Fluoroalkanesulfonamides were synthesized according to our previous publication.<sup>[9]</sup> Cl(CF<sub>2</sub>)<sub>2</sub>SO<sub>2</sub>F, FO<sub>2</sub>S(CF<sub>2</sub>)<sub>2</sub>O(CF<sub>2</sub>)<sub>2</sub>SO<sub>2</sub>F, FO<sub>2</sub>S(CF<sub>2</sub>)<sub>2</sub>O(CF<sub>2</sub>)<sub>4</sub>O(CF<sub>2</sub>)<sub>2</sub>SO<sub>2</sub>F, FO<sub>2</sub>S(CF<sub>2</sub>)<sub>2</sub>O(CF<sub>2</sub>)<sub>8</sub>O(CF<sub>2</sub>)<sub>2</sub>SO<sub>2</sub>F, and imidazolium iodides **3a–d** were prepared according to

the literature.<sup>[11]</sup> Other reagents used below were all purchased from commercial sources.

**Typical Procedure for the Preparation of 1a–c, 1f–j:** In a 1000 mL round-bottomed flask, I(CF<sub>2</sub>)<sub>2</sub>O(CF<sub>2</sub>)<sub>2</sub>SO<sub>2</sub>F (180 g, 95%, 0.401 mol) was added to a mixture of I(CF<sub>2</sub>)<sub>2</sub>O(CF<sub>2</sub>)<sub>2</sub>SO<sub>2</sub>NH<sub>2</sub> (155 g, 0.365 mol) and Et<sub>3</sub>N (300 mL) and heated at reflux for 29 h. After cooling, the resulting biphasic system was separated. The lower brown fluorine layer was diluted by CH<sub>2</sub>Cl<sub>2</sub> (700 mL), washed with H<sub>2</sub>O (6 × 400 mL), and dried with anhydrous Na<sub>2</sub>SO<sub>4</sub>. The solvent was evaporated, and the brown residue was dried in vacuo. After being acidified with concentrated H<sub>2</sub>SO<sub>4</sub>, the crude product was obtained by vacuum distillation. Vacuum redistillation afforded pure [H(CF<sub>2</sub>)<sub>2</sub>O(CF<sub>2</sub>)<sub>2</sub>SO<sub>2</sub>]<sub>2</sub>NH (**1b**) (110 °C/60 Pa, 182 g, 0.315 mol, 86%) as a white solid. <sup>1</sup>H NMR:  $\delta$  = 6.51 (tt,  $J$  = 52.1, 3.6 Hz, 2 H) ppm. <sup>19</sup>F NMR:  $\delta$  = -138.7 (d,  $J$  = 52.1 Hz, 4 F), -117.0 (s, 4 F), -89.1 (s, 4 F), -81.1 (t,  $J$  = 12.4 Hz, 4 F) ppm. MS (ESI):  $m/z$  (%) = 575.8 (100) [M - H]<sup>+</sup>. IR (KBr):  $\tilde{\nu}$  = 3580, 1629, 1426, 1333, 1287, 1148, 977, 858, 749, 616, 526 cm<sup>-1</sup>. C<sub>8</sub>H<sub>3</sub>F<sub>16</sub>NO<sub>6</sub>S<sub>2</sub> (577.22): calcd. C 16.65, H 0.52, N 2.43; found C 16.73, H 0.56, N 2.25.

**Typical Procedure for the Preparation of 1d, 1e, and 1k:** Cl(CF<sub>2</sub>)<sub>6</sub>O(CF<sub>2</sub>)<sub>2</sub>SO<sub>2</sub>F (5.87 g, 96%, 10.5 mmol) and Cl(CF<sub>2</sub>)<sub>6</sub>O(CF<sub>2</sub>)<sub>2</sub>SO<sub>2</sub>NH<sub>2</sub> (5.39 g, 10.1 mmol) were mixed in Et<sub>3</sub>N (10 mL). Then the mixture was heated at reflux for 50 h. After removing the upper Et<sub>3</sub>N layer, the lower brown fluorine residue was washed with H<sub>2</sub>O, dried in vacuum, acidified with concentrated H<sub>2</sub>SO<sub>4</sub>, and extracted by F113. The crude product was purified by column chromatography on silica gel by using dichloromethane/acetonitrile (4:1) as the eluent. Pure [Cl(CF<sub>2</sub>)<sub>6</sub>O(CF<sub>2</sub>)<sub>2</sub>SO<sub>2</sub>]<sub>2</sub>NH (**1e**) was obtained as a white solid (4.87 g, 4.66 mmol, 46%). <sup>19</sup>F NMR:  $\delta$  = -125.1 (m, 4 F), -121.7 (m, 4 F), -121.1 (m, 4 F), -120.0 (m, 4 F), -116.7 (s, 4 F), -82.7 (m, 4 F), -80.9 (m, 4 F), -68.5 (t,  $J$  = 12.3 Hz, 4 F) ppm. MS (ESI):  $m/z$  (%) = 1043.7 (100) [M - H]<sup>+</sup>. IR (KBr):  $\tilde{\nu}$  = 3650, 1369, 1342, 1207, 1147, 1099, 1047, 985, 887, 778, 706, 699, 683, 656, 624, 545, 516 cm<sup>-1</sup>. C<sub>16</sub>HCl<sub>2</sub>F<sub>32</sub>NO<sub>6</sub>S<sub>2</sub> (1046.17): calcd. C 18.37, H 0.10, N 1.34; found C 17.99, H <0.3, N 1.57.

**Typical Procedure for the Preparation of 2a–i:** In a 25 mL round-bottomed flask, **1b** (2.33 g, 4.04 mmol) was dissolved in CH<sub>3</sub>OH

(15 mL), and NaOH (0.165 g, 4.12 mmol) was added. The reaction mixture was then stirred at room temperature for several hours. After removing the solvent, the residue was extracted with ethyl ether (3 × 10 mL). The ether layer was evaporated, and the solution was dried in vacuum to give pure  $[\text{H}(\text{CF}_2)_2\text{O}(\text{CF}_2)_2\text{SO}_2]_2\text{NNa}$  (**2b**) as a white solid (2.25 g, 3.75 mmol, 93%).  $^1\text{H}$  NMR ( $\text{D}_2\text{O}$ ):  $\delta$  = 6.33 (tt,  $J$  = 52.1, 3.2 Hz, 2 H) ppm.  $^{19}\text{F}$  NMR ( $\text{D}_2\text{O}$ ):  $\delta$  = −135.8 (dt,  $J$  = 52.1, 4.2 Hz, 4 F), −114.2 (s, 4 F), −85.9 (m, 4 F), −78.7 (t,  $J$  = 12.4 Hz, 4 F) ppm. MS (ESI):  $m/z$  (%) = 575.8 (100)  $[\text{M} - \text{Na}]^-$ . IR (KBr):  $\tilde{\nu}$  = 1371, 1343, 1289, 1187, 1137, 1091, 994, 854, 771, 650, 624, 574, 527  $\text{cm}^{-1}$ .  $\text{C}_8\text{H}_2\text{F}_{16}\text{NNaO}_6\text{S}_2$  (599.20): calcd. C 16.04, H 0.34, N 2.34; found C 16.26, H 0.75, N 2.64.

**Typical Procedure for the Preparation of 4a–n:** Under vigorous stirring, a solution of **3a** (0.802 g, 3.58 mmol) in  $\text{H}_2\text{O}$  (10 mL) was added to a solution of **2e** (2.09 g, 3.47 mmol) in  $\text{H}_2\text{O}$  (10 mL), and the mixture was stirred at room temperature for 8 h. After removing the water layer, the lower phase was collected and washed with water (5 × 20 mL). The pure product **4h** was dried at 80 °C under reduced pressure to afford a light yellow liquid (2.22 g, 3.29 mmol, 95%).  $^1\text{H}$  NMR:  $\delta$  = 8.93 (s, 1 H), 7.67 (d,  $J$  = 1.5 Hz, 2 H), 6.52 (tt,  $J$  = 52.2, 3.6 Hz, 1 H), 4.04 (s, 6 H) ppm.  $^{19}\text{F}$  NMR:  $\delta$  = −139.9 (dt,  $J$  = 52.2, 4.0 Hz, 2 F), −127.2 (m, 2 F), −122.2 (m, 2 F), −118.1 (s, 2 F), −114.4 (t,  $J$  = 13.8 Hz, 2 F), −90.0 (m, 2 F), −82.3 (m, 2 F), −82.2 (m, 3 F) ppm. MS (ESI):  $m/z$  (%) = 97.1 (100)  $[\text{M}]^+$ , 577.8 (100)  $[\text{M}]^-$ . IR (KBr):  $\tilde{\nu}$  = 3166, 3132, 1578, 1425, 1355, 1286, 1177, 1078, 1031, 1009, 981, 874, 856, 748, 696, 649, 624, 591, 520  $\text{cm}^{-1}$ .  $\text{C}_{13}\text{H}_{10}\text{F}_{17}\text{N}_3\text{O}_5\text{S}_2$  (675.34): calcd. C 23.12, H 1.49, N 6.22; found C 22.87, H 1.50, N 6.20.

**Supporting Information** (see footnote on the first page of this article): NMR spectra for compounds **1a–k**, **2a–i**, and **4a–n**.

## Acknowledgments

We thank the Chinese Academy of Sciences (Hundreds of Talents Program), the National Natural Science Foundation (20772147, 20972179), and the Syngenta PhD Studentship Award for financial support.

- [1] a) T. Welton, *Chem. Rev.* **1999**, *99*, 2071–2083; b) J. Dupont, R. F. Souza, P. A. Z. Suarez, *Chem. Rev.* **2002**, *102*, 3667–3692; c) P. Wasserscheid, W. Keim, *Angew. Chem. Int. Ed.* **2000**, *39*, 3772–3789; d) R. Sheldon, *Chem. Commun.* **2001**, 2399–2407.
- [2] a) P. Wasserscheid, T. Welton, *Ionic Liquids in Synthesis*, Wiley-VCH, Weinheim, Germany, **2003**; b) A. Corma, H. Garcia, *Chem. Rev.* **2003**, *103*, 4307–4366; c) W. S. Miao, T. H. Chan,

- Acc. Chem. Res.* **2006**, *39*, 897–908; d) M. Smiglak, A. Metlen, R. Rogers, *Acc. Chem. Res.* **2007**, *40*, 1182–1192; e) R. Sheldon, *Chem. Commun.* **2001**, 2399–2407; f) M. Yoshizawa, A. Narita, H. Ohno, *Aust. J. Chem.* **2004**, *57*, 139–144; g) C. M. Gorden, *Appl. Catal. A* **2001**, *222*, 101–117; h) H. Zhao, S. Q. Xia, P. S. Ma, *J. Chem. Technol. Biotechnol.* **2005**, *80*, 1089–1096.
- [3] a) C. Ye, W. M. Liu, Y. X. Chen, L. G. Yu, *Chem. Commun.* **2001**, 2244–2245; b) F. Zhou, Y. Liang, W. Liu, *Chem. Soc. Rev.* **2009**, *38*, 2590–2599.
- [4] K. Binnemans, *Chem. Rev.* **2005**, *105*, 4148–4204.
- [5] K. Lava, K. Binnemans, T. Cardinaels, *J. Phys. Chem. B* **2009**, *113*, 9506–9511.
- [6] a) H. Sakaebe, H. Matsumoto, *Electrochem. Commun.* **2003**, *5*, 594–598; b) H. Nakagawa, S. Izuchi, K. Kuwana, T. Nukuda, Y. Aihara, *J. Electrochem. Soc.* **2003**, *150*, A695–A700; c) B. Garcia, S. Lavalley, G. Perron, C. Michot, M. Armand, *Electrochim. Acta* **2004**, *49*, 4583–4588; d) A. Guerfi, S. Duchesne, Y. Kobayashi, A. Vijh, K. Zaghib, *J. Power Sources* **2008**, *175*, 866–873; e) H. Matsumoto, H. Sakaebe, K. Tatsumi, M. Kikuta, E. Ishiko, M. Kono, *J. Power Sources* **2006**, *160*, 1308–1313; f) A. Lewandowski, A. Swiderska-Moczek, *J. Power Sources* **2009**, *194*, 601–609; g) T. D. J. Dunstan, J. Caja, US7582380 (B1), **2009**.
- [7] a) J. Foropoulos Jr., D. D. DesMarteau, *Inorg. Chem.* **1984**, *23*, 3720–3723; b) S. Singh, D. D. DesMarteau, *Inorg. Chem.* **1990**, *29*, 2982–2985; c) L.-Q. Hu, D. D. DesMarteau, *Inorg. Chem.* **1993**, *32*, 5007–5010; d) X. Hao, A. Yoshida, J. Nishikido, *J. Fluorine Chem.* **2006**, *127*, 193–199; e) B. H. Thomas, G. Shafer, J.-J. Ma, M.-H. Tu, D. D. DesMarteau, *J. Fluorine Chem.* **2004**, *125*, 1231–1240; f) L. Conte, G. Gambaretto, G. Caporiccio, F. Alessandrini, S. Passerini, *J. Fluorine Chem.* **2004**, *125*, 243–252; g) J. Zhang, D. D. DesMarteau, S. Zuberi, J.-J. Ma, L. Xue, S. M. Gillette, H. Blau, R. Gerhardt, *J. Fluorine Chem.* **2002**, *116*, 45–48.
- [8] C.-P. Zhang, Q.-Y. Chen, J.-C. Xiao, Y.-C. Gu, *J. Fluorine Chem.* **2009**, *130*, 671–673.
- [9] C.-P. Zhang, Z.-L. Wang, Q.-Y. Chen, C.-T. Zhang, Y.-C. Gu, J.-C. Xiao, *J. Fluorine Chem.* **2010**, *131*, 761–766.
- [10] H. Tokuda, S. Tsuzuki, M. Abu Bin Hasan Susan, K. Hayamizu, M. Watanabe, *J. Phys. Chem. B* **2006**, *110*, 19593–19600.
- [11] a) J.-C. Xiao, C.-P. Zhang, C. Yan, Z.-W. Qiang, CN101503382A, **2009**; b) W.-M. Qiu, D. J. Burton, *J. Fluorine Chem.* **1993**, *60*, 93–100; c) J. Zhang, D. D. DesMarteau, S. Zuberi, J.-J. Ma, L.-X. Xue, S. M. Gillette, H. Blau, R. Gerhardt, *J. Fluorine Chem.* **2002**, *116*, 45–48; d) C. Y. Guo, R. L. Kirchmeier, J. M. Shreeve, *J. Am. Chem. Soc.* **1991**, *113*, 9000–9001; e) *Acta Chim. Sin.* **1979**, *37*, 315–324; f) Y. Chu, H. Deng, J.-P. Cheng, *J. Org. Chem.* **2007**, *72*, 7790–7793.

Received: February 11, 2010  
Published Online: June 25, 2010

# Discrete, Base-Free, Cationic Alkaline-Earth Complexes – Access and Catalytic Activity in the Polymerization of Lactide

Yann Sarazin,<sup>\*[a]</sup> Valentin Poirier,<sup>[a]</sup> Thierry Roisnel,<sup>[a]</sup> and Jean-François Carpentier<sup>\*[a]</sup>

**Keywords:** Alkaline earth metals / Cations / Anions / Ring-opening polymerization / Lactides

Well-defined, base free cations of zinc and the alkaline-earth metals (Mg, Ca, Sr, Ba) supported by a multidentate phenolate ligand and stabilized by perfluorinated weakly coordinating counterions are readily available by simple procedures; the solid-state structures of the magnesium and calcium de-

rivatives were elucidated. Upon treatment with an excess of *i*PrOH, these complexes generate highly efficient binary catalytic systems for the immortal ring-opening polymerization of L-lactide, yielding poly(L-lactide)s with controlled architectures and molecular features.

## Introduction

Owing to the increasing interest in polymers from biological sources and catalytic systems to prepare them in an effective and rational fashion,<sup>[1]</sup> the last decade has witnessed the development of neutral discrete initiators (mostly complexes of the lanthanides, aluminum, or zinc stabilized by bulky ligands)<sup>[2]</sup> specifically tailored to promote the controlled ring-opening polymerization (ROP) of cyclic esters. Such enthusiasm can be paralleled with the polymerization of  $\alpha$ -olefins mediated by single-site group IV metallocenes. As it soon became apparent that the catalytically active species generated upon treatment with methylaluminoxane<sup>[3]</sup> consisted of base-free cationic metal species, efforts were devoted to the preparation of ion pairs in which a cationic group IV metal complex was associated to weakly coordinating anions such as  $B(C_6F_5)_4^-$ .<sup>[4]</sup> They eventually met with success, and many such complexes have appeared along the years. A similar trend – yet differently motivated – has recently emerged in the field of ROP, and a handful of well-defined cationic zinc,<sup>[5]</sup> magnesium,<sup>[5b,6]</sup> aluminum,<sup>[7]</sup> or lanthanide<sup>[8]</sup> compounds as alternative catalysts suitable for controlled polymerizations have been disclosed.<sup>[2d,9]</sup>

These examples are, however, strictly limited to metals of small to moderate size, and they do not extend to the larger alkaline-earth (Ae) elements calcium, strontium, and barium. Even though a few of their neutral complexes are now available to catalyze the transformation of small molecules,<sup>[10]</sup> well-defined, base-free cationic derivatives have so

far remained elusive. Such paucity can be attributed to the synthetic difficulties (which increase on going from neutral to cationic species) intrinsically related to the Ae elements: due to the large ionic radii ( $Ca^{2+}$  1.14,  $Sr^{2+}$  1.32,  $Ba^{2+}$  1.49 Å),<sup>[11]</sup> their complexes are usually kinetically labile and readily engage in detrimental equilibria of the Schlenk type. Itoh et al. synthesized Mg–Ba cations supported by macrocycle-containing phenoxy ligands, but the presence of coordinated Lewis bases (solvents, water) makes their use as catalysts or as models for catalytic reactions somewhat ill-advised.<sup>[12]</sup>

As part of studies aimed at developing Ae-based catalysts for the ROP of cyclic esters,<sup>[13]</sup> we report herein the first general procedures for the preparation of phenolate solvent-free Mg–Ba (and Zn) cationic complexes, their solid-state structures, and remarkable catalytic activity for the controlled immortal ROP of lactide (LA).

## Results and Discussion

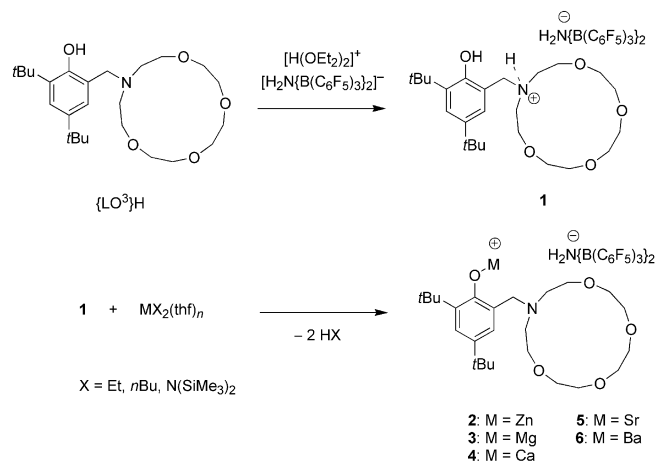
Itoh's proligand, 2-[(1,4,7,10-tetraoxa-13-azacyclopentadecan-13-yl)methyl]-4,6-di-*tert*-butylphenol ( $\{LO^3\}H$ ),<sup>[12]</sup> quantitatively reacts with Bochnann's acid,  $[H(OEt_2)_2]^+ [H_2N\{B(C_6F_5)_3\}_2]^-$ ,<sup>[14]</sup> in  $Et_2O$  to yield the doubly acidic, protonated  $\{LO^3\}H \cdot H^+ [H_2N\{B(C_6F_5)_3\}_2]^-$  (**1**) (Scheme 1), which readily crystallizes from a  $CH_2Cl_2$ /pentane mixture. The choice of the unusual  $[H_2N\{B(C_6F_5)_3\}_2]^-$  as our weakly coordinating counterion over of the more traditional  $[B(C_6F_5)_4]^-$  was motivated by its far better crystallization properties.<sup>[15]</sup>

Double protonolysis of the homoleptic precursors  $[MX_2(thf)_n] \{M = Zn, X = Et, N(SiMe_3)_2, n = 0; M = Mg, X = alkyl, n = 0; M = Ca, Sr, Ba, X = N(SiMe_3)_2, n = 2\}$  with **1** in  $Et_2O$  cleanly afforded the corresponding base-free cationic complexes **2–6** in a single-step procedure with good yields (> 70%). These salts were characterized by NMR

[a] Catalysis and Organometallics, UMR 6226 Sciences Chimiques de Rennes, CNRS – Université de Rennes 1, 35042 Rennes Cedex, France  
Fax: +33-2-23236939  
E-mail: yann.sarazin@univ-rennes1.fr  
jean-francois.carpentier@univ-rennes1.fr

Supporting information for this article is available on the WWW under <http://dx.doi.org/10.1002/ejic.201000558>.





Scheme 1. Synthesis of compounds 1–6.

spectroscopy (1- and 2D) and elemental analysis, which indicated that the coordination sphere around the metal cation was adequately filled by the ligand  $\{\text{LO}^3\}^-$  for all compounds (albeit in a different fashion according to the size of the metal, *vide infra*), and the presence of additional molecules of thf or Et<sub>2</sub>O was not required to yield stable cations. The <sup>19</sup>F NMR spectroscopic data were consistent with the absence of interaction between the cations and their counteranions, and therefore these compounds exist in solution as charge-separated ion pairs. In the <sup>1</sup>H NMR spectra of 1–6 recorded in CD<sub>2</sub>Cl<sub>2</sub>, the signals for the macrocycle show increasing levels of complexity on going from 1 through 2–3 to 4–6 (see the Supporting Information). The spectrum of 1 is essentially characterized by the presence of four sets of multiplets in the region 2.5–4.4 ppm, while seven sets of multiplets are present between 2.8 and 4.4 ppm in the cases of the structurally related 2 and 3. For the larger elements (4–6), several fairly well resolved signals are obtained in the region 2.2–4.6 ppm, some of which could be unambiguously assigned with the aid of 2D NMR spectra.

Compounds 2–6 proved surprisingly stable; no sign of decomposition was detected in their NMR spectra recorded over several hours. Recrystallization of 2–4 from CH<sub>2</sub>Cl<sub>2</sub>/pentane mixtures gave colorless crystals, and their structures were determined by X-ray diffraction methods. The Zn and Mg salts 2 and 3 were also prepared in high yields by protonolysis of the neutral heteroleptic precursors  $[\{\text{LO}^3\}\text{MX}]$  {M = Zn, N(SiMe<sub>3</sub>)<sub>2</sub>, or Et; M = Mg, X = alkyl} with  $[\text{H(OEt}_2\text{)]}^+[\text{H}_2\text{N}\{\text{B(C}_6\text{F}_5\text{)}_3\}_2\text{]}^-$ ; [16] this method was, however, not applicable to the larger elements, as in these cases we could not isolate the heteroleptic neutral precursors. These two procedures were also extended to other phenol-based proligands, for instance, to prepare species of the type  $[\{\text{LO}^x\}\text{H}\cdot\text{H}]^+[\text{H}_2\text{N}\{\text{B(C}_6\text{F}_5\text{)}_3\}_2\text{]}^-$  or  $[\{\text{LO}^x\}\text{M}]^+[\text{H}_2\text{N}\{\text{B(C}_6\text{F}_5\text{)}_3\}_2\text{]}^-$  (M = Zn, Mg, or Ca;  $\{\text{LO}^1\}$  = 4-*tert*-butyl-2,6-bis(morpholinomethyl)phenoxy,  $\{\text{LO}^2\}$  = 2,4-di-*tert*-butyl-6-(morpholinomethyl)phenoxy,  $\{\text{LO}^4\}$  = 2,4-di-*tert*-butyl-6-{[2-(methoxymethyl)pyrrolidin-1-yl]methyl}-phenoxy). [16]

Compounds 2 and 3 are isostructural and crystallize in the space group *P*1̄. A view of the cationic fragment in 3 (3<sup>+</sup>) is displayed in Figure 1. The structure of the counterion  $[\text{H}_2\text{N}\{\text{B(C}_6\text{F}_5\text{)}_3\}_2\text{]}^-$  is similar to that described in the literature with a range of H⋯F inter- and intramolecular stabilizing interactions. [14,15b] There is no contact between the metal center and neighboring fluorine atoms, which is consistent with the solution NMR spectroscopic data. The magnesium atom in 3<sup>+</sup> is thus six-coordinate and adopts a highly distorted trigonal-prismatic geometry. This unusual geometry for Mg is imposed by the tethered, semirigid nature of the multidentate  $\{\text{LO}^3\}^-$  ligand. The Mg–O distances to the macrocycle span the range 2.109(2)–2.222(2) Å and are marginally shorter than those observed in the methanol-containing analogue  $[\{\text{LO}^3\}\text{Mg}\cdot\text{CH}_3\text{OH}]^+[\text{BPh}_4\text{}]^-$ . [12] While the NOOOO core is perfectly planar in the latter compound, the absence of additional Lewis base in 3<sup>+</sup> strongly affects the geometry around the Mg cation, as the macrocycle is folded around the metal, with a dihedral angle of over 82° between the O67–O70–N73 and O61–O64–N73 planes (Figure 1, bottom). The Mg1–O81 distance of 1.900(2) Å to the σ-bonded oxygen atom (phenoxy fragment) in 3<sup>+</sup> is considerably shorter than those to the π-bonded ones (tethered macrocycle).

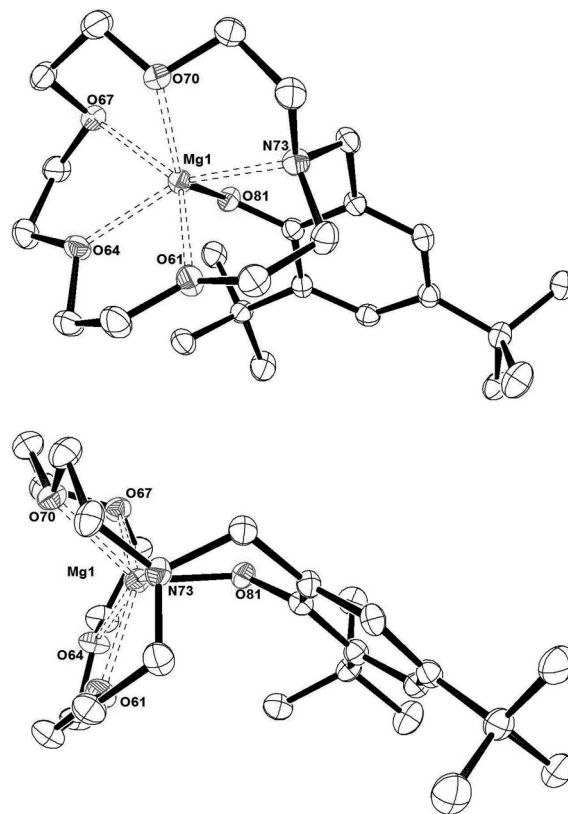


Figure 1. ORTEP diagram of the cationic fragment in 3 (3<sup>+</sup>) (thermal ellipsoids set at the 50% probability level): bottom view (top) and side view (bottom). The counterion and hydrogen atoms are omitted for clarity.

The solid-state structure of calcium derivative **4** shows no close contact between the cationic metal center and its counterion. Cationic fragment **4**<sup>+</sup> consists of a centrosymmetric Ca<sub>2</sub>O<sub>2</sub> bimetallic core, in which the two Ca atoms are bridged by the oxygen atoms of the phenoxy moieties [Ca1–O76 = 2.349(1), Ca1–O76<sup>i</sup> = 2.288(1) Å; Figure 2]. Each Ca atom is seven-coordinate, and the coordination sphere is completed by the N and the four O atoms of the anchored macrocycle. Instead of the expected pentagonal bipyramid, the geometry around the metal adopts a distorted capped trigonal prism arrangement. The distances between Ca and O [2.434(1)–2.541(1) Å] or N [2.551(1) Å]  $\pi$ -donors are comparable to those described for related compounds. Here also, the normally planar geometry of the aza-crown-ether tether is distorted [the angle between planes defined by N61–O70–O73 and N(61)–O(64)–O(67) is 78.25°] owing to its coordination to the large metal center, which does not sit inside the N61–O64–O67–O70–O73

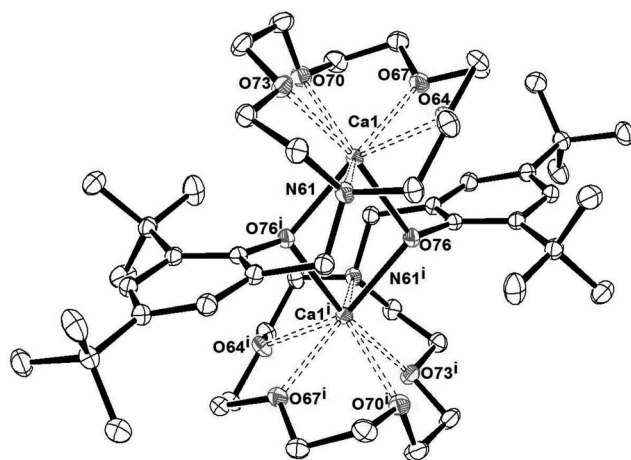


Figure 2. ORTEP diagram of the cationic fragment in **4** (**4**<sup>+</sup>) (thermal ellipsoids set at the 50% probability level). The counterion and hydrogen atoms are omitted for clarity.

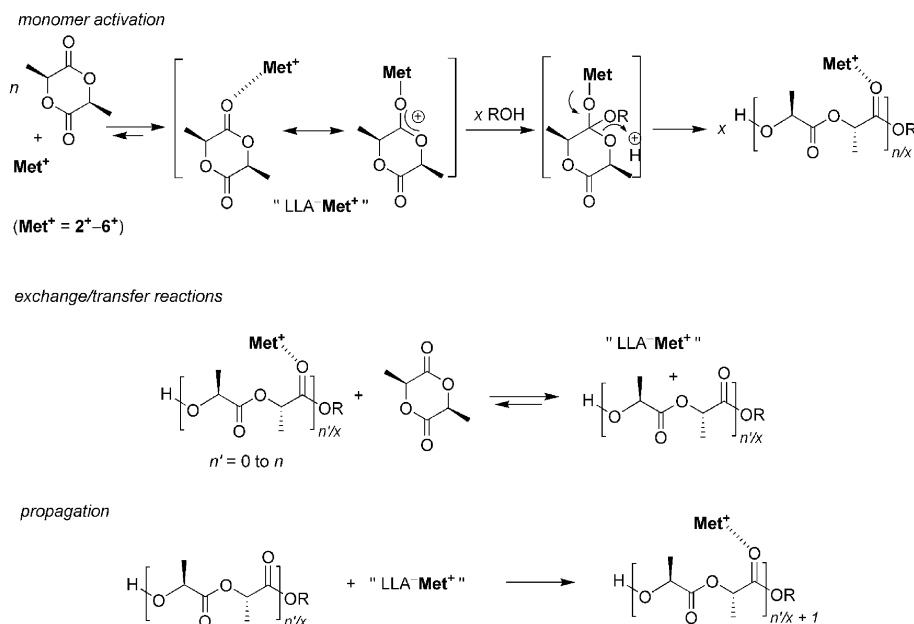
pocket but is clearly above (1.12 Å) the mean plane formed by these atoms.

With the exception of the yttrium system reported by Mountford et al. (which offered good control, but very limited activities),<sup>[8c]</sup> all cationic systems for the ROP of LA<sup>[5d,7a–7b,7d,8c]</sup> or  $\epsilon$ -caprolactone<sup>[5b,6,7c,7f,8a–8b]</sup> are severely hampered by low activities and poor control over the polymerization parameters, which is most likely due to the cationic mechanism probably involved (“activated chain-end”).<sup>[5b]</sup> By contrast, we found that the addition of *i*PrOH as an external initiator/transfer agent to compounds **2–6** generates binary catalysts for the controlled “immortal” ROP of L-LA, some of them featuring very high activities (Table 1).<sup>[17]</sup> At 100 °C, without alcohol (entry 1), the Zn-based salt **2** does not allow good control of the reaction. The production of polymer in this case results either from a cationic polymerization or from the presence of residual protic impurities in the monomer. However, upon addition of 10 equiv. of *i*PrOH, an efficient (albeit slow) system is generated (entries 3–4): the conversion of 1000 equiv. of monomer is complete within 16 h, and the resulting poly(L-LA)s (PLLAs) exhibit narrow molecular weight (MW) distributions ( $M_w/M_n = 1.08$ –1.25). The agreement between theoretical and experimental MWs was excellent, which indicated that reversible chain transfer between dormant and growing macromolecules characteristic of “immortal” ROP according to the so-called “activated monomer mechanism” was fast and efficient (Scheme 2).<sup>[18]</sup> The system displayed first-order dependence on monomer concentration, with an apparent propagation rate constant ( $k_{p,app}^{100}$ ) of 0.0041 min<sup>−1</sup>. Analysis of low-MW PLLA samples by NMR spectroscopy and MALDI-TOF mass spectrometry were consistent with the existence of a single family of polymer chains, all capped by –OH and –C(O)–OCH(CH<sub>3</sub>)<sub>2</sub> termini. Complete conversion of L-LA was ensured within 16 h when 5–50 equiv. of *i*PrOH were added (entries 2, 4, and 5); the MWs decreased with increasing alcohol loading and matched rigorously their expected values.

Table 1. Immortal ROP of lactide with complexes **2–6**.<sup>[a]</sup>

Entry	Initiator	LA/M <sup>+</sup> /OH	T <sup>re</sup> [°C]	Time [h]	Yield [%] <sup>[b]</sup>	$M_{n,theo}$ [g mol <sup>−1</sup> ] <sup>[c]</sup>	$M_{n,SEC}$ [g mol <sup>−1</sup> ] <sup>[d]</sup>	$M_w/M_n$
1	<b>2</b>	1000:1:0	100	3	65	93600	49400	1.70
2	<b>2</b>	1000:1:5	100	16	99	28600	31800	1.38
3	<b>2</b>	1000:1:10	100	3	60	8600	8400	1.08
4	<b>2</b>	1000:1:10	100	16	99	14300	13300	1.25
5	<b>2</b>	1000:1:50	100	16	97	2900	3200	1.15
6	<b>2</b> <sup>[e]</sup>	1000:1:10	100	16	95	13800	15800	1.13
7	<b>3</b>	500:1:10	100	5	28	2100	2500	1.08
8	<b>4</b>	1000:1:10	60	1	12	1900	2900	1.08
9	<b>4</b>	1000:1:10	60	2	28	4100	4800	1.08
10	<b>4</b>	1000:1:10	60	5	57	8300	8700	1.05
11	<b>4</b>	1000:1:10	60	8	75	10900	11600	1.05
12	<b>4</b>	1000:1:10	60	11	90	13000	12900	1.07
13	<b>5</b>	1000:1:10	30	1	48	6800	14000	1.20
14	<b>6</b>	1000:1:10	100	0.05	30	4400	11000	1.21
15	<b>6</b>	5000:1:50	100	0.5	77	11200	14800	1.70

[a] Polymerization in toluene with [L-LA]<sub>0</sub> = 2.0 M. [b] Isolated yield following reprecipitation. [c] Calculated from [L-LA]<sub>0</sub>/[*i*PrOH]<sub>0</sub> × monomer conversion ×  $M_{L-LA}$  +  $M_{iPrOH}$ , with  $M_{L-LA}$  = 144 g mol<sup>−1</sup> and  $M_{iPrOH}$  = 60 g mol<sup>−1</sup>. [d] Determined by size exclusion chromatography vs. polystyrene standards and corrected by a factor of 0.58.<sup>[19]</sup> [e] Nucleophile = BnNH<sub>2</sub>.



Scheme 2. Activated monomer mechanism for the immortal ROP of L-LA catalyzed by  $2^+ - 6^+/\text{ROH}$ .

The use of 10 equiv. of  $\text{BnNH}_2$  as a more nucleophilic initiator/transfer agent<sup>[8c]</sup> also provided an efficient binary catalyst, and full conversion of 1000 equiv. of L-LA was reached in 16 h (entry 6). Such amine end-capped PLLAs are not readily accessible with neutral catalysts operating by the usual "coordination-insertion" mechanism, as primary amines tend to lead to catalyst poisoning in this case.

Compounds **3** (entry 7), **5** (entry 13), and **6** (entries 14–15) also provided efficient catalytic systems. While the Mg-based system **3**/ROH was comparatively slow and only converted 500 or less equivalents of L-LA in a controlled fashion, the opposite problem was encountered with  $5^+$  and  $6^+$ , the cations of more electropositive elements Sr and Ba. Remarkably, these two systems proved extremely active, and at 100 °C they were plagued by transesterification reactions, which led to a broadening of the MW distributions at high monomer conversion. Thus, while the system **6**/*i*PrOH converted 30% of the monomer ( $[\text{L-LA}]/[\mathbf{6}]/[\textit{iPrOH}] = 1000:1:10$ ) in 3 min with good control (entry 14), full conversion took less than 30 min, but the resulting  $M_w/M_n$  values were above 2.0. The activity of these two systems could be tamed down to reassert control over the polymerization parameters ( $M_w/M_n \approx 1.20\text{--}1.40$ ) by decreasing the temperature and/or monomer conversion. Gratifyingly, **6** still afforded a satisfactory control for the ROP of up to 5000 equiv. of monomer, with as much as 50 equiv. of transfer agent (entry 15).

The best results were obtained with the cationic calcium  $4^+$  (entries 8–12). The binary system **4**/*i*PrOH allowed at 60 °C the complete conversion of L-LA ( $[\text{L-LA}]/[\mathbf{4}]/[\textit{iPrOH}] = 1000:1:10$ ) in a fully controlled fashion. The match between calculated and observed MWs was excellent, and the values  $M_w/M_n$  were systematically below 1.08. Efficient reversible chain transfer was further corroborated by NMR and MALDI-TOF-MS end-group analyses performed on a

low-MW PLLA sample. The MALDI-TOF mass spectrum also indicated that transesterification processes occurred extremely rapidly, as the Bernoullian distribution of a single population of chains with increments of 72 Da (i.e., half a lactide unit) was obtained. The kinetics were of first order in monomer concentration, and the apparent rate constant ( $k_{p,\text{app}}^{60} = 0.21 \text{ min}^{-1}$ ) was much higher than that with the Zn analogue, in spite of a lower polymerization temperature selected for the calcium cation. The unique ability of the highly Lewis acidic  $4^+$  to polymerize L-LA was illustrated with a comparative experiment: in a repeat of entry 10 but with  $\text{Ca}(\text{OTf})_2$  ( $\text{OTf} = \text{CF}_3\text{SO}_3^-$ ) instead of **4**, the attempted ROP of 1000 equiv. of monomer with the triflate salts did not produce any polymer.<sup>[20]</sup>

Within this family of cationic complexes, the order of activity follows the trend  $\text{Mg} < \text{Ca} < \text{Sr} < \text{Ba}$ , that is, the activity increases with the ionic radius and the electropositivity of the metal.<sup>[21]</sup> The particularly high activities displayed by  $4^+ - 6^+$  are likely the result of their exacerbated Lewis acidity, which we attribute to a combination of three factors: (1) the highly electropositive nature of Ca, Sr, and Ba, (2) the absence of solvent molecule(s) in the first coordination sphere of the cationic center, and (3) the noncoordinating nature of the  $[\text{H}_2\text{N}\{\text{B}(\text{C}_6\text{F}_5)_3\}_2]^-$  counterion.<sup>[4,14]</sup>

## Conclusions

In conclusion, we have developed a new, general, one-step protocol for the preparation of well-defined, base-free cations of zinc and the Ae elements, in which the metal center is stabilized by a sole (albeit multidentate) phenoxy ligand and a weakly coordinating anion. This procedure gives good to excellent yields, even for the larger elements Ca–Ba. We anticipate that it is extendable to a broad range



of phenol proligands. The stability of compounds **2–6** is particularly surprising, given the oxophilic and highly labile nature of these metals. The non-innocent choice of the weakly coordinating anion  $[\text{H}_2\text{N}\{\text{B}(\text{C}_6\text{F}_5)_3\}_2]^-$  has enabled the determination of the structures of base-free cationic complexes **Mg** and **Ca**. The first well-defined salts of the larger **Ae** for the (immortal) controlled ROP of **L-LA** have been disclosed, and the excellent activities and control displayed by the **Sr**-, **Ba**-, and especially **Ca**-based cations open up a new field of investigations for synthetic chemists.

## Experimental Section

**1:**  $[\text{H}(\text{OEt})_2]^+[\text{H}_2\text{N}\{\text{B}(\text{C}_6\text{F}_5)_3\}_2]^-$  (2.28 g, 1.91 mmol) was added in portions to a solution of  $[\text{LO}^3]\text{H}$  (0.84 g, 1.92 mmol) in  $\text{Et}_2\text{O}$  (100 mL) at room temperature. The colorless solution was stirred at room temperature for 1 h, and volatiles were then removed under vacuum to give a sticky foam. Repeated washings with pentane ( $3 \times 50$  mL) yielded a white powder, which was dried in vacuo to constant weight. Yield 2.47 g (87%).  $\text{C}_{61}\text{H}_{46}\text{B}_2\text{F}_{30}\text{N}_2\text{O}_5$  (1478.6): calcd. C 49.55, H 3.14, N 1.89; found C 49.63, H 3.08, N 1.84.  $^1\text{H}$  NMR (500.13 MHz,  $\text{CD}_2\text{Cl}_2$ , 298 K):  $\delta$  = 8.48 (br. s, 1 H, OH), 7.53 (d,  $^4J_{\text{HH}}$  = 2.3 Hz, 1 H,  $H_{\text{arom}}$ ), 7.09 (d,  $^4J_{\text{HH}}$  = 2.3 Hz, 1 H,  $H_{\text{arom}}$ ), 6.46 (s, 1 H,  $\text{NH}^+$ ), 5.71 (br. s, 2 H,  $\text{NH}_2$ ), 4.38 (d,  $^3J_{\text{HH}}$  = 5.6 Hz, 2 H, Ar- $\text{CH}_2$ -N), 3.90–3.55 (br. m, 16 H,  $H_{\text{cyc}}$ ), 3.56–3.27 (m, 4 H,  $H_{\text{cyc}}$ ), 1.48 [s, 9 H,  $\text{C}(\text{CH}_3)_3$ ], 1.33 [s, 9 H,  $\text{C}(\text{CH}_3)_3$ ] ppm.  $^{13}\text{C}\{^1\text{H}\}$  NMR (125.76 MHz,  $\text{CD}_2\text{Cl}_2$ , 298 K):  $\delta$  = 150.7 (*i*-C), 149.1 (C-F), 147.2 (C-F), 145.3 (*o*-C), 140.3 (C-F), 138.4 (C-F), 137.9 (C-F), 137.5 (*p*-C), 136.0 (C-F), 127.7 (*m*-C), 126.6 (*m*-C), 116.9 (*o*-C), 70.3, 69.3, 68.8, 63.5, (all  $C_{\text{cyc}}$ ), 58.9 (Ar- $\text{CH}_2$ -N), 55.3 (Ar- $\text{CH}_2$ -N- $\text{CH}_2$ ), 34.7 [ $\text{C}(\text{CH}_3)_3$ ], 34.6 [ $\text{C}(\text{CH}_3)_3$ ], 31.3 [ $\text{C}(\text{CH}_3)_3$ ], 30.4 [ $\text{C}(\text{CH}_3)_3$ ] ppm.  $^{19}\text{F}$  NMR (188.31 MHz,  $\text{CD}_2\text{Cl}_2$ , 298 K):  $\delta$  = –131.8 (d,  $^3J_{\text{FF}}$  = 19 Hz, *o*-F), –160.5 (t,  $^3J_{\text{FF}}$  = 19 Hz, *p*-F), –166.1 (t,  $^3J_{\text{FF}}$  = 19 Hz, *m*-F) ppm.  $^{11}\text{B}$  NMR (96.29 MHz,  $\text{CD}_2\text{Cl}_2$ , 298 K):  $\delta$  = –8.44 ppm.

**6:** In a standard procedure, a solution of **1** (0.40 g, 0.27 mmol) in  $\text{Et}_2\text{O}$  (15 mL) was added dropwise at room temperature to a solution of  $\text{Ba}[\text{N}(\text{SiMe}_3)_2]_2(\text{thf})_2$  (0.17 g, 0.28 mmol) in  $\text{Et}_2\text{O}$  (15 mL). The colorless solution was stirred at 20 °C for 90 min, and volatiles were removed in vacuo. The resulting oil was washed with cold pentane ( $2 \times 25$  mL) to give a white powder, which was dried under vacuum. Yield 0.38 g (0.23 mmol, 85%).  $\text{C}_{61}\text{H}_{44}\text{BaB}_2\text{F}_{30}\text{N}_2\text{O}_5$  (1613.9): calcd. C 45.40, H 2.75, N 1.74; found C 44.63, H 2.89, N 1.74.  $^1\text{H}$  NMR (500.13 MHz,  $\text{CD}_2\text{Cl}_2$ , 298 K):  $\delta$  = 7.42 (d,  $^4J_{\text{HH}}$  = 2.5 Hz, 1 H,  $H_{\text{arom}}$ ), 7.08 (d,  $^4J_{\text{HH}}$  = 2.5 Hz, 1 H,  $H_{\text{arom}}$ ), 5.71 (br. s, 2 H,  $\text{NH}_2$ ), 4.36 [d,  $^2J_{\text{HH}}$  = 11.5 Hz, 1 H, Ar- $\text{CH}(\text{H})$ -N], 3.95 (m, 2 H,  $H_{\text{cyc}}$ ), 3.83 (m, 1 H,  $H_{\text{cyc}}$ ), 3.74 (br. q, 3 H,  $H_{\text{cyc}}$ ), 3.58 (m, 1 H,  $H_{\text{cyc}}$ ), 3.53–3.31 (m, 6 H,  $H_{\text{cyc}}$ ), 3.26 [d,  $^2J_{\text{HH}}$  = 11.5 Hz, 1 H, Ar- $\text{CH}(\text{H})$ -N], 3.23–3.12 (m, 2 H,  $H_{\text{cyc}}$ ), 3.08 (m, 1 H,  $H_{\text{cyc}}$ ), 2.88 (m, 1 H,  $H_{\text{cyc}}$ ), 2.75 (m, 1 H,  $H_{\text{cyc}}$ ), 2.62 (m, 1 H,  $H_{\text{cyc}}$ ), 2.34 (m, 1 H,  $H_{\text{cyc}}$ ), 1.52 [s, 9 H,  $\text{C}(\text{CH}_3)_3$ ], 1.29 [s, 9 H,  $\text{C}(\text{CH}_3)_3$ ] ppm.  $^{13}\text{C}\{^1\text{H}\}$  NMR (125.76 MHz,  $\text{CD}_2\text{Cl}_2$ , 298 K):  $\delta$  = 157.9 (*i*-C), 149.3 (C-F), 146.9 (C-F), 140.6 (C-F), 138.8 (*p*-C), 138.1 (C-F), 137.7 (C-F), 137.6 (*o*-C), 135.7 (C-F), 127.5 (*m*-C), 125.6 (*m*-C), 124.0 (*o*-C), 70.6, 69.6, 69.5, 69.3, 69.2, 69.1, 68.5, 66.9 (all  $C_{\text{cyc}}$ ), 63.7 (Ar- $\text{CH}_2$ -N), 59.1 (N- $C_{\text{cyc}}$ ), 53.7 (N- $C_{\text{cyc}}$ ), 35.2 [ $\text{C}(\text{CH}_3)_3$ ], 34.1 [ $\text{C}(\text{CH}_3)_3$ ], 31.5 [ $\text{C}(\text{CH}_3)_3$ ], 31.4 [ $\text{C}(\text{CH}_3)_3$ ] ppm.  $^{19}\text{F}$  NMR (188.31 MHz,  $\text{CD}_2\text{Cl}_2$ , 298 K):  $\delta$  = –133.3 (d,  $^3J_{\text{FF}}$  = 19 Hz, *o*-F), –160.6 (t,  $^3J_{\text{FF}}$  = 19 Hz, *p*-F), –166.0 (t,  $^3J_{\text{FF}}$  = 19 Hz, *m*-F) ppm.  $^{11}\text{B}$  NMR (96.29 MHz,  $\text{CD}_2\text{Cl}_2$ , 298 K):  $\delta$  = –8.46 ppm.

CCDC-768296 (for **3**) and CCDC-768295 (for **4**) contain the supplementary crystallographic data for this paper. These data can be

obtained free of charge from The Cambridge Crystallographic Data Centre via [www.ccdc.cam.ac.uk/data\\_request/cif](http://www.ccdc.cam.ac.uk/data_request/cif).

**Supporting Information** (see footnote on the first page of this article): Full experimental procedures,  $^1\text{H}$  NMR spectra for compounds **1–6**, polymerization data, kinetic plots, characterization of various PLLA samples (NMR, MALDI-TOF and SEC analyses), and crystallographic data for **3** and **4**.

## Acknowledgments

The authors thank the Centre National de la Recherche Scientifique (CNRS), the Institut Universitaire de France (IUF), and Total Petrochemicals for funding this research.

- a) R. E. Drumright, P. R. Gruber, D. E. Henton, *Adv. Mater.* **2000**, *12*, 1841–1846; b) A.-C. Albertsson, I. K. Varma, *Adv. Polym. Sci.* **2002**, *157*, 1–40; c) S. Mecking, *Angew. Chem. Int. Ed.* **2004**, *43*, 1078–1085.
- a) B. J. O’Keefe, M. A. Hillmyer, W. B. Tolman, *J. Chem. Soc., Dalton Trans.* **2001**, 2215–2224; b) O. Dechy-Cabaret, B. Martin-Vaca, D. Bourissou, *Chem. Rev.* **2004**, *104*, 6147–6176; c) J. Wu, T.-L. Yu, C.-T. Chen, C.-C. Lin, *Coord. Chem. Rev.* **2006**, *250*, 602–626; d) C. A. Wheaton, P. G. Hayes, B. J. Ireland, *Dalton Trans.* **2009**, 4832–4846; e) M. J. Stanford, A. P. Dove, *Chem. Soc. Rev.* **2010**, *39*, 486–494.
- H. Sinn, W. Kaminsky, H. J. Vollmer, R. Woldt, *Angew. Chem.* **1980**, *92*, 396–402; *Angew. Chem. Int. Ed. Engl.* **1980**, *19*, 390–392.
- a) R. F. Jordan, *Adv. Organomet. Chem.* **1991**, *32*, 325–387; b) E. Y.-X. Chen, T. J. Marks, *Chem. Rev.* **2000**, *100*, 1391–1434; c) M. Bochmann, *J. Organomet. Chem.* **2004**, *689*, 3982–3998.
- a) M. D. Hannant, M. Schormann, M. Bochmann, *J. Chem. Soc., Dalton Trans.* **2002**, 4071–473; b) Y. Sarazin, M. Schormann, M. Bochmann, *Organometallics* **2004**, *23*, 3296–3302; c) M. D. Hannant, M. Schormann, D. L. Hughes, M. Bochmann, *Inorg. Chim. Acta* **2005**, *358*, 1683–1691; d) C. A. Wheaton, B. J. Ireland, P. G. Hayes, *Organometallics* **2009**, *28*, 1282–1285; e) C. A. Wheaton, P. G. Hayes, *Dalton Trans.* **2010**, *39*, 3861–3869.
- B. J. Ireland, C. A. Wheaton, P. G. Hayes, *Organometallics* **2010**, *29*, 1079–1084.
- a) N. Emig, H. Nguyen, H. Krautscheid, R. Réau, J.-B. Ca-zeaux, G. Bertrand, *Organometallics* **1998**, *17*, 3599–3608; b) J. Lewinski, P. Horeglad, M. Dranka, I. Justyniak, *Inorg. Chem.* **2004**, *43*, 5789–5791; c) S. Milione, F. Grisi, R. Centore, A. Tuzi, *Organometallics* **2006**, *25*, 266–274; d) S. Dagorne, F. Le Bideau, R. Welter, S. Bellemin-Laponnaz, A. Maisse-François, *Chem. Eur. J.* **2007**, *13*, 3202–3217; e) J.-T. Issenhuth, J. Pluinage, R. Welter, S. Bellemin-Laponnaz, S. Dagorne, *Eur. J. Inorg. Chem.* **2009**, 4701–4709; f) M. Haddad, M. Laghzaoui, R. Welter, S. Dagorne, *Organometallics* **2009**, *28*, 4584–4592; g) B. Lian, H. Ma, T. P. Spaniol, J. Okuda, *Dalton Trans.* **2009**, 9033–9042.
- a) H.-T. Sheng, H. Zhou, H.-D. Guo, H.-M. Sun, Y.-M. Yao, J.-F. Wang, Y. Zhang, Q. Shen, *J. Organomet. Chem.* **2007**, *692*, 1118–1124; b) D. Robert, M. Kondracka, J. Okuda, *Dalton Trans.* **2008**, 2667–2669; c) L. Clark, M. G. Cushion, H. E. Dyer, A. D. Schwarz, R. Duchateau, P. Mountford, *Chem. Commun.* **2010**, *46*, 273–275.
- a) A cationic silver complex for the ROP of **L-LA** has also been reported: M. K. Samantaray, V. Katiyar, D. Roy, K. Pang, H. Nanavati, R. Stephen, R. B. Sunoj, P. Ghosh, *Eur. J. Inorg. Chem.* **2006**, 2975–2984. For group 3 cations and their use for the polymerization of  $\alpha$ -olefins, styrene, and dienes, see: b) P. M. Zeimentz, S. Arndt, B. R. Elvidge, J. Okuda, *Chem. Rev.* **2006**, *106*, 2404–2433; c) X. Li, M. Nishiura, L. H. Hu, K. Mori, Z. M. Hou, *J. Am. Chem. Soc.* **2009**, *131*, 13870–13882.



- and references cited therein. For syntheses of group 13 cations, see: d) S. Dagorne, D. A. Atwood, *Chem. Rev.* **2008**, *108*, 4037–4071.
- [10] a) M. H. Chisholm, J. C. Gallucci, K. Phomphrai, *Inorg. Chem.* **2004**, *43*, 6717–6725; b) D. J. Darensbourg, W. Choi, O. Karoonnirun, N. Bhuvanesh, *Macromolecules* **2008**, *41*, 3493–3502; c) S. Harder, F. Feil, K. Knoll, *Angew. Chem. Int. Ed.* **2001**, *40*, 4261–4264; d) M. R. Crimmin, I. J. Casely, M. S. Hill, *J. Am. Chem. Soc.* **2005**, *127*, 2042–2043; e) S. Datta, M. T. Gamer, P. W. Roesky, *Organometallics* **2008**, *27*, 1207–1213; f) M. G. Davidson, C. T. O'Hara, M. D. Jones, C. G. Keir, M. F. Mahon, G. Kociok-Köhn, *Inorg. Chem.* **2007**, *46*, 7686–7688.
- [11] R. D. Shannon, *Acta Crystallogr., Sect. A* **1976**, *32*, 751–767.
- [12] S. Itoh, H. Kumei, S. Nagatomo, T. Kitagawa, S. Fukuzumi, *J. Am. Chem. Soc.* **2001**, *123*, 2165–2175.
- [13] V. Poirier, T. Roisnel, J.-F. Carpentier, Y. Sarazin, *Dalton Trans.* **2009**, 9820–9827.
- [14] S. J. Lancaster, A. Rodriguez, A. Lara-Sanchez, M. D. Hannant, D. A. Walker, D. L. Hughes, M. Bochmann, *Organometallics* **2002**, *21*, 451–453.
- [15] It is indeed known that, while the somewhat spherical, often disordered  $[\text{B}(\text{C}_6\text{F}_5)_4]^-$  tends to give oily salts, the presence of a dipole moment in  $[\text{H}_2\text{N}\{\text{B}(\text{C}_6\text{F}_5)_3\}_2]^-$  induces an orientation towards the cationic center that ultimately facilitates the crystallization process: a) I. Krossing, I. Raabe, *Angew. Chem. Int. Ed.* **2004**, *43*, 2066–2090; b) M. Bochmann, *Coord. Chem. Rev.* **2009**, *253*, 2000–2014 and references cited therein; c) Y. Sarazin, D. L. Hughes, N. Kaltsoyannis, J. A. Wright, M. Bochmann, *J. Am. Chem. Soc.* **2007**, *129*, 881–894.
- [16] The syntheses of  $\{\text{LO}^3\}\text{MX}$ ,  $[\{\text{LO}^x\}\text{H}\cdot\text{H}\]^+[\text{H}_2\text{N}\{\text{B}(\text{C}_6\text{F}_5)_3\}_2]^-$  and  $[\{\text{LO}^x\}\text{M}]^+[\text{H}_2\text{N}\{\text{B}(\text{C}_6\text{F}_5)_3\}_2]^-$  and their applications for catalytic purposes are beyond the scope of this communication and will be the object of a separate report.
- [17] It is noteworthy that *i*PrOH alone (i.e., in the absence of a metallic species) is not able to initiate the ROP of L-LA, while initiation due to the presence of residual traces of water can be ruled out on account of (1) the care taken in the purification of all solvents and L-lactide (Supporting Information), and (2) characterization of PLLA samples by the means of NMR and MALDI-TOF analyses, which confirmed that all macromolecules were truly initiated/end-capped by *i*PrOH.
- [18] a) T. Aida, S. Inoue, *Acc. Chem. Res.* **1996**, *29*, 39–48; b) N. Ajellal, J.-F. Carpentier, C. Guillaume, S. M. Guillaume, M. Helou, V. Poirier, Y. Sarazin, A. Trifonov, *Dalton Trans.*, DOI: 10.1039/c001226b.
- [19] M. Save, M. Schappacher, A. Soum, *Macromol. Chem. Phys.* **2002**, *203*, 889–899.
- [20]  $\text{Ca}(\text{OTf})_2$  promotes the ROP of cyclic carbonates: M. Helou, O. Miserque, J.-M. Brusson, J.-F. Carpentier, S. M. Guillaume, *ChemCatChem* **2010**, *2*, 306–313 and references cited therein.
- [21] For a similar trend with neutral complexes, see refs.<sup>[10a,13]</sup> and: a) M. H. Chisholm, J. Galucci, K. Phomphrai, *Chem. Commun.* **2003**, 48–49; b) Y. Sarazin, R. H. Howard, D. L. Hughes, S. M. Humphrey, M. Bochmann, *Dalton Trans.* **2006**, 340–350.

Received: May 20, 2010

Published Online: June 25, 2010

# Synthesis, Structural, Redox and Mössbauer Characterization of Four-Electron-Oxidized Tetrakis(cyclohexyl)iron(II)porphodimethene with Different Axial Ligations

Dibyendu Bhattacharya<sup>[a]</sup> and Sabyasachi Sarkar<sup>\*[a]</sup>

**Keywords:** Crystal engineering / Electron transfer / Iron / Porphyrinoids / Moessbauer spectroscopy

Monocationic  $\text{Fe}^{\text{II}}$  porphodimethene complexes,  $[\text{L}^{\Delta\Delta}\text{Fe}-\text{X}][\text{Y}]$  (**1**,  $\text{X} = \text{I}^-$  and  $\text{Y} = \text{I}_3^-$ ; **2**,  $\text{X} = \text{Br}^-$  and  $\text{Y} = [\text{Fe}^{\text{III}}\text{Br}_4]^-$ ;  $\text{L}^{\Delta\Delta}$  = tetrakis(cyclohexyl)porphodimethene), were achieved by induced electron-transfer reactions between the square-planar, intermediate-spin, iron(III)porphyrinogen complex  $[\text{Et}_4\text{N}][\text{LFe}^{\text{III}}]$  [ $\text{L}$  = tetrakis(cyclohexyl)porphyrinogen tetra-anion] and different oxidants. Single-crystal X-ray diffraction analysis reveals that **1** and **2** have a square-pyramidal geometry in which the iodide and bromide ligands occupy the axial position, respectively. Compound **1** exhibits an extended two-dimensional solid-state structure that comprises porpho-

dimethene cation and triiodide anion chain columns in a 1:1 ratio, which are packed alternately. Electrochemical assessment with cyclic voltammetry reveals reversibly accessible  $\text{Fe}^{\text{II/III}}$  oxidation states; however, the redox potential is nearly one volt more positive than that for a typical heme cofactor, which suggests the highly oxidizing nature of the tetrapyrrole framework in the four-electron-oxidized  $\text{L}^{\Delta\Delta}$  moiety. In addition, definitive experimental oxidation state and spin state assignments for the intermediate-spin  $[\text{Et}_4\text{N}][\text{LFe}^{\text{III}}]$  and high-spin  $\text{Fe}^{\text{II}}$  states of **1** and **2** were afforded by Mössbauer characterization.

## Introduction

In the years following the exploration of the redox processes in some enzymes and their model compounds that involve not only metal centers but also coordinated ligands,<sup>[1,2]</sup> several metal complexes with redox-active (non-innocent) ligands (e.g. porphyrins, pterins, flavins, quinines, dithiolenes, or phenoxyl-based systems) have been examined to determine the new aspects in synthetic chemistry and catalysis.<sup>[3]</sup> The commonalities of these types of compounds include (a) one-electron ligand-based redox couples and (b) frontier orbitals of mixed metal–ligand character.<sup>[1,3]</sup> The macrocyclic ligand “porphyrinogen” goes beyond those limitations in that (a) it reacts in discrete two-electron steps and (b) the orbitals that support the redox chemistry are cleanly localized on the organic part, in the formation or breaking of one or two spirocyclopropane rings ( $\Delta$ ), formed by  $\text{C}_\alpha\text{--C}_\alpha$  coupling between the adjacent carbon atoms of neighboring pyrroles.<sup>[2]</sup>

Iron is the most important transition metal found in biological systems and plays various roles in many important life processes.<sup>[4]</sup> Recently, we developed the direct incorporation of the ferric ion approach as an effective strategy for the simple one-pot synthesis of four-coordinate, square-planar iron(III) complexes  $[\text{Et}_4\text{N}][\text{LFe}^{\text{III}}]$  (where  $\text{L}$  = tetra-

kiscyclohexyporphyrinogen tetra-anion).<sup>[5]</sup> This method helps to offset the difficulties encountered in the biosynthesis of heme<sup>[6]</sup> and in other reported tedious metalation methods of porphyrinogens.<sup>[7,8]</sup>

The oxidation of  $[\text{Li}(\text{thf})_2][\text{L}'\text{Fe}^{\text{II}}]$  with excess copper(II) chloride as the oxidant was reported to lead to the formation of  $[\text{L}'^{\Delta\Delta}\text{Fe}^{\text{II}}\text{--Cl}][\text{CuCl}_5]$  ( $\text{L}'$  = *meso*-octamethylporphyrinogen tetraanion) with unprecedented metal cluster counteranions.<sup>[9]</sup> Furthermore, the reaction of  $[\text{Li}(\text{thf})_2][\text{L}'\text{Fe}^{\text{III}}]$  with excess  $\text{CuCl}_2$  led to the isolation of  $[\text{L}'^{\Delta\Delta}\text{Fe}^{\text{III}}\text{--Cl}][\text{FeCl}_4]$ . However, the synthesis procedures are complicated and the reported redox behaviors of the iron porphyrinogen complexes towards different oxidants are unclear and require further explanations. In this context, a cleaner oxidation of the iron porphyrinogen with the  $[(\text{cp})_2\text{Fe}]^+$  cation was reported, in which acetonitrile ( $\text{MeCN}$ ) was coordinated axially, which resulted in the isolation of the three-electron-oxidized dicationic entity,  $[\text{L}'^{\Delta\Delta}\text{Fe}^{\text{II}}\text{--MeCN}]^{2+}$ .<sup>[8]</sup> Recently,  $[\text{L}'^{\Delta\Delta}\text{Fe}\text{--MeCN}]^{2+}$  was used for the preparation of newer derivatives  $[\text{L}'^{\Delta\Delta}\text{Fe}\text{--X}]^+$ , where  $\text{X} = \text{Cl}^-$ ,  $\text{Me}_3\text{SiO}^-$ .<sup>[10]</sup> It is worth noting that all the above-mentioned redox reactions were studied with  $\eta^4$ -bound lithium ( $[\text{Li}(\text{thf})_2]^+$ ) or sodium ( $[\text{Na}(\text{thf})_2]^+$ ) cation bound organometallic entities. We believe that the substitution of such a  $\eta$ -bound counteranion by the tetraalkylammonium cation in metalloporphyrinogens dramatically alters the redox behavior of the purely anionic part to a greater extent than *meso*-substitution of the peripheral ligand, and as a result the redox chemistry could be different altogether.<sup>[2,11]</sup>

[a] Department of Chemistry, Indian Institute of Technology – Kanpur, Kanpur 208016, Uttar Pradesh, India  
Fax: +91-512-2597265  
E-mail: abya@iitk.ac.in

The development of a new and simple synthetic strategy that allows the isolation and characterization of porphyrinogen complexes with redox-active metals and a study of their reactivity have now rendered their experimental and theoretical description accessible.<sup>[8,11]</sup>

With these facts in mind and in conjunction with our exploration of a new route to the one-pot, direct Fe<sup>III</sup>-incorporated porphyrinogen complex synthesis,<sup>[5]</sup> we now report the simple and efficient one-pot synthesis of two new four-electron-oxidized iron(II)porphodimethene complexes [L<sup>ΔΔ</sup>Fe-X][Y] (**1**, X = I<sup>-</sup> and Y = I<sub>3</sub><sup>-</sup>; **2**, X = Br<sup>-</sup> and Y = (Fe<sup>III</sup>Br<sub>4</sub>)<sup>-</sup>; L<sup>ΔΔ</sup> = tetrakis(cyclohexyl)porphodimethene] from the direct Fe<sup>III</sup>-incorporated parent complex [Et<sub>4</sub>N][LFe<sup>III</sup>]. Compound **1** and **2** were further characterized by single-crystal X-ray diffraction analysis, cyclic voltammetry, and Mössbauer spectroscopy.

## Results and Discussion

### Synthesis of Complexes **1** and **2**

Treatment of [Et<sub>4</sub>N][LFe<sup>III</sup>] with three equivalents (or greater) of elemental iodine in dichloromethane (dcm) at room temperature gave **1** as the sole product in high yields (Scheme 1). However, **2** was obtained in a yield of only 35% because the iron for both the counteranion, [FeBr<sub>4</sub>]<sup>-</sup>, and [L<sup>ΔΔ</sup>Fe-Br] is provided by the parent complex. The authenticity of the compounds was confirmed by elemental analysis and IR and ESI-MS spectroscopy. The infrared spectrum of parent complex shows a sharp absorption band at 3073 cm<sup>-1</sup> (pyrrole aromatic C-H), and this band is significantly shifted to 3113 cm<sup>-1</sup> in **1** and **2**. This arises as a result of the formation of the cyclopropane ring, which causes structural changes in the porphyrinogen skeleton.<sup>[9,11]</sup> The ESI mass spectra of **1** and **2** show molecular ion peaks at *m/z* = 782.25 and 734.26, respectively. The structures of complexes **1** and **2** were further confirmed by single-crystal X-ray diffraction analysis. ORTEP diagrams of **1** and **2** are shown in Figure 1, and their pertinent crystallographic data can be found in Table 2. The core geometry is essentially square pyramidal; the four nitrogen atoms of porphodimethene are coordinated to the central Fe<sup>II</sup> atom with the axial ligation of a halide anion.

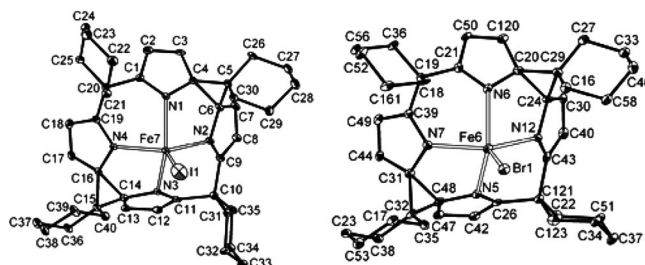


Figure 1. ORTEP plot of **1** (left) and **2** (right), with thermal ellipsoid drawn at the 30% probability level. Hydrogen atoms, solvent molecules, as well as counterions are omitted for clarity.

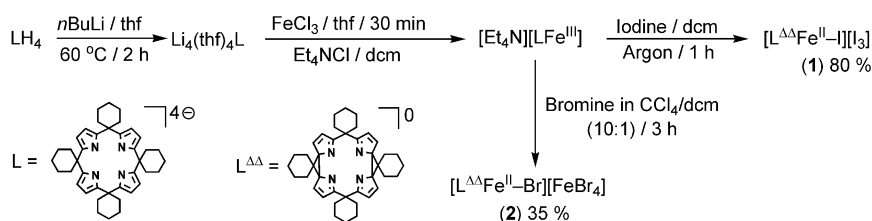
The formation of four-electron-oxidized products can be envisaged as occurring through a rare halogen-induced electron-transfer reaction across the Fe<sup>III</sup> porphyrinogen.<sup>[11,12]</sup> The halogens used in these reactions act as an external oxidant, which provoke the electron transfer between the Fe<sup>III</sup> center and the porphyrinogen anion (L<sup>4-</sup>). The four electrons that are released in the oxidation of L<sup>4-</sup> to L<sup>ΔΔ</sup> are shared by the one internal oxidant, Fe<sup>III</sup>, and by the three halides to yield product **1** and **2** (Scheme 1).

### Solid-State Structures of **1** and **2** by X-ray Crystallography

ORTEP diagrams of the cationic part of **1** and **2** are shown in Figure 1. The crystallographic data are provided in Table 2. Compounds **1** and **2** crystallize in the space group *P* $\bar{1}$  with two cationic molecules per asymmetric unit. The lattice of **1** contains one I<sub>3</sub><sup>-</sup>, one I<sub>2</sub> and two dcm molecules and **2** contains one [FeBr<sub>4</sub>]<sup>-</sup> and two acetone molecules.

The distance between the two pairs of adjacent C<sub>α</sub> atoms of the macrocycle in [L<sup>ΔΔ</sup>Fe<sup>II</sup>-X]<sup>+</sup> (where X = I<sup>-</sup> or Br<sup>-</sup>) is less than a single bond length [*d*(C<sub>α</sub>-C<sub>α</sub>) = 1.580(5) Å and 1.594(5) Å] and are smaller than those in [LFe<sup>III</sup>]<sup>+</sup>,<sup>[5]</sup> which suggests that the macrocycle is oxidised. The cyclopropane groups form nearly equilateral triangles with C<sub>α</sub>-C<sub>meso</sub>-C<sub>α</sub> angles of 63.3(6) and 62.8(7)° for **1** and **2**, respectively.

The presence of the spirocyclopropane rings distorts the macrocycle and the constituent pyrroles. The presence of alternating formal single and double bonds in the pyrroles is plainly evident by N=C double bonds {*d*<sub>av</sub>[N1-C1, N2-C9] = 1.309 Å}, which are significantly shorter than their neighboring N-C single bonds {*d*<sub>av</sub>[N1-C4, N2-C6] = 1.436 Å} in **1**. The C<sub>α</sub>-C<sub>α</sub> straps constrain the macrocycle

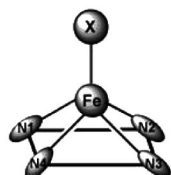


Scheme 1. Synthesis of four-electron-oxidized iron(II)porphodimethenes **1** and **2**.



along one axis, which causes the 4-N core to deform from a square to a rectangle {[N1–Fe7–N2] = 134.1° and [N2–Fe7–N4] = 132.1°} in **1**. The deformation in complex **2** (136.5°) is more severe. The ruffled conformation of the L<sup>4</sup>-macrocycle is replaced by a bowl conformation in L<sup>Δ</sup>, which is reminiscent of calixarenes<sup>[13]</sup> and calixpyrrole,<sup>[14]</sup> in which all the four pyrrole planes are tilted upwards relative to the 4-N plane. The conformational change from ruffle to bowl is accompanied by an upward movement of the Fe<sup>II</sup> center from the 4-N plane. Thus, the Fe<sup>II</sup> center has a five-coordinate, distorted, square-pyramidal coordination geometry with the four porphodimethene nitrogen atoms on the base of the square plane, while the axial halogen ligands occupy the apical site.

Figure 2 shows the distorted square-pyramidal coordination geometry in iron porphodimethenes. The structural features of these porphodimethenes are dependent on the nature of the counteranions; different Fe–N and Fe–axial bond lengths and angles can be obtained. The presence of interacting Cu<sub>4</sub>Cl<sub>5</sub><sup>−</sup> clusters influence the structural properties of the iron porphodimethene moiety, thus the iron atom may move slightly inward in [L<sup>Δ</sup>Fe<sup>II</sup>–Cl][(Cu<sub>4</sub>Cl<sub>5</sub>)].<sup>[9]</sup>



X	MeCN	Cl	Br	I
<i>d</i> (Fe–X), Å	2.064	2.185/2.25	2.395	2.447
<i>d</i> (Fe–N), <sup>a</sup> Å	2.116	2.192/2.161	2.170	2.173
<i>d</i> (Fe–4N plane) <sup>b</sup>	0.726	0.063/0.733	0.833	0.865
∠(N1–Fe–N4), <sup>c</sup> °	83.23	89.9/80.5	80.9	80.9
∠(N1–Fe–N3), <sup>d,e</sup> °	139.88	176.2/132.3	133.1	133.1
ref.	8	9/10	this work	this work

Note: <sup>a</sup>average distance. <sup>b</sup>distance between the mean N4 core and the Fe atom. <sup>c</sup>average of four angle. <sup>d</sup>average of two angle.

Figure 2. View of a displaced Fe<sup>II</sup> center in which different axial molecules/ions can be coordinated to form a distorted square-pyramidal coordination environment in Fe<sup>II</sup>porphodimethenes. The bond lengths and angles in the various compounds are presented.

Compounds **1** and **2** are of particular interest. Firstly, among these iron porphodimethenes, the N–Fe–N bond angles are not affected by the counteranions (133.1°).

Secondly, the Fe–N bond lengths are very similar, and the out-of-plane displacement of the Fe<sup>II</sup> center from 4-N core (0.833–0.866 Å) is therefore similar. Thus, our results establish the stable existence of and intrinsic metrics for [L<sup>Δ</sup>Fe<sup>II</sup>–X]<sup>+</sup> in the presence of an anionic axial ligand and in the absence of an interacting counterion.

The four-electron-oxidized macrocycle is a much weaker donor than the parent L<sup>4</sup>-porphyrinogen, as evidenced by the long Fe–N(pyrrole) bonds; the [Fe–N(pyrrole)] bond (1.896 Å, parent complex)<sup>[5]</sup> is 0.27 Å shorter than the Fe–N bond in compounds **1** and **2** [*d*<sub>av.</sub>(Fe–N) = 2.170 Å]. All four Fe–N distances in this [L<sup>Δ</sup>Fe<sup>II</sup>–X]<sup>+</sup> entity, however, are significantly longer than the corresponding distances in the previously reported dicationic MeCN axially coordinated complex, [L<sup>Δ</sup>Fe<sup>II</sup>–MeCN]<sup>2+</sup> (with cobalticborane, [(C<sub>2</sub>B<sub>9</sub>H<sub>11</sub>)<sub>2</sub>Co]<sub>2</sub>, as a counteranion).<sup>[8]</sup> However, there is good agreement in the increase in the Fe–axial bond length from MeCN > Cl > Br > I.<sup>[8–10]</sup>

Compound **1** exhibits an extended two-dimensional solid-state structure, which comprises a 1:1 ratio of porphodimethene cations and triiodide counterions. The anion component of the present derivatives is considered to be composed of triiodide anions and iodine molecule units. The polymeric anion of the zigzag chain lies along the *ab* and *ac* planes as illustrated in Figure 3. The triiodide anion unit was found to be linear and symmetric, and the I6–I7 bond length is 2.766(3) Å. The slightly bent nature of the triiodide anion was reported in the iodine-doped metallophthalocyanines.<sup>[15]</sup>

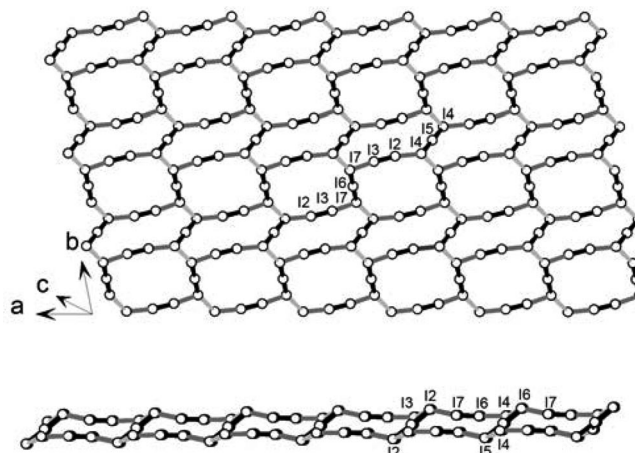


Figure 3. Polymeric anionic structure of the zigzag chain projected in the *ab* (top) and *ac* plane (below) in the triiodide-iodine salt in **1**.

The triiodide units are linked by the iodine molecule unit. The bridging I3–I7 distance is 3.236(3) Å, and the I1–I2–I3 angle is 87.7(2)°. The bond length is obviously shorter than the sum of the van der Waals radii for iodine atoms. The I–I distance in this iodine molecule unit is 2.743(5) Å, which is longer than that of usual iodine molecules (2.68 Å).<sup>[16]</sup> The bond lengths are in the range of other polyiodide anions<sup>[17]</sup> and similar to those in the reported polymeric penta-iodide anions in mixed-valence binuclear ferrocenium derivatives.<sup>[18]</sup>

The packing views projected in the (a) *ab* (b) *bc*, and (c) *ac* plane are shown in Figure 4. The cation and anion chain columns are packed alternately. In the cation column, the cyclohexyl rings do not overlap between neighboring cations but are stacked stepwise [Figure 4(b)]. The triiodide and free iodine molecules form a layer and the cationic part is trapped between the two layers of the triiodide-iodine network.

The shortest distance between a carbon atom in the pyrrole ring and the iodine atom is about 4.2 Å. The distance is close to the sum of the van der Waals radii for C(H)–I. That is, the interactions between the cation–anion columns are of the order of a “van der Waals interaction”.<sup>[19]</sup> Although the interaction is not so strong, it can be thought that a rigid polymeric anion structure controls the cation structure.

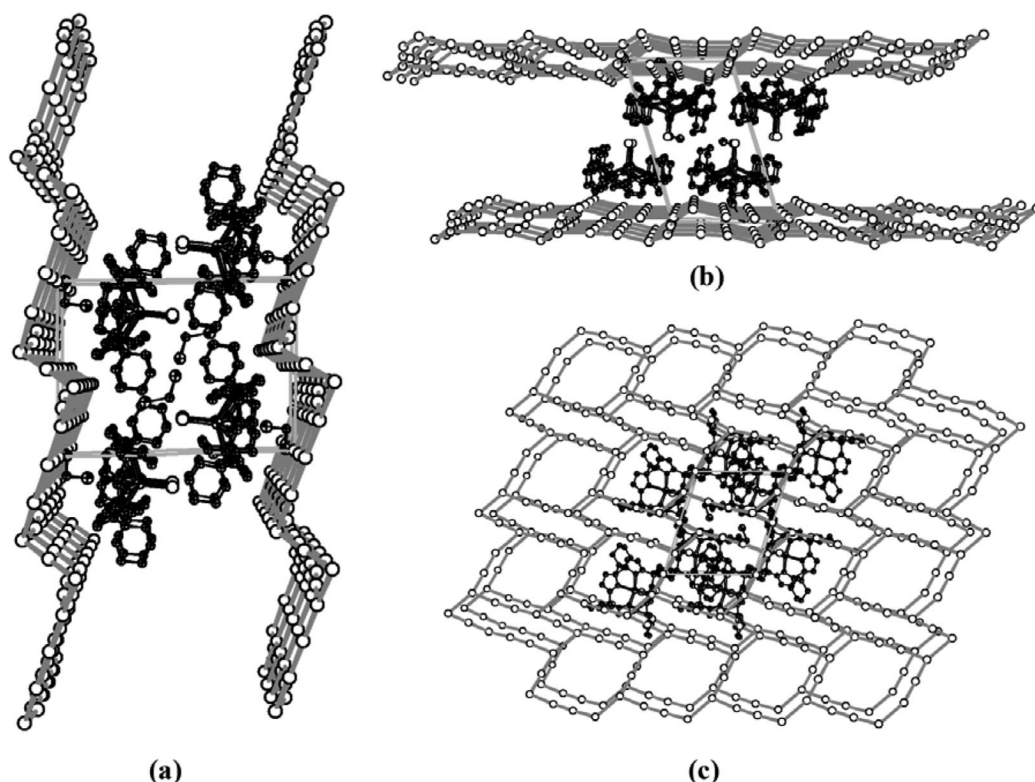


Figure 4. Perspective view projected in the (a) *ab* (b) *bc* and (c) *ac* plane of the complex **1**.

### Redox Potential

Figure 5 shows the cyclic voltammogram of complex **1** in acetonitrile. Reversible  $\text{Fe}^{\text{II/III}}$  waves are observed with  $E_{1/2} = +1.08$  and  $+1.36$  V (vs. Ag/AgCl electrode) for **1** and **2**, respectively, as verified by the linear plot of the cathodic and anodic current vs.  $\nu_{1/2}$  (scan rate,  $\nu = 100\text{--}1000$   $\text{mV s}^{-1}$ ). As the porphyrinogens are fully oxidized (predicted to respond normally to a pair of successive two-electron oxidations),<sup>[5]</sup> there are no ligand-centered oxidations expected for porphodimethenes. Therefore, reversible peaks with  $E_{1/2} = +0.56$  V in **1** results from the  $\text{I}^3/\text{I}^-$  couple in the absence of any ligand oxidation process.<sup>[11]</sup> The oxidation potential for the  $\text{Fe}^{\text{II/III}}$  couple in **2**, however, is more positively shifted, which is consistent with the greater electron-withdrawing nature of the axial bromide ion and related porphyrin complexes.

For comparison, the most difficult iron cofactors to reduce in biology are the ferredoxins, the reduction potential of the ferric form in porphyrinogen is  $-0.15$  V vs. Ag/AgCl.<sup>[5]</sup> With regard to their porphyrin relatives, however, iron(III)porphyrinogen is ca. 0.5 to 1.3 V more difficult to reduce than the heme cofactors (depending on the nature of the axial ligands).<sup>[5,20]</sup> In sharp contrast, owing to the highly oxidizing nature of the tetrapyrrole framework in the four-electron-oxidized porphodimethene ( $\text{L}^{\Delta\Delta}$ ) moiety, the  $\text{Fe}^{\text{II/III}}$  oxidation potential ( $E_{1/2} = +1.08$  V vs. Ag/AgCl) is nearly one volt more positive than that of a typical heme cofactor.<sup>[21]</sup>

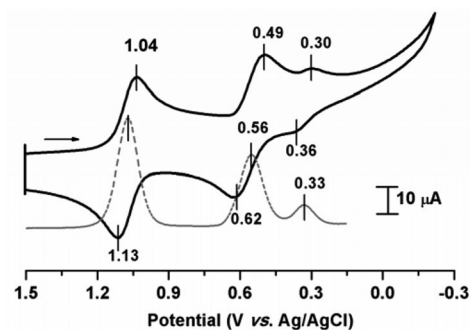


Figure 5. Cyclic voltammogram (solid black line) and differential pulse voltammogram (dotted gray line) (showing oxidation potential only) of **1** in MeCN (1 mM) in 0.1 M TBAPF<sub>6</sub> with scan rate of 100 mV/s vs. Ag/AgCl.

### Mössbauer Spectroscopy

Definitive experimental oxidation state and spin state assignments for the iron centers of  $[\text{Et}_4\text{N}][\text{LFe}^{\text{III}}]$  and the four-electron-oxidized iron porphodimethene complexes (**1** and **2**) were afforded by Mössbauer spectroscopy. Fitted  $^{57}\text{Fe}$  Mössbauer spectra of polycrystalline samples were recorded at 298 K, shown in Figure 6, and the results are summarized in Table 1.

Mössbauer data for square-planar  $\text{Fe}^{\text{III}}$  compounds in the literature is very scarce, and therefore, no benchmark is available for planar,  $S = 3/2$   $\text{Fe}^{\text{III}}$  compounds. Weighardt et al. recently described the tetrahedral  $\text{Fe}^{\text{III}}$  ( $d^5$ ,  $S_{\text{Fe}} = 3/2$ )

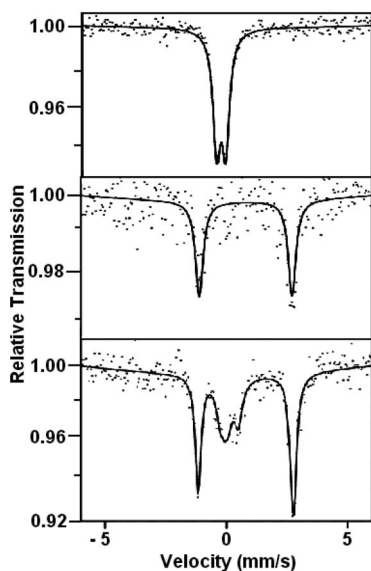


Figure 6. Fitted  $^{57}\text{Fe}$  Mössbauer spectra of solid  $[\text{Et}_4\text{N}][\text{LFe}^{\text{III}}]$  (top), solid **1** (middle), and solid **2** (bottom) at 298 K. Solid lines represent the best fits of the Lorentzian line shape. The vertical axis is an arbitrary transmission scale. Mössbauer parameters are given in Table 1.

Table 1. Fitted  $^{57}\text{Co}$  in Rh matrix Mössbauer data of  $[\text{Et}_4\text{N}][\text{LFe}^{\text{III}}]$ , **1**, and **2** at 298 K.

Complex	$S_{\text{Fe}}^{\text{[a]}}$	$\delta$ (mm s $^{-1}$ ) <sup>[b]</sup>	$ \Delta E_{\text{Q}} $ (mm s $^{-1}$ ) <sup>[c]</sup>	% <sup>[d]</sup>
$[\text{Et}_4\text{N}][\text{LFe}^{\text{III}}]$	3/2	0.15	0.38	100
<b>1</b>	2	0.88	3.91	100
<b>2</b>	2	0.90	3.92	96
	5/2 <sup>[e]</sup>	0.36	0.00	4

[a] Intrinsic spin state of central iron atom. [b] Isomeric shift vs.  $\alpha$ -Fe (298 K). [c] Quadrupole splitting. [d] Amount of major and minor component. [e]  $[\text{FeBr}_4]^-$  is noncommunicating and in the high-spin state.

complex coupled antiferromagnetically to the noninnocent  $\text{pda}^-$  ligand in  $[\text{Fe}^{\text{III}}(\text{pda}^{2-})(\text{pda}^-)]^0$ , [ $\text{pda} = N,N'$ -bis(pentafluorophenyl)- $o$ -phenylenediamido].<sup>[22]</sup> A discrete intermediate-spin ( $S_{\text{Fe}} = 3/2$ )  $\sigma$ -organoiron(III) complex in a truly four-coordinate environment has also been reported recently, in which four aromatic  $C$ -donor phenyl rings are coordinated,  $[\text{Li}(\text{thf})_4][\text{Fe}^{\text{III}}(\text{C}_6\text{Cl}_5)_4]$  ( $\text{C}_6\text{Cl}_5 =$  pentafluorophenyl).<sup>[23]</sup> The dominant contribution in both reported complexes is a doublet with a low isomer shift of  $IS = 0.20$ – $0.23$  mm/s and a large quadrupole splitting of  $\Delta E_{\text{Q}} \geq 3.00$  mm/s at 77 K, typical of a  $\text{Fe}^{\text{III}}$  entity in an  $S = 3/2$  or a spin-admixed state. We recently reported such a complex,  $[\text{Et}_4\text{N}][\text{LFe}^{\text{III}}]$ , and the oxidation and spin states were thoroughly characterized by magnetic moment measurements, electron spin resonance spectra and theoretical calculations.<sup>[5]</sup>

The Mössbauer spectrum of  $[\text{Et}_4\text{N}][\text{LFe}^{\text{III}}]$  exhibits a very narrow, quadrupole doublet ( $IS = 0.15$  mm/s,  $\Delta E_{\text{Q}} = 0.38$  mm/s) and is the first report of an intermediate spin,  $S = 3/2$ , square-planar inorganic  $\text{Fe}^{\text{III}}$  complex. The small values for both  $IS$  and  $\Delta E_{\text{Q}}$  for  $[\text{LFe}^{\text{III}}]^-$  are somewhat unexpected for an intermediate-spin  $\text{Fe}^{\text{III}}$  ion.<sup>[24]</sup> Such a low

$IS$  value, which indicates a high electron density around the iron nucleus and a low quadrupole value, accounts for the asymmetry around the iron neighbors. This can be explained by the fact that the *meso*-alkyl groups of the porphyrinogen provide flattened tetrahedral cage around  $\text{Fe}^{\text{III}}$ . The steric crowding of the  $C-H$  bonds frustrates the axial coordination of the metal center. The  $C-H \cdots \text{metal}$  interaction imposes a coordination asymmetry that induces intramolecular  $C-H$  bond activation.<sup>[25]</sup> For instance, axial agostic interactions have been suggested to be present between the  $\text{Fe}^{\text{III}}$  center and the remote methyl substituents of the porphyrinogen ring in  $[\text{Li}(\text{thf})_2][\text{L}'\text{Fe}^{\text{III}}]$ .<sup>[26]</sup>

The Mössbauer spectrum of the  $[\text{L}^{\Delta}\text{Fe}^{\text{II}}-\text{I}]^+$  cation ( $IS = 0.88$  mm/s,  $\Delta E_{\text{Q}} = 3.91$  mm/s) (Figure 6, middle) is very intriguing as well. The large quadrupole splitting clearly indicates a high-spin state,  $S_{\text{Fe}} = 2$ ;<sup>[27]</sup> this implies a higher symmetry around the iron neighbors. The Mössbauer spectrum of the dicationic entity  $[\text{L}^{\Delta}\text{Fe}^{\text{II}}-\text{MeCN}]^{2+}$  shows even a larger  $\Delta E_{\text{Q}}$  value, 4.66 mm/s.<sup>[8]</sup>

The Mössbauer spectrum of  $[\text{L}^{\Delta}\text{Fe}^{\text{II}}-\text{Br}][\text{Fe}^{\text{III}}\text{Br}_4]$  is complicated because of the presence of two iron centers in the molecule (Figure 6, below). Because of the two iron centers, an asymmetrical signal arises; the spectrum for  $[\text{L}^{\Delta}\text{Fe}^{\text{II}}-\text{Br}]^+$  present a similar isomeric shift and  $\Delta E_{\text{Q}}$  value as observed with the  $[\text{L}^{\Delta}\text{Fe}^{\text{II}}-\text{I}]^+$  moiety. This result supports the presence of two noncommunicating iron centers present in the crystal lattice. Consistent with the reported value, the counteranion  $[\text{FeBr}_4]^-$  is presented as a high spin  $\text{Fe}^{\text{III}}$  ( $S_{\text{Fe}} = 5/2$ ) state ( $IS = 0.36$  mm/s,  $\Delta E_{\text{Q}} = 0.00$  mm/s).<sup>[28]</sup> Therefore, the main feature of the spectrum with the large quadrupole splitting is likely to be resulting from  $[\text{L}^{\Delta}\text{Fe}^{\text{II}}-\text{Br}]^+$ , the sharp singlet (although of possibly insufficient intensity) at ca. 0.40 mm/s is likely to be from the  $[\text{FeBr}_4]^-$  anion, and the broad unresolved feature may be an impurity or possibly unreacted  $[\text{Et}_4\text{N}][\text{LFe}^{\text{III}}]$ .

## Conclusions

Two new four-electron-oxidised, high-spin  $\text{Fe}^{\text{II}}$  porphodimethenes were synthesized and characterized. Such a reaction can be viewed as an induced electron-transfer reaction between the parent  $\text{Fe}^{\text{III}}$  porphyrinogen and the halogens, where both the ligand and the metal centers are participants in the multielectron redox process; this is unique in the literature. Compound **1** shows an extended two-dimensional, solid-state structure that comprises porphodimethene cation and triiodide anion chain columns in a 1:1 ratio, which are packed alternately. The redox potentials of the reversible  $\text{Fe}^{\text{III/II}}$  couples are one volt more positive than that for a typical heme cofactor. Finally, the oxidation states and the spin states of the square-pyramidal  $\text{Fe}^{\text{II}}$  and square-planar  $\text{Fe}^{\text{III}}$  complexes were afforded by Mössbauer characterization.

## Experimental Section

**Materials and Physical Methods:** All reactions and manipulations were performed under a pure argon atmosphere by using modified Schlenk and vacuum-line techniques. Solvents, pyrrole, and cyclo-



hexanone were obtained from S. D. Fine Chemicals Ltd., India, and they were purified and dried before use by standard methods. Et<sub>4</sub>NCl, iodine, and bromine were obtained from Acros Organics. The ligand 5,10,15,20 tetrakis(cyclohexyl)porphyrinogen (L) was synthesized as reported earlier.<sup>[29]</sup> The lithium salt of the ligand was synthesized by using a standard procedure.<sup>[30]</sup> The parent complex [Et<sub>4</sub>N][LFe<sup>III</sup>] was prepared from our earlier reported procedure.<sup>[5]</sup> Electronic absorption spectra were recorded with a USB 2000 (Ocean Optics Inc.) UV/Vis spectrophotometer equipped with fiber optics. Infrared spectra were recorded on a Bruker Vertex 70 FTIR spectrophotometer as pressed KBr disks. Analysis for carbon, hydrogen, and nitrogen were carried with a Perkin–Elmer 2400 micro-analyser. Cyclic voltammograms were recorded with a BASi Epsilon EC bioanalytical systems Inc instrument, with a glassy carbon electrode as the working electrode, Pt wire as the auxiliary electrode, and an Ag/AgCl electrode as the reference electrode. All electrochemical experiments were performed under an argon atmosphere at 298 K. Potentials are referenced against internal ferrocene (Fc) and are reported relative to the Ag/AgCl electrode [ $E_{1/2}(\text{Fc}^+/\text{Fc}) = +0.49$  V vs. Ag/AgCl]. The cyclic voltammograms and differential pulse voltammograms (DPV) were measured with 0.1 M Bu<sub>4</sub>NPF<sub>6</sub> as the supporting electrolyte in CH<sub>3</sub>CN. A scan rate of 100 mV/s was employed.

**Mössbauer Spectroscopy:** Mössbauer spectra were recorded by using a conventional constant acceleration Mössbauer spectrometer (Wissenschaftliche Elektronik GmbH) with a <sup>57</sup>Co in Rh matrix as the Mössbauer source. The Doppler velocity was varied from –12.5 mm/s to +12.5 mm/s to cover the entire energy range corresponding to the magnetically split Mössbauer spectrum. The absorbers for Mössbauer spectroscopy were prepared from finely ground powder by pressing it in a copper ring with a diameter of 12 mm and by fixing the open ends with transparent tapes. Calibration spectra with natural iron foil were taken before and after each measurement at 298 K. Discrete doublets and hexaplets with Lorentzian peaks were fitted to the spectra by using a least-squares code developed at the Indian Institute of Technology, Kanpur, India. The isomer shift and the quadrupole splitting have an uncertainty of about 0.04 mm/s, whereas the hyperfine field has an uncertainty of 1 kOe.

**X-ray Crystal-Structure Determination of 1 and 2:** Suitable single crystals of **1** and **2** with dimensions of 0.30 × 0.30 × 0.15 mm and 0.25 × 0.20 × 0.15 mm, respectively, were selected for indexing and the collection of intensity data. Measurements were performed with graphite-monochromatized Mo-*K*<sub>α</sub> radiation ( $\lambda = 0.71073$  Å) on a Nonius Kappa CCD diffractometer. The unit cell parameters and crystal-orientation matrices were determined for two complexes by least-squares refinements of all reflections. The intensity data were corrected for Lorentz and polarization effects, and an empirical absorption correction was also employed by using the SAINT program.<sup>[31]</sup> Data were collected by applying the condition  $I > 2\sigma(I)$ . Intensity data were collected at 100(2) K within the limits  $0.95^\circ < \theta < 28.30^\circ$  for **1** and  $0.94^\circ < \theta < 28.42^\circ$  for **2**. All these structures were solved by direct methods and followed by successive Fourier and difference Fourier syntheses. Full-matrix least-squares refinements on  $F^2$  were carried out by using SHELXL-97 with anisotropic displacement parameters for all non-hydrogen atoms. Hydrogen atoms were constrained to ride on the respective carbon or nitrogen atoms with isotropic displacement parameters equal to 1.2 times the equivalent isotropic displacement of their parent atom in all cases. Complex neutral atom scattering factors were used throughout for all cases. All calculations were carried out by using the programs SHELXS 97,<sup>[32a]</sup> SHELXL97,<sup>[32b]</sup> PLATON 99,<sup>[33a]</sup> and ORTEP-3.<sup>[33b]</sup> The figures were generated by using the Dia-

mond 3.1e program. Details of the structure determinations are given in Table 2. CCDC-291418 (for **1**) and -761286 (for **2**) contain the supplementary crystallographic data for this paper. These data can be obtained free of charge from The Cambridge Crystallographic Data Centre via [www.ccdc.cam.ac.uk/data\\_request/cif](http://www.ccdc.cam.ac.uk/data_request/cif).

Table 2. Crystallographic data and structure refinement for **1** and **2**.

	<b>1</b>	<b>2</b>
Empirical formula	C <sub>46</sub> H <sub>60</sub> Cl <sub>4</sub> FeI <sub>6</sub> N <sub>4</sub>	C <sub>46</sub> H <sub>60</sub> Br <sub>5</sub> Fe <sub>2</sub> N <sub>4</sub> O <sub>2</sub>
$M_r$	1698.83	1315.35
Crystal system	triclinic	orthorhombic
Space group	$P\bar{1}$	$P\bar{1}$
$a$ (Å)	11.619(5)	13.2905(2)
$b$ (Å)	12.808(5)	24.1141(4)
$c$ (Å)	17.701(5)	15.0699(3)
$\alpha$ (°)	85.656(5)	90
$\beta$ (°)	73.024(5)	90
$\gamma$ (°)	71.922(5)	90
$V$ (Å <sup>3</sup> )	2394.7(15)	4829.73(14)
$Z$	2	4
$T$ (K)	100(2)	150(2)
$\lambda$ (Å)	0.71069	0.71073
$D_{\text{calcd.}}$ (g cm <sup>–3</sup> )	2.356	1.809
$\mu$ (mm <sup>–1</sup> )	4.707	5.076
$F(000)$	1594	2568
Goodness-of-fit	1.062	1.036
$R_1^{[a]}/wR_2^{[b]}$ [ $I > 2\sigma(I)$ ]	0.0357/0.0913	0.0285/0.0715
$R_1^{[a]}/wR_2^{[b]}$ (all data)	0.0473/0.0969	0.0443/0.0777

[a]  $R_1 = \sum ||F_o| - |F_c|| / \sum |F_o|$ . [b]  $wR_2 = \{\sum [w(F_o^2 - F_c^2)^2] / \sum [w(F_o^2)^2]\}^{1/2}$ .

**[<sup>LA</sup>Fe<sup>II</sup>–I]·I<sub>3</sub>·2CH<sub>2</sub>Cl<sub>2</sub> (**1**):** To a dcm solution of [Et<sub>4</sub>N][LFe<sup>III</sup>] (1.0 g, dissolved in 30 mL of dcm) was slowly added an iodine (1.0 g) solution in dcm (20 mL) over a period of 1 h, which resulted in a change in color of the solution to brown. The solution was filtered, and petroleum ether (40 mL, b.p. 40–60°) was added to the filtrate. On standing at 4 °C for 6 h, shining black crystals with a green hue appeared. These were filtered, washed with petroleum ether, and dried in vacuo to yield 1.4 g. (80%) of **1**. (–) ESI-MS (10% acetonitrile):  $m/z = 782.25$ . C<sub>46</sub>H<sub>60</sub>Cl<sub>4</sub>FeI<sub>6</sub>N<sub>4</sub> (1628.09): calcd. C 33.94, H 3.71, N 3.44; found C 33.53, H 3.63, N 3.67.

**[<sup>LA</sup>Fe<sup>II</sup>–Br][Fe<sup>III</sup>Br<sub>4</sub>]·2(CH<sub>3</sub>)<sub>2</sub>CO (**2**):** To a dcm solution of [Et<sub>4</sub>N][LFe<sup>III</sup>] (1.0 g, dissolved in 30 mL of dcm), was slowly added a bromine (1.0 g) solution in CCl<sub>4</sub> (20 mL) over a period of 3 h, which resulted in a change in color of the solution to deep brown. The solution was filtered and petroleum ether (40 mL) was added to the filtrate and kept at 4 °C for half an hour. A microcrystalline solid was collected by using G-3 frit and redissolved in acetone and layered with petroleum ether. On standing at 4 °C for 2 d shining bright red crystals appeared. These were filtered, washed with petroleum ether, and dried in vacuo. Yield 0.5 g (35%) of **2**. (–) ESI-MS (100% acetonitrile):  $m/z = 734.26$ . C<sub>46</sub>H<sub>60</sub>Br<sub>5</sub>Fe<sub>2</sub>N<sub>4</sub>O<sub>2</sub> (1212.22): calcd. C 45.58, H 4.99, N 4.62; found C 45.13, H 4.67, N 4.17.

## Acknowledgments

D. B. acknowledges the Indian Institute of Technology, Kanpur, for providing a Senior Teaching Fellowship, and S. S. is grateful for research funding from the Department of Science and Technology, New Delhi, (SR/S1/IC-09/2006).

[1] a) C. K. Jørgenson in *Oxidation Number and Oxidation States*, Springer, Heidelberg, Germany, 1969; b) A. H. Maki, N. Ed-



- elstein, A. Davison, R. H. Holm, *J. Am. Chem. Soc.* **1964**, *86*, 2799–2805; c) F. Thomas, *Eur. J. Inorg. Chem.* **2007**, 2379–2404; d) J. Bollinger, J. Martin, C. Krebs, *J. Inorg. Biochem.* **2006**, *100*, 586–605; e) H.-P. Hersleth, U. Ryde, P. Rydberg, C. H. Gorbitz, K. K. Andersson, *J. Inorg. Biochem.* **2006**, *100*, 460–476; f) B. A. Jazdzewski, W. B. Tolman, *Coord. Chem. Rev.* **2000**, *200–202*, 633–685; g) W. Kaim, *Dalton Trans.* **2003**, 761–768; h) M. D. Ward, J. A. McCleverty, *J. Chem. Soc., Dalton Trans.* **2002**, 275–288; i) W. Kaim, B. Schwederski, *Pure Appl. Chem.* **2004**, *76*, 351–3364.
- [2] D. Bhattacharya, S. Maji, K. Pal, S. Sarkar, *Inorg. Chem.* **2008**, *47*, 5036–5038.
- [3] a) M. R. Ringenberg, S. L. Kokatam, Z. M. Heiden, T. B. Rauchfuss, *J. Am. Chem. Soc.* **2008**, *130*, 788–789; b) C. J. Rolle, K. I. Hardcastle, J. D. Soper, *Inorg. Chem.* **2008**, *47*, 1892–1894; c) M. W. Bouwkamp, A. C. Bowman, E. Lobkovsky, P. J. Chirik, *J. Am. Chem. Soc.* **2006**, *128*, 13340–13341; d) C. Stanciu, M. E. Jones, P. E. Fanwick, M. M. Abu-Omar, *J. Am. Chem. Soc.* **2007**, *129*, 12400–12401; e) M. R. Haneline, A. F. Heyduk, *J. Am. Chem. Soc.* **2006**, *128*, 8410–8411; f) P. Chaudhuri, C. N. Verani, E. Bill, E. Bothe, T. Weyhermüller, K. Weighardt, *J. Am. Chem. Soc.* **2001**, *123*, 2213–2223; g) K. Chlopek, E. Bill, T. W. Ueller, K. Weighardt, *Inorg. Chem.* **2005**, *44*, 7087–7098; h) A. Mahammed, Z. Gross, *J. Am. Chem. Soc.* **2005**, *127*, 2883–2887; i) C. A. Joseph, P. C. Ford, *J. Am. Chem. Soc.* **2005**, *127*, 6737–6743.
- [4] a) S. J. Lippard, J. M. Berg in *Principles of Bioinorganic Chemistry*, University Science Books, Mill Valley, CA, **1994**; b) A. X. Trautwein, E. Bill, E. L. Bominaar, H. Winkler, *Struct. Bonding (Berlin)* **1991**, *78*, 71; c) J. Silver (Ed.), *Chemistry of Iron*, Blackie Academic & Professional, Glasgow, UK, **1993**.
- [5] D. Bhattacharya, S. Dey, S. Maji, K. Pal, S. Sarkar, *Inorg. Chem.* **2005**, *44*, 7699–7701.
- [6] a) G. H. Elder in *Iron in Biochemistry and Medicine II* (Eds.: A. Jacobs, M. Worwood), Academic Press, London, **1980**, pp. 245; b) R. Huszánk, O. Horváth, *Chem. Commun.* **2005**, *2*, 224–226.
- [7] a) C. Floriani, R. Floriani-Moro in *The Porphyrin Handbook* (Eds.: K. M. Kadish, K. M. Smith, R. Guilard), Academic Press, New York, **2000**, vol. 3, pp. 389; b) J. Judd, D. Jacoby, C. Floriani, A. Chiesi-Villa, C. Rizzoli, *Inorg. Chem.* **1992**, *31*, 1306–1308.
- [8] J. Bachmann, D. G. Nocera, *J. Am. Chem. Soc.* **2005**, *127*, 4730–4743.
- [9] S. De Angelis, E. Solari, C. Floriani, A. Chiesi-Villa, C. Rizzoli, *J. Am. Chem. Soc.* **1994**, *116*, 5702–5713.
- [10] J. Bachmann, J. M. Hodgkiss, E. R. Young, D. G. Nocera, *Inorg. Chem.* **2007**, *46*, 607–609.
- [11] D. Bhattacharya, S. Maji, K. Pal, S. Sarkar, *Inorg. Chem.* **2009**, *48*, 6362–6370.
- [12] a) H. Taube in *Electron Transfer Reaction of Complex Ions in Solution*, Academic Press, New York and London, **1970**; b) E. I. Stiefel, R. R. Chianelli in *Nitrogen Fixation* (Eds.: A. Müller, W. E. Newton), Plenum Press, New York, **1983**, pp. 341; c) S. S. Cohen, E. I. Stiefel, *Inorg. Chem.* **1985**, *24*, 4657–4662; d) S. Sarkar, M. A. Ansari, *J. Chem. Soc., Chem. Commun.* **1986**, 324–325; e) M. A. Ansari, J. Chandrasekharan, S. Sarkar, *Inorg. Chem.* **1988**, *27*, 763–764.
- [13] a) J. A. R. Navarro, B. Lippert, *Coord. Chem. Rev.* **2001**, *222*, 219–250; b) S. Y. Yu, H. Huang, H. B. Liu, Z. N. Chen, R. Zhang, M. Fujita, *Angew. Chem. Int. Ed.* **2003**, *42*, 686–690; c) M. J. Rauterkras, B. Krebs, *Angew. Chem. Int. Ed.* **2004**, *43*, 1300–1303.
- [14] a) S. Dey, K. Pal, S. Sarkar, *Tett. Lett.* **2007**, *48*, 5481–5485; b) P. A. Gale, P. Anzenbacher Jr., J. L. Sessler, *Coord. Chem. Rev.* **2001**, *222*, 57–102; c) P. A. Gale, J. L. Sessler, V. Kral, V. Lynch, *J. Am. Chem. Soc.* **1996**, *118*, 5140–5141; d) D.-W. Yoon, H. Hwang, C.-H. Lee, *Angew. Chem. Int. Ed.* **2002**, *41*, 1757–1759; e) K. A. Nielsen, J. O. Jeppesen, E. Levillain, J. Becher, *Angew. Chem. Int. Ed.* **2003**, *42*, 187–191.
- [15] J. Janczak, *Inorg. Chem.* **2003**, *42*, 3549–3558.
- [16] a) A. I. Kitaigorodskii, T. L. Khotsyanova, Y. T. Struchkov, *Zh. Fiz. Khim.* **1953**, *27*, 780–781; b) F. Van Bolhuis, B. P. Kostner, T. Migchelsen, *Acta Crystallogr.* **1967**, *23*, 90–91.
- [17] Structures of Interhalogen Compounds and Polyhalides: E. H. Wiebenga, E. E. Havigha, K. H. Boswijk, *Adv. Inorg. Chem. Radiochem.* **1961**, *3*, 133–169.
- [18] a) T.-Y. Dong, C.-C. Schei, M.-Y. Hwang, T.-Y. Lee, S.-K. Yeh, Y.-S. Wen, *Organometallics* **1992**, *11*, 573–582; b) T.-Y. Dong, C.-K. Chang, S.-H. Lee, L.-L. Lai, M. Y.-N. Chiang, K.-J. Lin, *Organometallics* **1997**, *16*, 5816–5825.
- [19] T.-Y. Dong, C.-H. Huang, C.-K. Chang, H.-C. Hsieh, S.-M. Peng, G.-H. Lee, *Organometallics* **1995**, *14*, 1776–1785.
- [20] a) S. G. Mayhew, D. Petering, G. Palmer, G. P. Foust, *J. Biol. Chem.* **1969**, *244*, 2830–2835; b) G. Backes, Y. Mino, T. M. Loehr, T. E. Meyer, M. A. Cusanovich, W. V. Sweeney, E. T. Adman, S.-L. Joann, *J. Am. Chem. Soc.* **1991**, *113*, 2055–2064.
- [21] a) P. Vogel, E. W. Knapp, *J. Biol. Chem.* **2003**, *278*, 51993–51997; b) R. J. Kassner, *Proc. Natl. Acad. Sci. USA* **1972**, *69*, 2263–2267.
- [22] M. M. Khusniyarov, E. Bill, T. Weyhermüller, E. Bothe, K. Harms, J. Sundermeyer, K. Wieghardt, *Chem. Eur. J.* **2008**, *14*, 7608–7622.
- [23] P. J. Alonso, A. B. Arauzo, J. Fornies, M. A. Garcia-Monforte, A. Martín, J. I. Martínez, B. Menjón, C. Rillo, J. J. Sáiz-Garitaonandia, *Angew. Chem.* **2006**, *45*, 6707–6711.
- [24] A. S. Attia, M. F. El-Shahat, *Polyhedron* **2007**, *26*, 791–796.
- [25] a) M. A. Baldo, D. F. O'Brien, Y. You, A. Shoustikov, S. Sibley, M. E. Thompson, S. R. Forrest, *Nature* **1998**, *395*, 151–154; b) M. A. Baldo, M. E. Thompson, S. R. Forrest, *Nature* **2000**, *403*, 750–753; c) S. Trofimenko, *Inorg. Chem.* **1973**, *12*, 1215–1221; d) D. Jacoby, C. Floriani, A. Chiesi-Villa, C. Rizzoli, *J. Chem. Soc., Chem. Commun.* **1991**, 790–792.
- [26] D. Jacoby, C. Floriani, A. Chiesi-Villa, C. Rizzoli, *J. Chem. Soc., Chem. Commun.* **1991**, 220–222.
- [27] a) N. Muresan, C. C. Lu, M. Ghosh, J. C. Peters, M. Abe, L. M. Henling, T. Weyhermüller, E. Bill, K. Wieghardt, *Inorg. Chem.* **2008**, *47*, 4579–4590; b) N. Habib, M. K. Ellison, B. Shaevitz, G. P. Gupta, W. R. Scheidt, *Inorg. Chem.* **2006**, *45*, 5284–5290; c) P. Ghosh, K. Stobie, E. Bill, E. Bothe, T. Weyhermüller, M. D. Ward, J. A. McCleverty, K. Wieghardt, *Inorg. Chem.* **2007**, *46*, 522–532.
- [28] a) C. A. Clausen, M. L. Good, *Inorg. Chem.* **1970**, *9*, 220–223; b) N. N. Greenwood, T. C. Gibb in *Mossbauer Spectroscopy*, Chapman and Hall, London, **1971**.
- [29] S. Dey, K. Pal, S. Sarkar, *Tetrahedron Lett.* **2006**, *47*, 5851–5854.
- [30] a) D. Jacoby, C. Floriani, A. Chiesi-Villa, C. Rizzoli, *J. Am. Chem. Soc.* **1993**, *115*, 3595–3602; b) R. Crescenzi, E. Solari, C. Floriani, A. Chiesi-Villa, C. Rizzoli, *J. Am. Chem. Soc.* **1999**, *121*, 1695–1706.
- [31] Bruker-Nonius, APEX-II and SAINT-Plus, Bruker AXS Inc., Madison, Wisconsin, USA, **2004**.
- [32] a) G. M. Sceldrick, *SHELXS97, Program for Solution of Crystal Structure*; University of Göttingen, Göttingen, Germany, **1997**; b) G. M. Sceldrick, *SHELXL97, Program for Crystal Structure Analysis (Release 97–2)*, University of Göttingen, Göttingen, Germany, **1997**.
- [33] a) A. L. Spek, *J. Appl. Crystallogr.* **2003**, *36*, 7–13; b) L. J. Farugia, *J. Appl. Crystallogr.* **1997**, *30*, 565.

Received: March 8, 2010  
Published Online: May 19, 2010

Topotactic Migration of Cationic Vacancies in  $\text{La}_{1-t}\text{Mn}_{1-t}\text{O}_3$ Raquel Cortés-Gil,<sup>[a]</sup> José M. Alonso,<sup>[b]</sup> M. Luisa Ruiz-González,<sup>[a]</sup> and José M. González-Calbet<sup>\*[a]</sup>**Keywords:** Lanthanum / Manganese / Perovskite / Microscopy / Surface chemistry

A reversible topotactic oxidizing–reducing process has been clearly evidenced in the annealing treatment followed to stabilize rhombohedral and orthorhombic  $\text{La}_{1-t}\text{Mn}_{1-t}\text{O}_3$  ( $0.016 \leq t \leq 0.038$ ) samples. The study of the surface evolution followed by characterization by scanning electron microscopy (SEM) and atomic force microscopy (AFM) gives

evidence for a diffusion mechanism of La and Mn cations through the grain boundaries which provides a fast pathway in the perovskite related compound; however, contrary to theoretical predictions, the overall cationic ratio (La:Mn 1:1) is kept.

## Introduction

$\text{LaMnO}_{3+\delta}$  systems exhibit a rich and complex chemistry showing unique behaviour among the  $\text{LaMO}_3$  (M = transition metal) perovskite compounds. Most of the transition metals are able to adopt several oxidation states, however  $\text{LaMnO}_3$  is the only compound of this series that shows a noteworthy oxygen excess. This has motivated extensive research moved by the need to increase basic knowledge as well as to find potential applications, such as catalysis, solid oxide fuel cells, oxygen sensors and, more recently, colossal magnetoresistance behaviour, based on nonstoichiometric phenomena.

The crystallochemical behaviour of  $\text{LaMnO}_{3+\delta}$  is complex and different approaches have been described. Early attempts to prepare  $\text{LaMnO}_3$  perovskite showed that it was oxidized when heated in air, requiring lower oxygen activities.<sup>[1]</sup> Although traditionally formulated as  $\text{LaMnO}_{3+\delta}$ , it is acknowledged that the perovskite structure cannot accept additional oxygen as interstitial due to size limitations.<sup>[2]</sup> Preliminary studies indicate the presence of La and Mn vacancies in a manganite formulated as  $\text{LaMnO}_{3.12}$ .<sup>[3]</sup> However, more recently, a detailed study by means of neutron diffraction coupled to high resolution electron microscopy and density measurements concluded that the defect chemistry of  $\text{LaMnO}_{3+\delta}$  should be described as equal numbers of La and Mn vacancies which are randomly distributed.<sup>[4]</sup> This disordered distribution contrasts to the related oxygen deficient  $\text{LaMnO}_{3-x}$  system, in which clusters of defects<sup>[4]</sup>

as well as new ordered superstructures,<sup>[5,6]</sup> have been detected due to short and long-range ordering. Oxygen vacancy ordering can be accommodated through the formation of new superlattices as, for instance,  $\text{LaMnO}_{2.75}$ ,<sup>[6]</sup> whereas symmetry changes have been described as a function of  $\delta$  values.  $\text{LaMnO}_3$  perovskite crystallizes with orthorhombic symmetry (S.G. *Pnma*, No. 62) while for higher values ( $\delta \geq 0.1$ ) rhombohedral symmetry has been recorded (S.G.  $R\bar{3}c$ , No. 167).

Since defects on  $\text{LaMnO}_3$  are Schottky-type rather than interstitials, the oxidative process provokes the appearance of  $\text{Mn}^{4+}$  and then the coexistence of  $\text{Mn}^{3+}$  and  $\text{Mn}^{4+}$ , which is related to the interesting magnetic and transport properties of this system.<sup>[7]</sup> This behaviour suggests that the oxidation and reduction processes in the so-called  $\text{LaMnO}_{3+\delta}$ , better formulated as  $\text{La}_{1-t}\text{Mn}_{1-t}\text{O}_3$  [ $t = \delta/(3+\delta)$ ], must be controlled by the presence of cationic vacancies. Diffusion processes in perovskites have been traditionally considered as being due to oxygen ion vacancies<sup>[8]</sup> as oxygen mobility is, in principle, faster than cationic mobility. Nevertheless, it should be noted that ion migration is a complex process influenced by many different factors such as temperature, ion size, vacancy concentration and higher order defects. In addition, extended defects, for instance grain boundaries, seem to play a prominent role since atoms in grain boundaries are known to be much more mobile than in the lattice.

The aim of this work is to study, by means of SEM and AFM techniques, the evolution of the surface of polycrystalline  $\text{La}_{1-t}\text{Mn}_{1-t}\text{O}_3$  as a function of cationic vacancy concentration induced by different thermal treatments.

## Results and Discussion

The starting sample, heated in air up to 1400 °C and labelled as A in Figure 1, is assigned as an orthorhombic

[a] Departamento de Química Inorgánica, Facultad de Químicas, Universidad Complutense, 28040 Madrid, Spain  
Fax: +34-91-3944352  
E-mail: jgcalbet@quim.ucm.es

[b] Instituto de Magnetismo Aplicado, UCM-CSIC-ADIF, Las Rozas, P. O. Box 155, 28230 Madrid, Spain

Supporting information for this article is available on the WWW under <http://dx.doi.org/10.1002/ejic.201000086>.

perovskite (S.G.  $Pnma$ ) according to previous results.<sup>[9]</sup> Annealing of this sample in air at 900 °C is accompanied by an orthorhombic–rhombohedral (S.G.  $R\bar{3}c$ , sample B) transition. After treatment in air at 1400 °C (sample C), the original orthorhombic symmetry is recovered. Cationic composition analysis indicates a La:Mn 1:1 ratio in all three samples. Iodometric analysis shows a 10%  $\text{Mn}^{4+}$  and 90%  $\text{Mn}^{3+}$  composition for both orthorhombic samples A and C. Annealing at 900 °C provokes an oxidation process (seen in sample B), which is reflected in the increase of the  $\text{Mn}^{4+}$  content to 24%. As a consequence, X-ray diffraction data show that the lattice volume (see Table 1) decreases as the  $\text{Mn}^{4+}$  concentration increases.<sup>[10]</sup> In parallel, thermogravimetric analysis indicates that sample B suffers a weight loss higher than that of samples A and C. As there is no interstitial oxygen, this behaviour can be only understood if the above samples exhibit different cationic vacancy concentrations. On the basis of both the Mn oxidation state and the La:Mn 1:1 ratio, and taking into account that, in all cases, the anionic sublattice is complete, samples A and C have a composition of  $\text{La}_{0.984}\text{Mn}_{0.984}\text{O}_3$ , whereas sample B can be formulated as  $\text{La}_{0.962}\text{Mn}_{0.962}\text{O}_3$ . At this point, it is worth stressing that the starting concentration of cationic vacancies is restored through an oxidation and reduction process.

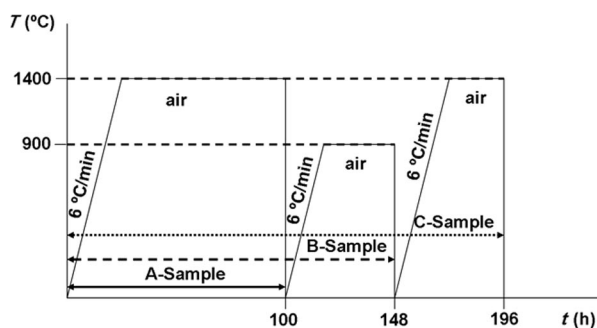


Figure 1. Schematic representation of the heating treatments undertaken to obtain samples A, B and C.

Table 1. Compositional characteristics and cell volume of  $\text{La}_{1-x}\text{Mn}_{1-x}\text{O}_3$  pellet as a function of different annealing temperatures.

Treatment	Composition	Cell volume [Å <sup>3</sup> ]	$\text{Mn}^{4+}$ Conc. (%)	$\text{Mn}^{3+}$ Conc. (%)
100 h, 1400 °C	$\text{La}_{0.984}\text{Mn}_{0.984}\text{O}_3$ (sample A)	60.405(6)	10	90
+ 48 h, 900 °C	$\text{La}_{0.962}\text{Mn}_{0.962}\text{O}_3$ (sample B)	59.972(8)	24	76
++ 48 h, 1400 °C	$\text{La}_{0.984}\text{Mn}_{0.984}\text{O}_3$ (sample C)	60.405(6)	10	90

In order to characterize the surface, a SEM study was performed. Figure 2 (parts a–c) shows representative SEM micrographs corresponding to samples A, B and C. From these images, the increase of the grain size at the lowest annealing temperature, 900 °C (sample B), is observed (Figure 2, b). The size enhancement is accompanied by an increase in the cationic vacancy concentration, which is in agreement with the composition analysis. Moreover, the

surfaces of samples A and C are very similar (see parts a and c in Figure 2). This fact underlies the importance of the temperature effect, independent of the pathway followed and, together with the composition study, suggests a reversible oxidation–reduction process through the 1400 → 900 → 1400 °C consecutive treatments as the initial surface is recovered at 1400 °C.

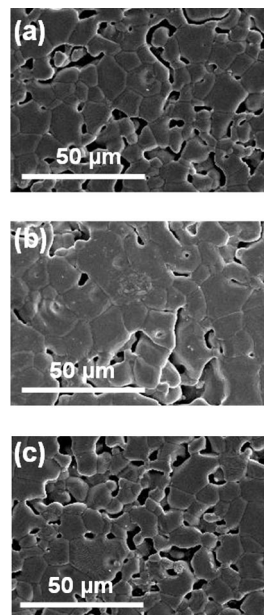


Figure 2. SEM micrographs of the  $\text{La}_{1-x}\text{Mn}_{1-x}\text{O}_3$  pellet after different heating processes: (a) A, (b) B and (c) C treatments (see Figure 1).

In order to investigate the composition on the pellet surface, analysis by X-ray energy dispersive spectroscopy (XEDS) was carried out. In all the three cases the La:Mn 1:1 ratio was kept. Furthermore, the surface map obtained by this characterization suggests a homogeneous La:Mn distribution. This analysis supports the absence of La or Mn rich phases in agreement with XRD data. This result contrasts with the predictions of Souza et al that suggest a higher tendency for La vacancy generation on the surface.<sup>[11]</sup>

In order to shed some light on the surface grain growth mechanism in this material, an AFM study was performed. Figure 3 depicts two AFM images corresponding to samples B and C. Differences concerning the grain boundaries as well as the size and shape of the grains are evident. In fact,  $\text{La}_{0.962}\text{Mn}_{0.962}\text{O}_3$  (sample B) exhibits a large grain size, in accordance with the SEM study, with polyhedral shape and flat boundaries including small inhomogeneities. On the contrary,  $\text{La}_{0.984}\text{Mn}_{0.984}\text{O}_3$  (sample C) shows a smaller grain size with a rounded and more homogeneous surface that is also in agreement with the SEM study. A more detailed topographic study was carried out by analyzing the surface height along and across the grains (Figure 4, a–f). Parts b and c of Figure 4 display the topographic changes found in two crystalline grains corresponding to  $\text{La}_{0.984}\text{Mn}_{0.984}\text{O}_3$  along the lines drawn in Figure 4 (a).



Level differences of about 200 nm were seen in both cases. Topographic analysis across some edges of different grains was carried out on the framed area in Figure 4 (a), as shown in the enlarged image d in Figure 4. In this case, sharper depth differences between the grains are evident (Figure 4, e) rising to the value of 650 nm. A 3D image corresponding to the area shown in part a of Figure 4 was generated (Figure 4, f) clearly showing the rounded morphology characteristic of  $\text{La}_{0.984}\text{Mn}_{0.984}\text{O}_3$ .

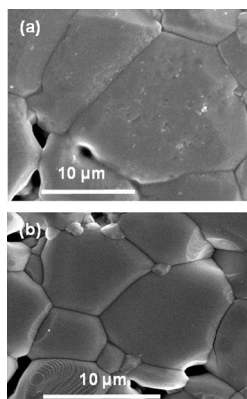


Figure 3. AFM micrographs corresponding to (a)  $\text{La}_{0.962}\text{Mn}_{0.962}\text{O}_3$  and (b)  $\text{La}_{0.984}\text{Mn}_{0.984}\text{O}_3$ .

Following the same procedure, a different topography of the surface has been found for  $\text{La}_{0.962}\text{Mn}_{0.962}\text{O}_3$  (sample B), after annealing  $\text{La}_{0.984}\text{Mn}_{0.984}\text{O}_3$  at 900 °C. The grains become flat with sharp edges (Figure 5, a). The topographic analysis along and across the grains (see lines marked in Figure 5, a) reveals a surface roughness of about 40 nm in each case (Figure 5, b–c). It is worth noting that the depth differences are of one order of magnitude less than those of  $\text{La}_{0.984}\text{Mn}_{0.984}\text{O}_3$ . Taking into account the lattice parameter of the cubic perovskite subcell (0.38 nm) it can be estimated that the grain boundaries in  $\text{La}_{0.962}\text{Mn}_{0.962}\text{O}_3$  are filled with around 1600 new perovskite unit cells.

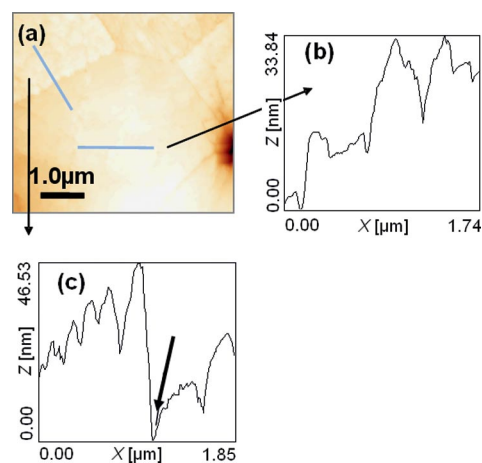


Figure 5. (a) AFM image corresponding to  $\text{La}_{0.962}\text{Mn}_{0.962}\text{O}_3$ . (b), (c) Surface profiles along the plotted areas in (a).

After final annealing at 1400 °C (sample C), the initial morphology is recovered as observed in Figure 6. The rounded morphology and the characteristic roughness, of the order of hundreds of nanometres, becomes evident (Figure 6, b–c). Figure 6 (d) shows the enlarged image corresponding to the framed area in Figure 6 (a) where the topographic analysis reveals similar depth values between the grains.

In summary, sample A,  $\text{La}_{0.984}\text{Mn}_{0.984}\text{O}_3$ , consists of rounded grains. After the same pellet is annealed and quenched at 900 °C, the surface is modified (sample B) exhibiting flat grains of  $\text{La}_{0.962}\text{Mn}_{0.962}\text{O}_3$  composition where the grain boundaries are filled. These experimental observations allow the proposal of a diffusion mechanism through the grain boundaries which provide fast cation diffusion paths in the perovskite related material. Under more oxidizing conditions (900 °C), La and Mn cations migrate from the bulk towards the crystal surface in order to react with oxygen and create new perovskite lattices on the surface.

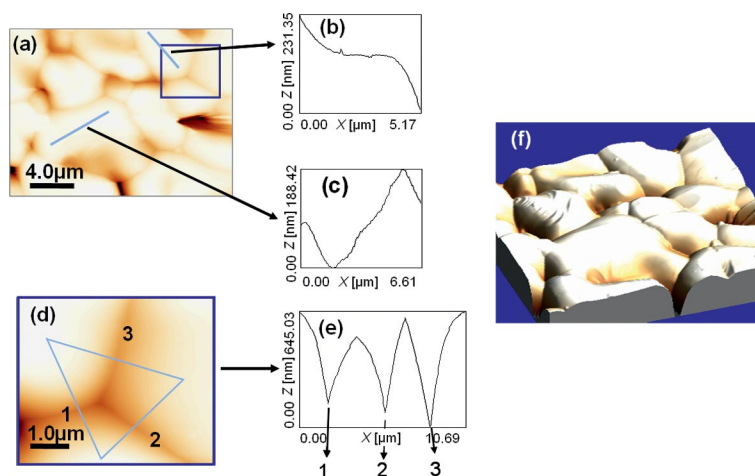


Figure 4. (a) AFM image corresponding to  $\text{La}_{0.984}\text{Mn}_{0.984}\text{O}_3$ ; (b), (c) surface profiles along the areas plotted in (a); (d) enlarged image of the framed area in (a); (e) analysis of the grains depth in (d); (f) detailed three dimensional representation of a  $\text{La}_{0.984}\text{Mn}_{0.984}\text{O}_3$  surface corresponding to the micrograph (a).



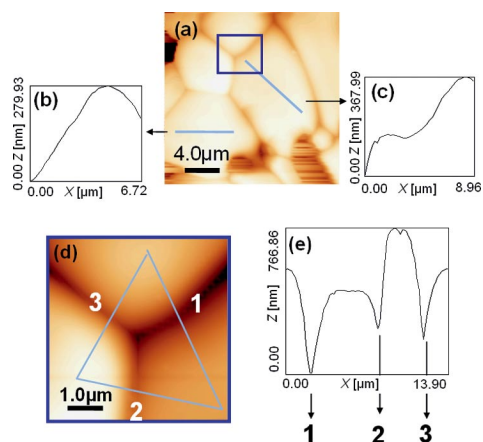


Figure 6. (a) AFM image corresponding to  $\text{La}_{0.984}\text{Mn}_{0.984}\text{O}_3$ . (b), (c) Surface profiles along the plotted areas in (a); (d) enlarged image of the framed area in (a), and (e) analysis of the grain depths.

Identical numbers of La and Mn cation vacancies are formed and randomly distributed over the lattice, ensuring that the La:Mn 1:1 ratio is always kept. This is the reason why at 900 °C the sample exhibits a higher cationic vacancy concentration compared to that at 1400 °C, despite exhibiting the same La:Mn ratio and oxygen content. As the final annealing at 1400 °C reinstates the original composition, the cationic diffusion process must be reversible. At this temperature the cationic vacancy concentration decreases as a consequence of La and Mn migration from the crystal surface to the bulk material returning to the initial  $\text{La}_{0.984}\text{Mn}_{0.984}\text{O}_3$  composition. The above process is depicted schematically in Figure 7.

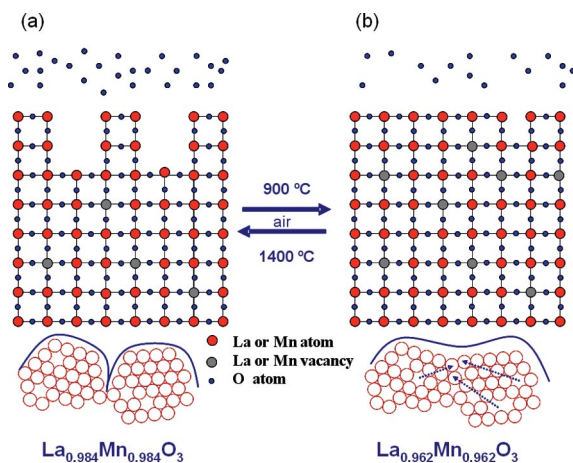


Figure 7. Schematic representation of the mechanism proposed for surface evolution as a function of the annealing temperature and sample composition. (a) Surface corresponding to  $\text{La}_{0.984}\text{Mn}_{0.984}\text{O}_3$  sample which exhibits depth grain boundaries (b) surface corresponding to  $\text{La}_{0.962}\text{Mn}_{0.962}\text{O}_3$  showing the filling of the grain boundaries as a consequence of the cationic diffusion at 900 °C. The reversible character of the process is indicated.

The cationic diffusion process has also been described in other related perovskite oxides.<sup>[12,13]</sup> The annealing process used to stabilize  $\text{SrTiO}_3$  in oxidative conditions gives rise to the formation of Sr-rich phases of the so-called Ruddlesden–

Popper type ( $\text{Sr}_{n+1}\text{Ti}_n\text{O}_{3n+1}$ ) and various forms of titanium oxide on the surface.<sup>[12]</sup> Phase segregation is also produced under reducing conditions giving rise to Ti-rich phases (such as  $\text{TiO}$  and  $\text{TiO}_2$ ). Obviously, the surface exhibits a drastically different composition compared to the bulk. Hence, although oxidizing and reducing processes in  $\text{SrTiO}_3$  and  $\text{La}_{0.984}\text{Mn}_{0.984}\text{O}_3$  are both tuned by the cationic diffusion, the final result is different since new chemical phases appear on the  $\text{SrTiO}_3$  surface while oxidation in  $\text{La}_{0.984}\text{Mn}_{0.984}\text{O}_3$  and reduction in  $\text{La}_{0.962}\text{Mn}_{0.962}\text{O}_3$  proceed through a reversible topotactic pathway.

Theoretical studies suggest that orthorhombic and rhombohedral perovskites in the La-Mn-O system exhibit a tendency towards La vacancy formation over Mn vacancy formation.<sup>[11]</sup> Nevertheless, since secondary phases such as  $\text{Mn}_x\text{O}_y$ ,  $\text{La}_2\text{O}_3$  and  $\text{La}_2\text{MnO}_4$  were not detected, even after a careful inspection at a local level by means of transmission electron microscopy, and the composition analysis always indicates a La:Mn 1:1 ratio, it seems reasonable to assume that the cationic vacancy concentration is always the same in both sublattices. This is in agreement with previous studies by Van Roosmalen et al.<sup>[4]</sup> and Huang et al,<sup>[14]</sup> suggesting that La and Mn cationic migration, as well as La and Mn vacancies, must be coupled in spite of the different cationic size. In fact, Schulz et al<sup>[15]</sup> suggest that the cation diffusion coefficients in  $\text{La}_{0.9}\text{Sr}_{0.1}\text{Ga}_{0.9}\text{Mg}_{0.1}\text{O}_{2.9}$  are very similar for all types of cations investigated including A and B site cations that are strongly dependent on temperature, similar to the material studied here.

## Conclusions

The morphology of the  $\text{La}_{1-x}\text{Mn}_{1-x}\text{O}_3$  surface is clearly altered when the sample is treated under different annealing conditions. The evolution of this surface can be followed by means of SEM and AFM by successive annealing of the same pellet. The surface of the as prepared pellet at 1400 °C exhibits rounded grains with abrupt changes in depth between them. Annealing at 900 °C provides a more oxidizing atmosphere and new perovskite lattice is formed filling the holes between grains as a consequence of the migration of La and Mn through these pathways and further recombination with the oxygen at the surface. As a result, the depth between grains decreases and they become flat. Annealing at higher temperature, 1400 °C, provides more reducing conditions and the surface roughness is recovered suggesting that the inverse cation diffusion progresses from the surface to the bulk. Therefore, reduction and oxidation in  $\text{La}_{1-x}\text{Mn}_{1-x}\text{O}_3$  are reversible topotactic processes, as the perovskite skeleton is preserved, controlled by migration of La and Mn cations through the grain boundaries.

## Experimental Section

A sample of  $\text{LaMnO}_3$  (nominal composition) was prepared by heating stoichiometric amounts of  $\text{La}_2\text{O}_3$  and  $\text{MnO}_2$  in air at 1400 °C for 100 h with intermediate milling. The as prepared sam-

ple underwent two consecutive annealing processes in air for 48 h, the first at 900 °C and the second at 1400 °C. Each thermal treatment was followed by final quenching to room temperature. The X-ray diffraction study was carried out with a Philips X'Pert (Cu- $K_{\alpha}$  radiation) diffractometer. Cationic composition analysis was performed by means of XEDS. Oxidation states were determined by iodometric analysis, following Fyfe's method.<sup>[16]</sup> Oxygen content was inferred by thermogravimetric analysis with a Cahn D-200 electrobalance equipped with a furnace and a two-channel register, allowing the simultaneous detection of the weight loss and the reaction temperature. The sample was heated in a H<sub>2</sub> (200 mbar) and He (300 mbar) atmosphere up to 800 °C at a rate of 6 °C/min.

The surface study was carried out with SEM (JEOL JSM 6400) and AFM (Nanotec Tapping mode VSxM software) microscopes. For this study the sample was pressed into a pellet (2 mm height  $\times$  18 mm diameter) followed by metallographic grinding with 320  $\mu$ m grit SiC paper and subsequent polishing with diamond paste of 3  $\mu$ m, 1  $\mu$ m and 0.25  $\mu$ m. Once prepared, the pellet was treated under the same heating conditions than the powdered sample, as shown in Figure 1.

**Supporting Information** (see also the footnote on the first page of this article): XEDS surface maps corresponding to SEM micrographs of samples B and C. The lanthanum and manganese maps suggest a surface homogeneous cationic distribution for both samples.

## Acknowledgments

Financial support by the Ministerio de Ciencia e Innovación through Research Project No. MAT2007-61954 is acknowledged. Fruitful discussions with Dr. M. A. García and Mr. I. Carabias are also acknowledged.

- [1] A. Wold, R. J. Arnott, *J. Phys. Chem. Solids* **1959**, 9, 176–180.
- [2] E. O. Wollan, W. C. Koehler, *Phys. Rev.* **1955**, 100, 545–563.
- [3] B. C. Tofield, W. R. Scott, *J. Solid State Chem.* **1974**, 10, 183–194.
- [4] J. A. M. Van Roosmalen, E. H. P. Cordfunke, R. B. Helmholtz, H. W. Zandbergen, *J. Solid State Chem.* **1994**, 110, 100–105; J. A. M. Van Roosmalen, E. H. P. Cordfunke, R. B. Helmholtz, H. W. Zandbergen, *J. Solid State Chem.* **1994**, 110, 106–108; J. A. M. Van Roosmalen, E. H. P. Cordfunke, R. B. Helmholtz, H. W. Zandbergen, *J. Solid State Chem.* **1994**, 110, 109–112; J. A. M. Van Roosmalen, E. H. P. Cordfunke, R. B. Helmholtz, H. W. Zandbergen, *J. Solid State Chem.* **1994**, 110, 113–117.
- [5] F. Abbattista, M. Lucco-Borlera, *Ceram. Int.* **1981**, 7, 137–141.
- [6] M. L. Ruiz-González, R. Cortés-Gil, J. M. Alonso, A. Hernandez, M. Vallet-Regí, J. M. González-Calbet, *Chem. Mater.* **2006**, 18, 5756–5763.
- [7] F. J. Palomares, F. Pigazo, J. J. Romero, R. Cuadrado, A. Arroyo, M. A. García, A. Hernandez, R. Cortés-Gil, J. M. González-Calbet, M. Vallet-Regí, J. M. González, J. M. Alonso, *Appl. Phys.* **2006**, 99, 08A702.
- [8] M. S. Islam, M. C. R. A. Cherry Catlow, *J. Solid State Chem.* **1996**, 124, 230–237.
- [9] F. Prado, R. D. Sánchez, A. Caneiro, M. T. Causa, M. Tovar, *J. Solid State Chem.* **1999**, 146, 418–427.
- [10] R. D. Shannon, *Acta Crystallogr., Sect. A* **1976**, 32, 751–767.
- [11] R. A. de Souza, M. S. Islam, E. Ivers-Tiffée, *J. Mater. Chem.* **1999**, 9, 1621–1627.
- [12] K. Szot, W. Speier, *Phys. Rev. B* **1999**, 60, 5909–5926.
- [13] R. Shiozaki, K. Takenaka, Y. Sawaki, S. Sugai, *Phys. Rev. B* **2001**, 63, 184419(1)–184419(5).
- [14] Q. Huang, A. Santoro, J. W. Lynn, R. W. Erwin, J. A. Borchers, J. L. Peng, R. L. Greene, *Phys. Rev. B* **1997**, 55, 14987–14999.
- [15] O. Schulz, M. Martin, C. Argirusis, G. Borchardt, *Phys. Chem. Chem. Phys.* **2003**, 5, 2308–2313.
- [16] W. S. Fyfe, *Anal. Chem.* **1951**, 23, 174–175.

Received: January 28, 2010

Published Online: June 16, 2010

# In Vitro Cytotoxic-Active Platinum(II) Complexes Derived from Carboplatin and Involving Purine Derivatives

Lukáš Dvořák,<sup>[a]</sup> Igor Popa,<sup>[a]</sup> Pavel Štarha,<sup>[a]</sup> and Zdeněk Trávníček<sup>\*[a]</sup>

**Keywords:** Platinum / Nucleobases / Cytotoxicity / Antitumor agents

Six platinum(II) complexes of the general formula [Pt(cbdc)-(HL<sub>n</sub>)<sub>2</sub>] (**1–6**; cbdc = cyclobutane-1,1-dicarboxylate and HL<sub>4</sub>–HL<sub>6</sub> = benzyl-substituted 6-benzylamino-2-chloro-9-isopropylpurine derivatives) have been synthesized by the reaction of [Pt(cbdc)(dmsO)<sub>2</sub>] with the corresponding HL<sub>n</sub> compound. The prepared complexes were characterized by elemental analysis and FTIR, Raman and NMR (<sup>1</sup>H, <sup>13</sup>C, <sup>15</sup>N and <sup>195</sup>Pt) spectroscopy. Based on the results of these techniques, it can be concluded that the central Pt<sup>II</sup> atom of the complexes **1–6** is coordinated to two oxygen atoms originating from the cyclobutane-1,1-dicarboxylate group and to two nitrogen atoms from two HL<sub>n</sub> molecules, that is, having a PtN<sub>2</sub>O<sub>2</sub> donor set. Detailed multinuclear and two-dimensional NMR studies indicated the N-7 atom to be the coordination site of the purine derivatives. The coordination mode was proven by a single-crystal X-ray analysis of the [Pt(cbdc)(dmsO)-

(HL<sub>7</sub>)]·H<sub>2</sub>O (**7a**·H<sub>2</sub>O) intermediate [HL<sub>7</sub> = 2-chloro-6-(2-methoxybenzyl)amino-9-isopropylpurine]. The geometry is slightly distorted square-planar and the central Pt<sup>II</sup> atom is coordinated to one bidentate cyclobutane-1,1-dicarboxylate dianion, one dmsO molecule through the sulfur atom and one HL<sub>7</sub> molecule through the N-7 atom of the purine ring, that is, with a PtNO<sub>2</sub>S donor set. The complexes **1–6** were tested for their in vitro cytotoxicity against K-562 (chronic myelogenous leukaemia) and MCF7 (breast adenocarcinoma) human cancer cell lines. Values of IC<sub>50</sub> (drug concentrations lethal for 50 % of the tumour cells) ranged from 4.5 to 14.1 μM for the K-562 cells and from 4.3 to 21.0 μM for the MCF7 cells. The in vitro cytotoxicities were in several cases comparable or even higher than those of therapeutically used platinum-based anticancer drugs, that is, cisplatin, carboplatin and oxaliplatin.

## Introduction

One of the best known platinum-based complexes used in the treatment of cancer is *cis*-diamminedichloridoplatinum(II) complex (cisplatin).<sup>[1]</sup> Since 1978 it has been used in chemotherapy against testicular, ovarian, oesophageal, lung, head, neck and other human malignancies.<sup>[2]</sup> However, the therapy itself is accompanied by several unwanted side-effects (e.g., nephrotoxicity and ototoxicity) and drug resistance. These limitations led to the preparation of new platinum(II) complexes, that is, diamminecyclobutane-1,1-dicarboxylatoplatinum(II) (carboplatin), (1*R*,2*R*)-diamminocyclohexaneoxalatoplatinum(II) (oxaliplatin) and diammineglycolatoplatinum(II) (nedaplatin), which have also been approved as platinum-based anticancer drugs. In the case of carboplatin and nedaplatin, the carrier N-donor ligands (NH<sub>3</sub>) are identical to those in cisplatin. However, the replacement of the chlorido-leaving ligands in cisplatin by the cyclobutane-1,1-dicarboxylate (carboplatin) or glycolate (nedaplatin) dianion led to the suppression of unwanted side-effects such as nephrotoxicity.<sup>[3]</sup>

The derivatives of 6-benzylamino-2-chloro-9-isopropylpurine (HL<sub>n</sub>) used for the preparation of the platinum(II) complexes **1–6** were chemically derived from a 6-benzylaminopurine (N6-benzyladenine, bap) skeleton. The latter represents one of the groups of plant growth regulators called cytokinins.<sup>[4]</sup> 6-Benzylamino-2-chloro-9-isopropylpurine itself is an inactive precursor of cyclin-dependent kinase (CDK) inhibitors such as 6-benzylamino-2-(3-hydroxypropylamino)-9-isopropylpurine (bohemine) or 6-benzylamino-2-(2-hydroxymethyl-1-propylamino)-9-isopropylpurine (roscovitine, ros).<sup>[5]</sup> These types of organic compounds have formerly been used in the synthesis of metallocomplexes, including platinum(II) and platinum(IV) complexes. Compounds *cis*-[PtCl<sub>2</sub>(HL)<sub>2</sub>], *trans*-[PtCl<sub>2</sub>(HL)<sub>2</sub>], [Pt(ox)(HL)<sub>2</sub>], [PtCl<sub>3</sub>(H<sup>+</sup>HL)], *cis*-[PtCl<sub>2</sub>(H<sup>+</sup>HL)<sub>2</sub>]-Cl<sub>2</sub> and [PtCl<sub>5</sub>(H<sup>+</sup>HL)] have been reported and their in vitro cytotoxic activity on selected human cancer cell lines have also been discussed (HL = variously substituted bap; H<sup>+</sup>HL = protonated form of bap derivatives; see ref.<sup>[6]</sup> and references cited therein). The best results were obtained for *cis*-[PtCl<sub>2</sub>(ros)<sub>2</sub>], the IC<sub>50</sub> (concentration of the tested compound lethal for 50 % of cells) values of which were equal to 1 μM for the K-562 (chronic myelogenous leukaemia), G-361 (malignant melanoma) and HOS (osteogenic sarcoma) human cancer cell lines and to 2 μM for the MCF7 (human breast adenocarcinoma) cells. The in vitro cytotoxicity of this complex exceeds that of cisplatin, the IC<sub>50</sub> values of

[a] Department of Inorganic Chemistry, Faculty of Science, Palacký University  
Tr. 17. listopadu 12, 77146 Olomouc, Czech Republic  
Fax: +420-585-634-357  
E-mail: zdenek.travnick@upol.cz

Supporting information for this article is available on the WWW under <http://dx.doi.org/10.1002/ejic.201000322>.

which were determined to be 3, 3, 5 and 11  $\mu\text{M}$ , respectively, for the above cell lines. With the exception of the above-mentioned compounds with 6-benzylaminopurine derivatives, complexes of the type  $[\text{Pt}(\text{1,4dach})(\text{L})_2]\text{X}$  involving different types of nucleobase or their derivatives ( $\text{L}$  = adenine, hypoxanthine, 9-methylguanine, cytosine and 1-methylcytosine) and 1,4-diaminocyclohexane (1,4dach) can be regarded as platinum(II) complexes with similar types of N-donor ligand;  $\text{X} = \text{SO}_4^{2-}$  or  $\text{Cl}_2^-$ ).<sup>[7]</sup>

A total number of 308 platinum(II) complexes involving the  $[\text{PtN}_2(\text{cbdc})]$  motif have been reported to date (SciFinder Scholar, 2004 edition). Moreover, 28 X-ray structures of platinum(II) square-planar complexes have been deposited at the Crystallographic Structural Database (CSD ver. 5.31, November 2009 update),<sup>[8]</sup> but only two of them, namely  $[\text{Pt}(\text{cbdc})(2\text{-mp})_2]$  and  $[\text{Pt}(\text{cbdc})(\text{hmi})_2]\cdot\text{H}_2\text{O}$ , have two unidentate N-donor heterocyclic ligands (2-methylpyridine, 2-mp; hexamethylenimine, hmi) coordinated to the  $\text{Pt}^{\text{II}}$  atom.<sup>[9]</sup> In relation to this, the complexes **1–6** represent the first ever prepared carboplatin-based complexes with two substituted purine molecules coordinated to the metal centre.

In this work we report the preparation and characterization of the platinum(II) complexes  $[\text{Pt}(\text{cbdc})(\text{HL}_n)_2]$  **1–6** bearing N-donor carrier ligands derived from 6-benzylamino-2-chloro-9-isopropylpurine ( $\text{HL}_n$ ) and the cyclobutane-1,1-dicarboxylate dianion (cbdc) as the leaving bidentate O-donor group. The complexes prepared were screened in an acetoxymethyl (AM) assay for their in vitro cytotoxicity against K-562 and MCF7 human cancer cell lines.

## Results and Discussion

### Synthesis

The 6-benzylamino-2-chloro-9-isopropylpurine derivatives ( $\text{HL}_n$ ), depicted in Scheme S1 (see the Supporting In-

formation), were synthesized from 2,6-dichloropurine, as shown in Scheme 1.<sup>[10]</sup>

A series of light-grey platinum(II) complexes **1–6** of the general formula  $[\text{Pt}(\text{cbdc})(\text{HL}_n)_2]$ , formally derived from carboplatin, were prepared by a general procedure with  $[\text{Pt}(\text{cbdc})(\text{dmsO})_2]$  as a key intermediate, which was allowed to react with 2 molequiv of the 6-benzylamino-2-chloro-9-isopropylpurine derivatives ( $\text{HL}_1\text{--HL}_6$ ) to give the final products of general formula  $[\text{Pt}(\text{cbdc})(\text{HL}_n)_2]$  (summarized in Scheme 1; dmsO = dimethyl sulfoxide).<sup>[11]</sup> The reactions were performed in distilled water/isopropyl alcohol (1:1, v/v) at 90 °C. The substitution of the two dmsO molecules proceeded in two steps, as reported for the reactions of  $[\text{Pt}(\text{cbdc})(\text{dmsO})_2]$  with 1,2-diaminocyclohexane (dach), aminocyclohexane (ach) and *n*-propylamine (pa).<sup>[11]</sup> In the

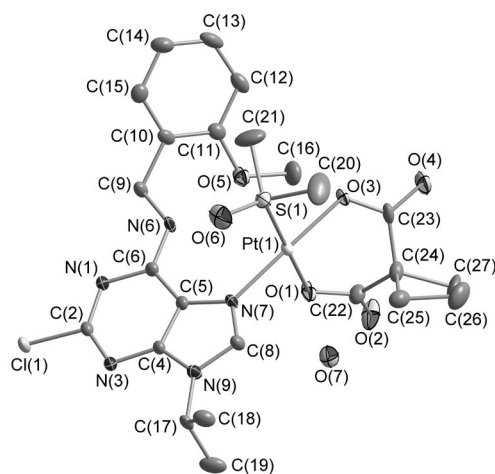
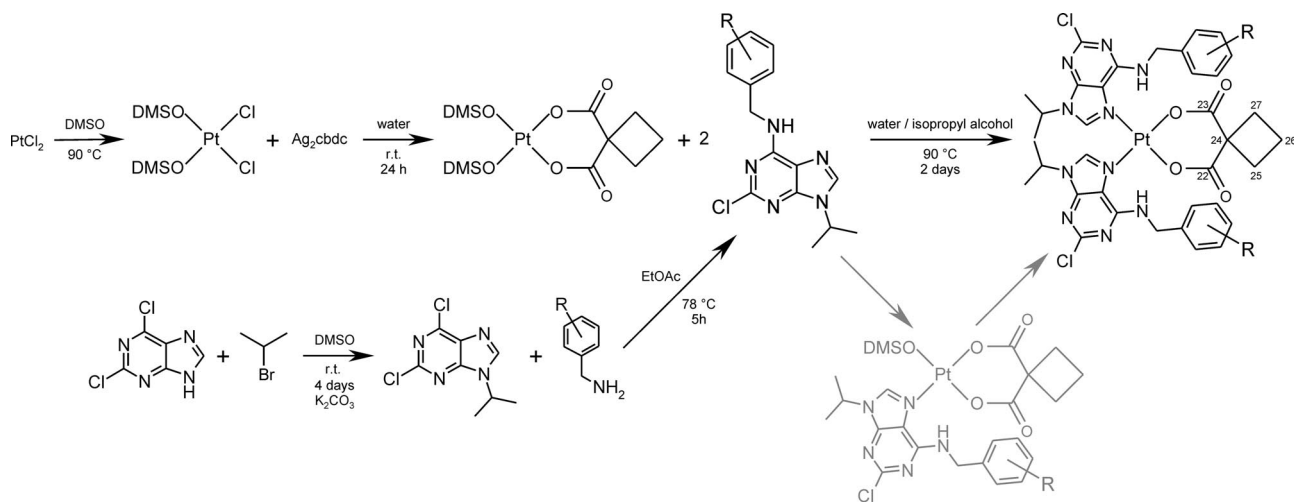


Figure 1. Molecular structure of  $[\text{Pt}(\text{cbdc})(\text{dmsO})(\text{HL}_7)]\cdot\text{H}_2\text{O}$  (**7a**· $\text{H}_2\text{O}$ ) with non-hydrogen atoms drawn as thermal ellipsoids at the 50% probability level. Hydrogen atoms have been omitted for clarity.



Scheme 1. Mechanism for the synthesis of 6-benzylamino-2-chloro-9-isopropylpurine derivatives ( $\text{HL}_n$ ) and the  $[\text{Pt}(\text{cbdc})(\text{HL}_n)_2]$  complexes **1–6** via the  $[\text{Pt}(\text{cbdc})(\text{dmsO})(\text{HL}_n)]$  intermediates (shown in grey).  $\text{R} = 5\text{-bromo-2-fluoro}$  ( $\text{HL}_1$ ; complex **1**),  $3,4\text{-dichloro}$  ( $\text{HL}_2$ ; **2**),  $3\text{-bromo}$  ( $\text{HL}_3$ ; **3**),  $2\text{-trifluoromethyl}$  ( $\text{HL}_4$ ; **4**),  $3\text{-trifluoromethyl}$  ( $\text{HL}_5$ ; **5**) and  $4\text{-trifluoromethyl}$  ( $\text{HL}_6$ ; **6**) derivatives of 6-benzylamino-2-chloro-9-isopropylpurine.



cases of the complexes **1–6**, the syntheses proceeded by a two-step reaction mechanism, the first stage involving the substitution of one dmsO molecule in the starting  $[\text{Pt}(\text{cbdc})(\text{dmsO})_2]$  complex by one  $\text{HL}_n$  molecule to form  $[\text{Pt}(\text{cbdc})(\text{dmsO})(\text{HL}_n)]$ . It is supposed that intermediates of this type are quite stable, probably due to the relative kinetic inertness of the latter complex and the intra- and intermolecular non-covalent interactions (e.g., hydrogen bonds) present both in the solid state and solution, which makes the substitution of the second dmsO molecule quite difficult and the whole process longer. The described mechanism was proven by determining the molecular (Figure 1) and crystal structures of  $[\text{Pt}(\text{cbdc})(\text{dmsO})(\text{HL}_7)] \cdot \text{H}_2\text{O}$  (**7a**· $\text{H}_2\text{O}$ ). Subsequently, the second dmsO ligand was substituted by another  $\text{HL}_n$  molecule to form the final product  $[\text{Pt}(\text{cbdc})(\text{HL}_n)_2]$  (see Scheme 1).

### FTIR and Raman Spectroscopy

Most of the bands observed in the FTIR spectra of **1–6** between 640 and 900  $\text{cm}^{-1}$  could be assigned to the purine skeletal vibrations of the coordinated  $\text{HL}_n$  molecules.<sup>[12]</sup> The very strong bands detected in the 1609–1621  $\text{cm}^{-1}$  region belong to  $\nu(\text{C}=\text{N})_{\text{ar}}$  vibrations. The weak-to-medium bands observed between 3050 and 3142  $\text{cm}^{-1}$  may be attributed to  $\nu(\text{C}-\text{H})_{\text{ar}}$  vibrations, whereas the maxima of the  $\nu(\text{C}-\text{H})_{\text{ar}}$  vibrations were detected in the 2873–2983  $\text{cm}^{-1}$  region. The  $\nu(\text{C}-\text{Cl})_{\text{al}}$  vibration is characterized by a band of medium or strong intensity with the maximum between 1163 and 1171  $\text{cm}^{-1}$ . Three bands with maxima at around 1480, 1530 and 1580  $\text{cm}^{-1}$  can be assigned to  $\nu(\text{C}=\text{C})_{\text{ar}}$  vibrations. The  $\nu_{\text{as}}(\text{C}=\text{O})$  vibration can be attributed to the band observed at 1679–1680  $\text{cm}^{-1}$ , which is the typical region for this vibration and it has previously been assigned to the carboxy groups of the cbdc dianion.<sup>[11,13]</sup> The bands observed for **1–6** in the 150–600  $\text{cm}^{-1}$  region, with maxima at 540–545 and 554–563  $\text{cm}^{-1}$ , could be assigned to the  $\nu(\text{Pt}-\text{N})$  and  $\nu(\text{Pt}-\text{O})$  stretching vibrations, respectively.<sup>[14]</sup> The presence of these two vibrations in the far-FTIR spectra indirectly confirmed the coordination of both types of organic ligands, that is,  $\text{HL}_1$ – $\text{HL}_6$  and cbdc, to the central  $\text{Pt}^{\text{II}}$  atom.

As can be seen from the data given in the Exp. Sect., only some of the above characteristic vibrations were detected in the Raman spectra of **2**, **3**, **5** and **6** (**1** and **4** were burnt under the laser beam). Nevertheless, it can be noted that the positions of the band maxima assignable to these vibrations for both the  $\text{HL}_n$  and cbdc ligands correlate well in the FTIR and Raman spectra of the particular complexes **1–6**. The bands with maxima at 3063–3140 and 2870–2987  $\text{cm}^{-1}$  can be assigned to  $\nu(\text{C}-\text{H})_{\text{ar}}$  and  $\nu(\text{C}-\text{H})_{\text{al}}$  vibrations, respectively.<sup>[15]</sup> The very strong skeletal vibration of the purine ring was detected in the range of 1338–1340  $\text{cm}^{-1}$ .<sup>[16]</sup>

### NMR Spectroscopy

All the signals of the free  $\text{HL}_n$  molecules detected in the  $^1\text{H}$  and  $^{13}\text{C}$  NMR spectra of the appropriate starting com-

pounds ( $\text{HL}_n$ ) were also found in the spectra of the complexes **1–6**. However, most of these signals were shifted as a consequence of the coordination of  $\text{HL}_n$  to the  $\text{Pt}^{\text{II}}$  atom and the formation of the final products **1–6**. The highest coordination shifts ( $\Delta\delta = \delta_{\text{complexes}} - \delta_{\text{ligand}}$ ) were found for the 8-H and 6-H signals in the  $^1\text{H}$  NMR spectra; these were shifted significantly more than for the other proton signals. Significant coordination shifts were also observed in the  $^{13}\text{C}$  NMR spectra for the C-5 and C-8 atoms of the purine moieties of  $\text{HL}_n$ : the C-5 signals are shifted upfield and the C-8 signals downfield by more than 3.0 ppm. These findings indirectly support the conclusion that the organic molecules  $\text{HL}_n$  are coordinated to the  $\text{Pt}^{\text{II}}$  atom through their N-7 atoms.

$^1\text{H}$ – $^{15}\text{N}$  gs-HMBC experiments were performed on **2–6** (unfortunately, signals from the nitrogen atoms in the structure of **1** were not detected) to confirm the above conclusion. Table 1 summarizes the chemical and coordination shifts obtained, the values of which correlate well for the individual nitrogen atoms for all the complexes. The largest values of  $\Delta\delta$  were found for the N-7 atom of the purine ring with values of around –110 ppm (Table 1). The coordination shifts for the N-1, N-3, N-6 and N-9 atoms are much smaller. These NMR results clearly prove that 6-benzylamino-2-chloro-9-isopropylpurine derivatives ( $\text{HL}_n$ ) are coordinated to the metal centre of the prepared platinum(II) complexes through the N-7 atom.

Table 1. Results of the  $^1\text{H}$ – $^{15}\text{N}$  gs-HMBC experiments given as chemical shifts with the coordination shifts ( $\Delta\delta = \delta_{\text{complexes}} - \delta_{\text{ligand}}$ ) given in parentheses.

	N1	N3	$\delta$ [ppm] N6	N7	N9
<b>1</b> <sup>[a]</sup>	–	–	–	–	–
<b>2</b>	232.7 (5.7)	225.3 (1.2)	96.3 (8.4)	129.3 (–109.4)	185.2 (7.1)
<b>3</b>	232.4 (7.1)	n.o. <sup>[b]</sup>	97.4 (7.7)	129.1 (–107.7)	184.9 (8.8)
<b>4</b>	230.8 (6.3)	n.o. <sup>[b]</sup>	92.4 (5.9)	128.0 (–109.3)	184.1 (7.2)
<b>5</b>	231.8 (4.0)	223.9 (–0.3)	97.3 (5.4)	129.0 (–111.6)	185.3 (6.2)
<b>6</b>	232.4 (4.4)	225.0 (–0.5)	96.5 (5.3)	129.0 (–112.0)	185.4 (6.4)

[a] Signals from the N-1, N-3, N-6, N-7 and N-9 atoms of **1** were not detected. [b] The N-3 signal was not observed for **3**,  $\text{HL}_3$  or **4**.

Signals characterizing the cyclobutane-1,1-dicarboxylate dianion were detected in both the  $^1\text{H}$  and  $^{13}\text{C}$  NMR spectra of **1–6** (see the Exp. Sect.) and these signals were refined by  $^1\text{H}$ – $^{13}\text{C}$  gs-HMQC and gs-HMBC 2D NMR experiments. The most characteristic signal of the coordinated cbdc dianion, which belongs to the C-22 and C-23 atoms of the two carboxy groups, was found at around 177.5 ppm.

The  $^{195}\text{Pt}$  NMR spectra of **1–6** exhibit signals between –1631 and –1620 ppm. Note that the  $^{195}\text{Pt}$  NMR chemical shifts of platinum(II) complexes with the formula  $[\text{Pt}(\text{cbdc})(\text{L})]$ , in which L symbolizes two monodentate or one bidentate N-donor ligand, namely amine, cyclopentylamine (cpa), 1,2-ethylenediamine (en), 1,2-diaminopropane (meen), *N,N*-dimethylethylenediamine ( $\text{Me}_2\text{en}$ ) and 1,2-diaminocyclohexane (dach), range from –1968 to –1647 ppm.<sup>[17]</sup> Thus, it can be said that the shifts for **1–6** approach the upper limit of  $^{195}\text{Pt}$  NMR chemical shifts of

the cited complexes. Moreover, these values are also similar to those obtained for oxalatoplatinum(II) complexes (ca. –1690 ppm) involving 6-benzylamino-2-chloro-9-isopropylpurine-based N-donor ligands.<sup>[6b]</sup>

### Single-Crystal X-ray Analysis of [Pt(cbdc)(dmsO)(HL<sub>7</sub>)]·H<sub>2</sub>O (7a·H<sub>2</sub>O)

Attempts to prepare single crystals of platinum(II) complexes 1–6 suitable for single-crystal X-ray analysis were unsuccessful. Nevertheless, very important findings about the compositions and coordination modes of these complexes were obtained by analysis of the [Pt(cbdc)(dmsO)(HL<sub>7</sub>)]·H<sub>2</sub>O (7a·H<sub>2</sub>O) intermediate, the molecular (Figure 1) and crystal (Figure 2) structures of which were determined by this important method (Table 2). Selected bond lengths and angles are presented in Table 3 and non-bonding contacts are given as a footnote in Figure 2.

Table 2. Crystal data and structure refinement details for [Pt(cbdc)(dmsO)(HL<sub>7</sub>)]·H<sub>2</sub>O (7a·H<sub>2</sub>O).

Molecular formula	C <sub>24</sub> H <sub>32</sub> ClN <sub>5</sub> O <sub>7</sub> PtS
Formula weight	765.15
Temperature [K]	120(2)
Wavelength [Å]	0.71073
Crystal system	orthorhombic
Space group	<i>Pbca</i>
Unit cell dimensions	
<i>a</i> [Å]	13.8086(3)
<i>b</i> [Å]	14.4052(3)
<i>c</i> [Å]	28.3693(5)
<i>α</i> [°]	90
<i>β</i> [°]	90
<i>γ</i> [°]	90
<i>V</i> [Å <sup>3</sup> ]	5643.1(2)
<i>Z</i> , <i>D</i> <sub>calc.</sub> [g cm <sup>−3</sup> ]	8, 1.801
Absorption coefficient [mm <sup>−1</sup> ]	5.193
Crystal size [mm]	0.40 × 0.35 × 0.30
<i>F</i> (000)	3024
<i>θ</i> range for data collection [°]	2.83 ≤ <i>θ</i> ≤ 25.00
Index ranges ( <i>h</i> , <i>k</i> , <i>l</i> )	−16 ≤ <i>h</i> ≤ 16 −17 ≤ <i>k</i> ≤ 12 −32 ≤ <i>l</i> ≤ 33
Reflections collected/unique ( <i>R</i> <sub>int</sub> )	44469/4960 (0.0393)
Max./min. transmission	0.3049/0.2305
Data/restraints/parameters	4960/0/363
Goodness-of-fit on <i>F</i> <sup>2</sup>	1.256
Final <i>R</i> indices [ <i>I</i> > 2σ( <i>I</i> )]	<i>R</i> <sub>1</sub> = 0.0285, <i>wR</i> <sub>2</sub> = 0.0616
<i>R</i> indices (all data)	<i>R</i> <sub>1</sub> = 0.0334, <i>wR</i> <sub>2</sub> = 0.0639
Largest peak/hole [e Å <sup>−3</sup> ]	0.822/−1.789

The [Pt(cbdc)(dmsO)(HL<sub>7</sub>)]·H<sub>2</sub>O (7a·H<sub>2</sub>O) complex has a distorted square-planar arrangement with a PtNO<sub>2</sub>S donor set and it contains one water molecule of crystallization (Figure 1). The donor atoms originate from 2-chloro-6-(2-methoxybenzyl)amino-9-isopropylpurine (HL<sub>7</sub>), the bidentate-coordinated cyclobutane-1,1-dicarboxylate dianion and the *S*-coordinated dmsO molecule. The coordination site of HL<sub>7</sub> is the N(7) atom of the purine moiety.

The HL<sub>7</sub> molecule consists of three aromatic systems, benzene (A), pyrimidine (B) and imidazole (C), with the biggest deviations from planarity being 0.003(5) Å for C(13), 0.018(4) Å for N(1) and 0.012(4) Å for C(5). The tor-

sion angles C(6)–N(6)–C(9)–C(10), C(5)–C(6)–N(6)–C(9) and N(6)–C(9)–C(10)–C(15) are equal to 165.1(4), 176.6(4) and –120.6(5)°, respectively. The dihedral angle formed by the benzene and purine rings is 53.62(13)°. Moreover, the dihedral angle between the purine ring and the basal plane formed by the atoms of the PtNO<sub>2</sub>S donor set was determined to be 87.34(8)°. The cyclobutane-1,1-dicarboxylate dianion is coordinated to the metal centre through its O(1) and O(3) atoms. The Pt–O bond lengths determined for 7a·H<sub>2</sub>O (Table 3) correlate well with those of the cyclobutane-1,1-dicarboxylatoplatinum(II) complexes deposited in the CSD,<sup>[8]</sup> which range from 1.977 to 2.065 Å (mean of 2.016 Å). The dihedral angle, typical of platinum(II) complexes coordinated to the cbdc dianion, formed by the basal plane (PtNO<sub>2</sub>S donor set) and the cyclobutane ring, is equal to 79.5(2)°. The dimethyl sulfoxide molecule is coordinated to the Pt<sup>II</sup> atom through its S(1) atom.

Table 3. Selected bond lengths and angles for 7a·H<sub>2</sub>O.

Bond lengths [Å]		Bond angles [°]	
Pt(1)–O(1)	2.018(3)	O(1)–Pt(1)–O(3)	89.89(13)
Pt(1)–O(3)	2.004(3)	O(1)–Pt(1)–N(7)	88.56(15)
Pt(1)–N(7)	2.011(4)	O(1)–Pt(1)–S(1)	178.00(11)
Pt(1)–S(1)	2.1819(12)	O(3)–Pt(1)–N(7)	178.45(15)
N(1)–C(2)	1.331(6)	O(3)–Pt(1)–S(1)	88.94(10)
N(1)–C(6)	1.346(6)	N(7)–Pt(1)–S(1)	92.60(12)
C(2)–N(3)	1.312(6)	Pt(1)–N(7)–C(5)	128.0(3)
N(3)–C(4)	1.353(6)	Pt(1)–N(7)–C(8)	125.3(3)
C(4)–C(5)	1.367(6)	Pt(1)–O(1)–C(22)	119.9(3)
C(4)–N(9)	1.372(6)	Pt(1)–O(3)–C(23)	119.8(3)
C(5)–C(6)	1.407(6)	Pt(1)–S(1)–C(20)	107.2(2)
C(5)–N(7)	1.380(6)	Pt(1)–S(1)–C(21)	108.7(2)
N(7)–C(8)	1.313(6)	Pt(1)–S(1)–O(6)	118.7(2)
C(8)–N(9)	1.350(6)	C(5)–N(7)–C(8)	106.6(4)
O(1)–C(22)	1.302(6)	N(7)–C(5)–C(4)	108.3(4)
O(3)–C(23)	1.308(6)	N(7)–C(5)–C(6)	134.3(4)
C(22)–O(2)	1.218(6)	N(7)–C(8)–C(9)	111.4(4)
C(22)–C(24)	1.520(7)	O(1)–C(22)–O(2)	121.3(5)
C(23)–O(4)	1.216(6)	O(1)–C(22)–C(24)	117.2(4)
C(23)–C(24)	1.525(7)	O(3)–C(23)–O(4)	121.1(5)
S(1)–C(20)	1.763(6)	O(3)–C(23)–C(24)	117.7(4)
S(1)–C(21)	1.745(6)		
S(1)–O(6)	1.455(4)		

A network of intra- and intermolecular hydrogen bonds and non-covalent contacts stabilize the crystal structure of 7a·H<sub>2</sub>O (Figure 2). As a consequence of the intramolecular N(6)–H(6)···O(5) hydrogen bond [*d*(D–H) = 0.8800 Å, *d*(H···A) = 2.435(4) Å, *d*(D···A) = 2.815(5) Å and <(DHA) = 106.5(3)°], the methoxy group is orientated towards the imidazole ring. The water molecule is involved in hydrogen bonds of the O–H···O type with the O(2) and O(4) atoms of two different 7a molecules to form the following hydrogen bonds: O(7)–H(7W)···O(4)<sup>i</sup> [*d*(D–H) = 0.89(7) Å, *d*(H···A) = 1.93(7) Å, *d*(D···A) = 2.767(6) Å and <(DHA) = 157(6)°] and O(7)–H(7V)···O(4)<sup>ii</sup> [*d*(D–H) = 0.81(7) Å, *d*(H···A) = 2.00(7) Å, *d*(D···A) = 2.806(6) Å and <(DHA) = 168(6)°] [Figure 2; symmetry codes: (i) 1 – *x*, *y* + 0.5, 0.5 – *z*; (ii) *x* + 0.5, *y*, 0.5 – *z*]. Finally, C–H···O, C–H···Cl, C···Cl and Cl···O non-covalent contacts were detected in the crystal structure of the complex 7a·H<sub>2</sub>O and their parameters are given in Table S1 of the Supporting Information.

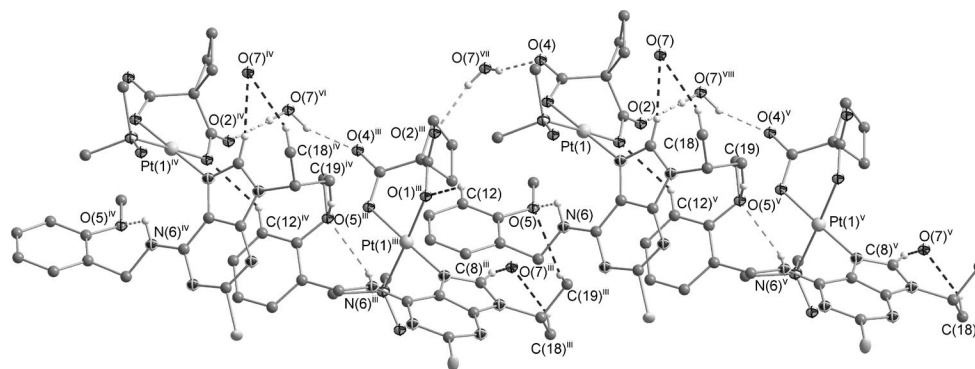


Figure 2. Part of the crystal structure of  $[\text{Pt}(\text{cbdc})(\text{dmsO})(\text{HL}_7)] \cdot \text{H}_2\text{O}$  (**7a**· $\text{H}_2\text{O}$ ) showing N–H...O and O–H...O hydrogen bonds (dashed light-grey lines) and C–H...O non-covalent contacts (dashed dark-grey lines). Hydrogen atoms not involved in hydrogen bonds have been omitted for clarity. Symmetry codes: (iii)  $0.5 - x, y - 0.5, z$ ; (iv)  $x, y - 1, z$ ; (v)  $0.5 - x, y + 0.5, z$ ; (vi)  $x - 0.5, y - 1, 0.5 - z$ ; (vii)  $1 - x, y - 0.5, 0.5 - z$ ; (viii)  $x - 0.5, y, 0.5 - z$ .

### In Vitro Cytotoxic Activity

The prepared complexes **1–6** were tested for their in vitro cytotoxic activity by performing a calcein AM assay on the chronic myelogenous leukaemia (K-562) and breast adenocarcinoma (MCF7) human cancer cell lines (Table 4).

Table 4.  $\text{IC}_{50}$  values ( $\mu\text{M}$ ) of the in vitro cytotoxicity of the complexes **1–6** and platinum-based anticancer drugs against K-562 (chronic myelogenous leukaemia) and MCF7 (breast adenocarcinoma) human cancer cell lines; the cells were exposed to the compounds for 72 h; experiments were repeated three-times.

Complex	$\text{IC}_{50}$ [ $\mu\text{M}$ ]		Ref.
	K-562	MCF7	
<b>1</b>	$9.5 \pm 2.5$	$9.0 \pm 2.3$	this work
<b>2</b>	$4.8 \pm 0.6$	$4.3 \pm 0.2$	this work
<b>3</b>	$4.5 \pm 1.0$	$5.0 \pm 0.3$	this work
<b>4</b>	$7.0 \pm 1.3$	$7.9 \pm 2.3$	this work
<b>5</b>	$14.1 \pm 3.3$	$21.0 \pm 1.4$	this work
<b>6</b>	$7.5 \pm 1.9$	$19.2 \pm 8.6$	this work
Cisplatin	4.7	10.9	[18a]
Carboplatin	60.0	250.0	[18b, 18c]
Oxaliplatin	8.8	18.2	[18a]

The results reveal very promising cytotoxic activities with  $\text{IC}_{50}$  values in the range of 4.5–14.1 and 4.3–21.0  $\mu\text{M}$  for the K-562 and MCF7 cell lines, respectively. In the case of the K-562 cells, complexes **2** and **3** have an in vitro cytotoxicity comparable to that of cisplatin. Moreover, these compounds, together with **4** and **6**, exceed the activity of oxaliplatin and all the tested substances are significantly more effective than carboplatin. As for the MCF7 human cancer cells, **1–6** are again more cytotoxic than carboplatin. The in vitro cytotoxic activities of the complexes **1–4** were evaluated as even higher than those of commercially used platinum-based drugs cisplatin and oxaliplatin.

### Conclusions

The seven novel  $[\text{Pt}(\text{cbdc})(\text{HL}_n)_2]$  (**1–6**) and  $[\text{Pt}(\text{cbdc})(\text{dmsO})(\text{HL}_7)] \cdot \text{H}_2\text{O}$  (**7a**· $\text{H}_2\text{O}$ ) cyclobutane-1,1-dicarboxylatoplatinum(II) complexes derived from carbopla-

tin have been prepared by a synthetic strategy with  $[\text{Pt}(\text{cbdc})(\text{dmsO})_2]$  as a key intermediate. The products obtained were fully characterized. Based on the results of various physicochemical techniques it can be concluded that the central  $\text{Pt}^{\text{II}}$  atom is tetracoordinated to two unidentate N-donor carrier ligands derived from 6-benzylamino-2-chloro-9-isopropylpurine ( $\text{HL}_1$ – $\text{HL}_6$ ) and the bidentate O-donor cyclobutane-1,1-dicarboxylate dianion (cbdc). Multi-nuclear and two-dimensional NMR studies proved the N-7 atom to be the coordination site of the  $\text{HL}_n$  ligands, which was also confirmed by single-crystal X-ray analysis of the  $[\text{Pt}(\text{cbdc})(\text{dmsO})(\text{HL}_7)] \cdot \text{H}_2\text{O}$  (**7a**· $\text{H}_2\text{O}$ ) intermediate.  $\text{IC}_{50}$  values for the in vitro cytotoxicity of the prepared platinum(II) complexes showed that several of the prepared complexes can be considered to have comparable or even higher in vitro cytotoxicity than the platinum-based anticancer drugs, that is, cisplatin, carboplatin and oxaliplatin.

### Experimental Section

**Materials:** The chemicals and solvents were purchased from commercial sources, namely Sigma–Aldrich, Acros Organics, Lachema and Fluka, and they were used as received.

The 6-benzylamino-2-chloro-9-isopropylpurine derivatives ( $\text{HL}_n$ ; see Scheme S1 in the Supporting Information) were synthesized from 2,6-dichloropurine according to previously reported procedures for the preparation of the 2,6,9-trisubstituted purine derivatives.<sup>[10]</sup> The synthetic strategy is given in Scheme 1. The molecules of  $\text{HL}_1$ – $\text{HL}_6$  were characterized by elemental analysis, melting-point determination and FTIR, Raman and NMR ( $^1\text{H}$ ,  $^{13}\text{C}$  and  $^{15}\text{N}$ ) spectroscopy. The results can be found in the Supporting Information. Yields ranged from 76–88%.

**Methods:** Chemical analysis (C, H, N) was performed with a Flash EA1112 Elemental Analyzer (ThermoFinnigan). The purities of the prepared organic compounds  $\text{HL}_1$ – $\text{HL}_7$  were determined with a Beckman HPLC. Melting points were determined with a Büchi B-540 melting-point apparatus with a temperature gradient of  $2^\circ\text{C min}^{-1}$ . The FTIR spectra were obtained with KBr pellets ( $400$ – $4000\text{ cm}^{-1}$ ) and by using the Nujol technique ( $150$ – $600\text{ cm}^{-1}$ ) with a Nexus 670 FT-IR device (ThermoNicolet). Raman spectroscopy was performed on the complexes **2**, **3**, **5** and **6** (**1** and **4** burned



under the laser beam) in the 150–3750 cm<sup>-1</sup> region with a FT-Raman Nicolet NXR 9650 spectrometer with a liquid-nitrogen-cooled NXE Genie germanium detector.

<sup>1</sup>H, <sup>13</sup>C and <sup>195</sup>Pt NMR spectra as well as <sup>1</sup>H–<sup>1</sup>H gs-COSY, <sup>1</sup>H–<sup>13</sup>C gs-HMQC and <sup>1</sup>H–<sup>13</sup>C gs-HMBC ([D<sub>7</sub>]DMF solutions) data were collected with a Bruker Avance 300 spectrometer for HL<sub>n</sub> and **1–6** {[Pt(cbdcdmsd)]<sub>2</sub> is insufficiently soluble in the used solvent}. <sup>1</sup>H–<sup>15</sup>N gs-HMBC experiments were performed on complexes **2–6** (at natural abundance) using the same device. Spectra were calibrated against SiMe<sub>4</sub> (for <sup>1</sup>H and <sup>13</sup>C) and K<sub>2</sub>PtCl<sub>4</sub> (D<sub>2</sub>O; for <sup>195</sup>Pt, –1628 ppm) and against the residual signals of the solvent (for <sup>15</sup>N, 104.7 ppm). The multiplicities in the proton spectra are defined as: s = singlet, d = doublet, t = triplet, quint = quintet, sept = septet, dd = doublet of doublets and m = multiplet.

**Synthesis of [Pt(cbdcdmsd)]<sub>2</sub>:** The silver(I) salt of cyclobutane-1,1-dicarboxylic acid (Ag<sub>2</sub>cbdc) and *cis*-[PtCl<sub>2</sub>(dmsd)]<sub>2</sub> were synthesized according to previously reported methods with cyclobutane-1,1-dicarboxylic acid (cbdc) and PtCl<sub>2</sub> used as starting compounds.<sup>[17a,19]</sup> The prepared *cis*-[PtCl<sub>2</sub>(dmsd)]<sub>2</sub> was dissolved in distilled water and an equimolar amount of Ag<sub>2</sub>cbdc was added to the solution.<sup>[11]</sup> The mixture was stirred in darkness at room temperature for 24 h. The solvent was evaporated and white crystals of [Pt(cbdcdmsd)]<sub>2</sub> formed (Scheme 1). Yield 88%. IR (Nujol):  $\tilde{\nu}$  = 567 (s, PtO) cm<sup>-1</sup>. IR (KBr):  $\tilde{\nu}$  = 1663 (CO) cm<sup>-1</sup>. C<sub>10</sub>H<sub>18</sub>O<sub>6</sub>PtS<sub>2</sub> (493.46): calcd. C 24.34, H 3.68; found C 24.42, H 3.96. M.p. 200–202 °C.

**Synthesis of [Pt(cbdcdmsd)]<sub>2</sub> **1–6**:** [Pt(cbdcdmsd)]<sub>2</sub> (0.2 mmol) was dissolved in distilled water (15 mL) and the appropriate 6-benzylamino-2-chloro-9-isopropylpurine derivative (HL<sub>n</sub>; 0.4 mmol) suspended in isopropyl alcohol (20 mL) was added (Scheme 1).<sup>[11]</sup> The mixture was stirred at 90 °C and a light-grey precipitate formed in 2 days. The product was removed by filtration, washed with cold distilled water and dried in the desiccator over silica gel.

**[Pt(cbdcdmsd)]<sub>2</sub> (**1**):** IR (Nujol):  $\tilde{\nu}$  = 563 (vs, PtO), 541 (vs, PtN) cm<sup>-1</sup>. IR (KBr):  $\tilde{\nu}$  = 3142 (w), 3095 (w), 3053 (w, CH<sub>ar</sub>), 2980 (m), 2933 (w), 2873 (w, CH<sub>al</sub>), 1679 (m, CO), 1621 (vs, CN), 1583 (s), 1540 (m), 1484 (s, CC), 1171 (m, CCl) cm<sup>-1</sup>. <sup>1</sup>H NMR ([D<sub>7</sub>]DMF):  $\delta$  = 9.38 (t, *J* = 6.4 Hz, 1 H, 6-H), 9.08 (s, 1 H, 8-H), 7.59 (s, 1 H, 15-H), 7.49 (d, *J* = 8.4 Hz, 1 H, 13-H), 7.32 (d, *J* = 7.7 Hz, 1 H, 12-H), 4.96 (d, *J* = 6.0 Hz, 2 H, 9-H), 4.87 (sept, *J* = 6.7 Hz, 1 H, 17-H), 2.86 (m, 2 H, 25-H<sup>a</sup>, 27-H<sup>a</sup>), 1.80 (m, 1 H, 26-H<sup>a</sup>), 1.67 (m, 2 H, 25-H<sup>b</sup>, 27-H<sup>b</sup>), 1.63 (d, *J* = 6.8 Hz, 6 H, 18-H, 19-H), 1.48 (m, 1 H, 26-H<sup>b</sup>) ppm. <sup>13</sup>C NMR ([D<sub>7</sub>]DMF):  $\delta$  = 177.4 (C-22, C-23), 155.3 (C-6), 153.7 (C-2), 150.1 (C-4), 144.0 (C-8), 141.9 (C-10), 132.3 (C-11), 130.8 (C-14), 130.6 (C-12), 129.7 (C-13), 128.8 (C-15), 116.5 (C-5), 56.8 (C-24), 49.9 (C-17), 44.3 (C-9), 31.4 (C-25, C-27), 22.1 (C-18, C-19), 15.9 (C-26) ppm. <sup>195</sup>Pt NMR:  $\delta$  = –1626 ppm. C<sub>36</sub>H<sub>34</sub>Br<sub>2</sub>Cl<sub>2</sub>F<sub>2</sub>N<sub>10</sub>O<sub>4</sub>Pt (1134.51): calcd. C 38.11, H 3.02, N 12.35; found C 37.74, H 2.82, N 12.57.

**[Pt(cbdcdmsd)]<sub>2</sub> (**2**):** IR (Nujol):  $\tilde{\nu}$  = 563 (v, PtO) cm<sup>-1</sup>. IR (KBr):  $\tilde{\nu}$  = 2980 (w, CH<sub>al</sub>), 1633 (vs, CN), 1586 (m, CC), 1169 (m, CCl) cm<sup>-1</sup>. Raman:  $\tilde{\nu}$  = 3123 (w), 3064 (m, CH<sub>ar</sub>), 2982 (s), 2942 (vs), 2873 (w, CH<sub>al</sub>), 1587 (s), 1535 (w), 1483 (m, CC), 1164 (m, CCl), 565 (w, PtO) cm<sup>-1</sup>. <sup>1</sup>H NMR ([D<sub>7</sub>]DMF):  $\delta$  = 9.44 (t, *J* = 6.4 Hz, 1 H, 6-H), 9.32 (s, 1 H, 8-H), 7.68 (d, *J* = 1.8 Hz, 1 H, 11-H), 7.58 (dd, *J* = 8.4, 1.8 Hz, 1 H, 14-H), 7.53 (d, *J* = 8.4 Hz, 1 H, 15-H), 4.96 (d, *J* = 6.2 Hz, 2 H, 9-H), 4.84 (sept, *J* = 6.8 Hz, 1 H, 17-H), 2.90 (m, 2 H, 25-H<sup>a</sup>, 27-H<sup>a</sup>), 1.80 (quint, *J* = 7.7 Hz, 1 H, 26-H<sup>a</sup>), 1.67 (m, 2 H, 25-H<sup>b</sup>, 27-H<sup>b</sup>), 1.62 (d, *J* = 6.8 Hz, 6 H, 18-H, 19-H), 1.47 (m, 1 H, 26-H<sup>b</sup>) ppm. <sup>13</sup>C NMR ([D<sub>7</sub>]DMF):  $\delta$  = 177.6 (C-22, C-23), 155.2 (C-6), 153.9 (C-2), 150.3 (C-4), 143.9 (C-8), 140.9 (C-10), 132.1 (C-12), 131.1 (C-15), 130.6 (C-13), 130.0 (C-

11), 128.5 (C-14), 116.7 (C-5), 56.8 (C-24), 49.8 (C-17), 44.1 (C-9), 31.4 (C-25, C-27), 22.1 (C-18, C-19), 15.8 (C-26) ppm. <sup>15</sup>N NMR ([D<sub>7</sub>]DMF):  $\delta$  = 232.7 (N-1), 225.3 (N-3), 185.2 (N-9), 129.3 (N-7), 96.3 (N-6) ppm. <sup>195</sup>Pt NMR:  $\delta$  = –1622 ppm. C<sub>36</sub>H<sub>34</sub>Cl<sub>6</sub>N<sub>10</sub>O<sub>4</sub>Pt (1078.51): calcd. C 40.09, H 3.18, N 12.99; found C 39.89, H 3.11, N 13.20.

**[Pt(cbdcdmsd)]<sub>2</sub> (**3**):** IR (Nujol):  $\tilde{\nu}$  = 554 (vs, PtO), 540 (vs, PtN) cm<sup>-1</sup>. IR (KBr):  $\tilde{\nu}$  = 3138 (w), 3092 (w), 3054 (w, CH<sub>ar</sub>), 2978 (m), 2936 (m), 2878 (w, CH<sub>al</sub>), 1679 (s, CO), 1620 (vs, CN), 1584 (vs), 1524 (m), 1477 (s, CC), 1166 (m, CCl) cm<sup>-1</sup>. Raman:  $\tilde{\nu}$  = 3140 (w), 3063 (m, CH<sub>ar</sub>), 2983 (s), 2942 (s), 2870 (w, CH<sub>al</sub>), 1679 (w, CO), 1583 (s), 1537 (w), 1484 (m, CC), 1166 (m, CCl), 540 (w, PtN) cm<sup>-1</sup>. <sup>1</sup>H NMR ([D<sub>7</sub>]DMF):  $\delta$  = 9.42 (t, *J* = 6.6 Hz, 1 H, 6-H), 9.31 (s, 1 H, 8-H), 7.65 (t, *J* = 1.7 Hz, 1 H, 11-H), 7.58 (dd, *J* = 7.9, 1.3 Hz, 1 H, 15-H), 7.47 (dd, *J* = 7.9, 2.0 Hz, 1 H, 13-H), 7.28 (t, *J* = 7.9 Hz, 1 H, 14-H), 4.94 (d, *J* = 6.4 Hz, 2 H, 9-H), 4.85 (sept, *J* = 6.8 Hz, 1 H, 17-H), 2.89 (m, 2 H, 25-H<sup>a</sup>, 27-H<sup>a</sup>), 1.79 (m, 1 H, 26-H<sup>a</sup>), 1.69 (m, 2 H, 25-H<sup>b</sup>, 27-H<sup>b</sup>), 1.62 (d, *J* = 6.7 Hz, 6 H, 18-H, 19-H), 1.48 (m, 1 H, 26-H<sup>b</sup>) ppm. <sup>13</sup>C NMR ([D<sub>7</sub>]DMF):  $\delta$  = 177.5 (C-22, C-23), 155.2 (C-6), 153.9 (C-2), 150.0 (C-4), 144.3 (C-8), 142.5 (C-10), 131.1 (C-13), 130.9 (C-14), 130.6 (C-15), 127.2 (C-11), 122.5 (C-12), 116.6 (C-5), 56.8 (C-24), 49.8 (C-17), 44.6 (C-9), 31.4 (C-25, C-27), 22.1 (C-18, C-19), 15.8 (C-26) ppm. <sup>195</sup>Pt NMR:  $\delta$  = –1621 ppm. C<sub>36</sub>H<sub>36</sub>Br<sub>2</sub>Cl<sub>2</sub>N<sub>10</sub>O<sub>4</sub>Pt (1098.53): calcd. C 39.36, H 3.30, N 12.75; found C 39.76, H 3.11, N 13.04.

**[Pt(cbdcdmsd)]<sub>2</sub> (**4**):** IR (Nujol):  $\tilde{\nu}$  = 562 (vs, PtO), 540 (vs, PtN) cm<sup>-1</sup>. IR (KBr):  $\tilde{\nu}$  = 3095 (w), 3050 (w, CH<sub>ar</sub>), 2982 (m), 2939 (w), 2883 (w, CH<sub>al</sub>), 1679 (m, CO), 1621 (vs, CN), 1583 (s), 1536 (w), 1482 (m, CC), 1163 (s, CCl) cm<sup>-1</sup>. <sup>1</sup>H NMR ([D<sub>7</sub>]DMF):  $\delta$  = 9.44 (t, *J* = 6.4 Hz, 1 H, 6-H), 9.42 (s, 1 H, 8-H), 7.74 (m, 3 H, 13-H, C14-H, 15-H), 7.48 (m, 1 H, 12-H), 5.64 (d, *J* = 6.0 Hz, 2 H, 9-H), 4.88 (sept, *J* = 7.0 Hz, 1 H, 17-H), 2.90 (m, 2 H, 25-H<sup>a</sup>, 27-H<sup>a</sup>), 1.80 (m, 1 H, 26-H<sup>a</sup>), 1.66 (d, *J* = 6.8 Hz, 6 H, 18-H, 19-H), 1.61 (m, 2 H, 25-H<sup>b</sup>, 27-H<sup>b</sup>), 1.43 (m, 1 H, 26-H<sup>b</sup>) ppm. <sup>13</sup>C NMR ([D<sub>7</sub>]DMF):  $\delta$  = 177.7 (C-22, C-23), 155.2 (C-6), 154.1 (C-2), 150.1 (C-4), 143.7 (C-8), 138.1 (C-10), 133.1 (C-14), 128.2 (C-15), 127.7 (C-13), 127.4, 123.8 (C-16), 126.7 (C-12), 116.6 (C-5), 56.9 (C-24), 49.9 (C-17), 41.4 (C-9), 31.5 (C-25, C-27), 22.1 (C-18, C-19), 15.8 (C-26) ppm. <sup>195</sup>Pt NMR:  $\delta$  = –1631 ppm. C<sub>38</sub>H<sub>36</sub>Cl<sub>2</sub>F<sub>6</sub>N<sub>10</sub>O<sub>4</sub>Pt (1076.73): calcd. C 42.39, H 3.37, N 13.01; found C 42.33, H 3.28, N 13.19.

**[Pt(cbdcdmsd)]<sub>2</sub> (**5**):** IR (Nujol):  $\tilde{\nu}$  = 560 (m, PtO), 542 (s, PtN) cm<sup>-1</sup>. IR (KBr):  $\tilde{\nu}$  = 3093 (w), 3050 (w, CH<sub>ar</sub>), 2982 (w), 2941 (w), 2884 (w, CH<sub>al</sub>), 1680 (m, CO), 1609 (vs, CN), 1583 (s), 1537 (w), 1484 (m, CC), 1166 (s, CCl) cm<sup>-1</sup>. Raman:  $\tilde{\nu}$  = 3072 (s, CH<sub>ar</sub>), 2987 (vs), 2946 (vs, CH<sub>al</sub>), 1609 (w, CN), 1579 (s), 1538 (m), 1480 (m, CC), 1170 (w, CCl) cm<sup>-1</sup>. <sup>1</sup>H NMR ([D<sub>7</sub>]DMF):  $\delta$  = 9.48 (t, *J* = 6.2 Hz, 1 H, 6-H), 9.31 (s, 1 H, 8-H), 7.88 (d, *J* = 7.9 Hz, 1 H, 15-H), 7.84 (s, 1 H, 11-H), 7.65 (d, *J* = 7.9 Hz, 1 H, 13-H), 7.55 (t, *J* = 7.9 Hz, 1 H, 14-H), 5.03 (d, *J* = 6.2 Hz, 2 H, 9-H), 4.83 (sept, *J* = 6.8 Hz, 1 H, 17-H), 2.89 (t, *J* = 8.0 Hz, 4 H, 25-H, 27-H), 1.78 (quint, *J* = 8.0 Hz, 2 H, 26-H), 1.61 (d, *J* = 6.8 Hz, 6 H, 18-H, 19-H) ppm. <sup>13</sup>C NMR ([D<sub>7</sub>]DMF):  $\delta$  = 177.6 (C-22, C-23), 155.1 (C-6), 154.0 (C-2), 150.0 (C-4), 144.8 (C-8), 141.2 (C-10), 132.3 (C-15), 130.8, 130.4, 130.0, 129.6 (C-12), 130.1 (C-14), 130.7, 127.1, 123.5, 119.9 (C-16), 125.1, 125.0 (C-11), 124.5, 126.4 (C-13), 116.6 (C-5), 56.8 (C-24), 49.8 (C-17), 44.8 (C-9), 31.4 (C-25, C-27), 22.1 (C-18, C-19), 15.8 (C-26) ppm. <sup>195</sup>Pt NMR:  $\delta$  = –1620 ppm. C<sub>38</sub>H<sub>36</sub>Cl<sub>2</sub>F<sub>6</sub>N<sub>10</sub>O<sub>4</sub>Pt (1076.73): calcd. C 42.39, H 3.37, N 13.01; found C 42.01, H 3.34, N 13.26.

**[Pt(cbdcdmsd)]<sub>2</sub> (**6**):** IR (Nujol):  $\tilde{\nu}$  = 560 (m, PtO), 545 (m, PtN) cm<sup>-1</sup>. IR (KBr):  $\tilde{\nu}$  = 3142 (w), 3097 (w), 3055 (w, CH<sub>ar</sub>), 2983



(w), 2939 (w), 2883 (w, CH<sub>al</sub>), 1679 (m, CO), 1618 (vs, CN), 1585 (s), 1530 (w), 1483 (m, CC), 1167 (m, CCl) cm<sup>-1</sup>. Raman:  $\tilde{\nu}$  = 3072 (s, CH<sub>ar</sub>), 2984 (s), 2945 (vs), 2876 (w, CH<sub>al</sub>), 1679 (w, CO), 1618 (m, CN), 1582 (s), 1534 (m), 1483 (m, CC), 1164 (m, CCl), 549 (w, PtN) cm<sup>-1</sup>. <sup>1</sup>H NMR ([D<sub>7</sub>]DMF):  $\delta$  = 9.47 (t,  $J$  = 6.2 Hz, 1 H, 6-H), 9.35 (s, 1 H, 8-H), 7.75 (d,  $J$  = 8.2 Hz, 2 H, 11-H, 15-H), 7.65 (d,  $J$  = 8.2 Hz, 2 H, 12-H, 14-H), 5.02 (d,  $J$  = 6.2 Hz, 2 H, 9-H), 4.84 (sept,  $J$  = 6.8 Hz, 1 H, 17-H), 2.90 (t,  $J$  = 8.0 Hz, 4 H, 25-H, 27-H), 1.80 (quint,  $J$  = 8.0 Hz, 2 H, 26-H), 1.62 (d,  $J$  = 6.8 Hz, 6 H, 18-H, 19-H) ppm. <sup>13</sup>C NMR ([D<sub>7</sub>]DMF):  $\delta$  = 177.7 (C-22, C-23), 155.2 (C-6), 154.0 (C-2), 150.0 (C-4), 144.6 (C-10), 143.8 (C-8), 130.8, 127.2, 123.6 (C-16), 129.4, 129.0, 128.6, 128.1 (C-13), 128.7 (C-11, C-15), 125.8, 125.8 (C-12, C-14), 116.7 (C-5), 56.8 (C-24), 49.8 (C-17), 44.6 (C-9), 31.4 (C-25, C-27), 22.1 (C-18, C-19), 15.8 (C-26) ppm. <sup>195</sup>Pt NMR:  $\delta$  = -1621 ppm. C<sub>38</sub>H<sub>36</sub>Cl<sub>2</sub>F<sub>6</sub>N<sub>10</sub>O<sub>4</sub>Pt (1076.73): calcd. C 42.39, H 3.37, N 13.01; found C 41.93, H 3.27, N 13.36.

**[Pt(cbdc)(dmsO)(HL<sub>7</sub>)]·H<sub>2</sub>O (7a·H<sub>2</sub>O):** The complex was prepared using the same synthetic strategy as in the cases of **1–6**, but in a shorter reaction time. The powder product obtained after 24 h was removed by filtration. It was found that the product contains a mixture of [Pt(cbdc)(HL<sub>7</sub>)<sub>2</sub>] and [Pt(cbdc)(dmsO)(HL<sub>7</sub>)] (**7a**). Recrystallization of this mixture gave crystals of [Pt(cbdc)(dmsO)(HL<sub>7</sub>)]·H<sub>2</sub>O (**7a**·H<sub>2</sub>O) suitable for a single-crystal X-ray analysis.

**Single-Crystal X-ray Analysis of [Pt(cbdc)(dmsO)(HL<sub>7</sub>)]·H<sub>2</sub>O (7a·H<sub>2</sub>O):** Diffraction data were collected with an Xcalibur™ 2 diffractometer (Oxford Diffraction Ltd.) with Mo-K $\alpha$  radiation (Monochromator Enhance, Oxford Diffraction Ltd.) and a Sapphire2 CCD detector at 100 K. Data collection and reduction were performed by using CrysAlis software.<sup>[20]</sup> The same software was used for data correction of the absorption effect by the empirical absorption correction using spherical harmonics as implemented in the SCALE3 ABSPACK scaling algorithm. Both structures were solved by direct methods using SHELXS-97 software and refined on  $F^2$  using the full-matrix least-squares procedure (SHELXL-97).<sup>[21]</sup> Non-hydrogen atoms were refined anisotropically. Hydrogen atoms were located in a difference map and refined with the riding model [C–H: 0.95 and 0.99 Å, N–H: 0.88 Å and  $U_{iso}(H)$  = 1.2  $U_{eq}(CH, CH_2, NH)$  or 1.5  $U_{eq}(CH_3)$ ]. The molecular and crystal structures were drawn using DIAMOND,<sup>[22]</sup> which was also used to interpret the additional structural parameters. The crystal data and structure refinement are summarized in Table 2.

CCDC-770266 contains the supplementary crystallographic data for this paper. These data can be obtained free of charge from The Cambridge Crystallographic Data Centre via [www.ccdc.cam.ac.uk/data\\_request/cif](http://www.ccdc.cam.ac.uk/data_request/cif).

**In Vitro Cytotoxic Activity:** Testing of the in vitro cytotoxicity was performed by a calcein acetoxymethyl (AM) assay on the breast adenocarcinoma (MCF7) and chronic myelogenous leukaemia (K-562) human cancer cell lines. Cell lines were kept in plastic tissue culture flasks and grown on Dulbecco's modified Eagle's cell culture medium (DMEM) under conditions of 37 °C, 5% CO<sub>2</sub> atmosphere and 100% humidity. The suspension (ca. 1.25 × 10<sup>5</sup> cells mL<sup>-1</sup>) of cancer cells was distributed between 96-well microtitre plates (Nunc) and preincubated (12 h). Diluted DMF solutions of the complexes **1–6** (final DMF concentration of 0.6%) were added to the suspensions of the cancer cells in concentrations of between 0.2 and 25  $\mu$ M. After 72 h of incubation, the cells were incubated for another hour with calcein AM. The fluorescence of the live cells was measured at 485/538 nm (excitation/emission) with Fluoroskan Ascent (LabSystems). Experiments were

repeated three times and the IC<sub>50</sub> values are given in Table 4 together with their standard deviations.

**Supporting Information** (see also the footnote on the first page of this article): The structural formulae of the 6-benzylamino-2-chloro-9-isopropylpurine derivatives (HL<sub>n</sub>), the results of elemental analyses, melting-point determinations and FTIR, Raman and NMR data (<sup>1</sup>H, <sup>13</sup>C and <sup>15</sup>N).

## Acknowledgments

This research was supported by the The Ministry of Education, Youth and Sports of the Czech Republic (Grant No. MSM6198959218). The authors thank Dr. Miroslava Matiková-Mařarová for measurement of the FTIR and Raman spectra and Dr. Vladimír Kryštof and Mrs. Dita Parobková for in vitro cytotoxicity testing.

- [1] B. Rosenberg, V. L. Camp, T. Krigas, *Nature* **1965**, *205*, 698–699.
- [2] R. B. Weiss, M. C. Christian, *Drugs* **1993**, *46*, 360–365.
- [3] M. J. Abrams, B. A. Murrer, *Science* **1993**, *261*, 725–730.
- [4] F. Skoog, H. Q. Hamzi, A. M. Szwedkowska, N. J. Leopard, K. L. Carraway, T. Fujii, J. P. Helgeson, R. N. Loepky, *Phytochemistry* **1967**, *6*, 1169–1192.
- [5] a) V. Brun, M. Legraverend, D. S. Grierson, *Tetrahedron Lett.* **2001**, *42*, 8161–8164; b) V. Brun, M. Legraverend, D. S. Grierson, *Tetrahedron Lett.* **2001**, *42*, 8165–8167.
- [6] a) L. Szűčová, Z. Trávníček, I. Popa, J. Marek, *Polyhedron* **2008**, *27*, 2710–2720; b) P. Štarha, Z. Trávníček, I. Popa, *J. Inorg. Biochem.*, doi:10.1016/j.jinorgbio.2010.02.005, in press.
- [7] S. Shamsuddin, M. S. Ali, K. H. Whitmire, A. R. Khokhar, *Polyhedron* **2007**, *26*, 637–644.
- [8] F. A. Allen, *Acta Crystallogr., Sect. B: Struct. Sci.* **2002**, *58*, 380–388.
- [9] a) M. J. Xie, Y. Yu, W. P. Liu, S. Q. Hou, Q. S. Ye, *Acta Crystallogr., Sect. E: Struct. Rep. Online* **2007**, *63*, m2589; b) M. S. Ali, J. H. Thurston, K. H. Whitmire, A. R. Khokhar, *Polyhedron* **2002**, *21*, 2659–2665.
- [10] a) G. B. Brown, V. S. Weliky, *J. Org. Chem.* **1958**, *23*, 125–126; b) C. H. Oh, S. C. Lee, K. S. Lee, E. R. Woo, C. Y. Hong, B. S. Yang, D. J. Baek, J. H. Cho, *Arch. Pharm. Pharm. Med. Chem.* **1999**, *332*, 187–190.
- [11] P. Bitha, G. O. Morton, T. S. Dunne, E. F. D. Santos, Y. Lin, S. R. Boone, R. C. Haltiwanger, C. G. Pierpoint, *Inorg. Chem.* **1990**, *29*, 645–652.
- [12] C. J. Pouchert, *The Aldrich Library of Infrared Spectra*, Aldrich Chemical Company Press, Milwaukee, WI, **1981**.
- [13] G. Bernhardt, H. Brunner, N. Gruber, C. Lottner, S. K. Pushpan, T. Tsuno, M. Zabel, *Inorg. Chim. Acta* **2004**, *357*, 4452–4466.
- [14] K. Nakamoto *Infrared and Raman Spectra of Inorganic and Coordination Compounds Part B: Applications in Coordination, Organometallic and Bioinorganic Chemistry*, Wiley, New York, **1991**.
- [15] a) H. Poel, G. Koten, K. Vrieze, *Inorg. Chem.* **1980**, *19*, 1145–1151; b) L. D. Via, O. Gia, S. M. Magno, A. Dolmella, D. Marton, V. Di Noto, *Inorg. Chim. Acta* **2006**, *359*, 4197–4206.
- [16] Z. Dhauadi, M. Ghomi, J. C. Austin, R. B. Girling, R. E. Hester, P. Mojzes, L. Chinsky, P. Y. Turpin, C. Coulombeau, H. Jobic, J. Tomkinson, *J. Phys. Chem.* **1993**, *97*, 1074–1084.
- [17] a) F. D. Rochon, G. Massarweh, *Inorg. Chim. Acta* **2006**, *359*, 4095–4104; b) M. Becker, R. E. Port, H. J. Zabel, W. J. Zeller, P. Bachert, *J. Magn. Reson.* **1998**, *133*, 115–122.
- [18] a) Z. Trávníček, I. Popa, M. Čajan, R. Zbořil, V. Kryštof, J. Mikulík, *J. Inorg. Biochem.* **2010**, *104*, 405–417; b) M. Carland, K. J. Tan, J. M. White, J. Stephenson, V. Murray, W. A. Denny, W. D. McFadyen, *J. Inorg. Biochem.* **2005**, *99*, 1738–1743; c)

- A. R. Ghezzi, M. Aceto, C. Cassino, E. Gabano, D. Osella, *J. Inorg. Biochem.* **2004**, *98*, 73–78.
- [19] J. H. Price, A. N. Williamson, R. F. Schramm, B. B. Wayland, *Inorg. Chem.* **1972**, *11*, 1280–1284.
- [20] *CrysAlis CCD* and *CrysAlis RED*, version 1.171.33.52, Oxford Diffraction Ltd., Abingdon, England, **2009**.
- [21] G. M. Sheldrick, *Acta Crystallogr., Sect. A* **2008**, *64*, 112–122.
- [22] K. Brandenburg, *DIAMOND*, rel. 3.1f, Crystal Impact GbR, Bonn, **2006**.

Received: March 22, 2010  
Published Online: June 15, 2010

# Dual Luminescent Dinuclear Gold(I) Complexes of Terpyridyl-Functionalized Alkyne Ligands and Their Efficient Sensitization of $\text{Eu}^{\text{III}}$ and $\text{Yb}^{\text{III}}$ Luminescence

Xiu-Ling Li,<sup>\*[a]</sup> Ke-Juan Zhang,<sup>[a]</sup> Juan-Juan Li,<sup>[a]</sup> Xin-Xin Cheng,<sup>[a]</sup> and Zhong-Ning Chen<sup>[b]</sup>

**Keywords:** Gold / Lanthanides / Dinuclear complexes / Sensitized luminescence / Alkynes

Reaction of  $(\text{tpyC}_6\text{H}_4\text{C}\equiv\text{CAu})_n$  [ $\text{tpyC}_6\text{H}_4\text{C}\equiv\text{CH} = 4'-(4\text{-ethynylphenyl})-2,2':6',2''\text{-terpyridine}$ ] with diphosphane ligands  $\text{Ph}_2\text{P}(\text{CH}_2)_x\text{PPh}_2$  ( $x = 2$  dppe, 3 dppp, 4 dppb, 5 dpppen, 6 dpbh) in  $\text{CH}_2\text{Cl}_2$  afforded the corresponding dual luminescent binuclear gold(I) complexes  $[(\text{tpyC}_6\text{H}_4\text{C}\equiv\text{CAu})_2(\mu\text{-dppe})]$  (**1**),  $[(\text{tpyC}_6\text{H}_4\text{C}\equiv\text{CAu})_2(\mu\text{-dppp})]$  (**2**),  $[(\text{tpyC}_6\text{H}_4\text{C}\equiv\text{CAu})_2(\mu\text{-dppb})]$  (**3**),  $[(\text{tpyC}_6\text{H}_4\text{C}\equiv\text{CAu})_2(\mu\text{-dpppen})]$  (**4**),  $[(\text{tpyC}_6\text{H}_4\text{C}\equiv\text{CAu})_2(\mu\text{-dpbh})]$  (**5**). Crystal structural analysis of complexes **1**· $2\text{CH}_2\text{Cl}_2$  and **2**· $2\text{CH}_2\text{Cl}_2$  show that the terpyridine moieties are free of coordination in these gold(I)-acetylide-phosphane complexes. Spectrophotometric titration

between complex **1** and  $[\text{Eu}(\text{tta})_3]$  [ $\text{Htta} = 2\text{-thenoyltrifluoroacetone}$ ] or  $[\text{Yb}(\text{hfac})_3(\text{H}_2\text{O})_2]$  [ $\text{Hhfac} = \text{hexafluoroacetylacetone}$ ] gave a 2:1 ratio between  $\text{Ln}(\beta\text{-diketonate})_3$  ( $\text{Ln} = \text{Eu}, \text{Yb}$ ) units and the complex **1** moiety, indicating the formation of  $\text{Au}_2\text{Ln}_2$  complexes. Both the luminescence titrations and the luminescence quantum yields of  $\text{Au}_2\text{Ln}_2$  ( $\text{Ln} = \text{Eu}, \text{Yb}$ ) solutions show that the energy transfer occurs efficiently from the binuclear gold(I) antennas **1–5** to  $\text{Eu}^{\text{III}}$  and  $\text{Yb}^{\text{III}}$  centers, and all complexes **1–5** are good energy donors for sensitization of visible and NIR luminescence of  $\text{Eu}^{\text{III}}$  and  $\text{Yb}^{\text{III}}$  ions.

## Introduction

Lanthanide(III) luminescence has attracted intensive research efforts because of its distinct advantages such as high color purity induced by narrow emission bands, long radiative lifetimes of the excited states in the range of microseconds to milliseconds, large Stokes' shifts, and relatively immovable emission positions.<sup>[1–2]</sup> Because of these advantages, lanthanide(III) complexes have been extensively applied to biomedical assays, optical communication, magnetic resonance imaging, lasers, and as components of the emitter layers in multilayer organic light-emitting devices (OLEDs), etc.<sup>[3–5]</sup> But direct excitation of the  $\text{Ln}^{\text{III}}$  centers always leads to inefficient luminescence because of the extremely weak absorption from Laporte-forbidden f-f transitions of the  $\text{Ln}^{\text{III}}$  ions.<sup>[1b]</sup> In order to improve the luminescence yields of  $\text{Ln}^{\text{III}}$  ions, one of the most feasible strategies is to use strong absorbing organic or d-block metallorganic antenna chromophores as ligands and sensitizers.<sup>[2a,6–8]</sup>  $\text{Ln}(\beta\text{-diketonate})_3$  moieties represent another efficient and well-investigated type of  $\text{Ln}^{\text{III}}$  co-ordinating unit. The two

coordinated water molecules in  $[\text{Ln}(\beta\text{-diketonate})_3(\text{H}_2\text{O})_2]$  compounds can be easily replaced by chelating chromophores such as phenanthroline or polypyridine, which results in highly luminescent ternary complexes.<sup>[6–7,8a,9]</sup>

With respect to energy-transfer processes and minimization of nonradiative deactivation in the d-f assembly, it is very advantageous to use polypyridine-functionalized alkynyl ligands to assemble d-f arrays because they contain both soft donors in the alkynyl positions and hard donors in the polypyridine moieties.<sup>[6–7,8a]</sup> The polypyridine unit can provide high coordination number and eliminate water molecules from the first coordination sphere of  $\text{Ln}^{\text{III}}$  centers effectively because of its good chelating ability. On the other hand, the good linearity and conjugacy of polypyridine-functionalized alkynyl ligands are favorable to the energy transfer from the antenna ligand to the  $\text{Ln}^{\text{III}}$  luminescence centers.<sup>[6–7,8a]</sup> A series of polypyridine-functionalized alkynyl ligands were utilized for the construction of d-block chromophores by incorporation with  $[\text{Ln}(\beta\text{-diketonate})_3(\text{H}_2\text{O})_2]$  compounds achieving sensitized lanthanide luminescence in our previous work.<sup>[2a,6–7]</sup>

Other important effects in achieving efficient energy transfer from the antennas to  $\text{Ln}^{\text{III}}$  ( $\text{Ln} = \text{Eu}, \text{Yb}$ ) centers include the energy match between the triplet state and the  $^5\text{D}_0$  energy level of the  $\text{Eu}^{\text{III}}$  ions,<sup>[9b,10]</sup> and the overlap degree between the emission bands of the antennas and the absorption spectra of  $\text{Yb}^{\text{III}}$ .<sup>[6]</sup> So whether the triplet states of the antennas can be determined easily, especially at room temperature, becomes very important to avoid a blind at-

[a] School of Chemistry and Chemical Engineering, Xuzhou Normal University, Xuzhou, Jiangsu 221116, China  
E-mail: lxl@fjirsm.ac.cn

[b] State Key Laboratory of Structural Chemistry, Fujian Institute of Research on the Structure of Matter, Chinese Academy of Sciences, Fuzhou, Fujian 350002, China

Supporting information for this article is available on the WWW under <http://dx.doi.org/10.1002/ejic.201000324>.

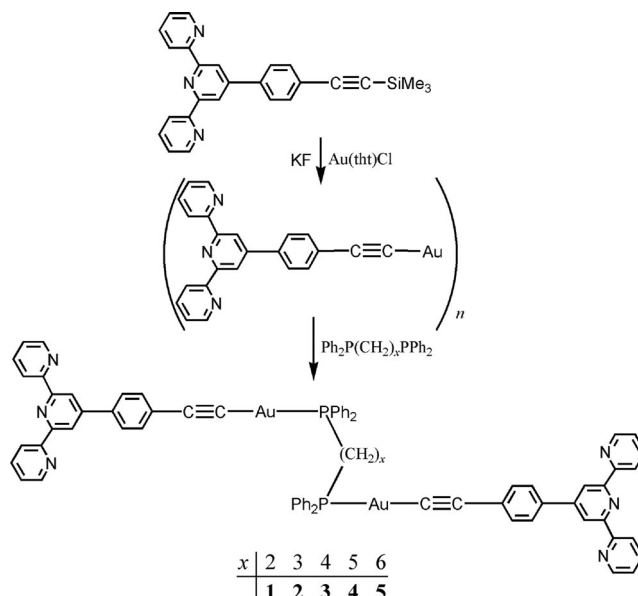


tempt. The organometallic Au<sup>I</sup> phosphane acetylides have exhibited easily observed phosphorescence emission properties due to the heavy atom effect of the Au<sup>I</sup> ions or aurophilic interactions,<sup>[7d,11–14]</sup> so that their triplet states can be easily concluded. In addition, their long phosphorescence lifetimes favor energy transfer.<sup>[6,7,11d,12b,14b]</sup> It has been reported that the Au<sup>I</sup> acetylide phosphane chromophores are favorable antenna chromophores for sensitization of lanthanide luminescence when using 5-ethynyl-2,2'-bipyridine as a bridging ligand in the Au<sub>4</sub>Ln<sub>4</sub> or Au<sub>2</sub>Ln<sub>2</sub> complexes, but the reported quantum yields of Eu<sup>III</sup> complexes are relatively low (0.010–0.012),<sup>[7d]</sup> and the triplet states of the antennas in dichloromethane solutions could not be observed at room temperature. In order to obtain an intensely phosphorescent system at room temperature, and understand further how to better match the triplet states of gold(I) antennas and the emitting levels of Ln<sup>III</sup> and figure out which Ln<sup>III</sup> ions may be sensitized efficiently, the conjugated degree of the alkyne system should be more extended because most phosphorescent systems at room temperature have a large conjugated degree apart from the heavy atom.<sup>[6,7d,11,14b]</sup> On the basis of this consideration, the terpyridyl-functionalized alkyne ligand 4'-(4-ethynylphenyl)-2,2':6',2''-terpyridine (tpyC<sub>6</sub>H<sub>4</sub>C≡CH) is a judicious choice, and a series of its intense room temperature phosphorescent Pt<sup>II</sup> complexes have been synthesized and used as efficient sensitized chromophores in our previous work.<sup>[6]</sup> For this work a series of binuclear gold(I)-alkynyl-phosphane complexes were prepared by depolymerization of polymeric (tpyC<sub>6</sub>H<sub>4</sub>C≡CAu)<sub>n</sub> with diphosphane ligands Ph<sub>2</sub>P(CH<sub>2</sub>)<sub>x</sub>PPh<sub>2</sub> (*x* = 2 dppe, 3 dppp, 4 dpbb, 5 dpppen, 6 dpbb) in CH<sub>2</sub>Cl<sub>2</sub>. The luminescence titrations and luminescence quantum yields of Au<sub>2</sub>Ln<sub>2</sub> (Ln = Eu, Yb) solutions demonstrate that all complexes **1–5** are good energy donors for sensitization of visible and NIR luminescence of Eu<sup>III</sup> and Yb<sup>III</sup> ions.

## Results and Discussion

### Syntheses of Gold(I) Complexes and Characterization

The dinuclear gold(I)-phosphane-acetylide complexes were prepared by general methods established previously<sup>[7d]</sup> through the reaction of diphosphane ligands with the corresponding gold(I) coordination polymer (tpyC<sub>6</sub>H<sub>4</sub>C≡CAu)<sub>n</sub> (Scheme 1) and purified by chromatography on short silica-gel columns using dichloromethane/methanol (100:2) as eluent. Recrystallization was carried out through slow diffusion of *n*-hexane into the corresponding concentrated dichloromethane solutions, from which pale yellow crystals of complexes **1·2CH<sub>2</sub>Cl<sub>2</sub>**, and **2·2CH<sub>2</sub>Cl<sub>2</sub>** suitable for X-ray diffraction were obtained. In the IR spectra, all the dinuclear gold(I)-phosphane-acetylide complexes **1–5** exhibit ν<sub>C≡C</sub> modes at about 2110 cm<sup>−1</sup>, which falls into the normal range of terminally σ-coordinated alkynyl ligands.<sup>[6,7]</sup> Lower frequency for the ν<sub>C≡C</sub> bands is not observed, indicating no π-coordination mode of the C≡C bond exists.<sup>[6,7,15–17]</sup>



Scheme 1. Synthetic routes to complexes **1–5**.

### Crystallographic Studies

The crystal structures of **1·2CH<sub>2</sub>Cl<sub>2</sub>** and **2·2CH<sub>2</sub>Cl<sub>2</sub>** were determined by single-crystal X-ray diffraction. Selected bond lengths and angles are presented in Table 1. The molecular structures of **1·2CH<sub>2</sub>Cl<sub>2</sub>** and **2·2CH<sub>2</sub>Cl<sub>2</sub>** are shown in Figures 1 and 2, respectively. Complexes **1·2CH<sub>2</sub>Cl<sub>2</sub>** and **2·2CH<sub>2</sub>Cl<sub>2</sub>** crystallize in the triclinic system with space group *P* $\bar{1}$  and monoclinic system with space group *C2/c*, respectively. Complex **1·2CH<sub>2</sub>Cl<sub>2</sub>** adopts a *trans* conformation. Complex **2·2CH<sub>2</sub>Cl<sub>2</sub>** adopts a *gauche* conformation with a P1–C71–C72–C71A torsion angle of 175(2)°. The Au<sup>I</sup> centers in the two complexes adopt quasilinear coordination geometries as reported in many gold(I)-acetylide-phosphane complexes,<sup>[11–14,17–19]</sup> and the C–Au–P angles are in the range of 177.2(4)–178.5(2)°, deviating slightly from 180°. The bond lengths of Au–P [2.271(2)–2.282(4) Å] and Au–C [1.971(12)–2.027(6) Å] are in good agreement with the lengths in analogous Au-acetylide systems.<sup>[11–14,17–20]</sup> The C≡C distances [1.162(10)–1.224(15) Å] are comparable to those in the similar dinuclear gold(I)-arylacetylide-phosphane complexes.<sup>[20]</sup> The intramolecular Au⋯Au distances are 7.078 Å in **1·2CH<sub>2</sub>Cl<sub>2</sub>** and 5.294 Å in **2·2CH<sub>2</sub>Cl<sub>2</sub>**, while the closest intermolecular Au⋯Au distances are 8.840 Å in **1·2CH<sub>2</sub>Cl<sub>2</sub>** and 6.556 Å in **2·2CH<sub>2</sub>Cl<sub>2</sub>**.

Table 1. Selected bond lengths [Å] and angles [°] for **1·2CH<sub>2</sub>Cl<sub>2</sub>** and **2·2CH<sub>2</sub>Cl<sub>2</sub>**.

<b>1·2CH<sub>2</sub>Cl<sub>2</sub></b>		<b>2·2CH<sub>2</sub>Cl<sub>2</sub></b>	
Au–P1	2.271(2)	Au1–P1	2.282(4)
Au–C23	2.027(6)	Au1–C1	1.971(12)
C22–C23	1.162(10)	C1–C2	1.224(15)
C23–Au–P1	178.5(2)	C1–Au1–P1	177.2(4)
C22–C23–Au	175.5(8)	C2–C1–Au1	173.8(11)
C19–C22–C23	178.7(8)	C3–C2–C1	179.4(14)

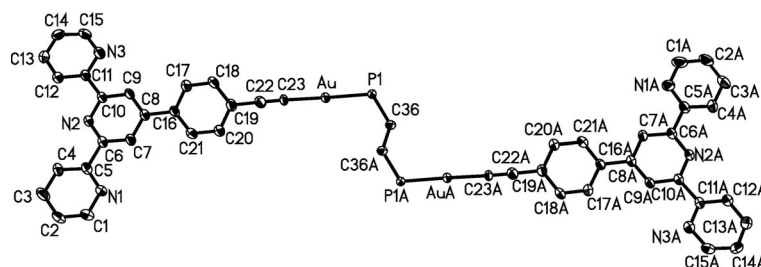


Figure 1. ORTEP drawing of  $1 \cdot 2\text{CH}_2\text{Cl}_2$  with atom labeling scheme showing 30% thermal ellipsoids. Phenyl rings of dppp,  $\text{CH}_2\text{Cl}_2$  molecules, and hydrogen atoms are omitted for clarity (symmetry code for A:  $-x - 2, -y - 1, -z - 1$ ).

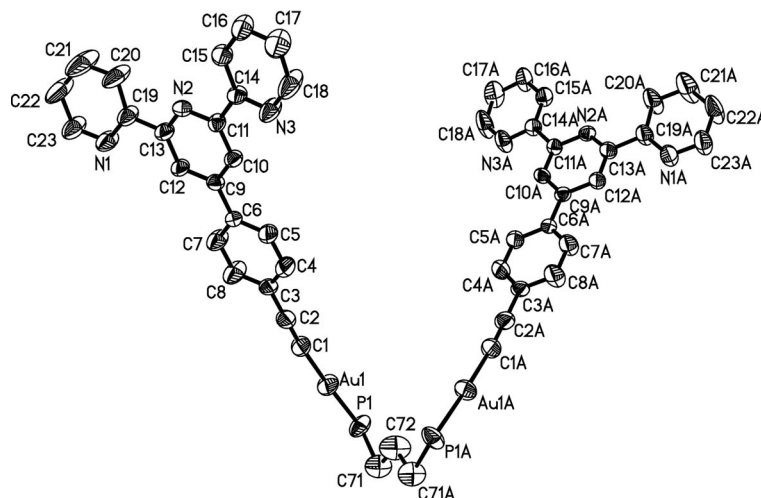


Figure 2. ORTEP drawing of  $2 \cdot 2\text{CH}_2\text{Cl}_2$  with atom labeling scheme showing 30% thermal ellipsoids. Phenyl rings of dppp,  $\text{CH}_2\text{Cl}_2$  molecules, and hydrogen atoms are omitted for clarity (symmetry code for A:  $-x + 1, y, 0.5 - z$ ).

These  $\text{Au} \cdots \text{Au}$  distances are much longer than  $3.6 \text{ \AA}$ ,<sup>[11d]</sup> indicating no intramolecular or intermolecular  $\text{Au} \cdots \text{Au}$  interaction in these complexes.

### C–H $\cdots$ Au Interaction

Weak X–H $\cdots$ M hydrogen bonds have received much attention in recent years, and they could be structurally significant in constructing supramolecular architectures, especially when no other classical hydrogen bonds and M $\cdots$ M interactions exist in a structure.<sup>[14b,19b–19d]</sup> As the metal centers act as Lewis bases, the electron-rich metals such as late transition metals in low oxidation states are favored. The X–H $\cdots$ M interactions with angles less than  $130^\circ$  have generally been excluded.<sup>[15,21]</sup> In the crystal structure of  $1 \cdot 2\text{CH}_2\text{Cl}_2$ , as shown in Figure 3, the molecules of **1** are linked through  $\text{C14} \cdots \text{H14A} \cdots \text{Au}$  ( $-x - 3, -y - 1, -z$ ) ( $d_{\text{H} \cdots \text{Au}} = 3.067 \text{ \AA}$ ,  $\angle \text{C} \cdots \text{H} \cdots \text{Au} = 154.7^\circ$ ) and  $\text{C27} \cdots \text{H27A} \cdots \text{Au}$  ( $x, y + 1, z$ ) ( $d_{\text{H} \cdots \text{Au}} = 3.163 \text{ \AA}$ ,  $\angle \text{C} \cdots \text{H} \cdots \text{Au} = 159.5^\circ$ ) interactions to produce 2-D layers, and the 2-D layers are reinforced through  $\pi \cdots \pi$  stacking interactions occurring between two exactly parallel pyridine rings consisting of six atoms (N2, C6–C10) and its symmetric ring at the  $-x - 3, -y - 2, -z$  position [intercentroid distance  $3.694(4) \text{ \AA}$ , per-

pendicular distance  $3.486(3) \text{ \AA}$ , offset  $1.222(3) \text{ \AA}$ ]. Similar weak interaction has been observed in the crystal structure of  $[\text{tpyC}_6\text{H}_4\text{C}\equiv\text{CAuPPh}_3]$ .<sup>[14b]</sup> The 2-D layers further interact with each other forming 3-D frameworks through  $\text{C25} \cdots \text{H25A} \cdots \text{Cl1}$  ( $-x - 2, -y, -z - 1$ ) weak hydrogen bonds [ $d_{\text{H} \cdots \text{Cl}} = 2.820 \text{ \AA}$ ,  $d_{\text{C25} \cdots \text{Cl}} = 3.658 \text{ \AA}$ ,  $\angle \text{C25} \cdots \text{H25A} \cdots \text{Cl1}$  ( $-x - 2, -y, -z - 1$ ) =  $151^\circ$ ] and  $\text{Cl2} \cdots \text{Cl2}$  ( $-x - 3, -y - 1, -z, 3.129 \text{ \AA}$ ) weak interactions (see Figure 4).<sup>[22]</sup> No obvious weak interaction was observed for  $2 \cdot 2\text{CH}_2\text{Cl}_2$ .

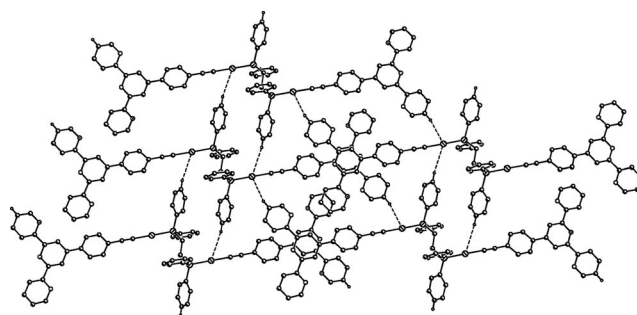


Figure 3. The 2-D layer of  $1 \cdot 2\text{CH}_2\text{Cl}_2$  induced by C–H $\cdots$ Au and  $\pi \cdots \pi$  interactions.  $\text{CH}_2\text{Cl}_2$  molecules and hydrogen atoms are omitted for clarity except H14A, H27A and their symmetrical atoms.

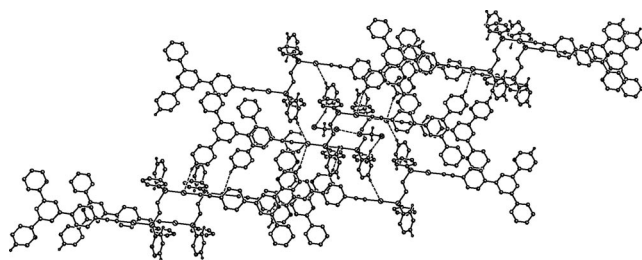


Figure 4. The 3-D framework of  $1 \cdot 2\text{CH}_2\text{Cl}_2$ . Phenyl rings of dppe and most hydrogen atoms are omitted for clarity.

## Photophysical Properties

### Absorption Spectra

UV/Vis absorption data for **1–5** in dichloromethane solution at 298 K are summarized in Table 2. The corresponding electronic absorption spectra are depicted in Figure 5. Though the spacers between two P donors in the diphosphane ligands change, the absorption spectra of complexes **1–5** are similar throughout the series, and they all display two distinct and intense absorption bands with one maxima at ca. 232 nm, and the other at ca. 315 nm with a shoulder absorption at ca. 303 nm. By comparison with the corresponding absorptions of the complexes  $[\text{Pt}\{\text{Ph}_2\text{P}(\text{CH}_2)_n\text{PPh}_2\}(\text{C}\equiv\text{CC}_6\text{H}_4\text{tpy})_2]$  ( $n = 1, 2$ , and 3) in our previous work and the analogous  $[\text{tpyC}_6\text{H}_4\text{C}\equiv\text{CAuPPh}_3]$  and  $[(\text{tpyC}_6\text{H}_4\text{C}\equiv\text{CAu})_2(\mu\text{-dppd})]$  {dppd = 1,10-bis(diphenylphosphanyl)decane} complexes reported by the Vicente group,<sup>[6,14b]</sup> the former higher energy bands arise primarily from diphosphane-centered transitions, and the latter lower energy bands are mainly due to intraligand (IL)  $\pi \rightarrow \pi^*$  transitions of the  $\text{C}\equiv\text{CC}_6\text{H}_4\text{tpy}$  units, mixed probably with

some Au orbital character. The low-energy absorption bands in complexes **1–5** display vibrational character with the vibronic spacings around  $1257\text{ cm}^{-1}$ , corresponding to vibrational stretching frequencies of the pyridyl in  $\text{C}\equiv\text{CC}_6\text{H}_4\text{tpy}$  units.<sup>[6]</sup> In addition, complexes **1–5** exhibit large molar absorption coefficients ( $\epsilon = 7.972 \times 10^4$  to  $1.130 \times 10^5$ ), which reveals their strong light-absorbing ability.<sup>[6,7d]</sup>

### Luminescence

The luminescence data, including emission wavelengths, lifetimes, and quantum yields of **1–5**, are presented in Table 3. The emission spectra of **1–5** in the solid state and in dichloromethane solution at 298 K are shown in Figures 6 and 7, respectively. All the dinuclear gold(I) complexes **1–5** exhibit dual emission bands both in the solid state and in dichloromethane solution at 298 K. Most low-energy bands for complexes **1–5** in the solid state and in the dichloromethane solution display vibronic character with spacings in the range of  $1225\text{--}1339\text{ cm}^{-1}$  which is typical of the  $\nu_{\text{C}\equiv\text{C}}$  and  $\nu_{\text{C}\equiv\text{N}}$  aromatic vibrational modes in the alkynyl ligands.<sup>[6,14b]</sup> As no obvious  $\pi \cdots \pi$  stacking and  $\text{Au} \cdots \text{Au}$  interactions are observed in the crystal structure of complex **2** and the emission bands of complexes **1–5** are similar, the low energy emissions may arise from intraligand character. Compared with the emission spectrum of  $\text{tpyC}_6\text{H}_4\text{C}\equiv\text{CH}$ , together with consideration of the smaller Stokes' shifts,<sup>[6]</sup> the high-energy emissions of binuclear gold(I) complexes **1–5** arise most probably from the  $^1(\pi \rightarrow \pi^*)$  excited state of the alkynyl ligand. With reference to the larger Stokes' shifts,<sup>[23]</sup> the vibrational spacings of typical  $\nu_{\text{C}\equiv\text{C}}$  and  $\nu_{\text{C}\equiv\text{N}}$  aromatic vibrational modes, and the emission properties of the reported gold(I)-alkynyl-phosphane complexes, especially those of  $[\text{tpyC}_6\text{H}_4\text{C}\equiv\text{CAuPPh}_3]$  and  $[(\text{tpyC}_6\text{H}_4\text{C}\equiv\text{CAu})_2(\mu\text{-dppd})]$ ,<sup>[7d,11,14b]</sup> the low-energy emission bands at ca. 490–540 nm of complexes **1–5** are tentatively assigned to the  $^3(\pi \rightarrow \pi^*)$  excited state of the acetylide ligand, mixed probably with some Au orbital character. In order to obtain deeper insight into the emissive properties, the radiation lifetime of the intense low-energy emission band at ca. 502 nm of complex **4** in dichloromethane solution was determined, and the long lifetime of 13.6  $\mu\text{s}$  further proves the triplet parentage of the low-energy band.<sup>[6]</sup> It is worth noting that the lower energy emission band at ca. 502 nm of complex **4** in dichloromethane solution is more obvious, and it is red-shifted 7–11 nm relative to those of complexes **1, 2, 3**, and **5**, indicating that a stronger interaction between  $\text{Au}^{\text{I}}$  and the  $\text{tpyC}_6\text{H}_4\text{C}\equiv\text{C}$  unit may exist in complex **4**, inducing stronger spin-orbital coupling and the increasing conjugated degree of the alkyne system. This can also be observed from the comparison between complex **1** and **2**. In complex **1**, the  $\text{Au}^{\text{I}}\text{--C}$  distance is  $2.027(6)\text{ \AA}$ , a little longer ( $0.056\text{ \AA}$ ) than that of  $1.971(12)\text{ \AA}$  in complex **2**, which indicates stronger interaction between  $\text{Au}^{\text{I}}$  and the  $\text{tpyC}_6\text{H}_4\text{C}\equiv\text{C}$  unit in complex **2**, and the phosphorescence emission of complex **2** in dichloromethane solution is more

Table 2. UV/Vis absorption data of **1–5** in dichloromethane solution at 298 K.

Compound	$\lambda$ [nm] ( $\epsilon$ [ $\text{M}^{-1}\text{cm}^{-1}$ ])
<b>1</b>	232 (103500), 301 (90230), 315 (96660)
<b>2</b>	232 (99500), 303 (85910), 315 (90340)
<b>3</b>	232 (113000), 303 (93080), 316 (96310)
<b>4</b>	232 (94400), 303 (79720), 314 (82880)
<b>5</b>	232 (104500), 302 (89550), 314 (93580)

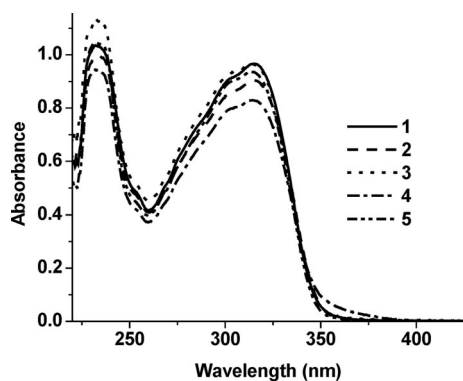


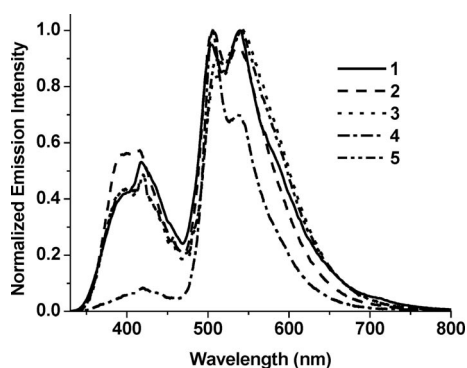
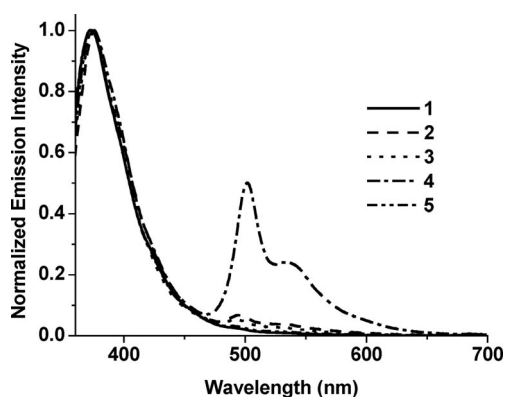
Figure 5. UV/Vis absorption spectra of **1–5** in dichloromethane solutions at 298 K.

obvious than that of complex **1**, and also a little red-shifted relative to that of complex **1**. In addition, the lower energy emission band at ca. 502 nm with a shoulder at 536 nm of complex **4** is close to that of 503 nm with a shoulder at 533 nm in  $[(\text{tpyC}_6\text{H}_4\text{C}\equiv\text{CAu})_2(\mu\text{-dppd})]$ , which is assigned to the intraligand  $^3(\pi\rightarrow\pi^*)$  excited state of the acetylide ligand.<sup>[14b]</sup>

Table 3. Luminescence data of **1–5**.

Compound	$\lambda_{\text{em}}$ [nm] (solid)	$\lambda_{\text{em}}$ [nm] ( $\tau_{\text{em}}$ [ $\mu\text{s}$ ]) ( $\text{CH}_2\text{Cl}_2$ )	$\Phi_{\text{em}}^{[a]}$
<b>1</b>	393 sh, 418	374	0.1089 <sup>[a]</sup>
	505 sh, 540	492 (w)	
<b>2</b>	394, 416 sh	377, 400	0.0745 <sup>[a]</sup>
	505, 540 sh	495 (w), 530 sh	
<b>3</b>	395, 420 sh	375	0.1419 <sup>[a]</sup>
	510, 544 sh	494, 529sh	
<b>4</b>	420	375	0.1331 <sup>[a]</sup>
	506, 540 sh	502 (13.6), 536 sh	
<b>5</b>	398, 420 sh	373	0.1340 <sup>[a]</sup>
	511, 541 sh	491, 525	

[a] The quantum yields in degassed  $\text{CH}_2\text{Cl}_2$  are determined relative to that of  $[\text{Ru}(\text{bpy})_3](\text{PF}_6)_2$  ( $\Phi = 0.062$ ) in degassed  $\text{CH}_3\text{CN}$ .<sup>[24]</sup>

Figure 6. Emission spectra of **1–5** in the solid state at room temperature.Figure 7. Emission spectra of **1–5** in fluid dichloromethane solution at room temperature.

## Spectrophotometric Titration

### Absorption Spectra Titration

The structural determination indicates the terpyridine units are free of coordination in complexes **1**·2 $\text{CH}_2\text{Cl}_2$  and

**2**·2 $\text{CH}_2\text{Cl}_2$ . These gold(I)-alkynyl-phosphane complexes can therefore be used as building blocks to react, through the polypyridine chelation, with  $\text{Ln}^{\text{III}}$  ions to form a  $\text{Au}_2\text{Ln}_2$  array as reported in our previous work.<sup>[6]</sup> We have tried our best to synthesize the  $\text{Au}_2\text{Ln}_2$  complexes, but no crystal suitable for single-crystal X-ray diffraction was obtained. So in order to explore how the UV/Vis absorption bands change when the dinuclear gold(I) complexes are coordinated to  $\text{Ln}^{\text{III}}$  ions, titrations were carried out by adding  $\text{Gd}(\text{hfac})_3(\text{H}_2\text{O})_2$  to the dichloromethane solution of complex **1**. It must be mentioned that because significant dissociation often occurs in very diluted solutions,<sup>[8f]</sup> the original total concentrations of  $\text{Au}_2$  units were kept at ca.  $1.0 \times 10^{-5} \text{ mol L}^{-1}$  and those of  $[\text{Gd}(\text{hfac})_3(\text{H}_2\text{O})_2]$  at ca.  $2.0 \times 10^{-5} \text{ mol L}^{-1}$ . Figure 8 (a) shows that the absorbance increases little by little, following the gradual addition of the dichloromethane solution of  $\text{Gd}(\text{hfac})_3(\text{H}_2\text{O})_2$  to that of **1**, and a graph of absorbance at 360 nm gives a smooth curve that fits well to a 2:1 binding ratio of  $\text{Gd}/\text{Au}_2$  (Figure 8, b), which is similar to those of  $[\{\text{Pt}(\text{PPh}_2(\text{CH}_2)_n\text{-PPh}_2)(\text{C}\equiv\text{CC}_6\text{H}_4\text{tpy})_2\}\{\text{Ln}(\text{hfac})_3\}_2]$  ( $n = 1$ , dpmp;  $n = 2$ , dppe;  $n = 3$ , dppp;  $\text{Ln} = \text{Eu}, \text{Nd}, \text{Yb}$ ) complexes in the previous work.<sup>[6]</sup>

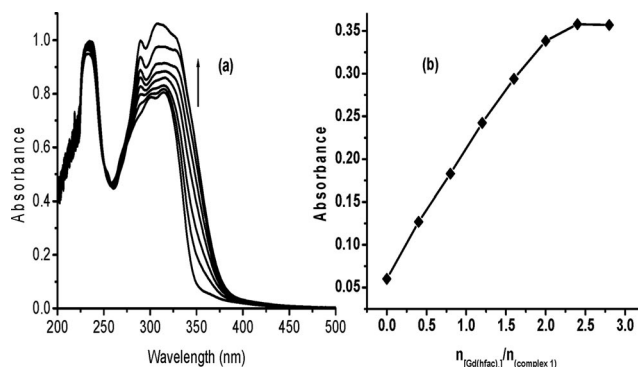


Figure 8. a: Changes in the UV/Vis absorption spectra by titration of **1** with  $\text{Gd}(\text{hfac})_3(\text{H}_2\text{O})_2$  in dichloromethane. b: Changes of absorbance at 360 nm vs. the ratio of  $\text{Gd}$  to  $\text{Au}_2$  moiety by titration of **1** with  $\text{Gd}(\text{hfac})_3(\text{H}_2\text{O})_2$  in dichloromethane.

## Luminescence Titration

For  $\text{Ln}^{\text{III}}$  complexes, both the singlet and triplet states of the ligand may transfer energy onto the  $\text{Ln}^{\text{III}}$  ions, but because of the short-lived character of the singlet state, energy transfer from it is often inefficient. So whether the energy gaps between the lowest triplets of the “metal complexes ligands” and  $\text{Ln}^{\text{III}}$  emitting levels are suitable for achieving sensitized luminescence of  $\text{Ln}^{\text{III}}$  is of primary importance. Though the triplet states of complexes **1–5** can not replace the triplet states of their corresponding  $\text{Gd}^{\text{III}}$  complexes, the easily determined triplet states of complexes **1–5** and their good luminescent properties at room temperature still make possible in a first step the following evaluations: (1) Whether complexes **1–5** can be used as sensitized chromophores for  $\text{Ln}^{\text{III}}$  luminescence; (2) which  $\text{Ln}^{\text{III}}$  ions may be



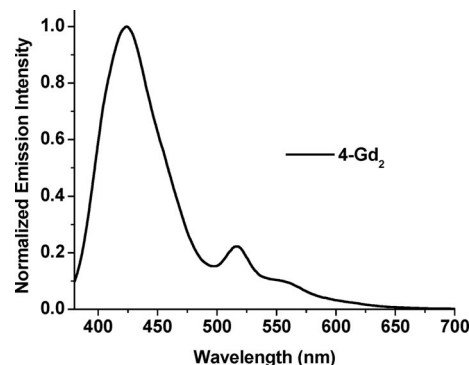
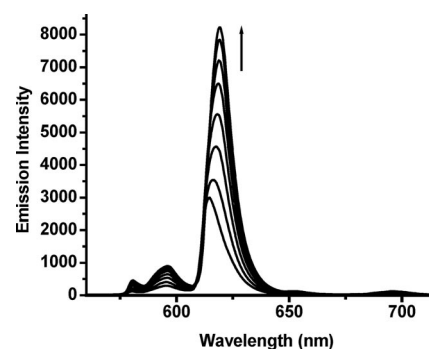
more efficiently sensitized. For example, all the triplet states of complexes **1–5** in dichloromethane solution in the range of 18904–20367 cm<sup>−1</sup> are lower than the emitting <sup>5</sup>D<sub>4</sub> transition of Tb<sup>III</sup> (20400 cm<sup>−1</sup>) and are therefore not expected to sensitize Tb<sup>III</sup> emission, but they all exceed to a sufficient extent the <sup>5</sup>D<sub>0</sub> level at 17241 cm<sup>−1</sup> (580 nm) of the corresponding Eu<sup>III</sup> complexes (see Table 4), so it is possible to use complexes **1–5** as antenna chromophores to achieve the sensitized luminescence of Eu<sup>III</sup> centers. In order to obtain more accurate data of the triplet states of the expected Au<sub>2</sub>Ln<sub>2</sub> complexes, the luminescence of the Au<sub>2</sub>Gd<sub>2</sub> dichloromethane solutions, which were prepared from complexes **1–5** and [Gd(hfac)<sub>3</sub>(H<sub>2</sub>O)<sub>2</sub>] according to the corresponding 1:2 ratio, were determined without O<sub>2</sub>. The lowest energy emitting state of Gd<sup>III</sup>, at 32150 cm<sup>−1</sup>, is too high to be excited by the antenna Au<sup>I</sup>-alkynyl chromophores used in this study. Consequently, the emission spectra of the Gd<sup>III</sup> complexes show exclusively Au<sup>I</sup>-alkynyl-centered emission. The corresponding data are summarized in Table 4. Only the triplet states of **4**-Gd<sub>2</sub> can be observed at room temperature. The emission spectrum of **4**-Gd<sub>2</sub> in dichloromethane solution is depicted in Figure 9. The energy gap between the triplet state of **4**-Gd<sub>2</sub> at about 19342 cm<sup>−1</sup> (517 nm) and the <sup>5</sup>D<sub>0</sub> energy level of Eu<sup>III</sup> is 2101 cm<sup>−1</sup>, which is suitable for efficient energy transfer to Eu<sup>III</sup> ions and prevention of possible energy back transfer.<sup>[25]</sup> Since complexes **1–5** are homologous, they are expected to behave as good energy donors to transfer energy to Eu<sup>III</sup> centers effectively. In order to observe how the Eu<sup>III</sup>-centered emission intensity changes when complexes **1–5** are coordinated to Eu(tta)<sub>3</sub>, emission titrations were carried out in the aerated dichloromethane solutions. Upon excitation at 300–380 nm, the Eu<sup>III</sup>-centered emission was enhanced greatly during the titration of [Eu(tta)<sub>3</sub>(H<sub>2</sub>O)<sub>2</sub>] by adding different amounts of complex **1**, following the different Au<sub>2</sub>/Eu ratios 0, 0.05, 0.10, 0.15, 0.20, 0.30, 0.40, and 0.50 (Figure 10). At a Au<sub>2</sub>/Eu ratio higher than 0.50, the Eu<sup>III</sup>-centered emission intensity decreased. The intensity of the Eu<sup>III</sup>-centered emission at a Au<sub>2</sub>/Eu ratio of 0.50 was 2.74-times that of [Eu(tta)<sub>3</sub>(H<sub>2</sub>O)<sub>2</sub>]. This large enhancement confirms the energy transfer from the [(tpyC<sub>6</sub>H<sub>4</sub>C≡CAu)<sub>2</sub>(μ-dppe)] unit to the Eu<sup>III</sup> center effectively.

The maximum excitation wavelength of Eu<sup>III</sup>-centered emission increased following the addition of [Eu(tta)<sub>3</sub>(H<sub>2</sub>O)<sub>2</sub>] to the dichloromethane solution of complex **1**, however it did not increase again when the Eu/Au<sub>2</sub> ratio was ca. 2.0 (Figure S1), confirming the 1:2 binding ratio between complex **1** and Eu(tta)<sub>3</sub>. The Eu<sup>III</sup>-centered emission quantum yields of **1**-Eu<sub>2</sub> to **5**-Eu<sub>2</sub> in dichloromethane solutions fall in the range 0.0400–0.0472, which is similar to those (0.0373–0.0445) of mononuclear Pt<sup>II</sup>-phosphane-alkynyl-Eu<sup>III</sup> complexes of the same alkyne ligand tpyC<sub>6</sub>H<sub>4</sub>C≡CH,<sup>[6]</sup> further confirming that the efficient energy transfer occurred from the [(tpyC<sub>6</sub>H<sub>4</sub>C≡CAu)<sub>2</sub>(μ-Ph<sub>2</sub>P(CH<sub>2</sub>)<sub>x</sub>PPh<sub>2</sub>)] (*x* = 2–6) series of units to the Eu<sup>III</sup> centers. The luminescence data, including emission wavelengths, lifetimes, and quantum yields of **1**-Ln<sub>2</sub> to **5**-Ln<sub>2</sub>, are presented in Table 4. All the Eu<sup>III</sup> solutions exhibit

Table 4. Luminescence data of **1**-Ln<sub>2</sub> to **5**-Ln<sub>2</sub> solutions at 298 K.

Solution	λ <sub>em</sub> [nm] (τ <sub>em</sub> [μs]) (CH <sub>2</sub> Cl <sub>2</sub> )	Φ <sub>em</sub> [a,b]
<b>1</b> -Eu <sub>2</sub>	618 (600.7)	0.0446 <sup>[a]</sup>
<b>2</b> -Eu <sub>2</sub>	618 (612.1)	0.0407 <sup>[a]</sup>
<b>3</b> -Eu <sub>2</sub>	618 (610.6)	0.0440 <sup>[a]</sup>
<b>4</b> -Eu <sub>2</sub>	618 (606.9)	0.0405 <sup>[a]</sup>
<b>4</b> -Gd <sub>2</sub>	398, 420 sh 511, 541 sh	
<b>5</b> -Eu <sub>2</sub>	618 (606.5)	0.0400 <sup>[a]</sup>
<b>1</b> -Yb <sub>2</sub>	980 (15.8)	0.0079 <sup>[b]</sup>
<b>2</b> -Yb <sub>2</sub>	980 (15.7)	0.0079 <sup>[b]</sup>
<b>3</b> -Yb <sub>2</sub>	980 (15.8)	0.0079 <sup>[b]</sup>
<b>4</b> -Yb <sub>2</sub>	980 (15.4)	0.0077 <sup>[b]</sup>
<b>5</b> -Yb <sub>2</sub>	980 (15.9)	0.0080 <sup>[b]</sup>

[a] The quantum yields in degassed CH<sub>2</sub>Cl<sub>2</sub> were determined relative to that of [Ru(bpy)<sub>3</sub>](PF<sub>6</sub>)<sub>2</sub> (Φ = 0.062) in degassed CH<sub>3</sub>CN.<sup>[24]</sup> [b] The quantum yields of Yb<sup>III</sup> complexes in dichloromethane solution at 298 K were estimated by the equation Φ = τ<sub>obs</sub>/τ<sub>0</sub>, in which τ<sub>obs</sub> is the observed emission lifetime and τ<sub>0</sub> is the radiative or “natural” lifetime of 2 ms. All the solutions containing Eu, Gd, and Yb were prepared from complexes **1** and [Eu(tta)<sub>3</sub>(H<sub>2</sub>O)<sub>2</sub>], [Gd(hfac)<sub>3</sub>(H<sub>2</sub>O)<sub>2</sub>], and [Yb(hfac)<sub>3</sub>(H<sub>2</sub>O)<sub>2</sub>] according to the corresponding ratio 1:2.

Figure 9. The emission spectrum of **4**-Gd<sub>2</sub> in dichloromethane solution at 298 K.Figure 10. Changes in Eu<sup>III</sup>-centered emission intensity upon titration of Eu(tta)<sub>3</sub>(H<sub>2</sub>O)<sub>2</sub> with complex **1** in dichloromethane upon excitation with 300 nm.

characteristic emission bands of Eu<sup>III</sup> ions at about 580, 596, 618, 652, and 695 nm for **1**-Eu<sub>2</sub> to **5**-Eu<sub>2</sub> solutions (prepared from [Eu(tta)<sub>3</sub>(H<sub>2</sub>O)<sub>2</sub>] and complexes **1–5** according to a 2:1 ratio) corresponding to the transitions <sup>5</sup>D<sub>0</sub>→<sup>7</sup>F<sub>0</sub>, <sup>7</sup>F<sub>1</sub>, <sup>7</sup>F<sub>2</sub>, <sup>7</sup>F<sub>3</sub>, <sup>7</sup>F<sub>4</sub>, respectively, with the dominant band at 618 nm (Figure S2).

Upon titration of  $[\text{Yb}(\text{hfac})_3(\text{H}_2\text{O})_2]$  with complex **1** in dichloromethane solution, a dramatic enhancement of  $\text{Yb}^{\text{III}}$  emission was observed with the  $\text{Au}_2/\text{Yb}$  ratios changing from 0, 0.10, 0.20, 0.30, 0.40 to 0.50 (Figure 11), which indicates that efficient energy transfer occurs from the  $\text{Au}_2$ -alkynyl unit to  $\text{Yb}^{\text{III}}$  centers. The intensity of  $\text{Yb}^{\text{III}}$ -centered emission at ca. 980 nm with the  $\text{Au}_2/\text{Yb}$  ratio at 0.50 was 3.37-times that of  $[\text{Yb}(\text{hfac})_3(\text{H}_2\text{O})_2]$ . All the  $\text{Au}_2\text{Yb}_2$  solutions (prepared from  $[\text{Yb}(\text{hfac})_3(\text{H}_2\text{O})_2]$  and complexes **1–5** according to a 2:1 ratio) exhibit the characteristic emission bands of  $\text{Yb}^{\text{III}}$  corresponding to the  $^2\text{F}_{5/2} \rightarrow ^2\text{F}_{7/2}$  transition at ca. 980 nm. The intrinsic quantum yields of  $\text{Yb}^{\text{III}}$  emission may be estimated by  $\Phi = \tau_{\text{obs}}/\tau_0$ , where  $\tau_{\text{obs}}$  is the observed emission lifetime and  $\tau_0$  is the “natural lifetime”.<sup>[6]</sup> The  $\text{Au}_2\text{Yb}_2$  solutions show emission lifetimes from 14.6–15.9  $\mu\text{s}$  and intrinsic quantum yields from 0.0073–0.0080 (see Table 4), which are comparable to those (0.0073–0.0080) of  $\text{Pt}^{\text{II}}$ -phosphane-alkynyl- $\text{Yb}^{\text{III}}$  complexes of the same alkyne ligand  $\text{tpyC}_6\text{H}_4\text{C}\equiv\text{CH}$  in our previous work.<sup>[6]</sup>

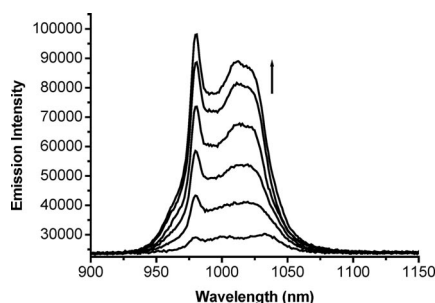


Figure 11. Changes of the  $\text{Yb}^{\text{III}}$ -centered emission intensity upon titration of  $[\text{Yb}(\text{hfac})_3(\text{H}_2\text{O})_2]$  with complex **1** in dichloromethane upon excitation with 330 nm.

## Conclusions

In conclusion, a series of dual luminescent binuclear gold(I) complexes of terpyridyl-functionalized alkyne ligands have been synthesized. Spectrophotometric titration and the quantum yields of  $\text{Ln}^{\text{III}}$  demonstrate that they can behave as good energy donors for sensitization of  $\text{Eu}^{\text{III}}$  and  $\text{Yb}^{\text{III}}$  emission, and as efficient chromophores, they are comparable to those of  $\text{Pt}^{\text{II}}$  complexes.<sup>[6]</sup>

## Experimental Section

**Materials and Reagents:** The reagents 1,2-bis(diphenylphosphanyl)ethane (dppe), 1,3-bis(diphenylphosphanyl)propane (dppp), 1,4-bis(diphenylphosphanyl)butane (dppb), 1,5-bis(diphenylphosphanyl)pentane (dpppen), 1,6-bis(diphenylphosphanyl)hexane (dppph), tetrahydrothiophene (tht), and  $\text{H}_3[\text{AuCl}_4]$  were commercially available without further purification. 4'-[4-{2-(trimethylsilyl)-1-ethynyl}phenyl]-2,2':6',2''-terpyridine ( $\text{tpyC}_6\text{H}_4\text{C}\equiv\text{CTMS}$ ), ( $\text{tpyC}_6\text{H}_4\text{C}\equiv\text{CAu}$ )<sub>n</sub>,  $[\text{Eu}(\text{tta})_3(\text{H}_2\text{O})_2]$ , and  $[\text{Ln}(\text{hfac})_3(\text{H}_2\text{O})_2]$  ( $\text{Ln} = \text{Gd}, \text{Yb}$ ) were prepared by the published methods.<sup>[26,7d,27]</sup> All solvents were purified and distilled using standard procedures before use except those for spectroscopic measurements which were of

spectroscopic grade. All other reagents were of analytical grade and were used as received.

**Preparation of Complexes:** All reactions were carried out under dry argon using Schlenk techniques at room temperature and a vacuum-line system unless specified.

**[( $\text{tpyC}_6\text{H}_4\text{C}\equiv\text{CAu}$ )<sub>2</sub>( $\mu$ -dppe)] (**1**):** Dppe (20.3 mg, 98%, 0.050 mmol) was added to a dichloromethane (15 mL) solution of ( $\text{tpyC}_6\text{H}_4\text{C}\equiv\text{CAu}$ )<sub>n</sub> (52.9 mg, 0.10 mmol) with stirring at room temperature for 30 min. The solution was concentrated and the product was purified by chromatography on a short silica-gel column using dichloromethane/methanol (100:2) as eluent. Addition of *n*-hexane to the concentrated solution gave the product as a pale yellow powder (yield 45 mg, 62%). Pale yellow crystals were obtained by layering *n*-hexane onto the concentrated dichloromethane solution in the absence of light.  $\text{C}_{72}\text{H}_{52}\text{Au}_2\text{N}_6\text{P}_2\cdot\text{CH}_2\text{Cl}_2$  (1542.06): calcd. C 56.87, H 3.53, N 5.45; found C 56.57, H 3.59, N 5.36. ESI-MS:  $m/z$  (%) = 1457.4 [ $\text{M} + \text{H}$ ]<sup>+</sup>, 1124.7 [ $\text{M} - \text{tpyC}_6\text{H}_4\text{C}\equiv\text{C}$ ]<sup>+</sup>. <sup>1</sup>H NMR ( $\text{CDCl}_3$ ):  $\delta$  = 8.75–8.72 (m, 8 H,  $\text{tpyC}_6\text{H}_4\text{C}\equiv\text{C}$ ), 8.67 (d, <sup>3</sup> $J_{\text{HH}}$  = 8.0 Hz, 4 H, H3'), 7.90–7.85 (m, 8 H,  $\text{tpyC}_6\text{H}_4\text{C}\equiv\text{C}$ ), 7.72–7.66 (m, 12 H,  $\text{tpyC}_6\text{H}_4\text{C}\equiv\text{C}$  and  $\text{PPh}_2$ ), 7.53–7.51 (m, 12 H,  $\text{PPh}_2$ ), 7.35 (m, 4 H, H5'), 2.70 (s, 4 H,  $\text{CH}_2$ ) ppm. IR spectrum (KBr):  $\tilde{\nu}$  = 2110 [ $\text{m}(\text{C}\equiv\text{C})$ ]  $\text{cm}^{-1}$ .

**[( $\text{tpyC}_6\text{H}_4\text{C}\equiv\text{CAu}$ )<sub>2</sub>( $\mu$ -dppp)] (**2**):** This compound was prepared by the same synthetic procedure as that of **1** except for using dppp instead of dppe. Color: pale yellow, yield: 43 mg, 59%. Pale yellow crystals were obtained by layering *n*-hexane onto the concentrated dichloromethane solution in the absence of light.  $\text{C}_{73}\text{H}_{54}\text{Au}_2\text{N}_6\text{P}_2$  (1471.15): calcd. C 59.58, H 3.70, N 5.71; found C 59.63, H 3.77, N 5.69. ESI-MS:  $m/z$  (%) = 1471.3 [ $\text{M} + \text{H}$ ]<sup>+</sup>, 1138.2 [ $\text{M} - \text{C}_6\text{H}_4\text{C}\equiv\text{C}$ ]<sup>+</sup>. <sup>1</sup>H NMR ( $\text{CDCl}_3$ ):  $\delta$  = 8.74–8.72 (m, 8 H, H3 and H6'), 8.67 (d, <sup>3</sup> $J_{\text{HH}}$  = 8.0 Hz, 4 H, H3'), 7.87 (td, <sup>3</sup> $J_{\text{HH}}$  = 8.0, <sup>4</sup> $J_{\text{HH}}$  = 2.0 Hz, 4 H, H4'), 7.84 (d,  $J$  = 7.2 Hz, 4 H,  $\text{tpyC}_6\text{H}_4\text{C}\equiv\text{C}$ ), 7.77–7.72 (m, 8 H,  $\text{tpyC}_6\text{H}_4\text{C}\equiv\text{C}$  and  $\text{PPh}_2$ ), 7.65–7.63 (m, 4 H,  $\text{PPh}_2$ ), 7.49–7.44 (m, 12 H,  $\text{PPh}_2$ ), 7.34 (m, 4 H, H5'), 2.87 (m,  $J$  = 4.5 Hz, 4 H,  $\text{PCH}_2$ ), 1.99 (m, 2 H,  $\text{PCH}_2\text{CH}_2$ ) ppm. IR spectrum (KBr):  $\tilde{\nu}$  = 2110 [ $\text{m}(\text{C}\equiv\text{C})$ ]  $\text{cm}^{-1}$ .

**[( $\text{tpyC}_6\text{H}_4\text{C}\equiv\text{CAu}$ )<sub>2</sub>( $\mu$ -dppb)] (**3**):** This compound was prepared by the same synthetic procedure as that of **1** except for using dppb instead of dppe. Color: pale yellow, yield: 45 mg, 61%.  $\text{C}_{74}\text{H}_{56}\text{Au}_2\text{N}_6\text{P}_2$  (1485.18): calcd. C 59.82, H 3.80, N 5.66; found C 59.52, H 3.85, N 5.60. ESI-MS:  $m/z$  (%) = 1152.1 [ $\text{M} - \text{tpyC}_6\text{H}_4\text{C}\equiv\text{C}$ ]<sup>+</sup>. <sup>1</sup>H NMR ( $\text{CDCl}_3$ ):  $\delta$  = 8.74–8.72 (m, 8 H, H3 and H6'), 8.67 (d, <sup>3</sup> $J_{\text{HH}}$  = 8.0 Hz, 4 H, H3'), 7.87 (td, <sup>3</sup> $J_{\text{HH}}$  = 7.6, <sup>4</sup> $J_{\text{HH}}$  = 2.0 Hz, 4 H, H4'), 7.84 (d,  $J$  = 8.0 Hz, 4 H,  $\text{tpyC}_6\text{H}_4\text{C}\equiv\text{C}$ ), 7.71–7.63 (m, 12 H,  $\text{tpyC}_6\text{H}_4\text{C}\equiv\text{C}$  and  $\text{PPh}_2$ ), 7.50–7.49 (m, 12 H,  $\text{PPh}_2$ ), 7.35 (ddd, <sup>3</sup> $J_{\text{HH}}$  = 8.0 and 4.8, <sup>4</sup> $J_{\text{HH}}$  = 1.2 Hz, 4 H, H5'), 2.44 (m, 4 H,  $\text{PCH}_2$ ), 1.83 (m, 4 H,  $\text{PCH}_2\text{CH}_2$ ) ppm. IR spectrum (KBr):  $\tilde{\nu}$  = 2110 [ $\text{m}(\text{C}\equiv\text{C})$ ]  $\text{cm}^{-1}$ .

**[( $\text{tpyC}_6\text{H}_4\text{C}\equiv\text{CAu}$ )<sub>2</sub>( $\mu$ -dpppen)] (**4**):** This compound was prepared by the same synthetic procedure as that of **1** except for using dpppen instead of dppe. Color: pale yellow, yield: 48 mg, 64%.  $\text{C}_{75}\text{H}_{58}\text{Au}_2\text{N}_6\text{P}_2$  (1499.21): calcd. C 60.07, H 3.90, N 5.61; found C 59.86, H 3.96, N 5.65. ESI-MS:  $m/z$  (%) = 1166.5 [ $\text{M} - \text{tpyC}_6\text{H}_4\text{C}\equiv\text{C}$ ]<sup>+</sup>. <sup>1</sup>H NMR ( $\text{CDCl}_3$ ):  $\delta$  = 8.73–8.72 (m, 8 H, H3 and H6'), 8.66 (d, <sup>3</sup> $J_{\text{HH}}$  = 8.0 Hz, 4 H, H3'), 7.87 (td, <sup>3</sup> $J_{\text{HH}}$  = 7.6, <sup>4</sup> $J_{\text{HH}}$  = 2.0 Hz, 4 H, H4'), 7.85 (d,  $J$  = 8.0 Hz, 4 H,  $\text{tpyC}_6\text{H}_4\text{C}\equiv\text{C}$ ), 7.74–7.64 (m, 12 H,  $\text{tpyC}_6\text{H}_4\text{C}\equiv\text{C}$  and  $\text{PPh}_2$ ), 7.49–7.46 (m, 12 H,  $\text{PPh}_2$ ), 7.35 (ddd, <sup>3</sup> $J_{\text{HH}}$  = 7.6 and 4.8, <sup>4</sup> $J_{\text{HH}}$  = 1.2 Hz, 4 H, H5'), 2.41 (m,  $J$  = 6.0 Hz, 4 H,  $\text{PCH}_2$ ), 1.69 [s, 6 H,  $\text{PCH}_2(\text{CH}_2)_3$ ] ppm. IR spectrum (KBr):  $\tilde{\nu}$  = 2109 [ $\text{m}(\text{C}\equiv\text{C})$ ]  $\text{cm}^{-1}$ .

**[( $\text{tpyC}_6\text{H}_4\text{C}\equiv\text{CAu}$ )<sub>2</sub>( $\mu$ -dpph)] (**5**):** This compound was prepared by the same synthetic procedure as that of **1** except for using dpph

instead of dppe. Color: pale yellow, yield: 76 mg, 90%.  $C_{76}H_{60}Au_2N_6P_2$  (1513.23): calcd. C 60.30, H 4.00, N 5.56; found C 60.01, H 4.03, N 5.47. ESI-MS:  $m/z$  (%) = 1180.9 [M –  $tpyC_6H_4C\equiv C$ ]<sup>+</sup>. <sup>1</sup>H NMR (CDCl<sub>3</sub>):  $\delta$  = 8.73–8.72 (m, 8 H, H3 and H6'), 8.66 (d, <sup>3</sup> $J_{HH}$  = 8.0 Hz, 4 H, H3'), 7.87 (td, <sup>3</sup> $J_{HH}$  = 7.8, <sup>4</sup> $J_{HH}$  = 2.0 Hz, 4 H, H4'), 7.83 (d,  $J$  = 8.4 Hz, 4 H,  $tpyC_6H_4C\equiv C$ ), 7.72–7.63 (m, 12 H,  $tpyC_6H_4C\equiv C$  and  $PPh_2$ ), 7.49–7.46 (m, 12 H,  $PPh_2$ ), 7.35 (ddd, <sup>3</sup> $J_{HH}$  = 7.6 and 4.8, <sup>4</sup> $J_{HH}$  = 1.2 Hz, 4 H, H5'), 2.43 (m,  $J$  = 7.5 Hz, 4 H,  $PCH_2$ ), 1.60 (s, 4 H,  $PCH_2CH_2$ ) ppm. 1.48 (m, 4 H,  $PCH_2CH_2CH_2$ ). IR spectrum (KBr):  $\tilde{\nu}$  = 2111 [m (C $\equiv$ C)] cm<sup>–1</sup>.

**Crystal Structure Determination:** Crystals suitable for X-ray diffraction studies of **1**·2CH<sub>2</sub>Cl<sub>2</sub> and **2**·2CH<sub>2</sub>Cl<sub>2</sub> were obtained by layering *n*-hexane onto the corresponding dichloromethane solution in the absence of light. Single crystals were sealed in capillaries with mother liquors. **1**·2CH<sub>2</sub>Cl<sub>2</sub> and **2**·2CH<sub>2</sub>Cl<sub>2</sub> were measured with a RIGAKU MERCURY CCD and RIGAKU SCXmini diffractometer, respectively, using the  $\omega$ -scan technique at room temperature with graphite-monochromated Mo- $K_\alpha$  radiation ( $\lambda$  = 0.71073 Å). The CrystalClear software package<sup>[28–29]</sup> and Bruker SAINT<sup>[30]</sup> were used for data reduction and empirical absorption correction, respectively. The structures were solved by direct methods. The heavy atoms were located from the E-map, and the rest of the non-hydrogen atoms were found in subsequent Fourier maps. The non-hydrogen atoms were refined anisotropically, whereas the hydrogen atoms were generated geometrically with isotropic thermal parameters. The structures were refined on  $F^2$  by full-matrix least-squares methods using the SHELXTL-97 program package.<sup>[31]</sup> The crystallographic data of **1**·2CH<sub>2</sub>Cl<sub>2</sub> and **2**·2CH<sub>2</sub>Cl<sub>2</sub> are summarized in Table 1.

CCDC-770767 (for **1**·2CH<sub>2</sub>Cl<sub>2</sub>) and CCDC-770768 (for **2**·2CH<sub>2</sub>Cl<sub>2</sub>) contain the supplementary crystallographic data for this paper. These data can be obtained free of charge from The Cambridge Crystallographic Data Centre via [www.ccdc.cam.ac.uk/data\\_request/cif](http://www.ccdc.cam.ac.uk/data_request/cif).

**Physical Measurements:** <sup>1</sup>H NMR spectra were measured with a Bruker Avance III (400 MHz) spectrometer with SiMe<sub>4</sub> as the internal reference. Infrared (IR) spectra were obtained from KBr pellets using a Bruker Optics TENSOR 27 FT-IR spectrophotometer. UV/Vis absorption spectra were recorded with a Purkinje General TU-1901 UV/Vis spectrophotometer. Elemental analyses (C, H, N) were carried out with a Perkin–Elmer model 240C elemental analyzer. Electrospray mass spectra (ES-MS) were performed with a Finnigan LCQ mass spectrometer using a dichloromethane/methanol mixture as the mobile phase. Steady-state excitation and emission spectra in the UV/Vis region were recorded with a Perkin–Elmer LS55 luminescence spectrometer with a red-sensitive photomultiplier type R928 or an Edinburgh F900 fluorescence spectrometer. The steady-state near-infrared (NIR) emission spectra were measured with an Edinburgh FLS920 fluorescence spectrometer equipped with a Hamamatsu R5509–72 supercooled photomultiplier tube at 193 K and a TM300 emission monochromator with NIR grating blazed at 1000 nm. The NIR emission spectra were corrected via a calibration curve supplied with the instrument. Emission lifetimes were determined with an Edinburgh Analytical Instrument (F900 fluorescence spectrometer) and the resulting emission was detected by a thermoelectrically cooled Hamamatsu R3809 photomultiplier tube. The emission quantum yields ( $\Phi$ ) in the UV/Vis region in degassed dichloromethane solutions at room temperature were calculated by  $\Phi_s = \Phi_r(B_r/B_s)(n_s/n_r)^2(D_s/D_r)$  using [Ru(bpy)<sub>3</sub>](PF<sub>6</sub>)<sub>2</sub> in acetonitrile as the standard ( $\Phi_{em}$  = 0.062), where the subscripts r and s denote reference standard and the sample solution, respectively; and  $n$ ,  $D$  and  $\Phi$  are the refractive

index of the solvents, the integrated intensity and the luminescence quantum yield, respectively.<sup>[24,32]</sup> The quantity  $B$  in the equation  $\Phi_s = \Phi_r(B_r/B_s)(n_s/n_r)^2(D_s/D_r)$  is calculated by  $B = 1 - 10^{-AL}$ , where  $A$  is the absorbance at the excitation wavelength and  $L$  is the optical path length. All the solutions used for determination of emission lifetimes and quantum yields were prepared after rigorous removal of oxygen by three successive freeze–pump–thaw cycles under vacuum in a 10-cm<sup>3</sup> round-bottomed flask equipped with a side arm 1-cm fluorescence cuvette and sealed from the atmosphere by a quick-release Teflon® stopper.<sup>[6b]</sup>

**Supporting Information** (see also the footnote on the first page of this article): Changes of the excitation spectra and the maximum excitation wavelength with the emission at 618 nm upon titration of complex **1** with [Eu(tta)<sub>3</sub>(H<sub>2</sub>O)<sub>2</sub>] in dichloromethane following different Eu/Au<sub>2</sub> ratios (Figure S1), and Eu<sup>III</sup>-centered emission spectra of **1**-Eu<sub>2</sub> in dichloromethane solution (Figure S2).

## Acknowledgments

This work was supported financially by the National Natural Science Foundation of China (NSFC) (20801047, 20931006, and 20772103), the Foundation of Xuzhou Normal University (07XLA07, KY2007039, and XGG2007034) and the QingLan Project of Jiangsu Province (08QLT001).

- [1] a) J. C. G. Bünzli, *Acc. Chem. Res.* **2006**, *39*, 53–61; b) J. C. G. Bünzli, C. Piguet, *Chem. Soc. Rev.* **2005**, *34*, 1048–1077; c) J. C. G. Bünzli, C. Piguet, *Chem. Rev.* **2002**, *102*, 1897–1928.
- [2] a) Z. N. Chen, Y. Fan, J. Ni, *Dalton Trans.* **2008**, 573–581; b) M. D. Ward, *Coord. Chem. Rev.* **2007**, *251*, 1663–1677; c) J. G. Mao, *Coord. Chem. Rev.* **2007**, *251*, 1493–1520; d) D. Parker, *Coord. Chem. Rev.* **2000**, *205*, 109–130; e) K. Kuriki, Y. Koike, Y. Okamoto, *Chem. Rev.* **2002**, *102*, 2347–2356; f) A. de Bettencourt-Dias, *Dalton Trans.* **2007**, 2229–2241.
- [3] a) Z. Zheng, *Chem. Commun.* **2001**, 2521–2529; b) F. X. Zang, Z. R. Hong, W. L. Li, M. T. Li, X. Y. Sun, *Appl. Phys. Lett.* **2004**, *84*, 2679–2681; c) D. Guo, C. Y. Duan, F. Lu, Y. Hasegawa, Q. J. Meng, S. Yanagida, *Chem. Commun.* **2004**, 1486–1487; d) X. Zhu, J. Lü, X. Li, S. Gao, G. Li, F. Xiao, R. Cao, *Cryst. Growth Des.* **2008**, *8*, 1897–1901.
- [4] a) T. Lazarides, N. M. Tart, D. Sykes, S. Faulkner, A. Barbieri, M. D. Ward, *Dalton Trans.* **2009**, 3971–3979; b) T. Lazarides, H. Adams, D. Sykes, S. Faulkner, G. Calogero, M. D. Ward, *Dalton Trans.* **2008**, 691–698; c) S. G. Baca, H. Adams, D. Sykes, S. Faulkner, M. D. Ward, *Dalton Trans.* **2007**, 2419–2430; d) F. Kennedy, N. M. Shavaleev, T. Koullourou, Z. R. Bell, J. C. Jeffery, S. Faulkner, M. D. Ward, *Dalton Trans.* **2007**, 1492–1499; e) T. Lazarides, M. A. H. Alamir, H. Adams, S. J. A. Pope, S. Faulkner, J. A. Weinstein, M. D. Ward, *Dalton Trans.* **2007**, 1484–1491; f) T. K. Ronson, H. Adams, L. P. Harding, S. J. A. Pope, D. Sykes, S. Faulkner, M. D. Ward, *Dalton Trans.* **2007**, 1006–1022.
- [5] a) A. P. S. Samuel, E. G. Moore, M. Melchior, J. Xu, K. N. Raymond, *Inorg. Chem.* **2008**, *47*, 7535–7544; b) M. Giraud, E. S. Andreiadis, A. S. Fisyuk, R. Demadrille, J. Pécaut, D. Imbert, M. Mazzanti, *Inorg. Chem.* **2008**, *47*, 3952–3954; c) C. P. Montgomery, B. S. Murray, J. N. Elizabeth, R. Pal, D. Parker, *Acc. Chem. Res.* **2009**, *42*, 925–937; d) E. G. Moore, A. P. S. Samuel, K. N. Raymond, *Acc. Chem. Res.* **2009**, *42*, 542–552; e) J. L. Worlinsky, S. Basu, *J. Phys. Chem. B* **2009**, *113*, 865–868; f) K. Hanaoka, K. Kikuchi, S. Kobayashi, T. Nagano, *J. Am. Chem. Soc.* **2007**, *129*, 13502–13509; g) H. Li, P. Liu, Y. Wang, L. Zhang, J. Yu, H. Zhang, B. Liu, U. Schubert, *J. Phys. Chem. C* **2009**, *113*, 3945–3949.
- [6] a) X. L. Li, F. R. Dai, L. Y. Zhang, Y. M. Zhu, Q. Peng, Z. N. Chen, *Organometallics* **2007**, *26*, 4483–4490; b) X. L. Li, L. X.



- Shi, L. Y. Zhang, H. M. Wen, Z. N. Chen, *Inorg. Chem.* **2007**, *46*, 10892–10900.
- [7] a) H. B. Xu, L. X. Shi, E. Ma, L. Y. Zhang, Q. H. Wei, Z. N. Chen, *Chem. Commun.* **2006**, 1601–1603; b) H. B. Xu, L. Y. Zhang, Z. L. Xie, E. Ma, Z. N. Chen, *Chem. Commun.* **2007**, 2744–2746; c) H. B. Xu, L. Y. Zhang, Z. H. Chen, L. X. Shi, Z. N. Chen, *Dalton Trans.* **2008**, 4664–4670; d) H. B. Xu, L. Y. Zhang, J. Ni, H. Y. Chao, Z. N. Chen, *Inorg. Chem.* **2008**, *47*, 10744–10752.
- [8] a) T. K. Ronson, T. Lazarides, H. Adams, S. J. A. Pope, D. Sykes, S. Faulkner, S. J. Coles, M. B. Hursthouse, W. Clegg, R. W. Harrington, M. D. Ward, *Chem. Eur. J.* **2006**, *12*, 9299–9313; b) P. D. Beer, F. Szemes, P. Passaniti, M. Maestri, *Inorg. Chem.* **2004**, *43*, 3965–3975; c) S. I. Klink, H. Keizer, F. C. J. M. van Veggel, *Angew. Chem. Int. Ed.* **2000**, *39*, 4319–4321; d) N. M. Shavaleev, L. P. Moorcraft, S. J. A. Pope, Z. R. Bell, S. Faulkner, M. D. Ward, *Chem. Eur. J.* **2003**, *9*, 5283–5291; e) N. M. Shavaleev, L. P. Moorcraft, S. J. A. Pope, Z. R. Bell, S. Faulkner, M. D. Ward, *Chem. Commun.* **2003**, 1134–1135; f) N. M. Shavaleev, G. Accorsi, D. Virgili, Z. R. Bell, T. Lazarides, G. Calogero, N. Armaroli, M. D. Ward, *Inorg. Chem.* **2005**, *44*, 61–72.
- [9] a) F. F. Chen, Z. Q. Bian, Z. W. Liu, D. B. Nie, Z. Q. Chen, C. H. Huang, *Inorg. Chem.* **2008**, *47*, 2507–2513; b) M. Shi, F. Li, T. Yi, D. Zhang, H. Hu, C. Huang, *Inorg. Chem.* **2005**, *44*, 8929–8936; c) H. Xin, M. Shi, X. C. Gao, Y. Y. Huang, Z. L. Gong, D. B. Nie, H. Cao, Z. Q. Bian, F. Y. Li, H. H. Chun, *J. Phys. Chem. B* **2004**, *108*, 10796–10800; d) H. Xin, M. Shi, X. M. Zhang, F. Y. Li, Z. Q. Bian, K. Ibrahim, F. Q. Liu, H. H. Chun, *Chem. Mater.* **2003**, *15*, 3728–3733.
- [10] a) M. Latva, H. Takalo, V.-M. Mikkala, C. Matachescu, J. C. Rodriguez-Ubis, J. Kankare, *J. Lumin.* **1997**, *75*, 149–169; b) N. M. Shavaleev, R. Scopelliti, F. Gumy, J. C. G. Bünzli, *Inorg. Chem.* **2009**, *48*, 6178–6191; c) D. S. Oxley, R. W. Walters, J. E. Copenhafer, T. Y. Meyer, S. Petoud, H. M. Edenborn, *Inorg. Chem.* **2009**, *48*, 6332–6334.
- [11] a) W. Lu, N. Zhu, C. M. Che, *J. Am. Chem. Soc.* **2003**, *125*, 16081–16088; b) C. M. Che, H.-Y. Chao, V. M. Miskowski, Y. Li, K. K. Cheung, *J. Am. Chem. Soc.* **2001**, *123*, 4985–4991; c) W. Lu, H. F. Xiang, N. Zhu, C. M. Che, *Organometallics* **2002**, *21*, 2343–2346; d) H. Y. Chao, W. Lu, Y. Li, M. C. W. Chan, C. M. Che, K. K. Cheung, N. Zhu, *J. Am. Chem. Soc.* **2002**, *124*, 14696–14706.
- [12] a) X. X. Lu, C. K. Li, E. C. C. Cheng, N. Y. Zhu, V. W. W. Yam, *Inorg. Chem.* **2004**, *43*, 2225–2227; b) V. W. W. Yam, S. W. K. Choi, K. K. Cheung, *Organometallics* **1996**, *15*, 1734–1739.
- [13] P. Li, B. Ahrens, A. D. Bond, J. E. Davies, O. F. Koentjoro, P. R. Raithby, S. J. Teat, *Dalton Trans.* **2008**, 1635–1646.
- [14] a) W. J. Hinks, M. A. MacDonald, M. C. Jennings, P. J. Puddephatt, *Organometallics* **2000**, *19*, 5063–5070; b) J. Vicente, J. Gil-Rubio, N. Barquero, P. G. Jones, D. Bautista, *Organometallics* **2008**, *27*, 646–659.
- [15] J. Vicente, M. T. Chicote, M. M. Alvarez-Falcón, *Organometallics* **2005**, *24*, 5956–5963.
- [16] S. S. Y. Chui, M. F. Y. Ng, C. M. Che, *Chem. Eur. J.* **2005**, *11*, 1739–1749.
- [17] M. A. MacDonald, R. J. Puddephatt, G. P. A. Yap, *Organometallics* **2000**, *19*, 2194–2199.
- [18] a) V. W. W. Yam, S. K. Yip, L. H. Yuan, K. L. Cheung, K. K. Cheung, *Organometallics* **2003**, *22*, 2630–2637; b) H. S. Tang, N. Zhu, V. W. W. Yam, *Organometallics* **2007**, *26*, 22–25; c) X. He, N. Zhu, V. W. W. Yam, *Organometallics* **2009**, *28*, 3621–3624.
- [19] a) J. Vicente, M. T. Chicote, M. M. Álvarez-Falcón, P. G. Jones, *Organometallics* **2005**, *24*, 2764–2772; b) J. Vicente, M. T. Chicote, M. M. Álvarez-Falcón, P. G. Jones, *Organometallics* **2005**, *24*, 4666–4675; c) J. Vicente, M. T. Chicote, M. M. Álvarez-Falcón, M. A. Fox, D. Bautista, *Organometallics* **2003**, *22*, 4792–4797; d) J. Vicente, M. T. Chicote, M. M. Álvarez-Falcón, P. G. Jones, *Chem. Commun.* **2004**, 2658–2659.
- [20] a) C. P. McArdle, S. Van, M. C. Jennings, R. J. Puddephatt, *J. Am. Chem. Soc.* **2002**, *124*, 3959–3965; b) N. C. Habermehl, M. C. Jennings, C. P. McArdle, F. Mohr, R. J. Puddephatt, *Organometallics* **2005**, *24*, 5004–5014; c) C. P. McArdle, M. J. Irwin, M. C. Jennings, J. J. Vittal, R. J. Puddephatt, *Chem. Eur. J.* **2002**, *8*, 723–734; d) C. P. McArdle, M. C. Jennings, J. J. Vittal, R. J. Puddephatt, *Chem. Eur. J.* **2001**, *7*, 3572–3583; e) M. J. Irwin, J. J. Vittal, R. J. Puddephatt, *Organometallics* **1997**, *16*, 3541–3547; f) G. Jia, R. J. Puddephatt, I. D. Scott, J. Vittal, *Organometallics* **1993**, *12*, 3565–3574.
- [21] J. Vicente, M.-T. Chicote, M. D. Abrisqueta, M. M. Alvarez-Falcón, *Organometallics* **2003**, *22*, 4327–4333.
- [22] E. M. Barranco, O. Crespo, M. C. Gimeno, A. Laguna, *Inorg. Chem.* **2000**, *39*, 680–687.
- [23] a) D. H. Waldeck, *Chem. Rev.* **1991**, *91*, 415–436; b) K. Haskins-Glusac, I. Ghiviriga, K. A. Abboud, K. S. Schanze, *J. Phys. Chem. B* **2004**, *108*, 4969–4978.
- [24] J. N. Demas, G. A. Crosby, *J. Phys. Chem.* **1971**, *75*, 991–1024.
- [25] L. N. Puntus, K. A. Lyssenko, M. Y. Antipin, J. C. Bunzli, *Inorg. Chem.* **2008**, *47*, 11095–11107.
- [26] V. Grosshenny, F. M. Romero, R. Ziessel, *J. Org. Chem.* **1997**, *62*, 1491–1500.
- [27] Y. Hasegawa, Y. Kimura, K. Murakoshi, Y. Wada, J. H. Kim, N. Nakashima, T. Yamanaka, S. Yanagida, *J. Phys. Chem.* **1996**, *100*, 10201–10205.
- [28] Rigaku & Molecular Structure Corporation, *CrystalClear*, Rigaku Corporation, Tokyo, Japan, and MSC, The Woodlands, Texas, USA, **2000**.
- [29] Rigaku, *CrystalClear*, Rigaku Corporation, Tokyo, Japan, **2005**.
- [30] Bruker SAINT, Bruker AXS Inc., Madison, Wisconsin, USA, **2001**.
- [31] G. M. Sheldrick, *SHELXL-97, Program for the Refinement of Crystal Structures*, University of Göttingen, Göttingen, Germany, **1997**.
- [32] J. V. Caspar, T. J. Meyer, *J. Am. Chem. Soc.* **1983**, *105*, 5583–5590.

Received: March 24, 2010  
Published Online: June 16, 2010



# pH-Responsive Switching of the Near-Infrared Absorption of the Water-Soluble Bis(*o*-diiminobenzosemiquinonato)platinum(II) Complex

Atsuko Masuya,<sup>[a]</sup> Nobuhiko Iki,<sup>\*,[a]</sup> Chizuko Kabuto,<sup>[b]</sup> Yasunori Ohba,<sup>[c]</sup> Seigo Yamauchi,<sup>[c]</sup> and Hitoshi Hoshino<sup>[a]</sup>

**Keywords:** Absorption / Platinum / Radicals / N ligands / Electronic structure

The electronic structure of a water-soluble near-infrared (NIR)-absorbing complex was determined to be singlet diradical  $[\text{Pt}^{\text{II}}(\text{L}^{\text{ISQ}})_2]^{2-}$  [ $\text{L}^{\text{ISQ}} = o\text{-diiminosulfobenzosemiquinonate radical}$ ] by X-ray diffraction and  $^1\text{H}$  NMR spectroscopy. Cyclic voltammetry (CV) showed redox reactions of  $[\text{Pt}^{\text{II}}(\text{L}^{\text{ISQ}})_2]^{2-}$  to give  $[\text{Pt}^{\text{II}}(\text{L}^{\text{ISQ}})(\text{L}^{\text{IBQ}})]^-$  ( $E_{1/2}^1 = -0.26$  V vs.  $\text{Fc}^+/\text{Fc}$ ) and  $[\text{Pt}^{\text{II}}(\text{L}^{\text{ISQ}})(\text{L}^{\text{PDI}})]^{3-}$  ( $E_{1/2}^2 = -1.46$  V) [ $\text{L}^{\text{IBQ}} = o\text{-diiminosulfobenzoquinonate}$ , ( $\text{L}^{\text{PDI}} = o\text{-phenylenediiminesulfonate}$ ].

The monoradical structure of the latter was confirmed by electron paramagnetic resonance (EPR) spectroscopy. Splitting of the reduction wave of  $[\text{Pt}^{\text{II}}(\text{L}^{\text{ISQ}})(\text{L}^{\text{IBQ}})]^-$  in CV and the weak EPR signal suggested the formation of a dimer. Because the rest potential of the solution exceeds  $E_{\text{pa}}^1$  at pH 4.0, the decrease in the NIR absorption at pH < 4.0 can be attributed to the oxidation of  $[\text{Pt}^{\text{II}}(\text{L}^{\text{ISQ}})_2]^{2-}$  followed by dimerization.

## Introduction

Near-infrared (NIR) light of 700–1200 nm effectively penetrates biological tissues and hence in vivo optical-imaging techniques based on NIR absorption, such as optical coherence tomography (OCT) and photoacoustic tomography (PAT), have received much attention.<sup>[1,2]</sup> In these techniques, NIR-absorbing organic dyes such as SDA7460 or Indocyanine Green play important roles as contrast agents improving the signal-to-noise ratio. Recently, Au nanocages have emerged as efficient NIR-absorbing contrast agents for OCT and PAT.<sup>[3,4]</sup>

One of the most effective ways to further enhance the contrasting ability of NIR-absorbing agents is to introduce a functional group that responds to a specific molecule or ion, the concentration of which in a particular targeted tissue or organ is different to that of the background. A target-responsive agent thus obtained is able to easily differentiate the NIR-absorption of the targeted region from that of the background. To our surprise, however, there seem to have been no investigations into target-responsive NIR-absorbing dyes for optical imaging. This situation is in contrast to the case of NIR fluorescent imaging in which tar-

get-responsive NIR fluorescent dyes have been designed by covalently joining a NIR fluorophore and a pH-,<sup>[5]</sup> pyrophosphate-,<sup>[6]</sup> or NO-responsive<sup>[7]</sup> modulator to enable selective enhancement of NIR fluorescence arising from the targeted area.

As a candidate for target-sensitive NIR-absorbing dyes, we investigated the platinum(II) complex with 3,5-dibromo-1,2-diaminobenzene and revealed the involvement of redox reactions in the NIR absorption.<sup>[8]</sup> More recently, we found that the complex did not display NIR absorption in aqueous solution, but did so strongly in hydrophobic media such as surfactant micelles and liposome bilayers.<sup>[9]</sup> Thus, the complex shows a response to the hydrophobicity of the microenvironment and could be applied as an NIR-absorbing contrasting agent to stain cell membranes. Notably, the complex per se exhibits responsive ability towards hydrophobicity without attaching any target-responsive functional group.

The response of this complex to hydrophobic environments posed the question as to whether a  $\text{Pt}^{\text{II}}$  complex of *o*-phenylenediamine derivatives exhibits NIR absorption in hydrophilic media. This prompted us to prepare a water-soluble  $\text{Pt}^{\text{II}}$  complex with an *o*-phenylenediamine derivative bearing a sulfo group. Herein we show the NIR absorption properties of the complex in aqueous solutions and also the unexpected pH-responsive switching of the NIR absorption. By using X-ray analysis, cyclic voltammetry (CV), spectroelectrochemistry, and electron paramagnetic resonance (EPR) spectroscopy we have been able to attribute the switching ability to a change in the electronic structure, which results from oxidation followed by dimerization of the complex.

[a] Graduate School of Environmental Studies, Tohoku University, 6-6-07 Aramaki-Aoba, Aoba-ku, Sendai, 980-8579, Japan  
Fax: +81-22-795-7293  
E-mail: iki@orgsynth.che.tohoku.ac.jp

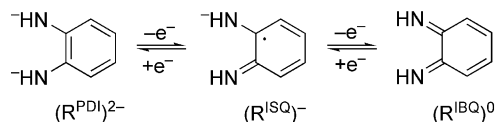
[b] School of Engineering, Tohoku University, 6-6-07 Aramaki-Aoba, Aoba-ku, Sendai, 980-8579, Japan

[c] Institute of Multidisciplinary Research for Advanced Materials, Tohoku University, 2-1-1 Katahira, Aoba-ku, Sendai, 980-8577, Japan

Supporting information for this article is available on the WWW under <http://dx.doi.org/10.1002/ejic.201000343>.

## Results and Discussion

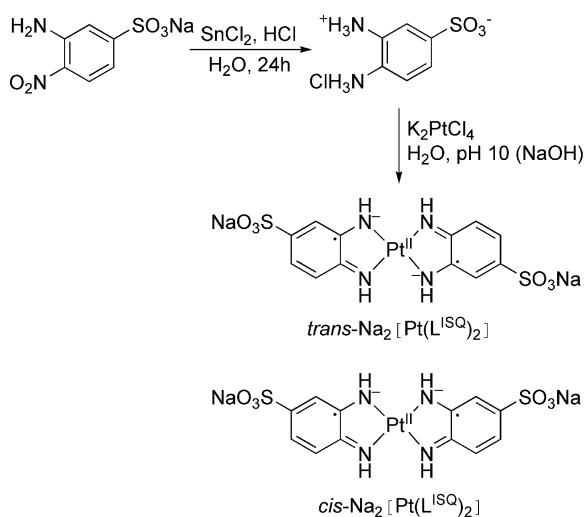
In this paper we have labeled the oxidation states of the *o*-phenylenediamine ligand ( $H_2R$ ) as shown in Scheme 1 and proposed by Wiegardt et al.<sup>[10]</sup> The aromatic closed-shell form is  $(R^{PDI})^{2-}$  (*o*-diiminophenolato ligand), the open-shell radical form is  $(R^{ISQ})^{\cdot-}$  (*o*-diiminoquinonate radical ligand), and the quinone-type closed-shell form is  $(R^{IBQ})^0$  (*o*-diiminobenzoquinone ligand).



Scheme 1. Oxidation states of *o*-phenylenediamine ( $H_2R^{PDI}$ ).

## Preparation of the Complex

To prepare the water-soluble  $Pt^{II}$  complex, we employed 3,4-diaminobenzenesulfonate [DABS,  $(H_2L^{PDI})^-$ ] produced by the reduction of 2-nitroaniline-4-sulfonate (Scheme 2). In accordance with the previously reported procedure for the preparation of the bis(*o*-diiminobenzoquinonato)-platinum(II) complex,<sup>[11]</sup>  $(H_2L^{PDI})^-$  was treated with  $K_2[PtCl_4]$  in aqueous solution in the presence of a base (pH 10, NaOH) at room temperature for 2 d to afford a green precipitate of  $Na_2[Pt^{II}(L^{ISQ})_2]$  in which the ligand was autoxidized during preparation. The assignment of the oxidation state of the ligand to  $(L^{ISQ})^{2-}$  was later confirmed by X-ray crystallography (see below). Both the *cis* and *trans* isomers (with respect to the positions of the sulfo groups) of the complex should be formed. The  $^1H$  NMR spectrum recorded in  $D_2O$  exhibits two sets of signals from the aromatic protons (Figure S1,  $\delta = 6.80$ – $7.40$  ppm), which suggests that *cis/trans* isomerization of  $Na_2[Pt^{II}(L^{ISQ})_2]$  is slow on the NMR timescale.



Scheme 2. Reaction scheme for the preparation of the ligand ( $H_3L^{PDI}$ ) and the  $Pt^{II}$  complex.

## UV/Vis/NIR Spectral Analysis

During the preparation of single crystals, we noticed that alkaline solutions of  $Na_2[Pt^{II}(L^{ISQ})_2]$  were a deep-blue color (see the picture in the Table of Contents). In fact, the complex exhibits very intense absorption at 705 nm ( $\epsilon = 1.1 \times 10^5 \text{ M}^{-1} \text{ cm}^{-1}$ ) in solution at pH 12 (Figure 1). Thus, the  $Pt^{II}$ -*o*-phenylenediamine complex exhibits NIR absorption even in aqueous solution, in contrast to the bis(3,5-dibromo-1,2-diiminobenzoquinonato) complex. We also noticed that the deep-blue color readily disappeared at lower pH, which prompted us to study the change with pH of the absorption spectra of  $[Pt^{II}(L^{ISQ})_2]^{2-}$  in aqueous solution (Figure 1). Upon lowering the pH from 12 to 7, the blue color of  $[Pt^{II}(L^{ISQ})_2]^{2-}$  is almost unchanged. In contrast, when the pH was reduced from 6 to 2.9, the color of the solution changed from deep blue to pale yellow with a steep decrease in the absorption at 705 nm (Figure 2) and a slight increase in the absorption bands at 420 and 822 nm (Figure 1). Upon decreasing the pH, the spectra show an instantaneous response to the change in pH. In contrast, upon increasing the pH, it takes very long time for the absorbance to equilibrate resulting in an apparent hysteresis within a limited time of measurement (ca. 1 min for each point; Figure 2). In any case, it is striking that the complex clearly exhibits switching of the NIR absorption properties at a pH of around 4.5, which implies that the complex can be used as a pH-responsive NIR-absorption probe. At the same time, the pH-responsive behavior poses the question as to how the complex responds to  $H^+$  despite the fact that the ligand does not have a proton-responsive functional group with a  $pK_a$  at 4.5. The long time required for equilibration upon increasing the pH ruled out simple acid dissociation as the cause of the color change because proton dissociation/association is usually very rapid. This prompted us to elucidate the electronic structure of the blue-colored complex to be designated as  $[Pt^{II}(L^{ISQ})_2]^{2-}$  and also the mechanisms of the NIR absorption and the pH-responsive behavior by using various characterization methods.

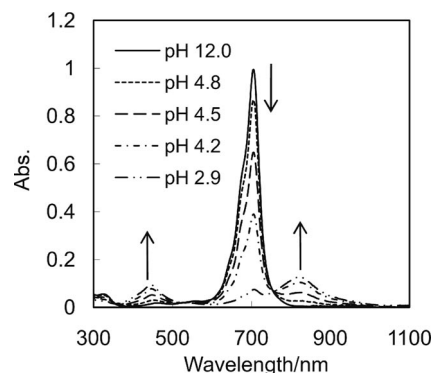


Figure 1. pH-dependent absorption spectra of an aqueous solution of  $Na_2[Pt^{II}(L^{ISQ})_2]$ .  $[Na_2[Pt^{II}(L^{ISQ})_2]] = 1.0 \times 10^{-5} \text{ M}$ ,  $I = 0.1$  (NaClO<sub>4</sub>), pH 2.9–12,  $N_2$  (pH was adjusted by the addition of  $H_2SO_4$  or NaOH solution).

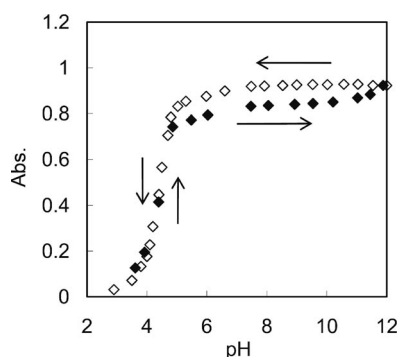


Figure 2. pH dependence of the absorbance of  $\text{Na}_2[\text{Pt}^{\text{II}}(\text{L}^{\text{ISQ}})_2]$  at 705 nm.  $[\text{Na}_2[\text{Pt}^{\text{II}}(\text{L}^{\text{ISQ}})_2]] = 1.0 \times 10^{-5} \text{ M}$ ,  $I = 0.1$  ( $\text{NaClO}_4$ ),  $\text{N}_2$ . The pH was first decreased from 12.0 to 2.9 (open diamond) and then increased from 2.9 to 11.9 (closed diamond).

### X-ray Analysis

As stated earlier, we were aware of the involvement of redox chemistry in the complexation between  $\text{Pt}^{\text{II}}$  and *o*-phenylenediamine ligands.<sup>[8]</sup> On the other hand, Wieghardt and co-workers<sup>[10]</sup> have shown that X-ray diffraction is the most reliable tool for assigning the redox state of the *o*-phenylenediamine ligands in the complex (Scheme 1) because it allows scrutiny of the lengths of the C–C and C–N bonds, which reflects the bond order, that is, the electronic structure (Table 1). To determine the structure of the NIR-absorbing complex, denoted as  $[\text{Pt}^{\text{II}}(\text{L}^{\text{ISQ}})_2]^{2-}$  in the previous section, we attempted to isolate single crystals of the sodium salt. However, the X-ray analysis revealed that the quality of the crystals was poor and the refinement of the structure failed, which was attributed to the loss of crystal water during the measurement. To expel water from the crystal lattice, we replaced the  $\text{Na}^+$  ion with a bulky and hydrophobic cation, *n*-propyltriphenylphosphonium ( $\text{PPrPh}_3^+$ ), by addition of the bromide salt to a solution of the complex at pH 10. Thus, we successfully obtained high quality single crystals suitable for X-ray analysis. The ORTEP diagram of  $(\text{PPrPh}_3)_2[\text{Pt}^{\text{II}}(\text{L}^{\text{ISQ}})_2]$  in Figure 3 shows that the complex adopts a square-planar coordination geometry with a *trans* configuration with respect to the posi-

tion of the sulfo groups. The space group is  $P2_1/c$  and the two ligands are crystallographically related by a center of symmetry. The complex has two counter-ions ( $\text{PPrPh}_3^+$ ) in the unit cell, which shows that the complex is dianionic. No water molecule was found in the crystal lattice, which justifies the introduction of the highly hydrophobic counter-ion and is also effective for the tight packing of the complex with  $\text{PPrPh}_3^+$  in the crystal lattice through  $\pi$ – $\pi$  interactions between the overlapping phenyl rings [the shortest distances are C2–C17 3.333(8) and C1–C17 3.482(8) Å]. In addition, two NH groups form hydrogen bonds with the sulfo group of the neighboring complex [ $\text{N1} \cdots \text{O3}$  3.028(6),  $\text{N2} \cdots \text{O2}$  3.023(6),  $\text{H1} \cdots \text{O3}$  2.21,  $\text{H2} \cdots \text{O2}$  2.14 Å].

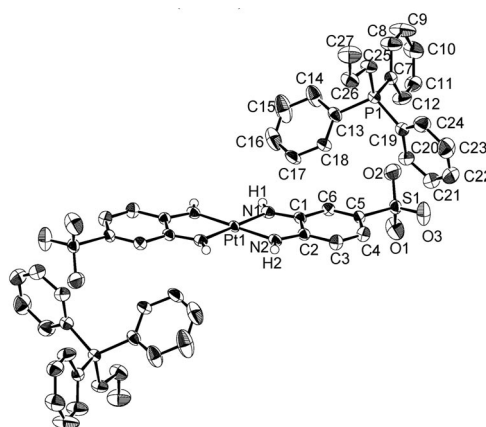


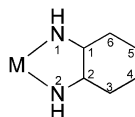
Figure 3. ORTEP diagram of  $(\text{PPrPh}_3)_2[\text{Pt}^{\text{II}}(\text{L}^{\text{ISQ}})_2]$  (at the 50% probability level). Open circles represent imine hydrogen atoms. All other hydrogen atoms have been omitted for clarity.

From the viewpoint of the assignment of the electronic structure of the complex, the electric charge on the DABS ligand in the complex is a convenient measure for distinguishing the oxidation states, as shown in Scheme 1. Anticipating the charge of  $\text{Pt}^{\text{II}}$  to be intact (2+), each ligand should be dianionic in the complex because the total charge of the complex is 2−. Because the sulfo group has one negative charge, the *o*-phenylenediimine part also possesses one negative charge. Therefore the ligand can be assigned to *o*-diiminosulfo benzosemiquinonate ( $\text{L}^{\text{ISQ}})^{2-}$ , as shown in

Table 1. Bond lengths of the three different oxidation states of the *o*-phenylenediamine ligand ( $\text{R}^{\text{IBQ}}$ ,  $\text{R}^{\text{ISQ}}$ , and  $\text{R}^{\text{PDI}}$ ) in the transition-metal(II) complexes and the ligand (L) in the  $[\text{Pt}^{\text{II}}\text{--DABS}]$  complex (assigned as  $[\text{Pt}^{\text{II}}(\text{L}^{\text{ISQ}})_2]^{2-}$  in this study).

	Bond length [Å]							Ref.
	C–N	C1–C2	C2–C3	C3–C4	C4–C5	C5–C6	C6–C1	
$\text{R}^{\text{IBQ}}$	1.30 <sup>[a]</sup>	1.45	1.43	1.34	1.43	— <sup>[b]</sup>	— <sup>[c]</sup>	[10]
$\text{R}^{\text{ISQ}}$	1.35 <sup>[a]</sup>	1.42	1.41	1.37	1.42	— <sup>[b]</sup>	— <sup>[c]</sup>	[10]
$\text{R}^{\text{PDI}}$	1.40 <sup>[a]</sup>	1.40	1.40	1.40	1.40	— <sup>[b]</sup>	— <sup>[c]</sup>	[10]
L in $[\text{Pt}^{\text{II}}\text{--DABS}]$	1.348(7) <sup>[d]</sup> 1.345(7) <sup>[e]</sup>	1.427(7)	1.409(7)	1.372(8)	1.403(8)	1.369(7)	1.416(7)	this study

[a] Average bond lengths of C1–N1 and C2–N2. [b] Same as C3–C4. [c] Same as C2–C3. [d] C1–N1. [e] C2–N2.





Scheme 2. Furthermore, the electronic structure was confirmed by scrutiny of the bond lengths of the aromatic ring (Table 1). The bond lengths of the aromatic rings can be differentiated into two shorter C–C bonds [C3–C4 1.372(8) and C5–C6 1.369(7) Å] and four longer ones [C1–C2 1.427(7), C2–C3 1.409(7), C4–C5 1.403(8), and C6–C1 1.416(7) Å]. In addition, the C–N bond lengths are N1–C1 1.348(7) and N2–C2 1.345(7) Å. By comparing the bond lengths in the three distinct oxidation states of the *o*-phenylenediamine ligands reported (Table 1),<sup>[10]</sup> the electronic structure of the present complex should be neither  $L^{PDI}$  with a fully aromatic hexagon structure nor  $L^{IBQ}$  with fully alternating double/single bonds. The bond lengths coincide well with that in *o*-diiminosulfobenzosemiquinonate ( $L^{ISQ}$ )<sup>2-</sup>.

Hence, the deep-blue complex that exists in alkaline solution can be formulated as  $[Pt^{II}(L^{ISQ})_2]^{2-}$  with a diradical structure to support the complexation scheme showing the involvement of autoxidation (Scheme 2). In addition, the <sup>1</sup>H NMR spectrum of  $(PPh_3)_2[Pt^{II}(L^{ISQ})_2]$  dissolved in DMSO shows peaks of ArH protons in the usual aromatic region ( $\delta$  = 6.87–7.31 ppm) with no paramagnetic shifts, which is also the case for  $Na_2[Pt^{II}(L^{ISQ})_2]$  (Figure S1). This indicates that the two radical centers are antiferromagnetically coupled and that the complex  $[Pt^{II}(L^{ISQ})_2]^{2-}$  should be a singlet (total spin quantum number,  $S_{Total}$  = 0 ground state). Wieghardt and co-workers assigned the intense NIR absorption of planar singlet diradical complexes of *o*-phenylenediamine derivatives with d<sup>8</sup> metals not to a  $\pi \rightarrow \pi^*$  or ligand-to-metal transition, but to ligand-to-ligand charge transfer (LLCT).<sup>[12]</sup> In a similar fashion, the intense NIR absorption of  $[Pt^{II}(L^{ISQ})_2]^{2-}$  at 705 nm can be assigned to LLCT.

## Electrochemistry

The cyclic voltammogram of  $Na_2[Pt^{II}(L^{ISQ})_2]$  recorded at a scan rate of 10 mVs<sup>-1</sup> in a DMSO solution containing 0.1 M  $(nBu_4N)ClO_4$  as supporting electrolyte exhibits three successive redox waves at  $E^1_{1/2}$  = -0.26,  $E^2_{1/2}$  = -1.46, and  $E^3_{1/2}$  = -2.08 V versus Fc<sup>+</sup>/Fc (Figure 4). Each redox wave shows reversible electron transfer in the redox series. Assuming each redox step to be a one-electron transfer reaction at the ligand center, the redox series can be depicted as in Scheme 3, in accordance with the redox behavior of analogous Pt<sup>II</sup> complexes with 3,5-di-*tert*-butyl-*o*-phenylenediamine.<sup>[10]</sup> Notably, the reduction wave at  $E^1_{1/2}$  exhibits scan-rate dependence (Figure S2). At scan rates of 10 and 20 mVs<sup>-1</sup>, one reduction peak appears, as in the case shown in Figure 4. On the other hand, at scan rates above 50 mVs<sup>-1</sup>, the reduction wave splits into two ( $E^1_{pc'}$  = -0.28 and  $E^1_{pc''}$  = -0.45 V). The splitting of the cathodic peak  $E^1_{pc}$  at high scan rates indicates that the oxidation of  $[Pt^{II}(L^{ISQ})_2]^{2-}$  to  $[Pt^{II}(L^{ISQ})(L^{IBQ})]^-$  is readily followed by a subsequent reaction to form another redox-active species. We suppose that  $[Pt^{II}(L^{ISQ})(L^{IBQ})]^-$  forms a dimer  $[Pt^{II}(L^{ISQ})_2]^{2-}$ , as shown in Equation (1), which is consistent with the results of the EPR measurement of  $[Pt^{II}(L^{ISQ})(L^{IBQ})]^-$  (see below).

(1)

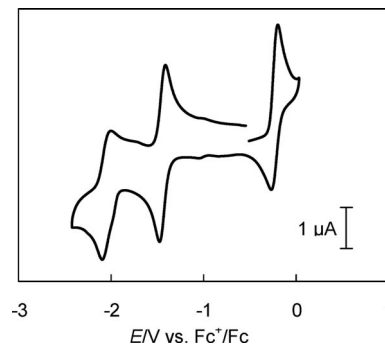
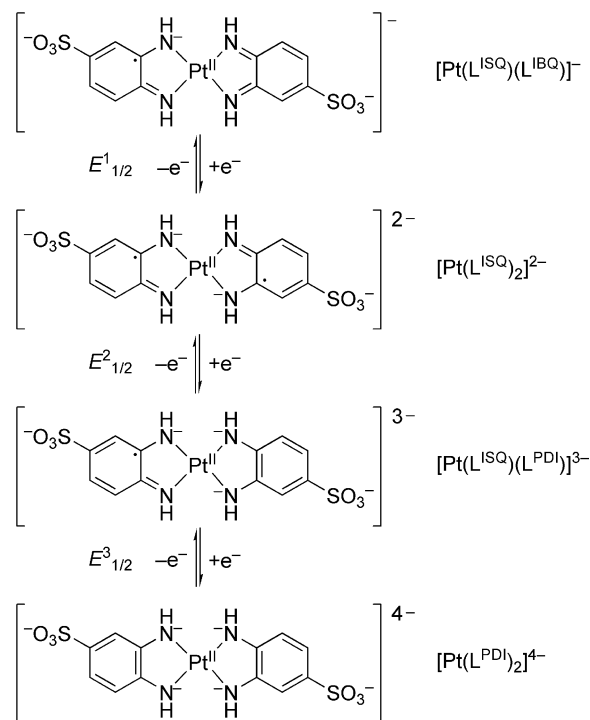


Figure 4. Cyclic voltammogram of  $Na_2[Pt^{II}(L^{ISQ})_2]$  in DMSO.  $[Na_2[Pt^{II}(L^{ISQ})_2]] = 1.0 \times 10^{-3}$  M,  $[(nBu_4N)ClO_4] = 0.10$  M, potential vs. Fc<sup>+</sup>/Fc, glassy carbon working electrode, Pt wire counter-electrode, a scan rate of 10 mVs<sup>-1</sup>.



Scheme 3. The ligand-centered redox series of  $Na_2[Pt^{II}(L^{ISQ})_2]$ .

At scan rates of 10 and 20 mVs<sup>-1</sup>, the dissociation of the dimer to monomer is faster than the CV scan rate and therefore only one reduction peak for the monomer is observed. At scan rates above 50 mVs<sup>-1</sup>, the dissociation of the dimer to the monomer is slower than the CV scan rate and thus a new reduction peak arising from the dimer at  $E^1_{pc''}$ , more negative than the  $E^1_{pc'}$  value for the monomer, is observed.

Absorption spectra of  $\text{Na}_2[\text{Pt}^{\text{II}}(\text{L}^{\text{ISQ}})_2]$  in DMSO solution were measured under controlled electrochemical potential (Figure 5). Without electrolysis,  $[\text{Pt}^{\text{II}}(\text{L}^{\text{ISQ}})_2]^{2-}$  displays a very intense absorption band at 724 nm ( $\epsilon = 1.1 \times 10^5 \text{ M}^{-1} \text{ cm}^{-1}$ ), very similar to that observed in aqueous solution (Figure 1), which suggests the same LLCT transition. Only a small bathochromic shift (19 nm) is observed in DMSO solution compared with the absorption in aqueous solution. Upon applying a potential of  $-0.05 \text{ V}$ , which corresponds to the one-electron oxidation of  $[\text{Pt}^{\text{II}}(\text{L}^{\text{ISQ}})_2]^{2-}$ , the absorption band at 724 nm disappears and others at 439 and 838 nm appear (Figure 5). Because these two absorption bands observed in DMSO closely resemble those observed in aqueous solution at low pH (Figure 1), the spectral change caused by oxidation of  $[\text{Pt}^{\text{II}}(\text{L}^{\text{ISQ}})_2]^{2-}$  corresponds well to the change caused by decreasing the pH of the solution. Hence, we can infer that the pH-responsive color change of  $[\text{Pt}^{\text{II}}(\text{L}^{\text{ISQ}})_2]^{2-}$  is caused by oxidation. It has been reported that upon lowering the pH, the bis(*o*-diiminobenzosemiquinonato)platinum(II) complex shows a color change similar to that of  $[\text{Pt}^{\text{II}}(\text{L}^{\text{ISQ}})_2]^{2-}$ , which is caused not by a change in the redox potential of the complex but by an increase in the rest potential of the solution at lower pH.<sup>[13]</sup> We also investigated the pH dependence of  $E^{1/2}$  of  $[\text{Pt}^{\text{II}}(\text{L}^{\text{ISQ}})_2]^{2-}$  upon decreasing the pH of the solution from 10.0 to 3.0 (Figure 6), which showed that the  $E^{1/2}$  value was almost constant, being in the narrow range of  $-0.19$  to  $-0.21 \text{ V}$ . This indicates that the complex does not accept or release protons in the pH range. On the other hand, the rest potential of the sample solution shows a large increase from  $-0.70$  to  $-0.10 \text{ V}$  and exceeds  $E^{1/2}$  at pH 4.0, which leads to the oxidation of  $[\text{Pt}^{\text{II}}(\text{L}^{\text{ISQ}})_2]^{2-}$ . Thus, the switching off of the NIR absorption at low pH is caused by a high rest potential of the solution, which causes the oxidation of  $[\text{Pt}^{\text{II}}(\text{L}^{\text{ISQ}})_2]^{2-}$  to a species such as  $[\text{Pt}^{\text{II}}(\text{L}^{\text{ISQ}})(\text{L}^{\text{IBQ}})]^-$  and the dimer  $[\{\text{Pt}^{\text{II}}(\text{L}^{\text{ISQ}})(\text{L}^{\text{IBQ}})\}_2]^{2-}$ . Therefore, upon increasing the pH, the dimeric species  $[\{\text{Pt}^{\text{II}}(\text{L}^{\text{ISQ}})(\text{L}^{\text{IBQ}})\}_2]^{2-}$  should eventually give  $[\text{Pt}^{\text{II}}(\text{L}^{\text{ISQ}})_2]^{2-}$  by reduction by the rest potential. Because dissociation of  $[\{\text{Pt}^{\text{II}}(\text{L}^{\text{ISQ}})(\text{L}^{\text{IBQ}})\}_2]^{2-}$  to the monomeric species  $[\text{Pt}^{\text{II}}(\text{L}^{\text{ISQ}})(\text{L}^{\text{IBQ}})]^-$  is slow, as shown by CV, the color change of the complex solution upon increasing the pH should be slow to attain equilibrium, as described earlier (Figure 2).

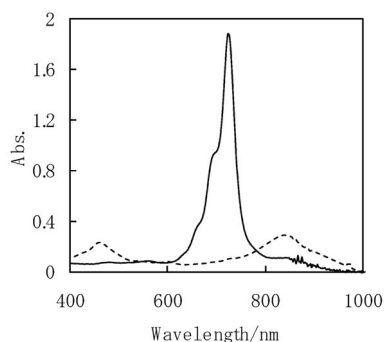


Figure 5. Absorption spectra of  $\text{Na}_2[\text{Pt}^{\text{II}}(\text{L}^{\text{ISQ}})_2]$  (solid line) and the electrochemically one-electron-oxidized species (dotted line) in DMSO.  $[\text{Na}_2[\text{Pt}^{\text{II}}(\text{L}^{\text{ISQ}})_2]] = 1.0 \times 10^{-4} \text{ M}$ ,  $[(n\text{Bu}_4\text{N})\text{ClO}_4] = 0.10 \text{ M}$ , potential vs.  $\text{Fc}^+/\text{Fc}$ , Pt mesh electrode, Pt wire counter-electrode, cell thickness: 1 mm.

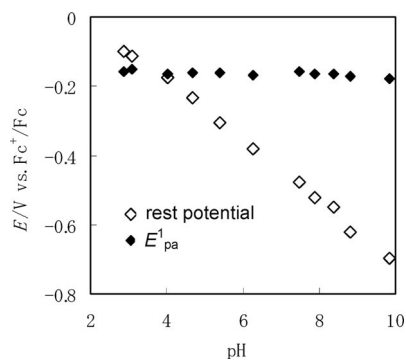


Figure 6. Dependence of  $E^{1/2}_{\text{pa}}$  of  $[\text{Pt}^{\text{II}}(\text{L}^{\text{ISQ}})_2]^{2-}$  and the rest potential of the solution on the apparent pH.  $[\text{Na}_2[\text{Pt}^{\text{II}}(\text{L}^{\text{ISQ}})_2]] = 1.0 \times 10^{-3} \text{ M}$ ,  $[(n\text{Bu}_4\text{N})\text{ClO}_4] = 0.10 \text{ M}$  in DMSO.

In addition, because  $E^{1/2}$  can be controlled by substituents, the pH-switching region of the NIR absorption is tunable. Namely, owing to the electron-withdrawing  $\text{SO}_3^-$  groups, the  $E^{1/2}$  value of  $[\text{Pt}^{\text{II}}(\text{L}^{\text{ISQ}})_2]^{2-}$  is larger than that of the bis(*o*-diiminobenzosemiquinonato)platinum(II) complex ( $E^{1/2} = -0.26$  to  $-0.28 \text{ V}$ ) in DMSO, which results in a color change at a lower pH of around 1 pH unit.<sup>[13]</sup>

## EPR Spectroscopy

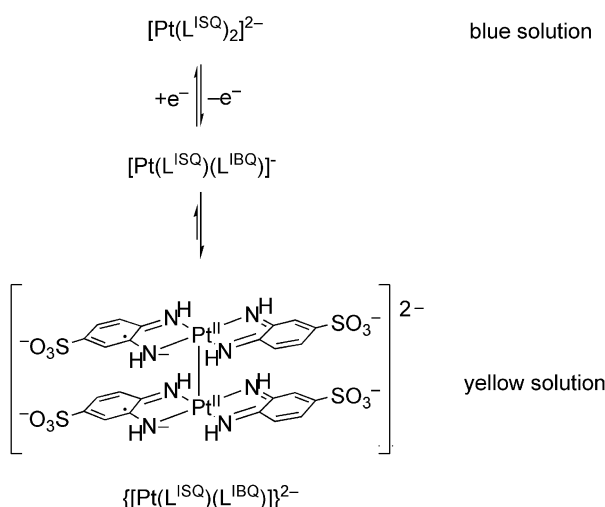
To clarify the electronic structures of the one-electron-oxidized and -reduced species of  $[\text{Pt}^{\text{II}}(\text{L}^{\text{ISQ}})_2]^{2-}$  shown in Scheme 3, we studied the chemically oxidized or reduced complexes by EPR spectroscopy. First, we recorded at room temperature and at 77 K the EPR spectrum of  $[\text{Pt}^{\text{II}}(\text{L}^{\text{ISQ}})(\text{L}^{\text{IBQ}})]^-$ , which seemed to exist at lower pH and be a precursor of the dimer at  $\text{pH} < 4.0$  (Table 2). At room temperature, the complex in DMSO exhibits a signal at  $g = 1.980$ , similar to the  $g$  values reported for  $[\text{M}^{\text{II}}(\text{R}^{\text{ISQ}})(\text{R}^{\text{IBQ}})]$ -type complexes (see Table 2), which supports the electronic structure of the present one-electron-oxidized complex as  $[\text{Pt}^{\text{II}}(\text{L}^{\text{ISQ}})(\text{L}^{\text{IBQ}})]^-$ . Notably, the signal intensity is as low as around 1% of what is expected from the solute concentration, which indicates that the concentration of paramagnetic species  $[\text{Pt}^{\text{II}}(\text{L}^{\text{ISQ}})(\text{L}^{\text{IBQ}})]^-$  in DMSO decreases significantly as a result of the formation of substantial amounts of the diamagnetic dimer  $[\{\text{Pt}^{\text{II}}(\text{L}^{\text{ISQ}})(\text{L}^{\text{IBQ}})\}_2]^{2-}$ . The DMSO solution at 77 K does not give any measurable EPR signal, which suggests that the complex is completely dimerized. Regardless of the temperature, the aqueous solution of the complex is EPR silent, which indicates that  $[\text{Pt}^{\text{II}}(\text{L}^{\text{ISQ}})(\text{L}^{\text{IBQ}})]^-$  completely dimerizes in aqueous solution at  $\text{pH} < 4.0$ . It may be said that the highly polar environment forces the monomer, which has a hydrophobic moiety, to dimerize [Equation (1)]. From above, one can conclude that the one-electron oxidation of the diamagnetic complex  $[\text{Pt}^{\text{II}}(\text{L}^{\text{ISQ}})_2]^{2-}$  should yield the paramagnetic complex  $[\text{Pt}^{\text{II}}(\text{L}^{\text{ISQ}})(\text{L}^{\text{IBQ}})]^-$  immediately followed by the formation of the

Table 2. EPR parameters for  $[M^{II}(R^{ISQ})(R^{IBQ})]$ -type complexes.

$M^{II}$	Ligand	Solvent	Temperature	$g$	Ref.
$Pt^{II}$	DABS	water	room temperature	—[a]	this study
		water	77 K	—[a]	this study
		DMSO	room temperature	1.980 <sup>[b]</sup>	this study
		DMSO	77 K	—[a]	this study
$Pt^{II}$	<i>o</i> -phenylenediamine	DMSO	room temperature	1.982	[11]
$Pd^{II}$	<i>o</i> -phenylenediamine	DMSO	room temperature	1.996	[11]
$Ni^{II}$	<i>o</i> -phenylenediamine	DMSO	room temperature	1.997	[11]
$Pt^{II}$	3,5-di- <i>tert</i> -butyl- <i>o</i> -phenylenediamine	$CH_3CN$	30 K	1.988 <sup>[c]</sup>	[10]

[a] EPR silent. [b] The intensity of the signal was quite low. [c]  $g_{iso}$  value.

diamagnetic dimer  $[\{Pt^{II}(L^{ISQ})(L^{IBQ})\}_2]^{2-}$  in aqueous solution (Scheme 4). This is consistent with the CV results, which reveal a reduction peak of the dimer species  $[\{Pt^{II}(L^{ISQ})(L^{IBQ})\}_2]^{2-}$  at high scan rates (Figure S2, b). Dimerization of  $[M^{II}(R^{ISQ})(R^{IBQ})]$ -type complexes is not peculiar to the present complex  $[\{Pt^{II}(L^{ISQ})(L^{IBQ})\}_2]^{2-}$ , but has been exemplified by several one-electron-oxidized complexes. For instance,  $[M^{II}(R^{ISQ})(R^{IBQ})]$ -type complexes such as bis(*o*-diiminobenzosemiquinonato)platinum(II), bis(*o*-diiminobenzosemiquinonato)palladium(II), and bis(*o*-diiminobenzosemiquinonato)nickel(II) display a low-intensity EPR signal only in DMSO solution at room temperature, which suggests the formation of the dimer (Table 2).<sup>[11]</sup> In addition, crystallographic evidence for bis(*o*-diiminobenzosemiquinonato)platinum(II),<sup>[13]</sup> bis(*N*-phenyl-*o*-diiminobenzosemiquinonato)platinum(II),<sup>[10]</sup> and bis(3,5-di-*tert*-butyl-*o*-diiminobenzosemiquinonato)nickel(II)<sup>[10]</sup> have shown that two  $[M^{II}(R^{ISQ})(R^{IBQ})]$  units are connected through  $M^{II}$ – $M^{II}$  interactions. Therefore one can anticipate that  $[\{Pt^{II}(L^{ISQ})(L^{IBQ})\}_2]^{2-}$  may adopt the same dimeric structure connected through a  $Pt^{II}$ – $Pt^{II}$  interaction.

Scheme 4. Reaction scheme for the pH-responsive switching of the NIR absorption of  $Na_2[Pt^{II}(L^{ISQ})_2]$ .

Secondly, we investigated one-electron-reduced species  $[Pt^{II}(L^{ISQ})(L^{PDI})]^{3-}$  obtained by reduction of  $[Pt^{II}(L^{ISQ})_2]^{2-}$  with a 10-fold amount of  $SnCl_2$  in alkaline DMSO, which shows a clear EPR signal at 77 K with the metal hyperfine

coupling for three principal directions (Figure 7, d). All three central lines of the rhombic signal are split into a doublet by coupling with  $^{195}Pt$  (33.7%,  $I = 1/2$ ). Simulations (Figure 7, a–c) were performed to determine the EPR parameters ( $g_x = 1.962$ ,  $g_y = 2.207$ ,  $g_z = 1.776$ ) and hyperfine coupling with  $^{195}Pt$  (33.7%,  $I = 1/2$ ;  $A_x^{195Pt} = 695$ ,  $A_y^{195Pt} = 259.5$ ,  $A_z^{195Pt} = 465$  MHz; for the assignment, see the Supporting Information). By using these  $g$  values and hyperfine coupling constants, we estimated the spin density at the central  $Pt^{II}$  to be 32.3% according to the method of Holm (see the Supporting Information).<sup>[14,15]</sup> The value is a reasonable estimate because the DFT calculation of the analogous  $[Pt^{II}(R^{ISQ})(R^{PDI})]$ -type square-planar complex of 2-anilino-4,6-di-*tert*-butylphenol indicated that the out-of-plane  $d_{xz}$  orbital of the  $Pt^{II}$  readily mixes with the  $p_z$  orbital of the ligand and thereby acquires some metal character (spin density: 23.7%).<sup>[16]</sup>

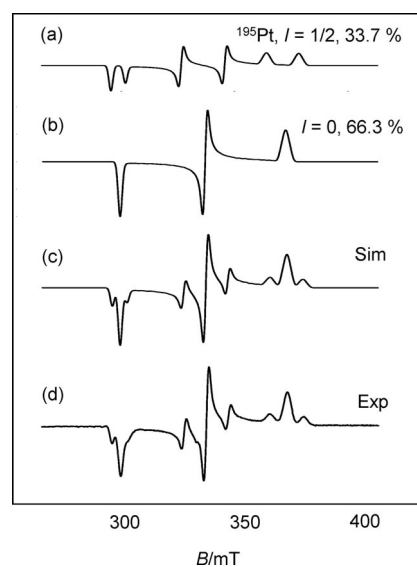


Figure 7. EPR spectrum of  $[Pt^{II}(L^{ISQ})(L^{PDI})]^{3-}$  at 77 K. (a) Simulated for  $^{195}Pt$ ,  $I = 1/2$ ; (b) simulated for  $I = 0$ ; (c) (a) + (b); (d) chemically generated  $[Pt^{II}(L^{ISQ})(L^{PDI})]^{3-}$  in frozen DMSO solution.  $[[Pt^{II}(L^{ISQ})_2]^{2-}] = 1.0 \times 10^{-3}$  M,  $[SnCl_2] = 1.0 \times 10^{-2}$  M, microwave frequency 9.23081 GHz, microwave power 10 mW, field modulation 5 G.

Thus, the EPR spectrum of the one-electron-oxidized species of  $[Pt^{II}(L^{ISQ})_2]^{2-}$  with a very weak signal of  $[Pt^{II}(L^{ISQ})(L^{IBQ})]^-$  at room temperature suggests the formation

of the dimer  $[\{\text{Pt}^{\text{II}}(\text{L}^{\text{ISQ}})(\text{L}^{\text{IBQ}})\}_2]^{2-}$ . Also, the EPR spectrum of the one-electron-reduced species of  $[\text{Pt}^{\text{II}}(\text{L}^{\text{ISQ}})_2]^{2-}$  confirms the paramagnetic structure of  $[\text{Pt}^{\text{II}}(\text{L}^{\text{ISQ}})(\text{L}^{\text{PDI}})]^{3-}$ . This EPR evidence for the imino radical electronic structure of  $[\text{Pt}^{\text{II}}(\text{L}^{\text{ISQ}})(\text{L}^{\text{IBQ}})]^-$  and  $[\text{Pt}^{\text{II}}(\text{L}^{\text{ISQ}})(\text{L}^{\text{PDI}})]^{3-}$ , which are both adjacent to  $[\text{Pt}^{\text{II}}(\text{L}^{\text{ISQ}})_2]^{2-}$  in the redox series (Scheme 3), in turn support the diradical structure of  $[\text{Pt}^{\text{II}}(\text{L}^{\text{ISQ}})_2]^{2-}$ .

## Conclusions

In this study we have successfully prepared a water-soluble singlet diradical complex  $[\text{Pt}^{\text{II}}(\text{L}^{\text{ISQ}})_2]^{2-}$  to show that strong absorption of NIR light can be achieved with a  $\text{Pt}^{\text{II}}$  complex in aqueous solution. It has also been clarified that the pH-dependent NIR absorption switching of  $[\text{Pt}^{\text{II}}(\text{L}^{\text{ISQ}})_2]^{2-}$  is caused by an increase in the rest potential of the solution that leads to its oxidation to form  $[\text{Pt}^{\text{II}}(\text{L}^{\text{ISQ}})(\text{L}^{\text{IBQ}})]^-$  immediately followed by dimerization to  $[\{\text{Pt}^{\text{II}}(\text{L}^{\text{ISQ}})(\text{L}^{\text{IBQ}})\}_2]^{2-}$ . Taking advantage of the high water solubility and the switching behavior, the diradical  $[\text{Pt}^{\text{II}}(\text{L}^{\text{ISQ}})_2]^{2-}$  complex can be applied as a highly sensitive NIR-absorbing contrast agent that responds to the pH and/or redox potential of its microenvironment.

## Experimental Section

**Materials and Methods:** Potassium tetrachloroplatinate(II) was purchased from Nacalai Tesque (Kyoto). Sodium 2-nitroaniline-4-sulfonate was purchased from Tokyo Chemical Industry Co., Ltd. (Tokyo). Tin(II) chloride dihydrate was purchased from Wako Pure Chemical Industries, Ltd. (Tokyo). All reagents were used without further purification.

The electronic spectra were recorded with Shimadzu UV-3100PC and JASCO V-570 spectrometers. The  $^1\text{H}$  NMR spectra were obtained with a Bruker DPX-400 spectrometer using  $\text{D}_2\text{O}$  or  $[\text{D}_6]$ -DMSO as solvents and (3-trimethylsilyl)propanesulfonic acid sodium salt (DSS) as an external standard for  $\text{D}_2\text{O}$ . Electrospray ionization mass spectrometry (ESI-MS) was performed with a Bruker APEX III Fourier-transform ion-cyclotron resonance mass spectrometer. The cyclic voltammetric measurements were performed with a Hokuto Denko HAB-151 using a glassy carbon working electrode, a  $\text{Ag}/\text{AgNO}_3$  reference electrode, and a Pt counter-electrode in DMSO solution containing 2 mM NaOH to dissolve the complex and 0.1 M  $(n\text{Bu})_4\text{NClO}_4$  as the supporting electrolyte under  $\text{N}_2$ . Potentials are referenced to the half-wave potential (+0.024 V) of the ferrocenium/ferrocene couple ( $\text{Fc}^+/\text{Fc}$ ). Spectroelectrochemistry was performed with Hokuto Denko HAB-151 and JASCO V-570 instruments using a spectroelectrochemical cell (light path length: 1 mm) with a Pt mesh working electrode, a Pt counter-electrode, and an  $\text{Ag}/\text{AgNO}_3$  reference electrode. The pH measurements were performed with a TOA HM-30V pH meter with a G51-5421C combined electrode. The EPR spectra were recorded with a Varian E112 spectrometer and simulated using a program written in our laboratory.

**$\text{H}_3\text{L}^{\text{PDI}}\cdot\text{HCl}$ :** A solution of sodium 2-nitroaniline-4-sulfonate (2.1 g) in water (15 mL) was added to a solution of  $\text{SnCl}_2\cdot 2\text{H}_2\text{O}$  (9.0 g) dissolved in a mixture of 66% (v/v) ethanol (30 mL) and

12 M HCl (10 mL). The reaction mixture was stirred at 0 °C for 24 h to give white precipitates. The crude product was filtered and recrystallized from heated 6 M HCl to give colorless crystals of 3,4-diaminobenzenesulfonic acid monohydrochloric acid ( $\text{H}_3\text{L}^{\text{PDI}}\cdot\text{HCl}$ , 0.12 g, 52% yield).  $^1\text{H}$  NMR (400 MHz,  $\text{D}_2\text{O}$ ):  $\delta$  = 6.88 (d,  $J$  = 8.18 Hz, 1 H, ArH), 7.17 (dd,  $J_1$  = 2.11,  $J_2$  = 8.17 Hz, 1 H, ArH), 7.21 (d,  $J$  = 2.08 Hz, 1 H, ArH) ppm.  $\text{C}_6\text{H}_9\text{ClN}_2\text{O}_3\text{S}$  (224.66): calcd. C 32.08, H 4.04, N 12.47, S 14.27, Cl 15.78; found C 31.85, H 3.95, N 12.38, S 13.98, Cl 15.46.

**$\text{Na}_2[\text{Pt}^{\text{II}}(\text{L}^{\text{ISQ}})_2]$ :** A solution of  $\text{K}_2[\text{Pt}^{\text{II}}\text{Cl}_4]$  (0.21 g) dissolved in water (ca. 5 mL) was added in small portions to an aqueous solution of  $\text{H}_3\text{L}^{\text{PDI}}\cdot\text{HCl}$  (0.22 g) in water (10 mL) and then aq. NaOH was added to adjust the pH to 10. Stirring the mixture at room temperature for 2 d gave a dark-green precipitate, which was collected by filtration, washed with cold water, and dried in vacuo to afford  $\text{Na}_2[\text{Pt}^{\text{II}}(\text{L}^{\text{ISQ}})_2]$  as a powder in both the *cis* and *trans* forms [0.27 g, 47% yield (total)].  $^1\text{H}$  NMR (400 MHz,  $\text{D}_2\text{O}$ ):  $\delta$  = 6.78/6.93 (d,  $J$  = 8.84/8.84 Hz, 1 H, ArH), 7.01/7.02 (dd,  $J_1$  = 1.92/2.00,  $J_2$  = 8.76/8.72 Hz, 1 H, ArH), 7.37/7.38 (d,  $J$  = 1.64/1.52 Hz, 1 H, ArH) ppm.  $^{13}\text{C}$  NMR (100 MHz,  $\text{D}_2\text{O}$ ):  $\delta$  = 119.1/119.2 (ArCH), 121.2/121.5 (ArCH), 121.5/122.5 (ArCH), 138.5/138.3 (ArC), 157.1/156.6 (ArC), 159.3/159.9 (ArC) ppm. Although the assignment was not clear, the intensities of the two signals of *cis*- and *trans*- $\text{Na}_2[\text{Pt}^{\text{II}}(\text{L}^{\text{ISQ}})_2]$  were in an approximate 1:1 ratio. MS (ESI): calcd. for  $[\text{M} - 2\text{Na}]^{2-}$  282.4844; found 282.4850; calcd. for  $[\text{M} - \text{Na}]^-$  587.9585; found 587.9595.

**$(\text{PPrPh}_3)_2[\text{Pt}^{\text{II}}(\text{L}^{\text{ISQ}})_2]$ :** *n*-Propyltriphenylphosphonium bromide ( $\text{PPrPh}_3\text{Br}$ ; 0.077 g) was added to a deep-blue aqueous solution of  $\text{Na}_2[\text{Pt}^{\text{II}}(\text{L}^{\text{ISQ}})_2]$  (0.056 g in 10 mL water), the pH of which had been adjusted to 10 with aqueous NaOH. Crude purple crystals were formed and collected by filtration, washed with cold water, and dried in vacuo to afford  $(\text{PPrPh}_3)_2[\text{Pt}^{\text{II}}(\text{L}^{\text{ISQ}})_2]$  (0.081 g, 75% yield) as a powder. The diffusion of acetone vapor to a methanolic solution of  $(\text{PPrPh}_3)_2[\text{Pt}^{\text{II}}(\text{L}^{\text{ISQ}})_2]$  afforded purple-colored single crystals of *trans*- $(\text{PPrPh}_3)_2[\text{Pt}^{\text{II}}(\text{L}^{\text{ISQ}})_2]$ .  $^1\text{H}$  NMR (400 MHz,  $[\text{D}_6]$ -DMSO):  $\delta$  = 1.07 (t,  $J$  = 7.27 Hz, 3 H,  $\text{CH}_2\text{CH}_3$ ), 1.56 (m, 2 H,  $\text{CH}_2\text{CH}_2\text{CH}_3$ ), 6.87 (dd,  $J_1$  = 1.64,  $J_2$  = 8.66 Hz, 1 H, ArH), 6.98 (d,  $J$  = 8.76 Hz, 1 H, ArH), 7.31 (s, 1 H, ArH), 7.77 (m, 12 H, ArH), 7.90 (m, 3 H, ArH), 10.0 (br., 2 H, NH) ppm. The two proton signals of the methylene moiety of  $\text{PPrPh}_3$  were not observed due to overlapping with the water peak.  $\text{C}_{54}\text{H}_{54}\text{N}_4\text{O}_6\text{P}_2\text{PtS}_2$  (1176.16): calcd. C 55.14, H 4.63, N 4.76, S 5.45; found C 54.81, H 4.80, N 4.80, S 5.20.

**X-ray Crystallography:** Single-crystal X-ray diffraction data were collected with a Bruker AXSII CCD diffractometer using  $\text{Mo-K}_\alpha$  radiation ( $\lambda$  = 0.71073 Å) employing a “Bruker Helios multilayered confocal mirror” as monochromator and a “Bruker TXS fine-focus rotating anode” as radiation source. Data integration and reduction were performed with the SAINT and XPREP software and the absorption correction was performed by the semi-empirical method with SADABS.<sup>[17]</sup> The structure was solved by the direct method using SHELXS-97<sup>[18]</sup> and refined by using least-squares methods on  $I^2$  with SHELXL-97.<sup>[18]</sup> The two NH protons were found as follows. The final difference Fourier map showed two peaks in the expected positions with N1–H1 of 0.82 Å and N2–N2 of 1.0 Å, which were first refined with the isotropic temperature factors. However, they did not converge to expected N–H distances. Therefore the positions were fixed in the amide geometry (N–H 0.88 Å) and only temperature factors were refined to give reasonable values ( $B_{\text{iso}}$  = 2.5 and 4.8 Å<sup>2</sup> for H1 and H2, respectively), thus proving clearly the existence of the N–H bonds. X-ray analysis



was undertaken using the free GUI software of Yadokari-XG 2009.<sup>[19]</sup> Crystal data and structure refinement for complex (PPrPh<sub>3</sub>)<sub>2</sub>[Pt<sup>II</sup>(L<sup>ISO</sup>)<sub>2</sub>] are summarized in Table 3.

Table 3. Crystallographic data for (PPrPh<sub>3</sub>)<sub>2</sub>[Pt<sup>II</sup>(L<sup>ISO</sup>)<sub>2</sub>].

Parameter	(PPrPh <sub>3</sub> ) <sub>2</sub> [Pt <sup>II</sup> (L <sup>ISO</sup> ) <sub>2</sub> ]
Empirical formula	C <sub>54</sub> H <sub>54</sub> N <sub>4</sub> O <sub>6</sub> P <sub>2</sub> S <sub>2</sub>
Formula mass	1176.16
Temperature [K]	173
Wavelength [Å]	0.71073
Crystal system	monoclinic
Space group	P2 <sub>1</sub> /c
Unit cell dimensions	
<i>a</i> [Å]	9.969 (2)
<i>b</i> [Å]	17.477 (3)
<i>c</i> [Å]	15.006 (3)
$\beta$ [°]	106.627 (2)
Volume [Å <sup>3</sup> ]	2505.3 (8)
<i>Z</i>	2
Density (calcd.) [g/cm <sup>3</sup> ]	1.559
Absorption coefficient [mm <sup>-1</sup> ]	3.003
<i>F</i> (000)	1188
Crystal size [mm <sup>3</sup> ]	0.10 × 0.05 × 0.04
Crystal color	purple
Reflections included in the refinement (total)	25674 (1.83° < $\theta$ < 26.50°)
Independent reflections	5196 [ <i>R</i> (int) = 0.0587]
Reflections with [ <i>I</i> > 2 $\sigma$ ( <i>I</i> )]	4408 [ <i>R</i> (int) = 0.0418]
Completeness to $\theta_{\max}$ [%]	99.9
Refined parameters	315
Final <i>R</i> indices [all data]	<i>R</i> <sub>1</sub> <sup>[a]</sup> = 0.0476, <i>wR</i> <sub>2</sub> <sup>[b]</sup> = 0.1025
Final <i>R</i> indices [ <i>I</i> > 2 $\sigma$ ( <i>I</i> )]	<i>R</i> <sub>1</sub> <sup>[a]</sup> = 0.0398, <i>wR</i> <sub>2</sub> <sup>[b]</sup> = 0.0979
GOF on <i>F</i> <sup>2</sup>	1.158
$\rho$ (max, min) [e Å <sup>-3</sup> ]	1.608, -1.731

[a]  $R_1(F) = \sum ||F_o| - |F_c|| / \sum |F_o|$ . [b]  $wR_2(F^2) = [\sum w(F_o^2 - F_c^2)^2 / \sum w(F_o^2)^2]^{1/2}$ .

CCDC-766406 contains the supplementary crystallographic data for this paper. These data can be obtained, free of charge, from The Cambridge Crystallographic Data Center at [www.ccdc.cam.ac.uk/data\\_request/cif](http://www.ccdc.cam.ac.uk/data_request/cif).

**Supporting Information** (see also the footnote on the first page of this article): <sup>1</sup>H NMR spectrum of Na<sub>2</sub>[Pt<sup>II</sup>(L<sup>ISO</sup>)<sub>2</sub>], cyclic voltammogram of Na<sub>2</sub>[Pt<sup>II</sup>(L<sup>ISO</sup>)<sub>2</sub>], EPR spectrum of [Pt<sup>II</sup>(L<sup>ISO</sup>)(L<sup>IBO</sup>)]<sup>+</sup>, and an estimation of the EPR parameters and spin density at the Pt<sup>II</sup> center.

## Acknowledgments

We thank Dr. F. Pichierri (Graduate School of Engineering, Tohoku Univ.) for useful discussions on the electronic structure of the complex.

- [1] C. Y. Xu, J. Ye, D. L. Marks, S. A. Boppert, *Opt. Lett.* **2004**, *29*, 1647–1649.
- [2] X. D. Wang, G. Ku, M. A. Wegiel, D. J. Bornhop, G. Stoica, L. H. V. Wang, *Opt. Lett.* **2004**, *29*, 730–732.
- [3] J. Chen, F. Saeki, B. J. Wiley, H. Cang, M. J. Cobb, Z. Y. Li, L. Au, H. Zhang, M. B. Kimmey, X. Li, Y. Xia, *Nano Lett.* **2005**, *5*, 473–477.
- [4] X. Yang, S. E. Skrabalak, Z. Y. Li, Y. Xia, L. H. V. Wang, *Nano Lett.* **2007**, *7*, 3798–3802.
- [5] B. Tang, F. Yu, P. Li, L. Tong, X. Duan, T. Xie, X. Wang, *J. Am. Chem. Soc.* **2009**, *131*, 3016–3023.
- [6] X. Huang, Z. Guo, W. Zhu, Y. Xie, H. Tian, *Chem. Commun.* **2008**, 5143.
- [7] Y. Gabe, Y. Urano, K. Kikuchi, H. Kojima, T. Nagano, *J. Am. Chem. Soc.* **2004**, *126*, 3357–3367.
- [8] H. Hoshino, K. Kiba, S. Eda, T. Yotsuyanagi, *Anal. Sci.* **1994**, *10*, 181–185.
- [9] Y. Terazono, Ph. D. Thesis, Tohoku University, **1999**.
- [10] D. Herebian, E. Bothe, F. Neese, T. Weyhermüller, K. Wieghardt, *J. Am. Chem. Soc.* **2003**, *125*, 9116–9128.
- [11] A. L. Balch, R. H. Holm, *J. Am. Chem. Soc.* **1966**, *88*, 5201–5209.
- [12] D. Herebian, K. Wieghardt, F. Neese, *J. Am. Chem. Soc.* **2003**, *125*, 10997–11005.
- [13] K. Konno, N. Matsushita, *Bull. Chem. Soc. Jpn.* **2006**, *79*, 1046–1053.
- [14] A. H. Maki, N. Edelstein, A. Davison, R. H. Holm, *J. Am. Chem. Soc.* **1964**, *86*, 4580–4587.
- [15] F. C. Senftleber, W. E. Geiger, *Inorg. Chem.* **1978**, *17*, 3615–3622.
- [16] X. Sun, H. Chun, K. Hildenbrand, E. Bothe, T. Weyhermüller, F. Neese, K. Wieghardt, *Inorg. Chem.* **2002**, *41*, 4295–4303.
- [17] a) *SMART, SAINT, and XPREP, Area Detector Control and Data Integration and Reduction Software*, Bruker Analytical X-ray Instruments Inc., Madison, WI, **1995**; b) G. M. Sheldrick, *SADABS, Empirical Absorption Correction Program for Area Detector Data*, University of Göttingen, Germany, **1996**.
- [18] G. M. Sheldrick, *SHELX97, Programs for Crystal structure Analysis*, University of Göttingen, **1998**.
- [19] K. Wakita, *Yadokari-XG, Software for Crystal Structure Analyses*, **2001**; Release of Software (Yadokari-XG 2009) for Crystal Structure Analyses; C. Kabuto, S. Akine, T. Nemoto, E. Kwon, *J. Cryst. Soc. Jpn.* **2009**, *51*, 218–224.

Received: March 28, 2010  
Published Online: June 16, 2010

# Quantum Chemical Design for Enhanced Second-Order NLO Response of Terpyridine-Substituted Hexamolybdates

Muhammad Ramzan Saeed Ashraf Janjua,<sup>[a]</sup> Wei Guan,<sup>[a]</sup> Likai Yan,<sup>[a]</sup> Zhong-Min Su,<sup>\*[a]</sup> Abdul Karim,<sup>[b]</sup> and Jamshed Akbar<sup>[b]</sup>

**Keywords:** Polyoxometalates / Organic–inorganic hybrid composites / Second-order polarizability / Charge transfer / Density functional calculations

A dramatic increase in the second-order nonlinear optical (NLO) response of terpyridine-substituted hexamolybdates has been observed from  $886.55 \times 10^{-30}$  esu (system **1**) to  $4622.92 \times 10^{-30}$  esu (system **7**). The dipole polarizabilities and second-order nonlinear optical (NLO) properties of terpyridine derivatives of hexamolybdates have been investigated by using time-dependent density functional theory (TDDFT). The quantum mechanical design suggests that  $[\text{Mo}_6\text{O}_{18}(\text{N}_4\text{C}_{25}\text{H}_{14}(\text{CF}_3)_2(\text{CN})_2)]^{2-}$  (system **7**) is the best

choice among all studied systems to improve nonlinearity. The electron-withdrawing ability of electron-acceptor groups (F, Cl, Br, I,  $\text{CF}_3$ , and CN) at the end of the terpyridine ligand directs the charge transfer (CT) from the POM cluster to the terpyridine segment along the *z* axis, which leads to an efficient second-order NLO molecular design. These small changes in molecular composition by substitution may have disproportionately huge effects on the NLO properties, which can be attributed to the so-called “butterfly effect”.

## Introduction

Polyoxometalates (POMs) are a versatile and diverse class of inorganic cluster systems recognized by fascinating structural, electrochemical, catalytic, magnetic, medicinal, and photophysical properties.<sup>[1–4]</sup> The development of rational methods for the modification and functionalization of POM systems may provide the means to fully exploit these desirable attributes. Preparation of POMs incorporating various main groups, organic, and organometallic fragments now constitutes a significant area of research, whose scope and pace continue to increase.<sup>[5]</sup>

The design and synthesis of second-order nonlinear optical (NLO) materials have been attracting more and more appreciation due to their potential implications in optoelectronics.<sup>[6–8]</sup> On the basis of experimental and theoretical research work, various principles and rules to enhance second-order NLO response have been developed, for example, the planar donor  $\pi$ -conjugated bridge acceptor (D- $\pi$ -A) model,<sup>[9]</sup> bond length alternation (BLA) theory,<sup>[10]</sup> auxiliary donors and acceptors model for heterocycles,<sup>[11–13]</sup> and twisted  $\pi$ -electron systems.<sup>[14–16]</sup> Directed by these strategies, large second-order NLO responses can be achieved by optimizing the D/A strength or elongating the conjugated

bridge.<sup>[17]</sup> In the past two decades, considerable efforts have been focused on the development of one-dimensional (1D) NLO materials. However, this work is also devoted to improve the nonlinearity of 1D systems.

Presently, POM-based organic–inorganic hybrid materials are the center of debate in our research group.<sup>[18–21]</sup> POMs have been found to be extremely versatile inorganic building blocks for constructing functionally active materials, and POM-based organic–inorganic hybrid compounds are the combination of POMs with organic ligands.<sup>[22–26]</sup> Several reasons make these hybrids excellent candidates for novel NLO materials. Firstly, they offer a wide range of metals with different coordination states and various organic groups which possess large  $\pi$ -conjugated systems.<sup>[27–29]</sup> Secondly, many of these compounds are known to possess intense low-lying electronic transitions.<sup>[22]</sup> Last but not least, POMs have been found to be extremely flexible building blocks as the non-centrosymmetric molecular structures can be achieved easily for such compounds.<sup>[22–29]</sup>

In the present work, we have designed different sorts of molecular systems by introducing various electron acceptors at the end of the terpyridine ligand. We performed TDDFT analysis on the terpyridine derivatives of hexamolybdates and have calculated remarkably enhanced first hyperpolarizabilities (second-order polarizabilities). The systems with enhanced second-order NLO response have been constructed by incorporation of different electron-withdrawing groups (F, Cl, Br, I,  $\text{CF}_3$ , and CN) at the endmost and lateral terminal positions (R and R<sup>1</sup>) of the terpyridine ligand. It is noteworthy that in all our studied systems the electron-accepting property of the POM cluster has been

[a] Institute of Functional Material Chemistry, Faculty of Chemistry, Northeast Normal University, Changchun 130024, P. R. China  
Fax: +86-431-8568-4009  
E-mail: Dr\_Janjua2010@yahoo.com  
zmsu@nenu.edu.cn

[b] Department of Chemistry, University of Sargodha, Sargodha 40100, Islamic Republic of Pakistan

changed, as it acts as a donor and the terpyridine ligand acts as an acceptor (D-bridge-A) by the charge-transport property of the  $\pi$ -conjugated bridge. This work may provide a basis to experimentalists for designing materials with enhanced NLO response.

## Results and Discussion

We have designed different types of systems by substituting various electron acceptors at the endmost and lateral terminal positions of the terpyridine ligand. After making calculations on numerous systems, we came to know that, interestingly, positions  $R^1$  and  $R$ , as shown in Figure 1, are most suitable to increase nonlinearity in terpyridine-substituted hexamolybdates. The  $\beta$  value of system **1** is calculated to be  $886.55 \times 10^{-30}$  esu. On the basis of this considerable NLO response of system **1**, we were inspired to design systems **2–7**, which show appealingly large second-order NLO responses as compared to system **1**. First of all, the geometrical optimization of systems **1–7** was carried out under the  $C_{2v}$  symmetry constraint, where the initial geometric data were obtained from the crystal structure.<sup>[30]</sup> The structures of these systems are depicted in Figure 1, and the optimized bond lengths and angles are compared in Table 1, which are in reasonable agreement with the reported experimental data. As shown in Figure 1, a hybrid structure incorporating a terpyridine ligand bearing various electron-acceptor moieties to a hexamolybdate cluster has been designed. The imido-functionalized hexamolybdate cluster exhibits features characteristic to other arylimido derivatives,<sup>[29a]</sup> such as a short Mo–N bond length, a linear/near-linear Mo1–N1–C1 bond angle, a closer distance of the central oxygen

(O1) to the imido-bearing Mo1 atom than to the other Mo (Mo2, Mo3, Mo4, Mo5, and Mo6) atoms. Moreover, C1–N1 and Mo1–N1 distances ( $\text{\AA}$ ) of the designed systems have also shown good consistency with the experimental values of system **1**. This agreement between experimental and calculated parameters of system **1** gives us confidence that the present study is consequential for this research, although the symmetry axis is along the  $z$  axis for our studied systems (**1–7**).

Table 1. Bond lengths ( $\text{\AA}$ ) and angles ( $^\circ$ ) calculated by DFT for systems **1–7**.

System	<b>1</b>	<b>2</b>	<b>3</b>	<b>4</b>	<b>5</b>	<b>6</b>	<b>7</b>
C1–N1	1.344 (1.375) <sup>[a]</sup>	1.340	1.340	1.339	1.339	1.336	1.335
Mo1–N1	1.820 (1.747)	1.824	1.824	1.823	1.824	1.829	1.831
Mo1–O1	2.222 (2.213)	2.221	2.221	2.220	2.221	2.220	2.222
Mo2–O1	2.364 (2.346)	2.364	2.364	2.364	2.364	2.363	2.363
Mo3–O1	2.368 (2.336)	2.368	2.368	2.367	2.367	2.367	2.367
Mo4–O1	2.364 (2.323)	2.364	2.364	2.364	2.364	2.363	2.363
Mo5–O1	2.368 (2.332)	2.368	2.368	2.367	2.367	2.367	2.367
Mo6–O1	2.439 (2.364)	2.442	2.442	2.443	2.444	2.447	2.446
C1–N1–Mo1	180 (175.83)	180	180	180	180	180	180

[a] Experimental values in parentheses are from ref.<sup>[30]</sup>

## Static Second-Order NLO Response

In order to have a better understanding of the second-order NLO response ( $\beta$ ), a knowledge of the dipole polarizability is also important. The average polarizability,  $\langle a \rangle$  is defined in [Equation (1)].

$$\langle a \rangle = 1/3 (a_{xx} + a_{yy} + a_{zz}) \quad (1)$$

There are three components of dipole polarizability  $a_{xx}$ ,  $a_{yy}$ , and  $a_{zz}$ . There exists  $C_{2v}$  symmetry in our studied systems, and the  $a_{zz}$  component has the largest value as compared to the  $a_{xx}$  and  $a_{yy}$  components, and the property of the studied compounds (**1–7**) is predominantly evaluated by the  $z$ -direction transition (Figure 1). The formula of dipole polarizability along the  $z$  direction is defined in Equation (2).

$$\alpha_{zz} \propto \frac{(M_z^{gm})^2}{E_{gm}} \quad (2)$$

Equation (2) shows that the  $a$  value is directly proportional to the transition moment and inversely proportional to the transition energy. The transition moment ( $M_z^{gm}$ ) and the corresponding dominant molecular orbital (MO) transitions of systems **1–7** are enlisted in Table 3. The average polarizability,  $\langle a \rangle$ , of the systems is in the following order: **7** > **6** > **5** > **4** > **3** > **2** > **1**, as shown in Table 2. The calculated dipole polarizability coefficients for systems **1–7** are listed in Table 2.

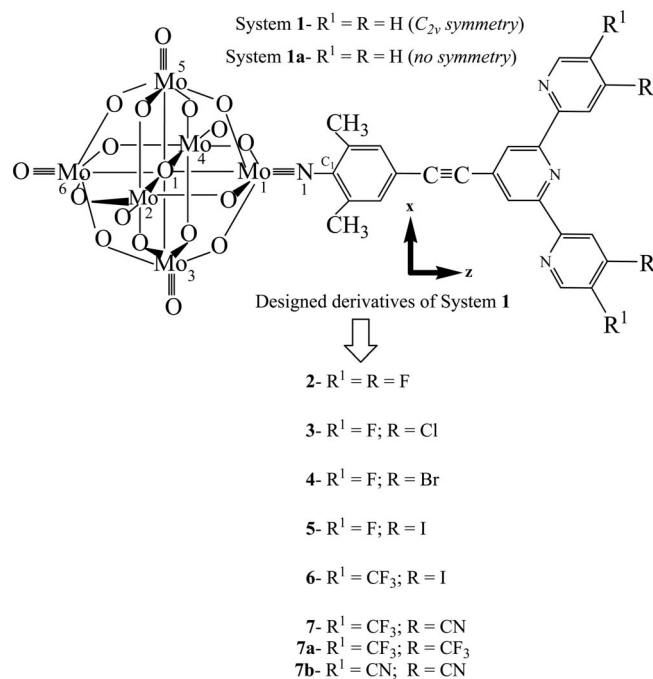


Figure 1. The orientation and calculation models of studied systems.

Table 2. The computed dipole polarizabilities ( $1 \times 10^{-24}$  esu) for systems 1–7.

System	$a_{xx}$	$a_{yy}$	$a_{zz}$	$\langle a \rangle$
1	105.73	65.22	285.01	151.98
2	106.76	65.08	320.90	164.25
3	108.66	66.90	334.51	170.02
4	109.97	68.32	342.30	173.53
5	110.69	68.40	348.60	175.90
6	123.53	71.82	415.19	203.51
7	135.89	70.09	476.00	227.32

The TDDFT results demonstrate that the electronic transitions in systems 2, 3, and 6 mainly occur from the POM (HOMO and HOMO-4) to the terpyridine ligand (LUMO+6) along the  $z$  direction. This tendency of charge transfer also occurs in system 4 (HOMO and HOMO-4 to LUMO+8), 5 (HOMO to LUMO+2 and LUMO+1), and 7 (HOMO and HOMO-4 to LUMO+2). The frontier molecular orbitals involved in the dominant electron transitions in systems 2–6 are shown in Figures 2 and 3, and all these transitions have  $A_1$  symmetry, as listed in Table 3.

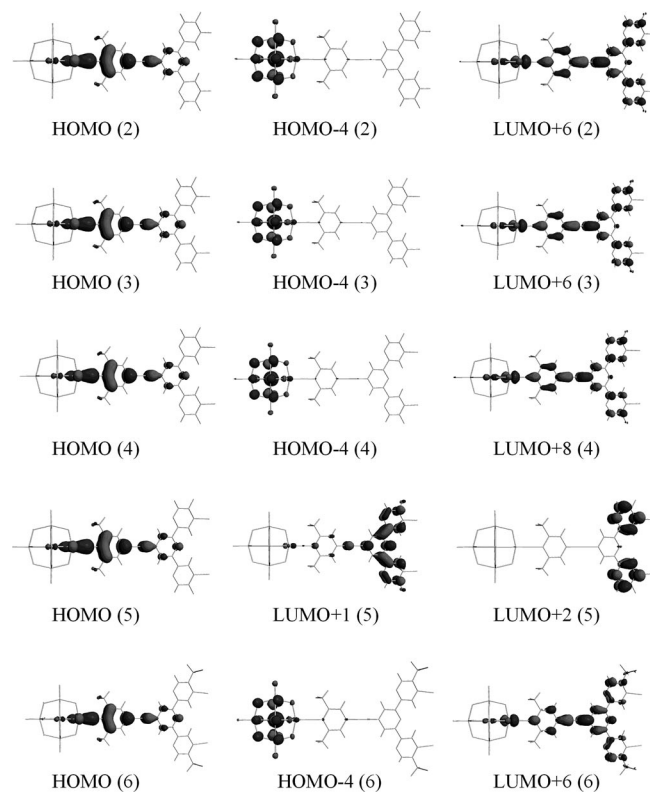


Figure 2. The frontier molecular orbitals of systems 2–6 involved in the dominant electron transitions.

The changes in the molecular structures modify the contribution of different orbitals to the electronic transitions. The dominant electronic transitions for the studied compounds have the same  $A_1$  symmetry, and the major charge transfer originates from the POM cluster to the terpyridine ligand along the  $z$  axis. This attribute indicates that the ter-

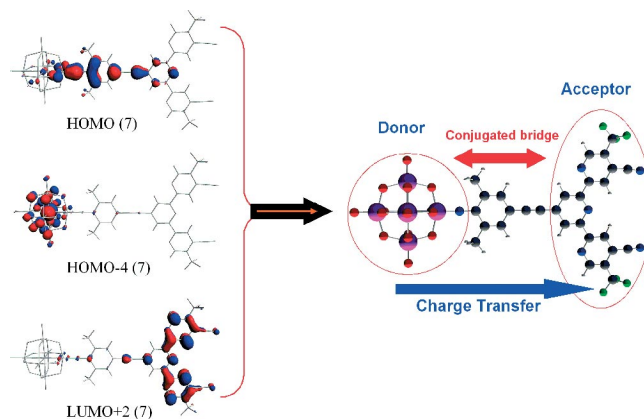


Figure 3. The frontier molecular orbitals of system 7 involved in the dominant electron transitions with D-A molecular configuration of the POM.

Table 3. Excitation energy (in eV), oscillator strengths ( $f$ ), symmetry (S), transition moment ( $M_z^{\text{gm}}$  = a.u.),<sup>[a]</sup> and corresponding dominant MO transitions of systems 2–7.

System	$E$	$f$	S	$M_z^{\text{gm}}$	MO transition
2	2.25	0.634	$A_1$	3.395	HOMO $\rightarrow$ LUMO+6 (59%) HOMO-4 $\rightarrow$ LUMO+6 (30%)
3	2.26	0.739	$A_1$	3.654	HOMO $\rightarrow$ LUMO+6 (64%) HOMO-4 $\rightarrow$ LUMO+6 (24%)
4	2.26	0.776	$A_1$	3.737	HOMO $\rightarrow$ LUMO+8 (66%) HOMO-4 $\rightarrow$ LUMO+8 (23%)
5	1.34	0.331	$A_1$	3.179	HOMO $\rightarrow$ LUMO+2 (54%) HOMO $\rightarrow$ LUMO+1 (39%)
6	2.14	0.525	$A_1$	3.168	HOMO $\rightarrow$ LUMO+6 (43%) HOMO-4 $\rightarrow$ LUMO+6 (20%)
7	1.04	0.387	$A_1$	3.884	HOMO $\rightarrow$ LUMO+2 (85%) HOMO-4 $\rightarrow$ LUMO+2 (7%)

[a]  $M_x^{\text{ng}} = M_y^{\text{ng}} = 0$

pyridine ligand acts as an acceptor and the POM (hexamolybdate) acts as a donor in our all designed systems. The direction and degree of charge transfer have been remarkably enhanced in system 7 relative to system 1, and all the system operate through a D- $\pi$ -bridge-A configuration. The direction of CT from the POM to the terpyridine segment has been reasonably improved by incorporation of F, Cl, Br, and I (2–5), while the presence of  $\text{CF}_3$  and CN (systems 6 and 7) have significantly enhanced the optical nonlinearity.

In our compounds, the direction of the dipole moment is along the  $z$  axis,  $\beta_{\text{vec}}$ , is defined in Equation (3).

$$\beta_{\text{vec}} = \sum_i \mu_i \beta_i / |\mu| \quad i = x, y, z \quad (3)$$

where  $\beta_i = (3/5) \sum_j = x, y, z \beta_{ijj}$

The computed  $\beta_{\text{vec}}$  values with their individual components for systems 1–7 are shown in Table 4. There are seven components of the second-order polarizability as a result of the  $C_{2v}$  symmetry. As we have mentioned that the  $\beta_{zzz}$  component has the largest value, the major share of the second-order polarizability is the  $\beta_{zzz}$  component, and the major charge transfer is also along the  $z$  direction. All the



systems (**2–7**) have larger second-order polarizability than system **1** as shown in Table 4, which indicates that all the studied systems have an excellent second-order NLO response.

Table 4. The computed static second-order polarizabilities and their individual components ( $1 \times 10^{-30}$  esu) for systems **1–7**.

System	$\beta_{zzz}$	$\beta_{yyz}$	$\beta_{xxz}$	$\beta_{zyy}$	$\beta_{zxy}$	$\beta_{xzx}$	$\beta_{zxx}$	$\beta_{vec}$
<b>1</b>	1444.80	1.87	30.72	1.87	1.87	30.72	30.72	886.55
<b>2</b>	1971.50	1.90	75.03	1.90	1.90	75.03	75.03	1229.21
<b>3</b>	2037.20	1.68	72.24	1.68	1.68	72.24	72.24	1266.79
<b>4</b>	2079.90	2.16	72.10	2.16	2.16	72.10	72.10	1292.63
<b>5</b>	2084.90	1.76	66.32	1.76	1.76	66.32	66.32	1291.93
<b>6</b>	3457.50	2.60	303.38	2.60	2.60	303.38	303.38	2258.32
<b>7</b>	6028.10	3.34	1672.60	3.34	3.34	1672.60	1672.60	4622.92

The computed  $\beta_{vec}$  values of the studied systems show that the NLO response is in the following order: **7** > **6** > **5**  $\approx$  **4** > **3** > **2** > **1**. The  $\beta_{zzz}$  component of system **7** has the highest value, as it shows the largest  $\beta_{vec}$  among systems **1–7**. However, in our systems the accepting ability of the terpyridine ligand has been enhanced by incorporation of various electron-withdrawing groups, which help to increase the optical nonlinearity in such types of organic–inorganic hybrid compounds.

In system **7**, the two  $CF_3$  groups at the lateral terminal position and the CN group at the endmost terminals of the terpyridine enhance the withdrawing ability of the terpyridine segment, so the  $\beta_{vec}$  value increases from  $886.55 \times 10^{-30}$  esu (system **1**) to  $4622.92 \times 10^{-30}$  esu (system **7**). System **7** offers maximal NLO response among all seven systems by establishing a D-bridge-A configuration, which also indicates that the POM acts as a donor in our all studied systems. The degree of charge transfer and the synergistic effect between the POM (D) and the terpyridine ligand have been strongly enhanced by introduction of different electron acceptors by various ways, particularly through the increased strength of the electron acceptor. Most importantly, for our studied organic–inorganic hybrid materials, nonlinearity has been appealingly improved by the introduction of the  $CF_3$  and CN simultaneously, which is helpful in enhancing the degree of charge transfer by decreasing the excited state energy, which leads to a remarkable increase in the first hyperpolarizability (see Figure 3 and Table 3).

Oudar and Chemla<sup>[31]</sup> formulated a simple link between molecular hyperpolarizability and electronic transition in low-lying crucial excited states. On the basis of the complex sum-over-states (SOS) expression, the paradigm two-level model can be defined by Equation (4).

$$\beta \propto \frac{\Delta\mu_{ge} \cdot f_{os}}{\Delta E_{ge}^3} \quad (4)$$

In Equation (4),  $\Delta\mu_{ge}$  is the dipole moment between the ground state (g) and the excited state (e),  $f_{os}$  is the oscillator strength, and  $\Delta E_{ge}$  is the transition energy. These factors ( $\Delta\mu_{ge}$ ,  $f_{os}$ , and  $\Delta E_{ge}$ ) are closely related with each other and governed by choice/strength of donor/acceptor along with conjugated bridge. The most favorable combination of these

factors can provide a larger  $\beta$  value. On the basis of this rule in the above model, we have designed different functionalized terpyridine derivatives of hexamolybdate systems by introducing different acceptors at the end of the terpyridine ligand. Overall, for our studied systems, low excitation energy along with high oscillator strength are the decisive factors to improve nonlinearity. The redshift of the absorption band indicates the substitution of the acceptor, which is much pronounced in system **7**. The excitation energy of system **7** is 1.04 eV, while that of system **2** is 2.25 eV, which indicates that a low-lying transition energy is a decisive factor towards enhanced NLO response in system **7**. Clearly, the excitation energy will tend to make a dominant contribution to the  $\beta_{vec}$  values of the studied compounds, as we have already illustrated that the  $\beta$  value is directly proportional to oscillator strength and inversely proportional to the transition energy.

In short, the large  $\beta_{vec}$  values come from the strong oscillator strength and small transition energy as shown in Table 3. The NLO response of systems **1–7** follows the order **7** > **6** > **5**  $\approx$  **4** > **3** > **2** > **1**, and it is obvious that system **7** offers the maximum  $\beta$  value by establishing a D-bridge-A configuration. It is also clear that substitution of a strong electron acceptor has a majestic influence on the second-order NLO properties in our studied systems. From these results, it can be concluded that incorporation of electron-acceptor groups at the end of the terpyridine ligand is helpful in enhancing nonlinearity and of course the  $\beta$  value as well. Therefore, larger  $\beta_{vec}$  values are generated, as electron transition occurs from the POM cluster to the terpyridine segment along the  $z$  axis.

It is generally believed that the low-lying HOMO–LUMO energy gap might enhance molecular second-order NLO properties. The HOMO–LUMO energy gaps of systems **1–7** decrease in the following order: **1** > **2** > **3**  $\approx$  **4**  $\approx$  **5** > **6** > **7**, while the NLO response increases accordingly as follows: **1** < **2** < **3** < **4**  $\approx$  **5** < **6** < **7**. Moreover, it can be seen from Figure 4 that the HOMO–LUMO energy gap of system **7** has a minimal value of 0.17 eV, which supports its highest nonlinearity in our studied systems; the incorporation of electron acceptors (F, Cl, Br, I,  $CF_3$ , and CN) are vital determinants for the larger  $\beta$  value. These POM-based organic–inorganic hybrid compounds can become an excellent kind of material in the second-order NLO field. The electron-acceptor in the terpyridine segment enhances the first hyperpolarizability, as the POM cluster acts as a donor and the terpyridine ligand acts as an acceptor in all the studied systems **1–7** (Figure 5).

On the basis of systems **1–7**, we were also inspired to probe into the following questions. First, all the systems have been optimized under the  $C_{2v}$  symmetry constraint; is there any role of torsion of the terpyridine ligand in modifying the charge-transfer? Second, what is the role of  $CF_3$  and CN at the end of the terpyridine ligand individually? In order to answer these questions, we investigated the behavior of the terpyridine ligand by optimizing the crystal system (**1a**) with original torsion (crystal system having no symmetry:  $C_1$ ) as illustrated in Figures 1 and 6. We found

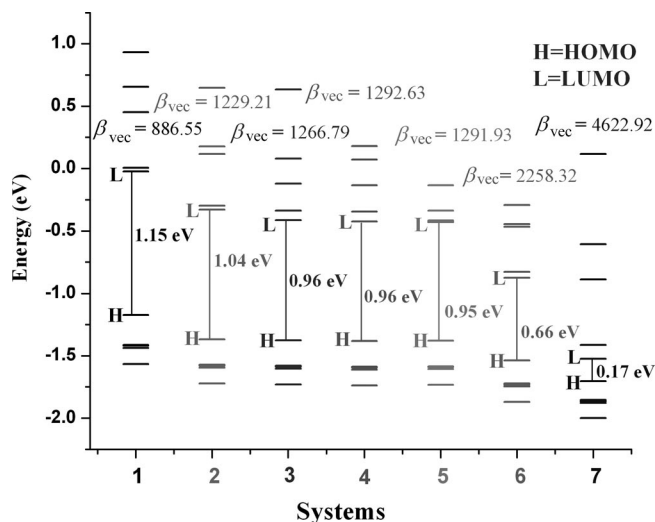


Figure 4. Molecular orbital energy diagram,  $\beta_{\text{vec}} \times 10^{-30}$  esu, and HOMO–LUMO energy gaps of systems 1–7.

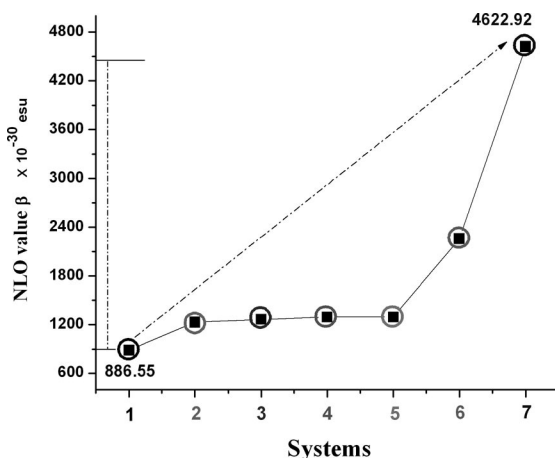


Figure 5. An incremental boost in NLO response ( $\beta \times 10^{-30}$  esu) from systems 1 to 7.

that, even with the torsion of the terpyridine ligand as in system **1a**, the direction of charge transfer was from the POM cluster to the terpyridine ligand, that is, HOMO  $\rightarrow$  LUMO+6 and HOMO-5  $\rightarrow$  LUMO+3, as shown in Figure 6 and Table 5. The  $\beta_{\text{vec}}$  value of system **1a** is calculated to be  $926.72 \times 10^{-30}$  esu, which is comparable with the  $\beta$  value of system **1** (system with  $C_{2v}$  symmetry), calculated to be  $886.55 \times 10^{-30}$  esu.

To further study the individual role of  $\text{CF}_3$  and CN, we also calculated systems **7a** and **7b**, as shown in Figures 1 and 6. On substituting  $\text{CF}_3$  (system **7a**) on both terminal positions R and R', the  $\beta_{\text{vec}}$  value was computed to be  $3060.89 \times 10^{-30}$  esu, while on substituting CN (system **7b**), the  $\beta_{\text{vec}}$  value was calculated to be  $3965.15 \times 10^{-30}$  esu (see Tables 5 and 6). From this it is clear to see that CN has more influence on enhancing NLO response as compared to  $\text{CF}_3$ , as shown in Table 6. Therefore, we may say that system **7** has the synergetic effect of the two substituents

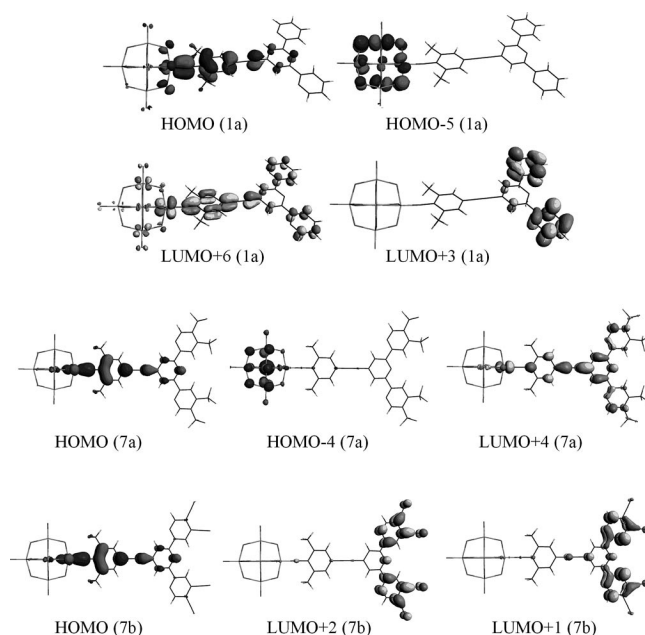


Figure 6. The frontier molecular orbitals of systems **1a**, **7a**, and **7b** involved in the dominant electron transitions.

Table 5. Excitation energy ( $E$  in eV), oscillator strengths ( $f$ ), symmetry ( $S$ ), transition moment ( $M_z^{\text{gm}}$  in a.u.),<sup>[a]</sup> and corresponding dominant MO transitions of systems **1a**, **7a**, and **7b**.

System	$E$	$f$	$S$	$M_z^{\text{gm}}$	MO transition
<b>1a</b> (Torsion)	2.35	0.554	$A_1$	3.099 <sup>[b]</sup>	HOMO $\rightarrow$ LUMO+6 (45%) HOMO-5 $\rightarrow$ LUMO+3 (32%)
<b>7a</b> ( $\text{CF}_3\text{-CF}_3$ )	2.08	0.413	$A_1$	2.842	HOMO $\rightarrow$ LUMO+4 (46%) HOMO-4 $\rightarrow$ LUMO+4 (43%)
<b>7b</b> (CN-CN)	1.01	0.373	$A_1$	3.889	HOMO $\rightarrow$ LUMO+2 (87%) HOMO $\rightarrow$ LUMO+1 (6%)

[a] Under  $C_{2v}$  symmetry constraint systems **7a** and **7b** have the maximum value of  $M_z^{\text{gm}}$ . [b]  $M_x^{\text{gm}} = 3.099$  for system **1a** (with torsion, no symmetry).

( $\text{CF}_3$  and CN) towards the maximal NLO value as compared to all the studied systems. The simultaneous presence of CN at the terminal position and  $\text{CF}_3$  at the lateral terminal position of the end terpyridine ligand has produced the  $\beta_{\text{vec}}$  value figured out to be  $4622.92 \times 10^{-30}$  esu (system **7**).

Table 6. The computed static second-order polarizabilities and their individual components ( $1 \times 10^{-30}$  esu) for systems **1a**, **7a**, and **7b**.

System	$\beta_{zzz}$	$\beta_{yyz}$	$\beta_{xxz}$	$\beta_{yyz}$	$\beta_{zyy}$	$\beta_{xzx}$	$\beta_{zxx}$	$\beta_{\text{vec}}$
<b>1a</b> (Torsion)	1511.10 <sup>[a]</sup>	–	–	–	–	–	–	926.72
<b>7a</b> ( $\text{CF}_3\text{-CF}_3$ )	4186.40	2.76	911.86	2.76	2.76	911.86	911.86	3060.89
<b>7b</b> (CN-CN)	4751.10	3.35	1853.50	3.35	2.16	3.35	1853.50	3965.15

[a] The tensor  $\beta_{yyy}$  has a maximum value computed to be  $1511.10 \times 10^{-30}$  because of no symmetry (with torsion).

In a few words, the small variations in the initial configuration of our studied system **1** have produced large variations in the long-term behavior of system **7**. So, the butterfly effect in quantum mechanics may encapsulate this idea, which leads to a remarkable increase in NLO response from  $886.55 \times 10^{-30}$  esu (system **1**) to  $4622.92 \times 10^{-30}$  esu (system **7**).

## Conclusions

We have successfully designed different molecular systems with significantly large molecular static second-order polarizability, particularly system **7** with a remarkably large NLO response, computed to be  $4622.92 \times 10^{-30}$  esu, which is more than 5.2 times that of system **1**. The presence of halogens (F, Cl, Br, or I) at the end of the terpyridine ligand has a considerably large effect on the  $\beta$  value, whereas the simultaneous existence of  $\text{CF}_3$  and CN at the end of the terpyridine segment has a very large effect on the second-order molecular response. Moreover, the direction of charge transfer from POM to terpyridine ligand is a vital determinant in designing highly efficient second-order NLO materials. Interestingly, the electron-accepting property of the POM cluster has been changed in presence of a  $\pi$ -conjugation bridge and a terpyridine segment: the POM turned out to be a donor and the terpyridine ligand acts as an acceptor in our all studied systems. These small changes made by incorporation of different acceptors in our studied systems have proven to have a disproportionately huge effect on NLO response, the so-called “butterfly effect” illustrates this point nicely. The present investigation provides important insight into the attractively large NLO properties of terpyridine-substituted hexamolybdates. This work may help experimentalists in designing remarkably large-second-order-NLO materials.

## Experimental Section

### Methodology

The DFT calculations were carried out by using the ADF2006.01 suite of programs.<sup>[32]</sup> The zero-order regular approximation (ZORA) was adopted in all the calculations to account for scalar relativistic effects.<sup>[33]</sup> The generalized-gradient approximation (GGA) was employed in the geometry optimizations by using the Beck<sup>[34]</sup> and Perdew<sup>[35]</sup> (BP86) exchange-correlation (XC) functional. For the calculations, we made use of the standard ADF TZP basis set, which is a triple- $\zeta$  plus polarization STO basis set. Triple- $\zeta$  plus polarization basis sets were used to describe the valence electrons of all atoms, whereas for the transition-metal molybdenum atom, a frozen core composed of 1s to 3spd shells was described by means of single Slater functions. In calculations of the polarizability, second-order polarizability, and excitation, the RESPONSE and EXCITATION modules<sup>[36]</sup> implemented in the ADF program were used on the basis of optimized geometries. The van Leeuwen–Baerends XC potential (LB94) was chosen for calculations of all the response properties.<sup>[37]</sup> The reliability of the LB94 potential to calculate polarizabilities and hyperpolarizabilities has already been proven and well-documented.<sup>[38–40]</sup> The adiabatic lo-

cal density approximation (ALDA) was applied for the evaluation of the first and second functional derivatives of the XC potential. Moreover, the value of the numerical integration parameter used to determine the precision of numerical integrals was 6.0. The functional and basis set choices for our studied organic–inorganic hybrid compounds were based on the research work that has already been reported.<sup>[41,42]</sup>

## Acknowledgments

The authors gratefully acknowledge the financial support from the National Natural Science Foundation of China (Project No. 20971020), Program for Changjiang Scholars and Innovative Research Team in University (IRT0714), Department of Science and Technology of Jilin Province (20082103), and Science Foundation for Young Teachers of Northeast Normal University (20090401). We also thank Yuhe Kan for computational support. M. R. S. A. J. acknowledges the Government of Pakistan and China Scholarship Council (CSC) for the award of a PhD scholarship for the period 2006–2010. He is very thankful to Saira Janjua and Muhammad Sareb Janjua for their endless sacrifice and cooperation for the successful completion of his PhD study.

- [1] M. T. Pope, A. Muller, *Angew. Chem. Int. Ed. Engl.* **1991**, *30*, 34–48.
- [2] M. T. Pope, *Heteropoly and Isopoly Oxometalates*, Springer, Berlin, **1983**, vol. 35, pp. 101–117.
- [3] Special issue on POMs: C. L. Hill (Guest Ed.), *Chem. Rev.* **1998**, *98*, issue 1.
- [4] M. T. Pope, A. Muller (Eds.), *Polyoxometalates: From Platonic Solids to Anti-Retroviral Activity*, Kluwer Academic Publishers, Dordrecht, The Netherlands, **1994**, p. 1–411.
- [5] P. Gouzerh, A. Proust, *Chem. Rev.* **1998**, *98*, 77–112.
- [6] P. G. Lacroix, *Eur. J. Inorg. Chem.* **2001**, *2*, 339–347.
- [7] S. Di Bella, *Chem. Soc. Rev.* **2001**, *30*, 355–366.
- [8] D. R. Kanis, M. A. Ratner, T. J. Marks, *Chem. Rev.* **1994**, *94*, 195–242.
- [9] J. Zyss, I. Ledoux, *Chem. Rev.* **1994**, *94*, 77–105.
- [10] F. Meyers, S. R. Marder, B. M. Pierce, J. L. Bredas, *J. Am. Chem. Soc.* **1994**, *116*, 10703–10714.
- [11] P. Rao Varanasi, A. K.-J. Jen, J. Chandrasekhar, I. N. N. Namboothiri, A. Rathna, *J. Am. Chem. Soc.* **1996**, *118*, 12443–12448.
- [12] E. M. Breitung, C. F. Shu, R. J. McMahon, *J. Am. Chem. Soc.* **2000**, *122*, 1154–1160.
- [13] I. D. Albert, T. J. Marks, M. A. Ratner, *J. Am. Chem. Soc.* **1997**, *119*, 6575–6582.
- [14] J. S. Yang, K. L. Liao, C. Y. Li, M. Y. Chen, *J. Am. Chem. Soc.* **2007**, *129*, 13183–13192.
- [15] H. Kang, A. Facchetti, P. Zhu, H. Jiang, Y. Yang, E. Cariati, S. Righetto, R. Ugo, C. Zuccaccia, A. Macchioni, C. L. Stern, Z. Liu, S. T. Ho, T. J. Marks, *Angew. Chem. Int. Ed.* **2005**, *44*, 7922–7925.
- [16] H. Kang, A. Facchetti, H. Jiang, E. Cariati, S. Righetto, R. Ugo, C. Zuccaccia, A. Macchioni, C. L. Stern, Z. Liu, S. T. Ho, E. C. Brown, M. A. Ratner, T. J. Marks, *J. Am. Chem. Soc.* **2007**, *129*, 3267–3270.
- [17] Y. Q. Shi, C. Zhang, H. Zhang, J. H. Bechtel, L. R. Dalton, B. H. Robinson, W. H. Steier, *Science* **2000**, *288*, 119–122.
- [18] L. K. Yan, G. C. Yang, W. Guang, Z. M. Su, R. S. Wang, *J. Phys. Chem. B* **2005**, *109*, 22332–22336.
- [19] a) L. K. Yan, M. S. Jin, J. Zhuang, C. G. Liu, Z. M. Su, C. C. Sun, *J. Phys. Chem. A* **2008**, *112*, 9919; b) M. R. S. A. Janjua, C. G. Liu, W. Guan, J. Zhuang, S. Muhammad, L. K. Yan, Z. M. Su, *J. Phys. Chem. A* **2009**, *113*, 3576–3587.
- [20] W. Guan, G. C. Yang, L. K. Yan, Z. M. Su, *Inorg. Chem.* **2006**, *45*, 7864–7868.

- [21] a) G. C. Yang, W. Guang, L. K. Yan, Z. M. Su, *J. Phys. Chem. B* **2006**, *110*, 23092–23098; b) L. K. Yan, Z. M. Su, W. Guan, M. Zhang, G. H. Chen, L. Xu, E. B. Wang, *J. Phys. Chem. B* **2004**, *108*, 17337–17343.
- [22] B. B. Xu, M. Lu, J. Kang, D. Wang, J. Brown, Z. H. Peng, *Chem. Mater.* **2005**, *17*, 2841–2851.
- [23] L. Xu, B. B. Xu, M. Lu, Y. G. Wei, Z. H. Peng, D. R. Powell, *Angew. Chem. Int. Ed.* **2002**, *41*, 4129–4132.
- [24] J. Kang, B. B. Xu, Z. H. Peng, X. D. Zhu, Y. G. Wei, D. R. Powell, *Angew. Chem. Int. Ed.* **2005**, *44*, 6902–6905.
- [25] B. B. Xu, Y. G. Wei, C. L. Barnes, Z. H. Peng, *Angew. Chem. Int. Ed.* **2001**, *40*, 2290–2292.
- [26] M. Lu, Y. G. Wei, B. B. Xu, C. F. C. Cheung, Z. H. Peng, D. R. Powell, *Angew. Chem. Int. Ed.* **2002**, *41*, 1566–1568.
- [27] R. J. Errington, S. S. Petkar, P. S. Middleton, W. McFarlane, W. Clegg, R. A. Coxall, R. W. Harrington, *J. Am. Chem. Soc.* **2007**, *129*, 12181–12196.
- [28] R. J. Errington, S. S. Petkar, P. S. Middleton, W. McFarlane, W. Clegg, R. A. Coxall, R. W. Harrington, *Dalton Trans.* **2007**, 5211–5222.
- [29] a) J. B. Strong, G. P. A. Yap, R. Ostrander, L. M. Liable-Sands, A. L. Rheingold, R. Thouvenot, P. Gouzerh, E. A. Maatta, *J. Am. Chem. Soc.* **2000**, *122*, 639–649; b) J. Zhuang, L. K. Yan, C. G. Liu, Z. M. Su, *Eur. J. Inorg. Chem.* **2009**, *31*, 2529–2535.
- [30] B. Xu, Z. Peng, Y. Wei, D. R. Powell, *Chem. Commun.* **2003**, 2562–2563.
- [31] a) J. L. Oudar, D. S. Chemla, *J. Chem. Phys.* **1977**, *66*, 2664–2668; b) J. L. Oudar, *J. Chem. Phys.* **1977**, *67*, 446–457.
- [32] a) Chemistry with ADF: G. te Velde, F. M. Bickelhaupt, E. J. Baerends, C. Fonseca Guerra, S. J. A. van Gisbergen, J. G. Snijders, T. Ziegler, *J. Comput. Chem.* **2001**, *22*, 931–967; b) C. Fonseca Guerra, J. G. Snijders, G. te Velde, E. J. Baerends, *Theor. Chem. Acc.* **1998**, *99*, 391–403; c) ADF**2008.01**, SCM, *Theoretical Chemistry*, Vrije Universiteit, Amsterdam, The Netherlands, <http://www.scm.com>.
- [33] E. van Lenthe, E. J. Baerends, J. G. Snijders, *J. Chem. Phys.* **1993**, *99*, 4597–4610.
- [34] A. D. Becke, *Phys. Rev. A* **1988**, *38*, 3098–3100.
- [35] J. P. Perdew, *Phys. Rev. B* **1986**, *33*, 8822–8824.
- [36] S. J. A. van Gisbergen, J. G. Snijders, E. J. Baerends, *Comput. Phys. Commun.* **1999**, *118*, 119–138.
- [37] R. van Leeuwen, E. J. Baerends, *Phys. Rev. A* **1994**, *49*, 2421–2431.
- [38] S. J. A. van Gisbergen, V. P. Osinga, O. V. Gritsenko, R. van Leeuwen, J. G. Snijders, E. J. Baerends, *J. Chem. Phys.* **1996**, *105*/7, 3142–3151.
- [39] S. J. A. van Gisbergen, J. G. Snijders, E. J. Baerends, *J. Chem. Phys. Rev. Lett.* **1997**, *78*, 3097–3100.
- [40] S. J. A. van Gisbergen, J. G. Snijders, E. J. J. Baerends, *Chem. Phys.* **1998**, *109*, 10657–10668.
- [41] a) M. R. S. A. Janjua, W. Guan, C. G. Liu, Z. M. Su, *Eur. J. Inorg. Chem.* **2009**, *34*, 5181–5188; b) W. Guan, G. C. Yang, L. K. Yan, Z. M. Su, *Eur. J. Inorg. Chem.* **2006**, *20*, 4179–4183.
- [42] a) Y. L. Si, C. G. Liu, E. B. Wang, Z. M. Su, *Theor. Chem. Account.* **2009**, *122*, 217–226; b) D. M.-L. Carey, A. Munoz-Castro, C. J. Bustos, J. M. Manriquez, R. Arratia-Perez, *J. Phys. Chem. A* **2007**, *111*, 6563–6567.

Received: April 19, 2010

Published Online: June 16, 2010



# An Acetate-Functionalized Tetranuclear Zirconium Sandwiching Polyoxometalate Complex

Wei Zhang,<sup>[a]</sup> Shu-Xia Liu,<sup>\*[a]</sup> Chun-Dan Zhang,<sup>[a]</sup> Rui-Kang Tan,<sup>[a]</sup> Feng-Ji Ma,<sup>[a]</sup>  
Shu-Jun Li,<sup>[a]</sup> and Yuan-Yuan Zhang<sup>[a]</sup>

**Keywords:** Polyoxometalates / Sandwich complexes / Zirconium / Clusters / Stabilization

The dimeric, zirconium-sandwiching compound  $K_4H_6[Zr_4(OH)_6(CH_3COO)_2(\alpha-PW_{10}O_{37})_2] \cdot 23H_2O$  (**1**) was obtained by the reaction of lacunary  $[PW_{11}O_{39}]^{7-}$  and  $ZrCl_4$  in a 1 M potassium acetate buffer. It was characterized by elemental and thermogravimetric analysis, X-ray crystallography, solution

$^{183}W$  NMR, FTIR, and UV spectroscopy, and cyclic voltammetry (CV). All the studies indicate that compound **1** is stable both in the solid state and in solution. The cyclic voltammograms indicate good electrocatalytic activity in the reduction of nitrite.

## Introduction

Polyoxometalates (POMs) are discrete molecular metal-oxo clusters with structural and compositional diversities and unique physicochemical properties that have a multitude of potential applications in many different areas.<sup>[1]</sup> Grafting or incorporating organometallic groups, lanthanides, or transition metals into the polyanion framework leads to large numbers of functionalized POM derivatives. Among them, the transition-metal-sandwiching POMs constitute one of the largest subclasses in this field. Moreover, in the transition-metal family, zirconium and hafnium compounds, including their oxides, have unique chemical and physical properties leading to their applications as, for example, oxygen sensors, fuel cells, catalysts, and catalyst supports.<sup>[2]</sup> In particular, they are very useful Lewis acid catalysts.<sup>[3]</sup> However, relative to those of other families of transition metals, the zirconium- or hafnium-based POMs are still less explored, so their synthesis attracts more and more interest in the field of POM chemistry.

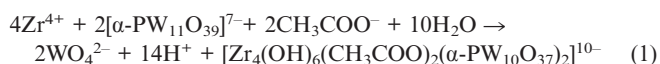
There were few well-characterized zirconium-containing POMs decades ago. In 1989, the first example of the zirconium-sandwiching POM, a trinuclear zirconium-containing Knoth type sandwich silicotungstate,  $[Zr_3(\mu_2-OH)_3(A-\beta-SiW_9O_{34})_2]^{11-}$ , was reported by Finke and co-workers.<sup>[4a]</sup> In recent years, there has been a dramatic advance in studies on various types of zirconium complexes in combination with several POMs, including zirconium-containing POMs with structures of the Keggin,<sup>[4b–4g]</sup> Wells–Dawson,<sup>[5]</sup> and

Lindqvist type.<sup>[6]</sup> However, zirconium-sandwiching POMs functionalized with organic ligands are still rare. Recently, Hill and co-workers reported chiral zirconium-containing Wells–Dawson type POMs functionalized with enantiomerically pure dicarboxylates such as tartrate and malate.<sup>[7]</sup> In our work, by utilizing  $ZrCl_4$  and monolacunary Keggin polyoxotungstates,  $K_7[PW_{11}O_{39}]$ , we successfully prepared an acetate-functionalized, tetranuclear, zirconium(IV)-sandwiching POM complex  $K_4H_6[Zr_4(OH)_6(CH_3COO)_2(\alpha-PW_{10}O_{37})_2] \cdot 23H_2O$  (**1**), which consists of two dilacunary  $[\alpha-PW_{10}O_{37}]^{8-}$  and a central tetranuclear  $[Zr_4(OH)_6(CH_3COO)_2]$  cluster. Compound **1** is stable in solution between pH 0 and 8.5. Herein we report the synthesis, molecular structure, and spectroscopic characterization of **1** in detail.

## Results and Discussion

### Synthesis and Stabilization

The formation of the polyoxoanion in **1** can be represented by Equation (1).



In this experiment, we used monolacunary polyoxotungstate  $K_7[PW_{11}O_{39}]$  as precursor; however, it disassembled to dilacunary  $[\alpha-PW_{10}O_{37}]^{8-}$  during the reaction. This could be explained by a POMs self-assembly mechanism.<sup>[8,9]</sup> Interestingly, the  $CH_3COOH/CH_3COO^-$  solution both acts as buffer and affords  $CH_3COO^-$  functionalized ligands. Moreover, as reported by Kortz et al., when the ratio of  $Zr^{4+}$  to POM precursor is changed from about 4:1 to 8:1,

[a] Key Laboratory of Polyoxometalates Science of Ministry of Education, College of Chemistry, Northeast Normal University, Changchun City, Jilin 130024, P. R. China  
Fax: +86-43185099328  
E-mail: liusx@nenu.edu.cn

Supporting information for this article is available on the WWW under <http://dx.doi.org/10.1002/ejic.201000043>.

the resulting product changes from tetranuclear to hexanuclear zirconium-sandwiching POM.<sup>[4f]</sup> However, in our study, we changed this ratio from 4:1 to 6:1, and from 8:1 to 10:1, but the product was still **1**. Therefore, in our experiment, the increase in  $\text{Zr}^{4+}$  concentration does not seem to change the product of the reaction, which shows that **1** is stable in solution and also has a loose synthetic restriction.

To further investigate the stability of compound **1** in aqueous solution, in situ UV spectroscopic measurements of **1** ( $4 \times 10^{-4} \text{ mol L}^{-1}$ ) were performed in aqueous solution. The UV spectra of **1** in aqueous solution all display similar absorption peaks at 252 nm between pH values of 0 and 8.5; however, the absorption begins to decrease at pH = 9 (Figure S5). Moreover, the UV spectrum of **1** in aqueous solution was also monitored from 0 d to 28 d, and the spectra all displayed one absorption peak, no obvious change being observed in four weeks (Figure S4). These results show that the aqueous solution of **1** is stable at pH 0–8.5 for at least four weeks.

### Description of the Crystal Structure

X-ray crystallography of **1** reveals that the polyoxoanion framework of **1** crystallizes in the triclinic space group  $C2v$ . Compound **1** is constructed from two dilacunar  $[\alpha\text{-PW}_{10}\text{O}_{37}]^{8-}$  subunits linked by a  $\text{Zr}_4(\text{OH})_6(\text{CH}_3\text{COO})_2$  central cluster, leading to a sandwich-type structure (Figure 1). During the reaction, the monolacunar polyoxotungstate  $\text{K}_7[\text{PW}_{11}\text{O}_{39}]$  precursor disassembles to dilacunar  $[\alpha\text{-PW}_{10}\text{O}_{37}]^{8-}$ , and all of the bond lengths and angles of the molecular structure in  $[\alpha\text{-PW}_{10}\text{O}_{37}]^{8-}$  are within the normal ranges and consistent with those described in the literature.<sup>[4c,4e,10]</sup> Each  $\text{Zr}^{4+}$  center is seven-coordinate and defined by three  $\mu_2\text{-OH}$  ligands, three oxygen atoms from  $[\alpha\text{-PW}_{10}\text{O}_{37}]^{8-}$ , and one oxygen atom from the  $\text{CH}_3\text{COO}^-$  ligand. It displays a distorted monocapped trigonal-prismatic coordination geometry. Four Zr centers are connected by  $\mu_2\text{-OH}$  and functionalized  $\text{CH}_3\text{COO}^-$  ligands to form a new tetranuclear cyclic cluster  $[\text{Zr}_4(\text{OH})_6(\text{CH}_3\text{COO})_2]$  (Figure 2), which constitutes the whole polyoxoanion framework of **1** with two  $[\alpha\text{-PW}_{10}\text{O}_{37}]^{8-}$  subunits. The cyclic structure of the  $[\text{Zr}_4]$  core in **1** differs from the adamantane-type structure and the rhombus-like structure observed in two other tetranuclear zirconium-substituted polyoxotungstates reported by Mizuno and co-workers and Xue and co-workers.<sup>[10b,4g]</sup> As the shape of the central cluster, the connection of the ligands, the coordination number of the Zr centers, and the protonation of bridged oxygen ligands are all different from each other. The Zr–O bond lengths range from 2.100 to 2.205 (Zr– $\text{O}_{\text{bridged}}$ ), 2.236 to 2.258 (Zr– $\text{O}_{\text{c}}$ ), and 2.091 to 2.158 (Zr– $\text{O}_{\text{w}}$ ) Å. The Zr–O–Zr angles range from 105.8(6) to 146.6(6)°, and the Zr...Zr separations range from 3.481 to 3.510 Å (Table S1 in the Supporting Information). The bridged ligands  $\text{CH}_3\text{COO}^-$  are undoubtedly connected to the Zr centers and stabilize the central  $[\text{Zr}_4(\text{OH})_6(\text{CH}_3\text{COO})_2]$  core. This further enhances the stabilization of the molecular structure. In ad-

dition, since **1** was synthesized under acidic conditions, it is common in POMs that six protons are used to balance the charge of **1**.

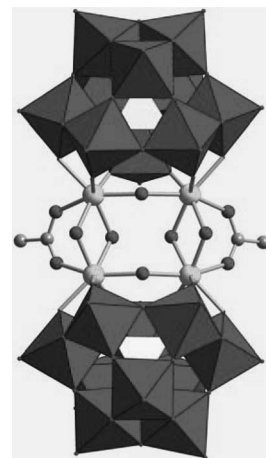


Figure 1. Main structural unit of **1**; octahedra:  $\text{WO}_6$ ; tetrahedra:  $\text{PO}_4$ ; large spheres: Zr; small spheres: O.

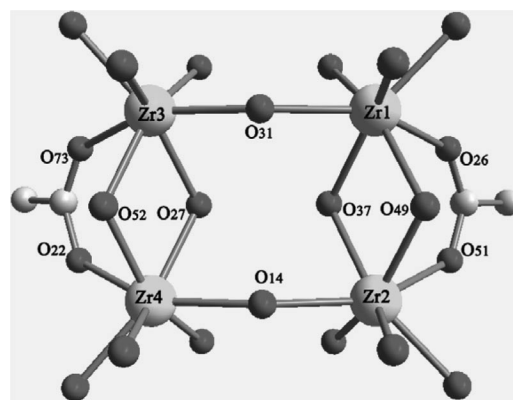


Figure 2. The connection modes of Zr in **1**.

The bond valence sum (BVS)<sup>[11]</sup> values of zirconium, tungsten, and phosphorus indicate that the respective valences are +4, +6, and +5. Notably, the BVS values of the six bridged oxygen atoms in the central cluster ( $\text{O}_{14}$ ,  $\text{O}_{27}$ ,  $\text{O}_{31}$ ,  $\text{O}_{37}$ ,  $\text{O}_{49}$ ,  $\text{O}_{52}$ ) are 0.990–1.201, suggesting that all these bridged oxygen atoms are monoprotonated. It has been reported that the protonated oxygen atoms play an important role in POMs-based catalysts.<sup>[12]</sup> Therefore, for compound **1**, the loose synthetic restriction, stabilization in solution, and large numbers of protonated bridged oxygen atoms are advantages for prospective catalytic applications.

### FTIR Spectroscopy and Thermogravimetric Analysis

The IR spectrum of **1** (Figure S2) shows the characteristic bands of the Keggin POM framework at 1065, 1038, 949, 779, 663  $\text{cm}^{-1}$ ; all correspond to the peaks of the heteropoly complex of the Keggin structure previously reported.<sup>[13]</sup> The resonances at 1541 and 1419  $\text{cm}^{-1}$  are assigned to the  $\nu_{\text{as}}(\text{C}=\text{O})$  and  $\nu_{\text{as}}(\text{C}-\text{O})$  stretching vibrations

of the  $\text{CH}_3\text{COO}^-$  ligands.<sup>[14]</sup> These results suggest that the  $\text{CH}_3\text{COO}^-$  ligands are coordinated to the Zr cations by means of the carboxyl oxygen atoms. The IR spectral results are in good agreement with the X-ray single-crystal structural analyses. Thermogravimetric (TG) measurements of **1** also supported its chemical composition (see Figure S3 in the Supporting Information). The TG curve of **1** shows a total weight loss of 8.65% in the range 20–460 °C, which agrees with the calculated value of 8.71% (Figure S1). The weight loss of 7.06% at 20–235 °C corresponds to the loss of 23 lattice and coordinated water molecules (calcd. 6.78%). The weight loss of 1.59% at 200–460 °C is due to the removal of two acetate ligands (calcd. 1.93%). Between 460–610 °C, a gradual decomposition of **1** is observed, and no weight loss is observed at temperatures higher than 610 °C.

### Solution $^{183}\text{W}$ NMR Spectrum

The crystallographic results show that, because of coordination with the  $\text{Zr}_4$  cluster, the ten  $\text{WO}_6$  octahedra are divided into six kinds according to the ratio 1:2:2:2:1:2. The  $^{183}\text{W}$  NMR spectrum of **1** in  $\text{D}_2\text{O}$  (Figure 3) shows a six-line spectrum with peaks at  $-166.7$  ( $1\text{ W} \times 2$ ),  $-159.4$  ( $2\text{ W} \times 2$ ),  $-152.1$  ( $2\text{ W} \times 2$ ),  $-130.6$  ( $2\text{ W} \times 2$ ),  $-116.6$  ( $1\text{ W} \times 2$ ), and  $-112.4$  ( $2\text{ W} \times 2$ ) ppm, in which the integrated intensities and the peak positions are all in accord with the coordination environment of tungsten atoms in the POM framework  $[\alpha\text{-PW}_{10}\text{O}_{37}]^{9-}$ . Thus, obviously, the molecular structure of **1** in the solid state is maintained in solution. The results of  $^{183}\text{W}$  NMR spectroscopic studies further confirm the stabilization of **1** in solution.

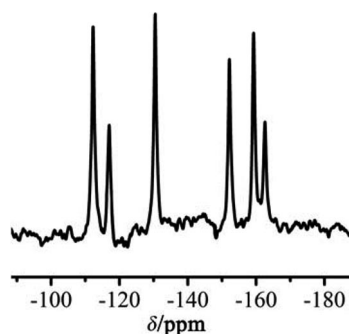


Figure 3.  $^{183}\text{W}$  NMR spectrum of **1** in  $\text{D}_2\text{O}$  at room temperature.

### Electrochemistry

The electrochemical behavior and the electrocatalytic properties for the  $\text{NO}_2^-$  salt of **1** were studied in a solution of  $0.5\text{ M H}_2\text{SO}_4 + 0.5\text{ M Na}_2\text{SO}_4$  in the potential range +200 to  $-1000\text{ mV}$  (scan rate:  $100\text{ mV s}^{-1}$ , Figure 4). There exist two reversible redox waves with midpoint potentials ( $E_{\text{mid}}$ ) of  $-632$  (II–II') and  $-775$  (III–III') mV, where  $E_{\text{mid}} = (E_{\text{pc}} + E_{\text{pa}})/2$ ,  $E_{\text{pc}}$  and  $E_{\text{pa}}$  being the cathodic and anodic peak potentials, respectively. The redox peaks II–II' and III–III' should be ascribed to the two consecutive two-electron pro-

cesses of W centers.<sup>[15,1b]</sup> In addition, the irreversible anodic peak I with a potential of  $-357\text{ mV}$  is assigned to the electrochemical signature of the  $\text{Zr}_{\text{core}}$  subunit,<sup>[10a]</sup> and its cathodic counterpart may be embedded in the reduction peak of W due to weakness of its signal.<sup>[16]</sup>

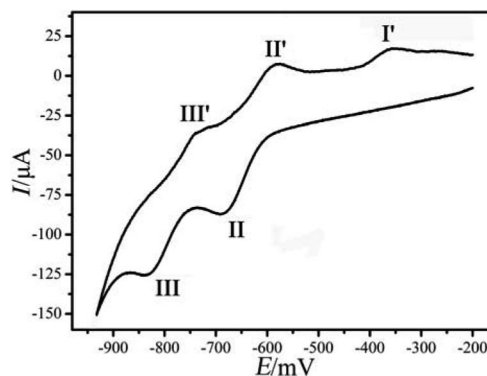


Figure 4. Cyclic voltammogram of **1** in  $0.5\text{ M H}_2\text{SO}_4 + 0.5\text{ M Na}_2\text{SO}_4$  at scan rates of  $100\text{ mV s}^{-1}$ ; the working electrode was glassy carbon, and the reference electrode was  $\text{Ag}/\text{AgCl}$ .

Catalytic reduction of  $\text{NO}_x$  species, especially of nitrite, by POMs, has become a classical test for their electrocatalytic activity. The electrocatalytic reduction of nitrate remains a challenge in the  $\text{NO}_x$  series, because a complete process requires several electrons. Therefore, electrocatalytic reduction of  $\text{NO}_2^-$  by **1** constitutes a further step in the investigation of its electrocatalytic activity. We found that **1** displays a notable electrocatalytic activity in the reduction of nitrite (Figure 5). On addition of  $\text{NO}_2^-$ , all the reduction peak currents increase, and the corresponding oxidation peak currents decrease dramatically, which indicates that both of the reduced species show electrocatalytic activities toward the reduction of nitrite. In comparison, no reduction of nitrate took place on the glassy carbon electrode in the absence of **1**.

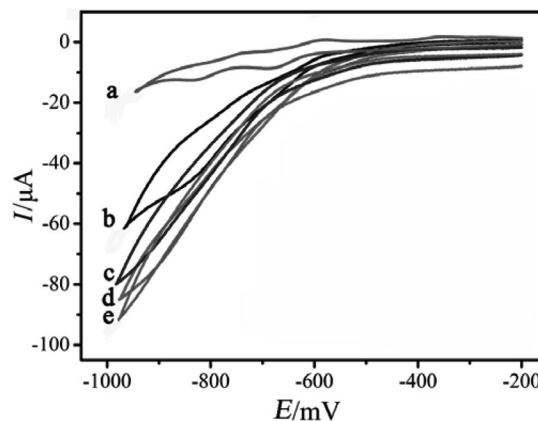


Figure 5. Cyclic voltammograms of **1** ( $1.0\text{ mM}$ ) in the  $0.5\text{ M H}_2\text{SO}_4/\text{Na}_2\text{SO}_4$  solution containing (a) 0, (b) 5, (c) 10, (d) 12, and (e)  $15\text{ mM NaNO}_2$ . Scan rate:  $100\text{ mV s}^{-1}$ ; the working electrode was glassy carbon, and the reference electrode was  $\text{Ag}/\text{AgCl}$ .



## Conclusions

We synthesized and structurally characterized an acetate-functionalized zirconium-containing POM  $\text{K}_4\text{H}_6[\text{Zr}_4(\text{OH})_6(\text{CH}_3\text{COO})_2(\text{PW}_{10}\text{O}_{37})_2]\cdot 23\text{H}_2\text{O}$  (**1**). As shown by UV/Vis and  $^{183}\text{W}$  NMR spectroscopy, **1** is stable over a wide pH range, and the stabilization of a solution of **1** can last for a long time. Examinations of cyclic voltammograms show an electrochemical signature for the  $\text{Zr}_{\text{core}}$  subunit and display electrocatalytic activity toward the reduction of nitrite. Furthermore, large numbers of protonated oxygen atoms are observed in the structure of the molecule, which is an important feature for prospective catalytic applications. In our next study, we will try to obtain new zirconium-containing complexes based on other kinds of vacant POMs and explore the catalytic applications of these complexes.

## Experimental Section

**Materials, Methods, and Instrumentation:** The lacunary POM precursor  $\text{K}_7[\text{PW}_{11}\text{O}_{39}]$  was synthesized according to the published literature,<sup>[17]</sup> and its purity was determined by IR spectroscopy. All other reagents were readily available from commercial sources and used as received without further purification. The IR spectra in KBr pellets were recorded in the range 400–4000  $\text{cm}^{-1}$  with an Alpha Centaur FTIR spectrophotometer. Elemental analyses (C, H and N) were performed with a Perkin–Elmer 2400 CHN Elemental Analyzer. K, P, Zr, and W were determined with a PLASMASPEC (I) ICP atomic emission spectrometer. Thermogravimetric analysis was carried out by using a Perkin–Elmer TGA7 instrument, with a heating rate of 10  $^{\circ}\text{C}/\text{min}$ , under a nitrogen atmosphere. UV/Vis absorption spectra were obtained by using a 752 PC UV/Vis spectrophotometer. The  $^{183}\text{W}$  NMR spectra were measured with an Avance-400 Bruker NMR spectrometers at an operating frequency of 16.66 MHz, with a 2.5 kHz sweep width, 50 s pulse width, and 5 s pulse delay, NS 58256, LB 10.00 Hz. Electrochemical measurements were performed with a CHI660B electrochemical workstation (Chenhua Instruments Co., Shanghai, China). A three-electrode system was employed in this study. The glassy carbon electrode ( $d = 3$  mm) was used as a working electrode, the Ag/AgCl electrode as a reference electrode, and the Pt coil as a counterelectrode. All potentials were measured and reported vs. Ag/AgCl. All the experiments were conducted at ambient temperature (25–30  $^{\circ}\text{C}$ ).

**$\text{K}_4\text{H}_6[\text{Zr}_4(\text{OH})_6(\text{CH}_3\text{COO})_2(\alpha\text{-PW}_{10}\text{O}_{37})_2]\cdot 23\text{H}_2\text{O}$  (**1**):** To a  $\text{CH}_3\text{COOH}/\text{CH}_3\text{COOK}$  buffer (20 mL, 1 M, pH 4.8) was added  $\text{ZrCl}_4$  (0.48 g, 1.02 mmol). After complete dissolution,  $\text{K}_7[\text{PW}_{11}\text{O}_{39}]$  (0.7 g, 0.24 mmol) was added. The solution was stirred for 1 h at 50  $^{\circ}\text{C}$ . Then it was cooled to room temperature and filtered. Evaporation of the solvent at room temperature resulted in needlelike colorless crystals of compound **1** after two weeks (yield 63% based on W).  $\text{C}_4\text{H}_{64}\text{K}_4\text{O}_{107}\text{P}_2\text{W}_{20}\text{Zr}_4$  (6084.71): calcd. C 0.81, H 1.09, K 2.59, P 1.03, W 60.40, Zr 5.98; found C 0.86, H 1.06, K 2.51, P 0.99, W 60.53, Zr 6.07.

**X-ray Structure Analysis:** Single-crystal X-ray diffractometry was conducted with a Bruker Smart Apex CCD diffractometer with  $\text{Mo-K}\alpha$  monochromated radiation ( $\lambda = 0.71073$  Å) at room temperature. The linear absorption coefficients, scattering factors for the atoms, and the anomalous dispersion corrections were taken from ref.<sup>[18]</sup> Empirical absorption corrections were applied. The structure was solved by the direct method and refined by the full-

matrix least-squares method on  $F^2$  by using the SHELXS-97 program<sup>[19]</sup>. Anisotropic thermal parameters were used to refine all non-hydrogen atoms except for some oxygen atoms. Those hydrogen atoms attached to lattice water molecules were not located. The composition and formula of **1** containing four potassium counterions and 23 hydrated water molecules were determined by complete elemental analysis and TG/DTA analysis. Through X-ray crystallography of the polyoxoanion in **1**, all four potassium cations and 20 hydrated water molecules per formula unit were identified unambiguously, but three hydrated water molecules were not determined because of disorder. The largest residual electron density was located less than 1.0 Å from the W addenda atoms and was most likely due to an imperfect absorption correction often encountered in the solution and refinement of polyoxotungstate structures. Anisotropic thermal parameters were used to refine all non-hydrogen atoms except for oxygen atoms O3, O4, O8, O12, O21, O28, O41, O52, and O58, which were refined by using isotropic thermal parameters. CCDC-753608 contains the supplementary crystallographic data for this paper. These data can be obtained free of charge from The Cambridge Crystallographic Data Centre via [www.ccdc.cam.ac.uk/data\\_request/cif](http://www.ccdc.cam.ac.uk/data_request/cif). The crystal data and structure refinement results of **1** are summarized in Table 1; selected bond lengths (in Å) and angles (in  $^{\circ}$ ) are given in Table S1.

Table 1. Crystal data and structural refinement for compound **1**.<sup>[a]</sup>

Formula	$\text{H}_{44}\text{C}_4\text{K}_4\text{O}_{103}\text{P}_2\text{W}_{20}\text{Zr}_4$
Formula weight / $\text{g mol}^{-1}$	5972.06
$T / \text{K}$	296 (2)
Wavelength / Å	0.71073
Crystal system	Triclinic
Space group	$P\bar{1}$
$a / \text{Å}$	13.1561 (8)
$b / \text{Å}$	20.2527 (13)
$c / \text{Å}$	23.4140 (15)
$\alpha / ^{\circ}$	106.2950 (10)
$\beta / ^{\circ}$	105.4350 (10)
$\gamma / ^{\circ}$	94.6460 (10)
$V / \text{Å}^3$	5689.7 (6)
$Z$	2
$D_{\text{calc}} / \text{Mg m}^{-3}$	3.490
$\mu / \text{mm}^{-1}$	20.751
$F(000)$	5217.6
Crystal size / mm	$0.205 \times 0.172 \times 0.138$
Goodness-of-fit on $F^2$	1.014
Final $R$ indices [ $I > 2\sigma(I)$ ]	$R_1 = 0.0755$ , $wR_2 = 0.1939$
$R$ indices (all data)	$R_1 = 0.0991$ , $wR_2 = 0.2077$

[a]  $R_1 = \sum |F_o| - |F_c| / \sum |F_o|$ ,  $wR_2 = \{\sum [w(F_o^2 - F_c^2)^2] / \sum [w(F_o^2)^2]\}^{1/2}$ .

**Supporting Information** (see footnote on the first page of this article): Additional structural view of **1**, IR spectrum, TG curve, UV spectra, and selected bond lengths and bond angles in **1**.

## Acknowledgments

This work was supported by National Nature Science Foundation of China (NSFC) (Grant Nos. 20871027 and 20973035), the Program for New Century Excellent Talents in University (NCET-07-0169), and the Program for Changjiang Scholars and Innovative Research Team in University.

- [1] a) M. T. Pope, A. Müller, *Angew. Chem. Int. Ed. Engl.* **1991**, 30, 34–48; b) M. Sadakane, E. Steckhan, *Chem. Rev.* **1998**, 98, 219–237; c) A. Müller, F. Peters, M. T. Pope, D. Gatteschi, *Chem. Rev.* **1998**, 98, 239–271; d) E. Coronado, C. J. Gómez-



- García, *Chem. Rev.* **1998**, *98*, 273–296; e) J. T. Rhule, C. L. Hill, D. A. Judd, R. F. Schinazi, *Chem. Rev.* **1998**, *98*, 327–357; f) S. T. Zheng, J. Zhang, G. Y. Yang, *Angew. Chem. Int. Ed.* **2008**, *47*, 3909–3913; g) J. P. Wang, P. T. Ma, J. Li, H. Y. Niu, J. Y. Niu, *Chem. Asian J.* **2008**, *3*, 822–833.
- [2] a) M. Gateshki, V. Petkov, G. Williams, S. K. Pradhan, Y. Ren, *Phys. Rev. B* **2005**, *71*, 224107-1–224107-8; b) M. Yashima, T. Hirose, S. Katano, Y. Suzuki, M. Kakihara, M. Yoshimura, *Phys. Rev. B* **1995**, *51*, 8018–8025.
- [3] a) K. Suzuki, S. Yamanoi *Lewis Acids in Organic Synthesis* (Ed.: H. Yamamoto), Wiley-VCH, Weinheim, Germany, **2000**, pp. 849–864; b) R. Hara, T. Takahashi, *Lewis Acids in Organic Synthesis* (Ed.: H. Yamamoto), Wiley-VCH, Weinheim, Germany, **2000**, pp. 865–881; c) K. Arata, *Adv. Catal.* **1990**, *37*, 165–211; d) O. A. Kholdeeva, G. M. Maksimov, R. I. Maksimovskaya, M. P. Vanina, T. A. Trubitsina, D. Y. Naumov, B. A. Kolesov, N. S. Antonova, J. J. Carbo, J. M. Poblet, *Inorg. Chem.* **2006**, *45*, 7224–7234.
- [4] a) R. G. Finke, B. Rapko, T. J. R. Weakley, *Inorg. Chem.* **1989**, *28*, 1573–1579; b) L. Cai, Y. Li, C. Yu, H. Ji, Y. Li, S. Liu, *Inorg. Chim. Acta* **2009**, *362*, 2895–2899; c) E. V. Radkov, V. G. Young Jr., R. H. Beer, *J. Am. Chem. Soc.* **1999**, *121*, 8953–8954; d) L. L. Chen, L. L. Li, B. Liu, G. L. Xue, H. M. Hu, F. Fu, J. W. Wang, *Inorg. Chem. Commun.* **2009**, *12*, 1035–1037; e) B. S. Bassil, M. H. Dickman, U. Kortz, *Inorg. Chem.* **2006**, *45*, 2394–2396; f) A. J. Gaunt, I. May, D. Collison, O. D. Fox, *Inorg. Chem.* **2003**, *42*, 5049–5051; g) L. L. Chen, Y. Liu, S. H. Chen, H. M. Hu, F. Fu, J. W. Wang, G. L. Xue, *J. Cluster Sci.* **2009**, *20*, 331–340.
- [5] a) X. Fang, C. L. Hill, *Angew. Chem. Int. Ed.* **2007**, *46*, 3877–3880; b) A. J. Gaunt, I. May, D. Collison, K. T. Holman, M. T. Pope, *J. Mol. Struct.* **2003**, *656*, 101–106; c) Y. Saku, Y. Sakai, K. Nomiya, *Inorg. Chem. Commun.* **2009**, *12*, 650–652; d) M. N. Sokolov, N. V. Izarova, E. V. Peresypkina, D. A. Mainichev, V. P. Fedin, *Inorg. Chim. Acta* **2009**, *362*, 3756–3762.
- [6] a) H. Carabineiro, R. Villanneau, X. Carrier, P. Herson, F. Lemos, F. R. Ribeiro, A. Proust, M. Che, *Inorg. Chem.* **2006**, *45*, 1915–1923; b) R. J. Errington, S. S. Petkar, P. S. Middleton, W. McFarlane, W. Clegg, R. A. Coxall, R. W. Harrington, *J. Am. Chem. Soc.* **2007**, *129*, 12181–12196.
- [7] a) X. Fang, T. M. Anderson, Y. Hou, C. L. Hill, *Chem. Commun.* **2005**, 5044–5046; b) X. Fang, T. M. Anderson, C. L. Hill, *Angew. Chem. Int. Ed.* **2005**, *44*, 3540–3544.
- [8] U. Kortz, S. Matta, *Inorg. Chem.* **2001**, *40*, 815–817.
- [9] B. S. Bassil, S. Nellutla, U. Kortz, A. C. Stowe, J. V. Tol, N. S. Dalal, B. Keita, L. Nadjo, *Inorg. Chem.* **2005**, *44*, 2659–2665.
- [10] a) B. S. Bassil, S. S. Mal, M. H. Dickman, U. Kortz, H. Oelrich, L. Walder, *J. Am. Chem. Soc.* **2008**, *130*, 6696–6697; b) Y. Kikukawa, S. Yamaguchi, K. Tsuchida, Y. Nakagawa, K. Uehara, K. Yamaguchi, N. Mizuno, *J. Am. Chem. Soc.* **2008**, *130*, 5472–5478.
- [11] a) N. E. Brese, M. O’Keeffe, *Acta Crystallogr., Sect. B* **1991**, *47*, 192–197; b) I. D. Brown, D. Altermatt, *Acta Crystallogr., Sect. B* **1985**, *41*, 244–247.
- [12] K. Kamata, K. Yonehara, Y. Sumida, K. Yamaguchi, S. Hikichi, N. Mizuno, *Science* **2003**, *300*, 964–966.
- [13] C. Rocchiccioli-Deltcheff, M. Fournier, R. Frank, R. Thouvenot, *Inorg. Chem.* **1983**, *22*, 207–216.
- [14] K. Wassermann, H. J. Lunk, R. Palm, J. Fuchs, N. Steinfeldt, R. Stoßser, M. T. Pope, *Inorg. Chem.* **1996**, *35*, 3273–3279.
- [15] T. McCormac, B. Fabre, G. Bidan, *J. Electroanal. Chem.* **1997**, *425*, 49–54.
- [16] a) G. L. Xue, X. M. Liu, H. S. Xu, H. M. Hu, F. Fu, J. W. Wang, *Inorg. Chem.* **2008**, *47*, 2011–2016; b) Y. Z. Zhen, Q. Shen, L. L. Li, G. L. Xue, H. M. Hu, F. Fu, J. W. Wang, *Inorg. Chem. Commun.* **2008**, *11*, 886–888.
- [17] E. Radkov, R. H. Beer, *Polyhedron* **1995**, *14*, 2139–2143.
- [18] N. F. M. Henry, K. Lonsdale (Eds.), *International Tables for X-ray Crystallography*, Kynoch Press, Birmingham, **1952**.
- [19] G. M. Sheldrick, *SHELXS-97, Program for the Refinement of Crystal Structures*, University of Göttingen, Germany, **1997**.

Received: January 18, 2010  
Published Online: June 16, 2010

## Anion-Induced Assembly of Hexacoordinate Rare-Earth(III) Complexes

Stefania Tanase,<sup>[a][‡]</sup> Silvia Sottini,<sup>[b]</sup> Valerie Marvaud,<sup>[c]</sup> Edgar J. J. Groenen,<sup>[b]</sup> and Lise-Marie Chamoreau<sup>[c]</sup>**Keywords:** Rare earths / Schiff bases / Structure elucidation / EPR spectroscopy / Magnetic properties

Rare-earth(III) complexes of the general formula  $[\text{RE}\{(\text{Hsal})_3\text{tren}\}_2](\text{CF}_3\text{SO}_3)_3 \cdot n\text{CH}_3\text{CN}$ , where RE is Eu (**1**), Gd (**2**), and Tb (**3**), and  $(\text{Hsal})_3\text{tren}$  is tris[2-(salicylideneimino)ethyl]amine, have been synthesized and structurally characterized. X-ray crystallographic studies show that the rare-earth(III) center is coordinated by six oxygen atoms that belong to the phenolato groups of two  $(\text{Hsal})_3\text{tren}$  ligand molecules to give an unusual hexacoordinate geometry. The molecular structure is stabilized by strong intramolecular interactions estab-

lished between the hydrogen atoms located on the three imino nitrogen atoms and the deprotonated phenol oxygen atoms of each ligand. Luminescence studies have indicated the presence of efficient nonradiative deactivation pathways in **1–3**, and only a weak ligand emission was observed ( $\lambda_{\text{exc}} = 275 \text{ nm}$ ,  $\lambda_{\text{em}} = 545 \text{ nm}$ ) in all cases. Temperature-dependent magnetic susceptibility studies have shown that crystal field effects are dominant for complex **3**, whilst small antiferromagnetic interactions have been observed in **2**.

## Introduction

In recent years, significant efforts have been made to design polydentate ligands for the coordination of rare-earth(III) ions.<sup>[1–4]</sup> These studies have been motivated by numerous applications of rare-earth(III) complexes in medicine,<sup>[5,6]</sup> catalysis,<sup>[7]</sup> materials science,<sup>[8,9]</sup> and molecular magnetism.<sup>[10]</sup> In particular, rare-earth(III) complexes with heptadentate tripodal Schiff base ligands have attracted considerable interest due to their potential application as magnetic resonance contrast agents.<sup>[11–21]</sup> A range of complexes have been prepared by template condensation of tris(2-aminoethyl)amine with various ring-substituted salicylaldehydes in the presence of different rare-earth(III) salts.<sup>[13,15–21]</sup> These complexes are seven-coordinate and they are remarkably stable toward air and moisture, apparently due to the efficient encapsulation of the rare-earth(III) ion in the  $\text{N}_4\text{O}_3$  cavity of the Schiff base ligand. When the complexes are prepared from nonsubstituted salicylaldehyde and a rare-earth(III) salt containing a monodentate, poorly coordinating anion, such as  $\text{Cl}^-$ , similar species are formed.<sup>[15,20,22]</sup> However, these species are labile and lose

the ligand in solvents that have strong donor properties.<sup>[15]</sup> Attempts to isolate rare-earth(III) complexes of tris[2-(salicylideneimino)ethyl]amine and  $(\text{Hsal})_3\text{tren}$  (Figure 1) by direct reaction with rare-earth(III) nitrates have shown that the absence of base favors the formation of nine-coordinate  $[\text{RE}\{(\text{Hsal})_3\text{tren}\}(\text{NO}_3)_3]$  species, whereas, in the presence of base, heptacoordinate species of the type  $[\text{RE}\{(\text{sal})_3\text{tren}\}]$  are formed.<sup>[15]</sup> During our studies on the synthesis of a series of rare-earth(III) complexes with Schiff base ligands, we have observed that the reaction of the free ligand  $(\text{Hsal})_3\text{tren}$  with  $\text{RE}(\text{CF}_3\text{SO}_3)_3 \cdot n\text{H}_2\text{O}$  (RE = Eu, Gd, Tb), both in the presence and absence of tetrabutylammonium hydroxide, led to the hexacoordinate complexes  $[\text{RE}\{(\text{Hsal})_3\text{tren}\}_2](\text{CF}_3\text{SO}_3)_3 \cdot n\text{CH}_3\text{CN}$  [RE = Eu (**1**), Gd (**2**) and Tb (**3**);  $n = 0.5$  or  $1.5$ ]. In this paper, we describe the synthesis, crystal structure, and properties of complexes **1–3**. Scheme 1 illustrates the anion effect on the type of the complexes obtained by the reaction of  $(\text{Hsal})_3\text{tren}$  with a variety of rare-earth(III) salts.

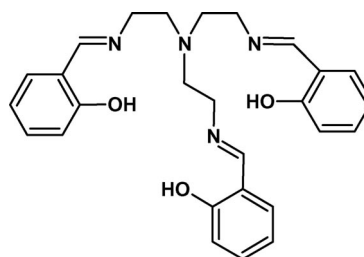
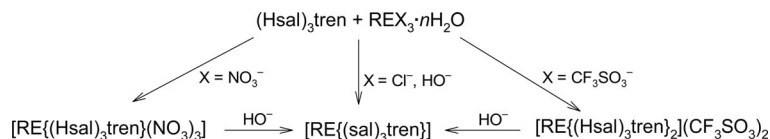


Figure 1. Structure of the ligand tris[2-(salicylideneimino)ethyl]amine.

- [a] Leiden Institute of Chemistry, Gorlaeus Laboratories, Leiden University, P. O. Box 9502, 2300 RA Leiden, The Netherlands  
 [b] Leiden Institute of Physics, Leiden University, P. O. Box 9504, 2300 RA Leiden, The Netherlands  
 [c] Laboratoire de Chimie Inorganique et Matériaux Moléculaires, C.N.R.S. UMR 7071, Case 42, Batiment F74 Université Pierre et Marie Curie, 4 place Jussieu, 75252 Paris Cedex 05, France  
 [‡] Current address: Van 't Hoff Institute for Molecular Sciences, University of Amsterdam, P. O. Box 94720, 1090 GE Amsterdam, The Netherlands  
 E-mail: s.grecea@uva.nl



Scheme 1. Anion effect on the type of mononuclear rare-earth(III) complexes of the (Hsal)<sub>3</sub>tren ligand.

## Results and Discussion

### Synthesis and Spectroscopic Characterization

The reaction of  $\text{RE}(\text{CF}_3\text{SO}_3)_3 \cdot 6\text{H}_2\text{O}$  ( $\text{RE} = \text{Eu}, \text{Tb}, \text{Gd}$ ) with (Hsal)<sub>3</sub>tren in a molar ratio of 1:1 in acetonitrile leads to the isolation of the complexes  $[\text{RE}\{(\text{Hsal})_3\text{tren}\}_2](\text{CF}_3\text{SO}_3)_n \cdot n\text{CH}_3\text{CN}$  ( $n = 0.5$  or  $1.5$ ) as microcrystalline solids, which is confirmed by elemental analysis and crystallographic studies. The IR spectra of **1** and **3** are almost identical; however, all the bands are slightly shifted ( $1\text{--}3\text{ cm}^{-1}$ ) in that of **2**. The broad band for the weak O–H stretching vibration of the ligand at approximately  $3005\text{ cm}^{-1}$  is replaced by a band at about  $3490\text{ cm}^{-1}$  in **1–3**, due to the N–H vibration of  $\text{C}=\text{N}^+\text{--H}$  moiety in the complexes. This band indicates that a hydrogen atom is still involved in intramolecular hydrogen bonding with the phenolic oxygen. All complexes show the typical four-band pattern of Schiff base ligands ( $1648\text{--}1477\text{ cm}^{-1}$ ). The characteristic  $\nu_{\text{S=O}}$  vibrations of the ionic triflate ions are observed at approximately  $1260\text{ cm}^{-1}$ . Positive ion electrospray mass spectrometric analysis of **1–3** in acetonitrile/water gave ion molecular peaks corresponding to the fragments  $[\text{RE}\{(\text{sal})_3\text{tren}\} + \text{H}]^+$  and  $[\text{RE}\{(\text{Hsal})_3\text{tren}\}(\text{H}_2\text{O})_3(\text{CF}_3\text{SO}_3)_2]^+$ . The UV/Vis absorption spectrum of the ligand shows characteristic bands at 276, 342 and  $425\text{ nm}$ . The spectral features observed for **1–3** are similar to those observed for the corresponding ligand. Excitation in the UV absorption bands ( $\pi \rightarrow \pi^*$  and  $n \rightarrow \pi^*$ ) of the free ligand does not result in an observable rare-earth(III)-based emission in **1–3**. This result points to the presence of efficient nonradiative deactivation pathways in the complexes. A weak ligand emission was observed ( $\lambda_{\text{exc}} = 275\text{ nm}$ ,  $\lambda_{\text{em}} = 545\text{ nm}$ ).

### Crystallographic Studies

X-ray crystallographic studies reveal that complexes **1** and **3** crystallize in the monoclinic space group  $P 2_1/n$ , and complex **2** crystallizes in the rhombohedral space group  $R\bar{3}$ . In all cases, the potentially heptadentate tripodal ligand, (Hsal)<sub>3</sub>tren, acts as a tridentate ligand with the rare-earth(III) ion surrounded by six oxygen atoms that belong to the phenolato groups of two ligand molecules. A perspective drawing of the complex cation,  $[\text{Eu}\{(\text{Hsal})_3\text{tren}\}_2]^{3+}$ , of **1** is shown in Figure 2. The coordination geometry around the rare-earth(III) ion can be described as slightly distorted octahedral. The mean value of the  $\text{RE--O}_{\text{phenoxo}}$  distances ( $2.267$ ,  $2.274$ , and  $2.271\text{ \AA}$  for **1**, **2**, and **3**, respectively) is in the range of those observed for rare-earth(III) complexes with similar Schiff base ligands.<sup>[11,13,15,18,19]</sup> The average

carbon–nitrogen bond lengths for the imino group is  $1.296$ ,  $1.290$ , and  $1.289\text{ \AA}$  for **1**, **2**, and **3**, respectively, in agreement with the  $\text{C}=\text{N}$  distance.<sup>[13,15,19]</sup> Hydrogen atoms located on the three imino nitrogen atoms of each ligand are involved in intramolecular hydrogen bonds with the deprotonated phenol oxygen atoms, indicating that a proton migration is involved during coordination, which is similar to other reports on Schiff base rare-earth(III) complexes (**1**: av.  $\text{N}\cdots\text{O} = 2.674\text{ \AA}$ ,  $\text{N--H}\cdots\text{O} = 131.5^\circ$ ; **2**: av.  $\text{N}\cdots\text{O} = 2.80\text{ \AA}$ ,  $\text{N--H}\cdots\text{O} = 131.9^\circ$ ; **3**: av.  $\text{N}\cdots\text{O} = 2.672\text{ \AA}$ ,  $\text{N--H}\cdots\text{O} = 131.3^\circ$ ).<sup>[13,31]</sup> The shortest intermolecular distances between the rare-earth(III) ions are  $12.783$ ,  $10.348$ , and  $13.253\text{ \AA}$  for **1**, **2**, and **3**, respectively (Table 1).

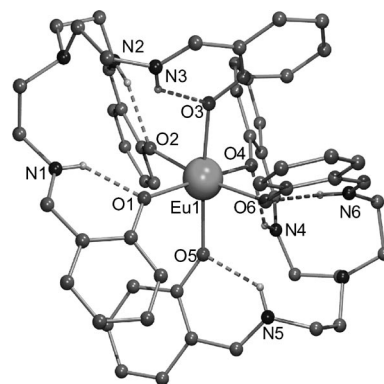


Figure 2. Molecular structure of the complex cation  $[\text{Eu}\{(\text{Hsal})_3\text{tren}\}_2]^{3+}$  in **1**. Hydrogen atoms not involved in hydrogen bonds were omitted for clarity.

### Temperature-Dependent Magnetic Susceptibility and EPR Studies

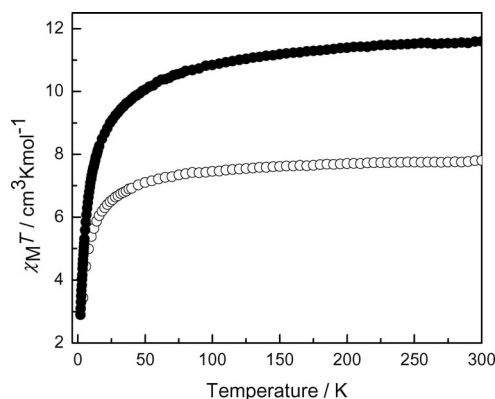
Temperature-dependent magnetic susceptibility data of compacted polycrystalline samples of **2** and **3** have been measured in the  $2\text{--}300\text{ K}$  temperature range in a  $0.1\text{ T}$  magnetic field (Figure 3).  $\text{Gd}^{\text{III}}$  has a  $^8\text{S}_{7/2}$  ground state that is located at some  $10^4\text{ cm}^{-1}$  below the first excited state and is not perturbed by crystal field effects.<sup>[32]</sup> Therefore, the  $7.80\text{ cm}^3\text{ K mol}^{-1}$  value of  $\chi_{\text{M}}T$  observed at  $300\text{ K}$  for **2** corresponds to the value expected for one  $\text{Gd}^{\text{III}}$  ion ( $7.88\text{ cm}^3\text{ K mol}^{-1}$ ). The  $\chi_{\text{M}}T$  value remains almost constant until  $100\text{ K}$ , and then it decreases gradually reaching a value of  $3.43\text{ cm}^3\text{ K mol}^{-1}$  at  $4\text{ K}$  (Figure 3). The temperature dependence of  $\chi_{\text{M}}^{-1}$  obeys the Curie–Weiss law,  $\chi_{\text{M}} = C/(T - \theta)$ , over the whole temperature range with  $C = 7.91\text{ cm}^3\text{ K mol}^{-1}$  and  $\theta = -5.5$ . The small negative value of the paramagnetic Curie–Weiss temperature can be attributed to the zero-field-splitting of the  $\text{Gd}^{\text{III}}$  ion as well as to

Table 1. Selected bond lengths and angles for  $[\text{RE}\{(\text{Hsal})_3\text{tren}\}_2](\text{CF}_3\text{SO}_3)_3 \cdot n\text{CH}_3\text{CN}$ .

Bond lengths / Å		Bond angles / °	
Compound 1			
Eu1–O2	2.250(4)	O2–Eu1–O5	99.23(13)
Eu1–O5	2.250(4)	O2–Eu1–O1	85.95(14)
Eu1–O1	2.268(3)	O5–Eu1–O1	89.75(14)
Eu1–O6	2.274(4)	O2–Eu1–O6	171.37(12)
Eu1–O4	2.279(4)	O5–Eu1–O6	86.14(13)
Eu1–O3	2.283(4)	O1–Eu1–O6	100.91(13)
		O2–Eu1–O4	87.38(14)
		O5–Eu1–O4	84.32(14)
		O1–Eu1–O4	170.27(14)
		O6–Eu1–O4	86.42(13)
		O2–Eu1–O3	88.45(14)
		O5–Eu1–O3	172.20(14)
		O1–Eu1–O3	89.39(14)
		O6–Eu1–O3	86.40(13)
		O4–Eu1–O3	97.52(13)
Compound 2			
Gd1–O1	2.269(3)	O1–Gd1–O1	86.27(10)
Gd1–O1	2.269(3)	O1–Gd1–O1	86.27(10)
Gd1–O1	2.269(3)	O1–Gd1–O1	86.27(10)
Gd1–O2	2.280(3)	O1–Gd1–O2	171.17(10)
Gd1–O2	2.280(3)	O1–Gd1–O2	89.40(11)
Gd1–O2	2.280(3)	O1–Gd1–O2	101.13(10)
		O1–Gd1–O2	89.40(11)
		O1–Gd1–O2	101.13(10)
		O1–Gd1–O2	171.17(10)
		O2–Gd1–O2	83.89(11)
		O1–Gd1–O2	101.13(10)
		O1–Gd1–O2	171.17(10)
		O1–Gd1–O2	89.40(10)
		O2–Gd1–O2	83.89(11)
		O2–Gd1–O2	83.89(11)
Compound 3			
Tb1–O6	2.255(4)	O6–Tb1–O1	98.97(15)
Tb1–O1	2.265(4)	O6–Tb1–O3	89.74(17)
Tb1–O3	2.273(4)	O1–Tb1–O3	86.02(18)
Tb1–O2	2.277(4)	O6–Tb1–O2	172.49(16)
Tb1–O4	2.278(4)	O1–Tb1–O2	88.44(16)
Tb1–O5	2.283(5)	O3–Tb1–O2	89.55(17)
		O6–Tb1–O4	86.19(15)
		O1–Tb1–O4	171.54(16)
		O3–Tb1–O4	100.78(16)
		O2–Tb1–O4	86.60(15)
		O6–Tb1–O5	84.64(17)
		O1–Tb1–O5	87.28(17)
		O3–Tb1–O5	170.49(17)
		O2–Tb1–O5	97.02(16)
		O4–Tb1–O5	86.53(16)

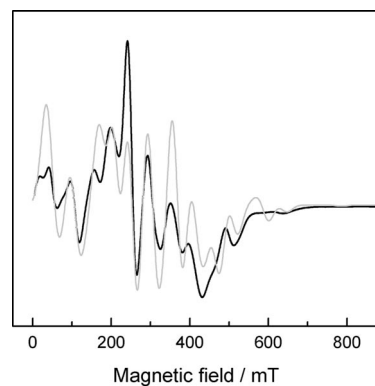
a very weak antiferromagnetic interaction between the  $\text{Gd}^{\text{III}}$  ions. Such antiferromagnetic behavior can be explained by the presence of a small amount of magnetically ordered (antiferromagnetic) clusters and is consistent with observations during EPR experiments (see below) that were prohibited at low temperature by the magnetic properties of the compound.

For  $\text{Tb}^{\text{III}}$ , the energy separation between the  $^{2\text{S}+1}\text{L}_\text{J}$  ground state and the first excited state is so large that only the ground state is thermally populated at room and low temperature.<sup>[32]</sup> However, the crystal field effect partly re-

Figure 3. Temperature dependence of  $\chi_M T$  for **2** (○) and **3** (●) in 0.1 T applied field.

moves the degeneracy of the  $^7\text{F}_6$  ground state, giving  $^{2\text{S}+1}\text{L}_\text{J}$  states, which further split into Stark levels by crystal field perturbation. For **3**, the  $\chi_M T$  value at 300 K is equal to  $12.19 \text{ cm}^3 \text{ K mol}^{-1}$ , which is slightly higher than the calculated value of  $11.82 \text{ cm}^3 \text{ K mol}^{-1}$  for the free  $\text{Tb}^{\text{III}}$  ion. From 300 to 4 K, the  $\chi_M T$  value decreases slowly to  $2.55 \text{ cm}^3 \text{ K mol}^{-1}$  (Figure 3); this behavior is typical of the depopulation of the Stark levels of  $\text{Tb}^{\text{III}}$  by lowering the temperature.<sup>[32]</sup>

Figure 4 shows the X-band EPR spectrum of a polycrystalline sample of **2**, resulting from the paramagnetic  $\text{Gd}^{\text{III}}$  ( $S = 7/2$ ) center. The resonances span a broad field range up to 800 mT. Figure 5 shows the J-band spectrum, which consists of an intense line at about  $g = 2$ , surrounded symmetrically by a number of weaker lines. A very weak line at half field is also observed. The shape of the J-band spectrum reveals that the Zeeman interaction is much larger than the zero-field splitting at 275 GHz, which allows an accurate determination of the  $g$  value from this spectrum. Starting from this value, we were able to simulate both the X- and J-band spectra with the following set of parameters: an isotropic  $g = 1.9912 \pm 0.0003$ , an axial zero-field-splitting tensor with  $D = 0.0697 \pm 0.0016 \text{ cm}^{-1}$ , and an axial fourth-order contribution of  $-0.0018 \pm 0.0006 \text{ cm}^{-1}$ . The latter contribution is of course too small to contribute sig-

Figure 4. Experimental (thick line) and simulated (thin line) X-band EPR spectrum of complex **2** at room temperature.



nificantly at J-band, but improves the simulation of the X-band spectrum. The simulated spectra reproduce the positions of the resonances well, but not the intensity. A value of  $g$  slightly lower than the free-electron value is commonly observed for  $\text{Gd}^{\text{III}}$  complexes. The  $4f^7$  ground-state configuration of  $\text{Gd}^{\text{III}}$  gives rise to a  $^8S_{7/2}$  term, and the small deviation from the free-electron value results from a slight admixture of an excited  $J = 7/2$  term that carries orbital angular momentum.<sup>[33]</sup> The significant second-order zero-field splitting reflects the fact that the symmetry of the coordination sphere of the  $\text{Gd}^{\text{III}}$  in complex **2** is lower than cubic, in agreement with the crystal structure described above.

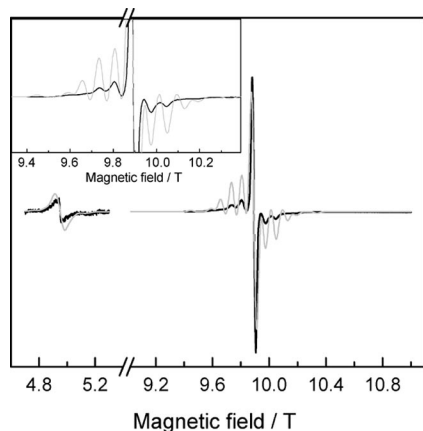


Figure 5. Experimental (thick line) and simulated (thin line) J-band EPR spectrum of complex **2** at room temperature. The intensity of the weak line at half field has been multiplied by a factor of 50. A magnified view of the region around  $g = 2$  is shown in the inset.

## Conclusions

We have shown that the ligand tris[2-(salicylideneimino)-ethyl]amine has a more versatile coordination chemistry than reported previously and is able to form unusual hexacoordinate rare-earth(III) complexes by an anion-induced assembly process. Mononuclear complexes with the general formula  $[\text{RE}\{(\text{Hsal})_3\text{tren}\}_2](\text{CF}_3\text{SO}_3)_3 \cdot n\text{CH}_3\text{CN}$  (where  $\text{RE}(\text{III}) = \text{Eu}, \text{Gd}, \text{or Tb}$ ) were synthesized and structurally characterized. In these compounds, the rare-earth(III) ion is surrounded by six oxygen atoms that belong to the phenolato groups of two  $(\text{Hsal})_3\text{tren}$  ligands to give an unusual hexacoordinate geometry, which is strongly stabilized by intramolecular interactions. Study of the luminescence properties revealed the presence of efficient nonradiative deactivation pathways and only a weak ligand emission was observed in all cases. Magnetic studies have shown that the crystal field effects are dominant for the complex with  $\text{Tb}^{\text{III}}$  (**3**). For the  $\text{Gd}^{\text{III}}$  derivative (**2**), small antiferromagnetic interactions were observed due to the presence of a small amount of magnetically ordered (antiferromagnetic) clusters, and the analysis of the EPR spectra indicated an isotropic  $g$  value and a small axial zero-field-splitting tensor for the  $\text{Gd}^{\text{III}}$  ion.

## Experimental Section

**Materials:** All reagents and solvents were purchased from Aldrich and were used as received unless otherwise stated. The ligand  $(\text{Hsal})_3\text{tren}$  has been synthesized according to the published procedure.<sup>[23]</sup>

**Synthesis:** To a solution of  $(\text{Hsal})_3\text{tren}$  (0.35 mmol) in  $\text{CH}_3\text{CN}$  (10 mL) was added  $\text{RE}(\text{CF}_3\text{SO}_3)_3 \cdot 6\text{H}_2\text{O}$  (0.35 mmol) dissolved in  $\text{CH}_3\text{CN}$  (10 mL). The yellow solution was stirred for 10 min and then filtered to remove any impurities. Slow diffusion of ethyl ether into the filtrate at  $4^\circ\text{C}$  resulted in the formation of yellow crystals after a few hours.

**[Eu $\{(\text{Hsal})_3\text{tren}\}_2](\text{CF}_3\text{SO}_3)_3 \cdot 1.5\text{CH}_3\text{CN}$  (**1**):** Yield: 252 mg (48%).  $\text{C}_{60}\text{H}_{64.5}\text{EuF}_9\text{N}_{9.5}\text{O}_{15}\text{S}_3$  ( $M = 1577.85 \text{ g mol}^{-1}$ ): calcd. C 45.67, H 4.12, N 8.43, S 6.10; found C 45.81, H 4.26, N 8.71, S 5.98. IR:  $\tilde{\nu}_{\text{max}} = 3492$  (w, br), 2946 (w), 2853 (w), 1648 (s), 1608 (s), 1544 (s), 1478 (s), 1450 (m), 1345 (m), 1266 (s), 1220 (s), 1156 (m), 1085 (w), 1030 (s), 1005 (m), 890 (m), 870 (m), 760 (m), 635 (m), 574 (m), 517 (w)  $\text{cm}^{-1}$ . UV/Vis ( $\lambda/\text{nm}$ ): 276, 340, 425. ESI-MS:  $m/z = 608.9$   $[\text{Eu}(\text{Hsal})\{(\text{sal})_2\text{tren}\}]^+$ , 963.1  $[\text{Eu}\{(\text{Hsal})_3\text{tren}\}(\text{H}_2\text{O})_3(\text{CF}_3\text{SO}_3)_2]^+$ .

**[Gd $\{(\text{Hsal})_3\text{tren}\}_2](\text{CF}_3\text{SO}_3)_3 \cdot 0.5\text{CH}_3\text{CN}$  (**2**):** Yield: 270 mg (47%).  $\text{C}_{58}\text{H}_{61.5}\text{F}_9\text{GdN}_{8.5}\text{O}_{15}\text{S}_3$  ( $1542.10 \text{ g mol}^{-1}$ ): calcd. C 45.18, H 4.02, N 7.72, S 6.24; found C 44.93, H 4.01, N 7.32, S 6.32. IR:  $\tilde{\nu}_{\text{max}} = 3490$  (w, br), 2946 (w), 2855 (w), 1644 (s), 1606 (s), 1542 (s), 1472 (s), 1452 (m), 1338 (m), 1251 (s), 1216 (s), 1150 (m), 1075 (w), 1026 (s), 1004 (m), 887 (m), 875 (m), 779 (m), 757 (m), 737 (m), 634 (m), 572 (m), 517 (w)  $\text{cm}^{-1}$ . UV/Vis ( $\lambda/\text{nm}$ ): 277, 320, 400. ESI-MS:  $m/z = 613.9$   $[\text{Gd}(\text{Hsal})\{(\text{sal})_2\text{tren}\}]^+$ , 968.1  $[\text{Gd}\{(\text{Hsal})_3\text{tren}\}(\text{H}_2\text{O})_3(\text{CF}_3\text{SO}_3)_2]^+$ .

**[Tb $\{(\text{Hsal})_3\text{tren}\}_2](\text{CF}_3\text{SO}_3)_3 \cdot 1.5\text{CH}_3\text{CN}$  (**3**):** Yield: 117 mg (21%).  $\text{C}_{60}\text{H}_{64.5}\text{F}_9\text{N}_{9.5}\text{O}_{15}\text{S}_3\text{Tb}$  ( $1584.81 \text{ g mol}^{-1}$ ): calcd. C 45.47, H 4.10, N 8.40, S 6.07; found C 45.62, H 4.33, N 8.62, S 6.21. IR:  $\tilde{\nu}_{\text{max}} = 3492$  (w, br), 2946 (w), 2853 (w), 1648 (s), 1608 (s), 1545 (s), 1478 (s), 1450 (m), 1345 (m), 1266 (s), 1220 (s), 1157 (m), 1085 (w), 1030 (s), 1005 (m), 890 (m), 870 (m), 760 (m), 638 (m), 574 (m), 517 (w)  $\text{cm}^{-1}$ . UV/Vis ( $\lambda/\text{nm}$ ): 275, 380, 510. ESI-MS:  $m/z = 614.9$   $[\text{Tb}(\text{Hsal})\{(\text{sal})_2\text{tren}\}]^+$ , 969.1  $[\text{Tb}\{(\text{Hsal})_3\text{tren}\}(\text{H}_2\text{O})_3(\text{CF}_3\text{SO}_3)_2]^+$ .

**Physical Characterization:** Elemental analysis for C, H and N was performed with a Perkin–Elmer 2400 series II analyzer. Infrared spectra ( $4000\text{--}300 \text{ cm}^{-1}$ ) were recorded with a Perkin–Elmer Paragon 1000 FTIR spectrometer equipped with a Golden Gate ATR device, using the reflectance technique. Ligand field spectra were obtained with a Perkin–Elmer Lambda 900 spectrophotometer using the diffuse reflectance technique, with  $\text{MgO}$  as a reference. Electrospray mass spectra (ESI-MS) in acetonitrile/water solution were recorded with a Thermo Finnigan AQA apparatus. DC magnetic data were recorded using a Quantum Design MPMS-5 SQUID susceptometer. The magnetic susceptibilities were measured from 2 to 300 K on polycrystalline samples in a gelatin capsule with an applied field of 0.1 T. Data were corrected for magnetization of the sample holder and for diamagnetic contributions, which were estimated from Pascal constants. Continuous-wave EPR spectra of complex **2** were obtained at room temperature for two microwave frequencies, X-band (9.49 GHz) and J-band (275 GHz). The X-band spectrum was measured on a polycrystalline powder and recorded with a Bruker Elexsys E 680 spectrometer, equipped with a standard  $\text{TE}_{102}$  cavity. The modulation amplitude and the microwave power amounted to 1 mT and 3.2 mW, respectively. The experiment at J-band used the same powder, which was dispersed in an eicosane matrix (Fluka, 99.8%) in order to avoid self-orientation of the microcrystals in the high magnetic field. The spectrum at this frequency was measured with a self-built

Table 2. Summary of the crystallographic data obtained for complexes 1–3.

	1	2	3
Empirical formula	C <sub>60</sub> H <sub>64.5</sub> EuF <sub>9</sub> N <sub>9.5</sub> O <sub>15</sub> S <sub>3</sub>	C <sub>58</sub> H <sub>61.5</sub> F <sub>9</sub> GdN <sub>8.5</sub> O <sub>15</sub> S <sub>3</sub>	C <sub>60</sub> H <sub>64.5</sub> F <sub>9</sub> N <sub>9.5</sub> O <sub>15</sub> S <sub>3</sub> Tb
Formula weight /g mol <sup>-1</sup>	1577.85	1542.10	1584.81
T /K	250(2)	250(2)	250(2)
Wavelength /Å	0.71073	0.71073	0.71073
Crystal system	monoclinic	trigonal	monoclinic
Space group	P2 <sub>1</sub> /n	R3	P2 <sub>1</sub> /n
a /Å	16.1696(11)	17.203(1)	16.129(2)
b /Å	23.0070(5)	17.203(1)	23.060(2)
c /Å	19.2260(17)	40.263(2)	19.178(2)
α /°	90	90	90
β /°	91.727(9)	90	92.028(14)
γ /°	90	120	90
V /Å <sup>3</sup>	7149.1(8)	10319.2(10)	7128.5(13)
Z	4	6	4
D <sub>calc</sub> /g cm <sup>-3</sup>	1.466	1.483	1.477
μ /mm <sup>-1</sup>	1.055	1.147	1.171
Crystal size /mm	0.33 × 0.31 × 0.25	0.14 × 0.13 × 0.13	0.24 × 0.22 × 0.17
Reflections collected	95034	15590	84414
Independent reflections	20510	6625	20767
Internal R factor	0.0840	0.0654	0.0884
Number of parameters	884	287	856
Goodness-of-fit S on F <sup>2</sup>	0.980	0.930	1.015
Largest peak and hole in final difference map /e Å <sup>-3</sup>	1.310 and -1.009	0.770 and -0.521	1.187 and -1.139
Final R indices [I > 2σ(I)]	R1 = 0.0588 wR2 = 0.1585	R1 = 0.0515 wR2 = 0.0982	R1 = 0.0665 wR2 = 0.1817
R indices (all data)	R1 = 0.1370 wR2 = 0.1967	R1 = 0.1619 wR2 = 0.1281	R1 = 0.1713 wR2 = 0.2253

spectrometer,<sup>[24]</sup> by using a microwave power of about 5.5 μW and a field modulation of 1.2 kHz with an amplitude of about 0.7 mT. For the measurement in the half-field region a microwave power of about 10 μW was used. Simulations of the EPR spectra were performed using the Matlab toolbox Easyspin.<sup>[25,26]</sup>

**X-ray Crystallography:** A single crystal of each compound was selected, mounted onto a glass fiber, and transferred in a cold nitrogen gas stream. Intensity data were collected with a Bruker-Nonius-Kappa-CCD with graphite-monochromated Mo-K<sub>α</sub> radiation. Unit-cell parameters determination, data collection strategy and integration were carried out with the Nonius EVAL-14 suite of programs.<sup>[27]</sup> Multiscan absorption correction was applied.<sup>[28]</sup> The structures were solved by direct methods using the SIR97 program<sup>[29]</sup> for 1 and 3, and the SHELXS-97 program<sup>[30]</sup> for 2. All three structures were refined anisotropically by full-matrix least-squares methods using the SHELXL-97 software package.<sup>[30]</sup> Hydrogen atoms of the C=N<sup>+</sup>-H moiety were found on the Fourier difference map for 2 (Table 2).

## Acknowledgments

The authors are grateful to Prof. Jan Reedijk for valuable discussions. This research was supported by a Veni grant from the Netherlands Organization for Scientific Research (NWO) to S. T. and the ECNetwork of Excellence Magmanet (No. 515767-2).

- [1] A. Chaudhary, R. V. Singh, *Rev. Inorg. Chem.* **2008**, *28*, 35–75.
- [2] W. K. Wong, X. Zhu, W. Y. Wong, *Coord. Chem. Rev.* **2007**, *251*, 2386–2399.
- [3] J. C. G. Bunzli, *Acc. Chem. Res.* **2006**, *39*, 53–61.
- [4] J. C. G. Bunzli, *Met. Ions Biol. Syst.* **2004**, *42*, 39–75.

- [5] K. W. Y. Chan, W. T. Wong, *Coord. Chem. Rev.* **2007**, *251*, 2428–2451.
- [6] P. Caravan, *Chem. Soc. Rev.* **2006**, *35*, 512–523.
- [7] J. L. C. Rowsell, O. M. Yaghi, *Microporous Mesoporous Mater.* **2004**, *73*, 3–14.
- [8] H. Iwanaga, *J. Polym. Sci. Techn.* **2008**, *21*, 165–172.
- [9] J. C. G. Bunzli, S. Comby, A. S. Chauvin, C. D. B. Vandevyver, *J. Rare Earths* **2007**, *25*, 257–274.
- [10] C. Benelli, D. Gatteschi, *Chem. Rev.* **2002**, *102*, 2369–2387.
- [11] L. W. Yang, S. Liu, E. Wong, S. J. Rettig, C. Orvig, *Inorg. Chem.* **1995**, *34*, 2164–2178.
- [12] U. Casellato, S. Tamburini, P. Tomasin, P. A. Vigato, M. Botta, *Inorg. Chim. Acta* **1996**, *247*, 143–145.
- [13] D. J. Berg, S. J. Rettig, C. Orvig, *J. Am. Chem. Soc.* **1991**, *113*, 2528–2532.
- [14] W. K. Wong, H. Z. Liang, J. P. Guo, W. Y. Wong, W. K. Lo, K. F. Li, K. W. Cheah, Z. Y. Zhou, W. T. Wong, *Eur. J. Inorg. Chem.* **2004**, 829–836.
- [15] A. Smith, S. J. Rettig, C. Orvig, *Inorg. Chem.* **1988**, *27*, 3929–3934.
- [16] S. Salehzadeh, S. M. Nouri, H. Keypour, *Asian J. Chem.* **2006**, *18*, 515–522.
- [17] S. Salehzadeh, S. M. Nouri, H. Keypour, M. Bagherzadeh, *Polyhedron* **2005**, *24*, 1478–1486.
- [18] S. Liu, L. W. Yang, S. J. Rettig, C. Orvig, *Inorg. Chem.* **1993**, *32*, 2773–2778.
- [19] S. Liu, L. Gelmini, S. J. Rettig, R. C. Thompson, C. Orvig, *J. Am. Chem. Soc.* **1992**, *114*, 6081–6087.
- [20] M. Kanesato, T. Yokoyama, O. Itabashi, T. M. Suzuki, M. Shiro, *Bull. Chem. Soc. Jpn.* **1996**, *69*, 1297–1302.
- [21] M. W. Essig, D. W. Keogh, B. L. Scott, J. G. Watkin, *Polyhedron* **2001**, *20*, 373–377.
- [22] M. Kanesato, T. Yokoyama, *Chem. Lett.* **1999**, 137–138.
- [23] A. Malek, G. C. Dey, A. Nasreen, T. A. Chowdhury, E. C. Alyea, *Synth. React. Inorg. Met.-Org. Chem.* **1979**, *9*, 145–155.

- [24] H. Blok, J. Disselhorst, S. B. Orlinskii, J. Schmidt, *J. Magn. Reson.* **2004**, *166*, 92–99.
- [25] S. Stoll, A. Schweiger, *J. Magn. Reson.* **2006**, *178*, 42–55.
- [26] S. Stoll, A. Schweiger, *Biol. Magn. Reson.* **2007**, *27*, 299–321.
- [27] A. J. M. Duisenberg, L. M. J. Kroon-Batenburg, A. M. M. Schreurs, *J. Appl. Crystallogr.* **2003**, *36*, 220.
- [28] R. H. Blessing, *Acta Crystallogr., Sect. A* **1995**, *51*, 33.
- [29] A. Altomare, M. C. Burla, M. Camalli, G. L. Cascarano, C. Giacovazzo, A. Guagliardi, A. G. G. Moliterni, G. Polidori, R. Spagna, *J. Appl. Crystallogr.* **1999**, *32*, 115–119.
- [30] G. M. Sheldrick, *Acta Crystallogr., Sect. A* **2008**, *64*, 112–122.
- [31] T. Gao, P. F. Yan, G. M. Li, G. F. Hou, J. S. Gao, *Inorg. Chim. Acta* **2008**, *361*, 2051–2058.
- [32] O. Kahn, *Molecular Magnetism*, John Wiley & Sons, New York, **1993**.
- [33] A. Abragam, B. Bleaney, *Electron Paramagnetic Resonance of Transition Ions*, Clarendon Press, Oxford, **1970**.

Received: January 21, 2010  
Published Online: June 23, 2010

# A $\mu_3$ -Alkoxo-Bridged Tetranuclear $[\text{Cu}_4\text{L}_2]$ Copper(II) Complex of a Hexadentate $\text{N}_2\text{O}_4$ Donor Ligand with a $[6 + 0]$ $\text{Cu}_4\text{O}_4$ Cubane Core: Synthesis, Crystal Structure, and Magnetic Properties

Dipankar Maity,<sup>[a]</sup> Atish D. Jana,<sup>[b]</sup> Mainak Debnath,<sup>[a]</sup> Nigel G. R. Hearn,<sup>[c,d]</sup> Ming-Han Sie,<sup>[e]</sup> Hon Man Lee,<sup>[e]</sup> Rodolphe Clérac,<sup>\*,[c,d]</sup> and Mahammad Ali<sup>\*,[a]</sup>

**Keywords:** Copper /  $\text{N}_2\text{O}_4$  donor ligands / Magnetic properties

A novel hexacoordinating non-Schiff base ligand ( $\text{H}_4\text{L}$ ) with  $\text{N}_2\text{O}_4$  donor atoms has been synthesized by simple Mannich reactions. The use of this ligand with  $\text{Cu}(\text{ClO}_4)_2 \cdot 6\text{H}_2\text{O}$  in different molar ratios as well as pH leads to the formation of a mononuclear species and a tetranuclear  $\text{Cu}^{\text{II}}$  complex possessing a cubane  $[\text{Cu}_4\text{L}_2]$  core with almost equal  $\text{Cu} \cdots \text{Cu}$  separation. In the presence of an excess amount of copper(II) ions and triethylamine at reflux, the mononuclear  $[\text{CuH}_2\text{L}]$

species can be converted into the tetranuclear one, whereas the reverse process was not observed even after prolonged reaction time. Both the complexes have been characterized by single-crystal X-ray diffraction and magnetic measurements. Magnetic studies reveal that complex **1** displays a paramagnetic Curie-type behavior whereas **2** displays a singlet-spin ground state induced by strong intramolecular antiferromagnetic interactions.

## Introduction

High-nuclearity transition-metal complexes have been attracting continuous interest due to their relevance in the research fields of metalloproteins to mimic polymetallic active sites,<sup>[1]</sup> molecular magnetism,<sup>[2,3]</sup> or the emerging science of nanomaterials.<sup>[4]</sup> The flexibility of the coordination sphere around  $\text{Cu}^{\text{II}}$ , in combination with steric and crystal packing forces, leads to a tremendous structural diversity of  $\text{Cu}^{\text{II}}$ -based systems. Indeed, these small structural changes at the molecular scale usually have significant effects on their magnetic properties.<sup>[5]</sup> Quite generally, transition-metal complexes with a cubane-type structure ( $\text{M}_4\text{L}_n$ ) possess intramolecular hydroxo, alkoxo, azido, sulfido, or iminato bridges<sup>[6–8]</sup> and constitute a very interesting class of compounds.<sup>[9,10]</sup> Their originality is often found in their high-spin ground state that is induced, for example, by the pseudo-orthogonality of the magnetic orbitals of the metal ions.<sup>[11–15]</sup>

In this work, we report on a mononuclear and a tetranuclear cubane<sup>[11,12,16]</sup>-type  $\text{Cu}^{\text{II}}$  complex based on a novel hexa-coordinating  $\text{N}_2\text{O}_4$  ligand. To the best of our knowledge, this constitutes the first report in which a hexa-coordinating  $\text{N}_2\text{O}_4$  donor ligand has been employed to generate a  $[6 + 0]$  cubane  $\text{Cu}_4\text{O}_4$  core.

## Results and Discussion

### Syntheses and Structural Characterizations

The hexadentate  $\text{H}_4\text{L}$  ligand was synthesized by simple Mannich condensation of *N,N'*-bis(2-hydroxyethyl)ethylenediamine with 2,4-di-*tert*-butylphenol and formaldehyde in MeOH. Straightforward reaction of this ligand with 1 equiv. of  $\text{Cu}(\text{ClO}_4)_2 \cdot 6\text{H}_2\text{O}$  in MeOH under reflux conditions [with 2 equiv. of triethylamine (TEA)] leads to **1**, whereas **2** is obtained when 2 equiv. of  $\text{Cu}(\text{ClO}_4)_2 \cdot 6\text{H}_2\text{O}$  were used in the presence of 4 equiv. of TEA. Compound **1** was found to be converted into **2** when 1 equiv. of **1** is reacted with 0.5 equiv. of  $\text{Cu}(\text{ClO}_4)_2 \cdot 6\text{H}_2\text{O}$  under reflux for an extended time (Scheme 1). The reverse was not observed, even in the presence of an excess amount of the ligand.

Compound **1** crystallizes in a monoclinic  $C2/c$  space group. Crystal structure analysis revealed that **1** is a monomeric species,  $[\text{Cu}^{\text{II}}(\text{H}_2\text{L})]$ , in which the copper(II) ion has a distorted-octahedral geometry with four oxygen and two nitrogen atoms of the  $\text{H}_2\text{L}$  ligands acting as donors (Figure 1). Two oxygen (O1 and O1\*; \*:  $1 - x$ ,  $y$ ,  $\frac{1}{2} - z$ ) and

[a] Department of Chemistry, Jadavpur University, Kolkata 700032, India  
E-mail: mali@chemistry.jdvu.ac.in

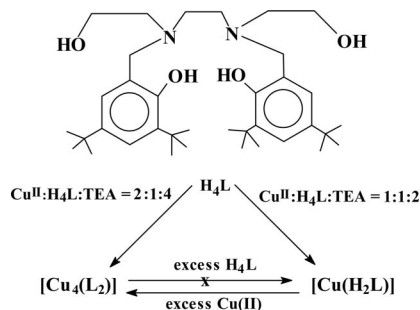
[b] Department of Physics, Sripat Singh College, Jiaganj, Murshidabad, W. B., 742123, India

[c] CNRS, Centre de Recherche Paul Pascal (CRPP), Equipe "Matériaux Moléculaires Magnétiques", 115 avenue du Dr. Albert Schweitzer, 33600 Pessac, France  
E-mail: clerac@crpp-bordeaux.cnrs.fr

[d] Université de Bordeaux, UPR 8641, 33600 Pessac, France

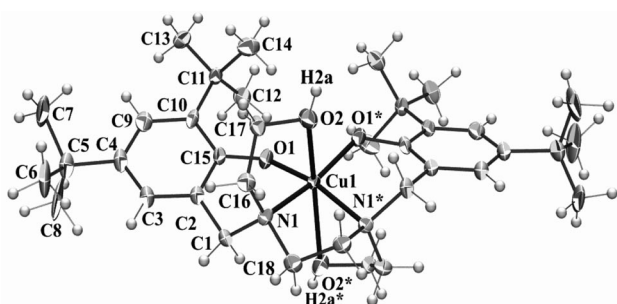
[e] National Changhua University of Education, Department of Chemistry, Changhua 50058, Taiwan





Scheme 1.

two nitrogen (N1 and N1\*) atoms occupy the equatorial positions, whereas the axial sites are occupied by two oxygen atoms (O2 and O2\*).

Figure 1. The ORTEP diagram of **1** with 30% ellipsoidal probability (\*:  $1 - x, y, \frac{1}{2} - z$ ).

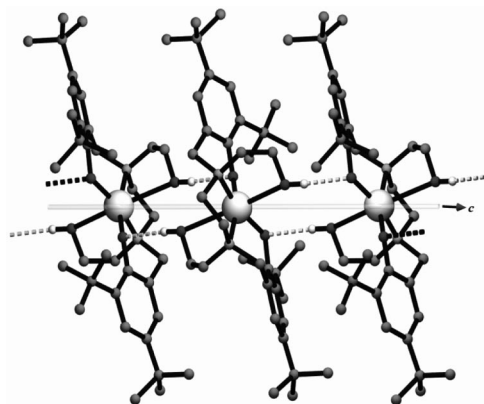
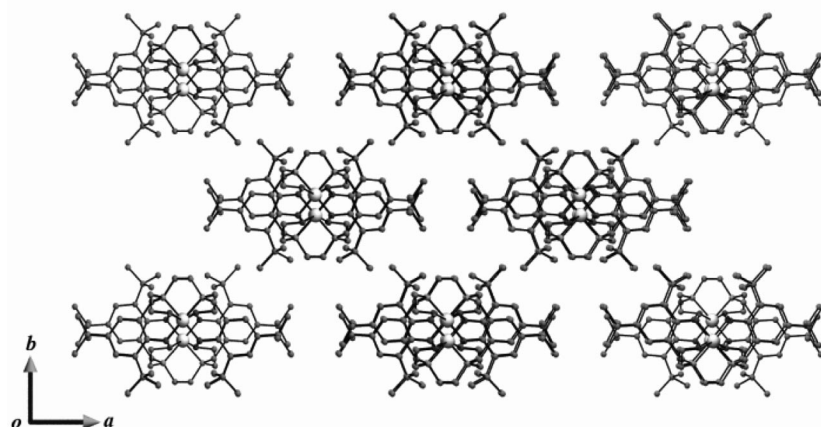
The four equatorial donor atoms (N1, N1\*, O1, O1\*) are slightly away from the mean-square plane. The deviations of the two N1 and two O1 atoms from the plane are  $+0.238, -0.238$  and  $+0.249, -0.249$  Å, respectively. The axial oxygen atoms (O2, O2\*) have a distance of 2.639 Å from the Cu center. The equatorial oxygen (O1, O1\*) and nitrogen (N1, N1\*) atoms are *trans* to each other in respect to the central Cu atom. The four opposite bond angles around the Cu site along the basal plane are equal, namely, the angle O1–Cu–N1 equals N1\*–Cu–O1\* ( $92.79^\circ$ ) and the angle O1–Cu–N1\* equals N1–Cu–O1\* ( $165.74^\circ$ ). All the important bond lengths and bond angles are listed in Table 1. It should be

noted that the axial oxygen atoms (O2, O2\*) remain protonated (H2a and H2a\*) under the experimental reaction conditions. This partial protonation on the ligand helps the columnar helical packing of mononuclear units (Figure 2). The complementary packing of the mononuclear unit and the equatorial-to-axial connection of adjacent mononuclear units through hydrogen-bonding interactions [O2–

Table 1. Selected bond lengths and angles for **2**.

Bond lengths [Å]		Bond angles [°]	
Cu1–O1	1.910(2)	O1–Cu1–O2	103.88(9)
Cu1–O2	2.639(2)	O1–Cu1–N1	92.80(10)
Cu1–N1	2.061(3)	O1–Cu1–O1 <sup>[a]</sup>	90.89(9)
Cu1–O1 <sup>[a]</sup>	1.910(2)	O1–Cu1–O2 <sup>[a]</sup>	90.31(9)
Cu1–O2 <sup>[a]</sup>	2.639(2)	O1–Cu1–N1 <sup>[a]</sup>	165.73(10)
Cu1–N1 <sup>[a]</sup>	2.061(3)	O2–Cu1–N1	75.42(9)
		O1 <sup>[a]</sup> –Cu1–O2	90.31(9)
		O2–Cu1–O2 <sup>[a]</sup>	159.87(8)
		O2–Cu1–N1 <sup>[a]</sup>	89.89(9)
		O1 <sup>[a]</sup> –Cu1–N1	165.73(10)
		O2 <sup>[a]</sup> –Cu1–N1	89.89(9)
		N1–Cu1–N1 <sup>[a]</sup>	86.99(11)
		O1 <sup>[a]</sup> –Cu1–O2 <sup>[a]</sup>	103.88(9)
		O1 <sup>[a]</sup> –Cu1–N1 <sup>[a]</sup>	92.80(10)
		O2 <sup>[a]</sup> –Cu1–N1 <sup>[a]</sup>	75.42(9)

[a]  $1 - x, y, \frac{1}{2} - z$ .

Figure 2. Intermolecular hydrogen-bonding interaction leading to the helical assembly of mononuclear units along the *c* axis in **1**.Figure 3. Packing arrangement of the helical columns in **1**.

H2A...O1<sup>a</sup>, O2–H2A 0.84 Å, H2A...O1<sup>a</sup> 2.08 Å, O2...O1<sup>a</sup> 2.922(7) Å; O2–H2A...O1 175°; a:  $x, -y, \frac{1}{2} + z$ ] are responsible for this helical assembly. The axis of the helix is the crystallographic  $c$  axis (Figures 2 and 3) and has a pitch length of 12.05 Å, which is equal to the length of the  $c$  axis. The packing arrangements of the helical columns are shown in Figure 3.

Complex **2** crystallizes in the  $P\bar{1}$  space group and consists of a discrete tetranuclear Cu<sup>II</sup> unit self-assembled by two L<sup>4-</sup> ligands to form a [Cu<sub>4</sub>O<sub>4</sub>] central cubane core (Figure 4). The central core of **2** consists of four alkoxo-bridged copper metal ions (Cu1, Cu2, Cu3, and Cu4) giving an approximately cubic array of alternating copper and oxygen atoms. Consequently, copper(II) centers are linked in a  $\mu_3$ -bridging fashion by an alkoxo-oxygen atom of the aliphatic backbone of the L<sup>4-</sup> ligands.

The  $\mu_3$ -bridging oxygen atoms are deprotonated, affording two tetra-anionic ligands and finally a neutral complex **2**, [Cu<sub>4</sub>L<sub>2</sub>]. Each amine phenolate acts as a hexadentate ligand leading to five- and six-membered chelate rings with bite angles of 85 and 93°, respectively. Each copper(II) center is pentacoordinate with an NO<sub>4</sub> donor set of atoms. The coordination environment is best described as square pyramidal with the basal plane occupied by the phenolate oxygen atom, imino nitrogen, and alkoxide oxygen atoms of the aliphatic part of one L<sup>4-</sup> ligand as well as an additional alkoxide oxygen atom of a second L<sup>4-</sup> ligand moiety. The apical position is occupied by an alkoxide oxygen atom of the second ligand molecule at a rather long donor distance (Table 2). The donor atoms of all basal coordination planes deviate by less than 4 pm from the corresponding mean planes of the related copper(II) centers and are only slightly displaced toward the apical ligand (0.07 to 0.15 Å).

The cubane-type complexes have been classified according to the Cu...Cu<sup>[17]</sup> and Cu–O<sup>[18]</sup> distances and they generally come in two categories, namely, type-I and type-II. A rare class type-III has also been reported.<sup>[11,12,16]</sup> According to the commonly adopted convention of classifying cubane structures, type-I cubane is characterized by two short and four long Cu...Cu distances (thus also called a [2 + 4] cubane), whereas, type-II possesses four short and two long

Table 2. Selected bond lengths and angles for **2**.

Bond lengths [Å]			
Cu1–O1	1.884(7)	Cu3–O4	1.982(6)
Cu1–O2	1.947(7)	Cu3–O5	1.876(6)
Cu1–O4	2.388(6)	Cu3–O6	1.941(6)
Cu1–O6	1.972(5)	Cu3–O8	2.442(7)
Cu1–N1	2.047(7)	Cu3–N3	2.038(8)
Cu2–O2	2.449(6)	Cu4–O2	1.969(6)
Cu2–O3	1.876(7)	Cu4–O6	2.434(7)
Cu2–O4	1.948(7)	Cu4–O7	1.881(6)
Cu2–O8	1.965(6)	Cu4–O8	1.942(6)
Cu2–N2	2.053(8)	Cu4–N4	2.053(7)
Bond angles [°]			
O1–Cu1–O2	171.7(3)	Cu1–O2–Cu2	89.1(3)
O1–Cu1–O4	100.0(2)	Cu1–O2–Cu4	109.6(3)
O1–Cu1–O6	94.9(3)	Cu1–O4–Cu2	90.9(2)
O2–Cu1–O4	88.0(2)	Cu1–O4–Cu3	90.9(2)
O2–Cu1–O6	84.9(3)	Cu2–O4–Cu3	108.4(3)
O4–Cu1–O6	75.9(2)	Cu1–O6–Cu4	92.6(3)
O2–Cu2–O3	102.8(3)	O7–Cu4–O8	169.2(3)
O2–Cu2–O4	86.3(2)	O6–Cu4–N4	109.5(3)
O2–Cu2–O8	72.9(2)	O2–Cu4–N4	166.2(3)
O3–Cu2–O4	170.8(3)	O7–Cu4–N4	95.4(3)
O3–Cu2–O8	95.6(3)	O8–Cu4–N4	81.3(3)
O4–Cu2–O8	86.1(3)	O6–Cu3–N3	81.3(3)
O4–Cu3–O5	94.5(3)	O8–Cu3–N3	113.0(3)
O4–Cu3–O6	87.0(2)	O1–Cu1–N1	96.1(3)
O4–Cu3–O8	73.4(2)	O2–Cu1–N1	82.9(3)
O5–Cu3–O6	172.2(3)	O4–Cu1–N1	110.9(3)
O5–Cu3–O8	101.8(3)	O6–Cu1–N1	165.7(3)
O6–Cu3–O8	86.0(2)	O2–Cu2–N2	111.9(2)
O2–Cu4–O6	73.0(2)	O3–Cu2–N2	96.6(3)
O2–Cu4–O7	97.1(2)	O4–Cu2–N2	80.6(3)
O2–Cu4–O8	85.4(2)	O8–Cu2–N2	165.4(3)
O6–Cu4–O7	104.7(3)	O4–Cu3–N3	166.1(3)
O6–Cu4–O8	86.2(3)	O5–Cu3–N3	96.1(3)

Cu...Cu distances (a [4 + 2] cubane). For the rare type-III geometry, all six Cu...Cu distances are nearly identical, a [6 + 0] cubane. The six Cu...Cu distances observed in **2** fall within a very short range of 3.104 to 3.200 Å and accordingly the present [Cu<sub>4</sub>O<sub>4</sub>] core structure should be classified as type-III or a [6 + 0] cubane. Two different groups of Cu–O–Cu bond angles at the bridging oxygen atoms are found: (i) a set of angles that fall between 89.1 and 92.6° and

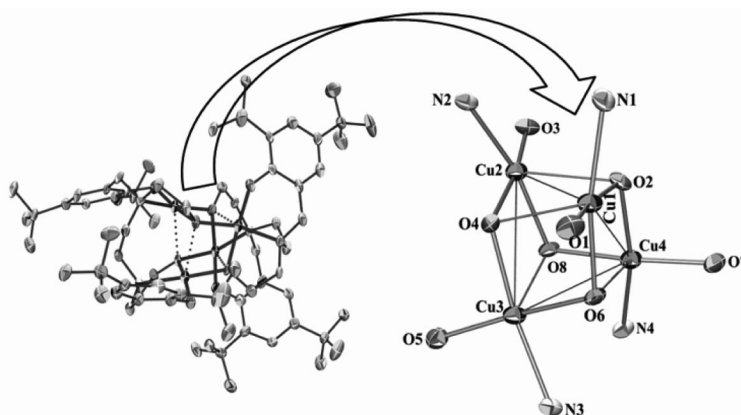


Figure 4. The ORTEP diagram (30% ellipsoidal probability) of the alkoxo-bridged cubane unit in **2** (solid bonds between Cu centers are within the 1.94–1.97 Å range and the dashed bonds are within the 2.39–2.45 Å range).

(ii) the other set of angles within the 106.1–109.6° range. The bridging angle of 89.1° is by far the smallest angle observed for alkoxo-bridged compounds in a  $[\text{Cu}_2\text{O}_2]$  fragment.<sup>[19–40]</sup> Intracomplex metal–metal separations in the present complex are Cu1–Cu2 3.104 Å, Cu1–Cu3 3.126 Å, Cu1–Cu4 3.200 Å, and Cu3–Cu4 3.146 Å (Table 1). The packing arrangement of the tetranuclear species is shown in Figure 4. To the best of our knowledge, this probably provides the first example in which a hexa-coordinating ligand with  $\text{N}_2\text{O}_4$  donor atoms forms a rare  $[6 + 0]$  cubane  $\text{Cu}_4\text{O}_4$  core without any exogenous bridging ligand (Figure 5).

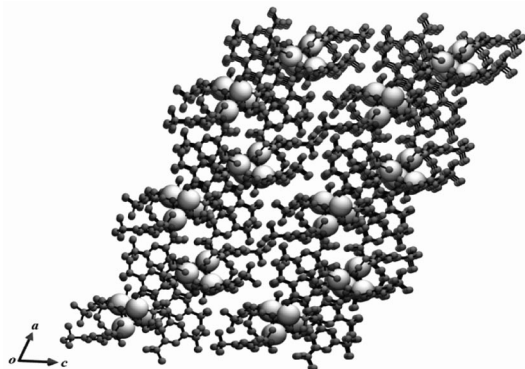


Figure 5. Packing diagram of complex **2**. The cubane cores are represented by white spheres.

### Electronic Spectra

The absorption spectrum of the monomeric complex shows a sharp peak at 430 nm ( $\epsilon = 8373 \text{ M}^{-1}\text{cm}^{-1}$ ) and a shoulder at 557 nm ( $\epsilon = 4303 \text{ M}^{-1}\text{cm}^{-1}$ ) corresponding to ligand-to-metal charge-transfer (LMCT) transitions. After prolonged treatment of the monomer in an excess amount of metal precursor and TEA, the tetramer is produced as seen by the LMCT absorption band at 457 nm ( $\epsilon = 8747 \text{ M}^{-1}\text{cm}^{-1}$ ). The conversion was not followed spectrophotometrically, as it occurs under prolonged reflux conditions, so only the absorbance of the initial and final states of the reaction solution were measured as shown in Figure 6.

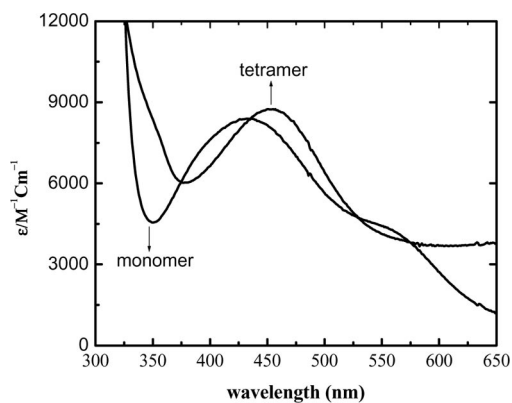


Figure 6. UV/Vis spectra for complexes **1** and **2** in MeCN.  $[\mathbf{1}] = [\mathbf{2}] = 5.0 \times 10^{-5} \text{ M}$ .

### Magnetic Properties

The magnetic properties of complexes **1** and **2** have been measured from 300 to 1.8 K at 1000 Oe (Figure 7). At room temperature, the product of the molar magnetic susceptibility and temperature ( $\chi T$ ) is 0.42 and  $1.24 \text{ cm}^3 \text{ K mol}^{-1}$  for **1** and **2**, respectively, which is in good agreement with the presence of one and four  $S = 1/2$   $\text{Cu}^{\text{II}}$  spins, respectively. The magnetic properties of **1** are relatively straightforward. The  $\chi T$  product stays constant all the way down to 1.8 K (Figure 7) as a textbook example of paramagnetic Curie behavior seen for magnetically isolated spins. This result is in good accord with the crystal structure of **1** (vide supra) that confirms the complete isolation of the monomeric  $\text{Cu}^{\text{II}}$  species. The  $\chi T$  product of  $0.42 \text{ cm}^3 \text{ K mol}^{-1}$  is thus the Curie constant and the deduced  $g$  factor is higher than 2, at approximately 2.1, as is often seen for  $\text{Cu}^{\text{II}}$  systems.

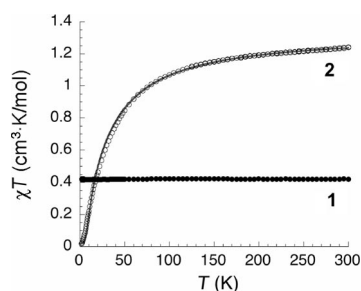
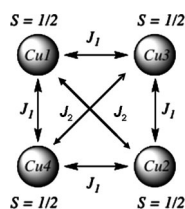


Figure 7. Temperature dependence of the  $\chi T$  product for complexes **1** (filled circles) and **2** (open circles) at 1000 Oe [with  $\chi$  being equal to magnetization ( $M$ )/magnetic field ( $H$ )]. The solid line is the best fit of the experimental data of **2** using the simplified tetranuclear Heisenberg model described in the text.

For **2**, the  $\chi T$  product at room temperature ( $1.24 \text{ cm}^3 \text{ K mol}^{-1}$ ) is slightly lower than the expected value of  $1.5 \text{ cm}^3 \text{ K mol}^{-1}$ , which is explained by the presence of intramolecular antiferromagnetic interactions as seen by the decrease of  $\chi T$  when lowering the temperature (Figure 7). At 1.8 K, the  $\chi T$  product reaches almost zero, at approximately  $0.02 \text{ cm}^3 \text{ K mol}^{-1}$ , as expected for a complex with a singlet ground state ( $S_T = 0$ ). Inspection of the crystal structure (vide supra) reveals that the used ligand is sufficiently bulky to efficiently separate the  $[\text{Cu}_4\text{O}_4]$  cores from each other, which implies extremely negligible intermolecular magnetic interactions. If, at a first stage, the slight differences in the Cu–O–Cu angles can be ignored, a close inspection of the  $[\text{Cu}_4\text{O}_4]$  core reveals two types of Cu–O bonds with different lengths: short Cu–O bonds of about 1.9 Å and long Cu–O bonds of about 2.4 Å. The short Cu–O bonds (ca. 1.9 Å) involve an oxygen atom bonded to copper in an equatorial position of its coordination sphere, whereas the long Cu–O bonds (ca. 2.4 Å) imply an oxygen atom in an axial position (Jahn–Teller axis). Consequently, two different pathways for the interactions between the  $\text{Cu}^{\text{II}}$  metal ions can be identified that are mediated by double oxygen bridges with short–short/short–long ( $J_1$ ) or two long–short ( $J_2$ ) Cu–O bond lengths. The spin/interaction topology is thus given by Scheme 2.





Scheme 2.

We have attempted to fit the  $\chi T$  data using a well-known model invoking a  $[\text{Cu}_4\text{O}_4]$  cubane that has pseudo- $S_4$  site symmetry that essentially treats the  $[\text{Cu}_4\text{O}_4]$  core as two coupled  $\text{Cu}^{\text{II}}$  dimer pairs.<sup>[41–42]</sup> The topology of the  $[\text{Cu}_4\text{O}_4]$  core is thus viewed as shown in Scheme 2 in which  $J_1$  is the exchange between two  $\text{Cu}^{\text{II}}$  sites forming a regular square and  $J_2$  is the cross exchange between the opposite vertex of the square. The isotropic exchange Hamiltonian based on this topology is shown in Equation (1)

$$H = -2J_1(\mathbf{S}_{\text{Cu}1} + \mathbf{S}_{\text{Cu}2}) \cdot (\mathbf{S}_{\text{Cu}3} + \mathbf{S}_{\text{Cu}4}) - 2J_2(\mathbf{S}_{\text{Cu}1} \cdot \mathbf{S}_{\text{Cu}2} + \mathbf{S}_{\text{Cu}3} \cdot \mathbf{S}_{\text{Cu}4}) \quad (1)$$

in which  $J_1$  and  $J_2$  are the exchange constants as shown in Scheme 2, and  $\mathbf{S}_i$  are the spin operators for each  $\text{Cu}^{\text{II}}$  metal ion for the “ $i$ ” site. By ignoring the contribution of anisotropy in the system and in the weak-field approximation, the resulting expression derived from the Van Vleck formula is [Equation (2)].

This analytical expression has been used to fit the experimental  $\chi T$  data measured at 1000 Oe but this approach leads to nondetermined  $J$  parameters for which the error on the values is larger than the values themselves. The present situation is a typical case of overparametrization found in fitting procedures, that is, an infinite number of ( $J_1$ ,  $J_2$ ) exchange parameter pairs could fit the experimental data. Therefore, the number of fitting parameters must be reduced to only two ( $J$  and  $g$ ) by considering  $J = J_1 = J_2$  as there is no structural justification to suppress one of the two interactions in the  $[\text{Cu}_4\text{O}_4]$  core. By using this simplified model, the experimental data are perfectly reproduced down to 1.8 K with  $J/k_B = -14.9(5)$  K and  $g = 2.0(1)$  (red line in Figure 7). It is worth mentioning that the obtained  $J$  parameter is an average value of  $J_1$  and  $J_2$ . The sign of the magnetic interaction confirms that this  $\text{Cu}^{\text{II}}$  tetramer complex possesses an  $S_T = 0$  spin ground state.

## Conclusion

In summary, using a simple Mannich-type reaction we have prepared a novel hexacoordinating bis(hydroxyethyl)-ethylenediamine-bis(phenolate) ligand. This new ligand is able to stabilize both mono- and tetranuclear  $\text{Cu}^{\text{II}}$  complexes depending on the ligand/metal ratio and pH conditions. The mononuclear complex, **1**, can be converted to the tetranuclear **2** by heating **1** at reflux with an excess amount of both the copper(II) ion and TEA. However the reverse process was not observed. The tetranuclear  $[\text{Cu}_4\text{O}_4]$  core in **2** possesses a  $[6 + 0]$ -type cubane conformation that was observed for the first time using a hexacoordinating ligand. Whereas **1** displays an expected paramagnetic Curie behavior, magnetic measurements reveal dominating antiferromagnetic interactions in **2**. Complex **2** belongs to a rare  $[6 + 0]$ -type cubane. Unlike the other  $[6 + 0]$ -type cubanes, which show overall ferromagnetic interactions arising from competing ferromagnetic and antiferromagnetic interactions propagating through two exchange pathways ( $J_1$  and  $J_2$ ) in  $S_4$  or  $C_2$  symmetries, complex **2** shows dominating antiferromagnetic interactions inducing an  $S_T = 0$  ground state.

## Experimental Section

**Materials:** Starting materials (reagent grade) for the synthesis of the  $\text{H}_4\text{L}$  ligand: 2,4-di-*tert*-butylphenol (Lancaster), formaldehyde (Merck India), and  $N,N'$ -bis(2-hydroxyethyl)ethylenediamine (Aldrich Chemicals) have been used as received. Solvents like methanol, ethanol, petroleum ether, and acetonitrile (Merck India) were of reagent grade and dried by standard methods before use.

**Synthesis of the  $\text{H}_4\text{L}$  Ligand:** This was prepared by using simple Mannich condensation.<sup>[43,44]</sup> In a typical procedure,  $N,N'$ -bis(2-hydroxyethyl)ethylenediamine (2.22 g, 15 mmol) in MeOH along with 2,4-di-*tert*-butylphenol (6.19 g, 30 mmol) and formaldehyde (3 mL, 41%, 35 mmol) was stirred for 2 d. The solution was kept in air to evaporate the solvent partially. A white solid appeared within 2 d. After filtration, the solid was washed with cold methanol and dried in air.

**Synthesis of  $[\text{Cu}(\text{H}_2\text{L})]$  (**1**):** *Caution!* Since perchlorate salts are potentially explosive, only small amounts of the materials should be handled with care.

The  $\text{H}_4\text{L}$  ligand (1.0 mmol) was added to a methanolic solution of  $\text{Cu}(\text{ClO}_4)_2 \cdot 6\text{H}_2\text{O}$  (1 mmol). Triethylamine (TEA; 2.0 mmol) was added and the resulting solution was heated at reflux for 6 h. On cooling, a green crystalline product was obtained. After filtration, the solid was washed with methanol and dried in air. Diffraction-quality crystals were obtained by very slow evaporation of a solution of the sample in dichloromethane at 5 °C. The composition of

$$\chi T = \frac{2N_A g^2 \mu_B^2}{k_B} \frac{2 \exp\left(\frac{2J_1}{k_B T}\right) + \exp\left(\frac{4J_1 - 2J_2}{k_B T}\right) + 5 \exp\left(\frac{4J_1 + 2J_2}{k_B T}\right)}{1 + 6 \exp\left(\frac{2J_1}{k_B T}\right) + \exp\left(\frac{4J_1 - 4J_2}{k_B T}\right) + 3 \exp\left(\frac{4J_1 - 2J_2}{k_B T}\right) + 5 \exp\left(\frac{4J_1 + 2J_2}{k_B T}\right)} \quad (2)$$



the complex was determined by elemental analysis based on  $C_{36}H_{58}CuN_2O_4$  (644.4): calcd. C 67.09, H 9.07, N 4.35; found C 67.21, H 9.15, N 4.46. IR:  $\tilde{\nu}$  = 3442 (br), 2957–2867 (s), 1429 (s), 1297–1255 (s), 833, 727  $cm^{-1}$ .

**Synthesis of  $[Cu_4L_2]$  (2):** Two methods can be used to synthesize compound **2**. Method (a): TEA (4.2 mmol) was added to a solution of  $H_4L$  (1.0 mmol, 0.584 mg) in dichloromethane (20 mL) and heated at reflux for 15 min.  $Cu(ClO_4)_2 \cdot 6H_2O$  (2 mmol) in acetonitrile (60 mL) was added dropwise to this hot solution. The resulting solution was heated at reflux for 6 h. After cooling down to room temperature, the solution was filtered and kept in refrigerator. After a week, dark brown block-shaped crystals formed and were filtered and washed with ice-cold methanol and dried in air. Method (b): Complex **1** (green product, 1.0 mmol) was dissolved in dichloromethane, and  $Cu(ClO_4)_2 \cdot 6H_2O$  (0.5 mmol) in acetonitrile (60 mL) was added dropwise. The resulting solution was heated at reflux for 24 h. After cooling down to room temperature, the solution was filtered and kept in the refrigerator. After a week, dark brown block-shaped crystals were obtained and filtered. The crystals were washed with ice-cold methanol and dried in air.

The composition of **2** was determined by elemental analysis as based on  $C_{72}H_{112}Cu_4N_4O_8$  (1415.86): calcd. C 61.07, H 7.97, N 3.96; found C 61.21, H 8.15, N 3.92. IR:  $\tilde{\nu}$  = 3442 (br), 2957–2867 (s), 1429 (s), 1297–1255 (s), 833, 727  $cm^{-1}$ .

**Physical Measurements:** Elemental analyses were carried out using a Perkin–Elmer 240 elemental analyzer. Infrared spectra (400–4000  $cm^{-1}$ ) were recorded from KBr pellets on a Nicolet Magna IR 750 series-II FTIR spectrophotometer.

**X-ray Crystallography:** Intensity data for complexes **1** and **2** were collected at 148(2) and 273(2) K on a smart CCD diffractometer using graphite-monochromatized Mo- $K_\alpha$  radiation ( $\lambda$  = 0.71073 Å) in  $\omega$ – $2\theta$  scan mode ( $2.75^\circ < 2\theta < 27.50^\circ$ ). As judged by the diffraction peaks, no decomposition of the crystals occurred during the data collection. The intensities were corrected for Lorentz and polarization effects and for absorption using the  $\psi$ -scan data. The structure was solved by direct methods using SHELXS-97<sup>[45]</sup> and was refined anisotropically on  $F^2$  using the full-matrix least-squares procedure of SHELXL-97<sup>[46]</sup> and hydrogen atoms were included in the model at their calculated positions with  $d(C-H)$  = 0.93–0.97 Å and  $U_{iso}(H)$  values of **1** with 5 equiv. of C for methyl protons and 1.2 equiv. of C for other protons at convergence [ $\sigma$  weights, i.e.,  $1/\sigma^2(F)$ ]. Structural data are summarized in Table 3.

**Magnetic Studies:** The magnetic susceptibility measurements were carried out with the use of a Quantum Design SQUID magnetometer MPMS-XL. This magnetometer works between 1.8 and 400 K for direct current (dc) applied fields ranging from –7 to 7 T. Measurements were performed with microcrystalline samples of **1** (16.99 mg) and **2** (9.74 mg). Before any measurement, the sample was checked for the presence of ferromagnetic impurities by measuring the magnetization as a function of the field at 100 K. For pure paramagnetic or diamagnetic systems, a perfect straight line is expected and is observed for these compounds, thus indicating the absence of any ferromagnetic impurities. The magnetic data were corrected for the sample holder and the diamagnetic contribution.

CCDC-746247 (for **1**) and -745854 (for **2**) contain the supplementary crystallographic data for this paper. These data can be obtained free of charge from The Cambridge Crystallographic Data Centre via [www.ccdc.cam.ac.uk/data\\_request/cif](http://www.ccdc.cam.ac.uk/data_request/cif).

Table 3. Crystal data and details of the structure determination.

	1	2
Formula	$C_{36}H_{58}CuN_2O_4$	$C_{72}H_{112}Cu_4N_4O_8$
Formula weight	644.38	1415.86
Crystal system	monoclinic	triclinic
Space group	$C2/c$ (no. 15)	$P\bar{1}$ (no. 2)
$a$ [Å]	18.6612(17)	14.8140(14)
$b$ [Å]	16.3168(15)	16.5896(17)
$c$ [Å]	12.0534(11)	19.2368(19)
$\alpha$ [°]	90	64.871(6)
$\beta$ [°]	90.974(5)	68.302(6)
$\gamma$ [°]	90	83.947(6)
$V$ [Å <sup>3</sup> ]	3669.6(6)	3969.4(7)
$Z$	4	2
$D$ (calcd.) [g cm <sup>–3</sup> ]	1.166	1.185
$\mu$ (Mo- $K_\alpha$ ) [mm]	0.632	1.106
$F(000)$	1388	1504
Temperature [K]	148	273
$\theta$ min., max. [°]	1.7, 28.9	1.4, 28.8
Dataset	–25;24; –21;22; –16;16	–19;19; –22;22; –25;25
Total, unique data	25714, 4555	60489, 20237
$R$ (int)	0.013	0.073
Observed data [ $I > 2\sigma(I)$ ]	1964	5196
$N$ (reflections)	4555	20237
$N$ (parameters)	205	817
$R^2$ <sup>[a]</sup>	0.0563	0.0866
$wR2$ <sup>[b]</sup>	0.1299	0.2715
$S$	0.87	0.86
Max., av. shift/error	0.00, 0.00	0.00, 0.00
Min., max. residual density [e Å <sup>–3</sup> ]	–0.35, 0.75	–0.81, 0.62

[a]  $R(F_o) = \Sigma |F_o| - |F_c| / \Sigma |F_o|$ . [b]  $wR2(F_o^2) = \{\Sigma [w(F_o^2 - F_c^2)^2] / \Sigma [w(F_o^2)^2]\}^{1/2}$ .

## Acknowledgments

Financial support from the Department of Science and Technology (ref. SR/S1/IC-35/2006), Defence Research and Development Organisation (ref. ERIP/ER/0503513/M/01/947), and Council of Scientific and Industrial Research New Delhi, India [ref. 01(2129)/07/EMR-II] are gratefully acknowledged. Financial support from the University of Bordeaux (in particular for the visiting professor position of M. A.), Centre National de la Recherche Scientifique (CNRS), Agence Nationale de la Recherche (ANR) (NT09\_469563, AC-MAGnets), European Network of Excellence “Molecular Approach to Nanomagnets and Multifunctional Materials” (MAGMANet, NMP3-CT-2005-515767), Région Aquitaine, GIS Materials in Aquitaine (COMET Project), and The Natural Sciences and Engineering Research Council of Canada (NSERC) are also gratefully acknowledged.

- [1] H. Oshio, N. Hoshino, T. Ito, M. Nakano, F. Renz, P. Gütllich, *Angew. Chem. Int. Ed.* **2003**, 42, 223–225; A. Caneschi, A. Cornia, S. J. Lippard, *Angew. Chem. Int. Ed. Engl.* **1995**, 34, 467–469.
- [2] D. Gatteschi, R. Sessoli, *Angew. Chem. Int. Ed.* **2003**, 42, 268–297.
- [3] W. Wernsdorfer, N. Aliaga-Alcalde, D. N. Hendrickson, G. Christou, *Nature* **2002**, 416, 406–409.
- [4] R. E. P. Winpenny, *Adv. Inorg. Chem.* **2001**, 52, 1–111; V. G. Makhankova, O. Y. Vassilyeva, V. N. Kokozay, B. W. Skelton, J. Reedijk, G. A. Vanalbada, L. Sorace, D. Gatteschi, *New J. Chem.* **2001**, 25, 685–689.
- [5] W. E. Hatfield, in: *Magnetostructural Correlations in Exchange Coupled Systems* (Eds.: R. D. Willett, D. Gatteschi, O. Kahn), Reidel, Dordrecht, The Netherlands, **1985**, pp. 555–602.

- [6] M. A. Halcrow, J. C. Huffman, G. Christou, *Angew. Chem. Int. Ed. Engl.* **1995**, *34*, 889–891.
- [7] M. A. Halcrow, J. S. Sun, J. C. Huffman, G. Christou, *Inorg. Chem.* **1995**, *34*, 4167–4177.
- [8] H. J. Mai, R. M. Köcker, S. Wocadlo, W. Massa, K. Dehnicke, *Angew. Chem. Int. Ed. Engl.* **1995**, *34*, 1235–1236.
- [9] J. M. Berg, R. H. Holm, in: *Iron-Sulfur Proteins*, vol. 4 (Ed.: T. G. Spiro), Wiley-Interscience, New York, **1982**, pp. 1–66.
- [10] R. H. Holm, S. Ciurli, J. A. Weigel, *Prog. Inorg. Chem.* **1990**, *38*, 1–74.
- [11] L. Mertz, W. Haase, *J. Chem. Soc., Dalton Trans.* **1978**, 1594–1598.
- [12] L. Schwabe, W. Haase, *J. Chem. Soc., Dalton Trans.* **1985**, 1909–1913.
- [13] J. W. Hall, W. E. D. Estes, R. P. Scaringe, W. E. Williams, *Inorg. Chem.* **1977**, *16*, 1572–1574.
- [14] J. Sletten, A. Sorensen, M. Julve, Y. Journaux, *Inorg. Chem.* **1990**, *29*, 5054–5058.
- [15] J. A. Bertrand, A. P. Ginsberg, R. I. Kaplan, C. E. Kirkwood, R. L. Martin, R. C. Sherwood, *Inorg. Chem.* **1971**, *10*, 240–246.
- [16] N. Matsumoto, I. Ueda, Y. Nishida, S. Kida, *Bull. Chem. Soc. Jpn.* **1976**, *49*, 1308–1312.
- [17] E. Ruiz, A. Rodriguez-Forteza, P. Alemany, S. Alvarez, *Polyhedron* **2001**, *20*, 1323–1327.
- [18] R. Mergehenn, W. Haase, *Acta Crystallogr., Sect. B* **1977**, *33*, 1877–1882.
- [19] J. A. Bertrand, E. Fujita, P. G. Eller, *Inorg. Chem.* **1974**, *13*, 2067–2071.
- [20] J. A. Bertrand, C. E. Kirkwood, *Inorg. Chim. Acta* **1972**, *6*, 248–252.
- [21] J. A. Bertrand, J. A. Kelley, *Inorg. Chim. Acta* **1970**, *4*, 203–209.
- [22] N. F. Curtis, F. W. B. Einstein, K. R. Morgan, A. C. Willis, *Inorg. Chem.* **1985**, *24*, 2026–2032.
- [23] M. Drillon, A. Grand, P. Rey, *Inorg. Chem.* **1990**, *29*, 771–774.
- [24] M. Handa, T. Idehara, K. Nakano, K. Kasuga, M. Mikuriya, N. Matsumoto, M. Kodera, S. Kida, *Bull. Chem. Soc. Jpn.* **1992**, *65*, 3241–3252.
- [25] T. Lindgren, R. Sillanpää, K. Rissanen, L. K. Thompson, C. J. O'Connor, G. A. van Albada, J. Reedijk, *Inorg. Chim. Acta* **1990**, *171*, 95–102.
- [26] N. Matsumoto, T. Tsutsumi, A. Ohyoshi, H. Ojkawa, *Bull. Chem. Soc. Jpn.* **1983**, *56*, 1388–1392.
- [27] G. S. Matuzenko, Y. A. Simonov, A. A. Dvorkin, Y. V. Yablokov, V. K. Voronkova, L. V. Mosina, B. Y. Kuyavskaya, M. A. Yampolskaya, N. V. Gerbeleu, *Zh. Neorg. Khim.* **1984**, *29*, 978–986.
- [28] M. Mikuriya, H. Ojkawa, S. Kida, *Bull. Chem. Soc. Jpn.* **1982**, *55*, 1086–1091.
- [29] M. Mikuriya, T. Harada, H. Ojkawa, S. Kida, *Inorg. Chim. Acta* **1983**, *75*, 1–7.
- [30] M. Mikuriya, K. Toriumi, T. Ito, S. Kida, *Inorg. Chem.* **1985**, *24*, 629–631.
- [31] M. Mikuriya, K. Toriumi, *Bull. Chem. Soc. Jpn.* **1993**, *66*, 2106–2108.
- [32] M. Mikuriya, H. Ojkawa, S. Kida, *Bull. Chem. Soc. Jpn.* **1981**, *54*, 2979–2982.
- [33] Y. A. Simonov, M. A. Yampolskaya, G. S. Matuzenko, V. K. Belskii, B. Y. Kuyavskaya, *Zh. Neorg. Khim.* **1986**, *31*, 941–946.
- [34] T. Tokii, M. Nakashima, T. Furukawa, Y. Muto, R. L. Lintvedt, *Chem. Lett.* **1990**, 363–366.
- [35] L. Walz, W. Haase, *J. Chem. Soc., Dalton Trans.* **1985**, 1243–1248.
- [36] L. Walz, H. Paulus, W. Haase, *J. Chem. Soc., Dalton Trans.* **1985**, 913–920.
- [37] M. A. Yampolskaya, A. A. Dvorkin, Y. A. Simonov, V. K. Voronkova, L. V. Mosina, Y. V. Yablokov, K. I. Turte, A. V. Ablov, T. I. Malinovskii, *Zh. Neorg. Khim.* **1980**, *25*, 174–179.
- [38] Y. Xie, W. Bu, X. Xu, H. Jiang, Q. Liu, Y. Xue, Y. Fan, *Inorg. Chem. Commun.* **2001**, *4*, 558–560.
- [39] G. D. Fallon, B. Moubaraki, K. S. Murray, A. M. van den Bergen, B. O. West, *Polyhedron* **1993**, *12*, 1989–2000.
- [40] T. Shiga, H. Oshio, *Sci. Technol. Adv. Mater.* **2005**, *6*, 565–570, and references cited therein.
- [41] A. Burkhardt, E. T. Spielberg, H. Görls, W. Plass, *Inorg. Chem.* **2008**, *47*, 2485–2493.
- [42] B. Abarca, R. Ballesteros, M. Chadlaoui, C. Ramirez de Arelano, J. A. Real, *Eur. J. Inorg. Chem.* **2007**, 4574–4578.
- [43] E. Y. Tshuva, I. Goldberg, M. Kol, Z. Goldschmidt, *Organometallics* **2001**, *20*, 3017–3028.
- [44] D. Maity, A. Ray, W. S. Sheldrick, H. Mayer-Figge, B. Bandyopadhyay, M. Ali, *Inorg. Chim. Acta* **2006**, *359*, 3197–3204.
- [45] G. M. Sheldrick, *Acta Crystallogr., Sect. A* **1990**, *46*, 467–473.
- [46] G. M. Sheldrick, T. R. Schneider, *Methods Enzymol.* **1997**, *277*, 319–343.

Received: January 29, 2010  
Published Online: June 22, 2010

# Weak Ferromagnetism Caused by a 2D Effect in Two New Cobalt(II)– and Nickel(II)–1,2-Bis(4-pyridyl)ethane (bpa) Polynuclear Compounds

Noelia de la Pinta,<sup>[a]</sup> Gotzon Madariaga,<sup>[b]</sup> Luis Lezama,<sup>[a]</sup> M. Luz Fidalgo,<sup>[c]</sup> and Roberto Cortés\*<sup>[c]</sup>

**Keywords:** Polynuclear structures / Magnetic properties / Structure-magnetism relationship / N ligands / Cyanato ligands / Cobalt / Nickel

The combination of bpa [1,2-bis(4-pyridyl)ethane] with the pseudohalide cyanato ( $\text{NCO}^-$ ) ligand leads to the preparation of two new isomorphous compounds exhibiting the general formula  $[\text{M}(\text{NCO})_2(\text{bpa})_2]_n$  [ $\text{M} = \text{Co}$  (**1**) and  $\text{M} = \text{Ni}$  (**2**)]. Both compounds consist of  $\text{M}-(\text{gauche-bpa})_2-\text{M}$  chains linked by

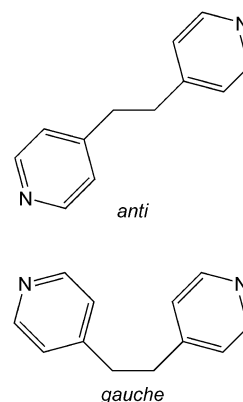
hydrogen bonds to give a global 2D network.  $\text{Co}^{\text{II}}$  and  $\text{Ni}^{\text{II}}$  ions are octahedrally coordinated to four bpa ligands and two terminal NCO groups. The two compounds exhibit slight antiferromagnetic interactions through bpa groups and a 2D effect leading to a ferromagnetic component.

## Introduction

The 4,4-dipyridyl-type organic groups are well known to be excellent spacers for the preparation of coordination polymers. Among these ligands, the flexibility of the 1,2-bis(4-pyridyl)ethane ligand (bpa) is especially remarkable and provides a clear advantage over other related rigid 4,4'-dipyridyl organic ligands.

The bpa ligand can adopt two different conformations, *anti* and *gauche* (Scheme 1), as a consequence of the freedom of rotation exhibited by the ethyl group. Both conformers are able to perform as coordinating ligands, either bridging or terminal, and/or as crystallisation molecules. As a result, bpa is characterised by a high capability to be incorporated into the structural framework, as illustrated by the increasing amount of bpa polymers reported during the last years.<sup>[1]</sup>

Our previous works with bpa concern four families of polymers where this ligand is combined with pseudohalides {azido ( $\text{N}_3$ ),<sup>[2]</sup> dicyanamido [ $\text{N}(\text{CN})_2$ ],<sup>[3]</sup> thiocyanato ( $\text{NCS}$ )<sup>[4]</sup> and cyanato ( $\text{NCO}$ )<sup>[5]</sup>}. The use of these ligands focuses on the generation of significant magnetic interactions through



Scheme 1. Conformations of the bpa ligand.

intermetallic bridges. It is worth mentioning that few examples of  $\text{M}-\text{L}-\text{bpa}$  [ $\text{L} = \text{NCS}$ <sup>[6]</sup> and  $\text{N}(\text{CN})_2$ <sup>[3,7]</sup>] can be found in the literature. For  $\text{L} = \text{N}_3$  and  $\text{NCO}$  the  $[\text{M}(\text{N}_3)_2(\text{bpa})]$  ( $\text{M} = \text{Mn}, \text{Fe}, \text{Co}$  and  $\text{Ni}$ )<sup>[2,8]</sup> and  $[\text{M}(\text{NCO})_2(\text{bpa})_2] \cdot \text{bpa}$  ( $\text{M} = \text{Mn}$  and  $\text{Co}$ )<sup>[5]</sup> compounds have been characterised to date.

In this context, this paper reports on the synthesis and magnetostructural characterisation of the polynuclear compounds  $[\text{M}(\text{NCO})_2(\text{bpa})_2]_n$  [ $\text{M} = \text{Co}$  (**1**) and  $\text{Ni}$  (**2**)]. These isomorphous compounds exhibit  $\text{M}-(\text{gauche-bpa})_2-\text{M}$  chains that are connected through hydrogen bonds to give a 2D global network. The metal ions are octahedrally coordinated, and this arrangement gives rise to a 2D effect showing a ferromagnetic component. The absence of direct intermetallic bridges through the cyanato groups precludes the existence of stronger magnetic interactions between the metallic centres.

[a] Departamento de Química Inorgánica, Fac. Ciencia y Tecnología, UPV/EHU, Apartado 644, 48080 Bilbao, Spain

[b] Departamento de Física de la Materia Condensada, Fac. Ciencia y Tecnología, UPV/EHU, Apartado 644, 48080 Bilbao, Spain

[c] Departamento de Química Inorgánica, Fac. Farmacia, UPV/EHU, Apartado 450, 01080 Vitoria, Spain  
Fax: +34-945-01-3019  
E-mail: roberto.cortes@ehu.es

Supporting information for this article is available on the WWW under <http://dx.doi.org/10.1002/ejic.201000134>.



## Results and Discussion

### Structural Analysis

Compounds **1** and **2** are isomorphous. At first sight both exhibit linear M–(bpa)<sub>2</sub>–M chains extending along the [010] direction (Figure 1) where the metallic ions are octahedrally coordinated. Four bpa groups occupy the equatorial positions of the coordinating sphere, whereas in the axial ones two N-bonded terminal cyanato ligands can be found for both compounds. The two bpa ligands, bridging octahedral metal ions, adopt the *gauche* conformation. The intermetal-

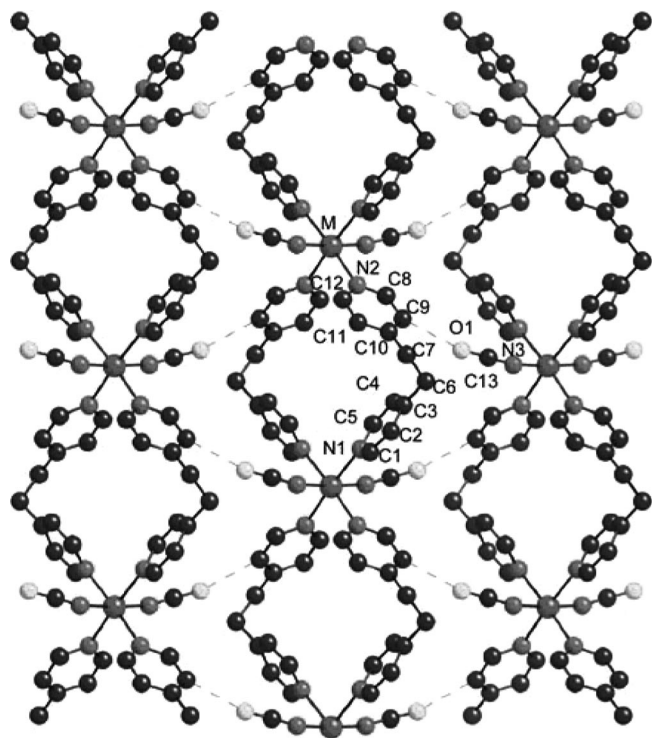


Figure 1. Packing of the chains for **1** and **2** on the *xy* plane to give a 2D global network. The discontinuous lines represent hydrogen bonds.

Table 1. Selected bond lengths [Å] and angles [°] for [M(NCO)<sub>2</sub>–(bpa)<sub>2</sub>] [M = Co (**1**) and Ni (**2**)].<sup>[a]</sup>

	Co ( <b>1</b> )	Ni ( <b>2</b> )
M–N(1)	2.201(4)	2.145(5)
M–N(2) <sup>ii</sup>	2.209(4)	2.147(5)
M–N(3)	2.099(3)	2.074(4)
N(3)–C(13)	1.150(5)	1.154(7)
C(13)–O(1)	1.214(6)	1.197(7)
N(1) <sup>i</sup> –M–N(1)	90.9(2)	90.6(3)
N(1)–M–N(2) <sup>iii</sup>	175.0(1)	175.5(2)
N(1)–M–N(2) <sup>ii</sup>	91.8(1)	92.0(2)
N(1)–M–N(3)	85.6(1)	86.2(2)
N(1)–M–N(3) <sup>i</sup>	92.0(1)	90.8(2)
N(2) <sup>ii</sup> –M–N(2) <sup>iii</sup>	85.9(2)	85.6(3)
N(2) <sup>iii</sup> –M–N(3)	90.1(1)	90.3(2)
N(2) <sup>ii</sup> –M–N(3)	92.5(1)	93.1(2)
N(3)–M–N(3) <sup>i</sup>	176.5(2)	175.4(3)
C(13)–N(3)–M	151.4(4)	151.5(5)
N(3)–C(13)–O(1)	179.3(6)	178.3(7)

[a] Symmetry transformations used to generate equivalent atoms: i =  $-x + 1, y, -z + 1/2$ ; ii =  $x, y - 1, z$ ; iii =  $-x + 1, y - 1, -z + 1/2$ .

allic distance through the bpa links is 9.95 Å for **1** and 9.87 Å for **2**. The torsion angle py–C–C–py for the bpa ligands is 68.0(5)° for **1** and 67.1(7)° for **2**. Similar low values of the torsion angles have been found for other M–(*gauche*-bpa)<sub>2</sub>–M chains.<sup>[4,5,9]</sup> With regard to the skew propeller configurations of the four coordinated pyridine moieties around the metal ion, the dihedral angle between the two independent pyridine moieties is 74.1(2)° and 72.6(3)° for compounds **1** and **2**, respectively.

Table 1 summarises the most significant bond parameters for **1** and **2**. As observed, the values for the bond angles are near to the ideal ones. The M–N<sub>bpa</sub> distance [2.201(4) Å for **1** and 2.145(5) Å for **2**] is slightly longer than the M–N<sub>NCO</sub> distance [2.099(3) Å for **1** and 2.074(4) Å for **2**]. The cyanato ligands are nearly linear [N–C–O 179.3(6)° for **1** and N–C–O 178.3(7)° for **2**].

These M–(bpa)<sub>2</sub>–M chains are connected through hydrogen bonds (Table 2) giving rise to a 2D global network shown in Figures 1 and 2. It is worth remarking that the

Table 2. Selected most important intermolecular hydrogen bonds for compounds **1** and **2**.<sup>[a]</sup>

<b>1</b>			
C9–H9 <sup>iv</sup>	C9...O1 <sup>iv</sup>	H9...O1 <sup>iv</sup>	C9–H9...O1
0.93	3.397(6)	2.54	154.2
C1–H1 <sup>v</sup>	C1...N3 <sup>v</sup>	H1...N3 <sup>v</sup>	C1–H1...N3
0.93	3.618(6)	2.88	137.3
<b>2</b>			
C9–H9 <sup>iv</sup>	C9...O1 <sup>iv</sup>	H9...O1 <sup>iv</sup>	C9–H9...O1
0.93	3.400(8)	2.4	154.3
C1–H1 <sup>v</sup>	C1...N3 <sup>v</sup>	H1...N3 <sup>v</sup>	C1–H1...N3
0.93	3.602(7)	2.87	136.8

[a] Symmetry transformations used to generate equivalent atoms: iv =  $-x + 1/2, y + 1/2, -z + 1/2$ ; v =  $x, -y, z - 1/2$ .

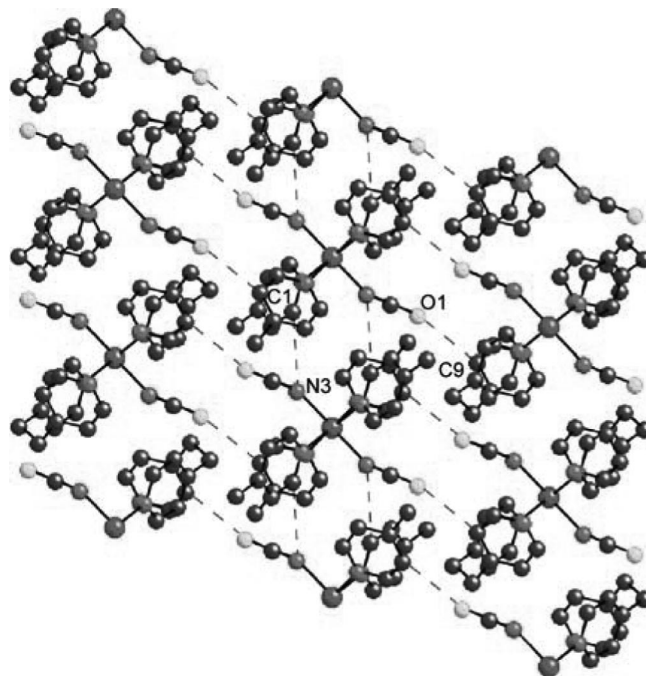


Figure 2. View along the [010] direction of structures **1** and **2**. The discontinuous lines represent the hydrogen bonds.



hydrogen bonds linking the N atoms of the cyanato groups with the C1 atom of the bpa groups connect molecular units related by  $x$ ,  $-y$ ,  $z - 1/2$  symmetry transformations, since the distance between metallic atoms related by this symmetry is the shortest one in these structures (6.999 Å for **1** and 6.959 Å for **2**).

### IR and UV/Vis Spectroscopy and Thermal Behaviour

A summary of the most important IR bands corresponding to compounds **1** and **2**, together with their tentative assignments,<sup>[10]</sup> are given in Table 3. As can be seen, the two spectra exhibit an intense absorption at about 2200 cm<sup>-1</sup>, which is associated with the asymmetric stretching mode of the cyanato ligand. A broad band of medium intensity at about 3500 cm<sup>-1</sup> for **1** (Figure S4) must be associated with the OH stretching vibrations of the atmospheric water.

Table 3. IR bands [cm<sup>-1</sup>] and assignments for compounds **1** and **2**.

	<b>1</b>	<b>2</b>
$\nu(\text{C-H})_{\text{bpa}}$	3200–2800	3200–2800
$\nu_{\text{as}}(\text{C-N})_{\text{NCO}}$	2193	2194
$\nu(\text{C}=\text{C})$ , $\nu(\text{C}=\text{N})_{\text{bpa}}$	1613	1611
$\nu(\text{ArC-C})_{\text{bpa}}$	1424	1416
$\nu(\text{C-O})_{\text{NCO}}$	1224	1222
$\delta_{\text{ep}}(\text{ArC-H})_{\text{bpa}}$	1069/1019	1071/1019
$\nu_{\text{fp}}(\text{ArC-H})_{\text{bpa}}$	809	819
$\delta(\text{NCO})_{\text{NCO}}$	635	625

The frequencies of the IR bands related to the bpa ligand in the compounds are very close to their positions in the free ligand (which are also displayed in Table 3), showing that the pyridyl rings behave similarly in the complexes. These results correlate well with similar coordinations of the ligands to the metal ions, as observed in the structure of isomorphous compounds.

The diffuse reflectance spectrum for compound **1** (Figure S6) exhibits three transitions attributed to spin-allowed transitions from  $^4\text{T}_{1\text{g}}(\text{F})$  to  $^4\text{T}_{2\text{g}}(\text{F})$  ( $\nu_1 = 9200 \text{ cm}^{-1}$ ),  $^4\text{A}_{2\text{g}}(\text{F})$  ( $\nu_2 = 18800 \text{ cm}^{-1}$ ) and  $^4\text{T}_{1\text{g}}(\text{P})$  ( $\nu_3 = 20300 \text{ cm}^{-1}$ ), as corresponds to high-spin octahedral Co<sup>II</sup>. At 35000 cm<sup>-1</sup> the spectrum shows a charge-transfer band. The values of  $Dq = 960 \text{ cm}^{-1}$  and  $B = 869 \text{ cm}^{-1}$  calculated from these transitions are common for octahedral Co<sup>II</sup> complexes.<sup>[11]</sup> The value of  $B$  is indicative of 89.5% of covalence for the Co–N bonds in compound **1**.

For **2** (Figure S7), the UV/Vis spectrum exhibits the typical transitions for octahedral Ni<sup>II</sup> compounds<sup>[12]</sup> with values of  $Dq = 1010 \text{ cm}^{-1}$ ,  $B = 1032 \text{ cm}^{-1}$  (99.1% covalence) and  $C = 2938 \text{ cm}^{-1}$  ( $C/B = 2.85$ ) calculated for spin-allowed transitions from  $^3\text{A}_{2\text{g}}(\text{F})$  to  $^3\text{T}_{2\text{g}}(\text{F})$  ( $\nu_1 = 10100 \text{ cm}^{-1}$ ),  $^3\text{T}_{1\text{g}}(\text{F})$  ( $\nu_2 = 16200 \text{ cm}^{-1}$ ),  $^3\text{T}_{1\text{g}}(\text{P})$  ( $\nu_3 = 29100 \text{ cm}^{-1}$ ) and the spin-forbidden transition from  $^3\text{A}_{2\text{g}}(\text{F})$  to  $^1\text{E}_{\text{g}}$  ( $\nu^*_1 = 13500 \text{ cm}^{-1}$ ).

The TG curves (Figures S8 and S9) obtained for **1** and **2** (25–600 °C), under argon, indicate the occurrence of two steps (Table 4). The first one, which corresponds to a weight loss of 36.82% (**1**) and 35.80% (**2**), takes place between 145 °C and 223 °C (**1**) and 175 °C and 255 °C (**2**) and can be attributed to one molecule of bpa. The second step takes place between 223 °C and 330 °C (**1**) and 255 °C and 375 °C (**2**) and corresponds to a weight loss of 46.88% (**1**) and 41.90% (**2**). This step can be associated with the pyrolysis of the other molecule of bpa and the two cyanato groups.

As seen for the thermal behaviour (Figure S8), the thermal decomposition for compound **2** starts at a higher temperature than for **1**. This is indicative of a slightly higher stability of the Ni compound that is also reflected in the shorter Ni–N bond lengths and the higher rate of covalency concluded by UV/Vis spectroscopy.

### ESR Spectroscopic and Magnetic Properties

ESR spectroscopic measurements were carried out at several temperatures over the range 2–300 K for compounds **1** and **2**. As expected for compound **2**, having a non-Kramer metallic ion, ESR spectra did not show any signals over the whole temperature range. For compound **1**, even if X-band isotropic spectra were recorded below 100 K, just those corresponding to temperatures lower than 30 K acquired rhombic resolution.

The spectrum at 4 K (Figure 3) can be described in terms of an effective spin doublet  $S = 1/2$ . The sum of the three observed  $g$  values,  $g_1 = 2.21$ ,  $g_2 = 2.75$  and  $g_3 = 7.70$ , are close to the theoretical value of 13 proposed by Abragam and Pryce<sup>[12]</sup>, which is consistent with the slightly distorted octahedral sphere around Co<sup>II</sup> in compound **1**.

The thermal variation of  $\chi_{\text{m}}$  for **1** shows a continuous increase from  $\chi_{\text{m}} = 12.24 \times 10^{-3} \text{ cm}^3 \text{ mol}^{-1}$  at room temperature. As observed in Figure 4, where  $\chi_{\text{m}}^{-1}$  and  $\chi_{\text{m}}T$  values vs. temperature are displayed, the Curie–Weiss law is obeyed down to 50 K with values of  $C_{\text{m}} = 4.10 \text{ cm}^3 \text{ K mol}^{-1}$ .

Table 4. Thermoanalytic data for compounds **1** and **2**.<sup>[a]</sup>

	Step	$T_i$	$T_f$	$\Delta T$	% $\Delta m_{\text{experimental}}$	% $\Delta m_{\text{theoretical}}$	Assignment (per unit formula)
[Co(NCO) <sub>2</sub> (bpa) <sub>2</sub> ] ( <b>1</b> )	1	145	223		36.82	36.02	Loss of one bpa molecule
	2	223	330		46.88	46.22	Pyrolysis other bpa molecule and two cyanato groups
	Total	145	330	185	83.70	82.24	
[Ni(NCO) <sub>2</sub> (bpa) <sub>2</sub> ] ( <b>2</b> )	1	175	255		35.80	36.04	Loss of one bpa molecule
	2	255	375		41.90	46.24	Pyrolysis other bpa molecule and two cyanato groups
	Total	175	375	200	77.70	82.28	

[a]  $T_i$  [°C] = initial temperature,  $T_f$  [°C] = final temperature,  $\Delta T = T_f - T_i$ , % $\Delta m_{\text{experimental}}$  = experimental mass loss percentage, % $\Delta m_{\text{theoretical}}$  = theoretical mass loss percentage.

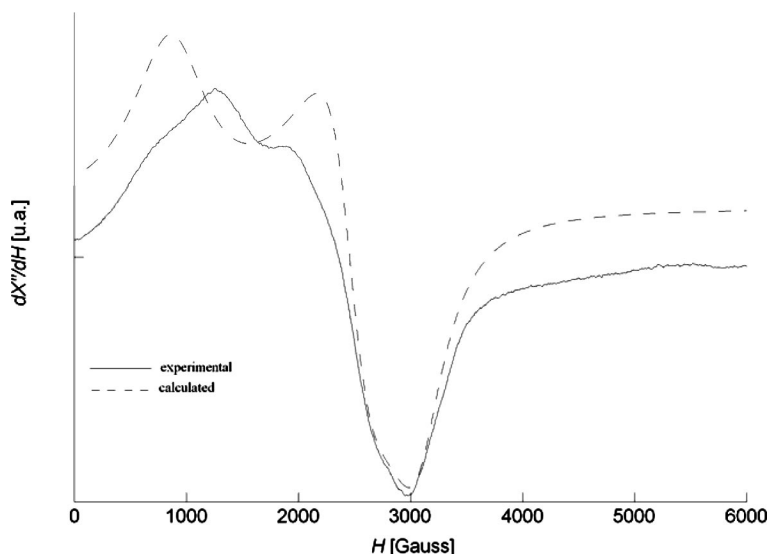


Figure 3. Experimental and calculated ESR powder spectra for **1** at 4 K.

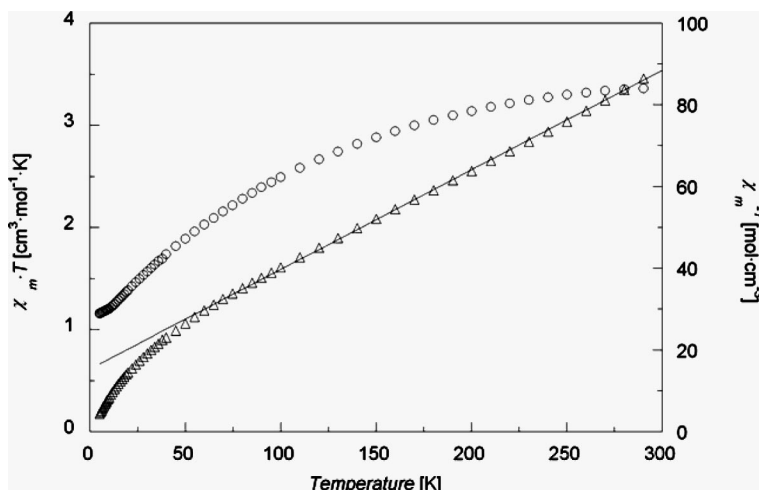


Figure 4. Thermal evolution of  $\chi_m T$  and  $\chi_m^{-1}$  for compound **1** and the corresponding Curie–Weiss curve.

and  $\theta = -63.0$  K. The decreasing values of  $\chi_m T$  (from  $\chi_m T = 3.36 \text{ cm}^3 \text{ K mol}^{-1}$  at room temperature) should be interpreted in terms of the spin-orbit coupling rather than considering significant antiferromagnetic interactions between the  $\text{Co}^{\text{II}}$  centres.

The magnetic susceptibility for **2** continuously increases from  $40.82 \times 10^{-3} \text{ cm}^3 \text{ mol}^{-1}$  at room temperature. Figure 5 shows the thermal variations of  $\chi_m^{-1}$  and  $\chi_m T$ . The inverse of  $\chi_m$  follows the Curie–Weiss law along the whole range of temperature ( $C_m = 1.23 \text{ cm}^3 \text{ K mol}^{-1}$  and  $\theta = -2.04$  K). The  $\chi_m T$  product slowly decreases with decreasing temperature from  $\chi_m T = 1.25 \text{ cm}^3 \text{ K mol}^{-1}$  at room temperature down to 33 K ( $\chi_m T = 1.15 \text{ cm}^3 \text{ K mol}^{-1}$ ). Upon further cooling, a slight increase of  $\chi_m T$  can be observed with a maximum at 12.6 K ( $\chi_m T = 1.22 \text{ cm}^3 \text{ K mol}^{-1}$ ). At lower temperatures, the  $\chi_m T$  values tend to zero. This anomaly will be discussed below.

The decrease of  $\chi_m T$  upon cooling for **2** should be attributed to the occurrence of slight antiferromagnetic interactions

between atoms connected through bpa ligands. Thus, if we consider the chains only, magnetic data for **2** can be treated on the basis of the Weng equation [Equation (1)] for the calculation of  $\chi_m T$  down to 33 K. This equation is applicable to linear chains with  $S = 1$  being based upon the spin Hamiltonian  $H = -\sum S_i S_{i+1}$ . The best fit (shown in Figure 5) has been carried out by using  $J = -0.8 \text{ cm}^{-1}$  and  $g = 2.21$  in agreement with very weakly coupled octahedral  $\text{Ni}^{\text{II}}$  ions.

$$\chi_m = \frac{N g^2 \beta^2}{kT} \left[ \frac{2 + A\alpha + B\alpha^2}{3 + C\alpha + D\alpha^2 + E\alpha^3} \right] \quad (1)$$

where  $A = 0.019$ ,  $B = 0.777$ ,  $C = 3.436$ ,  $D = 3.232$ ,  $E = 5.834$ ,  $\alpha = J/kT$ ;  $N$  and  $k$  are the Avogadro and Boltzmann constants, respectively,  $g$  is the Landé factor, and  $\beta$  is the Bohr magneton.

As observed, the theoretical fit (solid line) does not account for the anomaly at low temperatures. Assuming that

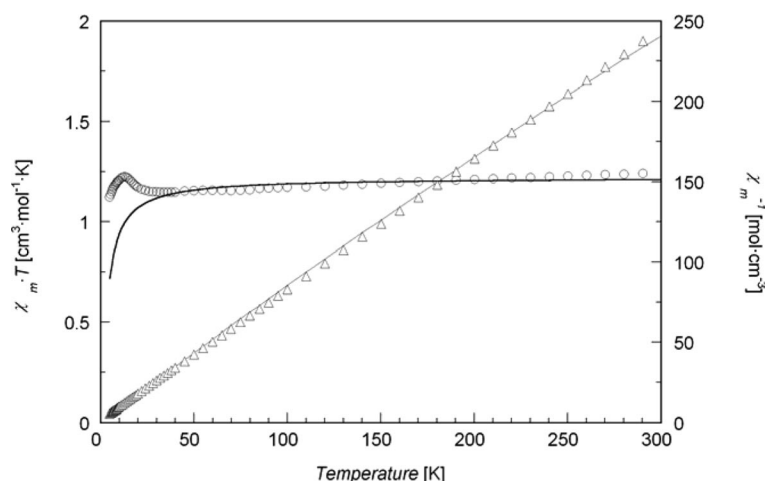


Figure 5. Thermal evolution of  $\chi_m T$  and  $\chi_m^{-1}$  for compound **2** and the corresponding theoretical Curie–Weiss curve.

the intrachain exchange through bpa only accounts for the occurrence of weak antiferromagnetic interactions, the low-temperature anomaly observed for **2** should be explained by considering a 2D effect related to the packing of the chains.

Figure 6 displays a 3D view of the metallic centres for **2** by considering the antiparallel coupling not only along the Ni–(bpa)<sub>2</sub>–Ni chains but also between consecutive centres connected through hydrogen bonds along the *x* and *z* directions. It is worth remarking that consecutive atoms along *z* are not magnetically equivalent (they are related by the *x*, *−y*, *z* + 1/2 symmetry transformation). On the other hand, the intermetallic distance between these atoms is the shortest one in the structure (6.959 Å): shorter than the distance through bpa ligands (9.869 Å) and the distance on the *xy* planes (10.593 Å). Taking into account these considerations, an interchain canting effect along *z* can be proposed. This canting could give rise to a weak ferromagnetic com-

ponent that accounts for the slight anomaly in the thermal variation of the  $\chi_m T$  product for **2**.

To definitively confirm the existence of a canting phenomenon, measurements at different magnetic fields should show a field dependence of the  $\chi_m T$  values in the anomaly, as thus occurs. Measurements at 0.1 T and 1 T have been performed and, as expected, the lower the field the larger the variation of  $\chi_m T$  in the anomaly.

Since compounds **1** and **2** are isomorphous, the absence of this effect for **1** can be explained by considering that the stronger decrease of effective magnetic moment ( $\mu_{\text{eff}}$ ) for Co<sup>II</sup>, due to the spin-orbit coupling, could be obscuring the weak ferromagnetic component.

## Conclusions

Compound **1** and **2** are new examples of the system M–bpa–L where M is a divalent cation and L is N<sub>3</sub>, NCO, NCS or N(CN)<sub>2</sub>. The structural features of all the compounds characterised indicate that only the azido pseudohalide can compete with bpa in the formation of intermetallic bridges. These compounds have bpa intermetallic bridges, so their magnetic interactions are insignificant. On the other hand, the bulkiness of the bpa ligand does not seem to be an impediment for the stabilisation of octahedral spheres consisting of four bpa groups and two pseudohalide ligands for M(1):bpa(2) compounds.<sup>[7c,7d,9c,9d,9e,13]</sup> This is because of the free rotation of the ethyl group.

In relation to M(1):bpa(2) compounds, some additional aspects should be remarked upon. Two polymorphous compounds of formula [Co(NCS)<sub>2</sub>(bpa)<sub>2</sub>] have been reported to date. One of them, by Park et al.,<sup>[14]</sup> consists of interpenetrated 2D units where each octahedral sphere is connected to another four through N,N'–bpa groups. On the contrary, for the second polymorphous compound<sup>[4,9b]</sup> each octahedral sphere is connected to another two through double N,N'–bpa bridges. This latter structural unit is common for the rest of M(1):bpa(2) compounds reported so far<sup>[4,5]</sup> (including compounds **1** and **2**). In fact, there are even more

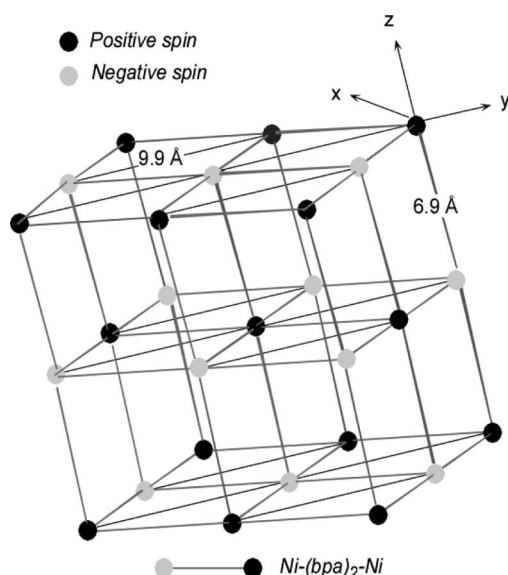


Figure 6. Chart of interactions proposed for compound **2**.

similarities among these structures since not only the resulting chains but also their packing on the *xy* planes are nearly identical for these compounds. What is novel in compounds **1** and **2** is the 2D global network observed in their structures, which gives rise to a 2D effect leading to the ferromagnetic component between the chains.

## Experimental Section

**Synthesis:** The synthesis of compound **1** was carried out by mixing an aqueous solution (10 mL) of KNCO (41 mg, 0.5 mmol) with an aqueous solution (20 mL) of Co(NO<sub>3</sub>)<sub>2</sub>·6H<sub>2</sub>O (73 mg, 0.25 mmol). After 30 min of stirring, a warm methanolic solution (20 mL) of 1,2-bis(4-pyridyl)ethane (bpa) (46 mg, 0.25 mmol) was added. The resulting solution was filtered off the precipitate and was left to stand at room temperature. Several days later, prismatic, pink, X-ray-quality single crystals were obtained. Compound **2** was similarly synthesised by using Ni(NO<sub>3</sub>)<sub>2</sub>·6H<sub>2</sub>O (73 mg, 0.25 mmol). In this case, prismatic, blue, X-ray-quality single crystals were obtained. Elemental analyses results were in good agreement with the structure. **1**: C<sub>26</sub>H<sub>24</sub>CoN<sub>6</sub>O<sub>2</sub> (511.4): calcd. C 61.06, H 4.73, N 16.43; found C 60.12, H 4.71, N 16.40. **2**: C<sub>26</sub>H<sub>24</sub>N<sub>6</sub>NiO<sub>2</sub> (511.2): calcd. C 61.09, H 4.73, N 16.44, found C 60.60, H 4.67, N 16.25.

**Physical Measurements:** Microanalyses were performed with a LECO CHNS-932 analyser. Infrared spectroscopy was performed with a MATTSON FTIR 1000 spectrophotometer over the 400–4000 cm<sup>−1</sup> region. Thermal analyses were obtained by using a TA Instruments SDT-2960 DSC-TGA unit at a heating rate of 5 °C. Diffuse reflectance spectra were recorded at room temperature with a CARY 2415 spectrometer over the range 5000–45000 cm<sup>−1</sup>. ESR spectroscopy was performed on powdered samples at the X-band frequency, with a Bruker ESR 300 spectrometer equipped with a standard OXFORD low-temperature device, which was calibrated by the NMR probe for the magnetic field. The frequency was measured with a Hewlett–Packard 5352B microwave-frequency computer. Magnetic susceptibilities and the magnetisation of powdered samples were carried out over the temperature range 1.8–300 K at values of up to 1000 G for the magnetic field by using a Quantum Design Squid magnetometer, equipped with a helium continuous-flow cryostat. The experimental susceptibilities were corrected for the diamagnetism of the constituent atoms (Pascal tables).<sup>[15]</sup>

**Crystal Structure Determination:** Single-crystal X-ray measurements for compounds **1** and **2** were performed at room temperature with an Enraf–Nonius CAD-4 automatic four-circle diffractometer with graphite-monochromated Mo-*K*<sub>α</sub> radiation ( $\lambda = 0.71070$  Å), operating in the  $\omega/2\theta$  scanning mode by using suitable crystals for data collection. Accurate lattice parameters were determined from the least-squares refinement of 25 well-centred reflections. Intensity data were collected in the  $\theta$  range 2.27–29.96° for compound **1**, and in the  $\theta$  range 2.28–30.08° for compound **2**. During the data collection, two standard reflections, periodically observed, showed no significant variation. Corrections for Lorentz and polarisation factors were applied to the intensity values. The structure was solved by heavy-atom Patterson methods using the program SHELXS97<sup>[16]</sup> and refined by a full-matrix least-squares procedure on  $F^2$  using SHELXL97.<sup>[17]</sup> Non-hydrogen atomic scattering factors were taken from the International Tables of X-ray Crystallography.<sup>[18]</sup> In Table 5 crystallographic data and processing parameters for compounds **1** and **2** are shown. The higher values of  $R_1$  and  $wR_2$  for compound **2** can be associated with the lower quality of the crystals formed. CCDC-206333 (**1**) and -206334 (**2**) contain

the supplementary crystallographic data for this paper. These data can be obtained free of charge from The Cambridge Crystallographic Data Centre via [www.ccdc.cam.ac.uk/data\\_request/cif](http://www.ccdc.cam.ac.uk/data_request/cif).

Table 5. Crystallographic data and refinements for compounds **1** and **2**.

Compound	<b>1</b>	<b>2</b>
Empirical formula	C <sub>26</sub> H <sub>24</sub> CoN <sub>6</sub> O <sub>2</sub>	C <sub>26</sub> H <sub>24</sub> N <sub>6</sub> NiO <sub>2</sub>
$M_r$ [g mol <sup>−1</sup> ]	511.4	511.2
Crystal system	monoclinic	monoclinic
Space group	<i>C2/c</i>	<i>C2/c</i>
<i>a</i> [Å]	18.814(3)	18.746(7)
<i>b</i> [Å]	9.945(3)	9.869(6)
<i>c</i> [Å]	13.995(2)	13.914(4)
$\beta$ [°]	107.77(1)	107.58(3)
<i>V</i> [Å <sup>3</sup> ]	2493.6(9)	2454(2)
$\rho_{\text{calcd.}}$ [g cm <sup>−3</sup> ]	1.362	1.384
$\rho_{\text{obsd.}}$ [g cm <sup>−3</sup> ]	1.40	1.43
$\mu$ [mm <sup>−1</sup> ]	0.723	0.826
<i>F</i> (000)	1060	1064
$\theta$ range [°]	2.27–29.96	2.28–30.08
Collected reflections	3699	3650
Independent reflections	3602	3554
Parameters	159	159
$R_1(F_o)^{[a]}$	0.076	0.1046
$wR_2(F_o^2)^{[b]}$	0.1774	0.205
$\Delta\rho_{\text{max}}/\Delta\rho_{\text{min}}$ [e Å <sup>−3</sup> ]	0.926/−0.935	1.494/−0.836

[a]  $R_1(F_o) = [(\sum |F_o| - |\sum F_c|)/(\sum F_o)]$ . [b]  $wR_2(F_o^2) = \{\sum [w(F_o^2 - F_c^2)^2]/\sum [w(F_o^2)^2]\}^{1/2}$ ;  $w = 1/[\sigma^2(F_o) + (0.03P)^2]$ ,  $P = (F_o^2 + 2F_c^2)/3$ .

**Supporting Information** (see footnote on the first page of this article): Structure views, IR and UV/Vis spectra, and TG curves for **1** and **2**.

## Acknowledgments

This work was supported by the Universidad del País Vasco (UPV/EHU) (00169.125-13956/2004), the Ministerio de Ciencia y Tecnología (MCYT) (CTQ2005-05778-PPQ) and the Gobierno Vasco (Project IT-282-07). N. d. l. P. thanks the UPV/EHU for financial support from “Convocatoria para la concesión de ayudas de especialización para investigadores doctores (2008)”.

- [1] a) M. Moon, I. Kim, M. S. Lah, *Inorg. Chem.* **2000**, *39*, 2710–2711; b) L. Carlucci, G. Ciani, D. M. Proserpio, S. Rizzato, *Chem. Commun.* **2000**, 1319–1320; c) L. Carlucci, G. Ciani, D. M. Proserpio, S. Rizzato, *J. Chem. Soc., Dalton Trans.* **2000**, 3821–3828; d) J. Lu, B. Moulton, M. J. Zaworotko, S. A. Bourne, *Chem. Commun.* **2001**, 861–862; e) J. Y. Lu, A. Babb, *Inorg. Chim. Acta* **2001**, *318*, 186–190; f) L. Carlucci, G. Ciani, D. M. Proserpio, S. Rizzato, *Chem. Commun.* **2001**, 1198–1199; g) M. J. Plater, M. R. St. J. Foreman, J. M. S. Skakle, *Cryst. Eng.* **2001**, *4*, 293–308; h) Z.-Y. Fu, X.-T. Wu, J.-C. Dai, L.-M. Wu, C.-P. Cui, S.-M. Hu, *Chem. Commun.* **2001**, 1856–1857; i) F. A. Almeida Paz, A. D. Bond, Y. Z. Khimyak, J. Klinowski, *New J. Chem.* **2002**, *26*, 381–383; j) Z.-Y. Fu, X.-T. Wu, J.-C. Dai, S.-M. Hu, W.-X. Du, H.-H. Zhang, R.-Q. Sun, *Eur. J. Inorg. Chem.* **2002**, 2730–2735; k) F. A. Almeida Paz, Y. Z. Khimyak, A. D. Bond, J. Rocha, J. Klinowski, *Eur. J. Inorg. Chem.* **2002**, 2823–2828; l) D. Ghoshal, T. K. Maji, G. Mostafa, T.-H. Lu, N. R. Chaudhuri, *Cryst. Growth Des.* **2003**, *3*, 9–11; m) J.-C. Dai, X.-T. Wu, S.-M. Hu, Z.-Y. Fu, J.-J. Zhang, W.-X. Du, H.-H. Zhang, R.-Q. Sun, *Eur. J. Inorg. Chem.* **2004**, 2096–2106; n) T. Sunahara, S. Onaka, M. Ito, H. Imai, K. Inoue, T. Ozeki, *Eur. J. Inorg. Chem.* **2004**, 4882–4890; o) T. K. Maji, M. Ohba, S. Kitagawa, *Inorg. Chem.* **2005**, *44*, 9225–



- 9231; p) C.-Y. Sun, X.-J. Zheng, S. Gao, L.-C. Li, L.-P. Jin, *Eur. J. Inorg. Chem.* **2005**, 4150–4159; q) S. Wang, H. Xing, Y. Li, J. Bai, Y. Pan, M. Scheer, X. You, *Eur. J. Inorg. Chem.* **2006**, 3041–3053; r) J. Lewinski, W. Bury, I. Justyniak, J. Lipkowski, *Angew. Chem. Int. Ed.* **2006**, 45, 2872–2875; s) K. Liang, H.-G. Zheng, Y.-Z. Li, X.-Q. Xin, *Inorg. Chem. Commun.* **2007**, 10, 1164–1167; t) W.-H. Zhang, Y.-L. Song, Z.-G. Ren, H.-X. Li, L.-L. Li, Y. Zhang, J.-P. Lang, *Inorg. Chem.* **2007**, 46, 6647–6660; u) P. Vaqueiro, M. L. Romero, *J. Am. Chem. Soc.* **2008**, 130, 9630–9631; v) Z. Fu, J. Yi, Y. Chen, S. Liao, N. Guo, J. Dai, G. Yang, Y. Lian, X. Wu, *Eur. J. Inorg. Chem.* **2008**, 628–634; w) L.-F. Ma, L.-Y. Wang, Y.-Y. Wang, M. Du, J.-G. Wang, *CrystEngComm* **2009**, 11, 109–117.
- [2] M. L. Hernández, M. G. Barandika, M. K. Urtiaga, R. Cortés, L. Lezama, M. I. Arriortua, *J. Chem. Soc., Dalton Trans.* **2000**, 79–84.
- [3] S. Martin, Ph. D. Thesis, **2002**.
- [4] M. L. Hernández, M. G. Barandika, M. K. Urtiaga, R. Cortés, L. Lezama, M. I. Arriortua, T. Rojo, *J. Chem. Soc., Dalton Trans.* **1999**, 1401–1406.
- [5] M. L. Hernández, M. K. Urtiaga, M. G. Barandika, R. Cortés, L. Lezama, N. De La Pinta, M. I. Arriortua, T. Rojo, *J. Chem. Soc., Dalton Trans.* **2001**, 3010–3014.
- [6] a) Q.-M. Wang, G.-C. Guo, T. C. W. Mak, *Chem. Commun.* **1999**, 1849–1850; b) M. J. Plater, M. R. S. J. Foreman, R. A. Howie, J. M. S. Skakle, *Inorg. Chim. Acta* **2001**, 318, 175–180; c) Y.-Y. Niu, H.-W. Hou, Q.-F. Zhang, X.-Q. Xin, H.-K. Fun, S. Chantapromma, I. A. Razak, *Acta Crystallogr., Sect. C* **2001**, 57, 526–527; d) G. Mahmoudi, A. Morsali, L.-G. Zhu, *Polyhedron* **2007**, 26, 2885–2893.
- [7] a) J. Carranza, C. Brennan, J. Sletten, F. Lloret, M. Julve, *J. Chem. Soc., Dalton Trans.* **2002**, 3164–3170; b) S. Dalai, P. S. Mukherjee, E. Zangrando, N. R. Chaudhuri, *New J. Chem.* **2002**, 26, 1185–1189; c) S. Dalai, P. S. Mukherjee, J. Ribas, C. Diaz, E. Zangrando, N. R. Chaudhuri, *Indian J. Chem., Sect. A: Inorg., Bio-inorg., Phys., Theor. Anal. Chem.* **2003**, 42, 2250–2255; d) T. K. Maji, R. Matsuda, S. Kitagawa, *Nat. Mater.* **2007**, 6, 142–148.
- [8] a) C. S. Hong, S.-K. Son, Y. S. Lee, M.-J. Jun, Y. Do, *Inorg. Chem.* **1999**, 38, 5602–5610; b) S. Konar, E. Zangrando, M. G. B. Drew, T. Mallah, J. Ribas, N. R. Chaudhuri, *Inorg. Chem.* **2003**, 42, 5966–5973.
- [9] a) C. Merz, M. Desciak, C. O'Brien, R. L. LaDuca, R. C. Finn, R. S. Rarig, J. A. Zubieta, *Inorg. Chim. Acta* **2004**, 357, 3331–3335; b) C. Seop Hong, Y. S. Youa, *Inorg. Chim. Acta* **2004**, 357, 2309–2314; c) T. Morita, Y. Asada, T. Okuda, S. Nakashima, *Bull. Chem. Soc. Jpn.* **2006**, 79, 738–744; d) M.-C. Suen, J.-C. Wang, *Struct. Chem.* **2006**, 17, 315–322; e) T. Morita, S. Nakashima, K. Yamada, K. Inoue, *Chem. Lett.* **2006**, 35, 1042–1043.
- [10] a) K. Nakamoto in *Infrared Spectra of Inorganic Compounds and Coordination Compounds*, New York, **1997**; b) E. Pretsch, T. Clerc, J. Seibl, W. Simon in *Tablas para la elucidación estructural de compuestos orgánicos por métodos espectroscópicos*, Barcelona, **1980**.
- [11] a) A. B. P. Lever in *Inorganic Electronic Spectroscopy*, Elsevier, London, **1984**; b) Y. Tanabe, S. Sugano, *J. Phys. Soc. Jpn.* **1954**, 9, 753.
- [12] A. Abragam, M. H. L. Pryce, *Proc. R. Soc. London, Ser. A* **1951**, 206, 173.
- [13] M. Kondo, M. Shimamura, S.-I. Noro, Y. Kimura, K. Uemura, S. Kitagawa, *J. J. Solid State Chem.* **2000**, 152, 113–119.
- [14] S. H. Park, K. M. Kim, S.-G. Lee, O.-S. Jung, *Bull. Korean Chem. Soc.* **1998**, 19, 79–82.
- [15] A. Earnshaw, *Introduction to Magnetochemistry*, Academic Press, London, **1968**.
- [16] G. M. Sheldrick, *SHELXS97, Program for the Solution of Crystal Structures*, University of Göttingen, Germany, **1997**.
- [17] G. M. Sheldrick, *SHELXL97, Program for the Refinement of Crystal Structures*, University of Göttingen, Germany, **1997**.
- [18] D. T. Cromer and J. T. Waber, *International Tables for X-ray Crystallography*, Kynoch Press, Birmingham, **1974**, vol. IV.

Received: February 4, 2010  
Published Online: June 17, 2010

# Ternary Rare Earth Inorganic–Organic Hybrids with a Mercapto-Functionalized Si–O Linkage and a Polymer Chain: Coordination Bonding Assembly and Luminescence

Kai Sheng,<sup>[a]</sup> Bing Yan,<sup>\*[a]</sup> Hai-Feng Lu,<sup>[a]</sup> and Lei Guo<sup>[a]</sup>

**Keywords:** Organic-inorganic hybrid composites / Rare earths / Polymers / Bridging ligands / Sulfur / Luminescence

A series of ternary organic/inorganic/polymer hybrid materials have been assembled on the basis of the coordination chemistry principle. Mercapto-functionalized MBA-Si from MBA (4-mercaptobenzoic acid) behaves as the first coordination unit, which forms sulfide linkages, resulting in an inorganic Si–O network after hydrolysis and copolycondensation with TEOS (tetraethoxysilane). The organic polymers PVPD [poly(4-vinylpyridine)] and PMMA [poly(methyl methacrylate)] play a role of the second coordination unit, whose or-

ganic polymeric C–C chain originates from addition polymerization of the monomers 4-VPD (4-vinylpyridine) and MMA (methyl methacrylate), respectively. These hybrids are characterized in detail to compare with the binary hybrids without an organic polymer unit, whose results reveal that the microstructure, the thermal stability, and especially the photoluminescence properties of the hybrid system are improved with the introduction of the polymer as the coligand.

## Introduction

The study on luminescent rare earth (especially  $\text{Eu}^{3+}$  and  $\text{Tb}^{3+}$ ) complexes has gained great interest during the past decades for their fascinating properties including high quantum efficiency, narrow emission bands, high color purity, large Stokes shifts, and long lifetime, which can be expected to have large potential applications in the fields of luminescent sensors, lasers, fluorescent probes, light-emitting diodes, optical amplifiers, and so on.<sup>[1]</sup> Nevertheless, due to their poor thermal stability and low mechanical resistances, rare earth complexes have been excluded from practical applications.<sup>[2]</sup> Therefore, many researchers incorporate rare earth complexes into an inert host (silica gel or polymer matrix) to construct organic–inorganic hybrids by using the sol–gel method<sup>[3,4]</sup> to combine remarkable mutual features of both organic and inorganic components.<sup>[5]</sup>

Typically, according to the interfacial force between the organic and inorganic phases of the hybrid materials, the synthetic procedures can be categorized into two main routes.<sup>[6]</sup> One is called the conventional doping method: the organic compound is dispersed or dissolved into an inorganic host through weak physical interactions (such as hydrogen bonding, van der Waals forces, or electrostatic forces)<sup>[7]</sup> and easily introduces inhomogeneity and leaching or clustering of the photoactive center, which results from

the high vibration energy of the hydroxy groups surrounding rare earth ions. The other synthesis method involving covalent bonds can avoid these shortcomings. The resulting hybrid materials show improved chemical stability and compatibility owing to the covalent linking of the two parts.<sup>[8]</sup> Thus, more and more attention has been paid to the chemically bonding method to construct organic–inorganic hybrid materials. Carlos et al. have done important work and have lately written a review on lanthanide-containing light-emitting organic–inorganic hybrids.<sup>[9]</sup> More recently, Binnemans gives a more extensive overview of the different types of lanthanide-based hybrid materials and compared their respective advantages and disadvantages.<sup>[10]</sup>

The critical step to assemble molecular-based hybrid materials is to design a functional molecular bridge that can coordinate rare earth ions and covalently bond to siloxanes.<sup>[11]</sup> Our group has realized six main modification paths, amino group, carboxyl group, hydroxy group, sulfonic group, and methylene group modification, and further introduced an organic polymer into the hybrid materials not only as a matrix but also as a component that can coordinate to the rare earth ions through the oxygen or nitrogen atom, as they have attractive properties such as low cost, light weight, easy to fabricate, and convenient to control various optical parameters.<sup>[12]</sup> In our organic/inorganic/polymer hybrid materials, the bridge molecule acts as small molecular ligand and the polymer acts as a macromolecular ligand or coligand.<sup>[13]</sup> Under these circumstances, both the small bridge molecules and the polymer can absorb excitation energy and transfer it to rare earth ions to obtain hybrid materials with excellent luminescent properties.

[a] Department of Chemistry, Tongji University, Siping Road 1239, Shanghai 200092, P. R. China  
Fax: +86-21-65982287  
E-mail: byan@tongji.edu.cn

Supporting information for this article is available on the WWW under <http://dx.doi.org/10.1002/ejic.201000273>.

In this paper, a mercapto-group-functionalized aromatic compound is selected for the preparation of the precursor, for the mercapto group is very active in many reactions.<sup>[14]</sup> Binary organic–inorganic hybrids based on 2-MBA (2-mercaptobenzoic acid) have been investigated in detail.<sup>[15]</sup> Here, we construct the ternary rare earth (Eu, Tb) organic/inorganic/polymeric hybrid materials based on 4-MBA by using a different polymer and the sol–gel method, and we synthesized the binary organic–inorganic hybrids simultaneously for comparison.

## Results and Discussion

The scheme for the synthesis process and the predicted compositions of the precursors and the binary and ternary hybrid materials are presented in Figure 1 and Figures S1 and S2 in the Supporting Information. As we know, it is very difficult to prove the exact structure of these kinds of noncrystalline hybrid materials, and it is hardly possible to solve the coordination behavior of rare earth ions. However, the main composition and their coordination effects can be predicted according to the rare earth coordination chemistry principle and the organic functional groups present. Considering the molecular structure of ligands 4-MBA-Si (P<sup>1</sup>, P<sup>2</sup>, P<sup>3</sup>), the carboxylate group remains after the mercapto modification of 4-MBA. So it can be assumed that the three COO<sup>-</sup> groups can provide six coordination sites from the chemical behavior of the aromatic carboxylates.<sup>[16]</sup> The S atom in the sulfide linkage is not coordinated to the rare earth ions because of its large steric hindrance and its weak coordination ability. For the ternary hybrids introduced by polymers PVPD [poly(4-vinylpyridine)] and PMMA [poly(methyl methacrylate)], the functional groups within them can provide one coordinated nitrogen atom (pyridine of PVPD) or oxygen atom (methacrylate of PMMA). Furthermore, according to the previous research of Horrocks,<sup>[17]</sup> it can be deduced that one or two water molecules may participate in the coordination of these hybrids. The prediction has also been confirmed by infrared spectra. Here it needs to be referred that the scheme is only to show the average coordination chemistry behavior around rare earth ions, which does not represent the exact structure of the hybrids.

The Fourier transform infrared spectra of the initial ligand MBA and the three precursors (P<sup>1</sup> denote MBA-TEPIC, P<sup>2</sup> denote MBA-APS and P<sup>3</sup> denote MBA-CPS, where TEPIC = 3-(triethoxysilyl)propyl isocyanate, APS = (3-aminopropyl)trimethoxysilane, and CPS = (3-chloropropyl)trimethoxysilane) are presented in Figure 2a. As is clearly seen, there exists a broad band centered at around 2934 and 2874 cm<sup>-1</sup> in the three precursors, which can be ascribed to the asymmetric stretching vibration and symmetric stretching vibration for the methylene (-CH<sub>2</sub>-) group of the coupling reagents. The vanishing of the  $\nu(\text{S-H})$  at 2541 cm<sup>-1</sup> for the three precursors compared to MBA and the appearance of the  $\nu(\text{C-S-C})$  at 696 cm<sup>-1</sup> suggest the modification of the coupling reagent. The large broad band

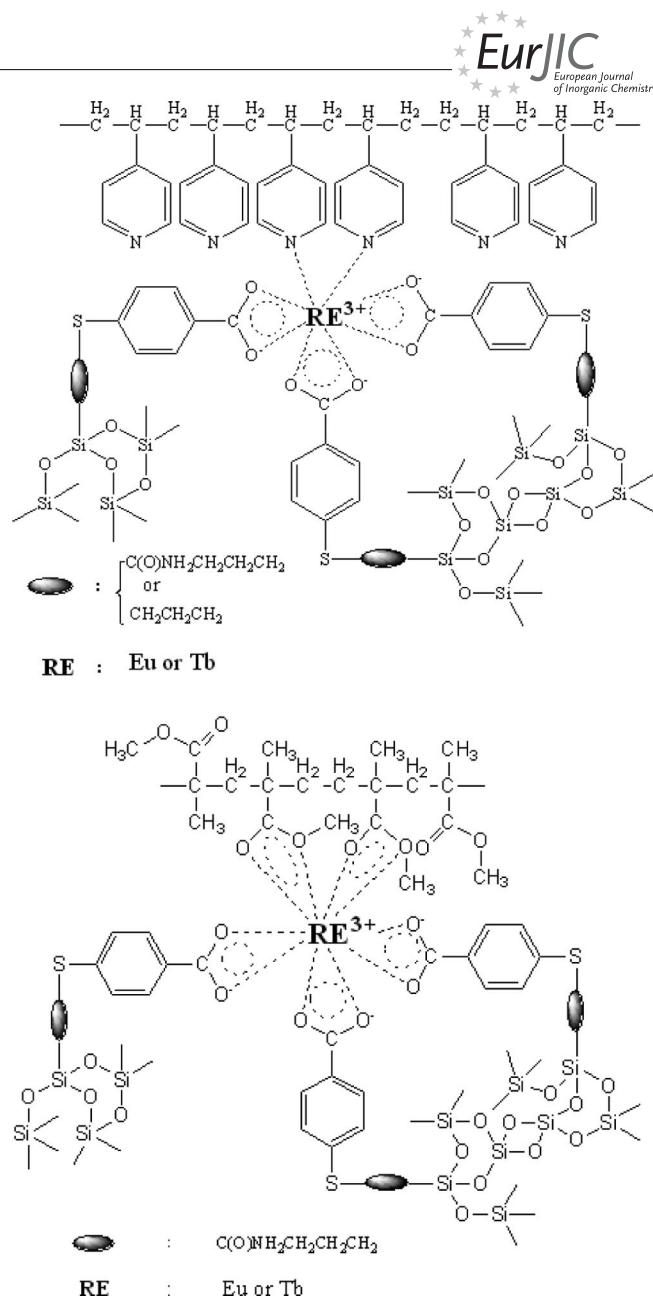


Figure 1. The predicted structure of the ternary hybrid materials.

at about  $3414\text{ cm}^{-1}$  and the low absorption peak at  $921\text{ cm}^{-1}$  in the three precursors are assigned to the stretching vibration and the out-of-plane bending vibration of O–H. The disappearance of the stretch vibration of (N=C=O) at  $2250\text{--}2275\text{ cm}^{-1}$  for P<sup>1</sup>, the  $\nu(\text{N–H})$  at  $1209\text{ cm}^{-1}$  for P<sup>2</sup>, and the  $\nu(\text{C–Cl})$  at  $800\text{ cm}^{-1}$  for P<sup>3</sup> indicate the coupling reagent is grafted onto MBA. Additionally, the existence of a stretching vibration of Si–C at  $1196\text{ cm}^{-1}$  and the stretching vibration of Si–O at  $1099$  and  $1047\text{ cm}^{-1}$  suggest the formation of the siloxane bonds. Figure 2b shows the FTIR spectra of selected hybrid materials. The two absorption bands at  $1594$  and  $1424\text{ cm}^{-1}$  correspond to the symmetric vibration and asymmetric vibration of the carbonyl group ( $\text{COO}^-$ ), respectively. The three absorption bands around  $2934\text{ cm}^{-1}$  are due to the  $-\text{CH}_2-$  vibration, and the broad band at  $3396\text{ cm}^{-1}$  corresponds to the O–H (vs). The strong

peak at  $1383\text{ cm}^{-1}$  is assigned to the stretching vibration of  $\text{NO}_3^-$ , which indicates the nitrate group is not coordinated to  $\text{RE}^{3+}$ . Further, there also exists the Eu–O vibration at  $545\text{ cm}^{-1}$  which suggests the carbonyl group  $\text{COO}^-$  is coordinated to the rare earth ions. For PVPD-Eu- $\text{M}^1$ , the Eu–N vibration is located at  $476\text{ cm}^{-1}$ .

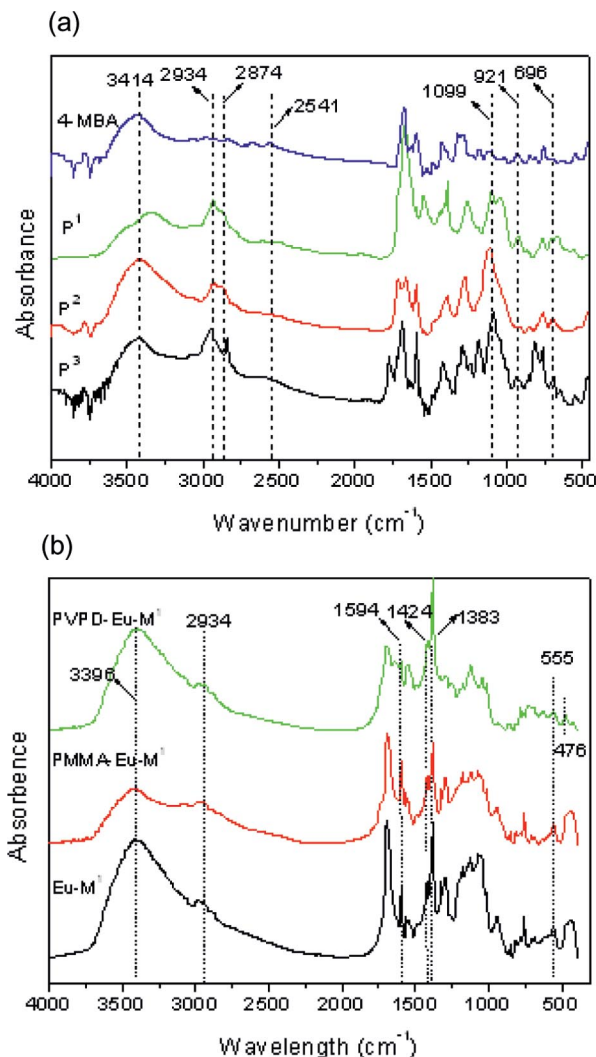


Figure 2. FTIR spectra of (a) the free ligand MBA and the three precursors MBA-Si ( $\text{P}^1$ ,  $\text{P}^2$ ,  $\text{P}^3$ , respectively) and (b) for the selected hybrids.

Figure 3 shows the ultraviolet absorption spectra ( $5 \times 10^{-4}\text{ M}$  DMF solution) of MBA,  $\text{P}^1$ ,  $\text{P}^2$ , and  $\text{P}^3$ . It is observed that there exists a broad absorption band for each compound (at 273, 264, 279, and 280 nm for MBA,  $\text{P}^1$ ,  $\text{P}^2$ , and  $\text{P}^3$ , respectively), which is ascribed to the major  $\pi$ – $\pi^*$  electronic transitions. Comparing the precursors with the original compound MBA, a blueshift (about 9 nm) of the absorption peak appears for  $\text{P}^1$ , whereas for  $\text{P}^2$  (about 6 nm) and  $\text{P}^3$  (about 7 nm) it shifted to a longer wavelength. This phenomenon indicates that the electron distribution of the conjugating system has changed after modification of MBA. Besides, we also can infer that the coupling reagents are grafted to MBA successfully.

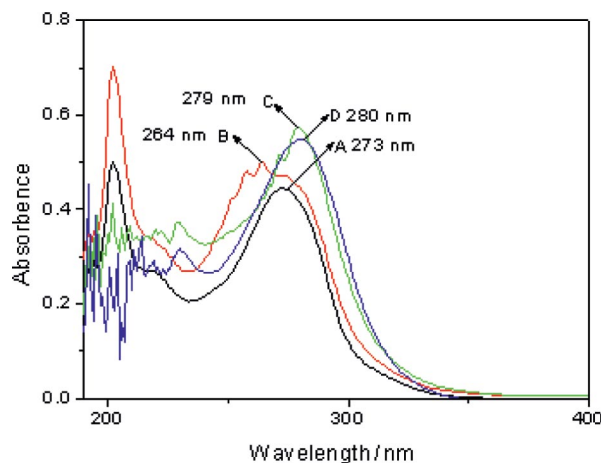


Figure 3. The ultraviolet absorption spectra of the free ligand MBA (A), precursors  $\text{P}^1$  (B), precursor  $\text{P}^2$  (C), and precursor  $\text{P}^3$  (D).

Figure S3 (Supporting Information) presents the X-ray diffraction (from  $10$  to  $70^\circ$ ) spectra of the selected hybrid materials Eu- $\text{M}^1$ , PVPD-Eu- $\text{M}^1$ , and PMMA-Eu- $\text{M}^1$ , which reveal that all the obtained hybrid materials are amorphous in the whole range. All the materials exhibit similar XRD patterns with a broad peak centered at around  $23^\circ$ , which is the characteristic diffraction of amorphous siliceous backbone material.<sup>[18]</sup> By comparison to the binary hybrids, there is no new diffraction peaks for the ternary hybrids with PVPD or PMMA, which show that the introduction of the macromolecular ligands in the hybrid system cannot affect the disordered silicon skeleton. Furthermore, there are many narrow weak peaks in these samples, corresponding to the incomplete hydrolysis–condensation of the excessive TEOS (tetraethoxysilane) molecules. TEOS molecules can carry on the hydrolysis–condensation process themselves or with a silane coupling reagent. If the hydrolysis–condensation process of the excessive TEOS molecules takes place among themselves, the ordered Si–O network can form a better crystal state. Then the narrow peaks appear, but the small amount of the ordered Si–O network brings the weak intensity. In addition, neither of the samples exhibit measurable amounts of the phase corresponding to the free ligands or the free salts, which can support the formation of the covalently bonded hybrids.

The DSC and TGA data for the ternary polymeric hybrid material PVPD-Eu- $\text{M}^1$  (Figure 4) shows 9% weight loss at  $170^\circ\text{C}$ , which is due to the loss of the residual and coordinated water molecule. Between  $170$  and  $600^\circ\text{C}$ , a weight loss of 37% is observed, which is ascribed to the decomposition of the organics in the material. Corresponding with this weight loss, are two obvious exothermic peaks at  $210$  and  $530^\circ\text{C}$  observed from the DSC curve, which is concordant with the pyrolysis of the material releasing energy. There are additional weight losses of 4% between  $600$  and  $800^\circ\text{C}$  and a very gradual loss of 1% at  $1000^\circ\text{C}$  without obvious absorbing and releasing energy in the DSC curve. The residual weight (49%) is mainly inorganic Si–O



networks ( $1090\text{ cm}^{-1}$  in FTIR). The results show that this kind of organic/inorganic/polymeric hybrid material is stable under  $210^\circ\text{C}$ . This thermal stability is higher than the pure complex and also better than the binary organic/inorganic hybrid material according to the literature.<sup>[15]</sup>

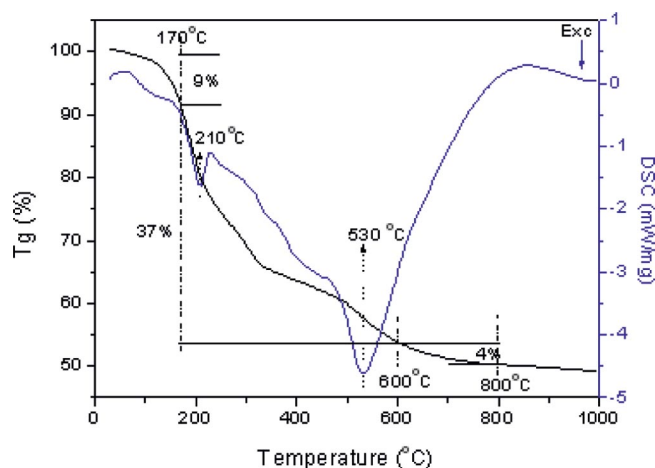


Figure 4. Selected DSC and TGA traces of the ternary hybrid material PVPD-Eu-M<sup>1</sup>.

Figure S4 (Supporting Information) and Figure 5 show the micrographs of the selected binary and ternary hybrid materials, respectively. It can be seen from the images of all hybrids that homogeneous systems are formed. Moreover, phase separation phenomenon cannot be observed, which always appears in the conventional doping method. By comparison with the binary and the ternary hybrid materials, we can observe distinct differences of the micro-morphology. For the binary hybrids, the microstructure exhibits the irregular shaped particles on the surface, whereas for the ternary hybrids, a more regular and uniform microstructure with ordered morphology on the surface can be obviously observed. This result verifies that the organic polymer (organic polymeric chains) may play an important role in the formation of the ultimate complicated hybrid system. For ternary hybrids, Figure 5a exhibits a petal-shaped, flake-layered, and globular structure. Figure 5b presents very ordered dendritic structure. Figure 5c,d show the perthitic structure with many small irregular particles on the surface. Figure 5e displays a regular and ordered globular structure. Figure 5f also has many ordered stripes with many small-sized uniform flake layers on the surface, which is amplified and clearly shown in Figure 5g for analysis. The luminescent center with the polymer is firstly accomplished by chelation not only through a small bridge molecule MBA-Si but also through macromolecular ligands PVPD or PMMA. Owing to the coordination effect and the steric hindrance of the polymer (as the terminal ligand), the structure of the luminescent center becomes rigid. Subsequently, the cohydrolysis and copolycondensation process is completed around the luminescent center. Therefore, it is easy to form a flake or globular structure. The flake structure can be stacked to petal shaped or layer shaped under different experimental conditions (polarity of the solvent,

for example). Moreover, the polymers PVPD or PMMA behave as the terminal ligand through simple chelation of the nitrogen or oxygen atom. The long organic chains supply the template effect to induce the cohydrolysis and copolycondensation process, which results in the long dendritic or stripe-shaped morphology. In summary, we can conclude that a more ordered and regular microstructure can be achieved with the introduction of the polymer.

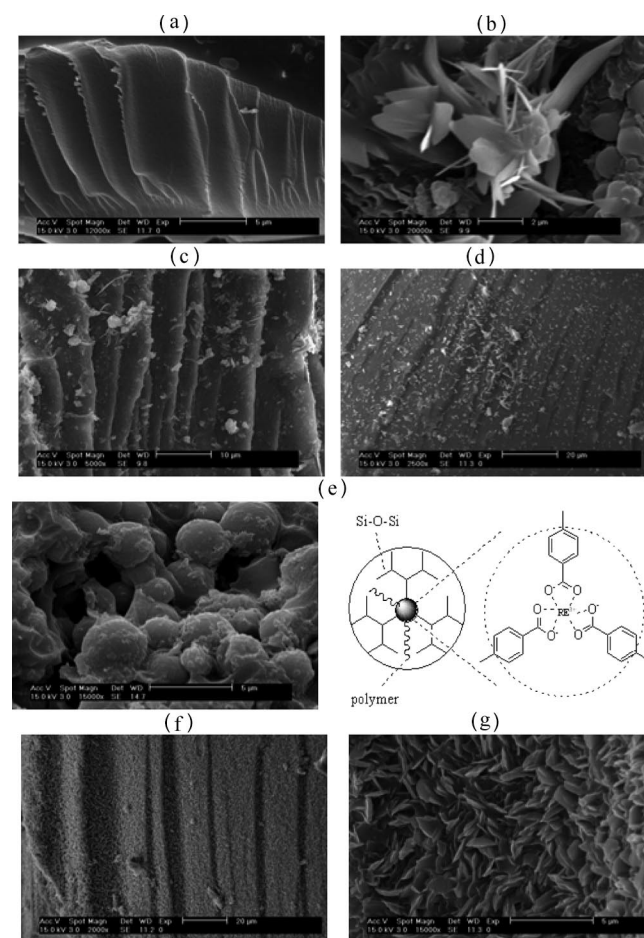


Figure 5. SEM images of the ternary hybrid materials: (a) PVPD-Eu-M<sup>1</sup>, (b) PMMA-Eu-M<sup>1</sup>, (c) PMMA-Eu-M<sup>2</sup>, (d) PVPD-Eu-M<sup>3</sup>, (e) PVPD-Tb-M<sup>1</sup>, (f) PMMA-Tb-M<sup>3</sup>, (g) amplified image of (f).

Figure S5 (Supporting Information) exhibits the UV/Vis diffuse reflection absorption spectra of selected europium and terbium hybrids. As can be seen, there is a large broad absorption band in each hybrid that is attributed to the  $\pi$ – $\pi^*$  electronic transition of the aromatic ring in the hybrid system. It is worth noting that the large broad band overlaps from 220 to 500 nm, which proves that not only the small molecular ligand MBA could absorb abundant energy in the UV/Vis region, but the macromolecular ligand PVPD or PMMA can also enhance the absorbance ability. This energy can be transferred to rare earth ions through the “antenna effect” and sensitize the rare earth ions.

Figure 6 show the selected excitation spectra of all the europium hybrid materials in the solid state at room temperature, which are preformed under the maximum wave-

length of 613 nm for  $\text{Eu}^{3+}$ . A broad absorption band in the range from 220 to 450 nm is attributed to the mercapto-modified Si–O linkage host.<sup>[19]</sup> Here, the organically modified Si–O hybrid hosts not only behaves as the host but also as the ligands for the coordination bonds between MBA-Si ( $\text{M}^1$ ,  $\text{M}^2$ ,  $\text{M}^3$ ) and  $\text{Eu}^{3+}$ .<sup>[20]</sup> The absorption of the photoactive organically modified group and the –Si–O– network both play a role in the energy transfer and luminescence of  $\text{Eu}^{3+}$  within the hybrid systems. It is noteworthy that the wide excitation bands should contain the charge transfer state of Eu–O between  $\text{Eu}^{3+}$  and the MBA-Si unit. Besides, the weak narrow lines located at 393 nm are probably due to transitions within the  $4f^6$  configuration of  $\text{Eu}^{3+}$  ( $^7\text{F}_0 \rightarrow ^5\text{L}_6$  transition) and overlapped with the wide excitation of the host.<sup>[21]</sup>

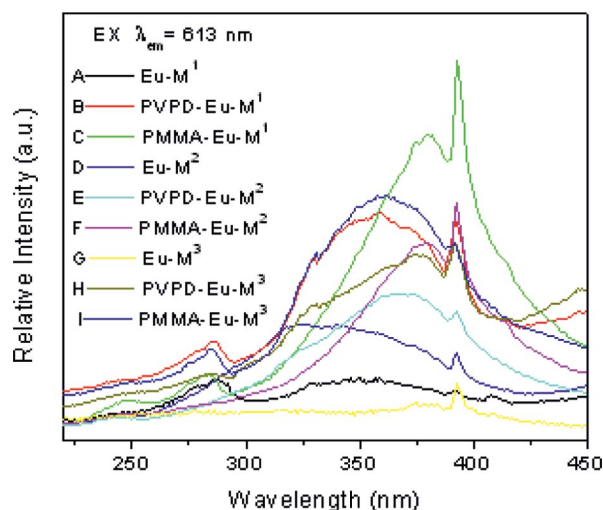


Figure 6. Selected excitation spectra of the europium hybrid materials; the curves from A to I denote Eu/Tb- $\text{M}^1$ , PVPD-Eu/Tb- $\text{M}^1$ , PMMA-Eu/Tb- $\text{M}^1$ , Eu/Tb- $\text{M}^2$ , PVPD-Eu/Tb- $\text{M}^2$ , PMMA-Eu/Tb- $\text{M}^2$ , Eu/Tb- $\text{M}^3$ , PVPD-Eu/Tb- $\text{M}^3$ , PMMA-Eu/Tb- $\text{M}^3$ , respectively.

Figure 7 presents the luminescence spectra of ternary europium and terbium organic/inorganic/polymeric hybrid materials in the visible range (from 550 to 700 nm for europium and from 400 to 600 nm for terbium). For europium hybrids, all the emission spectra display the characteristic  $\text{Eu}^{3+}$   $^5\text{D}_0 \rightarrow ^7\text{F}_J$  ( $J = 0-4$ ) intra- $4f^6$  transitions at 575, 589, 614, 649, and 700 nm, respectively.<sup>[19]</sup> Among these emission peaks, the orange emission at 589 nm and the predominant red emission at 614 nm (associated with  $^5\text{D}_0 \rightarrow ^7\text{F}_1$  and  $^5\text{D}_0 \rightarrow ^7\text{F}_2$  transitions, respectively) are obviously observed, whereas the other transitions are relatively weaker. The detailed luminescence data are shown in Table 1. As we know, the  $^5\text{D}_0 \rightarrow ^7\text{F}_2$  transition is the electric dipole transition with hypersensitivity to the local symmetry of the coordination sphere of the  $\text{Eu}^{3+}$  ions, whereas the magnetic dipole transition  $^5\text{D}_0 \rightarrow ^7\text{F}_1$  is practically independent of the host material, so the intensity ratio of the red and orange intensities is considered as the coefficient to the symmetry around  $\text{Eu}^{3+}$ . When the ratio is higher, the europium ion generally occupies a lower symmetry microenvironment,<sup>[22]</sup> and the data shown in Table 1 indicate that the europium ion may oc-

cupy the low symmetry sphere in ternary hybrids containing PMMA. For terbium hybrids, we can see that the narrow emission lines are recorded upon a broad emission band from 350 to 650 nm. The narrow lines are ascribed to the characteristic  $\text{Tb}^{3+}$  emission with peaks at 486, 542, 581, and 618 nm corresponding to  $^5\text{D}_4 \rightarrow ^7\text{F}_J$  ( $J = 6-3$ ), respectively, whereas the broad band are attributed to the emission of the organically modified Si–O group that is not transferred to the terbium ion.

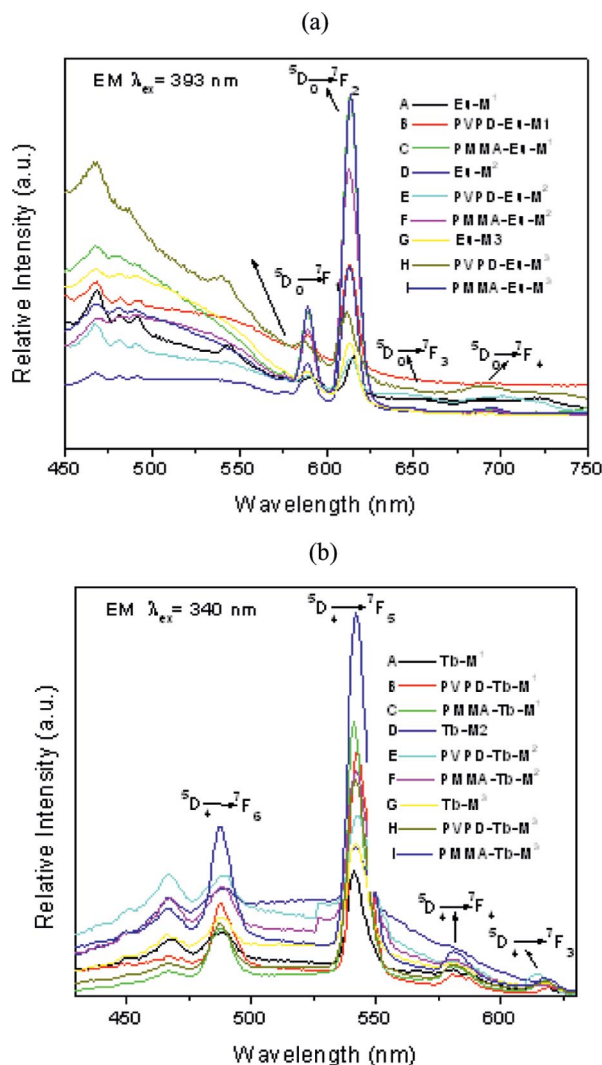


Figure 7. The emission spectra of (a) Eu hybrids and (b) Tb hybrids; the curves from B to J denote Eu/Tb- $\text{M}^1$ , PVPD-Eu/Tb- $\text{M}^1$ , PMMA-Eu/Tb- $\text{M}^1$ , Eu/Tb- $\text{M}^2$ , PVPD-Eu/Tb- $\text{M}^2$ , PMMA-Eu/Tb- $\text{M}^2$ , Eu/Tb- $\text{M}^3$ , PVPD-Eu/Tb- $\text{M}^3$ , PMMA-Eu/Tb- $\text{M}^3$ , respectively.

For further investigation of the photoluminescence properties, we measure the decay curves of all the europium and terbium hybrid materials at room temperature. All the typical decay curves can be described as a single exponential ( $\ln[S(t)/S_0] = -k_1t = -t/\tau$ ; Figure S6 in the Supporting Information shows the decay curve of the Eu- $\text{M}^1$  hybrids). The resulting luminescent lifetimes of the europium hybrids are summarized in Table 1. Furthermore, we selectively determined the emission quantum efficiency of the  $^5\text{D}_0$   $\text{Eu}^{3+}$  excited state for europium-containing hybrids on the basis of

Table 1. Luminescence efficiencies and lifetimes for the europium hybrid materials.

Hybrid Materials	$I_{02}/I_{01}$ <sup>[a]</sup>	$\tau$ [ms] <sup>[b]</sup>	$A_r$	$A_{nr}$	$\eta$ [%] <sup>[c]</sup>	$n_w$
Eu-M <sup>1</sup>	2.67	0.432	195	2120	8	~
PVPD-Eu-M <sup>1</sup>	3.77	0.485	224	1839	11	~2
PMMA-Eu-M <sup>1</sup>	3.65	1.052	241	951	25	~1
Eu-M <sup>2</sup>	2.21	0.478	176	1916	8	~2
PVPD-Eu-M <sup>2</sup>	3.49	0.618	228	1390	14	~1.5
PMMA-Eu-M <sup>2</sup>	3.52	0.794	229	1030	18	~1
Eu-M <sup>3</sup>	2.25	0.43	194	2132	8	~2
PVPD-Eu-M <sup>3</sup>	3.03	0.658	187	1333	12	~1.5
PMMA-Eu-M <sup>3</sup>	3.31	0.958	220	824	21	~1

[a] Integrated intensity of the  $^5D_0 \rightarrow ^7F_J$  emission curves. [b] For the  $^5D_0$  excited state of  $Eu^{3+}$ , whose error is  $\pm 50$   $\mu$ s. [c] For  $^5D_0$  quantum efficiency.

emission spectra and the lifetimes of the  $^5D_0$  emitting level. Assuming that only nonradiative and radiative processes are essentially involved in the depopulation of the  $^5D_0$  state,  $\eta$  can be defined by Equation (1).<sup>[23]</sup>

$$\eta = \frac{A_r}{A_r + A_{nr}} \quad (1)$$

Here,  $A_r$  and  $A_{nr}$  represent radiative and nonradiative transition rates, respectively.  $A_r$  can be obtained by summing over the radiative rates  $A_{0J}$  for each  $^5D_0 \rightarrow ^7F_J$  ( $J = 0-4$ ) transition of  $Eu^{3+}$ . Because  $^5D_0 \rightarrow ^7F_1$  belongs to the isolated magnetic dipole transition, it is practically independent of the chemical environments around the  $Eu^{3+}$  ion as an internal reference for the whole spectra; the experimental coefficients of spontaneous emission,  $A_{0J}$ , can be calculated according to the equation.<sup>[24,25]</sup> The emission intensity,  $I$ , taken as integrated intensity  $S$  of the  $^5D_0 \rightarrow ^7F_{0-4}$  emission curves. On the basis of the above discussion, the quantum efficiencies of the europium hybrid materials can be determined, as shown in Table 1. Seen from Equation (1), the value  $\eta$  mainly depends on the values of two factors: one is lifetime and the other is  $I_{02}/I_{01}$  (red/orange ratio). If the lifetime and red/orange ratio are large, the quantum efficiency must be high. As can be seen clearly from Table 1, the quantum efficiencies of the europium hybrid materials are determined in the order: PMMA-Eu-M > PVPD-Eu-M > PMAA-Eu-M for the same coupling reagent. That is, the ternary polymer-containing hybrids exhibit higher luminescence quantum efficiency than the binary hybrids, in particular, the ternary PMMA polymer-containing hybrids show the highest luminescence quantum efficiency, which are in accord with the order of luminescence intensities and lifetimes. The results reveal that with the introduction of the polymer as the macromolecule ligand or coligand, the luminescence properties of the overall hybrid system are improved by the increasing ratio of the radiative transitions. Here it is noteworthy that the absolute overall quantum yields had better be measured in order to show the real luminescent behavior, but here we merely want to compare the different hybrids relatively. The deep investigation needs to be underway.

To study the coordination environment surrounding the lanthanide ions, especially the influence caused by vibrations of water molecules according to Horrocks,<sup>[15]</sup> it is expected that the probable number of coordinated water molecules ( $n_w$ ) can be calculated by Equation (2).

$$n_w = 1.05 (A_{exp} - A_{rad}) \quad (2)$$

On the basis of the results, the coordination number of water molecules (Eu containing hybrid materials) can be estimated to be 1–2. The coordination water molecules produce severe vibrations of the hydroxy group, resulting in large nonradiative transitions and a decrease in the luminescent efficiency. The 4-MBA-Si (P<sup>1</sup>, P<sup>2</sup>, P<sup>3</sup>) bridge molecules provide three coordinated COO<sup>−</sup> groups to occupy the equal six coordination number and the functional group of polymers show the one coordinated N (PCPD) or O (PMMA) atom. So the total coordination number for the Eu (Tb) ion in the ternary hybrids is 8–9, which corresponds to rare earth coordination chemistry behavior.

## Conclusions

In summary, on the basis of coordination chemistry, ternary rare earth/organic/inorganic/polymeric hybrid materials containing both inorganic networks (Si–O–Si, first ligand) and organic polymeric C–C chains (second ligand) have been assembled. The small bridge molecule ligand precursor MBA-Si is constructed through mercapto functionalization with different coupling reagents and the polymer ligand is synthesized by polymerization reaction. The results reveal that the ternary hybrid materials present more regular morphology, stronger luminescence intensity, longer lifetimes, and higher quantum efficiency than the binary hybrids, indicating that the introduction of the polymer can induce the self-assembly process of the microstructure and sensitize the luminescence of the hybrid materials.

## Experimental Section

**Materials:** 4-Mercaptobenzoic acid (4-MBA), tetraethoxysilane (TEOS), and the three cross-linking reagents [3-(triethoxysilyl)propyl isocyanate (TEPIC), (3-aminopropyl)trimethoxysilane (APS), (3-chloropropyl)trimethoxysilane (CPS)] were all analytical reagents. Other starting reagents were used as received. Europium and terbium nitrates were obtained by dissolving the corresponding oxides in concentrated nitric acid.

**Synthesis of Precursors and Polymers:** Three precursors and the polymer are prepared according to ref.<sup>[13]</sup> and depicted in Figure S1 (Supporting Information).

**Precursor 1 (P<sup>1</sup>). Modification by TEPIC:** 4-MBA (1 mmol) was first dissolved in refluxing anhydrous THF by stirring, and then TEPIC (1 mmol) was added to the solution dropwise. The whole mixture was heated at reflux at 80 °C for 3 h under an atmosphere of argon in a covered flask. After cooling, the solvent was removed under reduced pressure, and then the residue was washed with hexane (3 × 20 mL). P<sup>1</sup> was obtained as a yellow oil. Yield: 0.34 g, 85%. C<sub>17</sub>H<sub>27</sub>NO<sub>6</sub>SSi (401.56): calcd. C 50.85, H 6.78, N 3.49; found C 50.53, H 6.87, N 3.56. <sup>1</sup>H NMR (400 MHz, CDCl<sub>3</sub>):  $\delta$  =



0.63 (t, 2-H,  $\text{CH}_2\text{Si}$ ), 1.25 (t, 9-H,  $\text{CH}_2\text{CH}_3$ ), 1.57 (m, 2-H,  $\text{CH}_2\text{CH}_2\text{CH}_2$ ), 3.20 (t, 2-H,  $\text{CH}_2\text{CH}_2\text{CH}_2$ ), 3.73 (q, 6-H,  $\text{CH}_2\text{CH}_3$ ), 7.35 (q, 1-H,  $-\text{C}_6\text{H}_4$ ), 7.42 (t, 1-H,  $\text{NH}$ ), 7.68 (d, 1-H,  $-\text{C}_6\text{H}_4$ ), 7.87 (q, 1-H,  $-\text{C}_6\text{H}_4$ ), 8.74 (d, 1-H,  $-\text{C}_6\text{H}_4$ ), 11.30 (s, 1-H,  $\text{OH}$ ) ppm.

**Precursor 2 ( $\text{P}^2$ ). Modification by APS:** 4-MBA (1 mmol) was first dissolved in refluxing pyridine by stirring, and then APS (1 mmol) was added to the solution dropwise. The whole mixture was heated at reflux at 100 °C for 8 h under an atmosphere of argon in a covered flask. After cooling, the solvent was removed under reduced pressure, and then the residue was washed with hexane ( $3 \times 20$  mL).  $\text{P}^2$  was obtained as a yellow oil. Yield: 0.31 g, 87%.  $\text{C}_{16}\text{H}_{26}\text{O}_5\text{SSi}$  (358.53): calcd. C 53.60, H 7.31; found C 53.23, H 7.23.  $^1\text{H}$  NMR (400 MHz,  $\text{CDCl}_3$ ):  $\delta$  = 0.66 (t, 2-H,  $\text{CH}_2\text{Si}$ ), 1.25 (t, 9-H,  $\text{CH}_2\text{CH}_3$ ), 1.71 (m, 2-H,  $\text{CH}_2\text{CH}_2\text{CH}_2$ ), 3.17 (t, 2-H,  $\text{CH}_2\text{CH}_2\text{CH}_2$ ), 3.54 (q, 6-H,  $\text{CH}_2\text{CH}_3$ ), 7.21 (q, 1-H,  $-\text{C}_6\text{H}_4$ ), 7.45 (d, 1-H,  $-\text{C}_6\text{H}_4$ ), 7.76 (q, 1-H,  $-\text{C}_6\text{H}_4$ ), 7.97 (d, 1-H,  $-\text{C}_6\text{H}_4$ ), 11.02 (s, 1-H,  $\text{OH}$ ) ppm.

**Precursor 3 ( $\text{P}^3$ ). Modification by CPS:** 4-MBA (1 mmol) was first dissolved in DMF by stirring, and then CPS (1 mmol) was added to the solution dropwise.  $\text{K}_2\text{CO}_3$  (0.01 g) was added as catalyst. The whole mixture was heated at reflux at 120 °C for 6 h under an atmosphere of argon in a covered flask. After filtration, the solvent was removed under reduced pressure, and then the residue was washed with hexane ( $3 \times 20$  mL).  $\text{P}^3$  was obtained as a yellow oil. Yield: 0.26 g, 83%.  $\text{C}_{13}\text{H}_{20}\text{O}_5\text{SSi}$  (316.45): calcd. C 49.34, H 6.37; found C 49.57, H 6.53.  $^1\text{H}$  NMR (400 MHz,  $\text{CDCl}_3$ ):  $\delta$  = 0.75 (t, 2-H,  $\text{CH}_2\text{Si}$ ), 1.89 (m, 2-H,  $\text{CH}_2\text{CH}_2\text{CH}_2$ ), 3.13 (t, 2-H,  $\text{CH}_2\text{CH}_2\text{CH}_2$ ), 3.61 (s, 9-H,  $\text{CH}_3$ ), 7.12 (q, 1-H,  $-\text{C}_6\text{H}_4$ ), 7.30 (d, 1-H,  $-\text{C}_6\text{H}_4$ ), 7.78 (q, 1-H,  $-\text{C}_6\text{H}_4$ ), 8.08 (d, 1-H,  $-\text{C}_6\text{H}_4$ ), 11.02 (s, 1-H,  $\text{OH}$ ) ppm.

**Synthesis of the Polymer PVPD (PMMA):** 4-Vinylpyridine (PVPD) [or methyl methacrylate (PMMA)] (1 mmol) was weighed and transferred into a separating funnel. It was then washed with 0.1 M sodium hydroxide solution to remove the inhibitor. After oscillating for 5 min and standing for 2 h, the water phase and upper oil phase were separated. The residual water was removed with anhydrous copper sulfate. After purification and reduced pressure distillation under a nitrogen atmosphere, the monomer was injected into a covered three mouth flask with azobisisobutyronitrile (AIBN) (or benzoyl peroxide, BPO) as an initiator. The mixture was dissolved in methanol [or blend-solvent (BS) of toluene and ethyl acetate] and maintained at 65 °C (or 70 °C) for 8 h (or 6 h) under flowing high-purity nitrogen. After removal of the solvent, a canary yellow and stringy liquid was obtained. The product was dried in a vacuum desiccator after recrystallization by using methanol and anhydrous ether (see Figure S1, Supporting Information).

**Synthesis of the Binary (Ternary) Rare Earth Inorganic/Organic/Polymeric Hybrid Materials:** The binary hybrids are prepared according to ref.<sup>[13]</sup> (Figure S2, Supporting Information). The typical procedure for the preparation of the ternary hybrid materials is as follows (Figure 1). The above-prepared precursor (1 mmol) was dissolved in dry ethanol with stirring, and then a stoichiometric amount of  $\text{Ln}(\text{NO}_3)_3 \cdot 6\text{H}_2\text{O}$  [corresponding amount of polymer (PVPD for example) with DMF solution] was added dropwise. After 3 h, TEOS and  $\text{H}_2\text{O}$  were added to the solution to allow a sol-gel process, and then one drop of diluted hydrochloric acid was added to promote hydrolysis. The molar ratio of  $\text{Ln}(\text{NO}_3)_3 \cdot 6\text{H}_2\text{O}$ /P/(Polymer)/TEOS/ $\text{H}_2\text{O}$  was 1:3:(3):6:24. After hydrolysis, an appropriate amount of hexamethylenetetramine was added to adjust to pH 6–7. The mixture was agitated magnetically in a covered Teflon beaker to obtain a single phase, and then it was aged at 65 °C for gelation in about 7 d. The final hybrid material named Eu- $\text{M}^1$  or Tb- $\text{M}^1$  (PVPD-Eu- $\text{M}^1$  or PVPD-Tb- $\text{M}^1$ ) was collected as mono-

lithic bulks and ground into powdered material for the photophysical studies.

**Physical Measurements:** All measurements were performed at room temperature. Infrared spectra were recorded with a Nexus 912 AO439 FTIR spectrophotometer. We mixed the compound with the dried potassium bromide (KBr) and then pressed into pellets. The spectra were collected over the range 4000–400  $\text{cm}^{-1}$  by averaging 32 scans at a maximum resolution of 8  $\text{cm}^{-1}$ .  $^1\text{H}$  NMR spectra were recorded in  $\text{CDCl}_3$  with a Bruker Avance-400 spectrometer with tetramethylsilane (TMS) as an internal reference. The ultraviolet absorption spectra ( $5 \times 10^{-4}$  M DMF solution) were recorded with an Agilent 8453 spectrophotometer. The UV/Vis diffuse reflection spectra of the powder samples were recorded with a BWS003 spectrophotometer. X-ray powder diffraction patterns were recorded by using a Rigaku D/max-rB diffractometer system equipped with a Cu anode in a  $2\theta$  range from 10 to 70°. Thermogravimetric analysis (TGA) and differential scanning calorimetry (DSC) traces were performed with a Netzsch STA 409 at a heating rate of 15 °C/min under a nitrogen atmosphere. The fluorescence spectra were obtained with a RF-5301 spectrophotometer equipped with a stabl-spec-xenon lamp (450 W) as the light source. Luminescent lifetimes were recorded with an Edinburgh FLS 920 phosphorimeter by using a 450-W xenon lamp as the excitation source (pulse width, 3  $\mu\text{s}$ ). The microstructures were checked by scanning electronic microscopy (SEM, Philips XL-30).

**Supporting Information** (see footnote on the first page of this article): Figures of the synthesis process of precursors or polymer, the binary hybrids, selected X-ray diffraction graph of hybrid materials, SEM of binary hybrids, UV/Vis diffuse reflection absorption spectra, and the decay curves of the hybrid materials.

## Acknowledgments

This work is supported by the National Natural Science Foundation of China (20971100) and the Program for New Century Excellent Talents in University (NCET-08-0398).

- [1] D. Parker, P. Kanthi-Senanayake, J. A. G. Williams, *J. Chem. Soc. Perkin Trans. 2* **1998**, 2129–2139; R. J. Curry, W. P. Gillin, *Curr. Opin. Solid State Mater. Sci.* **2001**, 5, 481–486; Y. X. Zheng, J. Lin, Y. J. Liang, Q. Lin, Y. N. Yu, Q. G. Meng, Y. H. Zhou, S. B. Wang, H. Y. Wang, H. J. Zhang, *J. Mater. Chem.* **2001**, 11, 2615–2619; J. C. G. Bünzli, C. Piguet, *Chem. Rev.* **2002**, 102, 1897–1928; J. Kido, Y. Okamoto, *Chem. Rev.* **2002**, 102, 2357–2368; T. Oyamada, Y. Kawamura, T. Koyama, H. Sasabe, C. Adachi, *Adv. Mater.* **2004**, 16, 1082–1086; C. M. G. dos Santos, P. B. Fernandez, S. E. Plush, J. P. Leonard, T. Gunnlaugsson, *Chem. Commun.* **2007**, 32, 3389–3391.
- [2] L. R. Matthews, E. T. Kobbé, *Chem. Mater.* **1993**, 5, 1697–1700.
- [3] Q. M. Wang, B. Yan, *J. Mater. Chem.* **2004**, 14, 2450–2454; Q. M. Wang, B. Yan, *Cryst. Growth Des.* **2006**, 5, 497–503; Q. M. Wang, B. Yan, *J. Photochem. Photobiol. A: Chem.* **2006**, 177, 1–6; B. Yan, Q. M. Wang, *J. Photochem. Photobiol. A: Chem.* **2008**, 197, 213–219; J. L. Liu, B. Yan, *J. Phys. Chem. B* **2008**, 112, 10898–10907; Y. Li, B. Yan, H. Yang, *J. Phys. Chem. C* **2008**, 112, 3959–3968; B. Yan, Q. M. Wang, *Cryst. Growth Des.* **2008**, 6, 1484–1489; H. F. Lu, B. Yan, J. L. Liu, *Inorg. Chem.* **2009**, 48, 3966–3975.
- [4] L. H. Wang, W. Wang, W. G. Zhang, E. T. Kang, W. Huang, *Chem. Mater.* **2002**, 12, 2212–2218; P. Lenaerts, A. Storms, J. Mullens, J. Dhaen, C. Görrler-Walrand, K. Binnemans, K. Driesen, *Chem. Mater.* **2005**, 17, 5194–5201; S. Moynihan, R. Van Deun, K. Binnemans, J. Krueger, G. von Papen, A. Kew-



- ell, G. Crean, G. Redmond, *Optical Mater.* **2007**, *29*, 1798–1808; B. Yan, X. F. Qiao, *J. Phys. Chem. B* **2007**, *111*, 12362–12374.
- [5] A. C. Franville, D. Zambon, R. Mahiou, S. Chou, Y. Troin, J. C. Cousseins, *J. Alloys Compd.* **1998**, *275–277*, 831–834; S. Capecci, O. Renault, D. G. Mon, M. Halim, M. Etchells, R. J. Dobson, O. V. Salata, V. Christou, *Adv. Mater.* **2000**, *12*, 1591–1594.
- [6] C. Sanchez, F. Ribot, *New J. Chem.* **1994**, *18*, 1007–1037.
- [7] L. D. Carlos, R. A. S. Ferreira, J. P. Rainho, V. D. Bermudez, *Adv. Funct. Mater.* **2002**, *12*, 819–823; L. N. Sun, H. J. Zhang, L. S. Fu, F. Y. Liu, Q. G. Meng, C. Y. Peng, J. B. Yu, *Adv. Funct. Mater.* **2005**, *15*, 1041–1048; P. P. Lima, R. A. S. Ferreira, R. O. Freire, P. F. A. Almeida, L. S. Fu, J. S. Alves, L. D. Carlos, O. L. Malta, *ChemPhysChem* **2006**, *7*, 735–746.
- [8] A. C. Franville, R. Mahiou, Y. Troin, D. Zambon, J. C. Cousseins, *Solid State Sci.* **2001**, *3*, 211–222; P. N. Minoofar, R. Hernandez, S. Chia, B. Dunn, J. I. Zink, A. C. Franville, *J. Am. Chem. Soc.* **2002**, *124*, 14388–14396; J. Choi, R. Tamaki, S. G. Kim, R. M. Laine, *Chem. Mater.* **2003**, *15*, 3365–3375; J. H. Harreld, A. Esaki, G. D. Stucky, *Chem. Mater.* **2003**, *15*, 3481–3489.
- [9] L. D. Carlos, R. A. S. Ferreira, V. D. Bermudez, J. L. S. Ribeiro, *Adv. Mater.* **2009**, *21*, 509–534.
- [10] K. Binnemans, *Chem. Rev.* **2009**, *109*, 4283–4374.
- [11] V. D. Bermudez, L. D. Carlos, M. C. Duarte, M. M. Silva, C. J. Silva, M. J. Smith, M. Assuncao, L. Alcacer, *J. Alloys Compd.* **1998**, *275*, 21–26; A. C. Franville, D. Zambon, R. Mahiou, S. Chou, Y. Troin, J. C. Cousseins, *J. Alloys Compd.* **1998**, *275–277*, 831–834; L. D. Carlos, V. D. Bermudez, R. A. S. Ferreira, *J. Non-Cryst. Solids* **1999**, *247*, 203–208; H. R. Li, J. Lin, H. J. Zhang, H. C. Li, L. S. Fu, Q. G. Meng, *Chem. Commun.* **2001**, 1212–1213; X. M. Guo, H. D. Guo, L. S. Fu, H. J. Zhang, L. D. Carlos, R. P. Deng, J. B. Yu, *J. Photochem. Photobiol. A: Chem.* **2008**, *200*, 318–324.
- [12] M. I. Sarwar, Z. Ahmad, *Eur. Polym. J.* **2000**, *36*, 89–94; D. Liu, Z. G. Wang, *Polymer* **2008**, *49*, 4960–4967.
- [13] N. Sabbatini, M. Guardigli, J. M. Lehn, *Coord. Chem. Rev.* **1993**, *123*, 201–208; J. Erotyak, A. Buzady, A. Kaszas, J. Kozma, I. Hornyak, *J. Lumin.* **1997**, *72*, 570–574; A. Beeby, S. Faulkner, *Chem. Phys. Lett.* **1997**, *266*, 116–122; V. Bekiari, P. Lianos, *Adv. Mater.* **1998**, *10*, 1455–1458; K. Driesen, R. V. Deun, C. Görrler-Walrand, K. Binnemans, *Chem. Mater.* **2004**, *16*, 1531–1535.
- [14] L. N. Nikolenko, V. A. Koptug, *Zh. Obshch. Khim.* **1955**, *25*, 1757–1760; M. Bandini, P. G. Cozzi, M. Giacomini, P. Melchiorre, S. Selva, A. Umani-Ronchi, *J. Org. Chem.* **2002**, *67*, 3700–3704; G. Tarzia, A. Duranti, A. Tontini, *J. Med. Chem.* **2003**, *39*, 2352–2360; S. Vijaikumar, K. Pitchumani, *J. Mol. Catal. A* **2004**, *217*, 117–120; F. Fringuelli, F. Pizzo, C. Vittorini, L. Vaccaro, *Eur. J. Org. Chem.* **2006**, *5*, 1231–1236.
- [15] B. Yan, H. F. Lu, *Inorg. Chem.* **2008**, *47*, 5601–5611; B. Yan, K. Qian, *J. Organomet. Chem.* **2009**, *694*, 3160–3166.
- [16] J. F. Ma, J. Z. Ni, *Prog. Chem.* **1996**, *8*, 264.
- [17] W. De W. Horrocks Jr., D. R. Sudnick, *J. Am. Chem. Soc.* **1979**, *101*, 334–340; W. De W. Horrocks Jr., D. R. Sudnick, *Acc. Chem. Res.* **1981**, *14*, 384–392.
- [18] L. D. Carlos, V. D. Bermudez, R. A. S. Ferreira, L. Marques, M. Assuncao, *Chem. Mater.* **1999**, *11*, 581–588; H. S. Hoffmann, P. B. Staudt, T. M. H. Costa, C. C. Moro, E. V. Benvenuti, *Surf. Interface Anal.* **2002**, *33*, 631–634; M. C. Goncalves, V. D. Bermudez, R. A. S. Ferreira, L. D. Carlos, D. J. Ostrovskii, J. Rocha, *Chem. Mater.* **2004**, *16*, 2530–2543.
- [19] M. D. Regulacio, M. H. Pablico, J. A. Vasquez, P. N. Myers, S. Gentry, M. Prushan, S. W. Tam-Changand, S. L. Stoll, *Inorg. Chem.* **2008**, *47*, 1512.
- [20] M. Kawa, J. M. J. Fréchet, *Chem. Mater.* **1998**, *10*, 286–296.
- [21] C. Y. Peng, H. J. Zhang, J. B. Yu, Q. G. Meng, L. S. Fu, H. R. Li, L. N. Sun, X. M. Guo, *J. Phys. Chem. B* **2005**, *109*, 15278–15287.
- [22] A. F. Kirby, D. Foster, F. S. Richardson, *Chem. Phys. Lett.* **1983**, *95*, 507–512.
- [23] R. A. S. Ferreira, L. D. Carlos, R. R. Gonçalves, S. J. L. Ribeiro, V. D. Bermudez, *Chem. Mater.* **2001**, *13*, 2991–2998; P. C. R. Soares-Santos, H. I. S. Nogueira, V. Félix, M. G. B. Drew, R. A. S. Ferreira, L. D. Carlos, T. Trindade, *Chem. Mater.* **2003**, *15*, 100–108.
- [24] M. H. V. Werts, R. T. F. Jukes, J. W. Verhoeven, *Phys. Chem. Chem. Phys.* **2002**, *4*, 1542–1548.
- [25] J. C. Boyer, F. Vetrone, J. A. Capobianco, A. Speghini, M. Bettinelli, *J. Phys. Chem. B* **2004**, *108*, 20137–20144.

Received: March 10, 2010

Published Online: June 21, 2010

## Three Novel Copper–Radical Complexes: Syntheses, Crystal Structures, and Magnetic Properties

Xiao-dan Chen,<sup>[a]</sup> Rong Rong,<sup>[b]</sup> Yun Wang,<sup>[b]</sup> Li-li Zhu,<sup>[b]</sup> Qi-hua Zhao,<sup>[b]</sup> Siau Gek Ang,<sup>[c]</sup> and Bai-wang Sun<sup>\*[a]</sup>

**Keywords:** Copper / Magnetic properties / Radicals / Structure elucidation

Three novel copper–radical complexes  $[\text{Cu}(\text{PhCOO})_2(\text{NITpPy})_2(\text{H}_2\text{O})_2]$  (**1**),  $[\text{Cu}_2(\text{Me}_3\text{CCOO})_4(\text{NITpPy})_2]$  (**2**), and  $[\{\text{Cu}_2(\text{Me}_3\text{CCOO})_4(\text{NITpPy})\}_n]$  (**3**) [ $\text{NITpPy}$  = 4,4,5,5-tetramethyl-2-(4-pyridyl)-2-imidazoline-1-oxyl 3-oxide] were synthesized and characterized structurally as well as magnetically. It is noteworthy that the syntheses of complexes **2** and **3** are similar except for the temperature of the reaction between  $\text{Cu}(\text{Me}_3\text{CCOO})_2 \cdot 2\text{H}_2\text{O}$  and the  $\text{NITpPy}$  radical li-

gand. Our magnetic study of complexes **1** and **2** reveals that the antiferromagnetic interactions occur with a  $J$  value around  $-10 \text{ cm}^{-1}$  between copper(II) and radicals when radicals use the pyridine nitrogen atom connected to the copper(II) ion. Yet the best-fit parameters of complex **3** reveal that significant ferromagnetic interactions ( $J_2 = 20.5 \text{ cm}^{-1}$ ) take place in the copper radical when radicals coordinate the copper(II) ion with nitroxide directly.

### Introduction

The design and synthesis of magnetic materials with a transition metal and organic bridging ligands have attracted considerable interest not only as bioinorganic model complexes and catalysts; they are also studied for their intriguing structural, magnetic, and spectral properties. The coordination chemistry of copper(II) complexes with various carboxylates has been investigated for a long time. This is because carboxylate is a versatile ligand with good binding ability and diversity among its bonding modes; in addition, carboxylate ligands can provide different super-exchange pathways that transmit magnetic interactions between paramagnetic metal atoms.<sup>[1,2]</sup>

On the other hand, the combination of paramagnetic metal ions and organic  $N$ -oxyl  $N'$ -oxides (nitronyl nitroxides) has attracted much more attention in the last decades.<sup>[3–5]</sup> However, the weakly basic character of nitronyl

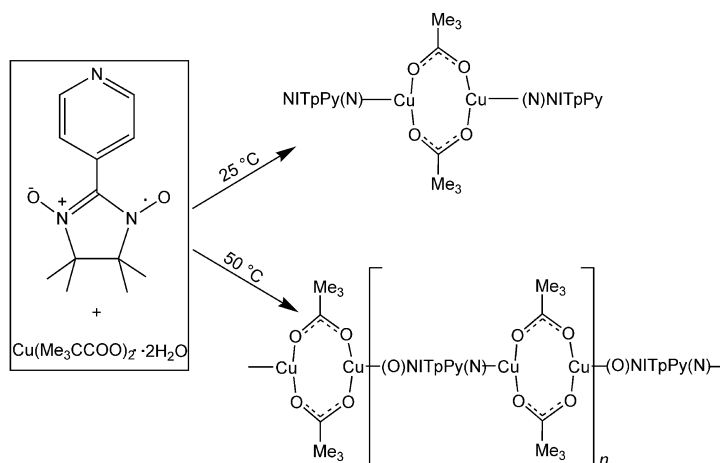
nitroxides strongly limits their coordination ability, which has inspired the development of functionalized nitronyl nitroxide radicals. To this end, many kinds of strong co-ligands have been employed in the synthesis of stable radicals, such as pyridine and imidazole.<sup>[6,7]</sup> Using these stable radicals, some discrete molecules, high-spin clusters, linear chains, and two-dimensional systems have been obtained and studied.<sup>[8–13]</sup> Among the functionalized nitroxide radical ligands, the pyridyl-substituted nitroxide radicals are extensively used to assemble metal–radical coupling complexes due to their donor nitrogen atoms. Recently, several polymeric metallic magnetic materials with pyridyl-substituted nitroxide radicals as the bridging ligands between metals have been reported, such as  $[\{\text{Cu}(\text{NITmPy})_2(\text{N}_3)_2\}_n]$ <sup>[14]</sup> and  $[\{\text{Cu}_2(\text{Me}_3\text{CCO}_2)_4(\text{NITmPy})\}_n]$ <sup>[15]</sup> [ $\text{NITmPy}$  = 4,4,5,5-tetramethylimidazoline-2-(3'-pyridyl)-1-oxyl 3-oxide]. However, reports on such systems are still scarce. To establish such complexes, we have tried to apply many kinds of different carboxylates in cooperation with  $\text{NITpPy}$  [4,4,5,5-tetramethyl-2-(4-pyridyl)-2-imidazoline-1-oxyl 3-oxide]. In this paper, we report three novel compounds that are discrete molecules:  $[\text{Cu}(\text{NITpPy})_2(\text{PhCOO})_2(\text{H}_2\text{O})_2]$  (**1**), paddle-wheel dicopper complex  $[\text{Cu}_2(\text{Me}_3\text{CCOO})_4(\text{NITpPy})_2]$  (**2**), and a chain complex  $[\{\text{Cu}_2(\text{Me}_3\text{CCOO})_4(\text{NITpPy})\}_n]$  (**3**). It is noteworthy that the synthesis conditions of complexes **2** and **3** are similar except for the temperature of the reaction between  $\text{Cu}(\text{Me}_3\text{CCOO})_2 \cdot 2\text{H}_2\text{O}$  and the  $\text{NITpPy}$  radical ligand. Complex **2** is synthesized at room temperature ( $25^\circ\text{C}$ ), whereas complex **3** is synthesized at  $50^\circ\text{C}$  (Scheme 1).

[a] Ordered Matter Science Research Center, Department of Chemistry and Chemical Engineering, Southeast University, Nanjing 210096, P. R. China  
Fax: +86-25-52090614  
E-mail: chmsunbw@seu.edu.cn

[b] Department of Chemistry, Key Laboratory of Medicinal Chemistry for Natural Resource Ministry of Education, Yunnan University, Kunming 650091, P. R. China

[c] Department of Chemistry, Faculty of Science, National University of Singapore, 3 Science Drive 3, Singapore 117543

Supporting information for this article is available on the WWW under <http://dx.doi.org/10.1002/ejic.201000005>.



Scheme 1.

## Results and Discussion

### Crystal Structure

Single-crystal X-ray analysis reveals that  $[\text{Cu}(\text{NITpPy})_2(\text{PhCOO})_2(\text{H}_2\text{O})_2]$  (**1**) crystallizes in the triclinic space group  $P\bar{1}$ . In the compound molecule, the crystallographically independent unit contains half a copper(II) ion, one benzoic acid molecule, one NITpPy ligand, and one aqua molecule. From the symmetrical operation, the structure of the complex shows a centrosymmetric mononuclear molecule (Figure 1, a). The copper(II) ion lies in a distorted octahedral coordination environment with two aqua oxygen atoms (O5, O5A); two oxygen atoms form two different  $\text{PhCO}_2^-$  (O1, O1A), which are located in the equatorial plane, as well as two nitrogen atoms (N1, N1A) from NITpPy ligands that occupy the axial positions. The atoms

of N2, N3, C13, O3, and O4 in the nitroxide group are nearly planar and form a dihedral angle of  $14.36(7)^\circ$  with the pyridine rings; the distances and angles in the nitroxide group are similar to those reported by Caneschi et al.<sup>[16]</sup> The whole benzoic acid molecule (Figure s1 in the Supporting Information) nearly occupies the same plane with a dihedral angle of  $0.528(3)^\circ$  between the phenyl ring and carboxylate, whereas it forms a dihedral angle of  $13.596(1)^\circ$  with the metal equatorial plane. In addition, the uncoordinated carboxylate oxygen atoms form intramolecular hydrogen bonds with the coordinated water molecules ( $\text{O5}\cdots\text{O2A}$   $2.6767(8)$  Å). The packing plot (Figure s1) shows there are face-to-face  $\pi$ – $\pi$  interactions between the aromatic rings of benzoic acid molecules with centroid–centroid distances of 3.67 Å on average and the closest intermolecular radical  $\text{N}\cdots\text{O}$ – $\text{N}$  distance is 3.96(3) Å, which indicates that there

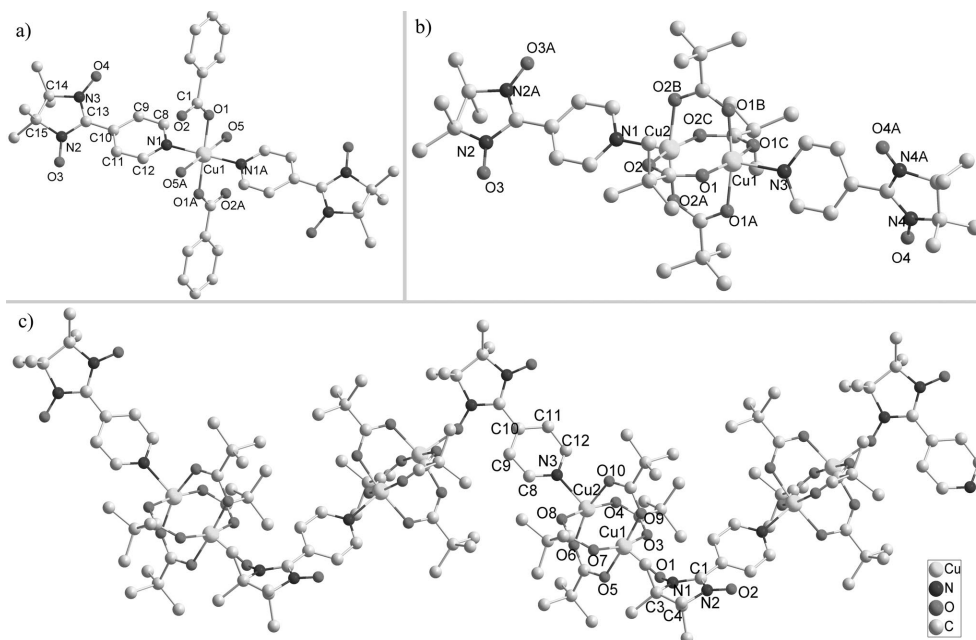


Figure 1. Perspective view of (a)  $[\text{Cu}(\text{NITpPy})_2(\text{PhCOO})_2(\text{H}_2\text{O})_2]$  (**1**), (b)  $[\text{Cu}_2(\text{Me}_3\text{CCO}_2)_4(\text{NITpPy})_2]$  (**2**), and (c)  $[\{\text{Cu}_2(\text{Me}_3\text{CCO}_2)_4(\text{NITpPy})\}_n]$  (**3**), with an atom- numbering scheme and the omission of all hydrogen atoms for clarity.

might be intermolecular magnetic interactions in complex **1**.

The crystal structure of  $[\text{Cu}_2(\text{Me}_3\text{CCO}_2)_4(\text{NITpPy})_2]$  (**2**) is illustrated in Figure 1 (b). In this dinuclear compound, the four oxygen atoms and one nitrogen atom bonded to the copper ion are located at the apices of a distorted square pyramid. The basal coordination sites are occupied by four oxygen atoms of four  $\text{Me}_3\text{CCO}_2^-$ , whereas the axial position is occupied by one nitrogen atom from the NITpPy group. The  $\text{Cu}^{\text{II}}$  ions are not coplanar with the basal plane, but have an out-of-plane displacement of 0.19(6) Å. The four carboxylate bridges between both copper ions form a paddle-wheel-type cage with a Cu–Cu distance of 2.62(2) Å, which is a typical value for dimeric copper(II) carboxylate adducts.<sup>[17]</sup> For complex **2**, the average bending angle ( $\phi_b$ ) of the OCO moieties of the carboxylato groups to the Cu–O···O–Cu plane is 2.71(7)°, which is possibly due to the intermolecular effects, because for an isolated dinuclear complex the symmetric structure without bending is expected to have the least intramolecular strain energy. Additionally, from the packing operation (Figure S2 in the Supporting Information), the nearest radical N–O···O–N distance between neighboring molecules is 4.28(5) Å, which shows that the intermolecular magnetic interactions in complex **2** cannot be ignored.

The X-ray crystal structure of  $[\{\text{Cu}_2(\text{Me}_3\text{CCO}_2)_4(\text{NITpPy})\}_n]$  (**3**) shows that the complex is an extended zig-zag chain of alternating dicopper(II) carboxylate and nitroxide elongated along the *a* axis (Figure 1c). In the paddle-wheel-type dimeric copper(II) carboxylate adducts, the Cu1–Cu2 distance is 2.62(4) Å, which is a typical value for dimeric copper(II) carboxylate adducts.<sup>[17]</sup> One of the paddle-wheel apical positions is occupied by the oxygen atom of the NO groups with a Cu1–O1 bond length of 2.26(5) Å, which is longer than the Cu–O(tempo) (tempo = 2,2,6,6-tetramethylpiperidine-1-oxyl) bond length of 1.946 Å in the previously reported dimeric  $[\text{Cu}_2(\text{Cl}_3\text{CCO}_2)_4(\text{tempo})_2]$ .<sup>[18,19]</sup> The other positions are occupied by the nitrogen atom of the pyridyl group with a Cu2–N3 length of 2.16(4) Å. The dihedral angle between the pyridine ring and the nitroxide group is 32.33(6)°, which is bigger than that in complex **1**. It possibly contributes to the effects of the radical O coordination to the copper(II) ion. In addition, the two NO groups of each NITpPy ligand have bond lengths of 1.27(4) and 1.26(7) Å for the coordinated and uncoordinated NO groups, respectively, as is generally observed.<sup>[20]</sup>

## Magnetic Properties

Variable-temperature, solid-state magnetic studies were performed on powdered crystalline samples of complexes **1–3** in a 2 kG (0.2 T) field and in a temperature range of 2.0–300 K. The temperature dependences of the molar magnetic susceptibility,  $\chi_M^{-1}$  and  $\chi_M T$ , for complexes **1**, **2**, and **3** are shown in Figure 2, Figure 3, and Figure 4, respectively. According to the  $\chi_M^{-1}T$  line, the magnetic behaviors of the three complexes follow the Curie–Weiss law  $\chi_M = C/(T - \theta)$

in a high temperature range, about 100–300, 50–300, and 140–300 K for complexes **1–3**, respectively, with a Curie constant (*C*) of 1.00, 1.16, and 2.00  $\text{cm}^3 \text{K mol}^{-1}$ , respectively, and a Weiss temperature ( $\theta$ ) of –7.09, –45.17, and –312.34 K, respectively.

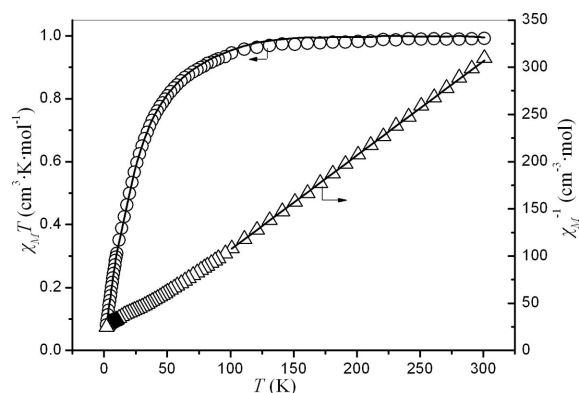


Figure 2. Temperature dependence of  $\chi_M T$  and  $\chi_M^{-1}$  of **1** at an applied field (*H*) of 20 kOe. The solid lines represent the best fit to the Curie–Weiss law and the calculated magnetic susceptibilities by the parameters reported in the text.

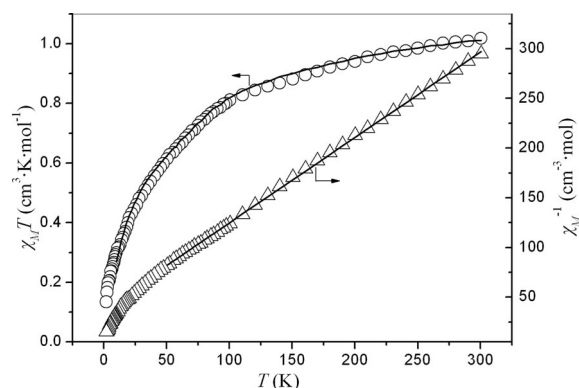


Figure 3. Temperature dependence of  $\chi_M T$  and  $\chi_M^{-1}$  of **2** at an applied field (*H*) of 20 kOe. The solid lines represent the best fit to the Curie–Weiss law and the calculated magnetic susceptibilities by the parameters reported in the text.

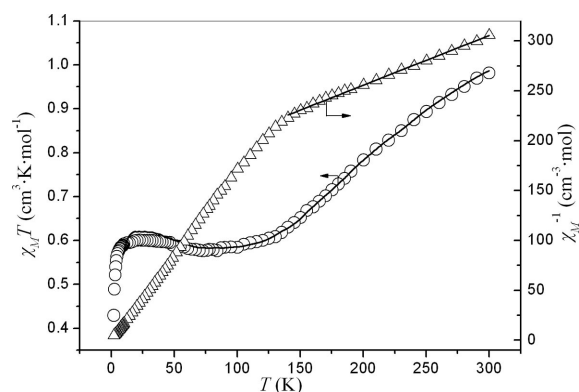


Figure 4. Temperature dependence of  $\chi_M T$  and  $\chi_M^{-1}$  of **3** at an applied field (*H*) of 20 kOe. The solid lines represent the best fit to the Curie–Weiss law and the calculated magnetic susceptibilities by the parameters reported in the text.



With regards to the  $\chi_M T$  versus  $T$  curve, the  $\chi_M T$  values of complexes **1–3** all decrease with a decrease in temperature.

For complex **1** (Figure 2), the  $\chi_M T$  value  $0.99 \text{ cm}^3 \text{ mol}^{-1} \text{ K}$  at 300 K is slightly lower than the value (1.125 for  $g = 2.0$ ) expected for three uncoupled spins ( $S = \frac{1}{2}$ ) of two nitronyl nitroxide radical ligands and one copper center, which reveals that there are antiferromagnetic interactions between the radical ligands and the copper(II) ion. With a decrease in temperature,  $\chi_M T$  decreases slightly and reaches a value of about  $0.94 \text{ cm}^3 \text{ mol}^{-1} \text{ K}$  at 100 K. However, at around 50 K,  $\chi_M T$  begins to drop sharply and finally reaches  $0.081 \text{ cm}^3 \text{ mol}^{-1} \text{ K}$  at 2 K, which is possibly due to the effect of intermolecular antiferromagnetic interactions.

To get more information from the magnetic data, we considered a central symmetric linear system of three  $S = \frac{1}{2}$  spins,  $S_1$ – $S_2$ – $S_3$ , in which  $S_1$  and  $S_3$  refer to the nitroxide sites and  $S_2$  refers to the copper(II) ion, with an exchange Hamiltonian of  $H = -2J(S_1 S_2 + S_2 S_3)$ .<sup>[21]</sup> Here we assumed  $g_{\text{Cu}} = g_{\text{rad}} = g$ , which was also adopted in analyzing the magnetic properties of complexes **2** and **3**. Equation (1), which was derived from the Van Vleck equation, was employed to fit the observed  $\chi_M T$  versus  $T$  plot by means of a least-squares method. Equation (2) shows the definition of  $\chi_M$ . Meanwhile, in consideration of the magnetic coupling between neighboring NITpPy radicals through the NO...ON pathway, the mean-field approximation,  $zJ'$  was employed. All the other symbols have the usual meaning.

$$\chi_o = \left( \frac{N\mu_B^2 g^2}{4kT} \right) \frac{1 + \exp(-2J/kT) + 10\exp(J/kT)}{1 + \exp(-2J/kT) + 2\exp(J/kT)} \quad (1)$$

$$\chi_M = \frac{\chi_o}{1 - \chi_o(zJ'/N\mu_B^2 g^2)} \quad (2)$$

The results best fitted to the experimental data yielded  $J = -10.89 \text{ cm}^{-1}$ ,  $zJ' = -0.52 \text{ cm}^{-1}$ , and  $g = 1.98$  for complex **1**. The solid line in Figure 2 represents the theoretical curve. The agreement factor ( $R$ ) is  $1.22 \times 10^{-5}$  ( $R$  was defined as  $\sum[(\chi_M)_{\text{obsd.}} - (\chi_M)_{\text{calcd.}}]^2 / \sum[(\chi_M)_{\text{obsd.}}]^2$ ).

In Figure 3, the  $\chi_M T$  value of complex **2** began to diminish visibly with a decrease in temperature from  $1.02 \text{ cm}^3 \text{ mol}^{-1} \text{ K}$  at 300 K to  $0.30 \text{ cm}^3 \text{ mol}^{-1} \text{ K}$  at 10 K. After that,  $\chi_M T$  showed an abrupt drop to  $0.13 \text{ cm}^3 \text{ mol}^{-1} \text{ K}$  at 2 K. The  $\chi_M T$  value of complex **2** at room temperature was much lower than that calculated for four noncorrelated  $S = \frac{1}{2}$  spins (1.5 for  $g = 2.0$ ). According to this and the clear decrease in  $\chi_M T$ , it suggests there are strong antiferromagnetic interactions in complex **2**.

To analyze the magnetic behavior of complex **2** more quantitatively, we considered a central symmetric linear tetramer of four  $S = \frac{1}{2}$  spins,  $S_1$ – $S_2$ – $S_3$ – $S_4$ , with the exchange Hamiltonian of  $H = -2J_1(S_1 S_2 + S_3 S_4) - 2J_2 S_2 S_3$ ,<sup>[21]</sup> in which two exchange coupling constants are obtained.  $S_2$  and  $S_3$  refer to copper(II) ions,  $S_1$  and  $S_4$  refer to the nitroxide sites of the NITpPy radicals, and  $J_1$  and  $J_2$  stand for the copper(II)–copper(II) and copper(II)–radical magnetic

interactions, respectively. According to a previous report,<sup>[4]</sup> the magnetic behavior based on the above isotropic Hamiltonian can be given as shown in Equation (3).

$$\chi_o = \left( \frac{2N\mu_B^2 g^2}{kT} \right) \frac{A}{B} \quad (3)$$

$$A = 10\exp(-E_1/kT) + 2\exp(-E_2/kT)$$

$$+ 2\exp(-E_3/kT) + 2\exp(-E_4/kT)$$

$$B = 5\exp(-E_1/kT) + 3[\exp(-E_2/kT) + \exp(-E_3/kT)$$

$$+ 2\exp(-E_4/kT)] + \exp(-E_5/kT) + \exp(-E_6/kT)$$

$$E_1 = -J_2 - J_1$$

$$E_2 = J_2 - J_1$$

$$E_3 = (J_2^2 + J_1^2)^{1/2}$$

$$E_4 = (J_2^2 + J_1^2)^{1/2}$$

$$E_5 = J_2 + (4J_2^2 - 2J_2 J_1 + J_1^2)^{1/2}$$

$$E_6 = J_2 - (4J_2^2 - 2J_2 J_1 + J_1^2)^{1/2}$$

Because of the intermolecular magnetic coupling, the molar susceptibility can be expressed by Equation (3). As a result, the best fit (10–300 K) with  $J_1 = -166.1 \text{ cm}^{-1}$ ,  $J_2 = -9.74 \text{ cm}^{-1}$ ,  $zJ' = -5.06 \text{ cm}^{-1}$ , and  $g = 2.16$  for **2** is obtained as the solid line in Figure 3. The agreement factor ( $R$ ) is  $2.23 \times 10^{-5}$ .

In Figure 4, the  $\chi_M T$  value of complex **3** was  $0.98 \text{ cm}^3 \text{ mol}^{-1} \text{ K}$  at 300 K, which is lower than the expected value (1.125 for  $g = 2$ ) for three noncoupled  $S = \frac{1}{2}$  spins, two from the dicopper ions and one from the NITpPy radical in **3**. In addition, it can be clearly seen from Figure 4 that the plot of  $\chi_M T$  versus  $T$  reveals three domains: (i) from 300 to about 120 K,  $\chi_M T$  rapidly decreases from 0.98 to 0.60, which is larger than for one independent  $S = \frac{1}{2}$  spin; (ii) between about 120 to 10 K, the  $\chi_M T$  value remains nearly unchanged with the decreasing temperature, and (iii) below 10 K,  $\chi_M T$  drops to approximately 0.42 at 2 K. In addition, the plot of  $\chi_M^{-1}$  versus  $T$  in the range 2–110 K essentially follows the Curie–Weiss law with a Curie constant ( $C$ ) of  $0.6 \text{ cm}^3 \text{ K mol}^{-1}$  and a Weiss constant ( $\theta$ ) of  $-0.59 \text{ K}$ . All of the above-mentioned phenomena are coincident with that described in a previous report of  $[\{\text{Cu}_2(\text{Me}_3\text{CCO}_2)_4(\text{NITmPy})\}_n]$ .<sup>[15]</sup>

In complex **3**, the crystal structure shows that two kinds of coordinate bonds link the  $\text{Cu}^{\text{II}}$ – $\text{Cu}^{\text{II}}$  cores by the trimethylacetic acid groups and by the radicals, which means three different coupling interactions occur in this chain  $\{\text{ON}[\text{N}-(J')\text{Cu1}-(J_1)\text{Cu2}-(J_2)\text{ON}][\text{N}-(J')\text{Cu1}'-(J_1)\text{Cu2}'-(J_2)\text{ON}]\text{N}-\}$ . As there is a lack of models for three different  $J$ -scheme chains, and the distances between copper(II) and the radical NO through the pyridyl ring are longer than  $7 \text{ \AA}$ , here we assume that the major variable-temperature magnetic susceptibilities are contributed by two kinds of interactions, between the Cu–Cu cores and the Cu–(O)radicals ( $S_1$ – $S_2$ – $S_3$ ) with the exchange Hamiltonian of  $H = -2J_1 S_1 S_2 - 2J_2 S_2 S_3$ , in which  $S_1$  and  $S_2$  refer to copper(II) ions and  $S_3$  refers to the nitroxide sites of the radical. Thus, an approximate fit is performed by employing Equation (3)<sup>[22]</sup> for complex **3**.

Additionally, the contributions of interactions between copper(II) and the radical through the pyridyl ring and interchain magnetic interactions are represented as  $zJ'$ , so Equation (2) was employed. Finally, an approximate fit performed by employing Equation (4) gave the best results (10–300 K) with  $J_1 = -151.7 \text{ cm}^{-1}$ ,  $J_2 = 20.5 \text{ cm}^{-1}$ ,  $zJ' = -3.57 \text{ cm}^{-1}$ , and  $g = 2.0$ . A solid line represents the calculated magnetic susceptibilities by the parameters above in Figure 4. The agreement factor ( $R$ ) is  $3.48 \times 10^{-4}$ .

$$\chi_o = \left( \frac{N\mu_B^2 g^2}{4kT} \right) \frac{1 + \exp(-E_1/kT) + 10 \exp(-E_2/kT)}{1 + \exp(-E_1/kT) + 2 \exp(-E_2/kT)} \quad (4)$$

$$E_1 = -(J_1^2 - J_1 J_2 + J_2^2)^{1/2}$$

$$E_2 = -(J_1 + J_2)/2 - (J_1^2 - J_1 J_2 + J_2^2)^{1/2}/2$$

Through the above studies of magnetic properties, it can be seen that the magnetic exchange interactions between the metal ion and the radical through the pyridyl rings are much weaker than the copper–copper magnetic interactions, which is presumably because of the long intramolecular distances between the oxygen atoms of the NO groups and the nearest copper(II) ion (longer than 7 Å). For complex **1**, the analysis results are coincident with previous reports.<sup>[23]</sup> In paddle-wheel dicopper systems like complex **2**, the radicals are usually looked upon as being two isolated spins in other reports,<sup>[24]</sup> from which a model could be applied to analyze complex **2** and a good fitting result might also be obtained. But by considering the interactions between copper(II) and the radical, the results are more comprehensive. For complex **3**, a similar system was studied in the literature,<sup>[15]</sup> in which the alternating chain model was employed first<sup>[25]</sup> to analyze the magnetic data of the linear complex  $[\{\text{Cu}_2(\text{Me}_3\text{CCO}_2)_4(\text{NITmPy})\}_n]$ , but the result was poor, so the interactions between copper(II) and the radical were omitted. However, the chain of complex **3** reported here, firstly, cannot be seen as an alternating chain model as introduced in the literature,<sup>[24]</sup> in which two interaction parameters ( $J$  and  $aJ$ ) were calculated. In complex **3**, the radical connecting the paddle wheels with the nitroxide and pyridine nitrogen has two different interactions with the two copper(II) ions ( $J_2$ ,  $J'$ , respectively), in which  $J'$  is just like the interactions between  $\text{Cu}^{\text{II}}$  and the radical in complexes **1** and **2**. Secondly,  $J_2$  here cannot be ignored in the way it was in the literature<sup>[15]</sup> since the copper(II)–(O)–NITpPy distance is definitely shorter than 5 Å, which reveals noticeable coupling interactions between the copper orbitals and the unpaired radical electron. Therefore, in this paper, complex **3** was analyzed as three spin units connected to the zigzag chain by the pyridyl rings. The interaction between the three spin units was taken together with interchain magnetic interactions as  $zJ'$  to simplify the model. The final fitting result also verified that there are significant ferromagnetic interactions in Cu–radical with  $J_2 = 20.5 \text{ cm}^{-1}$ ; the stable values of  $\chi_{\text{M}}T$  in the temperature range 120–10 K are probably due to the balance between the antiferromagnetic interactions of two copper(II) ions

and Cu–radical ferromagnetic interactions. As in complex **3**, the unpaired electron of the nitroxide radical delocalizes on the  $\pi$  orbital of the five-atom fragment (ONCNO),<sup>[26]</sup> which is orthogonal to the magnetic orbital  $d_{x^2-y^2}$  of the copper(II) ion and leads to the ferromagnetic interaction between copper(II) and the radical. The sharp decrease of  $\chi_{\text{M}}T$  below 10 K might be caused by the effect of interchain antiferromagnetic interactions.

## Conclusion

Three novel complexes were obtained successfully. The temperature of the reaction between  $\text{Cu}(\text{Me}_3\text{CCOO})_2 \cdot 2\text{H}_2\text{O}$  and the NITpPy radical is very essential to the synthesis, as the product will be complex **2** at room temperature (25 °C), whereas it will be complex **3** at 50 °C. The fitted parameters for the magnetic data study of complexes **1** and **2** provide evidence for the antiferromagnetic interaction between the copper(II) ion and NITpPy radicals that are connected by the pyridyl ring, whereas the magnetic data of complex **3** contains a nearly flat portion between 120 and 10 K of the  $\chi_{\text{M}}T$  versus  $T$  plot, which reveals that there are not solely antiferromagnetic interactions in the chain. With the model of Cu–Cu–(O)NITpPy, the best-fitted result reveals that there are ferromagnetic interactions ( $J_2 = 20.5 \text{ cm}^{-1}$ ) existing in Cu–radical when nitroxide radicals coordinate with the copper(II) ion directly.

## Experimental Section

**Synthesis:** All reagents and chemicals were purchased from commercial sources. The carboxylates,  $[\text{Cu}_2(\mu\text{-RCO}_2)_4(\text{H}_2\text{O})_2]$ , in which  $\text{R} = \text{C}_6\text{H}_5\text{-}$  or  $\text{Me}_3\text{C-}$ , were prepared as described previously.<sup>[27]</sup> Basic copper(II) carbonate (2.65 g, 12 mmol) and the carboxylic acid (1.46 g for benzoic acid, 1.23 g for pivalic acid; 12 mmol) were dissolved in water (ca. 100 cm<sup>3</sup>) at pH 5–6. The solution was allowed to stand at 25 °C for several days, giving precipitated products, which were recovered by means of reduced-pressure distillation and filtration. The nitronyl nitroxide (NITpPy) used in this work was synthesized as described previously.<sup>[6,7]</sup>

**[Cu(NITpPy)<sub>2</sub>(PhCOO)<sub>2</sub>(H<sub>2</sub>O)<sub>2</sub>] (1):** A solution of NITpPy (0.0235 g, 0.1 mmol) in methanol (5 mL) was added dropwise to a solution of  $\text{Cu}(\text{C}_6\text{H}_5\text{COO})_2 \cdot 2\text{H}_2\text{O}$  (0.068 g, 0.2 mmol) in methanol (15 mL). The mixture was stirred for 2 h in the dark and then filtered. The clear dark blue filtrate was allowed to stand at room temperature for 7 d, following which single crystals suitable for an X-ray diffraction analysis were obtained.  $\text{C}_{38}\text{H}_{46}\text{CuN}_6\text{O}_{10}$  (810.36): calcd. C 56.32, H 5.72, N 10.37; found C 56.14, H 5.52, N 10.14. IR (KBr):  $\tilde{\nu} = 3664.1\text{--}3138.7$ , 1604.5, 1558.7, 1456.5, 1365.4, 1315.1, 1138.8, 839.1, 706.7, 675.7 cm<sup>-1</sup>.

**[Cu(Me<sub>3</sub>CCOO)<sub>4</sub>(NITpPy)<sub>2</sub>] (2):**  $\text{Cu}(\text{Me}_3\text{CCOO})_2 \cdot 2\text{H}_2\text{O}$  (0.0556 g, 0.2 mmol) was dissolved with prolonged stirring at room temp. in methanol (15 mL). Then NITpPy (0.0936 g, 0.4 mmol) was dissolved in methanol (10 mL). Both solutions were mixed while stirring was continued for 2 h. Then the solutions were filtered. The clear dark blue filtrate was allowed to stand at room temperature for 5 d, following which single crystals suitable for an X-ray diffraction analysis were obtained.  $\text{C}_{44}\text{H}_{68}\text{Cu}_2\text{N}_6\text{O}_{12}$  (1000.15): calcd. C 52.84, H 6.85, N 8.40; found C 53.26, H 6.52, N 8.13. IR (KBr):  $\tilde{\nu}$

= 3583.5–3268.9, 2977.4, 1611.9, 1569.5, 1410.5, 1378.7, 1310.3, 1159.1, 821.7, 786.9, 657.7, 615.3 cm<sup>−1</sup>.

**[{Cu(Me<sub>3</sub>CCOO)<sub>4</sub>(NITpPy)<sub>2</sub>}<sub>n</sub>] (3):** Cu(Me<sub>3</sub>CCOO)<sub>2</sub>·2H<sub>2</sub>O (0.0556 g, 0.2 mmol) was dissolved with prolonged stirring at 50 °C in methanol (15 mL). Then NITpPy (0.0936 g, 0.4 mmol) was dissolved in methanol (10 mL). Both solutions were mixed while stirring was continued for 2 h. Then the solutions were filtered. The clear dark blue filtrate was allowed to stand at room temperature for 8 d, following which single crystals suitable for an X-ray diffraction analysis was obtained. C<sub>32</sub>H<sub>52</sub>Cu<sub>2</sub>N<sub>3</sub>O<sub>10</sub> (765.87): calcd. C 50.18, H 6.84, N 5.49; found C 50.54, H 6.50, N 5.24. IR (KBr):  $\tilde{\nu}$  = 3666.1–3326.3, 1610.5, 1550.7, 1396.5, 1317.4, 1217.1, 1168.8, 835.2, 777.3, 725.2 cm<sup>−1</sup>.

**Physical Measurements:** Elemental analyses for carbon, hydrogen, and nitrogen were carried out on a Vario-EL III elemental analyzer. Infrared spectra were recorded on a SHIMADZU IR prestige-21

FTIR-8400S spectrometer in the spectral range 4000–400 cm<sup>−1</sup>, with the samples in the form of potassium bromide pellets. Temperature-dependent magnetization (*M*–*T*) and magnetic hysteresis (*M* vs. *H*) (Figures 2–4) of three complexes were measured in the temperature range from 2 to 300 K using a Quantum Design vibrating sample magnetometer (VSM) in a physical property measurement system (PPMS). Data were corrected for the sample holder and diamagnetism was estimated from Pascal constants.

**X-ray Structure Determination:** The single-crystal X-ray diffraction data of the three complexes were recorded by using a Rigaku SCXmini diffractometer with the  $\omega$ -scan technique at 298 K with graphite-monochromated Mo-K $\alpha$  radiation ( $\lambda$  = 0.071073 nm). The lattice parameters were obtained by using the CrystalClear software.<sup>[28]</sup> The absorption correction was carried out by using a multiscan method. *N* independent reflections and *N*<sub>o</sub> with *I* > 2.0 $\sigma$ (*I*) were observed. The details of the data collection, crystallographic data, and reduction are summarized in Table S1 in the Supporting Information. The structure was solved by full-matrix least-squares methods using *F*<sup>2</sup> data. The SHELXS-97 and SHELXL-97 programs<sup>[29]</sup> were used for structure solution and refinement, respectively. Reliability factors were defined as  $R_1 = \Sigma(|F_o| - |F_c|)/\Sigma|F_o|$  and the function minimized was  $R_w = [\Sigma w(F_o^2 - F_c^2)^2/\Sigma w(F_o^4)]^{1/2}$ , where in the least-squares calculation the unit weight was used. All non-hydrogen atoms were refined anisotropically. The hydrogen atoms were inserted at their calculated positions and fixed at their positions. Selected bond lengths and angles of **1**, **2**, and **3** are listed in Table 1. The molecular graphics were prepared by using the DIAMOND program.<sup>[30]</sup>

CCDC-759170 (for **1**), -759171 (for **2**), and -759172 (for **3**) contain the supplementary crystallographic data for this paper. These data can be obtained free of charge from The Cambridge Crystallographic Data Centre via [www.ccdc.cam.ac.uk/data\\_request/cif](http://www.ccdc.cam.ac.uk/data_request/cif).

**Supporting Information** (see also the footnote on the first page of this article): The packing plots of complexes **1** and **2** are revealed in Figure S1; plots of the reduced magnetization for complexes **1**–**3** are shown in Figures S2–S4, respectively. Table S1 contains the crystal data and structure refinements for these three complexes and Table S2 shows the intermolecular hydrogen-bond information of **1**.

## Acknowledgments

This work was supported by the National Natural Science Foundation of China (project 20671019).

Table 1. Selected distances [Å], bond lengths [Å], and angles [°] for complexes **1**–**3**.

Complex 1			
Cu1–O1	1.967(4)	Cu1–N1	2.029(5)
Cu1–O5	2.630(5)		
O1A–Cu1–O1	180.00	N1–Cu1–N1A	180.00
O5A–Cu1–O5	180.00	O1A–Cu1–O5	96.38(2)
O1A–Cu1–N1	89.15(2)	O1–Cu1–O5	83.62(2)
O1–Cu1–N1	90.85(2)	N1–Cu1–O5	85.35(2)
N1A–Cu1–O5	94.65(2)		
Complex 2			
Cu1–O5	1.99(5)	Cu2–O6	1.98(7)
Cu1–O7	1.97(2)	Cu2–O8	1.96(7)
Cu1–O9	1.97(6)	Cu2–O10	1.95(2)
Cu1–O11	1.94(2)	Cu2–O12	1.94(9)
Cu1–N1	2.18(2)	Cu2–N1	2.20(7)
Cu1...Cu2	2.61(2)		
O11–Cu1–O7	169.8(5)	O12–Cu2–O10	90.0(4)
O11–Cu1–O9	89.0(4)	O12–Cu2–O8	168.0(4)
O7–Cu1–O9	88.8(6)	O10–Cu2–O8	88.6(4)
O11–Cu1–O5	89.8(4)	O12–Cu2–O6	89.6(4)
O7–Cu1–O5	90.2(4)	O10–Cu2–O6	170.0(4)
O9–Cu1–O5	167.7(4)	O8–Cu2–O6	89.8(4)
O11–Cu1–N1	96.0(3)	O8–Cu2–N4	95.6(4)
O7–Cu1–N1	94.2(3)	O12–Cu2–N4	96.0(4)
O9–Cu1–N1	95.9(3)	O10–Cu2–N4	96.4(4)
O5–Cu1–N1	96.4(3)	O6–Cu2–N4	93.9(4)
Complex 3			
Cu1–O5	1.92(7)	Cu2–O4	1.92(9)
Cu1–O9	1.93(4)	Cu2–O8	1.93(7)
Cu1–O3	1.96(1)	Cu2–O6	1.96(9)
Cu1–O7	1.97(5)	Cu2–O10	1.98(5)
Cu1–O1	2.26(5)	Cu2–N3	2.16(4)
Cu1...Cu2	2.62(4)		
O5–Cu1–O9	175.36(1)	O4–Cu2–O8	171.63(1)
O5–Cu1–O3	90.31(1)	O4–Cu2–O6	89.42(2)
O9–Cu1–O3	88.65(5)	O8–Cu2–O6	88.95(2)
O5–Cu1–O7	89.79(1)	O4–Cu2–O10	89.05(2)
O9–Cu1–O7	90.03(1)	O8–Cu2–O10	89.89(2)
O3–Cu1–O7	164.82(1)	O6–Cu2–O10	161.43(2)
O5–Cu1–O1	93.82(1)	O4–Cu2–N3	95.43(2)
O9–Cu1–O1	90.72(1)	O8–Cu2–N3	92.93(2)
O3–Cu1–O1	90.57(1)	O6–Cu2–N3	103.00(2)
O7–Cu1–O1	104.57(1)	O10–Cu2–N3	95.57(2)

- [1] K. Barthelet, D. Riou, G. Ferey, *Chem. Commun.* **2002**, 1492–1597.
- [2] J. F. Ma, J. Yang, G. L. Zheng, L. Li, J. F. Liu, *Inorg. Chem.* **2003**, 42, 7531–7534.
- [3] A. Alberola, E. Coronado, C. Gimenez-Saiz, C. J. Gomez-Garcia, F. M. Romero, A. Tarazon, *Eur. J. Inorg. Chem.* **2005**, 389–400.
- [4] Z. L. Liu, L. C. Li, D. H. Liao, Z. H. Jiang, S. P. Yan, *Cryst. Growth Des.* **2005**, 5, 783–789.
- [5] Z. L. Liu, Z. L. Lu, D. Q. Zhang, Z. H. Jiang, L. C. Li, C. M. Liu, D. B. Zhu, *Inorg. Chem.* **2004**, 43, 6620–6627.
- [6] K. Fegy, D. Luneau, T. Ohm, C. Paulsen, P. Rey, *Angew. Chem. Int. Ed.* **1998**, 37, 1270–1273.
- [7] E. F. Ullman, J. H. Siecki, D. G. B. Boocock, R. Darcy, *J. Am. Chem. Soc.* **1972**, 94, 7049–7059.
- [8] K. Fegy, D. Luneau, E. Belorizky, M. Novac, J. L. Tholence, C. Paulsen, T. Ohm, P. Rey, *Inorg. Chem.* **1998**, 37, 4524–4532.

- [9] K. Fegy, N. Sanz, D. Luneau, E. Belorizky, P. Rey, *Inorg. Chem.* **1998**, 37, 4518–4523.
- [10] M. Fettohi, M. Khaled, A. Waheed, S. Golhen, L. Ouahab, J. P. Sutter, O. Kahn, *Inorg. Chem.* **1999**, 38, 3967–3971.
- [11] G. Francese, F. M. Romero, A. Neels, H. Stoeckli-Evans, S. Decurtins, *Inorg. Chem.* **2000**, 39, 2087–2095.
- [12] D. Luneau, F. M. Romero, R. Ziessel, *Inorg. Chem.* **1998**, 37, 5078–5087.
- [13] J. Omata, T. Ishida, D. Hashizume, F. Iwasaki, T. Nogami, *Inorg. Chem.* **2001**, 40, 3954–3958.
- [14] L. C. Li, D. Z. Liao, Z. H. Jiang, S. P. Yan, *J. Chem. Soc., Dalton Trans.* **2002**, 1350–1353.
- [15] Y. H. Chung, H. H. Wei, *Inorg. Chem. Commun.* **1999**, 2, 269–271.
- [16] A. Caneschi, F. Ferraro, D. Gatteschi, P. Rey, R. Sessoli, *Inorg. Chem.* **1990**, 29, 1756–1760.
- [17] M. Kato, Y. Muto, *Coord. Chem. Rev.* **1988**, 92, 45–83.
- [18] L. C. Porter, M. H. Dickman, R. J. Doedens, *Inorg. Chem.* **1983**, 22, 1962–1964.
- [19] L. C. Porter, R. J. Doedens, *Inorg. Chem.* **1985**, 24, 1006–1010.
- [20] A. Caneschi, D. Gatteschi, P. Rey, *Prog. Inorg. Chem.* **1991**, 39, 331–429.
- [21] B. Chiari, O. Piovesana, T. Tarantelli, P. F. Zanazzi, *Inorg. Chem.* **1993**, 32, 4834–4838.
- [22] O. Kahn, *Molecular Magnetism*, VCH Publishers, New York, **1993**, p. 226.
- [23] H. H. Lin, H. H. Wei, G. H. Lee, Y. Wang, *Polyhedron* **2001**, 20, 3057–3062; I. Dasna, S. Golhen, L. Ouahab, M. Fettohi, O. Pena, N. Daro, J. P. Sutter, *Inorg. Chim. Acta* **2001**, 326, 37–46.
- [24] Y. H. Chung, H. H. Wei, G. H. Lee, Y. Wang, *Inorg. Chim. Acta* **1999**, 293, 30–36; I. Dasna, S. Golhen, L. Ouahab, O. Pena, N. Daro, J. P. Sutter, *New J. Chem.* **2000**, 24, 903–906; M. Mikiyama, H. Azuma, R. Nukada, Y. Sayama, K. Tanaka, J. W. Lim, M. Handa, *Bull. Chem. Soc. Jpn.* **2000**, 73, 2493–2498.
- [25] O. Kahn, *Molecular Magnetism*, VCH Publishers, New York, **1993**, p. 263.
- [26] A. Caneschi, D. Gatteschi, A. Grand, J. Laugier, L. Pardi, P. Rey, *Inorg. Chem.* **1988**, 27, 1031–1035.
- [27] R. B. R. C. Mehrotra, *Metal Carboxylates*, Academic Press, New York, **1983**.
- [28] Rigaku, *CrystalClear*, version 14.0, Rigaku Corporation, Tokyo, Japan, **2005**.
- [29] G. M. Sheldrick, *SHELXS97: Programs for Crystal Structure Analysis*, University of Göttingen, Germany, **1997**.
- [30] K. Brandenburg, *DIAMOND: Crystal and Molecular Structure Visualization*, version 3.1b, Crystal Impact GbR, Bonn, Germany, **2006**.

Received: January 3, 2010  
Published Online: June 16, 2010



# Click Chelators – The Behavior of Platinum and Palladium Complexes in the Presence of Guanosine and DNA

Aurélien Chevry,<sup>[a]</sup> Marie-Laure Teyssot,<sup>[a]</sup> Aurélie Maisoniai,<sup>[a]</sup> Pascale Lemoine,<sup>\*,[b]</sup> Bernard Viossat,<sup>[b]</sup> Mounir Traïkia,<sup>[a]</sup> David J. Aitken,<sup>[a][‡]</sup> Georges Alves,<sup>[c]</sup> Laurent Morel,<sup>[c]</sup> Lionel Nauton,<sup>[a]</sup> and Arnaud Gautier<sup>\*,[a]</sup>

**Keywords:** Platinum / Palladium / Click chemistry / Conformation analysis / DNA / Antitumor agents

Triazole chelators, synthesized by click chemistry, are convenient ligands for palladium(II) and platinum(II). Conformational changes induced by the complexation of these Pd<sup>II</sup> and

Pt<sup>II</sup> complexes with guanosine are similar to those of cisplatin. In addition, these complexes behave like cisplatin with regard to the relaxation of supercoiled plasmid DNA.

## Introduction

The emergence of “click chemistry” as a new paradigm for organic synthesis, invoking only simple, high-yielding and easily workable transformations, has facilitated an extraordinary expansion of the number of molecules available for medicinal chemistry.<sup>[1]</sup> Among these click reactions is the copper-catalyzed Huisgen [2+3] cycloaddition, also denoted as copper(I)-catalyzed azide–alkyne cycloaddition (CuAAC), which has received unrivalled attention, and has furnished an impressive array of new biologically relevant compounds.<sup>[2]</sup> In general, 1,2,3-triazole has proven itself useful for metal binding, and it is not surprising that such ligands find use in bioinorganic chemistry.<sup>[3]</sup> Schibli and co-workers take advantage of the binding properties of 1,2,3-triazole in a “click to chelate” approach to synthesize stable complexes of radionuclides that target tumors.<sup>[4]</sup> We also used the 1,2,3-triazole subunit to chelate platinum(II), and reported the cytotoxicity of this cisplatin analogue on cancer cell lines.<sup>[5]</sup>

Anticancer platinum drugs have enjoyed a long history since the discovery of cisplatin {*cis*-diaminedichloroplatinum(II)} by Rosenberg et al. in the 1960s.<sup>[6]</sup> Most of

the well known platinum-based anticancer compounds share the general formula *cis*-[PtX<sub>2</sub>(NH<sub>2</sub>R)<sub>2</sub>] in which R is an organic subunit, and X is a leaving group, usually a chloride. We have reported the chelation properties of the inverse and regular bidentate chelators such as (1,2,3-triazolyl)methylamine **1** for platinum(II) (Figure 1).<sup>[5]</sup> Our findings are in agreement with previous literature results, and show, in our hands, that complexes form easily from regular free aliphatic amine ligands; conversely, complexations from the corresponding inverse ligands are scarce, probably due to the lower electronic density at the C<sup>3</sup> atom of the 1,2,3-triazole moiety.<sup>[4,5]</sup> The *N,N* regular complexes of Pt<sup>II</sup> exhibit an IC<sub>50</sub> that is greater than that of the regular *N,O* complexes according to well known structure activity relationships of platinum complexes.<sup>[7]</sup> Our main concern now focuses on the propensity of **1** to form palladium chelates and to evaluate the behavior of the palladium and platinum chelates **2** and **3** in the presence of nucleotides and DNA.

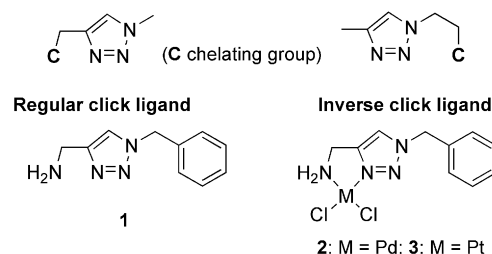


Figure 1. Schematic representation of regular and inverse click ligands and targeted complexes (C represents the chelating atom).

Indeed, even if palladium complexes have received less attention than their platinum analogs, recent studies have proved that this metal still retains some interest as depicted in Figure 2.<sup>[8]</sup>

[a] Clermont-Université, SEESIB, UMR CNRS 6504, Université Blaise Pascal, 24 avenue des Landais, 63177 Aubière Cedex, France  
E-mail: Arnaud.Gautier@univ-bpclermont.fr

[b] Université Paris 5, Faculté de Pharmacie, Laboratoire de cristallographie et RMN biologiques CNRS UMR-8015 4, avenue de l'observatoire, 75270 Paris Cedex 06, France  
E-mail: pascale.lemoine@univ-paris5.fr

[c] Clermont-Université, Université Blaise Pascal, GREd UMR 6247 CNRS, INSERM U931, 24 avenue des Landais, 63177 Aubière Cedex, France

[‡] Present address: Université Paris-Sud XI, Laboratoire de Synthèse Organique et Méthodologie, UMR8182 CNRS 15, rue Georges Clemenceau, 91405 Orsay Cedex, France

Supporting information for this article is available on the WWW under <http://dx.doi.org/10.1002/ejic.201000183>.

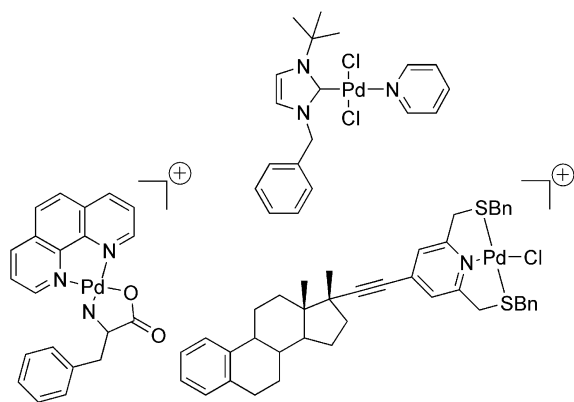


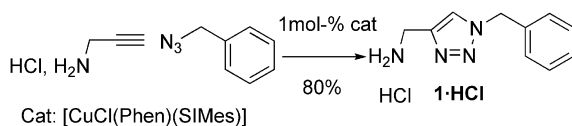
Figure 2. Some anticancer palladium(II) complexes.

Herein, we report the synthesis of the palladium complex **2** and its structural characteristics. We then determine if the candidates **2** and **3** behave like cisplatin in the presence of guanosine in terms of complexation, conformational behavior, and DNA affinity.

## Results and Discussion

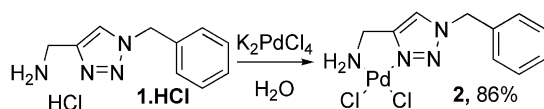
### Ligand Synthesis

The synthesis of **1** has been described previously, and uses tris(3-hydroxypropyltriazolylmethyl)amine (THPTA)/CuSO<sub>4</sub>/ascorbic acid] or [CuCl(SIMes)] – SIMes: 1,3-bis(2,4,6-trimethylphenyl)-4,5-dihydroimidazol-2-ylidene – as catalysts.<sup>[5]</sup> Alternatively, **1** can be easily synthesized from [CuCl(Phen)(SIMes)] – Phen: 1,10-phenanthroline – in good yields (Figure 3).<sup>[9]</sup>

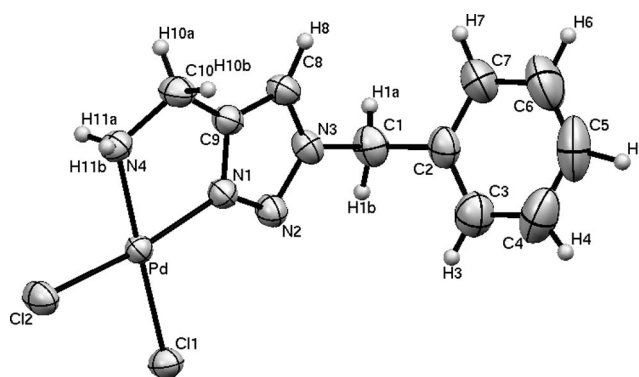
Figure 3. Synthesis of ligand **1**.

### Complexation

We were satisfied to observe that exposure of K<sub>2</sub>PdCl<sub>4</sub> to an aqueous solution of **1·HCl** resulted in the rapid formation of the expected neutral N<sub>2</sub>Cl<sub>2</sub> palladium complex **2**, which precipitated spontaneously from the reaction mixture (Figure 4). The reaction does not require the presence of the free amine **1** as was the case for the platinum complex **3**.<sup>[5]</sup>

Figure 4. Formation of complex **2**.

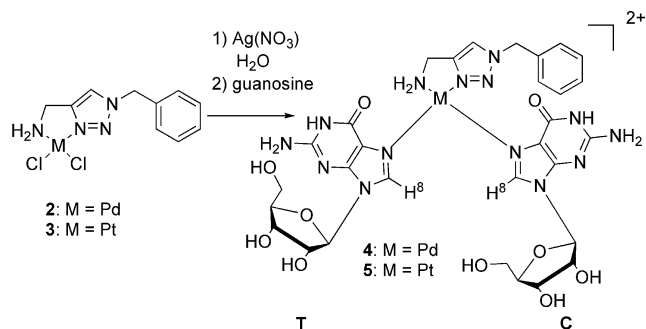
We succeeded in growing a single crystal of **2** by slow diffusion of ethanol into a saturated DMF solution of the complex, which was analyzed by X-ray diffraction. The ORTEP view presented in Figure 5 unambiguously proves the formation of a five-membered palladium chelate ring. Selected bond lengths and angles are summarized in Table 1. Similar to the platinum analog, the Pd<sup>II</sup> centre presents a distorted square-planar geometry, with an angle of 2° between the planes defined by N<sup>1</sup>–Pd–N<sup>4</sup> and Cl<sup>1</sup>–Pd–Cl<sup>2</sup>. The metal center bond lengths and angles fall into the usual ranges, although nonequivalence of the N–Pd bonds [N<sup>1</sup>–Pd: 2.000(2) Å; N<sup>4</sup>–Pd: 2.038(2) Å] and Pd–Cl bonds [Cl<sup>2</sup>–Pd: 2.270(1) Å; Cl<sup>1</sup>–Pd: 2.302(1) Å] is observed. The plane formed by the triazole ring atoms forms an angle of 7° with the plane defined by N<sup>1</sup>–Pd–N<sup>8</sup>.

Figure 5. ORTEP plot (50% thermal probability ellipsoids) of **2**.Table 1. Selected bond lengths and angles of complex **2**.

Distances [Å]			
N <sup>1</sup> –Pd	2.000(2)	Cl <sup>2</sup> –Pd	2.270(1)
N <sup>4</sup> –Pd	2.038(2)	H <sup>8</sup> –H <sup>10a</sup>	3.07(8)
Cl <sup>1</sup> –Pd	2.302(1)	H <sup>8</sup> –H <sup>10b</sup>	3.30(3)
Angles [°]			
N <sup>4</sup> –Pd–Cl <sup>2</sup>	90.35(5)	N <sup>1</sup> –Pd–Cl <sup>1</sup>	95.96(5)
N <sup>4</sup> –Pd–Cl <sup>1</sup>	176.90(5)	N <sup>1</sup> –Pd–Cl <sup>2</sup>	171.94(5)
N <sup>4</sup> –Pd–N <sup>1</sup>	81.69(7)	Cl <sup>1</sup> –Pd–Cl <sup>2</sup>	92.06(2)

### Guanosine Adducts of **2** and **3**

The reaction of the activated aqua form of the complexes **2** and **3** with guanosine was investigated. A suspension of each complex in water was reacted for two days in the presence of 2 equiv. of AgNO<sub>3</sub>, then filtered, and the resulting pale yellow solution was added to a suspension of 2.5 equiv. of guanosine in water (Figure 6). The solution was stirred overnight and filtered. For the palladium complex **4**, the product was used without further purification. In the case of the platinum complex **5**, the mixture was separated by preparative HPLC [MeOH/AcONH<sub>4</sub> (0.1 M), pH = 5.5; isocratic conditions], and the resulting platinum adduct was desalted with a dialysis membrane (cut-off 500).

Figure 6. Formation of complexes **4** and **5**.

The structures of complexes **4** and **5** were proved by  $^1\text{H}$  NMR spectroscopy (vide infra) and mass spectrometry. Peaks at  $m/z$  ( $z = +2$ ) 430 and 474 for compounds **4** ( $M = 860.19$ ) and **5** ( $M = 949.25$ ) respectively, were found in the mass spectra, accompanied by their isotopic signatures.

### Conformational Analysis

The pseudorotation model describes the conformational behavior of a nucleotide in solution by a fast equilibrium between two discrete conformers. T represents a twisted form, E an envelope form, and the superscript and subscript numbers refer to the atom in *endo* or *exo* configuration relative to  $\text{C}^5$  of the sugar, respectively, Figure 7.<sup>[10]</sup> In practice, a substituted five-membered ring rarely adopts a pure T or E form because of the asymmetric surroundings induced by the substituents. Each of the two conformers is mathematically characterized by two pseudorotation parameters, one phase coordinate ( $P$ ) and one puckering coordinate ( $\Phi_{\text{max}}$ ).<sup>[11]</sup> Several vectors in three-dimensional space

describe the system unambiguously: the coordinates are  $[P_N, \Phi_N, (1 - X)]$  and  $[P_S, \Phi_S, X]$ , where  $X$  is the molar fraction of the south component. The coordinates are calculated by a nonlinear regression calculation method based on NMR measurements of the time-averaged vicinal coupling constants (Pseurot program).<sup>[12]</sup>

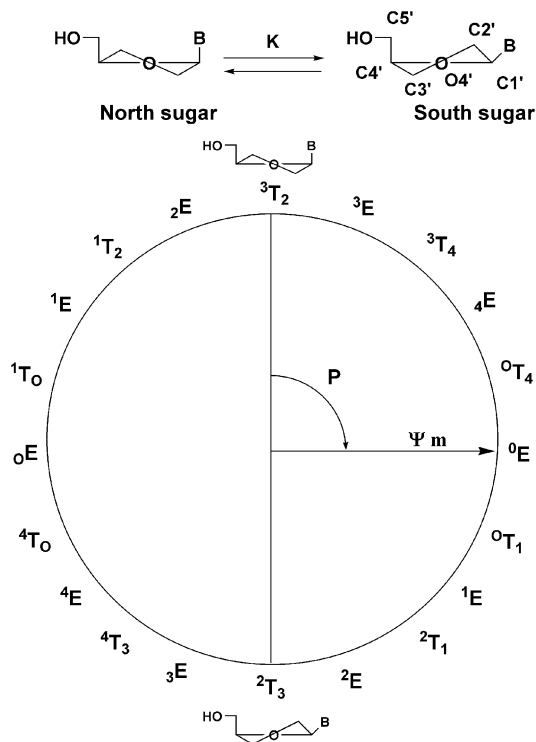
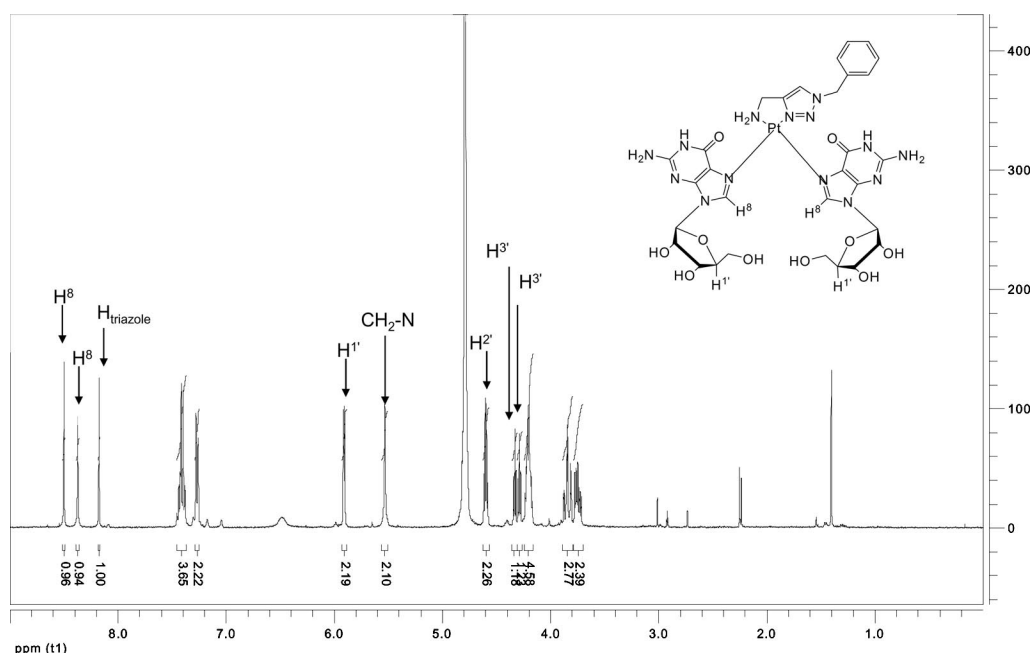


Figure 7. Discrete model and pseudorotational wheel of nucleosides.

Figure 8.  $^1\text{H}$  NMR of complex **5** in  $\text{D}_2\text{O}$  (300 K).

Plavec and Chattopadhyaya have reported a quantitative conformational study of the cisplatin–guanosine adduct.<sup>[13]</sup> They have demonstrated that, upon platination, the change of electronic character of the nucleobase is transmitted across the sugar ring and results in a shift of the north↔south ( $C3'endo \leftrightarrow C2'endo$ ) equilibrium as well as a reorientation of the nucleobase.

Overall, the parameters for the guanosine–cisplatin adduct and free guanosine are depicted in Table 2.

Table 2. Pseudorotational parameters and conformational equilibrium of the guanosine–cisplatin adduct.

	$P_N$	$\Phi_{\max S}$	$P_S$	$\Phi_{\max S}$	% sS	% anti
Guanosine	15	32	157	32	80	29
Cisplatin adduct	16	32	161	32	55	92

A detailed conformational analysis was undertaken on adducts **4** and **5** by NMR spectroscopy. The NMR spectrum of the platinum complex **5**, which is similar to that of complex **4**, is presented in Figure 8. It can be seen that a 1:2 (metal/guanosine) adduct forms almost exclusively. The spectrum displays two separate sets of signals for the nucleotides due to the asymmetry of the palladium complex (this nonequivalence is not observed in the case of the symmetrical cisplatin adduct).<sup>[13]</sup>

In terms of coupling constants, the two  $^1\text{H}$  NMR spectra reveal identical behavior for both sugars. We then attempted to assign each NMR peak for **4** and **5** using COSY, COSY-DQF (double-quantum filtered) and ROESY NMR experiments. Unfortunately, the lack of correlation between the nucleosides and the triazole subunit did not allow us to discriminate between the *cis* and *trans* sugar signals. However, each signal, regardless the nature of the sugar, was successfully assigned.

### Conformational Behavior of Complex 4

The coupling constants extracted from the NMR spectrum are collated in Table 3.

Table 3. Coupling constants of interest of complex **4**.

Coupling constants [Hz]					
$J_{H1'-H2'}$	$J_{H1'-H2'}$	$J_{H2'-H3'}$	$J_{H2'-H3'}$	$J_{H3'-H4'}$	$J_{H3'-H4'}$
4.8	4.8	4.8	4.8	4.9	4.9

Because of the presence of multiple overlapping signals due to the asymmetry of the ligand, we were unable to correctly extract the  $^1\text{H}$ – $^1\text{H}$  coupling constants of the furanose ring at different temperatures. This did not allow us to take advantage of the PSEUROT program to exactly determine the pseudorotational parameters and the equilibrium constants of the north and south conformers.<sup>[12]</sup> In order to gain a qualitative observation of the ribose conformational behavior, we used the simplest Altona–Sundaralingam equation that correlates the observed  $J_{H1'-H2'}$  and  $J_{H3'-H4'}$  coupling constants to the north↔south equilibrium, see Equation (1).<sup>[11b]</sup>

$$Ps = J_{H1'-H2'}/(J_{H1'-H2'} + J_{H3'-H4'}) \quad (1)$$

where  $Ps$  represents the population of the south conformer.

This calculation affords a south population of 49% (see data in Table 3), yielding close to a 1:1 ratio between the north and south conformers, a situation relatively close to that found for the cisplatin adduct.

With regard to the nucleobases orientations, the ROESY experiment reveals a strong correlation between the two guanosine  $H^8$  signals and the two overlapping signals of the anomeric  $H1'$ .<sup>[14]</sup> Based on the average distance for  $CH_2$ –N and  $H_{\text{triazole}}$  (3.19 Å) as a standard extracted from the X-ray data of **2**, the values of the two  $H^8$ – $H2'$  distances were found to be close to 2.6–2.7 Å, implying that each nucleobase is largely oriented to an *anti* conformation (80–90%) as found in the parent cisplatin adduct.

With the NMR observation in hand, a geometry optimization (Gaussian 03) for **4** was performed by DFT calculations [B3LYP/ 6-311G (C, N, O, H)/SDD (Pd)] in the gas phase to access its conformational parameters.<sup>[15]</sup> The choice of the basis set was dictated by the necessity to include the anomeric effect, which is taken into account by 6-311G, and to include the palladium atom that is not treated in this basis set, we used the Stuttgart/Dresden basis set (SDD) to gain a correspondence between the two triple- $\zeta$  basis.<sup>[16]</sup> For clarity purposes, each nucleoside was named according to its geometrical position from the triazole subunit in the square-planar complex. Thus, we named the nucleotide *trans* T and the nucleotide *cis* C according to Figure 6. Each possible conformer (T north C north, T north C south, T south C north, T south C south) was optimized, starting from *anti-anti* conformation of the two guanosine groups. The T north C north is presented in Figure 9 as a typical example and all the data of interest are collected in Tables 4 and 5.

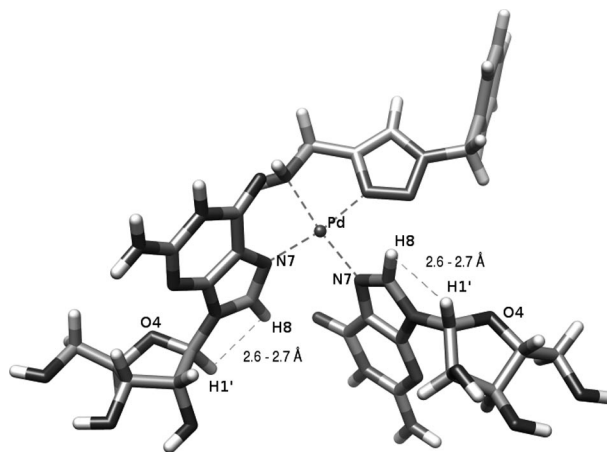


Figure 9. Geometry optimization of the T north C north conformer of **4**.

The results of the calculations reveal that palladium(II) retains its square-planar geometry correlating to bond lengths and angles already found in the structure of **2**. The  $H1'$ – $H^8$  distances calculated are in good agreement with the values found by the ROESY experiment and fall in the range typically found in the literature.<sup>[17]</sup>



Table 4. Calculated distances and angles of the palladium adduct **4**.

Distances [Å]	N <sup>1</sup> -Pd	N <sup>4</sup> -Pd	H <sup>1'</sup> -H <sup>8</sup> (T)	H <sup>1'</sup> -H <sup>8</sup> (C)
T north, C north	2.02	2.09	2.44	2.42
T north, C south	2.01	2.09	2.44	2.40
T south, C south	2.02	2.09	2.42	2.39
T south, C north	2.02	2.09	2.42	2.42
Angles [°]	N <sup>1</sup> -Pd-N <sup>4</sup>	N <sup>7</sup> -Pd-N <sup>7'</sup>		
T north, C north	80.6	93.8		
T north, C south	80.6	94.2		
T south, C south	80.6	93.8		
T south, C north	80.7	93.5		

Table 5. Calculated pseudorotational parameters of complex **4**.

Pseudorotational parameters [°]	$P_{(trans)}$	$\Phi_{max (trans)}$	$P_{(cis)}$	$\Phi_{max (cis)}$
T north, C north	46	39	45	38
T north, C south	46	39	164	40
T south, C south	153	35	164	40
T south, C north	152	35	44	39

Although some deviations from the cisplatin analogue are found, the computed pseudorotational parameters are in reasonable agreement with those found in literature.<sup>[13]</sup>

### Conformational Behavior of Complex **5**

The data extracted from the NMR spectra are collected in Table 6. There is no overlap of signals over a range of 20 °C, allowing us to extract nine coupling constants at three different temperatures.

Table 6. Coupling constants of interest in complex **5**.

	$J_{H^{1'}-H^{2'}}$ [Hz]	$J_{H^{2'}-H^{3'}}$ [Hz]	$J_{H^{3'}-H^{4'}}$ [Hz]
293 K	4.85	5.01	5.01
303 K	4.66	4.92	4.92
313 K	4.59	4.88	4.88

We then have nine physical data; a number superior to the seven parameters to be determined ( $P_N$ ,  $\Phi_N$ ,  $P_S$ ,  $\Phi_S$  and the three percentages). This gives an over-determined system and application of PSEUROT 6.3 furnishes the following pseudorotational and equilibrium parameters (Table 7).

Table 7. Pseudorotational and equilibrium parameters for complex **5**.

Pseudorotational parameters				
	$P_N$	$\Phi_N$	$P_S$	$\Phi_S$
	5.9	35	150	35.8
Equilibrium parameters				
$T$ [K]	293	303	313	
% south	49	48	48	
RMS [Hz] <sup>[a]</sup>	0.09	0.02	0.07	

[a] RMS: root mean square.

The results are similar to those found for the preceding palladium complex **4** and for the cisplatin adduct with a good overall root mean square (0.06 Hz).

With regard to the nucleobase orientations, results similar to those for **4** were found for compound **5** using the ROESY experiment. The distance of the two protons H<sup>8</sup>-H<sup>1'</sup> is found to be close to 2.6–2.7 Å, implying again that each nucleobase is largely oriented to an *anti* conformation (80–90%).

### Action of Complexes **2** and **3** on Supercoiled DNA

To ensure that DNA is also a target for these chelates, we examined the genotoxicity of **2** and **3** in vitro with the aid of the supercoiled pcDNA4TO plasmid. It is well known that upon platinum binding, a relaxation of the structure – easily visualized on gel electrophoresis – takes place. The behavior of our complexes was compared to that of cisplatin by agarose gel electrophoresis. Figure 10 presents the electrophoresis gel with the supercoiled plasmid as a blank in line 1. The endonuclease BamH1 was used to linearize the plasmid in line 2. Line 3 shows the effect of cisplatin, which is known to relax the supercoiled structure. Lines 4 and 5 depict the action of complexes **2** and **3** on the supercoiled plasmid respectively. From this experiment it is seen that the two complexes are able to relax the supercoiled structure of the plasmid.

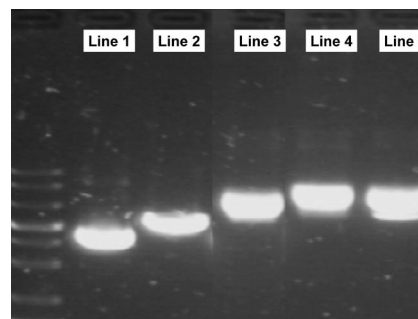


Figure 10. Action of **2** and **3** on plasmid DNA (1% agarose gel). Line 1: supercoiled plasmid blank, line 2: linearized plasmid by endonuclease BamH1, line 3: effect of cisplatin, line 4: effect of **2**, line 5: effect of **3**. (The blanks corresponding to water/NaClO<sub>4</sub> and water/DMF/NaClO<sub>4</sub> used for solubilising cisplatin and complexes **2** and **3** are similar to line 1).

### Conclusions

In conclusion, we have found that regular click chelators containing palladium or platinum can behave similar to cisplatin. Thus, guanosine adducts form easily and the conformational change produced by such complexation resembles that of cisplatin. Relaxation of DNA also takes place like the action of cisplatin.

### Experimental Section

**General:** The following procedures were used in all reactions unless otherwise noted. Reactions were stirred with a Teflon®-coated magnetic stirring bar. Removal of solvents was accomplished by evaporation on a Buchi rotary evaporator (water bath at 40 °C). All com-

mercially available reagents were used as received. NMR spectra were recorded in Fourier Transform mode with Bruker AVANCE 400 and 500 spectrometers at 25 °C. Chemical shifts are reported in ppm. Spin multiplicity is described by means of the following abbreviations: s = singlet, d = doublet, m = multiplet, and br. = broad. Coupling constants ( $J$ ) are reported in Hertz (Hz). Diffraction data were collected with an Enraf–Nonius CAD4 diffractometer at 293 K. The data collection and reduction were carried out with the CAD4 Express Enraf–Nonius CAD4 program package. All data were corrected for Lorentz-polarization effects and absorption corrections were made with Multi-Scan. The structures were solved through direct and Fourier methods and refined by full-matrix least-square methods based on  $F^2$  with the SIR92 and SHELXL-97 programs. Hydrogen atoms were located from a difference Fourier map and the same isotropic thermal parameters were then refined. The final least-square refinements ( $R1$ ) based on  $I > 2\sigma(I)$  converged to 0.0226. All calculations were conducted using DFT as implemented in the Gaussian 03 program. Geometry optimizations were performed using the restricted B3LYP exchange and correlation function and the triple- $\zeta$  6-311G(d,p) basis set for all atoms except for Pd (SDD basis set) [B3LYP/ 6-311G (C, N, O, H)/SDD (Pd)]. Harmonic frequency analysis based on analytical second derivatives was used to characterize the optimized geometries as local minima. Diffraction intensity data were collected at  $T = 293$  K with an Oxford-Diffraction XCALIBUR diffractometer [Mo- $K_\alpha$  radiation ( $\lambda = 0.7107$  Å)] with data collection and reduction by using the CrysAlis program package.<sup>[18]</sup> Data were corrected for Lorentz-polarization effects and empirical absorption corrections by using SCALE3 ABSPACK.<sup>[19]</sup> The structure was solved by direct methods with SIR-92<sup>[20]</sup> and refined by least-squares methods on  $F^2$  with SHELXL-97<sup>[21]</sup> incorporated in the WinGX package.<sup>[22]</sup> Hydrogen atoms were inserted at calculated positions with isotropic thermal parameters constrained to be 1.2 times the Ueq of the carrier atoms. The molecule was drawn by using CAMERON.<sup>[23]</sup>

### Procedures and Compounds

**1·HCl:**<sup>[5]</sup> Benzyl azide (266 mg, 2 mmol, 1.0 equiv.) and propargylamine hydrochloride (218 mg, 2.4 mmol, 1.2 equiv.) were mixed in a mixture of *tert*-butyl alcohol/H<sub>2</sub>O (2:1, 4 mL). 16 mg (0.04 mmol, 2 mol-%) of [CuCl(SiMes)] and 7.2 mg (0.04 mmol, 2 mol-%) of 1,10-phenanthroline were added sequentially. A color change to orange was observed, and the reaction was stirred for 12 h. The solvent was removed, and the resulting solid was taken up in ethanol. The resulting white solid was collected by filtration, and washed with diethyl ether to yield the desired pure triazole hydrochloride (358 mg, 80%).

**Palladium Complex 2:** 1·HCl (74.2 mg, 0.32 mmol, 1.0 equiv.) was dissolved in water (3 mL), and added to K<sub>2</sub>PdCl<sub>4</sub> (108 mg, 0.32 mmol, 1.0 equiv.) dissolved in water (2 mL). After a few minutes, a red brownish precipitate formed and the reaction was stirred 24 h. The precipitate was collected by filtration, washed with water (3 × 5 mL), MeOH (2 × 5 mL), ether (5 mL), and the resulting solid was dried in air to yield pure complex **2** (104 mg, 86%). Crystals were obtained by dissolving **2** in a minimum amount of DMF. Crystals were grown by slow diffusion of ethanol in a closed desiccator kept at 35 °C for two weeks. <sup>1</sup>H NMR ([D<sub>6</sub>]DMSO):  $\delta$  = 8.29 (s, 1 H, triazole), 7.40 (m, 5 H, Ar), 5.68 (s, 2 H, CH<sub>2</sub>), 5.58 (m, 2 H, CH<sub>2</sub>), 3.68 (m, 2 H, NH<sub>2</sub>) ppm. <sup>13</sup>C NMR ([D<sub>6</sub>]DMSO):  $\delta$  = 152.0, 134.6, 128.8, 128.6, 128.2, 122.3, 54.6, 40.4 ppm. C<sub>10</sub>H<sub>12</sub>Cl<sub>2</sub>N<sub>4</sub>Pd (365.6): calcd. C 32.86, H 3.31, N 15.33; found C 33.44, H 3.49, N 15.56.

**Palladium Complex 4:** Compound **2** (46 mg, 0.13 mmol, 1.0 equiv.) was stirred in D<sub>2</sub>O (2.5 mL) in the presence of AgNO<sub>3</sub> (53.9 mg,

0.31 mmol, 2.4 equiv.) in the absence of light for 2 d. The reaction mixture was passed through a Millipore filter to yield a pale yellow solution that was added to guanosine (89.9 mg, 0.31 mmol, 2.5 equiv.). The suspension was stirred for 24 h, and passed through a Millipore filter before being analyzed by <sup>1</sup>H NMR spectroscopy. <sup>1</sup>H NMR (D<sub>2</sub>O):  $\delta$  = 8.60 (s, 1 H, H<sup>8</sup>); 8.45 (s, 1 H, H<sup>8</sup>); 8.35 (s, 1 H, triazole), 7.60–7.48 (m, 3 H, Ar), 7.35 (m, 2 H, Ar), 6.05 (d,  $J$  = 4.5 Hz, 1 H, H<sup>1'</sup>), 6.01 (d,  $J$  = 4.5 Hz, 2 H, H<sup>1'</sup>), 5.62 (s, 2 H, CH<sub>2</sub>), 4.75 (t,  $J$  = 4.5 Hz, 1 H, H<sup>2'</sup>), 4.72 (t,  $J$  = 4.5 Hz, 1 H, H<sup>2'</sup>), 4.47 (t,  $J$  = 4.5 Hz, 1 H, H<sup>3'</sup>), 4.40 (t,  $J$  = 4.5 Hz, 1 H, H<sup>3'</sup>), 4.36 (m, 2 H, CH<sub>2</sub>), 4.33 (m, 2 H, CH<sub>2</sub>), 4.10–3.80 (m, 6 H, H<sup>4'</sup>, H<sup>5'</sup>, H<sup>5'</sup> of the two riboses) ppm.

**Platinum Complex 5:** Compound **3** (50.0 mg, 0.11 mmol, 1.0 equiv.) was stirred in H<sub>2</sub>O (2.0 mL) in the presence of AgNO<sub>3</sub> (47.0 mg, 0.28 mmol, 2.5 equiv.) in the absence of light for 3 d. The reaction mixture was passed through a Millipore filter to yield a pale yellow solution that was added to guanosine (77.9 mg, 0.28 mmol, 2.5 equiv.). The suspension was stirred 24 h and passed through a Millipore filter. The solution was then lyophilized, the mixture purified by C-18 preparative HPLC [MeOH/AcONH<sub>4</sub> (0.1 M): 75:25, pH = 5.5; isocratic conditions], and the fractions containing the adduct **5** were lyophilized. The resulting solid was dissolved in water (20 mL) and desalted using a dialysis membrane (cut-off: 500) to yield pure adduct **5** (30 mg). <sup>1</sup>H NMR (D<sub>2</sub>O):  $\delta$  = 8.55 (s, 1 H, H<sup>8</sup>); 8.25 (s, 1 H, H<sup>8</sup>); 8.05 (s, 1 H, triazole), 7.30–7.25 (m, 3 H, Ar), 7.10 (m, 2 H, Ar), 5.80 (d,  $J$  = 4.5 Hz, 1 H, H<sup>1'</sup>), 5.75 (d,  $J$  = 4.5 Hz, 2 H, H<sup>1'</sup>), 5.35 (s, 2 H, CH<sub>2</sub>), 4.45 (t,  $J$  = 4.5 Hz, 1 H, H<sup>2'</sup>), 4.42 (t,  $J$  = 4.5 Hz, 1 H, H<sup>2'</sup>), 4.25 (t,  $J$  = 4.5 Hz, 1 H, H<sup>3'</sup>), 4.20 (t,  $J$  = 4.5 Hz, 1 H, H<sup>3'</sup>), 3.90 (m, 2 H, CH<sub>2</sub>), 3.85 (m, 2 H, CH<sub>2</sub>), 3.75–3.70 (m, 6 H, H<sup>4'</sup>, H<sup>5'</sup>, H<sup>5'</sup> of the two riboses) ppm.

**DNA Gel Electrophoresis:** Three solutions (3 × 10<sup>−4</sup> M) of **2**, **3** and cisplatin were prepared in DMF and water. 1  $\mu$ L of each solution was added to 1.4  $\mu$ g of plasmid pcDNA 4T0 in the presence of 30  $\mu$ L NaClO<sub>4</sub> (10<sup>−2</sup> M) and incubated for 24 h at 37 °C. Samples were then analyzed by agarose (1%) electrophoresis and DNA was revealed with BET under UV light.

**Supporting Information** (see also the footnote on the first page of this article): <sup>1</sup>H, <sup>13</sup>C, and mass spectra of complexes **2** and **4**, <sup>1</sup>H, HPLC profile, and mass spectra of adduct **5**.

CCDC-647394 contains the supplementary crystallographic data. These data can be obtained free of charge from The Cambridge Crystallographic Data Centre via [www.ccdc.cam.ac.uk/data\\_request/cif](http://www.ccdc.cam.ac.uk/data_request/cif).

### Acknowledgments

We thank Aurélie Job for the purification of compound **5** and Bertrand Legeret for mass analysis.

- [1] H. C. Kolb, M. G. Finn, K. B. Sharpless, *Angew. Chem. Int. Ed.* **2001**, *40*, 2004–2021.
- [2] a) C. W. Tornøe, M. Meldal, *Peptides: The wave of the future* (Eds.: M. Lebl, R. A. Houghton); Kluwer Academic Publishers, Dordrecht, **2001**, pp. 263–264; b) C. W. Tornøe, C. Christensen, M. Meldal, *J. Org. Chem.* **2002**, *67*, 3057–3064; c) M. Meldal, C. W. Tornøe, *Chem. Rev.* **2008**, *108*, 2952–3015; d) V. D. Bock, H. Hiemstra, J. H. van Maarseveen, *Eur. J. Org. Chem.* **2006**, 51–68; e) H. C. Kolb, K. B. Sharpless, *Drug Des. Today* **2003**, *8*, 1128–1137.
- [3] For an excellent review, see: H. Struthers, T. L. Mindt, R. Schibli, *Dalton Trans.* **2010**, 39, 675–696.
- [4] a) T. L. Mindt, H. Struthers, L. Brans, T. Anguelov, C. Schweinsberg, V. Maes, D. Tourwé, R. Schibli, *J. Am. Chem.*

- Soc.* **2006**, 128, 15096–15097; b) T. L. Mindt, C. Müller, M. Melis, M. de Jong, M. R. Schibli, *Bioconjugate Chem.* **2008**, 19, 1689–1695; c) H. Struthers, B. Spingler, T. L. Mindt, R. Schibli, *Chem. Eur. J.* **2008**, 14, 6173–6183. Other examples: d) A. Nadler, C. Hain, U. Diederichsen, *Eur. J. Org. Chem.* **2009**, 27, 4593–4599; e) M. L. Bowen, C. Orvig, *Chem. Commun.* **2008**, 41, 5077–5091; f) R. M. Meudtner, M. Ostermeier, R. Goddard, C. Limberg, S. Hecht, *Chem. Eur. J.* **2007**, 13, 9834–9840; g) Interestingly, a collection of inverse click ligands has been amassed, but to date no studies of transition metals complexation were reported; for example see: D. Urankar, J. Kosmrlj, *J. Comb. Chem.* **2008**, 10, 981–985.
- [5] For part I, see: A. Maisonia, P. Serafin, M. Traïkia, E. Debiton, V. Théry, D. J. Aitken, P. Lemoine, B. Viossat, A. Gautier, *Eur. J. Inorg. Chem.* **2008**, 298–305.
- [6] B. Rosenberg, L. van Camp, T. Krigas, *Nature* **1965**, 205, 698–699.
- [7] a) M. J. Cleare, J. D. Hoeschele, *Bioinorg. Chem.* **1973**, 2, 187–210; b) J. Reedijk, *Inorg. Chim. Acta* **1992**, 873, 198–200.
- [8] a) E. J. Gao, Q. T. Liu, L. Y. Duan, *Russ. J. Coord. Chem.* **2007**, 33, 120–123; b) A. Jackson, J. Davis, R. J. Pither, A. Rodger, M. J. Hannon, *Inorg. Chem.* **2001**, 40, 3964–3973; c) S. Ray, R. Mohan, J. K. Singh, M. K. Samantaray, M. M. Shaikh, D. Panda, P. Ghosh, *J. Am. Chem. Soc.* **2007**, 129, 15042–15053; d) S. Fakih, W. C. Tung, D. Eierhoff, C. Mock, B. Krebs, *Z. Anorg. Allg. Chem.* **2005**, 631, 1397–1402; e) G. Zhao, H. Lin, S. Zhu, H. Sun, Y. Chen, *J. Inorg. Biochem.* **1998**, 70, 219–226; f) E. Amtmann, W. Friebolin, G. Schilling, A pharmaceutical preparation containing palladium complex compounds and the uses thereof for treating cancer and autoimmune disease, WO Patent 018043, **2004**.
- [9] M.-L. Teyssot, A. Chevy, M. Traïkia, M. El-Ghozzi, D. Avignant, A. Gautier, *Chem. Eur. J.* **2009**, 15, 6322–6326.
- [10] a) C. A. G. Haasnoot, F. A. A. M. de Leeuw, C. Altona, *Tetrahedron* **1980**, 36, 2783–2792; b) C. Altona, *Recl. Trav. Chim. Pays-Bas* **1982**, 101, 413–433.
- [11] a) C. Altona, M. Sundaralingam, *J. Am. Chem. Soc.* **1972**, 94, 8205–8212; b) C. Altona, M. Sundaralingam, *J. Am. Chem. Soc.* **1973**, 95, 2333–2344.
- [12] J. van Wijk, C. A. G. Haasnoot, F. A. A. M. de Leeuw, B. D. Huckriede, A. W. Hoekzema, C. Altona, *PSEUROT 6.3*, Leiden Institute of Chemistry, Leiden University, Leiden, The Netherlands, **1999**.
- [13] M. Polak, J. Plavec, A. Trifonova, A. Földesi, J. Chattopadhyaya, *J. Chem. Soc. Perkin Trans. 1* **1999**, 2835–2843.
- [14] The classical NOESY experiments were not adapted due to the molecular weight of **5** ( $M = 891$  g/mol). Indeed, on routine spectrometers, the NOE experiment is not effective for compounds of  $M = 500$ – $1000$  g/mol, and ROESY should be used. See: a) A. A. Bothner-By, R. L. Stephens, J. Lee, C. D. Warren, R. W. Jeanloz, *J. Am. Chem. Soc.* **1984**, 106, 811–813; b) A. Bax, D. G. Davis, *J. Magn. Reson.* **1985**, 63, 207–213; c) T. L. Wang, A. J. Shaka, *J. Magn. Res. A* **1992**, 114, 3157–3159. For the determination of the distances, see: d) E. Ammalahti, M. Bardet, D. Dalko, J. Cadet, *J. Magn. Res. A* **1996**, 122, 230–232.
- [15] a) M. J. Frisch, G. W. Trucks, H. B. Schlegel, G. E. Scuseria, M. A. Robb, J. R. Cheeseman, J. A. Montgomery, Jr., T. Vreven, K. N. Kudin, J. C. Burant, J. M. Millam, S. S. Iyengar, J. Tomasi, V. Barone, B. Mennucci, M. Cossi, G. Scalmani, N. Rega, G. A. Petersson, H. Nakatsuji, M. Hada, M. Ehara, K. Toyota, R. Fukuda, J. Hasegawa, M. Ishida, T. Nakajima, Y. Honda, O. Kitao, H. Nakai, M. Klene, X. Li, J. E. Knox, H. P. Hratchian, J. B. Cross, V. Bakken, C. Adamo, J. Jaramillo, R. Gomperts, R. E. Stratmann, O. Yazyev, A. J. Austin, R. Cammi, C. Pomelli, J. W. Ochterski, P. Y. Ayala, K. Morokuma, G. A. Voth, P. Salvador, J. J. Dannenberg, V. G. Zakrzewski, S. Dapprich, A. D. Daniels, M. C. Strain, O. Farkas, D. K. Malick, A. D. Rabuck, K. Raghavachari, J. B. Foresman, J. V. Ortiz, Q. Cui, A. G. Baboul, S. Clifford, J. Cioslowski, B. B. Stefanov, G. Liu, A. Liashenko, P. Piskorz, I. Komaromi, R. L. Martin, D. J. Fox, T. Keith, M. A. Al-Laham, C. Y. Peng, A. Nanayakkara, M. Challacombe, P. M. W. Gill, B. Johnson, W. Chen, M. W. Wong, C. Gonzalez, J. A. Pople, *Gaussian 03*, Revision D.01, Gaussian, Inc., Wallingford, CT, **2004**; b) for B3LYP method: A. J. Cohen, N. C. Handy, *Mol. Phys.* **2001**, 99, 607.
- [16] For calculation of the anomeric effect using the Gaussian program, see: C. Thibaudeau, P. Acharya, J. Chattopadhyaya, *Stereoelectronic Effects in Nucleotides and Nucleosides and Their Structural Implications*, Uppsala University Press, Uppsala, **2002**.
- [17] H. Rosemeyer, G. Toth, B. Golankiewicz, Z. Kazimierzczuk, W. Bourgeois, U. Kretschmer, H. P. Muth, F. Seela, *J. Org. Chem.* **1990**, 55, 5784–5790.
- [18] *CrysAlis RED*, Oxford Diffraction Ltd., version 1.171.31.5 (rel. 28-08-2006, CrysAlis171.NET) (compiled August 28, 2006, 13:05:05).
- [19] N. Walker, D. Stuart, *Acta Crystallogr., Sect. A* **1983**, 39, 158–166.
- [20] A. Altomare, G. Cascarano, C. Giacovazzo, A. Guagliardi, M. C. Burla, G. Polidori, M. Camalli, *J. Appl. Crystallogr.* **1994**, 27, 435–436.
- [21] G. M. Sheldrick, *SHELXL-97: Program for Crystal Structure Refinement*, University of Göttingen, Germany, **1997**.
- [22] WinGX-version 1.63.02: L. J. Farrugia, *J. Appl. Crystallogr.* **1999**, 32, 837–838.
- [23] D. J. Watkin, C. K. Prout, L. J. Pearce, *CAMERON*, Chemical Crystallography Laboratory, Oxford, UK, **1996**.

Received: February 15, 2010  
Published Online: June 21, 2010

# Synthesis, Structure and in Vitro Biological Screening of Palladium(II) Complexes of Functionalised Salicylaldimine Thiosemicarbazones as Antimalarial and Anticancer Agents

Prinessa Chellan,<sup>[a]</sup> Nelusha Shunmoogam-Gounden,<sup>[b]</sup> Denver T. Hendricks,<sup>[b]</sup> Jiri Gut,<sup>[c]</sup> Philip J. Rosenthal,<sup>[c]</sup> Carmen Lategan,<sup>[d]</sup> Peter J. Smith,<sup>[d]</sup> Kelly Chibale,<sup>[a,e]</sup> and Gregory S. Smith<sup>\*[a]</sup>

**Keywords:** Palladium / Salicylaldimine / Anticancer activity / Antimalarial activity / Thiosemicarbazone

A series of mononuclear salicylaldiminato(thiosemicarbazone)palladium(II) complexes of general formula  $[\text{Pd}(\text{saltsc-R})\text{PPh}_3]$ , ( $\text{H}_2\text{saltsc-R}$  = salicylaldehyde thiosemicarbazone;  $\text{R} = \text{H}$  (**5**), 3-*tert*-butyl (**6**), 3-methoxy (**7**), 5-chloro (**8**)) have been synthesized. The palladium complexes were prepared by the reaction of the appropriate salicylaldimine thiosemicarbazone with  $\text{Pd}(\text{PPh}_3)_2\text{Cl}_2$ . All complexes were characterised by a range of spectroscopic and analytical techniques. The molecular structures of **6–8** have been determined by single-crystal X-ray diffraction analysis. The salicylaldimine thiosemicarbazones coordinate to palladium in a tridentate manner, through the phenolic oxygen, imine nitrogen and thiolate sulfur, forming five- and six-membered chelate rings

within their structures. The fourth coordination site for these square-planar complexes is occupied by  $\text{PPh}_3$ . Biological activities of the thiosemicarbazone ligands and palladium complexes have been investigated toward the WHCO1 oesophageal cancer cell line and against two strains of the malaria parasite *Plasmodium falciparum*, W2 (chloroquine-resistant) and D10 (chloroquine-sensitive). The palladium(II) complexes show enhanced in vitro antiplasmodial activity in comparison with their thiosemicarbazone ligand precursors. On the other hand, in vitro anticancer activity studies on oesophageal cancer cell lines revealed a decrease in activity upon coordination of palladium to the thiosemicarbazone ligand.

## Introduction

Thiosemicarbazones are known for their pharmacological properties, particularly as antiparasitic,<sup>[1–4]</sup> antibacterial<sup>[5–8]</sup> and antitumoral<sup>[9,10]</sup> agents. Research into the structure and coordination chemistry of aliphatic, aromatic, heterocyclic and other types of thiosemicarbazones and their metal complexes is well-established.<sup>[11]</sup> Generally, thiosemicarbazones act as chelating agents for various metal ions, by bonding through the sulfur atom and the imine nitrogen atom. Cadmium,<sup>[12]</sup> mercury,<sup>[12]</sup> platinum,<sup>[13]</sup> cobalt<sup>[14]</sup> and palladium<sup>[15,16]</sup> are a few of the metals that have been complexed with various types of thiosemicarbazone ligands.

The study of the biological activity of transition metal complexes of thiosemicarbazones has emerged as an area of great interest, the premise being that coordination to a metal may affect biological activity.<sup>[17]</sup>

Several transition metal complexes of aromatic mono- and bidentate thiosemicarbazones have been studied for their anticancer activities.<sup>[18]</sup> Our current investigation of salicylaldehyde thiosemicarbazones stems from the incorporation of three donor atoms [O,N,S], increasing the coordination capacity of thiosemicarbazones, giving rise to chelating tridentate thiosemicarbazone metal complexes. Metal complexes of salicylaldehyde thiosemicarbazones have been studied for their antitumour activity in vitro and in some cases were found to be generally more active than the free ligand.<sup>[15,19]</sup> Das and Livingstone suggested that sulfur-containing ligands chelated to palladium(II) are better antitumour agents than those of other metals, as the palladium(II) chelates possess the proper lability to transport the metal to DNA, its primary target.<sup>[20]</sup> Palladium(II) complexes of aryl-derived thiosemicarbazones have been tested for antitumoral and anticancer activity against several cancer cell lines including, human and murine tumor cell lines that are resistant and sensitive to cisplatin,<sup>[21–23]</sup> human breast cancer<sup>[24]</sup> and bladder cancer.<sup>[24]</sup> In certain cases, the palladium(II) complexes were found to be better cytotoxic agents than cisplatin, as well as their free ligands. A tridentate

[a] Department of Chemistry, University of Cape Town, P. B. Rondebosch 7701, South Africa  
Fax: +27-21-6505195  
E-mail: Gregory.Smith@uct.ac.za

[b] Division of Medical Biochemistry, University of Cape Town, Anzio Road, Observatory 7925, South Africa

[c] Department of Medicine, San Francisco General Hospital, University of California, San Francisco, Box 0811, San Francisco, CA 94143, USA

[d] Division of Pharmacology, Department of Medicine, University of Cape Town, K45, OMB, Groote Schuur Hospital, Observatory 7925, South Africa

[e] Institute of Infectious Disease and Molecular Medicine, University of Cape Town, Rondebosch 7701, South Africa



phenanthrenequinone thiosemicarbazone palladium(II) complex was found to exhibit superior selectivity toward breast cancer cells which have previously shown resistance to conventional chemotherapies.<sup>[25]</sup> Overall, tridentate thiosemicarbazone Pd<sup>II</sup> complexes have exhibited antiproliferative activities that are comparable or better than their Pt<sup>II</sup> analogues.<sup>[26–28]</sup>

Reports on the use of thiosemicarbazone metal complexes as antimalarial agents are sparse. Copper(II), nickel(II) and iron(II) complexes of 2-acetyl pyridine-derived thiosemicarbazones have been screened for antimalarial activity.<sup>[29]</sup> The Cu<sup>II</sup> and Fe<sup>II</sup> complexes were found to exhibit modest activity compared to their free ligands while the Ni<sup>II</sup> complexes showed no activity. To the best of our knowledge, the investigation of thiosemicarbazone Pd<sup>II</sup> complexes as antimalarial agents has not been reported in the literature.

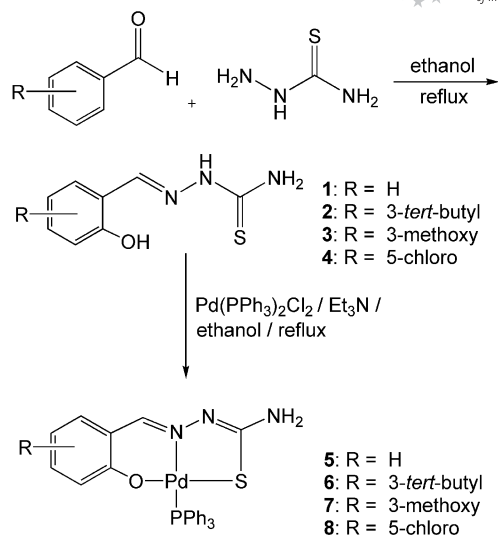
With the established biological activities of thiosemicarbazones, we decided to study the synthesis and characterisation of four mononuclear thiosemicarbazonepalladium(II) complexes, containing functionalized salicylaldehyde moieties and investigate the biological activity of the thiosemicarbazone ligands and their palladium(II) complexes against the WHCO1 oesophageal cancer cell line, as well as a sensitive and resistant strain of the malaria parasite *Plasmodium falciparum*.

## Results and Discussion

### Synthesis of Salicylaldimine Thiosemicarbazones 1–4 and Their Mononuclear Palladium(II) Complexes 5–8

The functionalised salicylaldehyde thiosemicarbazones 1–4 were prepared by Schiff base condensation reactions of the appropriate salicylaldehyde with thiosemicarbazide (Scheme 1). Thiosemicarbazones 1,<sup>[30]</sup> 3<sup>[31]</sup> and 4<sup>[32]</sup> are known compounds and their spectroscopic data and melting points correlate with the literature. The salicylaldimine thiosemicarbazone ligands 1–4 synthesised were treated with the precursor palladium(II) complex, *cis*-bis(triphenylphosphane)palladium dichloride (Scheme 1) to give the mononuclear salicylaldiminato(thiosemicarbazone)palladium(II) complexes 5–8. The complexes 5–8 are soluble in most organic solvents and show greater solubility when compared with the uncomplexed ligands 1–4.

The new salicylaldimine thiosemicarbazone ligand 2 shows similar spectral properties with the known compounds 1, 3 and 4.<sup>[30–32]</sup> Typically, the <sup>1</sup>H NMR spectrum of 2 shows a broad singlet for the hydroxy proton at  $\delta$  = 10.03 ppm and the hydrazinic proton occurs at  $\delta$  = 11.29 ppm. The imine proton, indicative of Schiff base condensation, is seen as a singlet at  $\delta$  = 8.28 ppm. In the <sup>13</sup>C NMR spectrum for ligand 2, the thione carbon is observed at  $\delta$  = 177.8 ppm and the hydroxy-substituted aromatic carbon at  $\delta$  = 155.3 ppm. In the <sup>1</sup>H NMR spectra for palladium(II) complexes 6–8, the imine proton is observed as a doublet at around 8.26 ppm. A coupling constant (<sup>4</sup>*J*) of 14.14 Hz is consistent with long range coupling of the imine



Scheme 1. Synthetic route to salicylaldiminato(thiosemicarbazone)palladium(II) complexes 5–8.

proton with the phosphorus nucleus of the triphenylphosphane co-ligand.<sup>[33]</sup> Peaks for the hydroxy proton and the hydrazinic proton of the free thiosemicarbazone ligand were not observed confirming coordination of the ligand via the phenolic oxygen and that sulfur coordinates to palladium in the thiolate form. All of the palladium complexes exhibit a singlet in their <sup>31</sup>P NMR spectra in the range between 24.00 and 26.00 ppm, with the exception of complex 7, which shows a singlet further upfield ( $\delta$  = 19.67 ppm) relative to the analogous complexes. The <sup>13</sup>C NMR spectra for 5–8 displays resonances due to the thiolate carbon at around 161 ppm and the imine carbon at around 171 ppm.

Infrared spectra for the salicylaldimine thiosemicarbazone ligands (1–4) show an absorption band assigned to the C=N stretching vibration at 1615 cm<sup>−1</sup>, confirming the formation of the thiosemicarbazone, Schiff-base product. For the mononuclear palladium(II) complexes 5–8, two absorption bands are observed in the imine region. This is consistent with the formation of a new imine bond within the thiosemicarbazone ligand, upon coordination of palladium to sulfur in the thiolate form. The lower frequency band, observed between 1610 and 1585 cm<sup>−1</sup>, is assigned to the imine bond coordinated to palladium. In all of the complexes two bands are observed for the N–H vibrations of the terminal amine between 3500 and 3250 cm<sup>−1</sup>. A third band for the hydrazinic N–H is not observed and this is consistent with the loss of the hydrazinic proton and formation of a new imine bond in the coordinated thiosemicarbazone ligand.

ESI mass spectrometry further confirmed the integrity of the new mononuclear palladium(II) complexes 6–8. The ESI spectrum of 6 and 7 reveals base peaks at *m/z* 617 and *m/z* 591 respectively for the [M – H]<sup>+</sup> ion. The spectrum of compound 8 displays a base peak for the mononuclear complex in its protonated form [M + H]<sup>+</sup> at *m/z* 597.

## Molecular Structures

The molecular structures of palladium complexes **6–8** have been determined using single-crystal X-ray crystallography. Single crystals suitable for X-ray diffraction of the palladium complexes were obtained by slow exaporation of either 1:1 dichloromethane/hexane or  $\text{CDCl}_3$ /hexane solutions. Crystallographic data are listed in Table 5 (see Exp. Section) and selected interatomic distances and bond angles are summarised in Table 1. The molecular structures of complexes **6–8** are shown in Figures 1, 2, and 3 respectively.

Table 1. Selected bond lengths [Å] and angles [°] for palladium(II) complexes **6–8**.

	<b>6</b>	<b>7</b>	<b>8</b>
Pd1–S1	2.2432(8)	2.2426(8)	2.2478(6)
Pd1–P1	2.2833(8)	2.2782(8)	2.2779(6)
Pd1–N3	2.028(3)	2.012(2)	2.0204(19)
Pd1–O1	2.014(2)	2.033(2)	2.0164(16)
C1–S1	1.754(3)	1.754(3)	1.751(3)
C1–N2	1.303(4)	1.304(4)	1.291(3)
C2–N3	1.294(4)	1.293(4)	1.294(3)
N3–Pd1–S1	84.16(8)	84.52(7)	84.09(6)
N3–Pd1–O1	93.03(10)	92.15(9)	93.15(7)
P1–Pd1–S1	93.41(3)	93.56(3)	92.27(2)
P1–Pd1–O1	89.41(7)	90.07(6)	90.43(5)

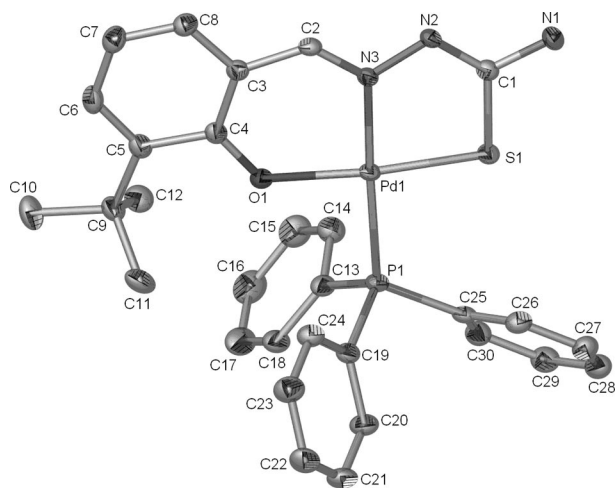


Figure 1. Molecular structure of complex **6** showing ellipsoids at the 40% probability level with hydrogen atoms and solvent molecules omitted for clarity.

For the palladium complexes **6–8**, the molecular structures show that the thiosemicarbazone ligand coordinates to the metal in the expected tridentate (O–N–S) fashion, via the phenolic oxygen, imine nitrogen and sulfur atom in a square-planar geometry, forming five- and six-membered chelate rings with the metal centre. The fourth coordination site is occupied by a triphenylphosphane ligand, coordinated to palladium *trans* to the nitrogen.

The bite angles formed between the metal and the coordinated ligands show that in each complex there is a slightly distorted square-planar arrangement around the metal. All of the bite angles around the metal in each complex are consistent with those observed for similar com-

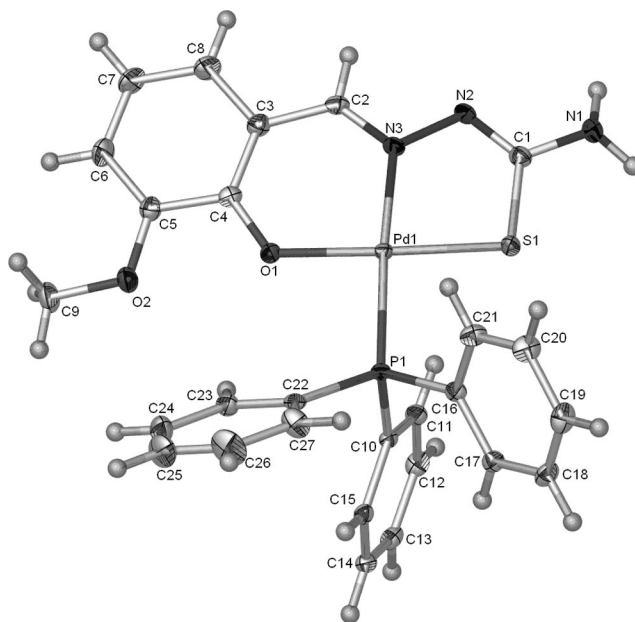


Figure 2. Molecular structure of complex **7** showing ellipsoids at the 40% probability level.

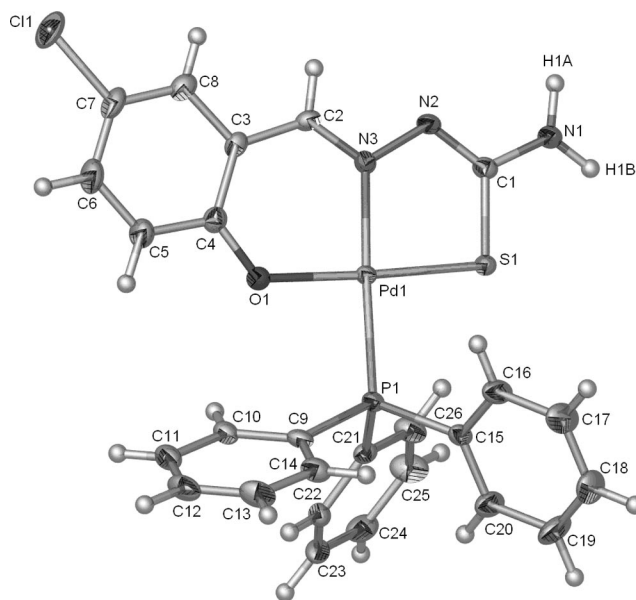


Figure 3. Molecular structure of complex **8** showing ellipsoids at the 40% probability level, with the solvent molecule ( $\text{CH}_2\text{Cl}_2$ ) omitted for clarity.

plexes.<sup>[15,34,35]</sup> The bite angle that shows the least deviation from 90° is the P(1)–Pd(1)–O(1); 89.41(7) for **8**, 90.07(6) for **7** and 90.43(5) for **6**. The *trans* angles O(1)–Pd(1)–S(1) and N(3)–Pd(1)–P(1) are close to linearity in all of the molecular structures with **8** showing the least deviation from 180°.

Inspection of the bond angles formed between the metal and the coordinated atoms show that they are consistent with analogous complexes.<sup>[15,35]</sup> The Pd(1)–N(3) bond length observed in **8** and **7** are slightly longer than that of **6**. This suggests there may be greater *trans* influence exerted

by the triphenylphosphane ligand in these two complexes.<sup>[34]</sup>

The C(1)–S(1) bond has a length of approximately 1.75 Å for all three complexes, closer to the expected bond length of a typical C–S single bond (1.82 Å) than that of a C=S double bond (1.56 Å),<sup>[36]</sup> confirming that sulfur coordinates to palladium in the thiolate form.<sup>[37]</sup> Further evidence of this is obtained from the bond lengths observed for the C(1)–N(2) bond. The approximate bond length of 1.30 Å in all of the molecular structures is similar to that of the C(2)–N(3) imine bond, indicating increased double bond character and formation of a new double bond between carbon and nitrogen in the thiosemicarbazone ligand upon coordination to palladium.<sup>[15,38,39]</sup>

### In Vitro Antimalarial Activity of Compounds 1–8

Compounds 1–8 were evaluated for in vitro antimalarial activity against both the chloroquine-resistant (W2) and -sensitive (D10) strains of *P. falciparum*, and the biological data are presented in Table 2. The control drugs used in the experiment were chloroquine (CQ) and artemisinin (ART) for the W2 strain and chloroquine for the D10 strain.

Table 2. In vitro antiplasmodial activity against *P. falciparum* strains in  $\mu\text{M}$  for compounds 1–8.

	W2	D10	D10
	IC <sub>50</sub> $\pm$ SD [ $\mu\text{M}$ ]	Percentage survival 10 mg/mL [%]	IC <sub>50</sub> $\pm$ SD [ $\mu\text{M}$ ]
CQ <sup>[a]</sup>	0.097 $\pm$ 0.92	–	0.0598 $\pm$ 0.0148
ART <sup>[b]</sup>	0.019 $\pm$ 2.30	–	–
1	> 20.0	56.18	–
2	> 20.0	102.59	–
3	> 20.0	48.62	–
4	> 20.0	107.21	–
5	8.87 $\pm$ 2.00	26.88	9.02 $\pm$ 0.342
6	13.74 $\pm$ 2.19	51.68	–
7	10.75 $\pm$ 0.44	33.47	5.64 $\pm$ 0.442
8	> 20.0	37.67	1.38 $\pm$ 0.0453

[a] CQ = chloroquine. [b] ART = artemisinin.

The palladium(II) complexes 5–7, with the exception of complex 8, generally showed superior antiplasmodial activity in comparison to the salicyldimine thiosemicarbazone ligands 1–4, against the chloroquine-sensitive (W2) strain of the parasite. For the chloroquine-sensitive (D10) strain, the compounds were first screened for percentage parasite survival at a single concentration, before determining the IC<sub>50</sub> values for selected compounds which were deemed to be active (Table 2). Generally, the palladium complexes showed enhanced activity over the analogous thiosemicarbazones against the D10 strain, and exhibited comparable antiplasmodial activity in the W2 strain. Although no clear structure–activity relationships can be gleaned from this study, it is interesting to note that for the D10 strain, the substituted aryl thiosemicarbazone palladium complexes are more active than the unsubstituted salicyldimine(thiosemicarbazone)palladium(II) complex 5. None of the free thiosemicarbazone ligands 1–4 showed ap-

preciable activity against either strain. It is evident that chelation of the ligand to palladium enhances antimalarial activity. The differences in antiplasmodial activities observed for the complexes suggest that, i. the aromatic ring of the coordinated thiosemicarbazone ligand may be involved in the mechanism of inhibition and ii. the effect of the aryl substituent is not electronic but may be attributed to steric effects.

### Antiproliferative Activity of Compounds 1–8 in Cancer Cell Lines

The salicylaldehyde-derived thiosemicarbazones ligands 1–4 and their corresponding Pd<sup>II</sup> complexes 5–8 were evaluated for their antiproliferative activity in vitro against the cancer cell line WHCO1, an oesophageal cancer cell line, using Doxorubicin as the control drug. The results of cytotoxic activity in vitro are expressed as IC<sub>50</sub>, the minimum compound concentration required for 50% inhibition of cell growth as compared to control untreated cells (Table 3).

Table 3. In vitro activity of compounds 1–8 [expressed as IC<sub>50</sub> ( $\mu\text{M}$ )] against the WHCO1 cancer cell line.

	IC <sub>50</sub> [ $\mu\text{M}$ ]	95% confidence interval
1	n/a <sup>[a]</sup>	n/a <sup>[a]</sup>
2	1.10	0.91–1.28
3	95.13	71.61–126.40
4	10.83	9.31–12.59
5	6.68	6.35–7.03
6	54.38	15.70–188.30
7	2.56	2.33–2.82
8	24.00	19.27–29.90
Doxorubicin	0.58	0.48–0.70

[a] n/a: not active at the measured concentration.

All the compounds, except thiosemicarbazone ligand 1, show cytotoxicity. The ligand, 3-*tert*-butyl-2-hydroxybenzaldehyde thiosemicarbazone (2), shows the best activity (IC<sub>50</sub> = 1.10  $\mu\text{M}$ ) out of all compounds screened against the WHCO1 cell line. Its corresponding complex 6, however, exhibits only moderate to weak cytotoxicity (IC<sub>50</sub> = 54.38  $\mu\text{M}$ ). Similarly, ligand 4 shows better activity than its corresponding complex 8. The poorer activity of these metal complexes as anticancer agents may be ascribed to their poor solubility in the cultivation medium since the metal complexes of 1 and 3 are poorly soluble under the conditions tested.

The palladium complex 7 is nearly 40 times more cytotoxic than the free ligand precursor 3, with IC<sub>50</sub> = 95.13  $\mu\text{M}$ . Generally, the coordination of the thiosemicarbazone to palladium may alter the lipophilic character of the complex, thus increasing the biological activity or it may be a synergistic effect, where the ligand dissociates within the cell and interacts with the ribonucleotide reductase enzyme while the free metal ion interacts with DNA.<sup>[24,40]</sup> In the case of complex 7, this enhanced activity may be attributed to the presence of the methoxy substituent. Interestingly, ligand 1 is not active at the maximum concentration used while its palladium complex 5 shows cytotoxicity. Coordination of

Table 4. IC<sub>50</sub> values for compounds **2**, **7** and **5** against several cancer cell lines.

Cell line	Ligand <b>2</b> IC <sub>50</sub> [μM]	95% confidence interval	Complex <b>7</b> IC <sub>50</sub> [μM]	95% confidence interval	Complex <b>5</b> IC <sub>50</sub> [μM]	95% confidence interval
WHCO1	1.10	0.91–1.28	2.56	2.33–2.82	6.68	6.35–7.03
WHCO5	4.03	3.47–4.69	2.11	0.69–6.39	n/a <sup>[a]</sup>	n/a <sup>[a]</sup>
WHCO6	6.32	5.05–7.92	12.23	5.40–27.70	43.13	15.00–124.00
KYSE30	3.02	2.21–4.13	1.48	1.11–1.96	3.76	2.63–5.39
KYSE70	7.98	6.66–9.56	n/a <sup>[a]</sup>	n/a <sup>[a]</sup>	10.28	8.14–12.97
KYSE180	7.27	6.46–8.19	5.23	n/d	6.43	5.40–7.65
KYSE410	7.46	6.48–8.59	46.02	23.51–90.11	n/a <sup>[a]</sup>	n/a <sup>[a]</sup>
KYSE450	1.64	1.33–2.02	2.19	1.42–3.36	4.11	2.86–5.91
CaSki	13.03	9.56–17.75	n/a <sup>[a]</sup>	n/a <sup>[a]</sup>	n/a <sup>[a]</sup>	n/a <sup>[a]</sup>
HeLa	0.91	0.79–1.06	n/a <sup>[a]</sup>	n/a <sup>[a]</sup>	70.61	61.81–80.67

[a] n/a: not active at the measured concentration.

thiosemicarbazone **1** to palladium clearly modifies its cytotoxic properties most likely by increasing its lipophilic nature. Of all the Pd<sup>II</sup> complexes tested, complex **7** shows the greatest cytotoxic activity with an IC<sub>50</sub> value of 2.56 μM.

Inspection of the results obtained for the free ligands **1**–**4** suggests that having a substituent on the aryl ring increases the activity of the compound, however, the degree of activation may be dependent on the position of the substituent, as well as the inductive effect of the substituent. Compound **3** has a strongly electron-donating substituent in position 3 on the ring yet it does not show any appreciable activity while thiosemicarbazone **2**, where the tertiary butyl group donates electron density into the ring to a lesser extent than **3**, shows the best activity. Compound **4** has an electron-withdrawing chloro substituent on the ring and it exhibits intermediate activity; better than **3**. This may be explained by the fact that the chloro group is in position 5 on the ring. It is possible that the position as well as the electronic nature of the aromatic substituent may influence the way the ligand interacts with targets inside the cell. Further studies regarding the structure–activity relationship of these compounds need to be undertaken in order to establish the actual effect of the aromatic substituent.

These observations, however, cannot be extended to their corresponding complexes which do not show particular structure–activity correlation with regard to the substituents on the ring. In a previous study, cisplatin has shown an IC<sub>50</sub> value of approximately 13 μM against the WHCO1 cell line.<sup>[41]</sup> The free ligands **2** and **4** as well as palladium complexes **5** and **7** all exhibit cytotoxicities lower than this value against this cell line.

The three compounds showing the best activities, thiosemicarbazone ligand **2** and palladium(II) complexes **5** and **7**, were then further tested in two additional oesophageal cancer cell lines of South African origin (WHCO5 and WHCO6), five oesophageal cancer cell lines of Japanese origin (KYSE30, KYSE70, KYSE180, KYSE410 and KYSE450) and two cervical cancer cell lines (CaSki and HeLa). The results are presented in Table 4 along with their activity against WHCO1.

The free thiosemicarbazone ligand **2**, showed good activity against all of the cell lines screened with the best activity observed in the cervical cancer cell line HeLa. Com-

plex **7** exhibited good IC<sub>50</sub> values against cell lines WHCO1, WHCO5, KYSE30, KYSE180 and KYSE450; intermediate activity against WHCO6 and negligible activity against KYSE410 cell lines. It did not show any activity against the remaining cell lines at the highest concentrations used. Complex **5** displayed good activity in only four of the oesophageal cancer cell lines tested; was not active in the CaSki line and showed negligible activity against the HeLa cell line.

Complex **5** and similar [O,N,S] tridentate thiosemicarbazone Pd<sup>II</sup> analogues have been previously screened for in vitro anticancer activity against the promyelocytic HL-60 and histiocytic lymphoma U-937 cell lines.<sup>[15]</sup> Most of these complexes exhibited IC<sub>50</sub> values less than 10 μM. In addition, they were found to be more potent cytotoxic agents than the clinical drugs cisplatin, BCNU [1,3-bis(2-chloroethyl)-1-nitrosourea], hydroxyurea and 5-FU (5-fluorouracil) which were also screened during the same experiments.<sup>[15]</sup> Similarly, in our studies, complex **5** has displayed activities lower than 10 μM in four of the oesophageal cell lines tested. Overall, thiosemicarbazone **2** was found to be a good cytotoxic agent, it consistently displayed good activity against all cell lines tested while the complexes **7** and **5** only exhibited cytotoxicity against selected cell lines.

### In Vitro Apoptosis Assay

Cytotoxic agents can induce cell death through various pathways that include necrosis and apoptosis. Apoptosis is a common process of programmed cell death and is the focus of current oncology research. This process involves a series of biochemical steps resulting in morphological changes to the cell membrane including cell shrinkage, nuclear fragmentation and chromosomal DNA fragmentation.<sup>[42]</sup> PARP (Poly Adenosine-Diphosphate Ribose Polymerase) is a known caspase substrate and cleavage of PARP into two distinct molecular fragments (116 kDa and 85 kDa) serves as a marker of apoptosis. Following the results of our in vitro cytotoxicity studies, we decided to further explore PARP cleavage by Western blot analysis, in order to determine the mode of cell death induced by thio-



semicarbazone ligand **2**, the most active compound from the series of ligands and complexes synthesised. Figure 4 shows the Western blot diagrams for this experiment.

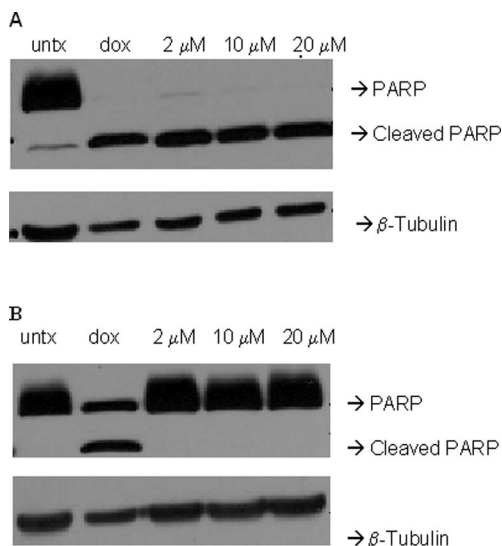


Figure 4. Western Blot diagrams for HeLa (A) and WHCO1 (B) cells treated with ligand **2** for 48 h. Dox represents the cells treated with 5  $\mu\text{M}$  doxorubicin for 48 h (positive control) and Untx represents the untreated cells (negative control).

HeLa cells treated with three concentrations of thiosemicarbazone **2** showed considerable cleavage of PARP whereas WHCO1 cells treated with this compound showed no PARP cleavage. Treatment of cells with 5  $\mu\text{M}$  doxorubicin served as a positive control. From these results it is evident that **2** kills HeLa cells via apoptosis. The mode of cell death in WHCO1 cells treated with **2** is clearly not apoptosis and it might be interesting to further investigate whether **2** triggers cell death in WHCO1 cells by necrosis, or autophagy (degradation of a cell by separating the contents from the rest of the cytoplasm).<sup>[43]</sup>

## Conclusions

The salicylaldimine thiosemicarbazones **1–4** were prepared by the condensation reaction of thiosemicarbazide and the appropriate salicylaldehyde derivatives. These thiosemicarbazone ligands were complexed with *cis*-bis(triphenylphosphane)palladium(II) dichloride to produce three new mononuclear thiosemicarbazone palladium complexes **6–8**. The new complexes were fully characterised by  $^1\text{H}$ ,  $^{13}\text{C}$  and  $^{31}\text{P}$  NMR and IR spectroscopy, elemental analysis and mass spectrometry. The molecular structures of **6–8** reveal a square-planar geometry around palladium, with the thiosemicarbazone ligand bonding in a tridentate manner, forming a five- and six-membered chelate ring. The palladium(II) complexes exhibit an enhanced antiplasmodial effect over the analogous thiosemicarbazone ligand precursors when tested against both chloroquine-resistant (W2) and chloroquine-sensitive (D10) strains of *P. falciparum*. The present study also shows that the palladium(II) complexes have moderate cytotoxic properties, and in some cases,

lower activities in comparison with the analogous thiosemicarbazone ligand. The thiosemicarbazone ligand **2**, containing the *tert*-butyl functionality, reveals cell death for HeLa cells to occur via apoptosis.

## Experimental Section

**General Procedures:** All complexation reactions were performed under an atmosphere of nitrogen or argon, using a dual vacuum/nitrogen line and standard Schlenk-line techniques. All reaction solvents were dried by refluxing under an inert atmosphere over the appropriate drying agent and all samples were dried under vacuum. Reagents and solvents were purchased from commercial suppliers.  $\text{PdCl}_2$  was kindly donated by Johnson–Matthey Inc. All purchased starting materials were used without further purification. The salicylaldimine thiosemicarbazone ligands **1**,<sup>[30]</sup> **3**,<sup>[31]</sup> and **4**,<sup>[32]</sup> and the palladium complexes, bis(triphenylphosphane)palladium(II) dichloride<sup>[44]</sup> and **5**,<sup>[15]</sup> were prepared according to the published literature procedures. Nuclear Magnetic Resonance (NMR) Spectra were recorded on a Varian Unity XR400 MHz ( $^1\text{H}$  at 399.95 MHz,  $^{13}\text{C}$  at 100.58 MHz,  $^{31}\text{P}$  at 161.90 MHz) or Varian Mercury XR300 ( $^1\text{H}$  at 300.08 MHz,  $^{13}\text{C}$  at 75.46 MHz,  $^{31}\text{P}$  at 121.47 MHz) MHz spectrometer at ambient temperature. Chemical shifts for  $^1\text{H}$  and  $^{13}\text{C}\{^1\text{H}\}$  NMR shifts are reported using tetramethylsilane (TMS) as the internal standard and  $^{31}\text{P}\{^1\text{H}\}$  spectra were measured relative to  $\text{H}_3\text{PO}_4$  as the external standard. Infrared absorptions (IR) were measured on a Perkin–Elmer Spectrum One FT-IR Spectrometer as KBr pellets. Microanalyses for C, H, N and S were carried out using a Fisons EA 110 elemental analyser and melting points were determined using a Kofler hot stage microscope (Reichert Thermovar). Mass Spectrometry determinations were carried out on all new compounds using electron spray ionisation on a Waters API Quattro Micro instrument in the positive mode.

**Salicylaldimine Thiosemicarbazone 2:** A solution of 3-*tert*-butyl-2-hydroxybenzaldehyde (0.520 g, 2.92 mmol) in ethanol (10 mL) was added dropwise to an equimolar amount of thiosemicarbazide (0.272 g, 2.98 mmol) in ethanol (20 mL). The reaction mixture was refluxed for 6 h. After cooling to room temperature, the product **2** precipitates out of solution as a white solid. The product is isolated by filtration, washed with ethanol and diethyl ether and dried in vacuo; yield 0.397 g (54%); m.p. 254–257  $^\circ\text{C}$ .  $^1\text{H}$  NMR (300 MHz, DMSO):  $\delta$  = 11.29 (s, 1 H, NNHCS), 10.03 (br. s, 1 H, OH), 8.28 (s, 1 H, HC=N), 7.99 (br. s, 2 H,  $\text{NH}_2$ ), 7.25 (m, 2 H, ArH), 6.86 (t,  $J$  = 7.69 Hz, 1 H, ArH), 1.40 [s, 9 H,  $\text{C}(\text{CH}_3)_3$ ] ppm.  $^{13}\text{C}$  NMR (75 MHz, DMSO):  $\delta$  = 177.8, 155.3, 147.0, 136.6, 129.3, 128.2, 119.1, 118.4, 34.3, 29.2 ppm. IR (KBr):  $\tilde{\nu}$  = 3419 (s, O–H), 3248 (s, N–H), 3164 (s, N–H), 3038 (s, N–H), 1614 (s, C=N), 1537 (s, C=C aromatics), 1488 (m, N–N), 1293 (m, N–CS–N) 1148 (m, C=S)  $\text{cm}^{-1}$ .  $\text{C}_{12}\text{H}_{17}\text{N}_3\text{OS}$  (251.36): calcd. C 57.34, H 6.81, N 16.72, S 12.76; found C 56.92, H 6.73, N 16.71, S 12.63.

**General Synthesis for the Palladium(II) Complexes 6–8:** The appropriate thiosemicarbazone ligand **2–4** (1 mol-equiv.) was added to dry ethanol (40  $\text{cm}^3$ ) under argon gas. The solution was heated to 60  $^\circ\text{C}$  with stirring. Triethylamine (2.1 mol-equiv.) was added followed by  $\text{Pd}(\text{PPh}_3)_2\text{Cl}_2$  (1 mol-equiv.). The mixture was refluxed under argon for five hours. During this time, the product precipitated as an orange solid. The product is isolated via filtration and washed with ethanol and diethyl ether, and dried in vacuo. All of the products were recrystallised from DCM/hexane.

**Spectroscopic Data for 6:** *cis*-Bis(triphenylphosphane)palladium(II) dichloride (0.530 g, 0.755 mmol) was treated with 3-*tert*-butyl-2-hy-

droxybenzaldehyde thiosemicarbazone (0.216 g, 0.837 mmol); yield 0.136 g (29%); m.p. 234–236 °C.  $^1\text{H}$  NMR (400 MHz,  $\text{CDCl}_3$ ):  $\delta$  = 8.26 (d,  $J$  = 14.14 Hz, 1 H,  $\text{HC}=\text{N}$ ), 7.70–7.77 (m, 6 H,  $\text{PPh}_3$ ), 7.38–7.48 (m, 9 H,  $\text{PPh}_3$ ), 7.20–7.37 (m, 2 H,  $\text{ArH}$ ), 6.57 (t,  $J$  = 8.82 Hz, 1 H,  $\text{ArH}$ ), 4.59 (s, 2 H,  $\text{NH}_2$ ), 0.744 [s, 9 H,  $\text{C}(\text{CH}_3)_3$ ] ppm.  $^{13}\text{C}$  NMR (100 MHz,  $\text{CDCl}_3$ ):  $\delta$  = 170.0, 162.2, 152.3, 140.3, 128.0–135.1, 118.0, 114.1 ppm.  $^{31}\text{P}$  NMR (162 MHz,  $\text{CDCl}_3$ ):  $\delta$  = 24.16 (1 P,  $\text{PPh}_3$ ) ppm. IR (KBr):  $\tilde{\nu}$  = 3464 (m, N–H), 3391 (m, N–H), 1634 (m, C=N), 1610 (s, C=N), 1593 (s, C=C aromatics)  $1435$  (s, N–N)  $\text{cm}^{-1}$ .  $\text{C}_{30}\text{H}_{30}\text{N}_3\text{O}_2\text{PPdS}$  (618.03): calcd. C 58.30, H 4.89, N 6.80, S 5.19; found C 57.73, H 4.91, N 6.39, S 4.69. ESI-MS:  $m/z$  617  $[\text{M} - \text{H}]^+$ .

**Spectroscopic Data for 7:** *cis*-Bis(triphenylphosphane)palladium(II) dichloride (0.516 g, 0.735 mmol) was treated with 2-hydroxy-3-methoxybenzaldehyde thiosemicarbazone (0.164 g, 0.728 mmol); yield 0.344 g (80%); m.p. 241–243 °C.  $^1\text{H}$  NMR (300 MHz,  $\text{CDCl}_3$ ):  $\delta$  = 8.24 (d,  $J$  = 13.87 Hz, 1 H,  $\text{HC}=\text{N}$ ), 7.49–7.81 (m, 6 H,  $\text{PPh}_3$ ), 7.26–7.49 (m, 9 H,  $\text{PPh}_3$ ), 6.96 (d,  $J$  = 8.06 Hz, 1 H,  $\text{ArH}$ ), 6.85 (d,  $J$  = 7.57 Hz, 1 H,  $\text{ArH}$ ), 6.56 (t,  $J$  = 7.79 Hz, 1 H,  $\text{ArH}$ ), 4.67 (s, 2 H,  $\text{NH}_2$ ), 3.57 (s, 3 H,  $\text{OCH}_3$ ) ppm.  $^{13}\text{C}$  NMR (75 MHz,  $\text{CDCl}_3$ ):  $\delta$  = 170.4, 150.9, 128.3–134.8, 126.5, 117.7, 115.5, 113.9, 56.6 ppm.  $^{31}\text{P}$  NMR (121.5 MHz,  $\text{CDCl}_3$ ):  $\delta$  = 19.67 (1 P,  $\text{PPh}_3$ ) ppm. IR (KBr):  $\tilde{\nu}$  = 3442 (m, N–H), 3308 (w, N–H), 1642 (m, C=N), 1592 (s, C=N), 1526 (s, C=C aromatics)  $1434$  (s, N–N)  $\text{cm}^{-1}$ .  $\text{C}_{27}\text{H}_{24}\text{N}_3\text{O}_2\text{PPdS}$  (591.96): calcd. C 54.78, H 4.09, N 7.10, S 5.42; found C 53.67, H 4.32, N 6.10, S 5.17. ESI-MS:  $m/z$  591  $[\text{M} - \text{H}]^+$ .

**Spectroscopic Data for 8:** *cis*-Bis(triphenylphosphane)palladium(II) dichloride (0.513 g, 0.732 mmol) was treated with 5-chlorosalicylaldehyde thiosemicarbazone (0.162 g, 0.706 mmol); yield 0.262 g (63%); m.p. 221–223 °C.  $^1\text{H}$  NMR (300 MHz,  $\text{CDCl}_3$ ):  $\delta$  = 8.13 (d,  $J$  = 13.62 Hz, 1 H,  $\text{HC}=\text{N}$ ), 7.66–7.75 (m, 6 H,  $\text{PPh}_3$ ), 7.26–7.55 (m, 9 H,  $\text{PPh}_3$ ), 7.23 (d,  $J$  = 2.75 Hz, 1 H,  $\text{ArH}$ ), 7.11 (dd,  $J$  = 2.76, 9.02 Hz, 1 H,  $\text{ArH}$ ), 6.59 (d,  $J$  = 9.02 Hz, 1 H,  $\text{ArH}$ ), 4.74 (s, 2 H,  $\text{NH}_2$ ) ppm.  $^{13}\text{C}$  NMR (75 MHz,  $\text{CDCl}_3$ ):  $\delta$  = 171.5, 161.2, 149.6, 128.3–134.7, 122.2, 118.7 ppm.  $^{31}\text{P}$  NMR (121.5 MHz,  $\text{CDCl}_3$ ):  $\delta$  = 25.23 (1 P,  $\text{PPh}_3$ ) ppm. IR (KBr):  $\tilde{\nu}$  = 3493 (N–H), 3385 (m, N–H), 3054 (w, C–N), 1605 (s, C=N), 1586 (m, C=N), 1529 (s, C=C aromatics),  $1433$  (s, N–N)  $\text{cm}^{-1}$ .  $\text{C}_{26}\text{H}_{21}\text{ClN}_3\text{O}_2\text{PPdS}$  (596.37): calcd. C 52.36, H 3.55, N 7.05, S 5.38; found C 51.96, H 3.55, N 5.83, S 4.76. ESI-MS:  $m/z$  597  $[\text{M} + \text{H}]^+$ .

**X-ray Crystallography:** X-ray single-crystal intensity data were collected on a Nonius Kappa-CCD diffractometer using graphite-mo-

nochromated Mo- $K_\alpha$  radiation. The temperature was controlled by an Oxford Cryostream cooling system (Oxford Cryostat). The strategy for the data collections was evaluated using the Bruker Nonius “Collect” program. Data were scaled and reduced using DENZO-SMN software [36,45]. The structure was solved by direct methods and refined employing full-matrix least-squares with the program SHELXL-97 [46,47] refining on  $F^2$ . Packing diagrams were produced using the program PovRay (<http://www.povray.org>) and graphic interface X-seed. [48] All non-H atoms were refined anisotropically. All the hydrogen atoms, except the amino hydrogen H1A and H1B, were included in idealised positions in a riding model with  $U_{\text{iso}}$  set at 1.2 or 1.5 times those of the parent atoms (Table 5).

**Crystal Data for 6–8:** CCDC-719352 (for 6), -719353 (for 7) and -719354 (for 8) contain the supplementary crystallographic data for this paper. These data can be obtained free of charge from The Cambridge Crystallographic Data Centre via [www.ccdc.cam.ac.uk/data\\_request/cif](http://www.ccdc.cam.ac.uk/data_request/cif).

### Biological Experiments

**Antimalarial Experiments:** Ring stage, W2-strain *P. falciparum* parasites (1% parasitaemia, 2% haematocrit) were cultured in 0.5 mL of medium in 48-well culture dishes. [49] Inhibitors from 10 mM stocks in DMSO were added to cultured parasites to give a final concentration of 20  $\mu\text{M}$ . From 48-well plates, 125  $\mu\text{L}$  of culture was transferred to two 96 well plates (duplicates). Serial dilutions (1:5) of inhibitors were made to final concentrations of 10  $\mu\text{M}$ , 2  $\mu\text{M}$ , 0.4  $\mu\text{M}$ , 80 nM, 16 nM and 3.2 nM. Cultures were maintained at 37 °C for 2 d after which the parasites were washed and fixed with 1% formaldehyde in PBS. After two days, parasitaemia was measured by flow cytometry using the DNA stain YOYO-1 as a marker for cell survival. [49]  $\text{IC}_{50}$  values for growth inhibition were determined with GraphPad Prism software from plots of percentage parasitemia of untreated control cultures against inhibitor concentration.

The test compounds were also tested in triplicate on one occasion against chloroquine-sensitive (CQS) strain of *Plasmodium falciparum* (D10). Continuous in vitro cultures of asexual erythrocyte stages of *P. falciparum* were maintained using a modified method of Trager and Jensen. [50] Quantitative assessment of antiplasmodial activity in vitro was determined via the parasite lactate dehydrogenase assay using a modified method described by Makler. [51] The samples were prepared to a 2 mg/mL stock solution in 10% DMSO and sonicated to enhance solubility. Samples were tested as a sus-

Table 5. Crystallographic data and structure refinement parameters for palladium complexes 6–8.

	6	7	8
Empirical formula	$\text{C}_{32}\text{H}_{30}\text{Cl}_6\text{D}_2\text{N}_3\text{O}_2\text{PPdS}$	$\text{C}_{27}\text{H}_{24}\text{N}_3\text{O}_2\text{PPdS}$	$\text{C}_{27}\text{H}_{23}\text{Cl}_3\text{N}_3\text{O}_2\text{PPdS}$
Formula mass	858.75	591.92	681.26
Crystal size	$0.18 \times 0.14 \times 0.14$ mm	$0.12 \times 0.11 \times 0.09$ mm	$0.20 \times 0.14 \times 0.08$ mm
Crystal system	monoclinic	monoclinic	monoclinic
Space group	$P2_1/n$	$C2/c$	$P2_1/c$
$a$	10.1900(2) Å	33.3399(7) Å	14.7145(4) Å
$b$	20.5408(4) Å	10.3708(2) Å	8.0414(1) Å
$c$	17.9344(3) Å	14.9613(2) Å	24.3591(6) Å
$\alpha$	90°	90°	90°
$\beta$	102.543°	102.0910°	101.151°
$\gamma$	90°	90°	90°
$V$	3664.27(12) Å <sup>3</sup>	5058.28(16) Å <sup>3</sup>	2827.88(11) Å <sup>3</sup>
$Z$	4	8	4
Calculated density	1.557 Mg/m <sup>3</sup>	1.555 Mg/m <sup>3</sup>	1.600 Mg/m <sup>3</sup>
$F(000)$	1728	2400	1368
$R$ indices, (for all data)	$R1 = 0.0476$ , $wR2 = 0.0887$	$R1 = 0.0362$ , $wR2 = 0.0628$	$R1 = 0.0528$ , $wR2 = 0.0883$

pension if not completely dissolved. Stock solutions were stored at  $-20^{\circ}\text{C}$ . Further dilutions were prepared on the day of the experiment. Chloroquine (CQ) was used as the reference drug in all experiments. Test samples were tested at one concentration ( $10\text{ }\mu\text{g/mL}$ ). CQ was tested at concentrations of 30, 15 and  $7.5\text{ ng/mL}$ .

### Anticancer Experiments

**Cell Lines and Cell Proliferation Assays:** The three oesophageal cancer cell lines, WHCO1, WHCO5 and WHCO6, were derived from biopsies of primary oesophageal squamous cell carcinomas (oesophageal cancer cells of South African origin)<sup>[52]</sup> and kindly provided by Professor Rob Veale (University of Witwatersrand, South Africa). The CaSki and HeLa cervical cancer cell lines were purchased from the American Type Culture Collection (Rockville, MD, USA) and the KYSE oesophageal squamous cell carcinoma cell lines, previously established by Shimada and co-workers,<sup>[53]</sup> were purchased from the German Resource Centre for Biological Material (<http://www.dsmz.de>). IC<sub>50</sub> determinations were carried out using the MTT [3-(4,5-Dimethylthiazol-2-yl)-2,5-diphenyltetrazolium bromide] assay. Briefly, 3000 cells were seeded per well in 96-well plates. Cells were incubated at  $37^{\circ}\text{C}$  under 5% CO<sub>2</sub> (24 h), after which aqueous DMSO solutions of each compound ( $10\text{ }\mu\text{L}$ , with a constant final concentration of DMSO: 0.2%) were plated at various concentrations. After 48 h incubation, observations were made, and MTT ( $10\text{ }\mu\text{L}$ ) solution added to each well. After a further 4 h incubation, solubilization solution ( $100\text{ }\mu\text{L}$ ) was added to each well, and plates were incubated overnight. Plates were read at 595 nm on a BioTek microplate reader.

**Western Blot Analysis:** Cells were harvested in  $60\text{ }\mu\text{L}$  of radioimmuno-precipitation assay buffer [ $150\text{ mmol/L}$  NaCl, 1% Triton X-100, 0.1% SDS,  $25\text{ mmol/L}$  Tris-HCl (pH 7.5), 1% sodium deoxycholate,  $1\text{ mmol/L}$  Na<sub>3</sub>VO<sub>4</sub>,  $20\text{ }\mu\text{g/mL}$  pepstatin,  $1\text{ mmol/L}$  phenylmethylsulfonyl fluoride] with protease inhibitor (Complete tablets, Roche), sonicated for 10 s with a probe sonicator (Heat System-Ultrasonics) and centrifuged for 15 min at  $13,000\text{ g}$ . The protein concentration of the lysates was determined using the BCA Protein Assay Kit (Pierce). Equal amounts of protein was electrophoresed on 10% SDS polyacrylamide gel at a constant current of 15 mA and electrophoretically transferred to a nitrocellulose membrane (Hybond-ECL; Amersham Pharmacia Biotech UK) at 100 V for 1 h. Membranes were incubated for 1 h with 5% fat-free dry milk in TBS with 0.1% Tween 20 to block nonspecific binding sites and then incubated with 1:1000 dilution of rabbit polyclonal primary antibody to poly (ADP ribose) polymerase (Santa Cruz Biotechnology) at  $4^{\circ}\text{C}$  overnight. The immunoreactivity was detected by using peroxidase-conjugated antirabbit secondary antibody and visualized by enhanced chemiluminescence (SuperSignal West Pico Chemiluminescent Substrate; Pierce). The blots were stripped before reprobing with antibody to  $\beta$ -tubulin (Santa Cruz Biotechnology).

### Acknowledgments

We gratefully thank the University of Cape Town, the National Research Foundation (NRF), the Medical Research Council (MRC) of South Africa and the Cancer Association of South Africa (CANSA) for financial support. AngloPlatinum Corporation and Johnson Matthey is acknowledged for the kind donation of palladium salts.

- [1] E. W. Ainscough, A. M. Brodie, W. A. Denny, G. J. Finlay, J. D. Ranford, *J. Inorg. Biochem.* **1998**, 70, 175–185.

- [2] H. Beraldo, D. Gambino, *Mini-Rev. Med. Chem.* **2004**, 4, 31–39.
- [3] D. S. Kalisnowski, D. R. Richardson, *Pharmacol. Rev.* **2005**, 57, 547–583.
- [4] D. S. Kalinowski, D. R. Richardson, *Chem. Res. Toxicol.* **2007**, 20, 715–720.
- [5] J. S. Casas, M. S. Garcia-Tasende, J. Sordo, *Coord. Chem. Rev.* **2000**, 209, 197–261.
- [6] M. A. Ali, S. E. Livingstone, *Coord. Chem. Rev.* **1974**, 13, 101–115.
- [7] M. J. M. Campbell, *Coord. Chem. Rev.* **1975**, 15, 279–319.
- [8] S. Padhye, G. B. Kauffman, *Coord. Chem. Rev.* **1985**, 63, 127–160.
- [9] A. G. Quiroga, C. N. Ranninger, *Coord. Chem. Rev.* **2004**, 248, 119–133.
- [10] S. N. Pandeya, J. R. Dimmock, *Pharmazie* **1993**, 48, 659–666.
- [11] T. S. Lobana, R. Sharma, G. Bawa, S. Khanna, *Coord. Chem. Rev.* **2009**, 253, 977–1055.
- [12] A. A. El-Asmy, O. A. El-Gammal, H. S. Saleh, *Spectrochimica Acta Part A: Mol. Biomol. Spec.* **2008**, 71, 39–44.
- [13] S. Halder, R. J. Butcher, S. Bhattacharya, *Polyhedron* **2007**, 26, 2741–2748.
- [14] R. M. El-Shazly, G. A. A. Al-Hazmi, S. E. Ghazy, M. S. El-Shahawi, A. A. El-Asmy, *J. Coord. Chem.* **2006**, 59, 845–849.
- [15] S. Halder, S.-M. Peng, G.-H. Lee, T. Chatterjee, A. Mukherjee, S. Dutta, U. Sanyal, S. Bhattacharya, *New J. Chem.* **2008**, 32, 105–114.
- [16] T. Stringer, P. Chellan, B. Therrien, N. Shunmoogam-Gounden, D. T. Hendricks, G. S. Smith, *Polyhedron* **2009**, 28, 2839–2846.
- [17] Z. Iakovidou, E. Mioglou, D. Mourelatos, A. Kotsis, M. A. Demertzis, A. Papageorgiou, J. R. Miller, D. Kovala-Demertzi, *Anticancer Drugs* **2001**, 12, 65–70.
- [18] A. Garoufis, S. K. Hadjikakou, N. Hadjiladis, *Metall-therapeutic Drugs and Metal-based Diagnostic Agents: The Use of Metals in Medicine* (Eds.: M. Gielen, E. R. T. Tiekink), John Wiley & Sons Ltd, **2005**, chapter 21, p. 399, and references cited therein.
- [19] D. Kovala-Demertzi, M. A. Demertzis, J. R. Miller, C. Papadopoulou, C. Dodorou, G. Filousis, *J. Inorg. Biochem.* **2001**, 86, 555–563.
- [20] M. Das, S. E. Livingstone, *Br. J. Cancer* **1978**, 37, 463–466.
- [21] A. G. Quiroga, J. M. Perez, I. Lopez-Solera, J. R. Masaguer, A. Luque, P. Roman, A. Edwards, C. Alonso, C. Navarro-Ranninger, *J. Med. Chem.* **1998**, 41, 1399–1408.
- [22] A. G. Quiroga, J. M. Perez, C. Alonso, C. Navarro-Ranninger, *Appl. Organomet. Chem.* **1998**, 12, 809–813.
- [23] A. G. Quiroga, J. M. Perez, E. I. Montero, C. Alonso, C. Navarro-Ranninger, *J. Inorg. Biochem.* **1999**, 75, 293–301.
- [24] D. Kovala-Demertzi, A. Alexandratos, A. Papageorgiou, P. N. Yadav, P. Dalezis, M. A. Demertzis, *Polyhedron* **2008**, 27, 2731–2738.
- [25] S. Padhye, Z. Afrasiabi, E. Sinn, J. Fok, K. Mehta, N. Rath, *Inorg. Chem.* **2005**, 44, 1154–1156.
- [26] J. Patole, S. Padhye, M. S. Moodbidri, N. Shirsat, *Eur. J. Med. Chem.* **2005**, 40, 1052–1055.
- [27] A. G. Quiroga, L. Cubo, P. J. S. Miguel, V. Moneo, A. Carnero, C. Navarro-Ranninger, *Eur. J. Inorg. Chem.* **2008**, 1183–1187.
- [28] D. Kovala-Demertzi, P. N. Yadav, M. A. Demertzis, M. Coluccia, *J. Inorg. Biochem.* **2000**, 78, 347–354.
- [29] J. P. Scovill, D. L. Klayman, D. G. Franchino, *J. Med. Chem.* **1982**, 25, 1261–1265.
- [30] I. D. Kostas, F. J. Andreadaki, D. Kovala-Demertzi, C. Prentzas, M. A. Demertzis, *Tetrahedron Lett.* **2005**, 46, 1967–1970.
- [31] A. P. Kumar, *Anal. Lett.* **2008**, 41, 1022–1037.
- [32] I. Yilmaz, *Heteroat. Chem.* **2003**, 14, 617–621.
- [33] J. Albert, J. Granell, J. Sales, M. Fon-Bardia, X. Solans, *Organometallics* **1995**, 14, 1393–1404.

- [34] R. Prabhakaran, S. V. Renukadevi, R. Karvembu, R. Huang, J. Mautz, G. Huttner, R. Subashkumar, K. Natarajan, *Eur. J. Inorg. Chem.* **2008**, 43, 268–273.
- [35] T. S. Lobana, G. Bawa, A. Castineiras, R. J. Butcher, *Inorg. Chem. Commun.* **2007**, 10, 506–509.
- [36] L. E. Shutton, *Tables of Interatomic Distances and Configurations in Molecules and Ions (Supplement)*, The Chemical Society, **1965**, London.
- [37] Z. Afrasiabi, E. Sinn, J. Chen, Y. Ma, A. L. Rheingold, L. N. Zakharov, N. Rath, S. Padhye, *Inorg. Chim. Acta* **2004**, 357, 271–278.
- [38] P. N. Yadav, M. A. Demertzis, D. Kovala-Demertzi, S. Skouloulika, D. X. West, *Inorg. Chim. Acta* **2003**, 349, 30–36.
- [39] L. Papathanasis, M. A. Demertzis, P. N. Yadav, D. Kovala-Demertzi, C. Prentjas, A. Castineiras, S. Skouloulika, D. X. West, *Inorg. Chim. Acta* **2004**, 357, 4113–4120.
- [40] D. Kovala-Demertzi, A. Domopoulou, M. A. Demertzis, G. Valle, A. Papageorgiou, *J. Inorg. Biochem.* **1997**, 68, 147–155.
- [41] J. Rajput, J. R. Moss, A. T. Hutton, D. T. Hendricks, C. E. Arndse, C. Imrie, *J. Organomet. Chem.* **2004**, 689, 1553–1568.
- [42] S. W. Lowe, A. W. Lin, *Carcinogenesis* **2000**, 21, 485–495.
- [43] M. Kundu, C. B. Thompson, *Annu. Rev. Pathol. Mech. Dis.* **2008**, 3, 427–455.
- [44] W. A. Hermann, A. Slazer, *Synth. Meth. Organomet. Inorg. Chem.* **1996**, 1, 160.
- [45] Z. Otwinowski, W. Minor, *Methods in Enzymology, Macromolecular Crystallography* (Eds.: C. W. Carter Jr., R. M. Sweet), Academic Press, **1997**, vol. 276, part A, pp. 307–326.
- [46] G. M. Sheldrick, *SADABS*, University of Göttingen, Germany, **1996**.
- [47] G. M. Sheldrick, *SHELXL-97 and SHELXS-97, Program for Crystal Structure Refinement*, University of Göttingen, Germany, **1997**.
- [48] L. J. Barbour, *J. Supramol. Chem.* **2001**, 1, 189–191.
- [49] P. S. Sijwali, P. J. Rosenthal, *Proc. Natl. Acad. Sci. USA* **2004**, 101, 4384–4389.
- [50] W. Trager, J. B. Jensen, *Science* **1976**, 193, 673–675.
- [51] M. T. Makler, J. M. Ries, J. A. Williams, J. E. Bancroft, R. C. Piper, B. L. Gibbins, D. J. Hinrichs, *Am. J. Trop. Med. Hyg.* **1993**, 48, 739–741.
- [52] R. B. Veale, A. L. Thornley, *S. Afr. J. Sci.* **1989**, 85, 375–379.
- [53] Y. Shimada, M. Imamura, T. Wagata, N. Yamaguchi, T. Tobe, *Cancer* **1992**, 69, 227–284.

Received: March 19, 2010

Published Online: June 15, 2010



# A Cu<sup>II</sup>Ni<sup>II</sup> Complex with Ethylenediamine: Crystal Structure and Ferromagnetic Behaviour of an Aqua-Bridged Heterometallic Chain Containing Ambidentate Ni(OAc)<sub>4</sub><sup>2-</sup> Blocks

Oksana V. Nesterova,<sup>[a]</sup> Svitlana R. Petrusenko,<sup>[a]</sup> Dmytro S. Nesterov,<sup>\*,[a]</sup>  
Vladimir N. Kokozay,<sup>[a]</sup> Brian W. Skelton,<sup>[b]</sup> Julia Jezierska,<sup>[c]</sup> Wolfgang Linert,<sup>[d]</sup> and  
Andrew Ozarowski<sup>[e]</sup>

**Keywords:** Copper / Nickel / Chain structures / Direct synthesis / Ferromagnetic behaviour / High-field EPR spectroscopy

A one-pot reaction of copper powder and nickel and ammonium acetates in a CH<sub>3</sub>OH solution of ethylenediamine (en) yields a unique 1D aqua-bridged polymer [Cu(en)<sub>2</sub>(μ<sub>2</sub>-H<sub>2</sub>O)<sub>2</sub>-Ni(OAc)<sub>4</sub>]<sub>n</sub>·4nH<sub>2</sub>O (**1**) with an ambidentate Ni(OAc)<sub>4</sub><sup>2-</sup> fragment that has not been previously characterized. The basic structural motif of **1** contains a previously unreported heterometallic M(μ<sub>2</sub>-H<sub>2</sub>O)M' aqua-bridge chain with alternating

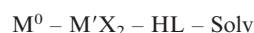
metal atoms. A complex system of N/O–H...O hydrogen bonds strengthens the polymeric chains and links them into a supramolecular three-dimensional network. Variable-temperature magnetic susceptibility measurements of **1** revealed a weak ferromagnetic coupling ( $J = 1.1 \text{ cm}^{-1}$ ) between the paramagnetic copper(II) and nickel(II) ions, which is transmitted through the oxygen bridges.

## Introduction

In the search for novel molecular-based magnetic materials with ferromagnetic coupling, considerable efforts have been devoted to the design and preparation of heterometallic complexes.<sup>[1]</sup> The most commonly used approach to achieve such systems has been based on a strict orthogonality of singly-occupied molecular orbitals of the interacting paramagnetic centres.<sup>[2]</sup> Factors such as bridging-ligand shape, bridging angles and out-of-plane shift of the hydrogen atoms on the bridge<sup>[3]</sup> are crucial for the appearance of ferromagnetic interactions and should be carefully controlled in order to avoid disruption of the rigorous symmetry requirements. The pathway used to obtain these intriguing species is based, essentially, on the self-assembly of specifically designed precursors that act as ligands together with a transition-metal complex with available coordination sites. Whereas the main reaction relies on the assembly of

preformed building blocks, the synthesis proceeds in several steps. Furthermore, the self-assembly process depends on different factors such as the nature of the ligand,<sup>[4]</sup> the counterions,<sup>[5]</sup> the noncovalent interactions (e.g. van der Waals, hydrogen-bonding, ionic or coordinative interactions)<sup>[6]</sup> and the crystallization conditions.<sup>[7]</sup> This approach is widely used in the synthesis of high-nuclearity transition-metal systems<sup>[8]</sup> as well as for polymeric complexes of various dimensionalities.<sup>[9]</sup> However, the search for novel synthetic methodologies is still one of the challenges in modern coordination chemistry.

We have previously reported on a synthetic strategy named “direct synthesis of coordination compounds” (DS), which is based on the one-step self-assembly of building blocks formed in situ:<sup>[10]</sup>



where  $M^0 = \text{Cu, Zn, Fe, Mn}$ ;  $M' = \text{Cr–Ni, Zn, Pb, Cd}$ ;  $X = \text{halide, NCS, OAc, NO}_3$ . The specific conditions during DS (such as kinetic effect of the metal dissolution, special metal/anion ratio) allowed us to prepare a series of heterometallic complexes.<sup>[10]</sup> In particular, we obtained a series of heterometallic Cu<sup>II</sup>M<sup>II</sup> ( $M = \text{Zn, Cd}$ ) complexes showing quasi-linear chain structures based on Zn(OAc)<sub>4</sub><sup>2-</sup> building blocks<sup>[11a]</sup> and 2D structures built from polymeric ladder-like  $[\{\text{Cd}_2(\text{OAc})_6\}^{2-}]_n$ <sup>[11b]</sup> anions and mixed-ligand anionic  $[\text{CdCl}_2(\text{OAc})_2]^{2-}$ ,  $[\text{CdI}(\text{OAc})_3]^{2-}$ ,  $[\text{CdI}_2(\text{OAc})_2]^{2-}$  and  $[\{\text{Cd}_2(\text{NCS})_6(\text{OAc})_2\}^{2-}]_n$  fragments,<sup>[11c]</sup> as well as a recently obtained Ni<sup>II</sup>/Cd<sup>II</sup> complex possessing a double-stranded zigzag chain structure.<sup>[11d]</sup>

[a] Department of Chemistry, National Taras Shevchenko University,  
Volodymyrska str. 64, Kyiv 01601, Ukraine  
Fax: +380-44-286-2467  
E-mail: nesterov@univ.kiev.ua

[b] Chemistry, School of Biomedical, Biomolecular and Chemical Sciences, The University of Western Australia,  
Crawley, WA 6009, Australia

[c] Faculty of Chemistry, University of Wrocław,  
14 Joliot-Curie Str., 50-383 Wrocław, Poland

[d] Institute of Applied Synthetic Chemistry, Vienna University of Technology,  
Getreidemarkt 9/163-AC, 1060 Vienna, Austria

[e] National High Magnetic Field Laboratory, Florida State University,  
1800 E. Paul Dirac Drive, Tallahassee, Florida 32310, USA

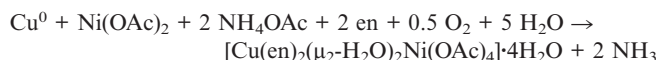
Continuing our systematic studies, we present here the preparation of a novel  $\text{Cu}^{\text{II}}\text{Ni}^{\text{II}}$  complex starting from elemental copper and nickel and ammonium acetates in a methanol solution of ethylenediamine in open air. The use of an aprotic chelating ligand, such as ethylenediamine, which has been broadly applied in supramolecular design because of its capability to form  $[\text{M}(\text{en})_2]^{2+}$  building blocks,<sup>[12]</sup> promotes the bridging function of the anions in the resulting polymeric structures.

We describe here the synthesis, characterization, spectroscopic and magnetic properties of the heterometallic complex  $[\text{Cu}(\text{en})_2(\mu_2\text{-H}_2\text{O})_2\text{Ni}(\text{OAc})_4]_n \cdot 4n\text{H}_2\text{O}$ , which contains the ambidentate  $[\text{Ni}(\text{OAc})_4]^{2-}$  building block that, according to the Cambridge Structural Database (CSD),<sup>[13]</sup> has not been previously structurally characterized for any transition metal. To the best of our knowledge, compound **1** represents the first example of a consecutive arrangement of two different transition metals  $\text{M}(\mu_2\text{-H}_2\text{O})\text{M}'$  through an aqua bridge, which serves as a basis for the resulting polymeric chain.

## Results and Discussion

### Synthesis and Spectroscopic Characterization

The coordination polymer was synthesized in a one-step reaction from copper powder and nickel and ammonium acetates in a methanol solution of ethylenediamine, using the molar ratio  $\text{Cu}/\text{Ni}(\text{OAc})_2/\text{NH}_4\text{OAc}/\text{en} = 1:1:2:3$ . The small excess of en is necessary for the formation of the complex and the use of a stoichiometric ratio of initial reagents of 1:1:2:2 did not lead to crystallisation. The reaction proceeds in the following way:



The IR spectrum of compound **1** confirmed the presence of ethylenediamine. Four characteristic frequencies,  $\nu(\text{NH})$ ,  $\nu(\text{CH})$ ,  $\nu(\text{CN})$  and  $\nu(\text{CC})$ , can easily be identified at 3130, 2910, 1045 and 930  $\text{cm}^{-1}$ , respectively, whereas the  $\delta(\text{NH}_2)$  absorption of en is obscured by stretching vibrations of the carboxylate groups. Although the difference in wave-numbers,  $\Delta = 155 \text{ cm}^{-1}$ , between the antisymmetric (1585  $\text{cm}^{-1}$ ) and symmetric (1430  $\text{cm}^{-1}$ )  $\nu(\text{CO})$  stretching frequencies is attributable to the existence of bridging acetate ligands,<sup>[14]</sup> this is not in agreement with the results from the X-ray analysis, which revealed a monodentate coordination mode of the carboxylate groups. Such a difference could be explained by the participation of monodentate acetate groups in a complex system of strong intra- and intermolecular hydrogen bonds resulting in a decrease of the  $\nu_{\text{as}}(\text{CO})$  and an increase of the  $\nu_{\text{s}}(\text{CO})$  stretching frequencies.

The diffuse-reflectance spectrum of the compound exhibits a high-intensity, broad peak with a maximum at 18150  $\text{cm}^{-1}$ , involving d–d transitions in a distorted octahedral environment around both copper(II) and nickel(II) atoms.<sup>[15]</sup> The shoulder at 26125  $\text{cm}^{-1}$  can be attributed to

the spin-allowed transition  ${}^3\text{A}_{2g} \rightarrow {}^3\text{T}_{1g}(\text{P})$  for the  $\text{Ni}^{\text{II}}$  centre. The spectrum also displays a ligand-to-metal charge-transfer transition at 38200  $\text{cm}^{-1}$ .

### Structure Description

The crystal structure of the complex consists of infinite one-dimensional chains of alternating cationic  $\text{Cu}(\text{en})_2^{2+}$  and anionic  $\text{Ni}(\text{OAc})_4^{2-}$  building blocks linked together through the oxygen atoms of the bridging water molecules, forming infinite one-dimensional chains (Figure 1). Examples of binding of the two transition metal atoms by means of one bridging water molecule into a polymeric structure are quite rare and, according to the CSD,<sup>[13]</sup> has been reported only in three homometallic cobalt  $\{[\text{Co}(\text{dmmba})_2(\text{H}_2\text{O})_3] \cdot \text{H}_2\text{O} \text{ (Hdmmba} = 2,6\text{-dimethoxybenzoic acid)},^{[16a]}$   $[\text{Co}(\mu\text{-H}_2\text{O})(\text{H}_2\text{O})_2\text{L}_2] \text{ (HL} = 3\text{-hydroxy-4-methoxybenzoic acid)}^{[16b]}$  and manganese  $\{[\text{Mn}(\text{OOCCH}_2\text{CH}_2\text{Fc})_2(\mu_2\text{-OH}_2)(\text{dmf})_2]\}_n^{[16c]}$  (Fc = ferrocenyl group) complexes. Hence, as far as we are aware, the presented compound is the first heterometallic complex containing the structural motif  $\{ -\text{M}(\mu_2\text{-H}_2\text{O})\text{M}' - \}_n$ .

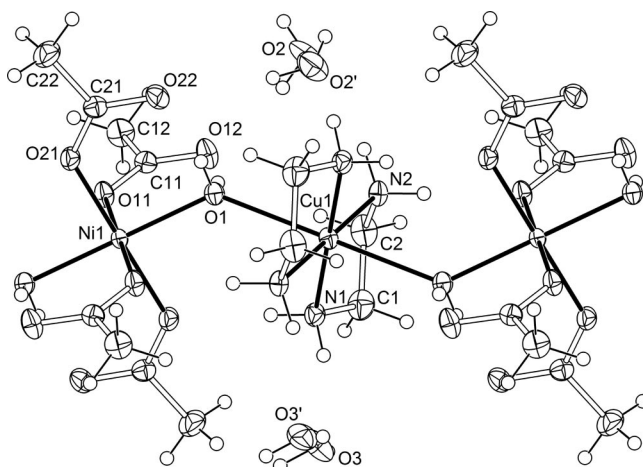


Figure 1. Fragment of the aqua-bridged chain of **1** with the atom-numbering scheme.

The closest intrachain  $\text{Cu} \cdots \text{Ni}$  distance is 4.244(1) Å, whereas the  $\text{Cu} \cdots \text{Cu}$  and  $\text{Ni} \cdots \text{Ni}$  separations are 8.488(2) Å. The copper(II) atoms are in a distorted-octahedral coordination environment consisting of four nitrogen atoms of en molecules forming the basal plane [ $\text{Cu}-\text{N}$  2.005(2), 2.014(2) Å; Table 1] and the oxygen atoms of the bridging water molecules [ $\text{Cu}-\text{O}$  2.535(2) Å] occupying the apical positions. The bond lengths and angles in the chelate rings are similar to those found in the literature.<sup>[17]</sup>

The nickel(II) atom is situated on a crystallographic inversion centre and has a slightly distorted octahedral environment with the  $\text{O}_6$  donor set formed by four monodentate acetate groups [ $\text{Ni}-\text{O}$  2.0694(17), 2.0649(17) Å] in equatorial positions and two  $\text{H}_2\text{O}$  molecules [ $\text{Ni}-\text{O}_{\text{H}_2\text{O}}$  2.0874(17) Å] in the apical positions. It should be noted that the title compound represents a first example of the am-

Table 1. Selected geometrical parameters (distances [Å] and angles [°]) for **1**.

Cu(1)–N(1)	2.005(2)	Ni(1)–O(11)	2.0694(17)
Cu(1)–N(2)	2.014(2)	Ni(1)–O(21)	2.0649(17)
Cu(1)–O(1)	2.535(2)	Ni(1)–O(1)	2.0894(17)
N(1)–Cu(1)–N(2)	84.91(9)	O(11)–Ni(1)–O(21)	89.63(7)
N(1)–Cu(1)–O(1)	87.33(7)	O(11)–Ni(1)–O(1)	92.62(7)
N(2)–Cu(1)–O(1)	93.52(6)	O(21)–Ni(1)–O(1)	92.81(7)

bidentate [Ni(OAc)<sub>4</sub>]<sup>2–</sup> fragment, which (according to the CSD) has not been previously structurally characterized for a transition metal. Similar fragments have been found in the complexes [Pt(dach)(OAc)<sub>4</sub>]<sup>[18a]</sup> [dach = (±)-*trans*-1,2-diaminocyclohexane] and K<sub>4</sub>[Cu(OAc)<sub>4</sub>(OAc)<sub>2</sub>](HOAc)<sub>2</sub>·(H<sub>2</sub>O)<sub>2</sub>,<sup>[18b]</sup> but here the Pt(OAc)<sub>4</sub> fragment is not ambidentate (the chelating organic molecules occupy the equatorial positions), and in the Cu complex the acetate ligands are asymmetrically bound to two different Cu<sup>II</sup> atoms. The absence of data for crystal structures containing the ambidentate [M(OAc)<sub>4</sub>]<sup>2–</sup> may not be accidental and may demonstrate its low thermodynamic stability. The existence of the ambidentate [Ni(OAc)<sub>4</sub>]<sup>2–</sup> in the presented complex is presumably caused by its participation in a complex system of hydrogen bonds. Indeed, all the acetate oxygen atoms take part in hydrogen bonding (Table 2) and in this way additionally strengthen the chains and join them into a supramolecular three-dimensional framework. The molecular shape of the cationic building block may also influence the final structure. The [Cu(en)<sub>2</sub>]<sup>2+</sup> cations can be considered as templating agents for the overall structure, as has been demonstrated previously.<sup>[19]</sup>

Table 2. Hydrogen-bonding interactions (distances [Å] and angles [°]) in **1**.<sup>[a]</sup>

D–H...A	D–H	H...A	D...A	D–H...A
N(1)–H(1A)...O(3)	0.92	2.20	3.090(10)	163.8
N(1)–H(1B)...O(21) <sup>a</sup>	0.92	2.04	2.944(3)	168.7
N(2)–H(2D)...O(11) <sup>b</sup>	0.92	2.00	2.917(3)	177.3
O(1)–H(1AO)...O(12)	0.83(2)	1.80(3)	2.616(3)	168(3)
O(1)–H(1BO)...O(22)	0.81(3)	1.81(3)	2.610(3)	171(4)
O(2)–H(2AO)...O(12)	0.83(4)	1.98(5)	2.773(7)	160(9)
O(2')–H(2CO)...O(12)	0.85(4)	1.98(6)	2.724(8)	145(9)
O(3)–H(3AO)...O(22) <sup>c</sup>	0.84(4)	1.90(4)	2.706(9)	158(7)
O(3')–H(3CO)...O(22) <sup>c</sup>	0.81(4)	2.02(8)	2.716(9)	143(11)

[a] Symmetry transformations used to generate equivalent atoms: (a) 2 – x, 1 – y, 1 – z; (b) x – 1, y, z; (c) x, y + 1, z.

## EPR Spectroscopy

The powder EPR spectrum of the complex at 9.58 GHz shows a very broad, unresolved line at 77 K. A narrow signal at about 3000 G should be assigned to the Cu<sup>II</sup> admixture. Frozen solutions of the compound in dmf as well as in water/ethylene glycol (3:1) exhibit spectra of two species resulting from the equilibrium between two Cu<sup>II</sup> complexes labelled as **I** and **II** in Figure 2. The intensity ratio of the two spectra depends on the solvent: complex **I** is dominant in a water/glycol solution, whereas **II** is dominant in dmf.

The EPR parameters derived by computer simulations of the spectra are:  $g_{\parallel} = 2.206$ ,  $g_{\perp} = 2.045$  and  $A_{\parallel} = 204 \times 10^{-4} \text{ cm}^{-1}$ ,  $A_{\perp} = 25 \times 10^{-4} \text{ cm}^{-1}$  for sim I (assigned to complex **I**);  $g_{\parallel} = 2.256$ ,  $g_{\perp} = 2.050$  and  $A_{\parallel} = 182 \times 10^{-4} \text{ cm}^{-1}$ ,  $A_{\perp} = 20 \times 10^{-4} \text{ cm}^{-1}$  for sim II (assigned to complex **II**). The parameters of **I** are typical for a Cu<sup>II</sup> complex with two en ligands, whereas those for complex **II** (with a significantly increased  $g_{\parallel}$  and decreased  $A_{\parallel}$  in comparison to **I**) indicate that the Cu<sup>II</sup> ion is coordinated by one en ligand (with solvent molecules completing the Cu<sup>II</sup> coordination sphere) in agreement with the parameters observed previously for model complexes<sup>[20a,20b]</sup> and according to differences in  $g_{\parallel}$  and  $A_{\parallel}$  allowing us to distinguish between N<sub>4</sub> or N<sub>2</sub> donor sets in the Cu<sup>II</sup> basal plane.<sup>[20]</sup> The spectra indicate a much greater stability of the [Cu(en)<sub>2</sub>]<sup>2+</sup> units in water/glycol than in dmf.

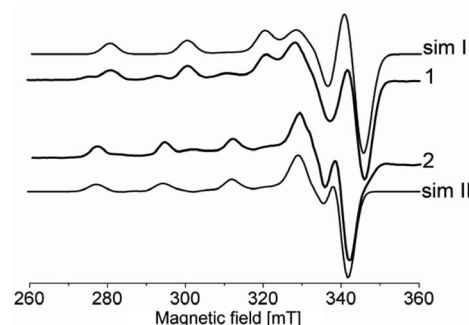


Figure 2. Frozen-solution EPR spectra of [Cu(en)<sub>2</sub>(μ<sub>2</sub>-H<sub>2</sub>O)<sub>2</sub>Ni(OAc)<sub>4</sub>]·4H<sub>2</sub>O in water/ethylene glycol (1) and dmf (2) together with the spectra simulated by using the parameters given in the text for the particular, **I** and **II**, species in equilibrium.

The high-frequency, high-field EPR spectrum of the powdered complex revealed a significant degree of dynamics in the system with the spectral features changing rapidly with temperature over a very narrow range. The spectrum

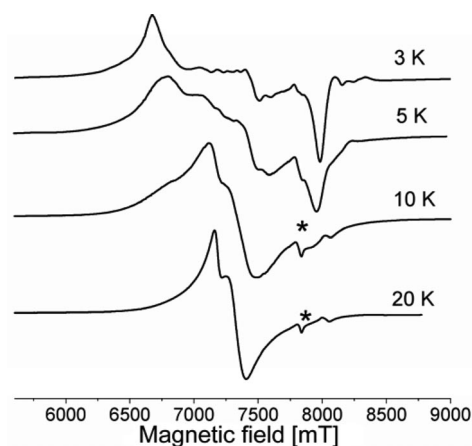


Figure 3. Temperature dependence of HF (224 GHz) EPR spectra of powdered [Cu(en)<sub>2</sub>(μ<sub>2</sub>-H<sub>2</sub>O)<sub>2</sub>Ni(OAc)<sub>4</sub>]·4H<sub>2</sub>O (the asterisk indicates the position of the signal from the monomeric Cu<sup>II</sup> admixture). The spectrum does not change much between 30 K and room temperature.

is extremely temperature-dependent at the lowest temperatures (Figure 3), whereas at higher temperatures it collapses to a narrow spectrum exhibiting no zero-field splitting features with  $g_{\parallel} = 2.23$  and  $g_{\perp} = 2.18$ . A trace of monomeric  $\text{Cu}^{\text{II}}$  with  $g_{\perp} = 2.04$  is also visible. If the strong, broad signal is from separate  $\text{Ni}^{\text{II}}$  ions then the signal from the separate  $\text{Cu}^{\text{II}}$  ions should also be observed with comparable intensity. Hence, the strong and broad signal cannot be a result of the separate  $\text{Ni}^{\text{II}}$  ions but rather from the Cu–Ni chain.

### Magnetic Properties

The results from magnetic susceptibility measurements are plotted as effective magnetic moment ( $\mu_{\text{eff}}$ ) vs. temperature in Figure 4. The complex shows a room-temperature magnetic moment of 3.6 B.M. This is very close to the spin-only value for two uncoupled spins that is obtained according to the expression:

$$\mu = \sqrt{g_1^2 S_1(S_1 + 1) + g_2^2 S_2(S_2 + 1)}$$

The high-field EPR spectrum at room temperature indicates that the  $g_{\text{average}}$  value is 2.2 and the formula gives  $\mu_{\text{eff}} = 3.65$  B.M. for  $S_1 = 1/2$ ,  $S_2 = 1$  and  $g_1 = g_2 = g_{\text{average}}$ . The increase of magnetic moment in the low-temperature region (up to 4.4 B.M.) is indicative of weak ferromagnetic interactions. The interpretation of the magnetic data was based on the dimetallic ordered ring  $(\text{CuNi})_N$  model (where  $N$  is the number of CuNi units) developed by Kahn and co-workers for a ferromagnetic interaction in the Cu/Ni chain<sup>[21]</sup> with the use of the following spin Hamiltonian:

$$H = -J \sum_{i=1}^{2N} S_i S_{i+1}$$

where for each  $i$ ,  $S_{2i-1} = S_{\text{Cu}}$  and  $S_{2i} = S_{\text{Ni}}$ . Their calculations resulted in the tabulated dependence of  $\chi_m T(4/g^2)$  on  $kT/|J|$  for  $N = 2, 3, 4, \infty$  and  $0.3 \leq kT/|J| \leq 4$ . The inter- and extrapolation of the tabulated data (for  $N = \infty$ ) yields the numerical equations that were fitted to the experimental data. The best fit, obtained by setting  $J = 1.1 \text{ cm}^{-1}$  and  $g = 2.14$ , resulted in  $R = 5.81 \times 10^{-4}$ , where  $R$  is the agreement factor defined as  $\Sigma[(\chi T)_{\text{obsd}} - (\chi T)_{\text{calcd}}]^2 / \Sigma[(\chi T)_{\text{obsd}}]^2$ . Unfortunately, this approach neglects the effects due to the zero-field splitting, difference between the  $g$  factors of Cu and Ni and anisotropic interactions. However, it is clear that the increase in the magnetic moment at the lowest temperatures is not due to the zero-field splitting on  $\text{Ni}^{\text{II}}$  or to the Zeeman energy becoming comparable to  $kT$  as both these effects lead to a decrease of the magnetic moment with decreasing temperature. Also, the magnetization at 2 K is saturated at  $3.14 N\mu_B$ , confirming the  $S = 3/2$  ground state and ferromagnetic interaction between  $\text{Ni}^{\text{II}}$  and  $\text{Cu}^{\text{II}}$  spin carriers.

The CSD search reveals 57 heterometallic Cu/Ni complexes of a polymeric nature. A large number of these complexes contain nickel in the form of a low-spin diamagnetic

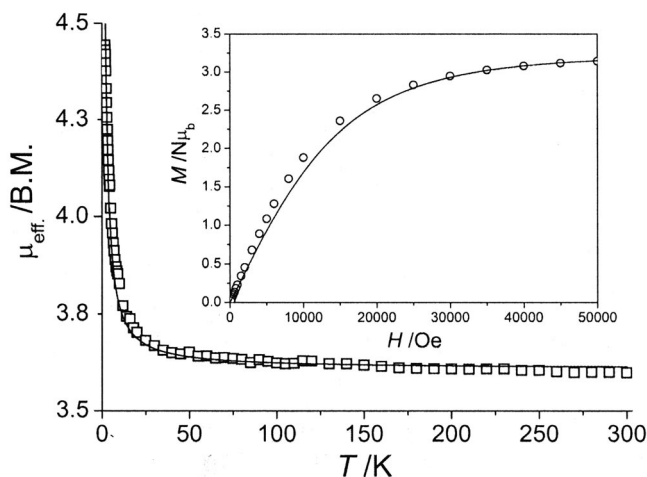


Figure 4. Plot of the effective magnetic moments vs. temperature for **1**. Squares are the experimental points, whereas the solid line was calculated from  $g_{\text{av}} = 2.14$  and  $J = 1.1 \text{ cm}^{-1}$  (see text). The inset shows experimental  $M$  vs.  $H$  plot (circles) and calculated for 2 K and  $g = 2.14$  (solid line).

$[\text{Ni}(\text{CN})_4]^{2-}$  block and thus could only show Cu $\cdots$ Cu interactions. Five compounds were found to possess antiferromagnetic or nearly paramagnetic properties.<sup>[22]</sup> Since all these complexes differ greatly in their exchange pathways, a comparative study seems to be unfeasible. There are also a few examples of Cu/Ni complexes with significant ferromagnetic interactions,<sup>[12a,23a]</sup> but no alternating chains can be identified in their crystal structures (at least from a magnetic point of view). The 3D-polymeric complex  $[\text{Ni}(\text{cyclam})(\mu_{1,3}\text{-dca})_2\text{Cu}(\mu_{1,5}\text{-dca})_2]$  (cyclam = 1,4,8,11-tetraazacyclotetradecane) shows an overall antiferromagnetic behaviour,<sup>[23b]</sup> although the authors suggest the presence of weak ferromagnetically coupled alternating Cu/Ni chains within the crystal framework (to the best of our knowledge, these results have not been interpreted). Only one recent compound was found to exhibit all the desired features: the 1D-coordination polymer  $[\text{Ni}(\text{cyclam})][\text{Cu}(\text{tfadt})_2]$  (tfadt = 3-trifluoromethylacrylonitrile-2,3-dithiolate) possesses a ferromagnetic coupling<sup>[23c]</sup> of  $J_{\text{CuNi}} = 3.5 \text{ cm}^{-1}$ , comparable to the value reported in this paper. The exchange pathway (Cu–S–C–N–Ni) is quite different from that observed in **1** (Cu–O–Ni), and hence a direct comparison of the geometrical parameters cannot be made.

Considering both molecular and polymeric Cu/Ni complexes containing the Cu–X–Ni fragment [but not Cu–(X)<sub>2</sub>–Ni], which is closest to the Cu–O–Ni exchange pathway in **1**, we found five complexes whose structural and magnetic properties are summarized in Table 3. It is noticeable that the absolute value of the exchange parameter decreases with the increase of the Cu–O–Ni angle, whereas the ferromagnetic interaction corresponds to higher angle values. However, the additional bridging between the copper and nickel centres in **5** and **6** could affect the magnetic exchange. Finally, the lack of data does not allow us to obtain reliable statistics, and we would like to refrain from making conclusions from such limited data.



Table 3. Selected geometrical parameters and magnetic exchange values for **1** and literature examples.

	$d(\text{Cu}\cdots\text{Ni})$ [Å]	$d(\text{Cu}-\text{O})$ [Å]	$d(\text{Ni}-\text{O})$ [Å]	$\angle(\text{Cu}-\text{O}-\text{Ni})$ [°]	$J$ [cm <sup>-1</sup> ]	Additional Cu $\cdots$ Ni bridging	Ref.
<b>1</b>	4.24	2.54	2.09	133.0	1.1	—	—
<b>2</b>	4.42	2.61	2.15	135.9	1.1	—	[24]
<b>3</b>	4.10	2.56	2.08	123.7	-0.5	—	[25]
<b>4</b>	3.65	1.96	2.10	127.9	-31	—	[26]
<b>5</b>	3.43	1.84	2.09	121.6	-142	Cu-N-O-Ni	[27]
<b>6</b>	3.45	1.92	2.08	119.7	-500	Cu-N=O-Ni	[28]

## Conclusions

The spontaneous self-assembly approach and its particular case – the direct synthesis – is known as an extremely effective pathway for the generation of unprecedented coordination compounds, and the present work confirms this strategy. The synthetic procedure described here allowed us to obtain a heterometallic Cu/Ni complex possessing a combination of several uncommon features. Firstly, the metal ions and water molecules form an alternating chain, which was found to be the first example (according to CSD) of a heterometallic 1D-coordination polymer based on  $\{-\text{M}(\mu_2\text{-H}_2\text{O})\text{M}'-\}_n$  fragments. Also, the presented compound contains unique ambidentate  $[\text{Ni}(\text{OAc})_4]^{2-}$  blocks. The magnetic properties of this compound are also unexpected. Whereas the overwhelming majority of Cu/Ni complexes show antiferromagnetic or paramagnetic behaviour, our complex possesses weak ferromagnetic properties. In view of the fact that there is only one ferromagnet possessing a true chain Cu/Ni structure, the complex reported here represents an extremely rare example of the ferromagnetically coupled (and at the same time crystallographically confirmed) 1D Cu/Ni polymer.

## Experimental Section

All chemicals were of reagent grade and used as received. All experiments were carried out in air. Elemental analyses for metals were performed by atomic absorption spectroscopy by the Department of Chemistry, National Taras Shevchenko University of Kyiv and with a vario EL III Universal CHNOS Elemental Analyzer (for C, H, N) in the Department of Chemistry, University of Wrocław.

**Synthesis of  $[\text{Cu}(\text{en})_2(\mu_2\text{-H}_2\text{O})_2\text{Ni}(\text{OAc})_4]\cdot 4\text{H}_2\text{O}$ :** Copper powder (0.16 g, 0.0025 mol),  $\text{Ni}(\text{OAc})_2\cdot 4\text{H}_2\text{O}$  (0.62 g, 0.0025 mol),  $\text{NH}_4\text{OAc}$  (0.39 g, 0.005 mol),  $\text{CH}_3\text{OH}$  (25 mL) and ethylenediamine (0.5 mL, 0.0075 mol) were heated to 50–60 °C and stirred magnetically for about 3 h. Dark violet crystals formed immediately after cooling of the resulting solution. The crystals were filtered, washed with *i*PrOH and dried in vacuo at room temperature. Yield: 0.83 g, 56%.  $\text{C}_{12}\text{H}_{40}\text{CuN}_4\text{NiO}_{14}$  (586.72): calcd. C 24.57, H 6.87, Cu 10.83, N 9.55, Ni 10.01; found C 24.6, H 6.9, Cu 11.0, N 9.7, Ni 10.1. The compound is sparingly soluble in dmsO, dmf and water and is indefinitely stable in air.

**Physical Measurements:** Infrared spectra were recorded by using KBr discs with a Spectrum BX-FTIR “Perkin–Elmer” spectrophotometer in the 4000–400 cm<sup>-1</sup> region. UV/Vis spectra were recorded with a Perkin–Elmer Lambda 900 spectrophotometer by using the diffuse-reflectance technique. EPR spectra were recorded

with a Bruker ESP 300E (Bruker, Germany) spectrometer operating at X-band and equipped with a Bruker NMR gaussmeter ER 035M and a Hewlett–Packard microwave frequency counter HP 5350B. High-frequency EPR spectra were recorded with a home-built spectrometer at the EMR facility of NHMFL.<sup>[29]</sup> The instrument is a transmission-type device in which waves are propagated in cylindrical light-pipes. The microwaves were generated with a Gunn oscillator, operating at  $95 \pm 3$  GHz. Higher frequencies (by a factor 2, 3 or 4) were obtained by using a Schottky diode based multiplier and appropriate high-pass filters. A phase-locked oscillator (Virginia Diodes) operating at a frequency of  $13 \pm 1$  GHz and generating its harmonics, of which the 4th, 8th, 16th, 24th and 32nd were available, was also used. A superconducting magnet (Oxford Instruments) capable of reaching a field of 17 T was employed. Magnetic susceptibility data were measured with a SQUID magnetometer (Quantum Design MPMSXL-5) over the temperature range 1.8–300 K at a magnetic induction of 0.5 T. The corrections for diamagnetism of the constituent atoms were calculated from the Pascal constants.<sup>[30]</sup> Experimental susceptibilities were also corrected for temperature-independent paramagnetism (TIP) ( $260 \times 10^{-6}$  cm<sup>3</sup> mol<sup>-1</sup>).

**X-ray Structure Determination:**  $\text{C}_{12}\text{H}_{40}\text{CuN}_4\text{NiO}_{14}$  ( $M_r = 586.7$  g mol<sup>-1</sup>),  $T = 150(2)$  K, triclinic,  $P\bar{1}$ ,  $a = 8.488(2)$  Å,  $b = 8.782(2)$  Å,  $c = 8.799(2)$  Å,  $\alpha = 91.632(4)^\circ$ ,  $\beta = 102.516(4)^\circ$ ,  $\gamma = 96.535(4)^\circ$ ,  $V = 635.2(3)$  Å<sup>3</sup>,  $Z = 1$ ,  $\mu(\text{Mo-K}\alpha) = 1.645$  mm<sup>-1</sup>,  $\rho_{\text{calcd.}} = 1.534$  g cm<sup>-3</sup>, 5906 reflections measured ( $\theta_{\text{max}} = 29.0^\circ$ ), 3037 unique ( $R_{\text{int}} = 0.020$ ) and of these 2550 had  $I > 2\sigma(I)$ . The final residuals were  $R_1 = 0.034$  [ $I > 2\sigma(I)$ ] and  $wR_2 = 0.087$  (all data) for 205 parameters. Data collection was by means of a Bruker SMART CCD diffractometer with subsequent full-matrix refinement on  $F^2$  using the program SHELXL-97<sup>[31]</sup> after multi-scan absorption corrections ( $T_{\text{max/min}} = 1/0.84$ ). Anisotropic displacement parameters were employed for the non-hydrogen atoms. The hydrogen atoms of the bridging water molecule were clearly observed in later difference maps. Two solvent water molecules were modelled as being disordered over two pairs of sites with the occupancy factors set at 0.5 after a trial refinement. Water-molecule H-atom parameters were refined with restrained geometries. All remaining H-atoms were added at calculated positions and refined by use of a riding model with isotropic displacement parameters based on that of the parent atom. CCDC-665382 contains the crystallographic data for this paper. These data can be obtained free of charge from The Cambridge Crystallographic Data Centre via [www.ccdc.cam.ac.uk/data\\_request/cif](http://www.ccdc.cam.ac.uk/data_request/cif).

## Acknowledgments

This work was supported in part by the Fundamental Research Fund of Ukraine (Project 28.3/017) and by the National High Magnetic Field Laboratory (NHMFL). The NHMFL is funded by the National Science Foundation (NSF) through the Cooperative

Agreement No. DMR-0654118, by the State of Florida and by the Department of Energy (DOE). Further thanks for financial support go to the Austrian Science Foundation (FWF Project 19335-N17).

- [1] S. Tanase, J. Reedijk, *Coord. Chem. Rev.* **2006**, *250*, 2501–2510; E. J. L. McInnes, S. Piligkos, G. A. Timco, R. E. P. Winpenny, *Coord. Chem. Rev.* **2005**, *249*, 2577–2590; S. A. Kozimor, B. M. Bartlett, J. D. Rinehart, J. R. Long, *J. Am. Chem. Soc.* **2007**, *129*, 10672–10674; W.-G. Wang, A.-J. Zhou, W.-X. Zhang, M.-L. Tong, X.-M. Chen, M. Nakano, C. C. Beedle, D. N. Hendrickson, *J. Am. Chem. Soc.* **2007**, *129*, 1014–1015; L. Engelhardt, C. Martin, R. Prozorov, M. Luban, G. A. Timco, R. E. P. Winpenny, *Phys. Rev. B* **2009**, *79*, 014404–014412; B. Gillon, C. Mathoniere, E. Ruiz, S. Alvarez, A. Cousson, T. M. Rajendiran, O. Kahn, *J. Am. Chem. Soc.* **2002**, *124*, 14433–14441; R. Clérac, H. Miyasaka, M. Yamashita, C. Coulon, *J. Am. Chem. Soc.* **2002**, *124*, 12837–12844.
- [2] O. Kahn, *Molecular Magnetism*, VCH, Weinheim, **1993**; V. Gadet, T. Mallah, I. Castro, M. Verdaguer, P. Veillet, *J. Am. Chem. Soc.* **1992**, *114*, 9213–9214; D. Gatteschi, O. Kahn, J. S. Miller, F. Palacio, Eds.; *NATO Advanced Study Institute Series E*; Plenum: New York, **1991**, vol. 198, 281.
- [3] M. K. Saha, F. Lloret, I. Bernal, *Inorg. Chem.* **2004**, *43*, 1969–1975; E. Ruiz, P. Alemany, S. Alvarez, J. Cano, *J. Am. Chem. Soc.* **1997**, *119*, 1297–1303; E. Ruiz, P. Alemany, S. Alvarez, J. Cano, *Inorg. Chem.* **1997**, *36*, 3683–3688; E. Ruiz, S. Alvarez, P. Alemany, *Chem. Commun.* **1998**, 2767–2768.
- [4] E. K. Brechin, *Chem. Commun.* **2005**, 5141–5153; A. M. Kirillov, M. N. Kopylovich, M. V. Kirillova, M. Haukka, M. F. C. Guedes da Silva, A. J. L. Pombeiro, *Angew. Chem. Int. Ed.* **2005**, *44*, 4345–4349; L. M. Wittick, K. S. Murray, B. Moubarak, S. R. Batten, L. Spiccia, K. J. Berry, *Dalton Trans.* **2004**, 1003–1011; G. A. Seisenbaeva, S. Gohil, V. G. Kessler, *J. Mater. Chem.* **2004**, *14*, 3177–3190.
- [5] R. Vilar, *Angew. Chem. Int. Ed.* **2003**, *42*, 1460–1477; L. Zhao, V. Niel, L. K. Thompson, Z. Xu, V. A. Milway, R. G. Harvey, D. O. Miller, C. Wilson, M. Leech, J. A. K. Howard, S. L. Heath, *Dalton Trans.* **2004**, 1446–1455.
- [6] D. L. Reger, R. F. Semeniuc, V. Rassolov, M. D. Smith, *Inorg. Chem.* **2004**, *43*, 537–554; L. J. Prins, D. N. Reinhoudt, P. Timmerman, *Angew. Chem. Int. Ed.* **2001**, *40*, 2382–2426; B. Moulton, M. J. Zaworotko, *Chem. Rev.* **2001**, *101*, 1629–1658; D. L. Reger, R. F. Semeniuc, I. Silaghi-Dumitrescu, M. D. Smith, *Inorg. Chem.* **2003**, *42*, 3751–3764; C. J. Janiak, *J. Chem. Soc., Dalton Trans.* **2000**, 3885–3896.
- [7] J. K. Bera, K. R. Dunbar, *Angew. Chem. Int. Ed.* **2002**, *41*, 4453–4457; C. Janiak, L. Uehlin, He.-P. Wu, P. Klufers, H. Piotrowski, T. G. Scharmann, *J. Chem. Soc., Dalton Trans.* **1999**, 3121–3131.
- [8] R. E. P. Winpenny, in *Compr. Coord. Chem. II* (Eds.: J. A. McCleverty, T. J. Meyer), Elsevier Pergamon, Oxford, **2004**, vol. 7, pp. 125–175; X.-Y. Chen, Y. Bretonniere, J. Pecaut, D. Imbert, J.-C. Bulnzi, M. Mazzanti, *Inorg. Chem.* **2007**, *46*, 625–637; A. Aukauloo, X. Ottenwaelde, R. Ruiz, Y. Journaux, Y. Pei, E. Riviere, M. C. Munoz, *Eur. J. Inorg. Chem.* **2000**, 951–957; C. N. Verani, E. Rentschler, T. Weyhermüller, E. Bill, P. Chaudhuri, *J. Chem. Soc., Dalton Trans.* **2000**, 4263–4271.
- [9] A. Rodriguez-Dieguez, R. Kivekas, R. Sillanpaa, J. Cano, F. Lloret, V. McKee, H. Stoeckli-Evans, E. Colacio, *Inorg. Chem.* **2006**, *45*, 10537–10551; Q.-F. Zhang, W.-H. Leung, X.-Q. Xin, H.-K. Fun, *Inorg. Chem.* **2000**, *39*, 417–426; R. Song, K. M. Kim, Y. S. Sohn, *Inorg. Chem.* **2003**, *42*, 821–826; C. Paraschiv, M. Andruh, S. Ferlay, M. W. Hosseini, N. Kyritsakas, J.-M. Planeix, N. Stanica, *Dalton Trans.* **2005**, 1195–1202; Q.-F. Zhang, Y. Niu, W.-H. Leung, Y. Song, I. D. Williams, X. Xin, *Chem. Commun.* **2001**, 1126–1127.
- [10] A. D. Garnovskii, B. I. Kharissov, *Direct Synthesis of Coordination and Organometallic Compounds*, Elsevier Science Amsterdam, **1999**; V. V. Semenaka, O. V. Nesterova, V. N. Kokozay, V. V. Dyakononko, O. V. Shishkin, R. Boca, J. Jezierska, *Dalton Trans.* **2010**, 39, 1734–1739; O. V. Nesterova, S. R. Petrusenko, V. N. Kokozay, B. W. Skelton, J. Jezierska, W. Linert, A. Ozarowski, *Dalton Trans.* **2008**, 1431–1436; D. S. Nesterov, V. N. Kokozay, B. W. Skelton, *Eur. J. Inorg. Chem.* **2009**, 5469–5473; E. A. Buvaylo, V. N. Kokozay, O. Y. Vassilyeva, B. W. Skelton, I. L. Eremenko, J. Jezierska, A. Ozarowski, *Inorg. Chem.* **2009**, *48*, 11092–11097; D. S. Nesterov, V. N. Kokozay, B. W. Skelton, J. Jezierska, A. Ozarowski, *Dalton Trans.* **2007**, 558–564.
- [11] a) O. V. Pryma, S. R. Petrusenko, V. N. Kokozay, B. W. Skelton, O. V. Shishkin, T. S. Teplytska, *Eur. J. Inorg. Chem.* **2003**, 1426–1432; b) O. V. Pryma, S. R. Petrusenko, V. N. Kokozay, O. V. Shishkin, M. V. Zhigalko, *Inorg. Chem. Commun.* **2003**, *6*, 896–899; c) O. V. Nesterova, A. V. Lipetskaya, S. R. Petrusenko, V. N. Kokozay, B. W. Skelton, J. Jezierska, *Polyhedron* **2005**, *24*, 1425–1434; d) O. V. Nesterova, S. R. Petrusenko, V. N. Kokozay, B. W. Skelton, J. Jezierska, W. Linert, A. Ozarowski, *Dalton Trans.* **2008**, 1431–1436.
- [12] a) L. Shen, Y.-Z. Xu, *J. Chem. Soc., Dalton Trans.* **2001**, 3413–3414; b) M. Ohba, N. Fukita, H. Okawa, *J. Chem. Soc., Dalton Trans.* **1997**, 1733–1738; c) M. Clemente-León, E. Coronado, J. R. Galán-Mascarós, C. J. Gómez-García, Th. Woiike, J. M. Clemente-Juan, *Inorg. Chem.* **2001**, *40*, 87–94; d) Z.-M. Wang, B.-W. Sun, J. Luo, S. Gao, C.-S. Liao, C.-H. Yan, Y. Li, *Inorg. Chim. Acta* **2002**, *332*, 127–134; e) O. Kahn, E. Bakalbassis, C. Mathoniere, M. Hagiwara, K. Katsumata, L. Ouahab, *Inorg. Chem.* **1997**, *36*, 1530–1531.
- [13] *Cambridge Structural Database (CSD)*, Version 5.30, Sep **2009**; F. H. Allen, *Acta Crystallogr., Sect. B* **2002**, *58*, 380–388.
- [14] G. B. Deacon, R. J. Phillips, *Coord. Chem. Rev.* **1980**, *33*, 227–250.
- [15] A. B. P. Lever, *Inorganic Electronic Spectroscopy*, 2nd ed., Elsevier Science Amsterdam, Oxford, New York, Tokyo, **1984**.
- [16] a) L. Strinna Erre, G. Micera, F. Cariati, G. Ciani, A. Sironi, H. Kozloski, J. Baranowski, *J. Chem. Soc., Dalton Trans.* **1988**, 363–367; b) T. Glowinski, H. Kozłowski, L. Strinna Erre, B. Gulinati, G. Micera, A. Pozzi, S. Bruni, *J. Coord. Chem.* **1992**, *25*, 75–84; c) L.-K. Li, Z.-Y. Cao, H.-W. Hou, *J. Coord. Chem.* **2008**, *61*, 2105–2112.
- [17] B. J. Hathaway, *Compr. Coord. Chem.* (Eds.: G. Wilkinson, R. D. Gillard, J. A. McCleverty), Pergamon Press, Oxford, **1987**, vol. 5, pp. 533–774; A. F. Wells, *Structural Inorganic Chemistry*, 5th ed., Clarendon Press, Oxford, **1986**.
- [18] a) K. M. Kim, Y.-A. Lee, S. S. Lee, Y. S. Sohn, *Inorg. Chim. Acta* **1999**, *292*, 52–56; b) V. Kh. Sabirov, M. A. Porai-Koshits, Yu. T. Struchkov, *Koord. Khim.* **1994**, *20*, 691–700.
- [19] D. B. Leznoff, B. Y. Xue, R. J. Batchelor, F. W. B. Einstein, B. O. Patrick, *Inorg. Chem.* **2001**, *40*, 6026–6034; R. W. Matthews, M. McPartlin, I. J. Scowen, *Chem. Commun.* **1996**, 309–310.
- [20] a) V. G. Makhankova, A. O. Beznischenko, V. N. Kokozay, R. I. Zubatyuk, O. V. Shishkin, J. Jezierska, A. Ozarowski, *Inorg. Chem.* **2008**, *47*, 4554–4563; b) B. N. Kolarz, D. Jermakowicz-Bartkowiak, J. Jezierska, W. Apostoluk, *React. Funct. Polym.* **2001**, *48*, 169–179; c) J. Peisach, W. E. Blumberg, *Arch. Biochem. Biophys.* **1974**, *165*, 691–708.
- [21] M. Verdaguer, M. Julve, A. Michalowicz, O. Kahn, *Inorg. Chem.* **1983**, *22*, 2624–2629.
- [22] J. Long, L.-M. Chamoreau, C. Mathoniere, V. Marvaud, *Inorg. Chem.* **2009**, *48*, 22–24; R. H. Ismayilov, W.-Z. Wang, G.-H. Lee, S.-M. Peng, *Dalton Trans.* **2006**, 478–491; A. Bienko, J. Kłak, J. Mroziński, S. Domagala, B. Korybut-Daszkiewicz, K. Woźniak, *Polyhedron* **2007**, *26*, 5030–5038; E. Colacio, I. B. Maimoun, F. Lloret, J. Suárez-Varela, *Inorg. Chem.* **2005**, *44*, 3771–3773; F. Sapina, E. Escrivá, J. V. Folgado, A. Beltrán, D. Beltrán, A. Fuertes, M. Drillon, *Inorg. Chem.* **1992**, *31*, 3851–3858.
- [23] a) F. Sapina, E. Escrivá, J. V. Folgado, A. Beltrán, D. Beltrán, A. Fuertes, M. Drillon, *Inorg. Chem.* **1992**, *31*, 3851–3858; b)

- E. Colacio, I. B. Maimoun, F. Lloret, J. Surez-Varela, *Inorg. Chem.* **2005**, *44*, 3771–3773; c) O. Jeannin, R. Clerac, T. Cauchy, M. Fourmigue, *Inorg. Chem.* **2008**, *47*, 10656–10661.
- [24] C. Diaz, J. Ribas, R. Costa, J. Tercero, M. Salah El Fallah, X. Solans, M. Font-Bardía, *Eur. J. Inorg. Chem.* **2000**, 675–681.
- [25] W.-L. Liu, Y. Zou, C.-L. Ni, Y.-Z. Li, Q.-J. Meng, *J. Mol. Struct.* **2005**, *751*, 1–6.
- [26] A. Fuertes, C. Miravittles, E. Escrivá, E. Coronado, D. Beltrán, *J. Chem. Soc., Dalton Trans.* **1987**, 1847–1851.
- [27] S. Zhan, C. Hu, X. Chen, Q. Meng, C. Lu, G. Wang, P. Zheng, *Polyhedron* **1999**, *18*, 2035–2039.
- [28] E. Colacio, J. M. Dominguez-Vera, A. Escuer, R. Kivekaes, A. Romerosa, *Inorg. Chem.* **1994**, *33*, 3914–3924.
- [29] A. K. Hassan, L. A. Pardi, J. Krzystek, A. Sienkiewicz, P. Goy, M. Rohrer, L.-C. Brunel, *J. Magn. Reson.* **2000**, *142*, 300–312.
- [30] E. König, *Magnetic Properties of Coordination and Organometallic Transition Metal Complexes*, Springer, Berlin, **1966**.
- [31] G. M. Sheldrick, *Acta Crystallogr., Sect. A* **2008**, *64*, 112–122.

Received: February 22, 2010  
Published Online: June 16, 2010